Universidad de Granada

Alkaline activation of clays for the consolidation of earthen architecture

Tesis Doctoral 2014

Kerstin Elert

Dpto. Mineralogía y Petrología

Editor: Editorial de la Universidad de Granada
Autor: Kerstin Elert
D.L.: GR 1923-2014
ISBN: 978-84-9083-094-9

ugr | Universidad de Granada

La doctoranda Kerstin Elert y los directores de la tesis Eduardo Sebastian Pardo y Carlos Rodriguez Navarro, garantizamos, al firmar esta tesis doctoral, que el trabajo ha sido realizado por el doctorando bajo la dirección de los directores de la tesis y hasta donde nuestro conocimiento alcanza, en la realización del trabajo, se han respetado los derechos de otros autores a ser citados, cuando se han utilizado sus resultados o publicaciones.

Granada, a 15 de Marzo de 2014

Director/es de la Tesis

Fdo.: Eduardo M. Sebastián

Fdo.: CARLOS RODRIGUEZ NAVARRO

Doctorando

Fdo.: Kerstin Elert

Acknowledgement

First of all I would like to thank my Ph.D. advisors Eduardo M. Sebastián Pardo and Carlos M. Rodríguez Navarro for their continuous support and guidance during all these years.

I would like to express my special appreciation to Manuel Rodriguez Gallego for answering patiently all my questions regarding mineralogy, crystallography and chemistry.

I am also thankful to Fernando J. Nieto García for sharing his broad knowledge on clay mineralogy and clay analysis.

I am indebted to José Daniel Martin Ramos for his assistance with XRD analysis and the interpretation of XRD patterns.

I would like to extend my thanks to Encarnación Ruiz-Agudo for being available to solve many of my doubts related to chemical issues and her assistance with the titration of alkaline solutions.

Special thanks to Francisco Javier Huertas Puerta for sharing his extensive knowledge on clay reactivity and for supplying some of the clay samples used in this study.

In addition, I would like to thank Francisca Martinez-Ruiz for her advice during preparation and analysis of clay minerals.

I am grateful to Jorge Rodriguez Navarro and Alejandro Rodriguez Navarro for answering all my questions regarding chemistry and crystallography.

Thanks also to Guiseppe Cultrone and Carolina Cardell Fernández for sharing their knowledge on the conservation of monuments and computer related issues.

Furthermore, I would like to thank Eduardo Molina and Ana Rizzi for their assistance with color and compression strength measurements.

I have to extend my thanks to the staff of the CIC-UGR, the IACT-CSIC and the Department of Mineralogy and Petrology, namely to Alicia González Segura (FESEM), Maria del Mar Abad Ortega and Javier Cifuentes Melchor (TEM), Conception Hernández Castilla (sample preparation), Bendición Funes Martin (Particle Size Analysis), Miguel Ángel Salas Peregrin (TG-FTIR), Juan Santamarina Urbano (XRD), Maria Carmen Niembro Bueno (XRF), Isabel Nieto García, Emilia Abarca Gonzalez, Jesus Montes Rueda and Agustin Rueda Torres (sample preparation).

Finally, I would like to thank all members of the Department of Mineralogy and Petrology (UGR), especially Miguel Ortega Huertas for his continuous help and support.

Index

Abstract

Thesis: Alkaline activation of clays for the consolidation of earthen architecture

Introduction

Earth is one of the oldest construction materials man has used. For instance, the remains of adobe structures of the city of Jericho date back to 8000 B.C (Houben and Guillaud 1994). Examples can be found in many countries and a great variety of earthen structures exists in Spain, including important monuments like the Alhambra in Granada, the "Murallas de Niebla" in Huelva or rural houses in Castilla-León and Aragón. Furthermore, earth is still one of the most employed construction materials in developing countries. In fact, nearly one third of the world´s population lives in buildings made of earth (Ren and Kagi 1995).

Earthen architecture (i.e. buildings and archaeological remains) is strongly affected by physical and chemical weathering (Brown y Clifton 1978). Clays are one of the main components of soil, acting as binder for the other constituents such as sand and silt. Alteration due to swelling and contraction of smectites or other expandable clays in contact with water has an important effect on the durability of earthen constructions since it may cause fissures, cracks and granular disintegration or may even result in the total loss of the structure (Rodriguez-Navarro et al. 1998). It can be deduced from the above that water of different sources (rain, condensation, capillary rise) is the most important extrinsic factor in the deterioration of earthen architecture.

At present, the majority of historic buildings and archaeological remains made of earth exhibits important conservation problems which require consolidation. A recent survey showed that one of the most demanded aspects requested by specialists in charge of the conservation of earthen architecture was the development of new consolidation treatments that could be applied in situ to these sensitive materials. These treatments should be both efficient and durable (Palumbo et al. 1999).

Historically, additives such as blood, alum, manure, bones, animal fat or vegetable oil, asphalt or lime were used to increase the materials cohesion, and in some cases to confer a certain hydrophobicity to adobe and rammed earth constructions (Lunt 1980). In modern construction lime, cement or asphalt emulsion may be used. However, many of these additives might not be suitable from a conservation point of view because they cause severe discoloration, could act as nutrients for insects and microorganism or modify physical characteristics of the earthen structure which in turn might result in increased degradation.

A great variety of products have been employed in architectural conservation, including natural resins, synthetic polymers, silicones, alcoxysilanes, lime and Portland cement (Oliver 2008). Frequently, treatments had only limited success and, occasionally, led to a total failure due to esthetical, chemical or physico-mechanical incompatibility of the product or, simply, due to limited penetration. Most importantly, treatments often only diminished the alteration effects but did not tackle the cause of the problem, the expansion and contraction of the clay minerals. Treatments, thus, were ineffective over the long run because the action of expandable clays continued as a result of changes in the moisture content of the earthen structure and destroyed the consolidation capacity of the applied product. Doehne and Price (2010) concluded that in the case of clay-rich stones the focus of conservation treatments should be on reducing clay swelling and not on increasing strength. The same applies to earthen materials.

The above shows the urgent need for the development of a more effective method that allows the in situ consolidation of earthen architecture by reducing the swelling capacity of clays. The swelling capacity could be reduced by transforming clays into non-expandable binding materials such as calcium silicate hydrates or other aluminiosilicates with cementing capacity, i.e. amorphous aluminosilicates or zeolitic phases. This transformation could be achieved by using an alkaline activator which reacts with clay minerals at high pH. $Ca(OH)_2$, NaOH or KOH might be suitable as alkaline activators.

As mentioned above lime has been used since ancient times as a stabilizer for earthen architecture. Its stabilizing effect involves pozzolanic reactions with aluminosilicates and their transformation into calcium silicate hydrate (CSH) or calcium aluminate hydrate (CAH) compounds and zeolitic phases which were recognized in antique roman mortars (Roy 1999). NaOH and KOH are also suitable for the alkaline activation of aluminosilicates. Both have been widely employed in the synthesis of zeolites since the mid-1930s (Flanigen et al. 2010). More recently the geochemistry that yielded the synthesis of zeolites has been applied for the production of alkaline activated cements. These new cements show high mechanical strength and water resistance due to the formation of an amorphous phase, i.e., a zeolite precursor. This phase formed upon dissolution of aluminiosilicates at high pH (Davidovits 1994). In conclusion, the above mentioned CSH, CAH and zeolitic phases act as cementing agents and could improve the durability and mechanical strength of earthen architecture.

Objectives

The main objective of this study is the evaluation of alkaline activation as an alternative consolidation treatment for clayey material such as rammed earth or adobe. The conservation needs of earthen structures like the Alhambra or the historic city walls of Granada could be addressed using this consolidation technique.

Consolidation treatments for earthen architecture are generally applied at room *T*. The curing of alkali-activated cements, on the other hand, is commonly performed at temperatures ≥ 30 °C. Zeolite synthesis is carried out at even higher temperatures ≥ 60 °C. Thus, an important aspect of this study is the evaluation of the extent of mineral transformation under high pH conditions at room *T*. Furthermore, mainly kaolinite (frequently metakaolinite) has been used for the preparation of alkali-activated cements and the synthesis of zeolites. Thus, other clay minerals commonly present in earthen structures, such as smectites or illite, have to be included in this investigation in order to study their reactivity under high pH conditions. In addition, the influence of the clays structural and compositional characteristics on the effectiveness of alkaline activation, e.g. trioctahedral- (saponite) versus dioctahedral smectite (montmorillonite), has to be addressed.

The evaluation will also have to consider factors influencing the effectiveness of alkaline activation as a consolidation method, including the interference of soil organic matter with the alkaline activation of clays or the efficacy of different activator solutions, e.g. $Ca(OH)_2$, NaOH and KOH.

In the preparation of alkali-activated cements and in the synthesis of zeolites, clay minerals are directly mixed with the alkaline solution. In contrast, alkaline activation in a conservation treatment has to be performed by impregnation with the consolidating solution, as it is commonly done when applying conventional consolidation treatments. Thus, it has to be determined whether an adequate penetration can be achieved in adobe blocks using alkaline solutions and whether the alkaline solution concentration is sufficiently high within the earthen structure to promote mineral transformation and stabilization. The suitability and performance of this consolidation method as an in situ treatment has to be evaluated. The ultimate goal of this Ph.D. thesis is to determine whether alkaline treatments can improve the water resistance and mechanical properties of earthen materials.

Materials and methods

Previous mineralogical studies of earthen constructions in the Granada area, including the city walls of Granada and the rammed earth walls of the

Alhambra, confirmed the presence of illite, kaolinite and smectite as main clay minerals, with minor amounts of chlorite and paragonite (de la Torre et al., 1996, Ontiveros et al., 1999). The bibliographic review of the mineralogical composition of earthen constructions revealed that these minerals, maybe with the exception of paragonite which is a mineral of rather rare occurrence, are the most common in the majority of earthen structures around the world (Houben and Guillaud, 1994). For our study we chose the soil from the nearby hills (Alhambra Formation) which was historically used as a construction material for most rammed earth structures in Granada (de la Torre et al., 1996, Ontiveros et al., 1999).

Preliminary results demonstrated certain difficulties in identifying mineralogical changes in the Alhambra Formation soil upon alkaline attack due to the presence of various clay minerals in this soil (Elert et al. 2008). Thus, pure clays, namely kaolinite, montmorillonite, saponite and illite, were included in this study in order to determine their reactivity as well as to enable the application of our results to soils with different clay mineral composition. The above mentioned pure clay minerals as well as soil from the Alhambra Formation have, therefore, been used as starting materials for alkaline activation in this study.

In order to evaluate the reactivity of the different clay minerals, 5 g of powdered clay samples (< 2 µm fraction) were subjected to alkaline activation using 100 ml of the following solutions:

a) 0.025 M $Ca(OH)_2$, this concentration corresponds to a saturated solution at room *T*.
b) 0.4 M NaOH
c) 0.4 M KOH
d) 5 M NaOH
e) 5 M KOH

Note that solutions with similar concentrations are commonly used in zeolite synthesis (Breck 1974) and for the preparation of alkaline activated cements (Xu and Van Deventer 2000).

The clay samples were kept in tightly capped polypropylene bottles and stored in the laboratory at 20 °C. Bottles were stirred periodically. Samples for analysis were taken at predetermined time intervals.

A wide variety of analytical techniques have been employed in order to study the chemical, compositional and morphological characteristics of the tested clay minerals before and after alkaline activation. These techniques include X-ray fluorescence (XRF), X-ray diffraction (XRD), field emission scanning electron microscopy (FESEM), transmission electron microscopy (TEM), elemental analysis, thermogravimetric analysis (TG) coupled with

Fourier transform infrared spectroscopy (FTIR) for evolved gas analysis, particle size analysis and nitrogen sorption (BET).

Furthermore, soil from the Alhambra Formation was used to prepare adobe test blocks which were treated by impregnation with the various alkaline solutions as a proxy to an in situ treatment. Afterwards, the adobe samples were submitted to further testing in order to evaluate the efficiency of the treatment. Hydric and mechanical properties of untreated and treated adobe test blocks were evaluated using water absorption tests, mercury intrusion porosimetry (MIP), compressive strength and drilling resistance tests. Furthermore, color measurements were performed to determine color change due to alkaline activation.

The limited bibliographic evidence (Lunt 1980, Claret et al. 2002) regarding a possible inhibiting effect on clay reactivity caused by organic matter in soils, motivated the study of the clay transformation in the case of Alhambra Formation soil with and without organic matter. For this purpose one batch of the clay was treated with H_2O_2 prior to alkaline activation in order to remove organic matter.

Preliminary studies revealed the possibility of salt formation during alkaline treatments. Excess alkali reacted with atmospheric CO_2 and formed carbonates which might be potentially damaging to porous materials. In order to evaluate the damage potential of the observed salts, a study was performed using a common test method where calcarenite prisms were partially immersed in different salt solutions including Na_2SO_4, Na_2CO_3, K_2CO_3 and $KHCO_3$. Note that calcarenite prisms had to be used because adobe blocks would not have withstood the action of the water-based solutions.

Results and discussion

The experimental results of this study have clearly shown that clay minerals can be transformed into cementing materials using alkaline solutions at room *T*. These cementing materials included zeolite precursors, zeolites, CSH phases and calcite. Additionally, some clay minerals experienced transformation into mixed-layer clays.

The response towards alkaline activation was not the same for the different clay minerals tested here. Kaolinite and dioctahedral smectite dissolved and transformed readily. Saponite experienced a slower transformation into a smectite-chlorite interstratification which still showed expansion and did not transform into zeolites. The highly crystalline illite tested here, on the other hand, only suffered minor chemical modifications. The different response of the various clay minerals can be related to structural and compositional characteristics (Sposito 1984, Schoonheydt and Johnston

2006). Kaolinite, a 1:1 clay, showed extensive dissolution because >AlOH groups at the gibbsite layer additional to the hydroxyl groups at broken edges, steps and defect sites contributed to the clays overall reactivity (Huertas et al. 1999). In contrast, the contribution of the basal layer to the reactivity of 2:1 clay minerals is limited and dissolution takes mainly place at the edge surfaces. The lower reactivity of illite if compared with montmorillonite, both diactahedral 2:1 clays, can be explained considering compositional differences. Illite has a much higher net charge due to isomorphic substitution in the tetrahedral layer which is compensated by K^+. In montmorillonite, on the other hand, layer charge is mainly caused by octahedral substitution and is compensated by Na^+. The compositional differences result in a more stable structure in the case of illite which commonly has a higher crystallinity and lower specific surface area than montmorillonite and does not experience intracrystalline swelling. Montmorillonite, in contrast swells readily in polar solvents and offers a much larger surface area for reaction (Newman and Brown 1987, Sposito 1984). Saponite, being an expandable clay, showed lower reactivity under alkaline conditions. This is thought to be due to the presence of mainly Mg in its octahedral layer (Becerro et al. 2009). Furthermore, isomorphic substitution commonly occurs in the tetrahedral layer and is compensated by Ca^{2+} or Mg^{2+} which might add to the clay´s stability (Newman and Brown 1987).

Whereas extensive zeolite formation was observed in kaolinite and montmorillonite, no zeolites were detected in the case of saponite which is thought to be due to the low Al content of this clay mineral. In illite samples treated with KOH, some zeolites were detected. However, kaolinite present as an impurity in illitic clay seemed to have been the source material for these zeolites.

The clay minerals of the Alhambra Formation soil, a mixture of kaolinite, smectite, illite and paragonite, generally showed a similar transformation path as observed for the pure clays. However, kaolinite experienced a faster dissolution in the case of the Alhambra Formation soil, because the crystallinity of this kaolinite was lower than the one of the pure clay.

Apart from the mineral composition, the soil organic matter content might have an important influence on the successfulness of the alkaline treatment. Our results indicate that mineral dissolution and transformation was delayed as a result of the presence of organic matter. The organic matter content was 1 wt% in the case of the Alhambra Formation soil.

The different response of the various clay minerals tested here as well as the influence of organic matter on the efficiency of the treatment shed light on an important aspect to be considered prior to the application of any

consolidation treatment. A detailed study of the earthen materials mineral composition and organic matter content is necessary. For example, a high concentration of saponitic clays or an elevated organic matter content may render this treatment inefficient.

This study further revealed that when saturated $Ca(OH)_2$ solution was used, a high enough pH could not be maintained to promote adequate mineral dissolution and transformation. Highly concentrated NaOH and KOH solutions, in contrast, resulted in extensive transformation in the case of the majority of clay minerals tested here. In general it can be concluded that a sufficiently high pH well above 10 has to be maintained during the treatment to ensure adequate mineral dissolution and transformation.

Comparing the zeolitic phases formed using the different alkaline solutions, the structure directing role of Na^+ and K^+ was evident (Barrer 1982). When NaOH was used a faujasite-type zeolite and a hydroxysodalite formed. In the case of KOH, zeolite K-I as well as zeolite K-F and/or a chabazite-type zeolite were observed independent of the clay mineral used as the starting material.

As indicated above, both, NaOH and KOH solutions were both effective in producing mineralogical changes. However, salt crystallization tests evidenced that sodium carbonates, which have been observed to form during the alkaline treatment with NaOH, have a much higher damaging potential than potassium carbonate and/or bicarbonate. The later phases might form as a byproduct of the KOH treatment. Considering these results, it can be concluded that KOH solutions are preferable for the use in conservation treatments.

Treatments of adobe test blocks with highly alkaline solutions showed that an improvement in water resistance was achieved. A comparative study using concentrated KCl solutions allowed us to verify that the observed improved resistance was due to clay mineral dissolution and transformation at high pH into amorphous aluminosilicate phases with cementing properties. Cationic exchange or the osmotic effect exerted by highly concentrated electrolytes, on the other hand, seemed to have played a negligible role in this improvement. The mineralogical and morphological study of the treated adobe test blocks led us to the conclusion that amorphous phases, possibly zeolite precursors which formed after 50 days of curing, served as cementing material and improved mechanical strength. Crystalline zeolitic phases were not observed in the treated adobe test blocks. It is believed that the formation of zeolites, which would require longer treatment durations, is not necessary in order to achieve a considerable strength increase.

Conclusions

Our research proved that the application of alkaline solutions for the consolidation of earthen structures can be regarded as a valuable alternative to conventional consolidation treatments. The majority of the tested clay minerals experienced extensive dissolution and transformation upon alkaline activation using NaOH and KOH. Furthermore, adobe test blocks showed a significant improvement in water resistance and mechanical strength after impregnation with NaOH or KOH and curing for 50 days at room *T*. However, salt crystallization tests indicated that KOH would be preferable because potassium carbonates are less damaging than sodium carbonates. This study further revealed that the soil`s organic matter content has to be taken into consideration because it might have an retardation effect on clay dissolution and transformation reactions. In any case, a detailed study of the earthen material`s mineral composition and organic matter content is necessary to ensure the viability of an alkaline treatment.

Several aspects were identified which deserve further research. These include the possible use of less concentrated alkaline solutions to control the risk of carbonate formation due to excess alkali as well as to reduce treatment cost and environmental impact; the testing of adobe blocks prepared from soil with high smectite or organic matter content to evaluate the feasibility of this treatment method under adverse conditions; or the preparation of conservation mortars using a mixture of soil and an alkaline solution.

Finally, the positive outcome of the laboratory results should be confirmed by an in situ study in the field. For this purpose adobe test walls or, ideally, pilot areas in historic earthen structures could be treated with alkaline solutions and their performance monitored over long periods of time.

Bibliography

Barrer, R.M., *Hydrothermal Chemistry of Zeolites*, Academic Press, London (1982) 360pp.

Becerro, A., Mantovani, M., Escudero, A., Mineralogical stability of phyllosilicates in hyperalkaline fluids: Influence of layer nature, octahedral occupation and presence of tetrahedral Al, *American Mineralogist* **94** (2009) 1187-1197.

Breck, D.W., *Zeolite molecular sieves – Structure, chemistry and use*, John Wiley and Sons, Inc., New York (1974).

Brown, P.W. and Clifton, J.R. Adobe I: the properties of adobe, *Studies in Conservation*, **23** (1978) 139-146.

Claret, F., Bauer, A., Schäfer, T., Griffault, L., Lanson, B., Experimental investigation of the interaction of clays with high-pH solutions: A case study from the Callavo-Oxfordian formation, Muese-Haute Marne Underground Laboratory (France), *Clays and Clay Minerals* **50** (2002) 633-646

Davidovits, J., Geopolymers: Man-made rock geosynthesis and the resulting development of very early high strength cement, *Journal of Materials education* **16** 2&3 (1994) 91-139

de la Torre, M.J.; Sebastián E., Rodríguez J., A study of the wall material in the Alhambra (Granada, Spain), *Cement and Concrete Research* **26** (1996) 825-839

Doehne, E., Price, C.A., *Stone Conservation - An overview of current research*, The Getty Conservation Institute, Los Angeles ISBN 9781606060469 (2010) 158pp.

Elert, K., Sebastian, E., Valverde, I., Rodriguez-Navarro, C., Alkaline treatment of clay minerals from the Alhambra Formation: Implications for the conservation of earthen architecture, *Applied Clay Science* **39** (2008) 122-132.

Flanigen, E.M., Mumpton, F.A., Commercial properties of natural zeolites, *Mineralogy and Geology of Natural Zeolites*, Mineralogical Society of America Short Course Notes **4** 1977, 165-175.

Huertas, F.J., Chou, L., Wollast, R.,, Mechanism of kaolinite dissolution at room temperature and pressure: Part II. Kinetic Study, *Geochimica et Cosmochimica Acta* **63** (1999) 3261-3275.

Houben, H., Guillaud, H., *Earth construction: a comprehensive guide*. CRA Terre-EAG, Intermediate Technology Publication, London (1994) 362 pp.

Lunt, M.G., Stabilised soil blocks for building, *Building Research Establishment, Overseas Building Notes*, No. **184** (1980) 127-144.

Newman, A.C.D., Brown, G., The chemical constitution of clay, *Chemistry of clays and clay minerals,* Mineralogical Society Monograph No.6, A.C.D. Newman (ed.) Longman Scientific & Technical, London (1987) 1-128.

Oliver, A., Conservation of nondecorated earthen materials, *Terra a Literature Review - An overview of research in earthen architecture conservation*, Avrami, E., Guillaud, H., Hardy, M. (eds.) J. Paul Getty Trust, Los Angeles (2008) 159 pp.

Ontiveros Ortega E., Sebastián Pardo E., Valverde Espinosa I., Deterioration in XI-XIV century Arab ramparts (Granada, Spain). *Materials and Structures* **32** (1999) 45-51.

Palumbo G., Ginell W. S., Rodríguez-Navarro C. *Earthen architecture research survey: Analysis report*. Getty Conservation Institute, Los Angeles (1999).

Ren, K.B., Kagi, D.A., Upgrading the Durability of Mud Bricks by Impregnation, *Building and Environment* **30** (1995) 433-440.

Rodriguez-Navarro, C., Sebastian, E., Doehne, E., Ginell, W.S., The role of sepiolite-palygorskite in the decay of ancient Egyptian limestone sculptures, *Clays and Clay Minerals* **46** (1998) 414-422.

Roy, D.M., Alkali-activated cements. Opportunities and challenges, *Cement and Concrete Research* **29** (1999) 249-254.

Schoonheydt, R.A., Johnston, C.F., Chapter 5. Surface and interface chemistry of clay minerals, *Handbook of Clay Science*, Bergaya, F., Theng, B.K.G., Lagaly, G., (eds.), Elsevier, Oxford (2006) 139-172.

Sposito, G., *The surface chemistry of soils*, Oxford University Press, New York (1984).

Xu, H., van Deventer, J.S.J., The geopolymerisation of alumino-silicate minerals, *International Journal of Mineral Processing* **59** (2000) 247-266.

Resumen

Tesis: La activación alcalina de arcillas para la consolidación de la arquitectura de tierra

Introducción

La tierra es uno de los materiales de construcción más antiguos utilizado por el hombre. Por ejemplo, los restos de estructuras de adobe de la ciudad de Jericó, datan del año 8000 a.c. (Houben y Guillaud 1994). Se pueden encontrar ejemplos de su uso en muchos países y en España existen una gran variedad de estructuras de tierra, incluyendo importantes monumentos como la Alhambra de Granada, las " Murallas de Niebla " en Huelva o las casas rurales de Castilla, León y Aragón. Además, la tierra sigue siendo uno de los materiales de construcción más utilizados en los países en desarrollo. De hecho, casi un tercio de la población mundial vive en edificios hechos de tierra (Ren y Kagi 1995).

La arquitectura de tierra (tanto edificios como restos arqueológicos) se encuentra gravemente afectada por procesos de alteración física y química (Brown y Clifton, 1978). Las arcillas son uno de los principales componentes del suelo o de la tierra empleada en la construcción de estructuras de adobe (ladrillos secados al sol) o tapial (tierra apisonada). Las arcillas actúan como aglutinante de los otros constituyentes tales como la grava, la arena y el limo. La alteración debida a la expansión y contracción de esmectitas o de otras arcillas expansivas en contacto con el agua tiene un efecto importante en la durabilidad de construcciones de tierra, ya que dicha expansión puede causar fisuras, grietas y desintegración granular o incluso puede ocasionar la ruina total de la estructura (Rodríguez-Navarro et al. 1998). De lo anterior se deduce que el agua, de diferentes orígenes (lluvia, condensación, ascenso capilar), es el factor extrínseco más importante en el deterioro de la arquitectura de tierra.

En la actualidad, la mayoría de los edificios históricos y restos arqueológicos hechos de tierra presenta importantes problemas de conservación que requieren su consolidación. Una encuesta reciente mostró que uno de los aspectos más demandados por los restauradores responsables de la conservación de la arquitectura de tierra era el desarrollo de nuevos tratamientos de consolidación que se pudieran aplicar in situ en estos materiales tan sensibles. Estos tratamientos debían ser a la vez eficaces y duraderos (Palumbo et al. 1999).

Históricamente se han utilizado aditivos tales como la sangre, el alumbre, el estiércol, huesos, grasa animal o aceite vegetal, asfalto o cal para aumentar la cohesión de tales materiales, y en algunos casos para conferir una cierta hidrofobicidad al adobe y a las construcciones de tapial (Lunt

1980). En las construcciones modernas se han usado cal, cemento o incluso emulsiones de asfalto para la estabilización de la tierra. Sin embargo, muchos de estos aditivos podrían ser inadecuados desde el punto de vista de la conservación debido a que causan cambios severos de color, pueden actuar como sustancias nutritivas para insectos y microorganismos o pueden modificar las características físicas de la estructura de tierra, lo que a su vez puede provocar un aumento de su degradación.

Se han empleado una gran variedad de productos en la conservación arquitectónica, incluyendo resinas naturales, polímeros sintéticos, siliconas, alcoxisilanos, cal y cemento Portland (Oliver 2008). A menudo, dichos tratamientos han tenido un éxito muy limitado y, en ocasiones, han sido un fracaso total debido a su incompatibilidad estética, química o físico-mecánica o, simplemente debido a una penetración limitada. Pero el problema más importante que presentan es que generalmente sólo maquillan los efectos de la alteración sin frenar la causa del problema; en este caso, la expansión y la contracción de los minerales de la arcilla. Los tratamientos convencionales han sido, por tanto, ineficaces a largo plazo debido a que la acción de las arcillas expansivas continua como resultado de los cambios en la HR y destruye la capacidad consolidante del producto aplicado. Doehne y Price (2010) sugieren que, en el caso de las piedras ricas en arcillas, el enfoque de los tratamientos de conservación debe ser el de reducir la expansión de la arcilla y no el aumento de la resistencia mecánica. Este mismo principio es aplicable en el caso de la conservación de estructuras de tierra.

Lo expresado demuestra la urgente necesidad del desarrollo de un método más eficaz que permita la consolidación in situ de la arquitectura de tierra mediante la reducción de la capacidad de expansión de las arcillas. La capacidad de expansión se podría reducir mediante la transformación de las arcillas en materiales no expansivos tales como silicato de calcio hidratado u otros aluminosilicatos con capacidad cementante, es decir, aluminosilicatos amorfos o fases zeolíticas. Esta transformación se puede lograr mediante el uso de un activador alcalino que reacciona con los minerales de la arcilla a pH elevado. $Ca(OH)_2$, NaOH o KOH podrían, ser por tanto, adecuados como activadores alcalinos.

Como se mencionó anteriormente, la cal se ha utilizado desde la antigüedad como un estabilizante de estructuras de tierra. Su efecto estabilizador implica reacciones puzolánicas con aluminosilicatos y su transformación en silicatos de calcio hidratados (CSH) o aluminatos de calcio hidratados (CAH) así como fases zeolíticas, fases reconocidas en morteros antiguos romanos (Roy 1999). NaOH y KOH también son adecuados para la activación alcalina de aluminosilicatos. Estas bases han sido ampliamente utilizadas en la síntesis de zeolitas desde mediados de la década de 1930

(Flanigen et al. 2010). Más recientemente, la geoquímica que conduce a la síntesis de zeolitas se ha aplicado para la producción de cementos activados alcalinamente. Estos nuevos cementos muestran una alta resistencia mecánica y elevada resistencia al agua debido a la formación de fases amorfas, es decir, precursoras de zeolitas. Estas fases se forman a partir de la disolución de silicatos de aluminio a pH elevado (Davidovits 1994). Fases como CSH, CAH así como fases zeolíticas podrían actuar como agentes cementantes mejorando la durabilidad y la resistencia mecánica de la arquitectura de tierra.

Objetivos

El objetivo principal de este estudio es la evaluación de la activación alcalina como un tratamiento alternativo para la consolidación de materiales arcillosos como tapial o adobe. Las necesidades de conservación de estructuras de tierra como la Alhambra o las murallas de la ciudad de Granada se podrían afrontar mediante esta técnica de consolidación.

Los tratamientos de consolidación de la arquitectura de tierra se aplican generalmente a *T* ambiente. El curado de cementos activados alcalinamente, por otro lado, se realiza comúnmente a temperaturas ≥ 30 ° C. La síntesis de zeolitas se lleva a cabo a temperaturas incluso más altas ≥ 60 ° C. Por lo tanto, un aspecto importante de este estudio es la evaluación de la transformación mineralógica a pH elevado y a *T* ambiente. Además, para la preparación de los cementos activados alcalinamente y la síntesis de zeolitas se ha utilizado principalmente caolinita (frecuentemente metacaolinita). Por lo tanto, deben ser incluidos en esta investigación otros minerales de la arcilla comúnmente presentes en las estructuras de tierra, tales como esmectitas o ilita, para así estudiar su reactividad en condiciones de pH muy alcalino. Además, se analiza la influencia de las características estructurales y composicionales de las arcillas sobre la eficacia de la activación alcalina. Por ejemplo: las esmectitas trioctaédricas (saponita) frente a esmectitas dioctaédricas (montmorillonita).

La evaluación también tendrá que considerar los factores que influyen en la eficacia de la activación alcalina como método de consolidación, incluyendo la interferencia del contenido de materia orgánica del suelo en dicho proceso, o la eficacia de diferentes soluciones activadoras, por ejemplo, $Ca(OH)_2$, NaOH y KOH .

En la preparación de cementos activados alcalinamente y en la síntesis de zeolitas, los minerales de la arcilla se mezclan directamente con la solución alcalina. Sin embargo, la activación alcalina como tratamiento de conservación tiene que ser realizada por impregnación con la solución activadora, como se hace comúnmente durante la aplicación de tratamientos de consolidación

convencionales. Por lo tanto, se tiene que determinar si se puede lograr una penetración adecuada en los bloques de adobe utilizando soluciones alcalinas, y si la concentración de la solución alcalina es suficientemente alta dentro de las estructuras de tierra como para promover la transformación de los minerales de la arcilla y así conseguir una adecuada estabilización. La idoneidad y eficacia de este método de consolidación como tratamiento in situ serán evaluados mediante la aplicación de soluciones alcalinas en bloques de adobe. El objetivo final de esta tesis doctoral es determinar si los tratamientos alcalinos pueden mejorar la resistencia al agua y las propiedades mecánicas de construcciones elaborados con tierra.

Materiales y métodos

Estudios previos confirmaron la presencia de ilita, caolinita y esmectita como principales minerales de la arcilla, con pequeñas cantidades de clorita y paragonita en construcciones de tierra de la zona de Granada, incluyendo sus murallas históricas y las estructuras de tapial de la Alhambra (de la Torre et al., 1996, Ontiveros et al., 1999). La revisión bibliográfica reveló que estos minerales, tal vez con la excepción de la paragonita que es un mineral poco abundante, son los más comunes en la mayoría de las estructuras de tierra de todo el mundo (Houben y Guillaud, 1994). Para nuestro estudio hemos elegido la tierra de las colinas cercanas (Formación Alhambra) utilizada históricamente como material de construcción en estructuras de tapial de Granada (De la Torre et al., 1996, Ontiveros et al., 1999).

Los resultados preliminares demostraron ciertas dificultades en la identificación de los cambios mineralógicos producidos por el ataque alcalino de la tierra de la Formación Alhambra debido a la presencia de varios minerales de la arcilla (Elert et al. 2008). Por ello, se incluyeron el estudio de arcillas puras, es decir, caolinita, montmorillonita, saponita e ilita, con el fin de determinar su reactividad monomineralica y que permitiera la aplicación de nuestros resultados a otras estructuras de tierra con distinta composición mineralógica a la de la Formación Alhambra. En este estudio los minerales de la arcilla puros antes mencionados, así como la tierra de la Formación Alhambra, han sido utilizados como materiales de partida para la activación alcalina.

Para evaluar la reactividad de los diferentes minerales de la arcilla, 5 g de arcilla en polvo (fracción < 2 micras) se activaron alcalinamente utilizando 100 ml de las siguientes soluciones:

a) 0.025 M de $Ca(OH)_2$, esta concentración corresponde a una solución saturada a *T* ambiente.
b) 0.4 M de NaOH
c) 0.4 M de KOH
d) 5 M de NaOH
e) 5 M de KOH

Hay que tener en cuenta que las soluciones con concentraciones similares se utilizan comúnmente en la síntesis de zeolita (Breck 1974) y en la preparación de cementos alcalinos activado (Xu y Van Deventer 2000).

Las muestras de arcilla se mantuvieron en botes de polipropileno herméticamente cerrados y almacenados en el laboratorio a 20 ºC. Los botes se agitaron periódicamente. Se tomaron muestras para análisis a intervalos de tiempo predeterminados.

Una amplia variedad de técnicas analíticas han sido empleadas con el fin de estudiar el quimismo, composición y características morfológicas de los minerales de la arcilla antes y después de la activación alcalina. Estas técnicas incluyeron: fluorescencia de rayos-X (XRF), difracción de rayos-X (DRX), microscopía electrónica de barrido con fuente de emisión de campo (FESEM), microscopía electrónica de transmisión (TEM), análisis elemental, análisis termogravimétrico (TG) con espectroscopía de infrarrojos (FTIR) de gases emitidos, análisis del tamaño de partícula y sorción de nitrógeno (BET).

Además, se utilizó la tierra de la Formación Alhambra para preparar bloques de adobe que fueron posteriormente tratados por impregnación con las diversas soluciones alcalinas como una aproximación a un tratamiento in situ. Posteriormente, los bloques fueron sometidos a varios ensayos con el fin de evaluar la eficacia del tratamiento. Las propiedades hídricas y mecánicas de los bloques sin tratar y tratados se evaluaron mediante ensayos de absorción de agua, porosimetría de inyección de mercurio (MIP), resistencia a compresión y pruebas de resistencia al taladrado. Por otra parte, se realizaron mediciones espectrofotométricas sobre bloques de adobe tratados para establecer posibles cambios de color debido al tratamiento de activación alcalina.

Un exhaustivo análisis bibliográfico permitió determinar que el conocimiento sobre el posible efecto inhibidor de la materia orgánica en suelos sobre la reactividad de las arcillas era muy limitado (Claret et al. 2002). Dicha falta de información motivó el estudio de la transformación de las arcillas de la tierra de la Formación Alhambra en presencia y ausencia de materia orgánica. Para ello, parte de la arcilla se trató con H_2O_2 antes de la activación alcalina con el fin de eliminar la materia orgánica.

Los estudios preliminares revelaron que existía la posibilidad de que se formasen sales durante los tratamientos alcalinos. Los álcalis en exceso

pueden reaccionar con el CO_2 atmosférico y formar carbonatos potencialmente perjudiciales para los materiales porosos. Con el fin de evaluar el potencial de daño de dichas sales, se realizó un ensayo de cristalización de sales consistente en la inmersión parcial de prismas de calcarenita en diferentes soluciones de Na_2SO_4, Na_2CO_3, K_2CO_3 y $KHCO_3$. Hay que tener en cuenta que se tuvieron que utilizar prismas de calcarenita porque los bloques de adobe no hubieran resistido la acción de las soluciones.

Resultados y discusión

Los resultados experimentales de este estudio demostraron que los minerales de la arcilla pueden ser transformadas en materiales cementantes usando soluciones alcalinas a *T* ambiente. Estos materiales cementantes incluyen fases precursoras de zeolitas, zeolitas, fases de tipo CSH y calcita. Adicionalmente, algunos minerales de la arcilla experimentaron una transformación en minerales de la arcilla interestratificados.

La respuesta a la activación alcalina no fue la misma para los diferentes minerales de la arcilla incluidos en este ensayo. La caolinita y la esmectita dioctaédrica se disolvieron y se transformaron fácilmente. La saponita experimentó una modificación más lenta, ocasionando la formación de un interestratificado esmectita-clorita que todavía mostró expansión. Este mineral de la arcilla no se transformó en zeolitas. La ilita usada en este estudio era altamente cristalina y por tanto poco reactiva, por lo que sólo sufrió modificaciones químicas menores. Las diferentes respuestas de los minerales de la arcilla estudiados están relacionadas con sus características estructurales y su composición (Sposito 1984, Schoonheydt y Johnston 2006). La caolinita, una arcilla de laminas tipo 1:1, mostró una extensa disolución debido a la existencia de grupos >AlOH en la capa gibsítica, además de los grupos hidroxilo de los bordes, peldaños y sitios con defectos cristalinos que contribuyen a la reactividad global de las arcillas (Huertas et al. 1999). En contraste, la contribución de la capa basal a la reactividad de los minerales de la arcilla de laminas tipo 2:1 es limitada y la disolución tiene lugar principalmente en las superficies de los bordes. La menor reactividad de la ilita, si se compara con la montmorillonita, ambas arcillas dioctaédricas, puede explicarse teniendo en cuenta sus diferencias composicionales. La ilita tiene una carga neta mucho mayor debida a la sustitución isomorfica en la capa tetraédrica, que es compensada por la entrada de K^+ en la intercapa. En la montmorillonita, por otra parte, la carga es originada principalmente por la sustitución octaédrica y compensada por la entrada de Na^+. Las diferencias en la composición dan como resultado una estructura más estable en el caso de ilita, que comúnmente tiene una mayor cristalinidad y menor superficie

específica que la montmorillonita. Además, la ilita no experimenta expansión intracristalina. La montmorillonita, por el contrario se expande fácilmente en presencia de disolventes polares y ofrece un área superficial mucho más elevada para la reacción (Newman y Brown 1987, Sposito 1984). La saponita, siendo una arcilla expansiva, mostró una reactividad más baja en condiciones alcalinas. Esto se debe a la presencia mayoritaria de Mg en su capa octaédrica (Becerro et al. 2009). Además, la sustitución isomorfica comúnmente se produce en sus capas tetraédricas y se compensa con Ca^{2+} o Mg^{2+}. Estas dos características contribuyen a aumentar la estabilidad de esta arcilla (Newman y Brown 1987).

Mientras que en el caso de la caolinita y montmorillonita se observó una formación masiva de zeolitas, en el caso de la saponita estas no se detectaron. Esto se debe posiblemente al bajo contenido en Al de este mineral de la arcilla. En las muestras de ilita tratadas con KOH, se detectaron algunas zeolitas. Sin embargo, estas fases posiblemente se formaron a partir de caolinita presente como impureza.

Los minerales de la arcilla de la tierra de la Formación Alhambra, una mezcla de caolinita, esmectita, ilita y paragonita, en términos generales mostraron una transformación similar a la observada en el caso de las arcillas puras. Sin embargo, la caolinita experimentó una disolución más rápida en el caso de la tierra de la Formación Alhambra, debido a que su cristalinidad era menor que la de la misma arcilla pura.

Además de la composición mineral, el contenido de materia orgánica puede tener una influencia importante en la eficacia del tratamiento alcalino. Nuestros resultados indican que la disolución y la transformación de los minerales de la arcilla se retrasaron debido a la presencia de materia orgánica. El contenido en materia orgánica de la tierra de la Formación Alhambra era del 1 % en peso.

La diferente respuesta de los distintos minerales de la arcilla, así como la influencia de la materia orgánica en la eficacia del tratamiento alcalino, arroja luz sobre un aspecto importante a considerar antes de aplicar este tratamiento de consolidación. Es necesario, un estudio detallado de la composición mineralógica y del contenido de materia orgánica de la tierra. Así por ejemplo, una alta concentración de arcillas saponíticas o un contenido de materia orgánica elevado pueden hacer que este tratamiento sea ineficaz.

Este estudio reveló además que el uso de soluciones saturadas de $Ca(OH)_2$ no produce un pH lo suficientemente alto como para promover la disolución de los minerales de la arcilla y su transformación en fases cementantes. Por el contrario, las soluciones concentradas de NaOH y KOH provocaron una extensa transformación de la mayoría de los minerales de la arcilla analizados en este estudio. En general se puede concluir que un pH

suficientemente alto, muy por encima de 10, tiene que ser mantenido durante el tratamiento para asegurar la adecuada disolución de los minerales de la arcilla y su transformación.

Comparando las fases zeolíticas formadas usando diferentes soluciones alcalinas, se puso claramente de manifiesto el papel del Na^+ y K^+ como iones que dirigen el desarrollo de estructuras zeoliticas (Barrer 1982). Cuando se utilizó NaOH se formaron zeolitas de tipo faujasita e hidroxi-sodalita. En el caso de KOH, se generaron zeolitas de tipo K-I y K-F y/o una zeolita de tipo chabazita, independientemente del mineral de la arcilla utilizado como material de partida.

Como se indicó anteriormente, tanto el NaOH como el KOH fueron eficaces en la producción de cambios mineralógicos. Sin embargo, los ensayos de cristalización de sales mostraron que el carbonato de sodio formado como subproducto del tratamiento alcalino con NaOH, tiene un potencial dañino mucho más alto que el carbonato o bicarbonato de potasio formados tras el tratamiento con KOH. Teniendo en cuenta estos resultados, se puede concluir que las soluciones de KOH son preferibles para su uso en los tratamientos de conservación.

Los tratamientos de bloques de adobe con soluciones altamente alcalinas mostraron que se logró una notable mejoría en la resistencia al agua. Un estudio comparativo utilizando una solución concentrada de KCl nos permitió verificar que la mejora de la resistencia observada fue debida a la disolución de los minerales de la arcilla y su transformación a un pH elevado en fases aluminosilicatadas amorfas con propiedades cementantes. El intercambio catiónico o el efecto osmótico ejercido por electrolitos altamente concentradas, por otra parte, parecen haber desempeñado un papel insignificante en esta mejora. El estudio mineralógico y morfológico de los bloques de adobe tratados nos llevó a la conclusión de que las fases amorfas, posiblemente precursores de zeolitas, que se formaron después de 50 días de curado, sirvieron como material cementante y mejoraron la resistencia mecánica. No se observaron fases zeolíticas cristalinas en los bloques de adobe tratados. Se cree que la formación de zeolitas, para lo que se requerirían tratamientos más largos, no es necesaria para aumentar la resistencia de los bloques de adobe.

Conclusiones

Nuestra investigación demuestra que la aplicación de soluciones alcalinas para la consolidación de estructuras de tierra puede ser considerada como una valiosa alternativa a los tratamientos convencionales de consolidación. La mayoría de los minerales de la arcilla incluidos en este

estudio experimentaron un notable grado de disolución y transformación tras la activación alcalina con NaOH y KOH. Además, los bloques de adobe mostraron una mejora significativa de su resistencia al agua y de su resistencia mecánica después de la impregnación con NaOH o KOH y su curado durante 50 días a *T* ambiente.

Sin embargo, los ensayos de cristalización de sales indicaron que el KOH sería preferible porque los carbonatos de potasio formados como posible subproducto del tratamiento alcalino son menos dañinos que los carbonatos de sodio. Este estudio reveló además que el contenido de materia orgánica de la tierra tiene que ser considerado, ya que podría tener un efecto de retardo en la disolución de las arcillas y en las reacciones de transformación. En cualquier caso, es necesario un estudio previo detallado de la composición mineralógica y del contenido de materia orgánica para garantizar la viabilidad de un tratamiento alcalino.

Además, se identificaron varios aspectos a considerar de cara a futuras investigaciones. Estos incluyen el posible uso de soluciones alcalinas menos concentradas para reducir el riesgo de la formación de carbonatos debido al exceso de álcalis, así como los costes de tratamiento e impacto ambiental; ensayos de bloques de adobe preparados a partir de tierra con alto contenido en esmectita o materia orgánica para evaluar la viabilidad de este método de tratamiento bajo condiciones adversas, o la preparación de morteros de restauración utilizando una mezcla de tierra y solución alcalina.

Por último, el resultado positivo de los resultados de laboratorio debe ser confirmado mediante un estudio in situ, en el terreno. Para este propósito se podrían construir replicas de muros de adobe o bien, idealmente, aplicar el tratamiento en áreas piloto de estructuras de tierra históricas, monitorizando el rendimiento de la consolidación durante largos períodos de tiempo.

Referencias

Barrer, R.M., *Hydrothermal Chemistry of Zeolites*, Academic Press, London (1982) 360pp.

Becerro,A., Mantovani, M., Escudero, A., Mineralogical stability of phyllosilicates in hyperalkaline fluids: Influence of layer nature, octahedral occupation and presence of tetrahedral Al, *American Mineralogist* **94** (2009) 1187-1197.

Breck, D.W., *Zeolite molecular sieves – Structure, chemistry and use*, John Wiley and Sons, Inc. New York 1974.

Brown, P.W. and Clifton, J.R. Adobe I: the properties of adobe, *Studies in Conservation*, **23** (1978) 139-146.

Claret, F., Bauer, A., Schäfer, T., Griffault, L., Lanson, B., Experimental investigation of the interaction of clays with high-pH solutions: A case study from the Callavo-Oxfordian formation, Muese-Haute Marne Undergraund Laboratory (France), *Clays and Clay Minerals* **50** (2002) 633-646.

Davidovits, J., Geopolymers: Man-made rock geosynthesis and the resulting development of very early high strength cement, *Journal of Materials education* **16** 2&3 (1994) 91-139.

de la Torre, M.J.; Sebastián E., Rodríguez J., A study of the wall material in the Alhambra (Granada, Spain), *Cement and Concrete Research* **26** (1996) 825-839.

Doehne, E., Price, C.A., *Stone Conservation - An overview of current research*, The Getty Conservation Institute, Los Angeles ISBN 9781606060469 (2010) 158pp.

Elert, K., Sebastian, E., Valverde, I., Rodriguez-Navarro, C., Alkaline treatment of clay minerals from the Alhambra Formation: Implications for the conservation of earthen architecture, *Applied Clay Science* **39** (2008) 122-132.

Flanigen, E.M., Mumpton, F.A., Commercial properties of natural zeolites, in Mineralogy and Geology of Natural Zeolites, *Mineralogical Society of America Short Course Notes* **4** 1977, 165-175.

Huertas, F.J., Chou, L., Wollast, R.,, Mechanism of kaolinite dissolution at room temperature and pressure: Part II. Kinetic Study, *Geochimica et Cosmochimica Acta* **63** (1999) 3261-3275.

Houben, H., Guillaud, H., *Earth construction: a comprehensive guide*. CRA Terre-EAG, Intermediate Technology Publication, London (1994) 362 pp.

Lunt, M.G., Stabilised soil blocks for building, *Building Research Establishment, Overseas Building Notes*, No. 184 (1980) 127-144.

Newman, A.C.D., Brown, G., The chemical constitution of clay, *Chemistry of clays and clay minerals, Mineralogical Society Monograph No.6*, Newman, A.C.D. (ed.), Longman Scientific & Technical, London (1987) 1-128.

Oliver, A., Conservation of nondecorated earthen materials, *Terra a Literature Review - An overview of research in earthen architecture conservation*, Avrami, E., Guillaud, H., Hardy, M. (eds.) J. Paul Getty Trust, Los Angeles (2008) 159 pp.

Ontiveros Ortega E., Sebastián Pardo E., Valverde Espinosa I., Deterioration in XI-XIV century Arab ramparts (Granada, Spain). *Materials and Structures* **32** (1999) 45-51.

Palumbo G., Ginell W. S., Rodríguez-Navarro C. *Earthen architecture research survey: Analysis report*. Getty Conservation Institute, Los Angeles 1999.

Ren, K.B., Kagi, D.A., Upgrading the Durability of Mud Bricks by Impregnation, *Building and Environment* **30** (1995) 433-440.

Rodriguez-Navarro, C., Sebastian, E., Doehne, E., Ginell, W.S., The role of sepiolite-palygorskite in the decay of ancient Egyptian limestone scultures, *Clays and Clay Minerals* **46** (1998) 414-422.

Roy, D.M., Alkali-activated cements. Opportunities and challenges, *Cement and Concrete Research* **29** (1999) 249-254.

Schoonheydt, R.A., Johnston, C.F., Chapter 5. Surface and interface chemistry of clay minerals, *Handbook of Clay Science*, Bergaya, F., Theng, B.K.G., Lagaly, G., Elsevier, Oxford (2006) 139-172.

Sposito, G., *The surface chemistry of soils*, Oxford University Press, New York (1984).

Xu, H., van Deventer, J.S.J., The geopolymerisation of alumino-silicate minerals, *International Journal of Mineral Processing* **59** (2000) 247-266.

1. Introduction

This section includes a description of the history and technology of earthen architecture as well as the mechanism of its degradation. Subsequently, we present a general overview of the different approaches followed in the past to stabilize and consolidate earthen structures. Research needs in the field of earthen architecture conservation are also outlined. Special emphasis is given to the reduction of clay swelling by alkaline activation as a means to consolidate earthen materials. Finally, the objectives of this research are presented.

1.1. Earthen architecture - History and technology

Earth is one of the oldest construction materials man has used: Remains of adobe structures of the city of Jericho (West Bank, Palestinian Territories) date back to 8000 B.C (Houben and Guillaud 1994, Figure 1-1). Other early adobe structures have been excavated at the Neolithic site of Catalhöyük in Turkey (Figure 1-2). Many historic earthen buildings and archaeological remains, in some cases entire cities, can be found all over the world, e.g.: Chan-Chan in Peru (Figure 1-3), Joya de Ceren in El Salvador, Shiban in Yemen, the great mosque of Djénné in Mali (Figure 1-4), the Rebkung monastery in Tibet, Arg-e Bam in Iran (Figure 1-5), part of the Great Wall in China or the Chateau of Reyrieux in France (Figure 1-6).

Figure 1-1. Adobe remains of the city of Jericho (Palestinian Territories, 8000 B.C., www.biblearchaeology. org).

Figure 1-2. Neolithic site at Catalhöyük in Turkey (www.define-isaretleri.com).

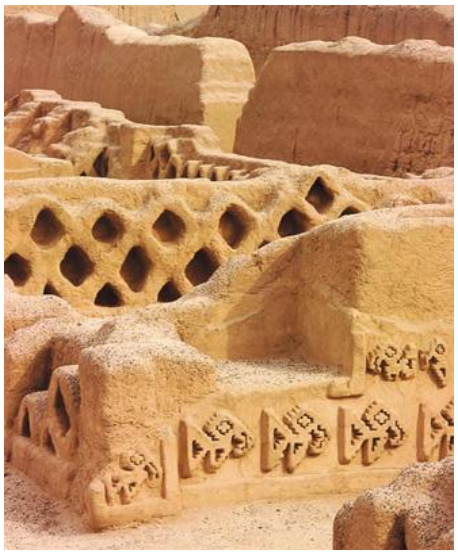

Figure 1-3. Adobe remains of the Pre-Columbian city of Chan-chan in Peru (www.journeylatin america.co.uk).

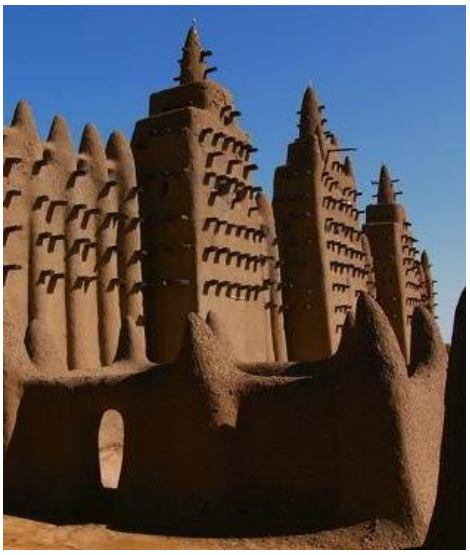

Figure 1-4. The great mosque of Djénné in Mali (www.home. earthlink.net).

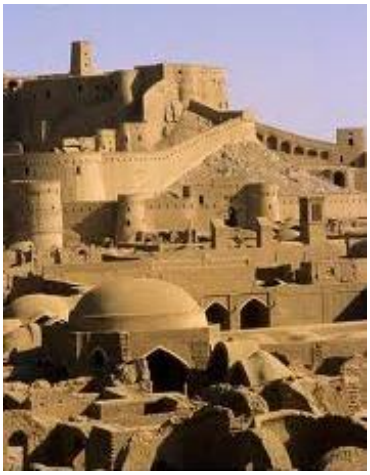

Figure 1-5. Citadel Arg-e Bam in Iran before the earthquake in 2003 (www.visualphoto. com).

Figure 1-6. 19th century Chateau Reyrieux in France (www.reyrieux.fr).

A great variety of examples of earthen architecture can also be found in Spain, including important monuments like the Alhambra in Granada, the "Murallas de Niebla" in Huelva (Figure 1-7) or rural houses in Castilla-León and Aragón (Figure 1-8). Furthermore, earth is still one of the most employed construction materials in developing countries. Ren and Kagi (1995) indicated that nearly one third of the world`s population lives in buildings made of earth.

Figure 1-7. City wall in Niebla, Huelva, Spain (www.arteguias.com).

Figure 1-8. Earth walled house in ecovillage Amayuelas, Palencia, Spain (Jimenez Delgado and Cañas Guerrero 2006).

The two most important construction techniques used in earthen architecture are adobe and rammed earth. Adobe refers to unburned bricks made of a mixture of earth, clay and sand, often with the addition of organic material (straw, animal hair, pieces of rope or manure). The mixture is shaped into bricks using frames and dried in the sun (Figure 1-9).

Figure 1-9. Different stages of the manufacturing of adobe bricks (www.communityrebuilds.worldpress.com).

Adobe buildings are similar to cob and mudbrick buildings. The same mixture used to make bricks, without the addition of fibrous material, is used as mortar or as plaster on interior and exterior walls (Figure 1-10 and 1-11). Some ancient cultures used lime-based plasters and renders to protect the earthen structure against rain damage (Houben and Guillaud 1994).

Figure 1-10. Construction of an adobe wall (www.es.wikipedia.org).

Figure 1-11. Renewal of the surface coating of an adobe wall in Chamisal, New Mexico (www.en. wikipedia.org).

Rammed earth, also known as *taipa* (Portuguese), *tapial* (Spanish), *pisé de terre* or simply *pisé* (French), is a technique used in the construction of walls. It is an ancient building method that has seen a revival in recent years as people seek low-cost, more sustainable building materials and more environmental friendly building methods. Building a rammed earth wall involves compressing a damp mixture of earth that has suitable proportions of sand, gravel and clay into an externally supported wooden frame. Damp material is poured into the frame and compressed. The compression of material is done in layers of 10 to 15 cm thickness to gradually build up the wall to the required height (Figure 1-12). The compression was historically done by hand with a long ramming pole. Once the wall is completed the frame is removed. Walls take some time to dry out completely, and may take years to completely cure if they contain additives such as lime. Compression strength, thus, increases with increasing curing time.

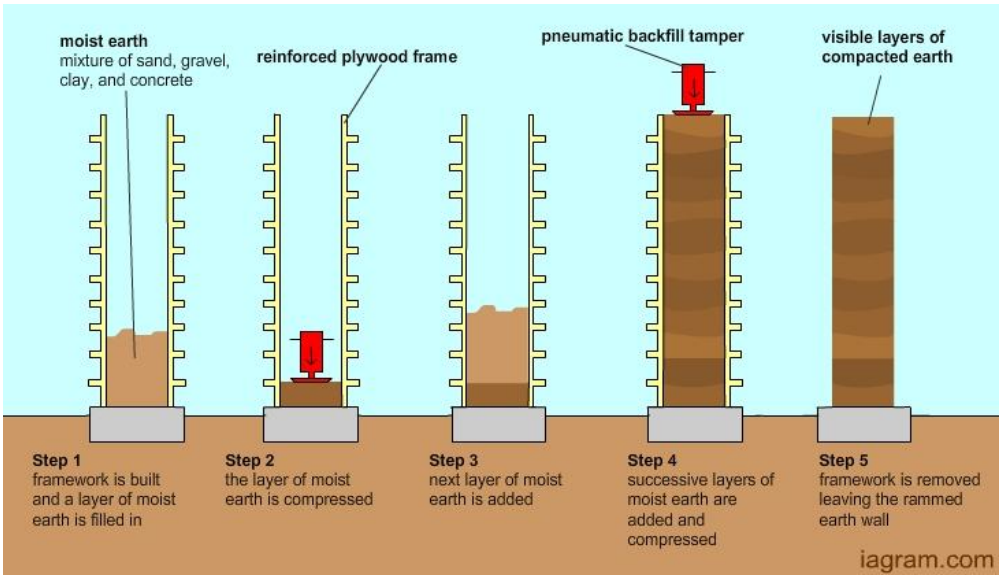

Figure 1-12. Different stages of the construction of a rammed earth wall (www.modernsustainable.blogspot.com).

A different type of rammed earth wall, called "calicostrado" (Figure 1-13), is documented in various buildings in Granada dating from the Nasrid period in the 13th and 14th century. These walls have a higher lime content in the outer part and a more clayey core. These walls were constructed in a similar manner as described above, only using a mixture with higher lime content in the outer part of the walls (Sebastian and Cultrone 2010). Furthermore, rammed earth walls in combinations with rocks or bricks (Figure 1-14) are also documented (Sebastian Pardo 2003).

Figure 1-13. "Tapia calicostrada" Castell Vell de Castellón de la Plana, Spain (Font and Hidalgo 2011).

Figure 1-14. Rammed earth wall with rock foundation, Paderne Castle, Algarve, Portugal (www.globedia.com).

1.2. Alteration of earthen architecture

Earthen architecture (i.e. buildings and archaeological remains) is strongly affected by physical and chemical alteration due to mineralogical, composional and structural characteristics of the construction material (Brown y Clifton 1978, Brown et al. 1979, Heathcote 1995). Clays are one of the main components of soil, acting as binder for the other constituents such as sand and silt. Especially, alteration due to swelling and contraction of smectites or other expandable clay minerals in contact with water has an important effect on the durability of earthen constructions. Clay swelling can be divided into intracrystalline swelling which only occurs in the so-called "expandable clays", such as smectites, and osmotic swelling which results in smaller swelling stresses but might affect non-expandable clay minerals as well (Pashley and Quirk 1984). However, illite will be affected to a much lower degree by osmotic swelling than smectites, and kaolinite will hardly experience any swelling at all (Foster 1955). The difference in the response towards water of various clay minerals is documented in Figure 1-15. The adobe block prepared with 25 wt.% smectite (saponite) and 75 wt.% standardized sand experienced complete destruction after immersion in water for 4 minutes, while the block prepared using kaolinite (same mixing ratio than in the first case) suffered only minor material loss.

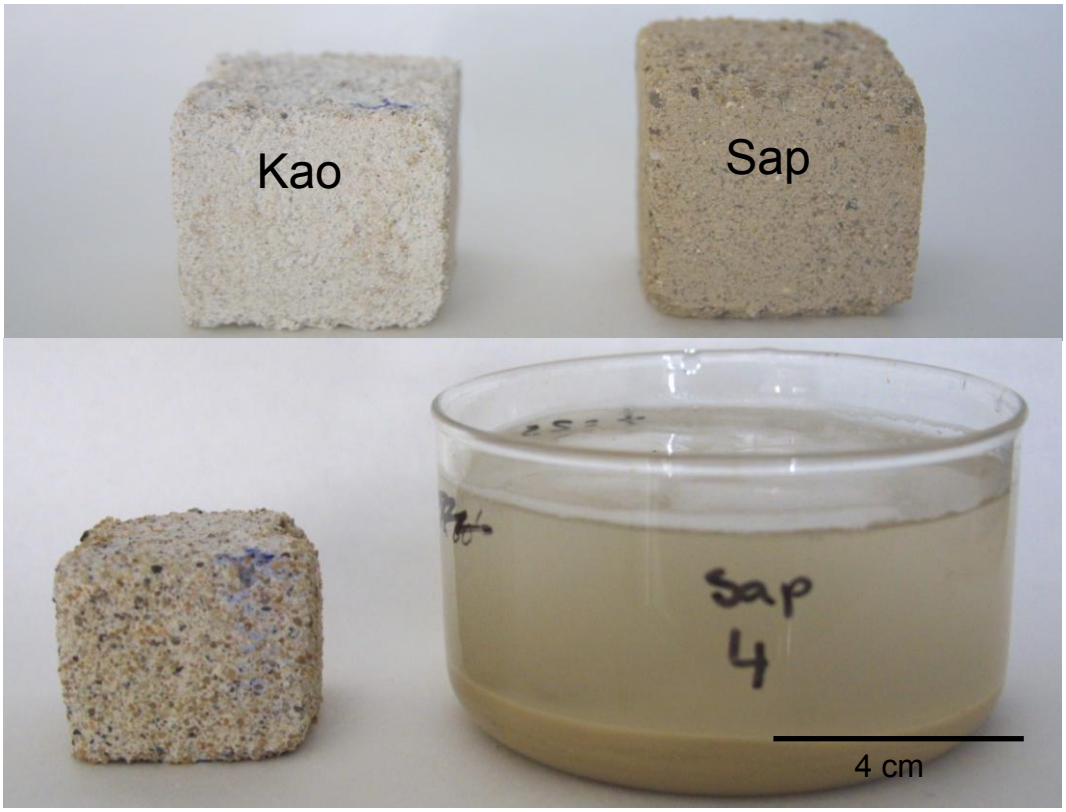

Figure 1-15. Adobe blocks prepared using kaolinite or saponite before and after immersion in water for 4 minutes.

According to Madsen and Müller-Vonmoos (1989) the first phase of swelling (intracrystalline swelling) involves the hydration of exchangeable interlayer cations (Figure 1-16). Intracrystalline swelling is limited to water vapour adsorption at a RH below 100 % (Norrish 1954). During intracrystalline swelling, montmorillonite can double its volume and swelling pressures of more than 100 N/mm^2 might be created (Madsen and Müller-Vonmoos 1989). The second phase of swelling takes place when clay is in direct contact with water. Osmotic swelling is a result of the difference between the ion concentration at the surface of the clay layers and in the pore water (Madsen and Müller-Vonmoos 1989, Figure 1-17). Since the interlayer cations are fixed electrostatically by the negative charge of the layers, concentration equilibrium can only be reached through the penetration of water into the space between the clay layers (C_1) where the ion concentration is higher than in the pore water (C_2). Osmotic swelling can result in a complete layer separation, for example in the case of sodium montmorillonite, but swelling pressure is much lower than in the case of intracrystalline swelling. Commonly it is not higher than 2 N/mm^2 (Madsen and Müller-Vonmoos 1989). During osmotic swelling Na-montmorillonite might take up 10 g H_2O/g clay and augments its volume by around 20 times (Norrish 1954).

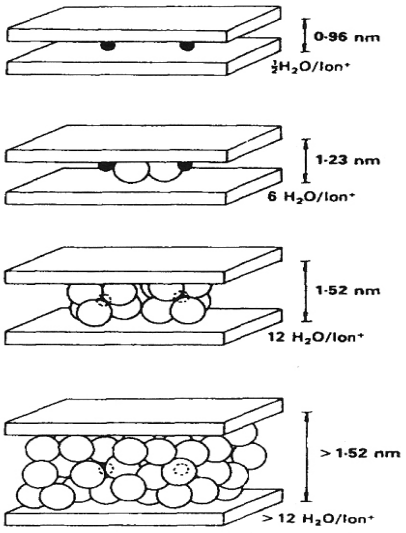

Figure 1-16. Intracrystalline swelling of sodium mont-morillonite (Madsen and Müller-Vonmoos 1989).

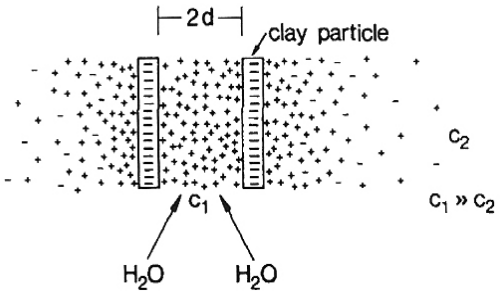

Figure 1-17. Two negatively charged clay layers with ion cloud. The difference between the ion concentration (C_1 and C_2) gives rise to osmotic swelling (Madsen and Müller-Vonmoos 1989).

As can be deduced from the above, water is the most important extrinsic factor in the deterioration of earthen architecture due to its interaction with clays. The action of water of different sources (rain, condensation, capillary rise) followed by evaporation can cause severe damage to earthen architecture including fissures, cracks (Figure 1-18) and granular disintegration or may even result in the total loss of the structure (Rodriguez-Navarro et al. 1997, 1998, Houben and Guillaud 1994). The presence of soluble salts might increase the destructive action of water. Salts may crystallize upon evaporation of water as efflorescence (Figure 1-19) or subflorescence, the later causing significant damage due to granular disintegration or scaling (Goudie and Viles 1997).

Other damaging extrinsic factors include erosion due to wind or rain (Figure 1-20), thermal shrinkage and expansion, air pollution, activity of plants or animals (Figure 1-21), seismic activity, inadequate conservation materials (Portland cement) or treatments (migration of the evaporation front or redistribution of loads upon excavation of archaeological sites), human activity (visitors, vandalism and wars) and lack of maintenance.

Figure 1-18. Drying cracks in an earthen structure in Djénné, Mali (www.flickr.com).

Figure 1-19. Salt efflorescence caused by Portland cement used in a conservation intervention (Castillo de Santa Catalina, Granada, Spain).

Figure 1-20. Wind erosion, Chan-chan in Peru (es.wikipedia.org).

Figure 1-21. Plant growth and damage due to capillary rise, Albayzin, Granada, Spain.

1.3. Stabilization and consolidation of earthen architecture

At present, the majority of historic buildings and archaeological remains made of earth exhibits important conservation problems which require consolidation. A recent survey showed that one of the most demanded aspects requested by specialists in charge of the conservation of earthen architecture was the development of new consolidation treatments that could be applied in situ to these sensitive materials of great value. These treatments should be both efficient and durable (Palumbo et al. 1999).

Historically, additives such as blood, alum, manure, bones, animal fat or vegetable oil, asphalt or lime were used to increase the materials cohesion, and in some cases to confer a certain hydrophobicity to adobe and rammed earth constructions. In modern construction lime, cement or asphalt emulsion may be used (Lunt 1980, Ashurst and Ashurst 1988).

The addition of lime for soil stabilization has a very long tradition and was used in the construction of roads in ancient Mesopotamia and Egypt (Bell 1996). Today slaked lime is applied massively for soil stabilization in the field of foundation and pavement engineering (Mohamed 2000, Kinthia et al. 1999, Rogers and Glendinning 1997, Rajasekaran et al. 1997). The use of $Mg(OH)_2$ solutions for the stabilization of expandable clays has also been proposed (Xeidakis 1996). In conservation interventions where the reconstruction of architectural elements (adobe or rammed earth) is necessary a lime-earth-mixture might be appropriate. However, the low solubility of $Ca(OH)_2$ and $Mg(OH)_2$ has limited their use as a consolidant where the in situ application is required.

Armbrust and Dickerson (1971) compared the efficiency of various commercial products for the consolidation of soil, including asphalt emulsion, solutions of carboxymethyl cellulose, polyvinyl acetate, polyvinyl alcohol, gypsum, polyarcrylamide and latex emulsion. The majority of these products has also been applied in the field of architectural conservation (Houben and Gillard 1994, Matero and Bass 1994). Furthermore, other products such as silicon resin and alkoxysilanes have been used. Often, treatments had only limited success and, occasionally, led to a total failure due to esthetical, chemical or physico-mechanical incompatibility of the products. In many cases the applied product did not penetrate sufficiently into the earthen material or reverse migration upon solvent evaporation occurred which resulted in the formation of superficial films and, sometimes, accelerated deterioration of the earthen structure (Coffman et al. 1990, Chiari 1990). According to Oliver (2008) asphalt and bitumen have only very limited application in the conservation of earthen architecture because they can cause severe discoloration. Other natural organic consolidants such as plant juices, animal products or resins may age very rapidly and require frequent

retreatment (Oliver 2008). Synthetic polymers, on the other hand, have high thermal expansion coefficients if compared to adobe and might cause superficial detachment upon temperature change. Besides, many treatments using synthetic polymers or alkoxysilanes cannot be applied to wet surfaces because the product might form glossy, fragile crusts without any consolidation effect (Chiari 1990).

Most importantly, treatments generally do not tackle the cause of the problem but rather only diminish the alteration effects, thus being ineffective over longer periods of time. Doehne and Price (2010) summarized findings of two independent studies where clay-rich stone was treated with ethyl silicate. This treatment resulted in an initial strength increase. However, this improvement was lost after several wet/dry cycles. It can be concluded that the decrease in efficiency over time was most probably due to continuous expansion and contraction of the clay minerals which destroyed the consolidation capacity of the applied product. The same authors suggested that for clay-rich stones the focus should be on reducing clay swelling and not on increasing strength. The same applies in the case of earthen architecture consolidation.

1.4. Reduction of clay swelling and consolidation of earthen architecture in situ

The above shows the urgent need for the development of an alternative, more effective method that allows the in situ consolidation of earthen architecture by reducing the swelling capacity of clays. Swelling capacity could be reduced by transforming the clay into non-expandable binding materials such as calcium silicate hydrates or other aluminiosilicates with cementing capacity, i.e. amorphous aluminosilicates or zeolitic phases. $Ca(OH)_2$, NaOH or KOH might be suitable as alkaline activators.

As mentioned above lime has been used since ancient times as a stabilizer for earthen architecture. In fact, lime with the addition of fired brick powder has been used in hydraulic mortars since Phoenician times. The Greek used tuff from the Santorini Island as a pozzolanic additive for the preparation of hydraulic lime mortars and the Romans further improved this technology, using volcanic ash from the region of Pozzuoli near Naples, hence the name pozzolana. Pozzolanic materials contain highly reactive silica and alumina which generate new products (calcium silicates and aluminates) with binding or cementing properties when combined with $Ca(OH)_2$ and water (Rodriguez-Navarro 2012). Pozzolanic materials include volcanic ash, calcined earth or clays (metakaolin), fired brick powder, unfired clays, tuff, zeolites and industrial by-products such as blast furnace slag, fly ash or rice husk (He et al. 1995, Roy 1999, Mertens et al. 2009, Wongpa et al. 2010).

Pozzolanic reactions occur at a high pH (>12) which is created upon dissolution of $Ca(OH)_2$. At this pH clay minerals or other aluminosilicates are partially dissolved and transformed into amorphous calcium silicate hydrate (CSH) gel, crystalline tobermorite-type phases, calcium aluminate hydrate (CAH) compounds or zeolite-like phases. These phases have been recognized in antique roman mortars (Eades and Grim 1960, Eades at al. 1962, Diamond et al.1964, Wild et al. 1987, Liebig and Althaus 1997, Merlino et al.1999, Roy 1999, Boardman et al. 2001). They can act as cementing agents and improve the durability and mechanical strength of earthen architecture. This is demonstrated by the soundness and resistance of ancient lime-amended rammed earth structures ("tapial calicostrado") such as the Alhambra fortress (de la Torre et al. 1996). Furthermore, the formation of calcite upon carbonation of portlandite ($Ca(OH)_2$) will add to this improvement. Calcium carbonate has cementing properties and confers mechanical strength to lime stabilized soils. The same effect has been observed in lime mortars (Cazalla et al. 2000). Apart from the above, the expected immediate effect of the addition of lime to soil is the exchange of interlayer cations, especially Na^+, for Ca^{2+}. The presence of Ca^{2+} as the dominant cation will induce flocculation of clay

minerals which will result in a reduction of the clays swelling capacity (Bell 1996).

Besides $Ca(OH)_2$, NaOH and KOH are also considered suitable for the alkaline activation of aluminosilicates and have been widely applied in the synthesis of zeolites since the mid-1930s (Flanigen et al. 2010). Al and Si sources for zeolite synthesis include glasses, salts, clay minerals and feldspathoids (Barrer 1982), as well as industrial waste products such as coal ashes and slags (Inada et al. 2005). However, zeolite synthesis takes generally place at relatively high *T* (≥ 60 °C) and *P* (autoclave), reaction conditions which are not applicable in architectural conservation interventions.

More recently the geochemistry that yields the synthesis of zeolites has been applied for the production of alkaline activated cements which are termed geopolymers (Davidovits 1994), low temperature aluminosilicate glass (Rahier et al. 1996a) or hydroceramics (Palomo et al. 1999). Often comparisons are drawn between zeolite chemistry and geopolymer chemistry due to the similarities between the two systems, and the geopolymeric gel phase is frequently described as a zeolitic precursor (Rees et al. 2008). These new cements are produced by the alkaline activation of aluminium silicates, with or without alkaline silicate solutions, at very high pH, and 1 atm pressure. Commonly, alkaline activated cements are cured at *T* between 60-90 °C (Barbosa et al. 2007, Hos et al. 2002, Lecomte et al. 2003, Palomo et al. 1999, Rahier et al. 1996, Rowles and O´Connor 2003, Swanepoel and Strydom 2002, Wang et al. 2005). Lower curing temperatures between 30-50 °C are less frequent (Lee and van Deventer 2004, van Jaarsfeld et al. 2002, Duxson et al. 2005a) and very few data of geopolymers produced at room *T* exist (Davidovits 1994, Lee and van Deventer 2002). Thermally activated clays or other natural aluminiosilicates, as well as industrial by-products such as blast furnace slag or fly ash can be used for the production of alkaline activated cements. Davidovits (1994) coined the term geopolymers which refers to materials formed by polycondensation of polysialates. Polysialates are amorphous or poorly crystalline and are formed by SiO_4 and AlO_4 tetrahedra. They are structurally and chemically similar to tectosilicates such as zeolites and feldspathoids. As in the case of zeolites, the charge deficit caused by substitution of Si^{4+} for Al^{3+} is compensated by the incorporation of alkaline cations such as Na and K. Various authors (Davidovits 1994, Barbosa and MacKenzie 2003, Duxson et al. 2005a) state the exceptional properties of alkali-activated cements regarding chemical resistance (acid and sulphate attack) as well as physical-mechanical resistance (salt attack, freeze-thaw cycles, thermal shock or mechanical stress). Roy (1999) offered an exhaustive review on the beginnings and evolution of alkaline activation techniques. The author emphasized the importance of alkali-activated cements as an

alternative material for Portland cement in construction as well as in the storage of toxic and radioactive waste.

Davidovits (1994) indicated that it would be possible to obtain a material with great water resistance and mechanical strength by alkaline activation of kaolinite at room *T*. This result motivated the application of the same technique to the field of architectural conservation, as an alternative to conventional consolidation treatments, which will be evaluated in this research project.

1.5. Objectives of the research project

The main objective of this study is the evaluation of alkaline activation as an alternative consolidation treatment for clayey material such as rammed earth or adobe. The conservation needs of earthen structures, such as the Alhambra fortress and the historic city walls of Granada (Figure 1-22 and 1-23), could be addressed using this consolidation technique.

Consolidation treatments for earthen architecture are generally applied at room *T*. The curing of alkali-activated cements, on the other hand, is commonly performed at temperatures ≥ 30 °C. As mentioned earlier, zeolite synthesis is carried out at even higher temperatures ≥ 60 °C. Thus, an important aspect of this study is the evaluation of the extent of the mineral transformation under high pH conditions at room *T*. Furthermore, mainly kaolinite (frequently metakaolinite) has been used for the preparation of alkali-activated cements and the synthesis of zeolites. Thus, other clay minerals commonly present in earthen structures, such as smectites or illite, have to be included in this investigation to study their reactivity under high pH conditions. Futhermore, the influence of the clays structural and compositional characteristics on the effectiveness of alkaline activation, e.g. trioctahedral- (saponite) versus dioctahedral smectite (montmorillonite), has to be addressed.

The evaluation will also have to consider factors influencing the effectiveness of alkaline activation as a consolidation method, including the interference of the soil organic matter content with the alkaline activation of clays or the efficacy of different activator solutions, e.g. $Ca(OH)_2$, NaOH and KOH.

In the preparation of alkali-activated cements and in the synthesis of zeolites, clay minerals are directly mixed with the alkaline solution. In contrast, alkaline activation in a conservation treatment has to be performed by impregnation with the consolidating solution, as it is commonly done when applying conventional consolidation treatments. Thus, it has to be determined whether an adequate penetration depth can be achieved in adobe blocks using alkaline solutions and whether the alkaline solution concentration is sufficiently high to promote mineral transformation and stabilization. The suitability and performance of this consolidation method as an in situ treatment will be evaluated by applying alkaline solutions to adobe blocks. The ultimate goal of this PhD thesis is to determine whether alkaline treatments can improve the water resistance and mechanical properties of earthen materials.

Figure 1-22. Tapial of the Alhambra. View from the "Cuesta de los Chinos", Granada, Spain.

Figure 1-23. Historic city wall in the Albaizin, Granada, Spain. View from the “Mirador de San Cristobal”.

2. Materials and methods

2.1. Raw materials

Previous mineralogical studies of earthen constructions in the Granada area, including the city walls of Granada and the rammed earth walls of the Alhambra, confirmed the presence of illite, kaolinite and smectite as main clay minerals, with minor amounts of paragonite and chlorite (de la Torre et al., 1996, Ontiveros et al., 1999). The bibliographic review of the mineralogical composition of earthen constructions revealed that these minerals, maybe with the exception of paragonite which is a mineral of rather rare occurrence, are the most common in the majority of earthen structures around the world (Houben and Guillaud, 1994). This is not surprising since they are also the most common clay minerals in soils (Grim, 1968; Velde, 1992), the raw material used for the construction of adobe and rammed earth structures. For our study we chose the soil from the nearby hills (Alhambra Formation) which was historically used as a construction material for most rammed earth structures in Granada (de la Torre et al., 1996, Ontiveros et al., 1999).

Preliminary results demonstrated certain difficulties in identifying mineralogical changes in the Alhambra Formation soil upon alkaline attack due to the presence of various clay minerals in this soil (Elert et al. 2008). Thus, additional to the Alhambra Formation soil, pure clays, namely kaolinite, montmorillonite, saponite and illite, were included in this study in order to determine their reactivity, as well as to enable the application of our results to soils with different clay mineral composition.

Based on preliminary results it was concluded that the rate of alkaline activation using 0.4 M NaOH and 0.4 M KOH solutions was to low to obtain reliable results in a reasonable length of time (Elert et al. 2008). Moreover, the pH, an important factor for assuring the effectiveness of the alkaline attack, dropped significantly after only a short period of time due to the interaction between clay minerals and the alkaline solution of relatively low concentration. Thus, in order to achieve unambiguous results and to avoid a drastic drop in pH over time, 5 M NaOH and 5 M KOH solutions were employed. Note that solutions of similar concentrations are commonly used in zeolite synthesis (Barrer et al. 1968, Breck 1974, Rios Reyes et al. 2013) and for the preparation of alkaline cements (Xu and Van Deventer 2000).

Subsequently, soil from the Alhambra Formation was used to prepare adobe blocks, to be treated by impregnation with the various alkaline solutions as a proxy to an in situ treatment. Afterwards, the adobe samples were submitted to further testing in order to evaluate the efficiency of the treatment.

2.1.1. Kaolinite

The material used is a kaolin from a clay deposit close to Cervo (Lugo, Spain), kindly supplied by Sargadelos (Cervo, Spain). The studied kaolin sample is sold under the commercial name "Super Standard Porcelain" and has a kaolinite content of 93 % according to the supplier. Kaolin is named after a hill in China (Kao-ling) from which this material was mined for centuries. It is a common 1:1 dioctahedral phyllosilicate mineral found throughout the world in highly-weathered environments. It forms from the alteration of aluminum-rich silicate minerals such as feldspars. Pure deposits are mined for porcelain.

2.1.2. Dioctahedral smectite (montmorillonite)

The starting material used in this study is a smectite from Cabo de Gata (Serrata de Nijar, Almeria, Spain), kindly supplied by F.J. Huertas Puertas (IACT-CSIC). Bentonites from the Cabo de Gata volcanic region have been commercialized since the 1950s. The origin of the bentonite rock is associated with hydrothermal alteration processes of tuffaceous volcanic rocks. The bentonites are of high quality, with a smectite content generally around 90%. The major mineral is a dioctahedral Fe- and Mg-smectite, accompanied by minor amounts of plagioclase, quartz, calcite, K-feldspar and traces of biotite and disordered tridymite. These smectites are always dioctahedral and belong to the beidellite-montmorillonite-nontronite series (Caballero et al., 2005).

2.1.3. Trioctrahedral smectite (saponite)

The saponite used is in this study is from the Yunclillos deposit, kindly supplied by Tolsa, S.A. (Madrid, Spain). The Yunclillos saponite deposit is situated in the Madrid Basin which extends over the provinces of Madrid and Toledo in the center of Spain. This saponite is very pure and only small amounts of quartz and sepiolite are observed as impurities (Merchan et al., 1998). Saponite is less common in nature than montmorillonite. Saponite is a tetrahedrally charged trioctrahedral smectite, originated as a product of the hydrothermal alteration and weathering of basalts and ultramafic rocks (Toranzo et al. 1997).

2.1.4. Illite

The illite used in this study is from the Beavers Bend State Park (Oklahoma, USA), kindly supplied by F.J. Huertas Puertas (IACT-CSIC). The sample is an illitic clay from an outcrop composed of alternating, discontinuous layers of fine sandstone and claystone (Mankin and Dodd, 1961). This clay, which was proposed as a standard reference material, is composed of a well-crystallized 2M-type illite with a minor amount of chlorite

(Chaudhuri and Brookins 1979). Gaudette et al., (1966) determine that the Beavers Bend illite is exceptionally pure and does not contain mixed-layer material.

2.1.5. Alhambra Formation soil

The Alhambra Formation outcrops at the east margin of the Granada Basin, forming an angular discontinuity over the underlying formations. It constitutes a good example of a fluvial (delta-fan) debris-flow deposit. It is made up of poorly sorted conglomerates and fluvial sand facies from Pleistocene-Early Pliocene age. In the distal areas, the deposit sequence shows “canal” facies with a predominantly inverse grain-size sequence. The delta-fan which originates such shallow marine deposit was supplied with sediments from both the Sierra Nevada area and the nearby calcareous reliefs. During the Pleistocene-Holocene, deposits tended to be characterized by abundant secondary red clays, associated with an intense weathering event, calcareous crusts, and fluvial sediments (clays, gravels and sands) forming a well-developed flooding plain (Martin 2000, Cultrone 2001, Azanon et al. 2003).

Soil samples were collected from the “Llano de la Perdiz”, an area close to the Alhambra Fortress, which belongs to the Alhambra Formation (Figure 2-1 and 2-2a and b).

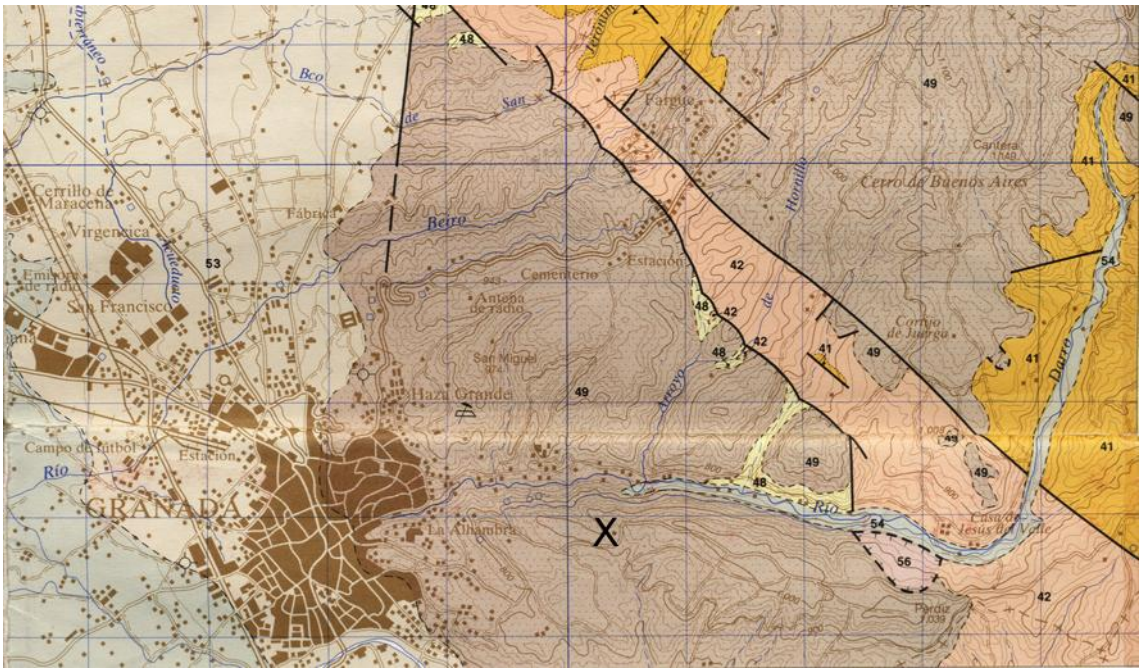

Figure 2-1. Geologic map (E. 1:50.000, 1009, Granada, Instituto Geologíco y Minero de España 1988) showing the Alhambra formation outcrops towards the East of the urban area. The X marks the zone where soil samples were collected. Legend: 41 = "Pinos Genil Formation ", conglomerates and sands; 42 = micaceous silt, sand and gravel; 48 = clays, red silts and conglomerates; 49 = "Alhambra conglomerate", conglomerates and sands,; 53 = red clays, gravel and sands, paleosoils; 54 = fluvial; 56 = detrital deposits.

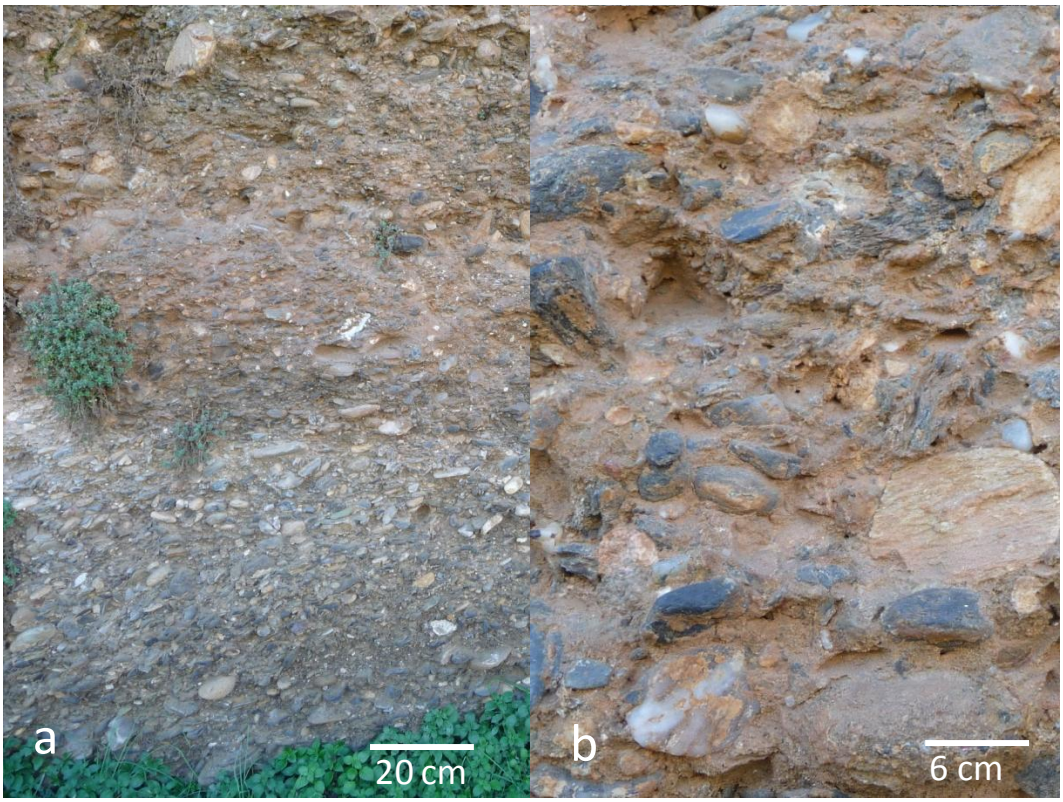

Figure 2-2. a) The Alhambra Formation soil; b) Detail (Fuente del Avellano, Granada, Spain).

2.2. Separation and analysis of the clay fraction

The sample preparation for the compositional analysis of the clay fraction (< 2 μm) of the Alhambra Formation soil and pure clays has been carried out according to the recommendations by Moore and Reynolds (1989). The study of the clay fraction requires the previous elimination of carbonates, which would mask some of the x-ray reflections of the clay minerals. In order to eliminate the carbonates, the sample was attacked with acetic acid. The concentration of the acetic acid was progressively increased up to 1 N. The sample was stirred to favour a homogeneous attack. After decarbonation was completed, excess acetate anions were removed by washing the sample with tap water.

All samples, (i.e., Alhambra Formation soil and pure clay minerals) were treated with a dispersant (sodium hexametaphosphate, Calgon) and the clay fraction was separated by centrifugation based on the Stokes law using a Kubota KS8000. Centrifugation time was 100 sec. at 1.000 rpm. This process was repeated 4 times in order to obtain a representative sample of the clay fraction. The clay fraction in suspension was pipetted on glass slides to allow the preparation of oriented clay mineral aggregates. In this manner the laminar clay particles were oriented with the c axis perpendicular to the glass slide surface, favouring the (00*l*) reflections. Four oriented aggregates (OA) of each raw clay sample were prepared for x-ray diffraction analysis: one aggregate without any further treatment (air-dried), one treated with ethylene glycol (EG) at 60 ºC for 48 h (Burton 1955), a third treated with dimethyl sulfoxide (DMSO) at 80 ºC for 48 h (Gonzalez Garcia and Sanchez Camazano 1968), and a forth submitted to thermal treatment at 550 ºC for 90 minutes.

2.3. Preparation of adobe samples

For the preparation of adobe bricks the fraction < 1 mm of the Alhambra Formation soil was used, which was separated from the bulk sample by sieving. Adobe bricks 4 x 4 x 4 cm in size were prepared by mixing 100 g of soil with 30 g of water. This mixture was poured into a wooden mold (Figure 2-3) which was previously wetted and covered with washed sand to facilitate demolding. After demolding, the sand was removed with a brush. The blocks were dried in the laboratory at ~ 20 ºC and ~ 45 % relative humidity.

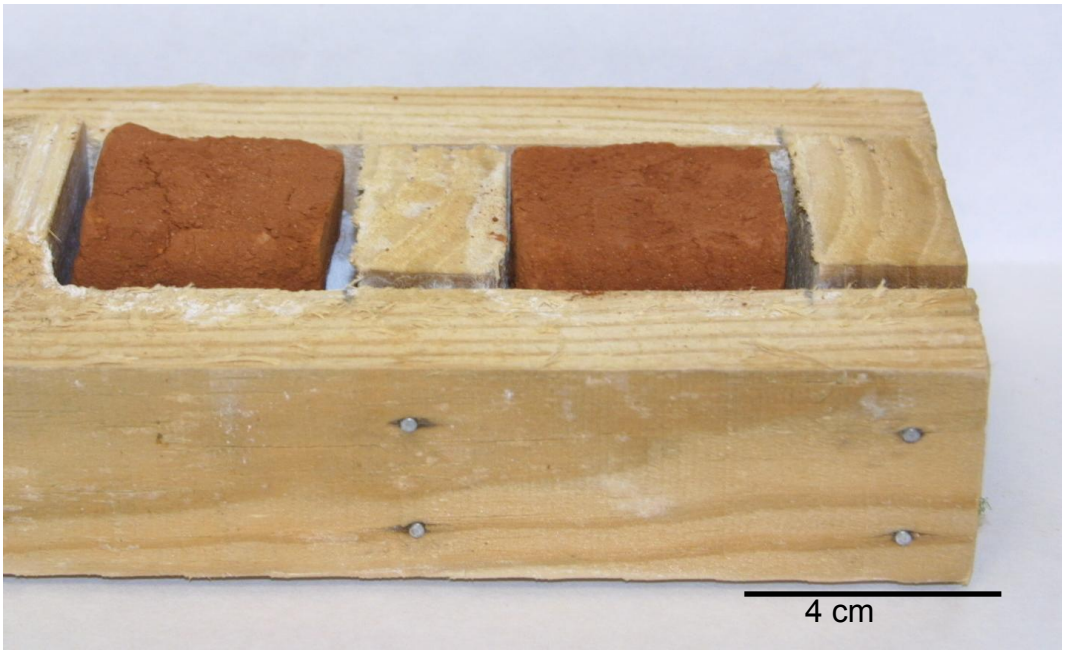

Figure 2-3. Preparation of adobe blocks using a wooden mold.

2.4. Alkaline activation using $Ca(OH)_2$, NaOH and KOH

After completion of the mineralogical characterization, powdered clay samples (< 2 μm fraction) were subjected to alkaline activation. All alkalis used here were reagent grade, Sigma-Aldrich Chemie GmbH, Germany. In all experiments a sample of 5 g (dry weight) was mixed with 100 ml of alkaline solution:

a) 0.025 M $Ca(OH)_2$, this concentration corresponds to a saturated solution at room *T* (Boynton, 1980).
b) 0.4 M NaOH
c) 0.4 M KOH
d) 5 M NaOH
e) 5 M KOH

The clay samples were kept in tightly capped polypropylene bottles and stored in the laboratory at 20 °C. Bottles were stirred periodically. Samples for analysis were taken at predetermined time intervals (i.e., 1, 3, 7, 14 days, 1, 2, 4, 6 months, 1, 4.5 and 6 years). The extracted samples were washed with deionized water until a pH of around 7 was reached. Afterwards, the alkaline-treated clay suspensions were deposited on glass slides to prepare oriented aggregates.

The adobe blocks were treated with 5 M NaOH and 5 M KOH solutions as well as with saturated $Ca(OH)_2$ solution by total immersion. The weight difference between adobe brick samples before and after alkaline activation (immersion for 20 min.) was measured in order to determine the amount of solution absorbed in each case (Table 2-1). Material loss was considered when determining the alkaline solution up-take.

Table 2-1. Average weight increase (weight %) of adobe blocks following immersion in alkaline solutions for 20 minutes.

5 M NaOH	5 M KOH	0.025 M $Ca(OH)_2$
6.6	7	6

Samples treated with NaOH and KOH showed only very little material loss whereas in the case of the sample treated with $Ca(OH)_2$ the material loss was more significant. Taking the material loss into consideration only little difference in solution up-take can be observed for the various alkaline solutions. Each adobe brick was placed in the alkaline solution for 20 minutes and afterwards stored in sealed polyethylene zip-lock bags to prevent premature drying and facilitate the reaction between clay minerals and

alkaline activator (Figure 2-4). The blocks were cured at ~20 ºC and 85% relative humidity. The samples weight was controlled during storage in order to detect premature drying, which was not the case. After 50 days the bags were opened to facilitate slow drying until a stable weight was reached.

Figure 2-4. Adobe blocks treated with alkaline solution were stored in plastic bags for 50 days to insure curing and avoid premature drying.

2.5. Sample analysis

Raw clays (i.e., soil from the Alhambra Formation and pure clays) and treated clay samples were subjected to chemical, mineralogical and textural analysis. These analyses included the characterization of newly formed phases as well as remaining clay minerals.

2.5.1. XRF

Elemental analysis was performed using a commercial wavelength dispersive X-ray fluorescence instrument (BRUKER S4 Pioneer, IACT-CSIC) equipped with an Rh anode X-ray tube (60 kV, 150 mA) and three analyzer crystals (OVO-55, LiF 200 and PET). For the detection of light elements a gas flow proportional counter and for heavy elements a scintillation counter were used. Quantification was made by the fundamental parameters method using SpectraPlus software. Samples were prepared as follows: Five grams of powdered sample was mixed with 0.5 grams of binder (Hoechst wax C micropowder) and homogenized in an agata mortar. To obtain a XRF-pellet, a small metallic sample holder made of aluminium with a diameter of about 4 cm was used. The pellets were pressed at 90 bars in a Nannetti hydraulic press for 30 s. To determine loss on ignition (LOI), samples were heated up to 900°C for 1 hour.

2.5.2. XRD

The mineralogical composition of the starting materials as well as of newly formed phases was determined by means of X-ray diffraction. XRD patterns were collected using either a Phillips PW 1547 diffractometer with Cu-Kα radiation (λ=1.5418 Å); 40 kV voltage; 40 mA intensity; exploration range of 3º to 60º 2θ; and goniometer speed of 0.01º $2\theta s^{-1}$ or X´Pert PRO (PANalytical B.V., The Netherlands) with Cu-Kα radiation; Ni filter; 45 kV voltage; 40 mA intensity; spinner on; exploration range of 3º to 60º 2θ and goniometer speed of 0.05º $2\theta s^{-1}$ (Dept. Min. and Petr. - UGR).

OA were used in order to study the raw clay samples. Ethylene glycol (EG) and dimethyl sulfoxide (DMSO) allowed the identification of expandable clays with a d-spacing of 12-14 Å which changed to ~17 Å in the case of EG and ~19 Å in the case of DMSO; whereas the thermal treatment reduced the d-spacing to 9.6 – 9.8 Å. The main Bragg peaks of chlorite and caolinite coincide, chlorite having a d-spacing of 7.16 Å and kaolinite of 7.10-7.20 Å. Therefore, both were differentiated using the doublet at 3.58 Å for kaolinite and 3.55 Å for chlorite (Moore and Reynolds 1989). Moreover, the DMSO treatment might cause the expansion of kaolinite changing the d-spacing from 7.16 Å to 11.18

Å, thus, allowing the differentiation from chlorite. Finally, the thermal treatment at 550 ºC results in the destruction of kaolinite, confirming, therefore, the presence or absence of chlorite.

The crystallite size of untreated and treated clay minerals was calculated using the 001 reflection according to the Scherrer equation from peak broadness analysis using X-powder12 (Martin Ramos 2004).

Qualitative analysis of minerals was performed with the help of X-powder12 software (Martin Ramos 2004). The obtained reflections were compared with Power Data Files of the "Joint Committee of Power Diffraction Standards". OA were also used in the case of treated clay samples. In the case of the adobe brick samples, powder XRD has been employed to detect newly formed phases after alkaline treatment.

Semiquantitative analysis of the Alhambra Formation soil (whole sample and < 1 mm fraction) was done using powder XRD. In the case of the clay fraction of Alhambra Formation soil and pure clays oriented aggregates were used. The integrated area of the main reflection (i.e., that with maximum intensity) of each mineral phase was measured and normalized by its reflection power (Table 2-2). The obtained values are given as percentage with respect to the entire mineral content. The quantitative analysis regarding the actual mineral content has an error of 5% in the case of the bulk sample and 5-10% the case of the clay fraction. Because of its elevated inaccuracy this method is considered semiquantitative.

Table 2-2. Main reflections and reflection power of minerals*.

Mineral	Main Reflection (Å)	Reflection power
Powder XRD		
Quartz	3.34	1.43
Clay fraction	4.45	0.09
Calcite	3.03	1.05
Dolomite	2.89	1.08
Feldspars	3.18	1.03
Oriented aggregate		
Illite	9.98	0.36
Paragonite	9.80	0.36
Smectite	12.5-14	0.93
Chlorite/ Kaolinite	7.1/ 7.16	0.98

* XRD Laboratory (Dept. of Min. and Petr. - UGR), determined using the Internal Standard Method.

2.5.3. FESEM

The morphology and qualitative composition of both, the clay fraction and reaction products formed upon alkaline treatment were studied by means of field emission scanning electron microscopy (FESEM; Leo Gemini 1530 or AURIGA, Carl Zeiss SMT, CIC-UGR) coupled with EDS microanalysis (INCA-200, Oxford). Prior to FESEM analysis, samples were carbon-coated (Hitachi) for compositional (qualitative) analyses and textural studies.

2.5.4. TEM

This technique has been used for the characterization of the starting material and, in particular, for the study of the transformation of minerals after alkaline activation where XRD and FESEM did not allow an unambiguous identification.

Compositional and morphological changes were examined using a transmission electron microscope (Philips CM20, CIC-UGR) equipped with an EDAX solid-state ultrathin window energy dispersive X-ray (EDS) detector. The acceleration voltage of the microscope was 200kV and a lens aperture of 40 μm was used as a compromise between amplitude and phase contrast for the images. The identification of new phases was facilitated collecting SAED (selected area electron diffraction) patterns prior to quantitative analytical electron microscopy (AEM) analysis. AEM analyses were performed in scanning TEM mode using a 10 nm diameter beam and 20 x 100 nm scanning area. A short counting time of 15-30 s was used for volatile elements (K and Na) and a longer counting time of 50-100 s for non-volatile ones. A low-background condenser aperture and an analytical Be sample holder were employed to improve spectrum quality. Ms, Ab, Bt, Sps, Ol, Ttn, KFds and $CaSO_4$-$MnSO_4$ standards were used to obtain *k*-factors allowing X-ray intensities to be corrected by the thin-film method (Lorimer and Cliff, 1976). Average errors for analyzed elements expressed as a percentage of atomic proportions are 6 (Na), 3 (Mg), 2 (Al), 4 (K), 4 (Ca), 5 (Ti), 3 (Mn), and 3 (Fe). Errors due to K and Na loss during AEM analysis were corrected by determining K and Na at 15-30 and 50-100 s beam-exposure time and scaling K and Na concentrations back to zero seconds as described by Worden et al. (1987). The structural formula of clay minerals and newly formed phases was calculated based on AEM data. In the case of newly formed zeolitic phases, formulae were adjusted considering the structural formulae of the phases previously identified with XRD. Note that in the case of most zeolites, TEM-AEM data were only considered qualitatively. Due to the crystal thickness of zeolites, absorption of the X-rays emitted by the elements is likely to occur. This effect is generally more significant in the light-weight elements, leading to

lower concentrations of Na and K relative to heavier elements such as Si and Al. Thus, the proportions of cations, especially Na and K, in structural formulae of zeolites will be underestimated (personal communication, Nieto Garcia, F., 11.10.13). The structural formulae were calculated assuming that all iron is ferrous (Fe^{2+}), since AEM analysis does not allow a distinction between ferrous and ferric iron.

Prior to TEM analysis samples were dispersed in ethanol, sonicated for 30 s and deposited on Formvar© and carbon-film coated copper grids. In some cases, gold grids instead of standard copper grids were used to avoid overlapping of the *K* band of Na and the *L* band of Cu (Drief et al., 2001).

2.5.5. Elemental analysis

Elemental analysis of nitrogen, carbon, hydrogen and sulfur was performed to verify organic carbon content using a Fisons Carlo Erba EA 1108 CHNS O equipped with TCD detection system (CIC-UGR). The samples were heated to 1020 ºC during 800 s and calculations were carried out employing Eager 200 software.

2.5.6. Thermogravimetric analysis

The thermal decomposition of clays and the amount of organic matter in the Alhambra Formation soil was determined using thermogravimetric analysis (TG) on a Shimadzu TGA-50H coupled with Fourier transform infrared spectroscopy (FTIR; Nicolet 550, CIC-UGR) for evolved gas analysis. Analyses were performed using air (100 ml/min flow rate), at a constant heating rate of 20 ºC/min (25-950 ºC).

2.5.7. pH evolution

The pH evolution during the alkaline attack was monitored using a pH-meter Stick Piccolo HI 1280 (Hanna Instruments, Dept. Min. and Petr. - UGR).

2.5.8. Titration

In order to verify the concentration of alkaline solutions used for the experiments, acid-base titration was performed using 905 Titrando, Metrohm (Dept. Min. and Petr. - UGR). This instrument also allowed the determination of the initial pH of the alkaline solutions.

2.5.9. Penetration depth of consolidants

In order to evaluate the efficiency of the consolidation treatment, the penetration depth of the alkaline solution was determined using a pH indicator (alizarin red). Treated adobe blocks were split in half and the indicator solution was applied by brushing.

2.5.10. Porosimetry

The total pore volume and the pore size distribution of adobe blocks was determined using mercury intrusion porosimetry (MIP). The instrument used was a Micromeritics Autopore III 9410 porosimeter (Dept. Min. and Petr., UGR). This instrument can generate pressures of up to 414 MPa and measures pores between 0.003-360 μm diameter. Before analysis, samples (about 2 g) were oven-dried for 24 h at 95 °C. The average porosity was calculated based on 4 measurements.

2.5.11. Nitrogen sorption

Nitrogen sorption isotherms of powdered clay samples before and after alkaline activation were obtained at 77 K on a TriStar 3000 equipment from Micromeritics (Dept. Min. and Petr., UGR). About 0.2 g of sample was degassed at 150 °C for 3 h prior to analysis using a sample degas system (VacPrep 061, Micrometrics, Dept. Min. and Petr., UGR). Note that the pretreatment at 150 °C might induce structural changes in some newly formed phases in the case of alkali activated samples, thus, altering the nitrogen adsorption results. However, Ismail et al. (2013) demonstrated that changes due to collapse of pores were limited to C-S-H-type gel. The main reaction products in our study were zeolites which generally show good thermal stability. Only in rare cases dehydration accompanied with contraction has been reported to take place at < 150 °C (Cruciani 2006). The surface area of untreated and treated clay samples was determined applying the BET method (Brunauer, Emmett and Teller, 1938).

2.5.12. Particle size analysis

Particle size analysis of powder samples dispersed in alcohol was performed using a Mastersizer 2000LF of Malvern Instruments (CIC-UGR). This instrument measures particles in the range 0.02 – 1500 μm using laser diffraction.

2.5.13. Hydric behaviour and water resistance

To evaluate the hydric properties and the water resistance of untreated and treated adobe blocks, samples were immersed in water and the weight gain was determined at fixed time intervals. The material loss upon immersion was considered when calculating the water uptake. The free water absorption (A_b) was calculated as follows:

$A_b = 100\ [M_L - M_0)/\ M_0]$

Where M_L and M_0 are the mass of the sample at immersion time t, and at time t = 0, respectively. The water absorption rate of untreated and treated samples is defined as the slope of the line which is drawn using the best fit to the initial linear section of the curve of free water absorption plotted against the square root of time.

The experiment was performed in duplicate in order to validate test results.

2.5.14. Compressive strength

Compressive strength was measured using an Incotecnic-Matest hydraulic press, kindly provided by Argos Derivados del Cemento S.L., Granada. The measurement was done according to UNE-EN 10-15 (2000).

2.5.15. Drilling Resistance

The drilling resistance was determined using a Drilling Resistance Measurement System (DRMS, Sint Technology, Italy, (Dept. Min. and Petr., UGR)) which allows the continuous measurement of the force necessary to drill a hole in the adobe block under constant operating conditions. The drilling parameters were: 15 mm maximum depth, 20 mm/min penetration rate, 200 rpm revolution speed and a diamond-tip 5 mm diameter drill bit. Macor®, a machinable glass ceramic, was used at regular intervals for calibration (Pamplona et al. 2007).

2.5.16. Color measurement

Color measurements of untreated adobe blocks and blocks subjected to alkaline activation have been performed in order to detect possible color changes upon treatment. Color measurements were carried out with a spectrophotometer CM-700d, Konika Minolta (Dept. Min. and Petr., UGR), using illuminant D65, 10º observer and 8 mm measurement area.

Color changes were determined using the CIE-LAB system. Lightness is defined as L*, and a* (red-green) and b* (yellow-blue) are the chromatic

coordinates. Reds have positive a* values, whereas greens have negative a* values. Similarly, yellows have positive b* values and blues have negative b* values. The total color variation, ΔE, was determined using the following formula: $\Delta E = [(\Delta L^*)^2+(\Delta a^*)^2+(\Delta b^*)^2]^{(1/2)}$

2.5.17. Salt crystallization test

After the treatment of soils with alkaline solutions, unreacted alkali might react with atmospheric CO_2 to form carbonates, namely Na_2CO_3, K_2CO_3 and $KHCO_3$. In order to evaluate the damaging character of these carbonates, a salt crystallization study was performed using calcarenite from Santa Pudia, Granada. This calcarenite was selected because it is a quite homogeneous material with a well known susceptibility to salt damage in the laboratory and in the field. In addition, this stone has been extensively characterized with regards to composition, mineralogy and pore system. The calcarenite from Santa Pudia has a porosity of 32.2 % as determined by MIP (Ruiz-Agudo et al. 2007). According to Ruiz-Agudo et al. (2007) and Benavente et al. (2004) the susceptibility to salt weathering of the Santa Pudia calcarenite is due to the high proportion of mesopores (pore radius = 2-50 nm) connected to larger macropores. Note that it was not possible to use adobe blocks in this test because they would not have withstood prolonged immersion in water-based solutions.

Four stone prisms (3x3x25 cm) were placed in glass dishes filled with 300ml of different saturated salt solutions (Figure 2-5). The stone blocks were partially immersed in the salt solution and crystallization occurred in the upper non-immersed stone areas following capillary rise and evaporation. The salt solutions included Na_2SO_4, Na_2CO_3, K_2CO_3 and $KHCO_3$. Na_2SO_4 is one of the most widely used salts in laboratory studies of salt weathering as well as in durability tests of building materials and has been proven to be extremely destructive. In this study it was included as a reference. The surface of the salt solutions was covered with paraffin in order to promote the migration of the salt solution through the pore system of the stone, to avoid creeping of the salt and to reduce solution evaporation (Rodriguez-Navarro and Doehne 1999). The samples were kept in the laboratory at 20 ºC and 35-50 % RH.

The weight loss due to evaporation of the salt solution was recorded and at the same time pictures were taken to document the damage evolution over time. To determine the damage, material that was lost from the stone surface following salt crystallization was weighed after the salt was removed by washing with distilled water. Total weight loss was expressed as percentage of the original weight of the stone block.

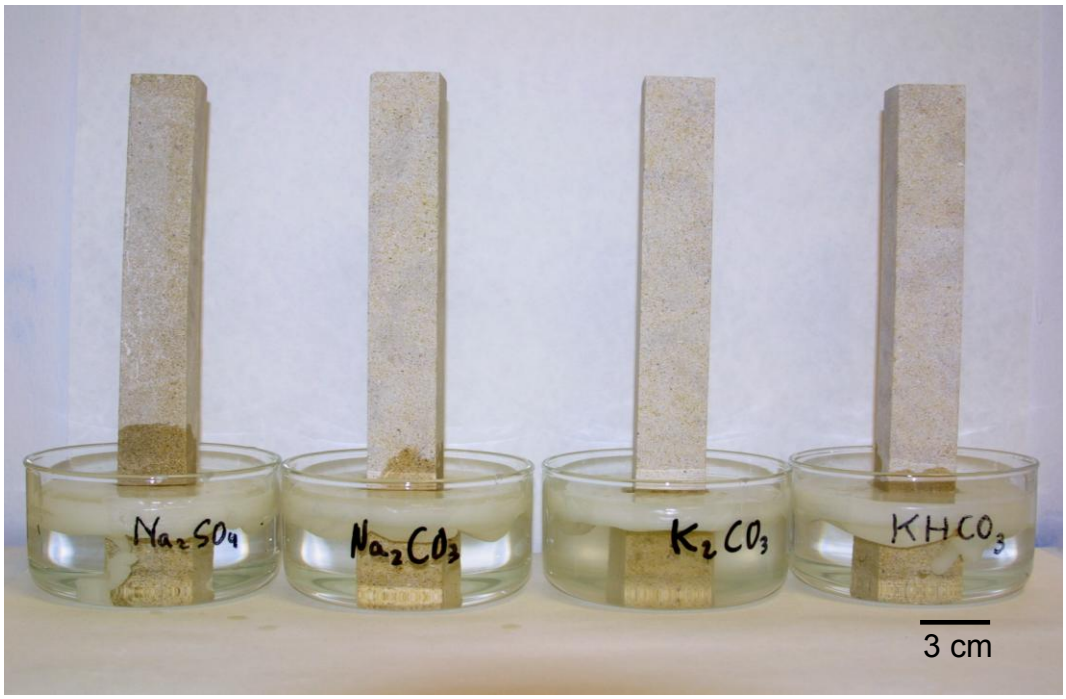

Figure 2-5. Calcarenite prisms partially immersed in the different salt solutions at the beginning of the test.

3. Results

In sections 3.1.-3.4. results regarding the characterization of tested pure clay minerals, including kaolinite, montmorillonite, saponite and illite, are presented. Furthermore, their mineral evolution upon alkaline activation with 5 M NaOH and 5 M KOH was studied. After that, results regarding the chemical, mineralogical and structural properties of the tested Alhambra Formation soil before and after alkaline activation using saturated $Ca(OH)_2$ solution, 0.4 and 5 M NaOH and 0.4 and 5 M KOH are presented (section 3.5). Subsequently, the pH evolution (section 3.6) upon alkaline activation and the influence of organic matter content on mineral dissolution and transformation (section 3.7) were determined. Next, the evaluation of an in situ application of alkaline solution to adobe test blocks is included in section 3.8. Finally, possible adverse effects of the consolidation treatment using alkaline solutions were examined. Salt crystallization tests were performed and their outcome is reported in section 3.9.

3.1. Characterization of kaolinite

The following section includes the characterization of the untreated kaolinite and the study of its mineralogical evolution upon alkaline activation using 5 M NaOH and 5 M KOH.

3.1.1. Untreated kaolinite

3.1.1.1. XRF

X-ray fluorescence analysis (Table 3-1) of the < 2 μm fraction of the untreated sample showed a high silica and aluminia content typical for kaolinite. However, the relatively high amount of K_2O as well as the minor content of sodium, magnesium, iron and calcium, suggest the presence of some impurities which was confirmed by XRD (see below). The XRF results are in agreement with published data for kaolinitic clays from this region (Conde-Pumpido et al. 1988). The following structural formula was calculated based on XRF results: $(Na_{0.02}K_{0.05}Ca_{0.02})Si_{2.04}(Al_{1.88}Mg_{0.01}Fe_{0.02})O_5(OH)_4$

Table 3-1. XRF results of the starting material (wt %)

Material	SiO_2	Al_2O_3	Fe_2O_3	Na_2O	MgO	K_2O	CaO	Loss on Ignition	Total
Kaolinite	47.43	37.09	0.61	0.18	0.19	0.91	0.17	13.4	99.98
Kaolinite*	48.50	35.70	1.14	0.04	0.36	0.68	0.08	13.1	99.60

* Conde-Pumpido et al. (1988)

3.1.1.2. XRD

OA treated with EG revealed the existence of minor amounts of smectite (showing a small Bragg peak at 16.85 Å) as well as illite, in addition to kaolinite (Figure 3.1.). The d_{001} of kaolinite expanded from 7.2 Å to 11.27 Å upon DMSO treatment and collapsed after the heat treatment at 550°C (Figure 3-1). Such an expansion is characteristic for kaolinite (Gonzalez Garcia and Sanchez Camazono 1968). The sample contained about 95 % kaolinite, 5 % illite and <1 % smectite as calculated using XRD data, thus, confirming suppliers data stating a kaolinite content of 93 % (Seminario de Sargadelos, personal communication, 2005). The samples Bragg peaks matched those of kaolinite JPDF card no. 060221.

The crystallite size of the kaolinite was 36 nm. This value suggests a high crystallinty of the kaolinite. Average crystallite sizes reported by Pardo et al. (2011) for kaolinite range between 22.2 and 40.5 nm.

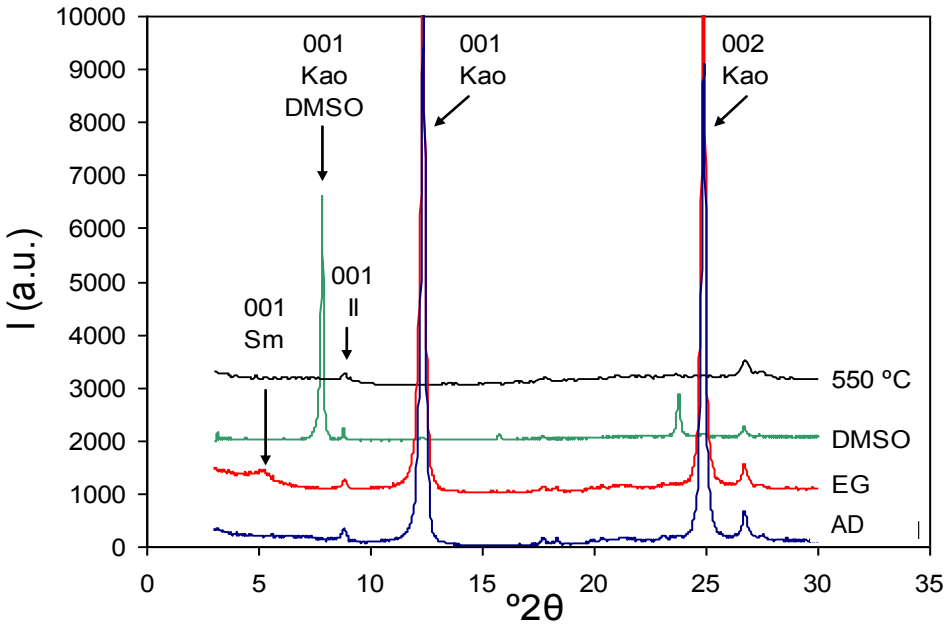

Figure 3-1. XRD patterns of kaolinite. OA air-dried (AD), treated with EG, DMSO and thermal treatment. Sm = smectite, Kao = kaolinite, Il = illite.

3.1.1.3. FESEM

The FESEM image (Figure 3-2) shows the typical blocky structure of hexagonal crystals of kaolinite formed by staking of (Si) tetrahedral and (Al) octahedral sheets along the *c*-axis (Goldman et al. 1990). Halloysite can also be appreciated. The microanalysis results, showing only Al and Si, confirmed the high purity of the kaolinite crystals.

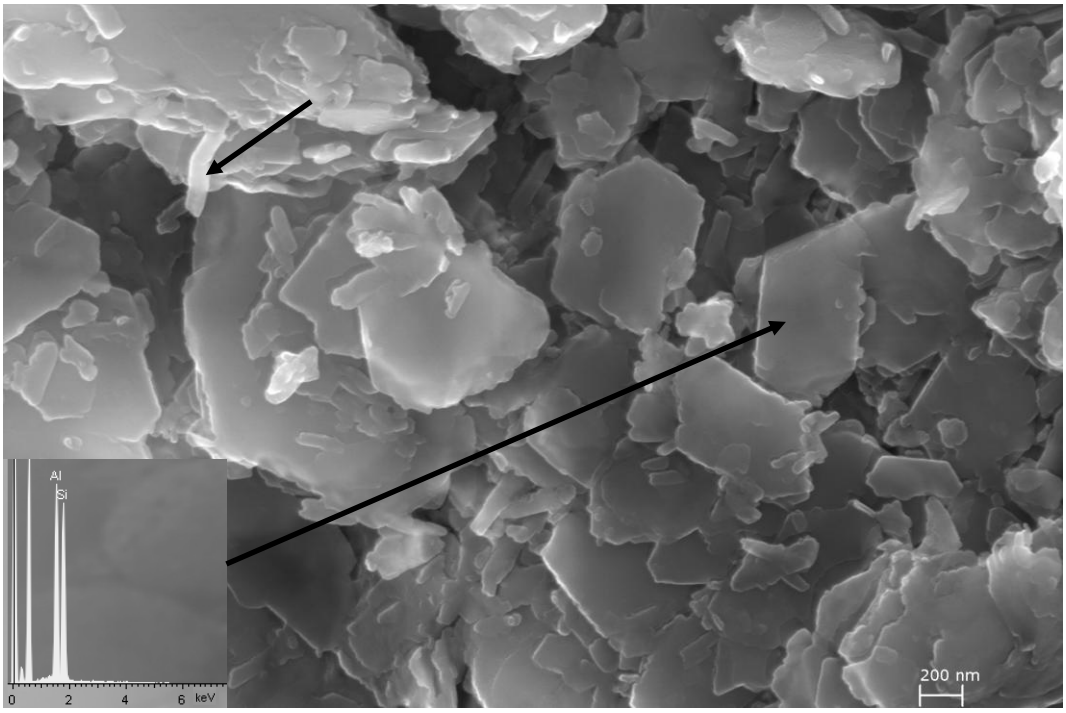

Figure 3-2. FESEM image and EDS spectrum of untreated kaolinite. Halloysite can be detected (arrow) as well.

3.1.1.4. TEM

The TEM image (Figure 3-3) of the untreated sample shows the typical hexagonal crystals of kaolinite together with halloysite, a fibrous polymorph of kaolinite. TEM-AEM analysis (inset, Figure 3-3) revealed the high purity of kaolinite/halloysite (Sebastian Pardo et al. 1983). Note that the sample was tilted 40 ° to prove the fibrous character of halloysite (Figure 3-4). The following average structural formula was calculated from TEM-AEM analysis data: $Si_{1.94}(Al_{2.07}Fe_{0.01})O_5(OH)_4$

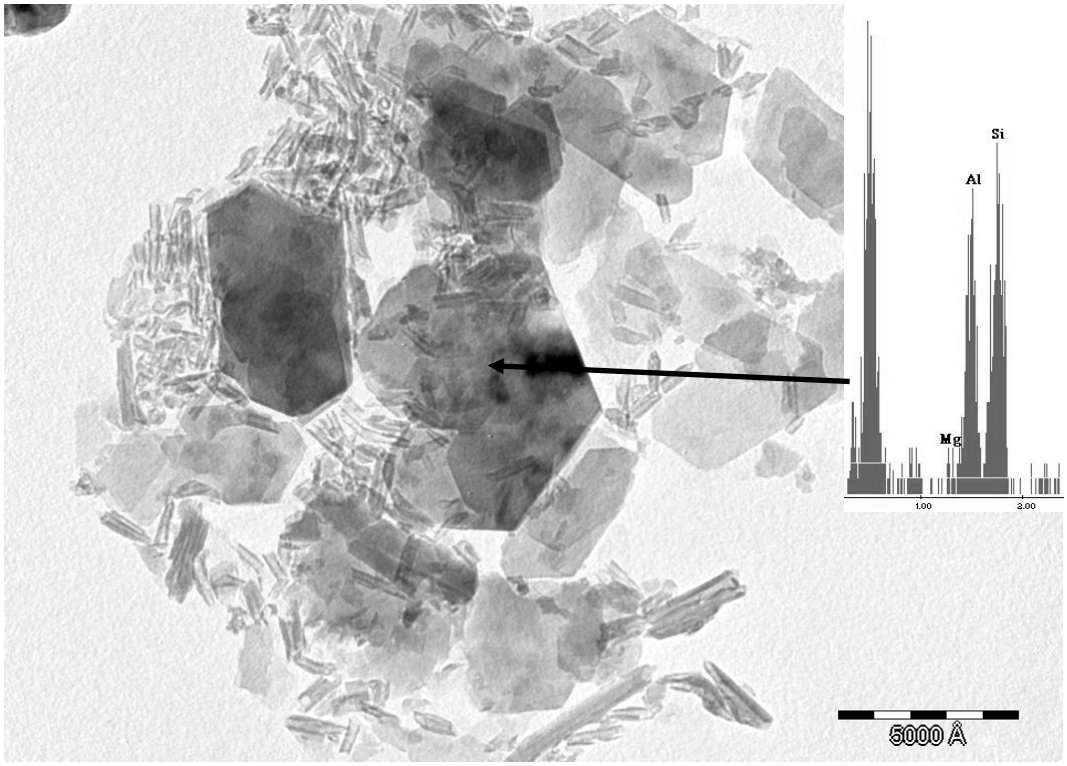

Figure 3-3. TEM image of untreated kaolinite. General aspect of the sample.

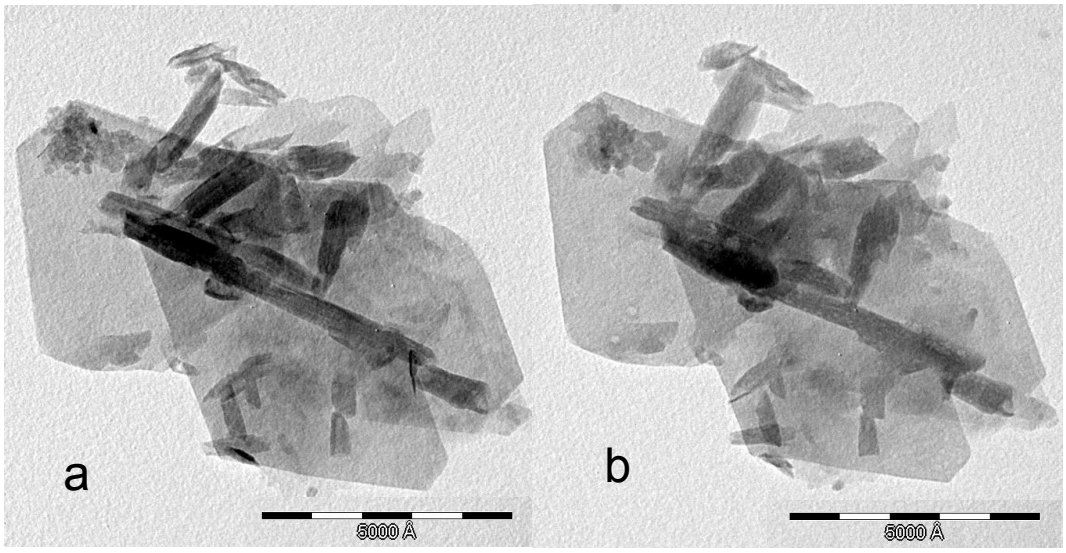

Figure 3-4. TEM images of untreated kaolinite. The image on the right (b) shows the clay particles in (a) after 40 ° tilting to prove the fibrous character of the halloysite crystals.

3.1.1.5. Nitrogen sorption

The BET surface area of the untreated kaolinite was 23.79 ± 0.09 m²/g. This value seems to be typical for kaolinite (Goldman et al. 1990, Celis et al. 1996, Bereznitski et al. 1998, Sanders et al. 2010). Murray and Lyons (1960) and Coles and Young (2002) reported a surface area range for kaolinite of 8-50 m²/g. However, in our case, the actual surface area of the kaolinite might have been slightly lower and was positively influenced by the presence of halloysite. Note that the specific surface area of the latter is higher than the one of kaolinite. The reported range is 35-70 m²/g (Goldman et al. 1990).

The Nitrogen sorption isotherm was of type II which is standard for a non-porous or macroporous (> 50 nm) adsorbent and common for kaolinite (Figure 3-5). The contribution of micro (< 2 nm) or mesopores (2-50 nm) was very limited (Celis et al. 1998, Kuila and Prasad 2013). A quite narrow, type H3 hysteresis loop was observed, which is typical for aggregates of plate-like particles and indicative for the presence of fine, slit-shaped macropores (Sing et al. 1985, Kuila and Parsad 2013).

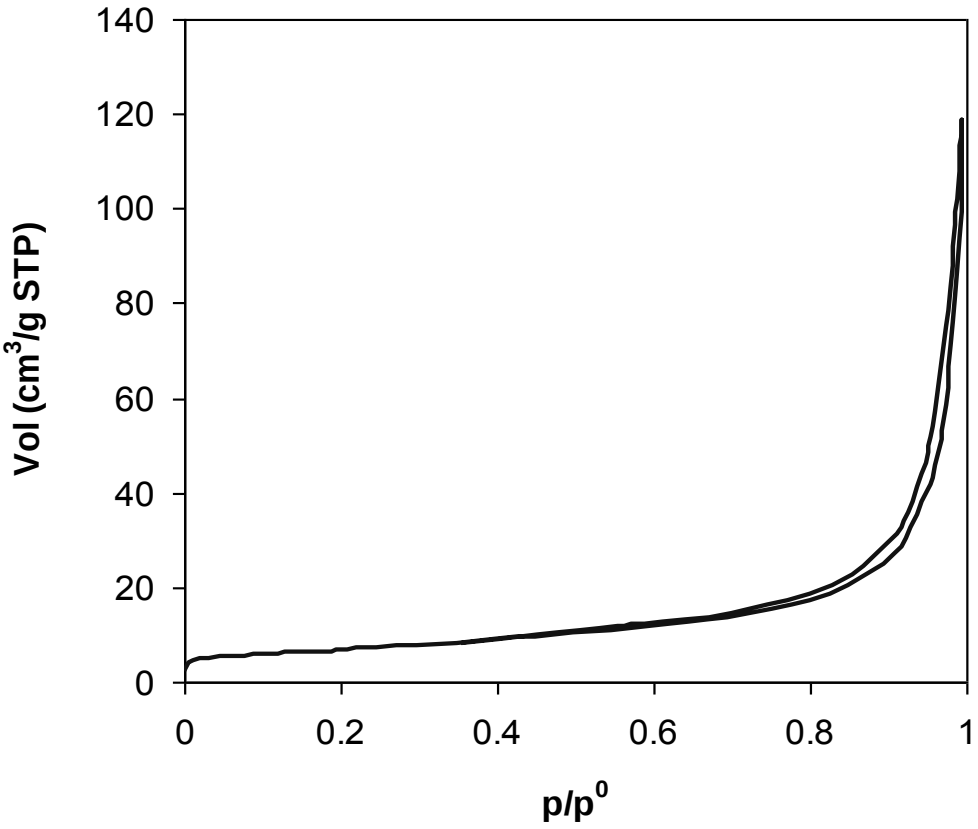

Figure 3-5. Nitrogen sorption isotherm of untreated kaolinite.

3.1.1.6. Particle size analysis

Kaolinite particles are generally larger and have a lower surface-to-volume ratio than other clays. The thickness of stacks of kaolinite range from 0.05-2 μm, resulting in a typically blocky structure (Goldman et al. 1990). The kaolinite studied here showed a particle size maximum at 140 nm and a secondary maximum between 0.5 – 3 μm (Figure 3-6). Young (2006) reported a particle size range between 0.3-4 μm for kaolinite and Franco et al. (2004) presented particle size distribution curves, showing a maximum at 0.5 μm. The relative small average particle size observed here is attributed to the presence of a significant amount of halloysite in the sample.

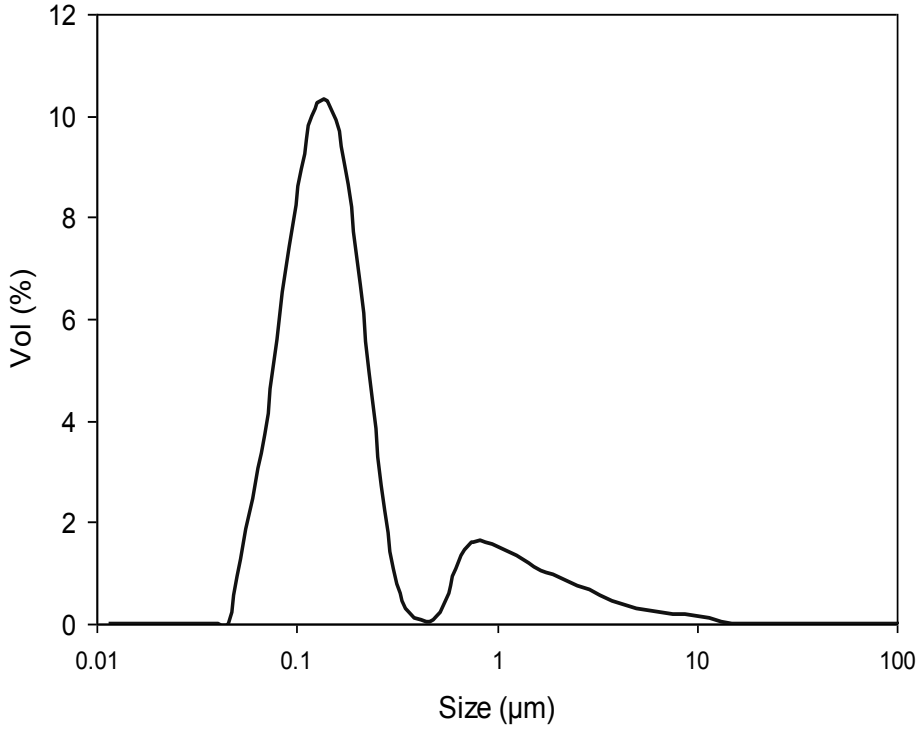

Figure 3-6. Particle size distribution of untreated kaolinite.

3.1.1.7. TG

The thermogravimetric curve showed a continuous loss of adsorbed water of 2 wt% from about 30°C to 450 °C (Figure 3-7). At this *T* the dehydroxylation of the kaolinite began. The total weight loss amounted to 13.4 wt%. The thermogravimetric curve and the total weight loss were very similar to data reported for kaolinite by Bain and Morgan (1969). The higher weight loss of about 11.4 wt% due to dehydroxylation in the case of kaolinite, a 1:1 clay, when compared to 2:1 clays can be explained by the larger number of structural hydroxyl groups per unit in the case of kaolinite.

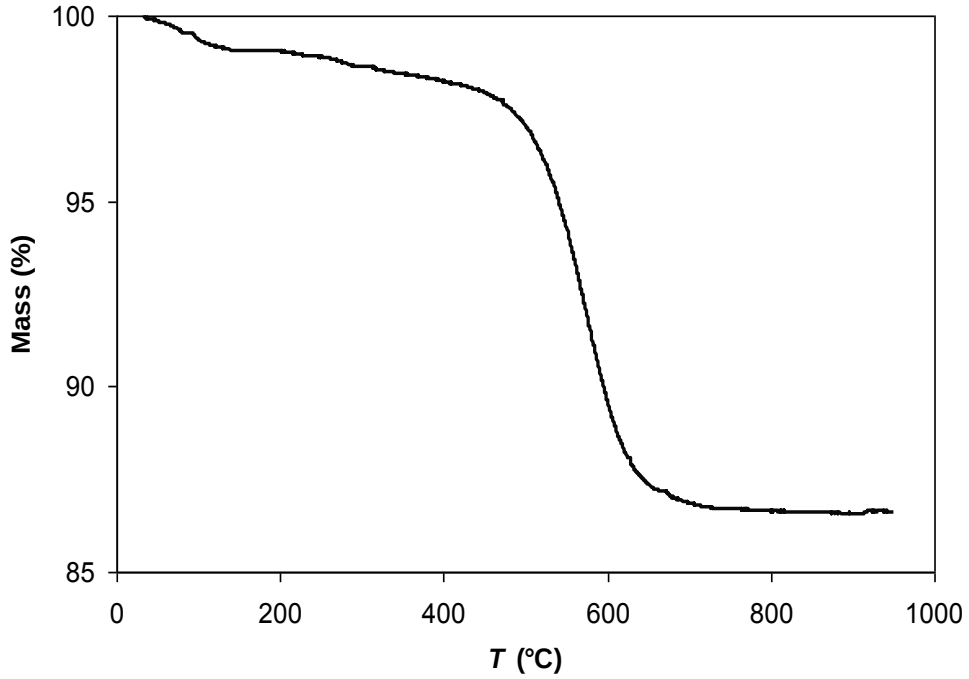

Figure 3-7. Thermogravimetric curve of untreated kaolinite.

3.1.2. Kaolinite treated with NaOH

3.1.2.1. XRD

XRD analyses demonstrated that a new zeolitic phase appeared after 2 months of treatment with 5 M NaOH. The new phase corresponded to zeolite X, a synthetic analogue of faujasite, which crystallizes in the cubic system and has the following formula: $Na_2Al_2Si_{2.5}O_9 \cdot 6.2H_2O$ (JPDF card no. 380237, see Figure 3-8, blue line pattern). The structural formula does not coincide with EDS microanalysis results which showed the presence of Ca instead of Na. However, different cations such as Ca, K and Na can enter the tetrahedral framework of this zeolite without causing severe changes in the diffraction pattern (Prokofev et al. 2013).

After six months, an additional zeolitic phase was identified which corresponds to a sodalite-type zeolite with the following formula: $Na_{2.16}Al_2Si_{1.68}O_{7.44} \cdot H_2O$ (JPDF card no.311271, see Figure 3-9, red line pattern). Sodalite-type zeolites and zeolite X are common reaction products in the zeolite synthesis using kaolinite and NaOH solution (Barrer et al. 1968).

After 1 year of treatment no additional phases were identified and the intensity of the kaolinite Bragg peaks at 7.19 Å and 3.59 Å diminished significantly, indicating a nearly complete destruction of the mineral.

The sample treated for 6.1 years revealed that the sodalite-type zeolite was now the dominant phase. At the same time, kaolinite and the faujasite-type zeolite disappeared completely.

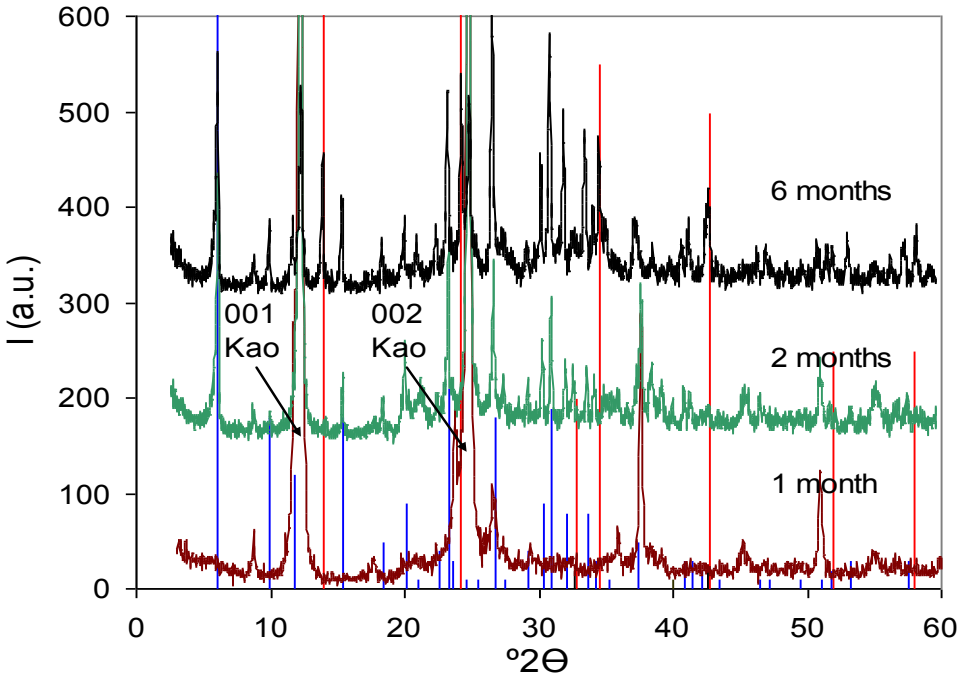

Figure 3-8: Mineralogical evolution of kaolinite treated with 5 M NaOH for different periods of time. The faujasite-type zeolite X (JPDF card no. 380237, blue line pattern) appeared after 2-months treatment and the sodalite-type zeolite (JPDF card no.311271, red line pattern) appeared after 6 months of treatment, Kao = kaolinite.

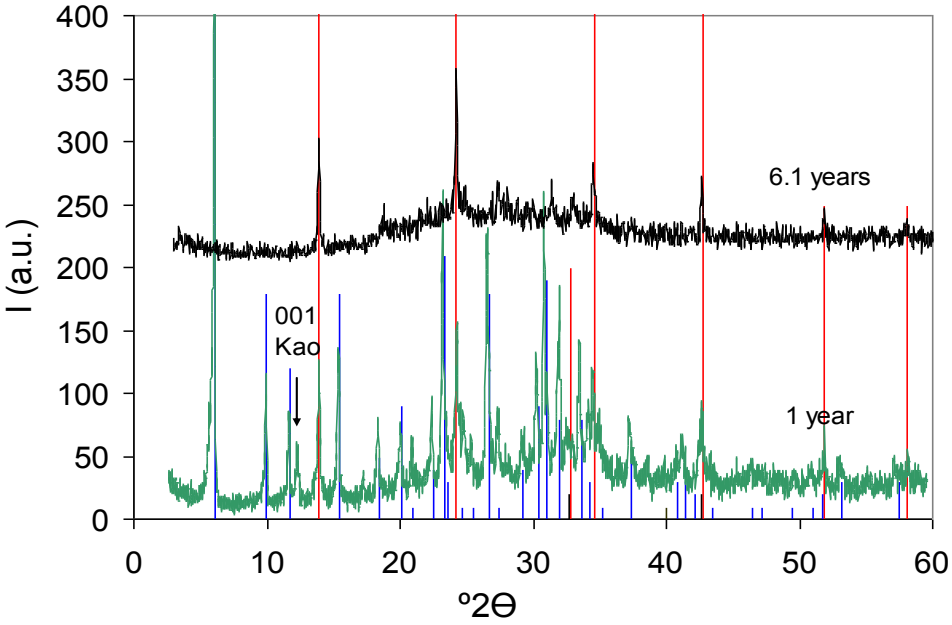

Figure 3-9: Mineralogical evolution of kaolinite treated with NaOH for different periods of time. Kaolinite and the faujasite-type zeolite X (blue line pattern, JPDF card no. 380237) disappeared after 6.1 years of treatment whereas the sodalite-type zeolite remained (red line pattern, JPDF card no.311271), Kao = kaolinite.

3.1.2.2. FESEM

FESEM images of the sample treated for 2 months confirmed the presence of a newly formed cubic phase compatible with a faujasite-type zeolite. Unreacted kaolinite particles were also visible (Figure 3-10). The microanalysis of the cubic phase showed Si, Al, Ca and a small amount of Mg (Figure 3-11).

The chemical composition of the faujasite-type zeolite changed after 6 months of treatment. The microanalysis of the cubic phase now revealed the presence of Na, Al, Si and small concentrations of Ca and Mg (inset, Figure 3-12). Barrer et al. (1969) reported a higher thermodynamic affinity for Ca^{2+} than for Na^{+} in zeolite X. Thus, the formation of a zeolite initially high in Ca was not surprising. However, over time Ca^{2+} seems to have been exchanged for Na^{+} due to the high concentration of Na in the alkaline solution. For comparison, Figure 3-13 shows an identical faujasite-twin crystal from a quarry in Germany. The FESEM images of the sample treated for 6 months also revealed an additional phase, showing polysynthetic twinning which resulted in a star-shaped morphology (Figure 3-14). The microanalysis of this phase evidenced the presence Na, Si and Al. This result is consistent with XRD data, pointing to the formation of a sodalite-type zeolite with cubic symmetry. Deng et al. (2006) published a SEM image of sodalite with a similar morphology as the one synthesized in this study (Figure 3-15). Figure 3-16 shows the general aspect of the sample after 6-month-treatment, both, the faujasite- and sodalite-type zeolites can be observed.

After one year of treatment FESEM analyses did not show any additional phases. However, it seems that the ratio between the sodalite-type and the faujasite-type zeolite increased (Figure 3-17).

Further treatment of up to 6.1 years confirmed this tendency; the only zeolite observed was the sodalite-type (Figure 3-18). These results are consistent with XRD data. Note that the size of the sodalite-type zeolite crystals had increased significantly over time.

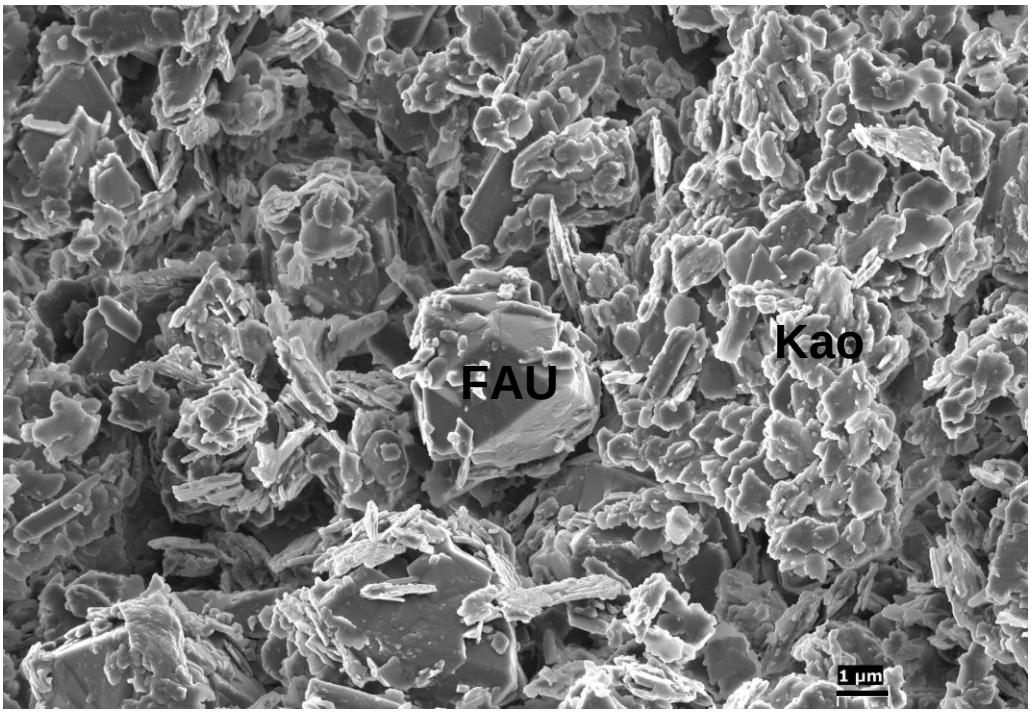

Figure 3-10. FESEM image of kaolinite treated with 5 M NaOH for 2 months. Unreacted kaolinite particles (Kao) and a newly formed, faujasite-type zeolite (FAU) can be observed.

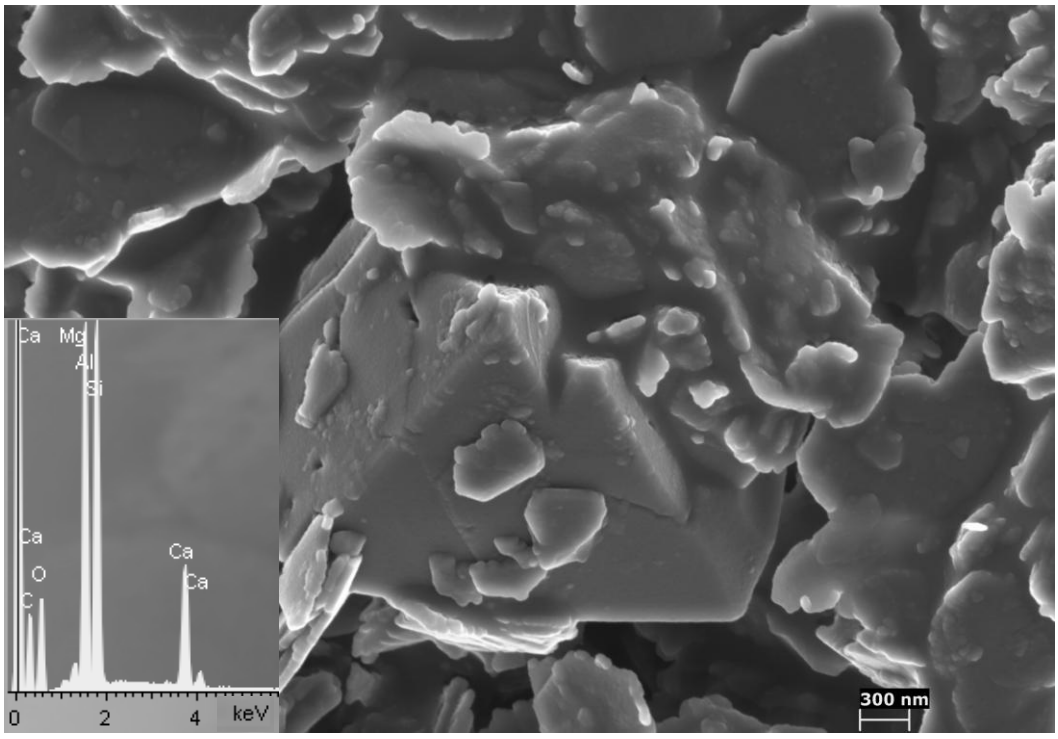

Figure 3-11. FESEM image showing a detail of the newly formed zeolite in kaolinite samples treated with 5 M NaOH for 2 months. The EDS spectrum (inset) confirms the formation of a Ca-zeolite, consistent with the chemistry of a faujasite-type zeolite.

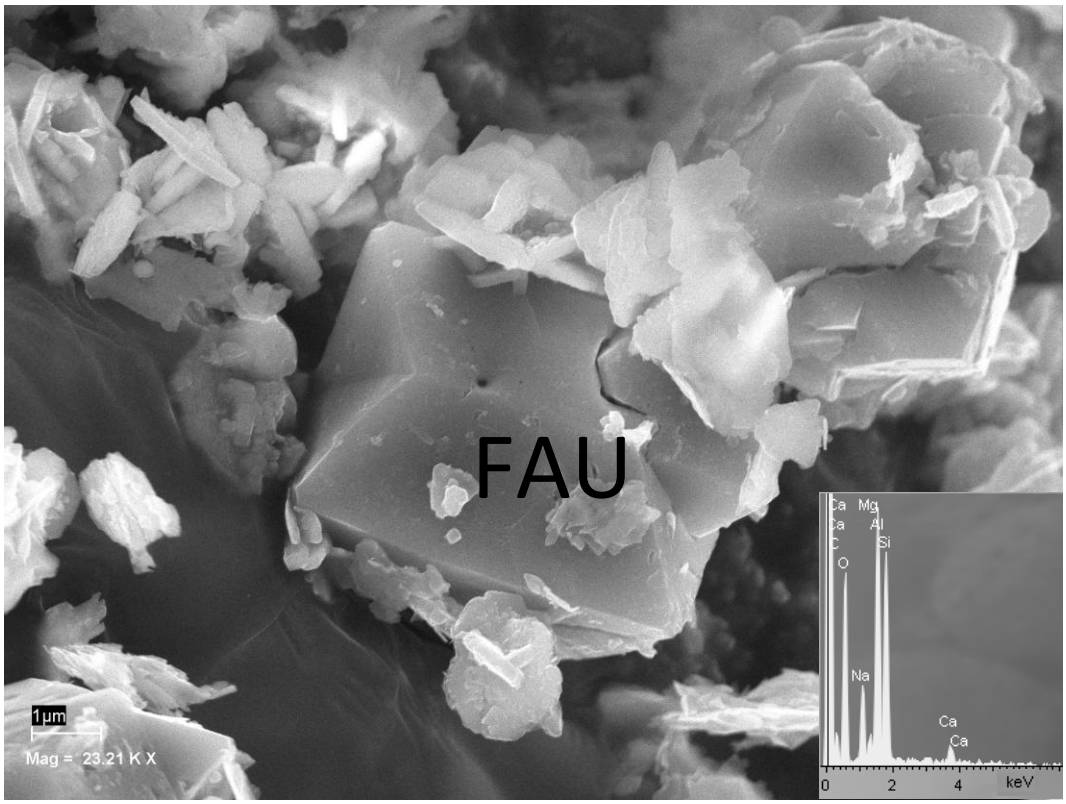

Figure 3-12. FESEM image of a newly formed, cubic phase (FAU, faujasite-type zeolite) in kaolinite samples treated with 5 M NaOH for 6 months. EDS spectrum in inset.

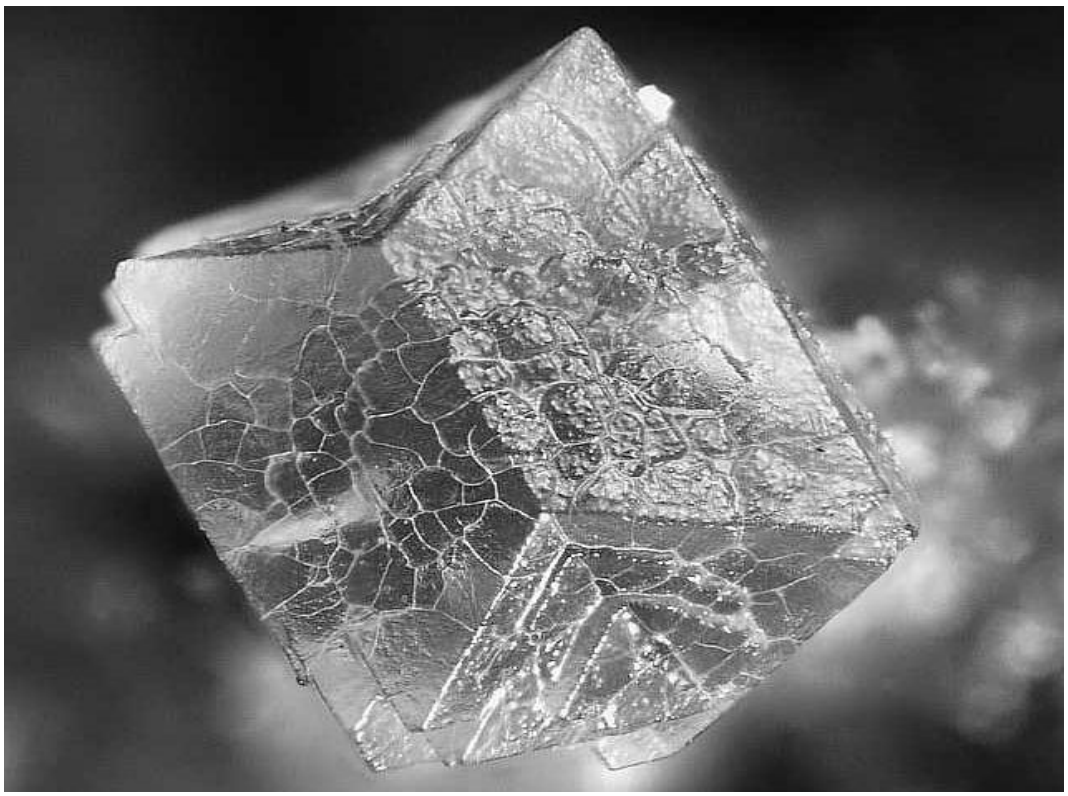

Figure 3-13.Faujasite-twin from Quarry I, Limberg near Sasbach, Kaiserstuhl, Baden, Germany. Field of view ca.1.5 mm, © Volker Betz (www.zeolite-collection.eu, accessed 21.9.12)

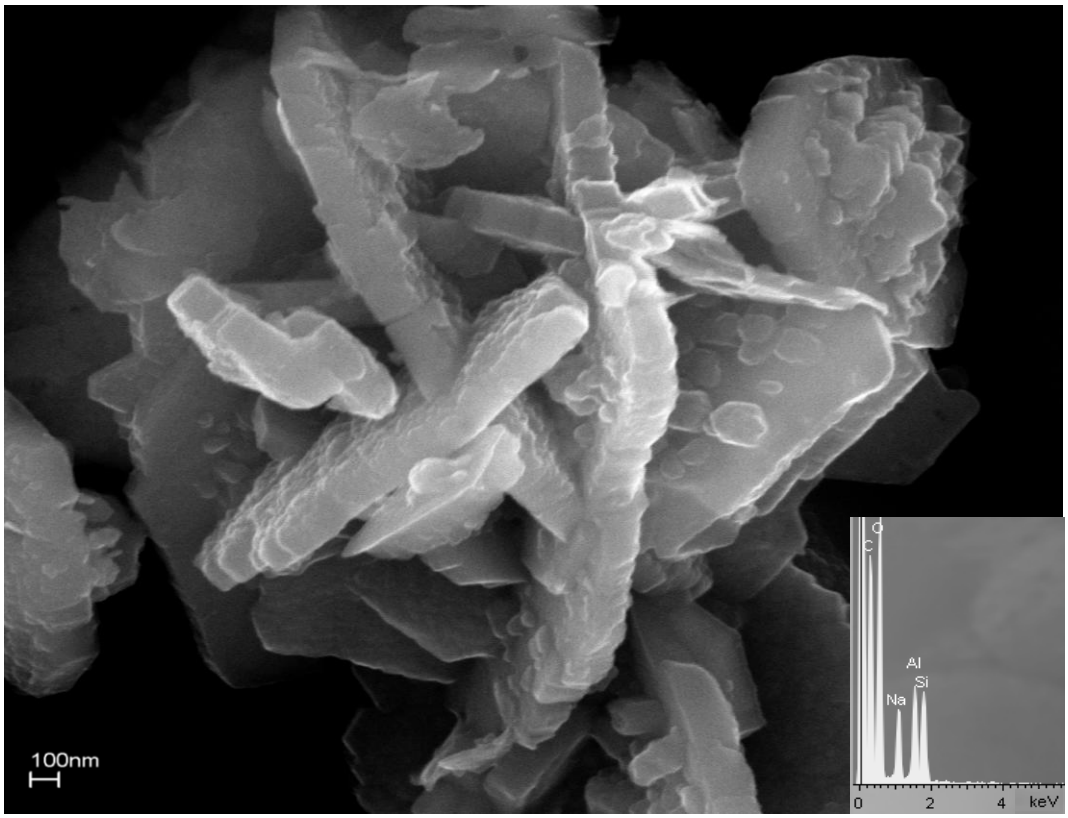

Figure 3-14. FESEM image of a newly formed phase in kaolinite samples treated with 5 M NaOH for 6 months. The EDS spectrum (inset) confirms the formation of a Na-zeolite, consistent with the composition of a sodalite-type zeolite.

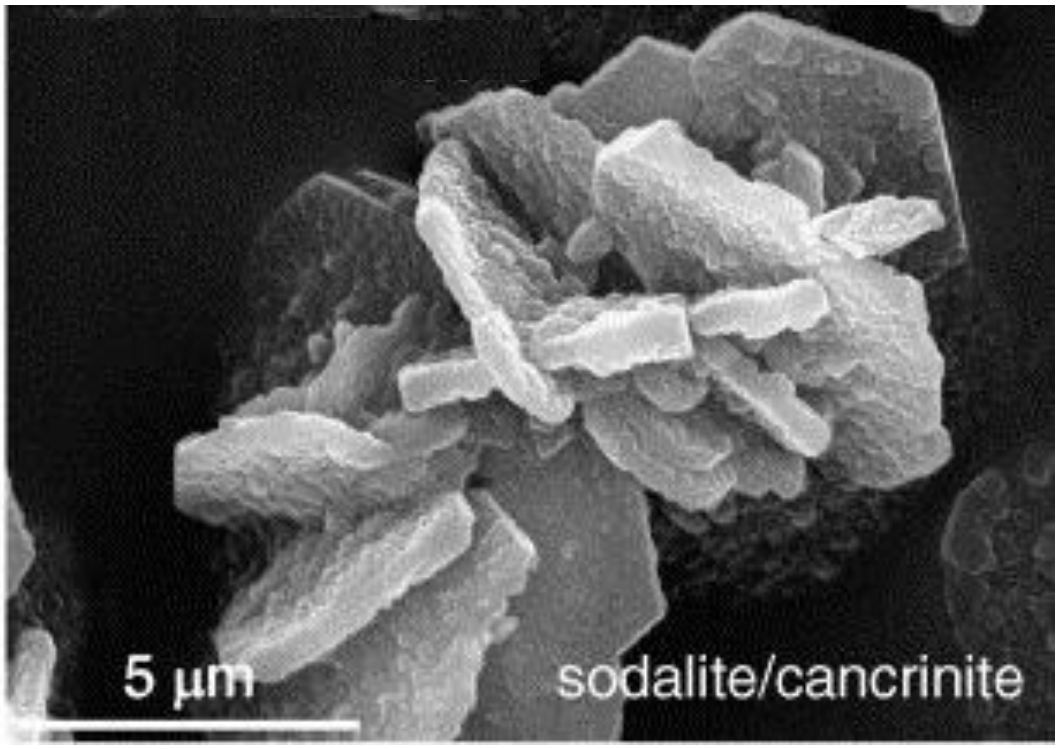

Figure 3-15. SEM image of sodalite/cancrinite synthesized from sodium silicate and aluminate treated with 1 M NaOH at 80 °C (Deng et al. 2006).

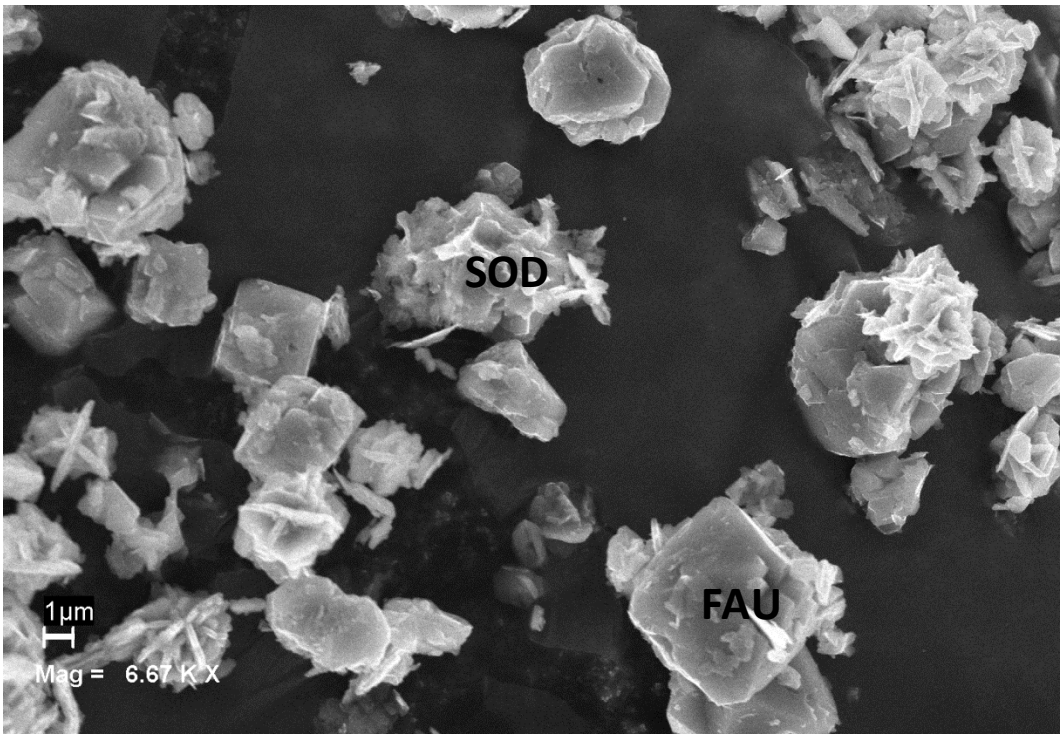

Figure 3-16. FESEM image of kaolinite treated with 5 M NaOH for 6 months. Sodalite- (SOD) and faujasite-type (FAU) zeolites can be observed.

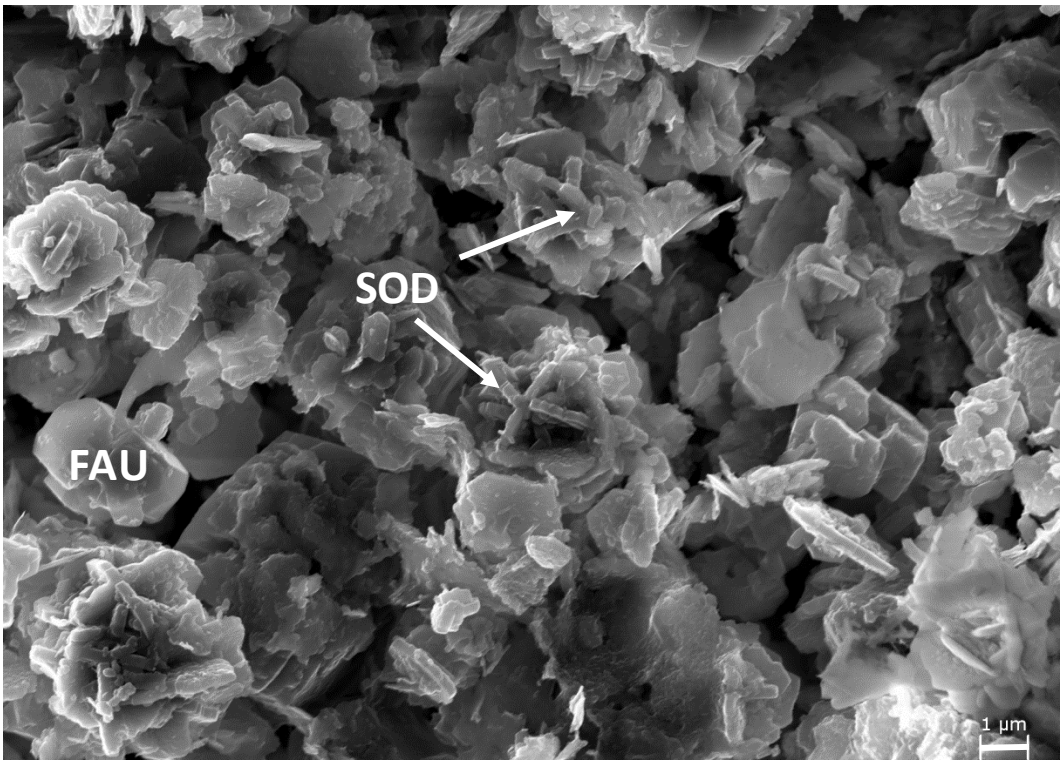

Figure 3-17. FESEM image of kaolinite treated with 5 M NaOH for 1 year. Sodalite- (SOD) and faujasite-type (FAU) zeolites can be observed.

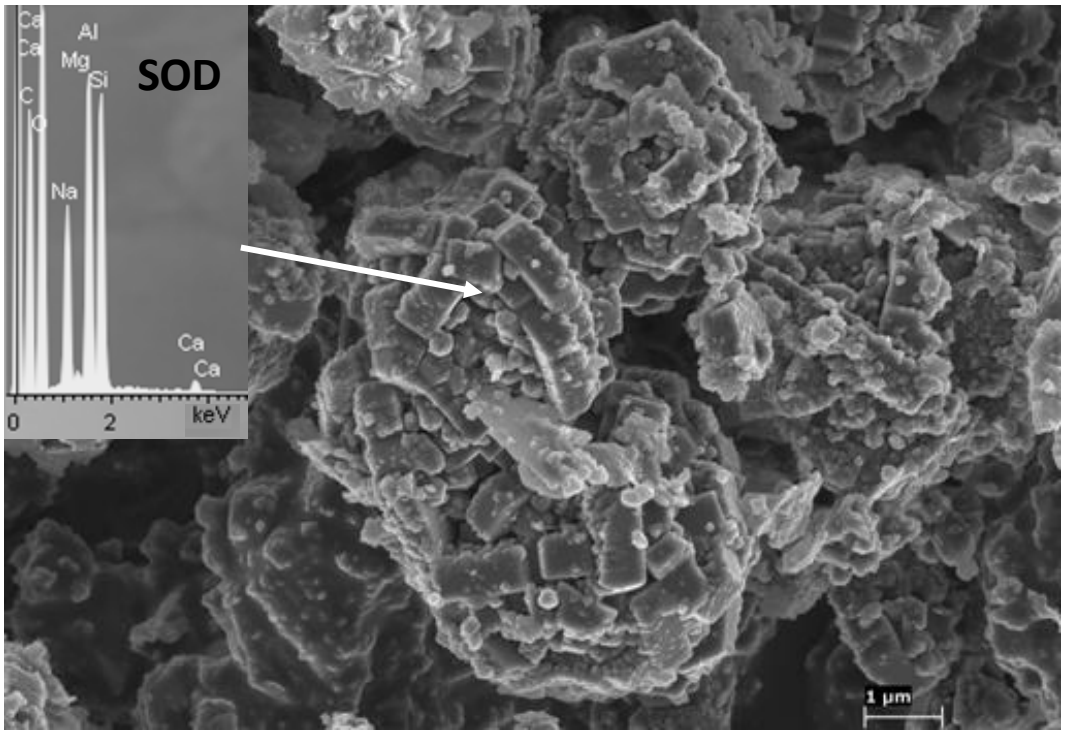

Figure 3-18. FESEM image of kaolinite treated with 5 M NaOH for 6.1 years. The faujasite-type zeolite seems to have disappeared, leaving only the sodalite-type zeolite (SOD). Note that the size of SOD crystals has increased significantly over time (EDS in inset).

3.1.2.3. TEM

The TEM image (Figure 3-19) shows that the amount of kaolinite/ halloysite seemed to have experienced a drastic reduction after alkaline treatment for 1 year with 5 M NaOH. This is in agreement with XRD data. The image further confirms the presence of newly formed phases, possibly sodalite-type and faujasite-type zeolites. Figure 3-20 shows a phase which might be compatible with a faujasite-twin crystal previously detected with FESEM. TEM-AEM analysis results (inset, Figure 3-20) revealed the presence of Si, Al, Ca and small amounts of Na and Mg. Furthermore, a nearly amorphous phase was detected with a comparatively high Na concentration after 1 year of treatment (insets, Figure 3-21). It is speculated that this phase contains rests of poorly crystalline kaolinite and halloysite together with a zeolitic precursor.

Figure 3-22 shows a sodalite-type zeolite together with an aggregate of nanosized crystals after 6.1 years of treatment. The nanosized crystals were rich in Si, Al and Mg. The chemical composition (Table 3-3) is close to a chlorite-type mineral, however, very poor in Fe and with an octahedral cation deficit (Newman and Brown, 1987). Mg was most likely released upon smectite dissolution. Note that smectite was present as impurity in the original clay.

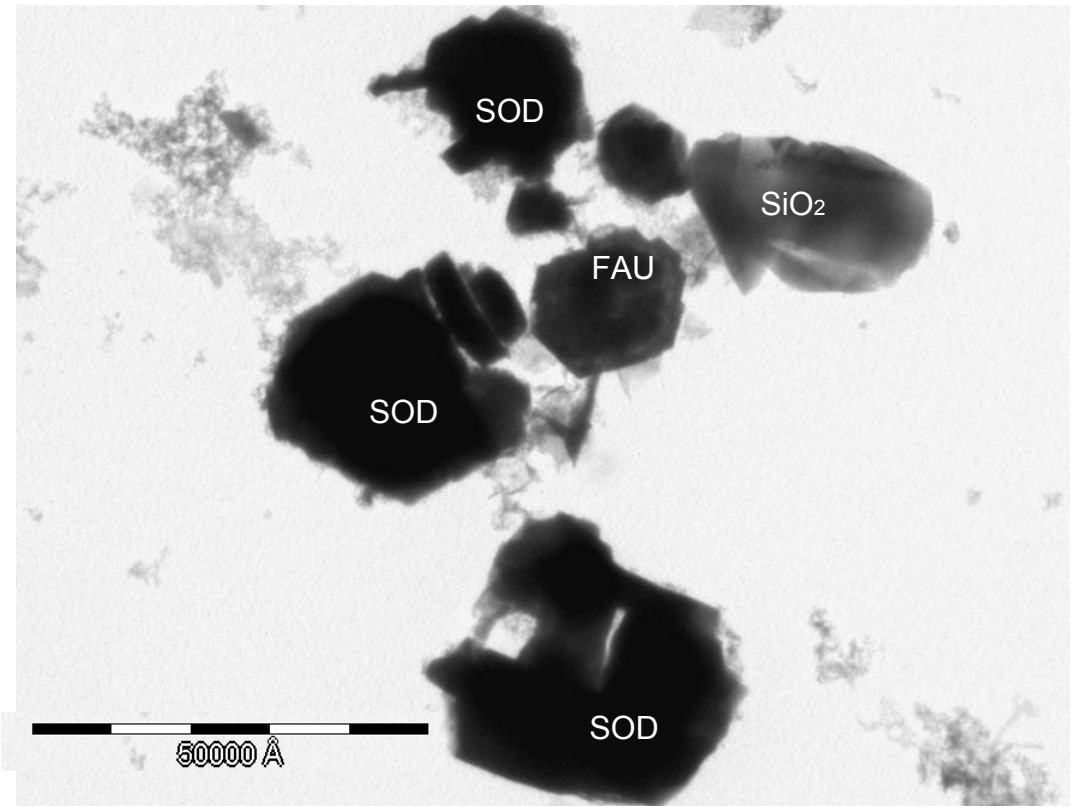

Figure 3-19. TEM image. General aspect of newly formed phases in kaolinite treated with 5 M NaOH for 1 year. SOD = sodalite, FAU= faujasite.

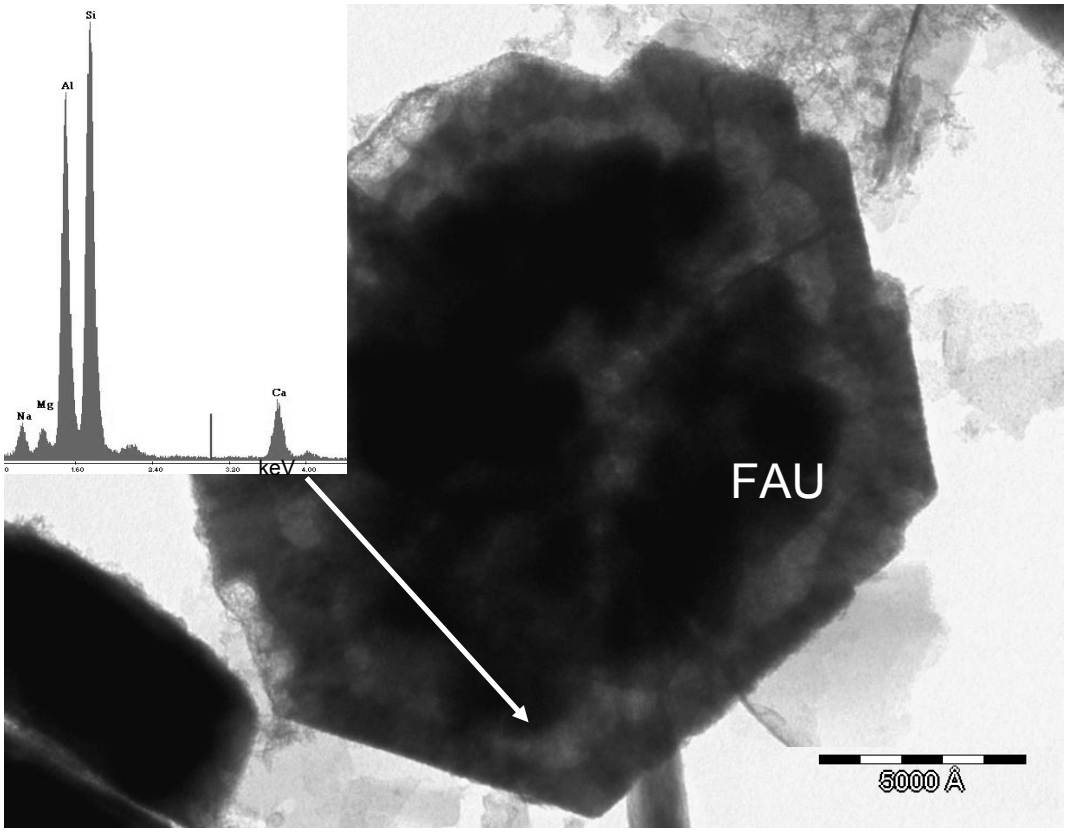

Figure 3-20. TEM image of a newly formed phase, possibly a faujasite-twin crystal, in kaolinite treated with 5 M NaOH for 1 year. The inset shows the TEM-AEM spectrum. FAU = faujasite.

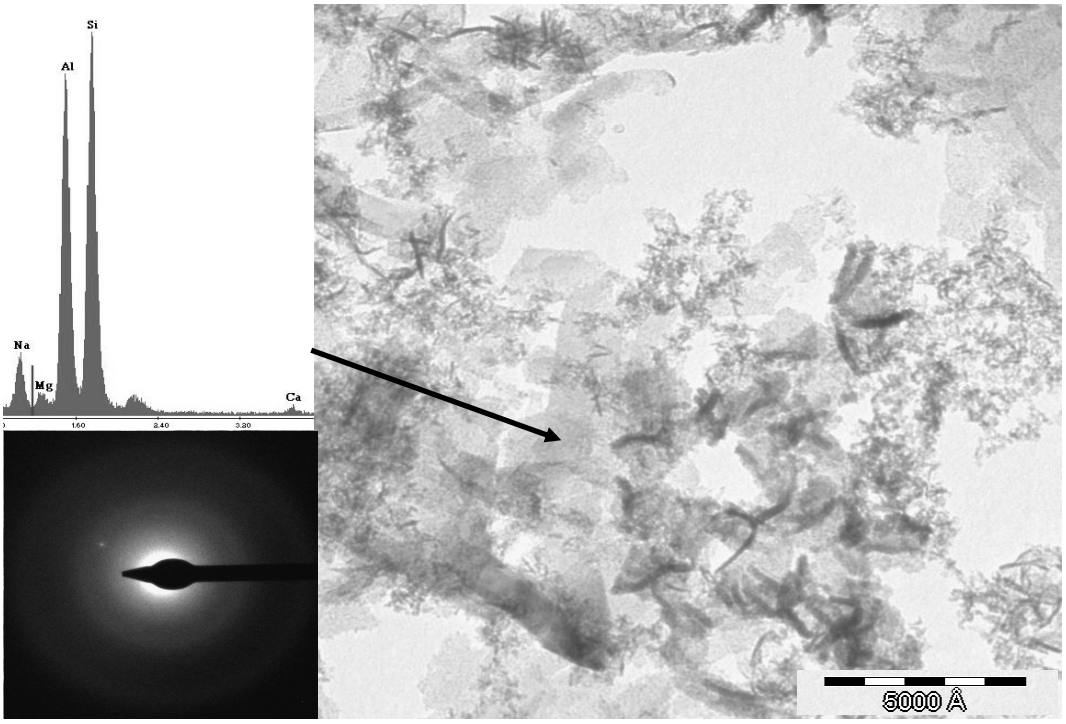

Figure 3-21. TEM image of newly formed amorphous phase in kaolinite treated with 5 M NaOH for 1 year. The SAED pattern reveals the nearly amorphous character of this phase, and the TEM-AEM spectrum shows the presence of Si, Al, Na and minor amounts of Mg and Ca (insets).

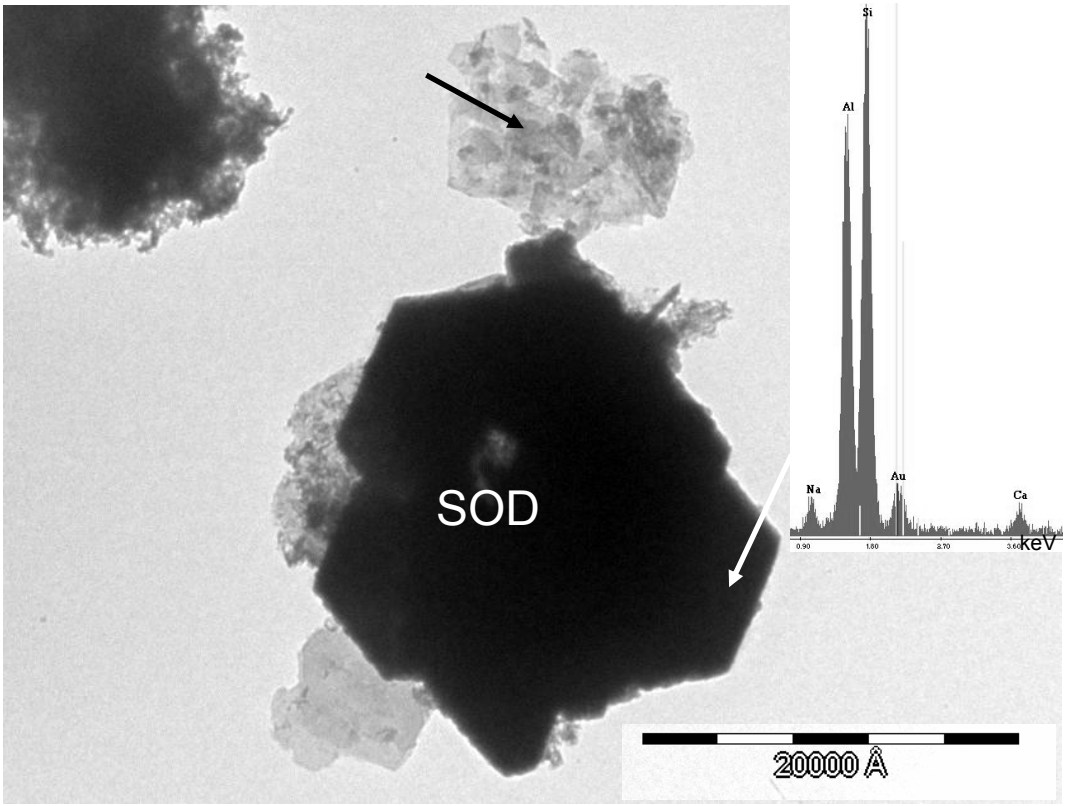

Figure 3-22. TEM image of the kaolinite sample treated with 5 M NaOH for 6.1 years. A sodalite-type zeolite (SOD, EDS in inset) and an aggregate of nanosized crystals (arrow) can be observed (see Table 3-3).

Table 3-3. Structural formulae of newly formed phase (Figure 3-22, arrow) in kaolinite treated with 5 M NaOH for 6.1 years.

Structural formulae of nano-size crystals based on $O_{10}(OH)_8$										
Analysis	Si	^{IV}Al	^{VI}Al	Mg	Fe	Σoct.cat.[1]	K	Ca	Na	Σint.cha.[2]
1	2.86	1.14	2.12	3.19	0.08	5.39	0.00	0.00	0.24	0.24
2	3.24	0.76	2.09	2.72	0.25	5.06	0.22	0.12	0.00	0.46

[1] Sum of octahedral cations

[2] Sum of interlayer charge

3.1.2.4. Nitrogen sorption

The surface area of kaolinite activated with 5 M NaOH experienced a drastic increase (Table 3-4) after 6-month treatment. This increase coincided with the formation of faujasite- and sodalite-type zeolites, as evidenced by XRD and FESEM. After 1-year treatment the surface area further increased. The increase in surface area is assumed to be due to the presence of faujasite. Sutarno and Arryanto (2007) reported a BET surface area of around 400 m^2/g for faujasite synthesized using fly ash and NaOH. According to Novembre et al. (2004) the specific surface area of synthesized zeolite Na-X (synthetic analogue of faujasite) obtained by the BET method was 339 m^2/g. The sodalite-type zeolite, however, did not contribute to the surface area increase because the BET surface area of sodalite is only 22.8 m^2/g (Li et al. 2007). These results are in agreement with the findings of this study, showing a drastic decrease in surface area after prolonged alkaline activation for 6.1 years. At this point XRD and FESEM data revealed that the faujasite-type zeolite had disappeared and the sodalite-type zeolite was now the dominant phase.

The shape of the nitrogen sorption isotherm (type II) and the hysteresis loop (type H3) of kaolinite did not experience any significant changes upon alkaline activation using 5 M NaOH (Figure 3-23).

Table 3-4. BET surface area of untreated kaolinite and kaolinite treated with 5 M NaOH

Treatment time	Surface area (m^2/g)
0	23.79 ± 0.09
6 months	273.33 ± 6.70
1 year	320.92 ± 8.50
6.1 years	16.77 ± 0.14

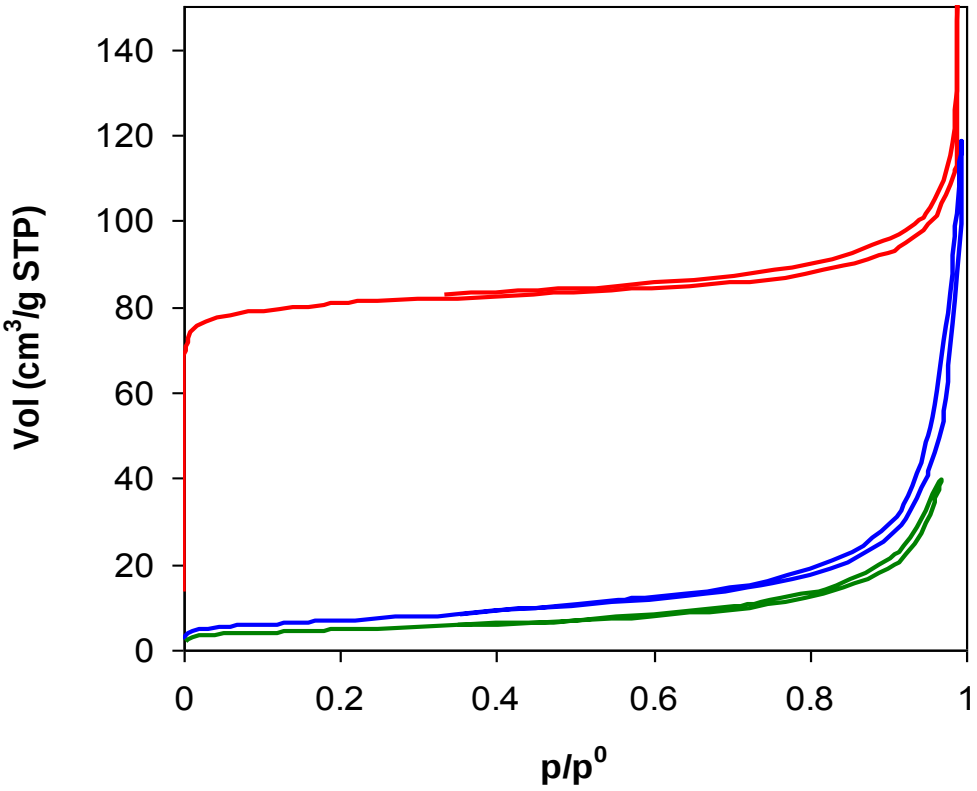

Figure 3-23. Nitrogen sorption isotherms of untreated kaolinite (blue), treated with NaOH for 6 months (red) and 6.1 years (green).

3.1.3. Kaolinite treated with KOH

3.1.3.1. XRD

XRD analyses demonstrate that a new zeolitic phase appeared after 2-month treatment with KOH. The low intensity Bragg peaks coincide with those of zeolite K-I (sometimes denominated zeolite H) which was synthesized by Barrer et al. (1968) using kaolinite and 1.8-4.0 M KOH at T < 100 °C. This phase has the following formula: $KAlSiO_4 \cdot 2H_2O$ (JPDF card no.220793, see Figure 3-24, red line pattern). Bauer et al. (1998) have also detected zeolite K-I as one of the reaction products in the case of kaolinite treated with 2 M KOH at 80 °C after 1 month treatment.

After 6-month treatment the above mentioned zeolitic phase was clearly identified due to an increase in the Bragg peaks intensities. However, a second zeolitic phase appeared which could not be identified unambiguously. Some of the Bragg peaks of this second phase matched those of K-chabazite (zeolite G, $K_2Al_2SiO_6 \cdot H_2O$, JPDF card no. 120194, blue line pattern). Barrer et al. (1968) also reported the formation of a near-chabazite phase (zeolite K-G). The researchers stated that the near-chabazite phase consistently formed with zeolite K-I as the main product upon synthesis using kaolinite and KOH.

The hump between 25° and 35° 2θ in the XRD pattern of the sample treated for 6 month is often associated with structurally disordered compounds and might suggest the formation of an amorphous aluminosilcate gel, for example a zeolitic precursor (Fernandez-Jimenez et al. 2008). However, in our case we can not rule out that the hump could be related to the thinness of the clay sample giving rise to the contribution of the amorphous glass sample holder to X-ray scattering.

After 1-year treatment a small amount of kaolinite remained. However, the intensity of the Bragg peak at 7.19 Å as well as at 3.59 Å diminished significantly. At this point, the chabazite-type zeolite could be identified unambiguously.

After 4.7 years kaolinite was no longer detectable and the Bragg peak intensities of the zeolite K-I and the chabazite-type zeolite increased.

Further treatment for a total of 6.1 years resulted in the reduction of the Bragg peak intensities of K-I zeolite (red line pattern), indicating the metastable character of this phase (Barrer 1982). Additionally, a third zeolitic phase was detected (Figure 3-25). The new phase corresponded to edingtonite-type zeolite K-F with a tetragonal symmetry and the following formula: $KAlSiO_4 \cdot 1.5H_2O$ (JPDF card no. 380216). Zeolite K-F (Barrer et al. 1968, Barrer and Mainwaring 1972, Belver et al. 2002) and zeolite G (chabazite-type zeolite, Breck 1974) have been previously reported to form together with zeolite K-I from kaolinite or metakaolinite treated with KOH.

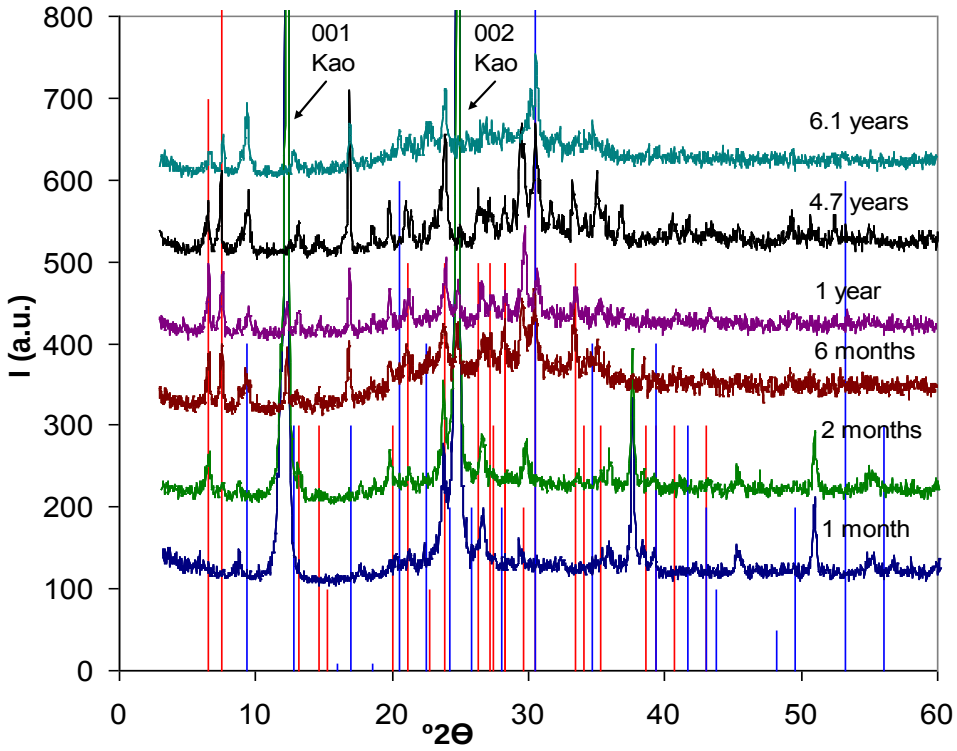

Figure 3-24. Mineralogical evolution of kaolinite treated with KOH for different periods of time. Red line pattern: K-I zeolite (JPDF card no. 220793); Blue line pattern: K-chabazite (JPDF card no. 120194). Kao = kaolinite

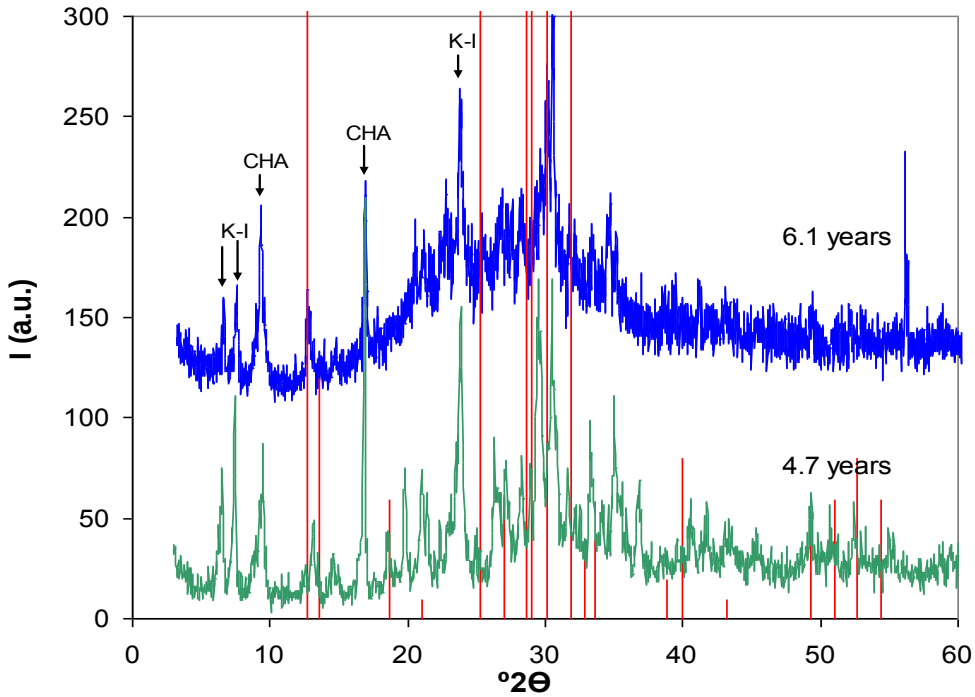

Figure 3-25. XRD patterns of kaolinite treated with KOH for 4.7 and 6.1 years. Red line pattern: Zeolite K-F (JPDF card no. 380216). K-I = zeolite K-I, CHA = chabazite.

3.1.3.2. FESEM

According to Barrer et al. (1968) zeolite K-I, i.e., the phase previously identified with XRD, crystallizes rapidly as very small hexagonal plates. After 2 months of treatment with 5 M KOH, the formation of an aggregate of nanocrystals was observed (Figure 3-26) which might correspond to zeolite K-I. EDS microanalysis showed the presence of K and Ca in addition to Si and Al (inset, Figure 3-26).

After 6 months of treatment, a lens-shaped chabazite-type zeolite with ~ 2 μm diameter was detected together with the aggregate previously described (Figure 3-27). The rhombohedral crystals of the chabazite-type zeolite showed penetration-twinning. Fernandez et al. (2010) published a SEM image (Figure 3-28) of similar chabazite crystals showing polysynthetic twinning.

Figure 3-29 shows the textural features of the sample after 1 year of treatment. EDS microanalysis showed the presence of Si, Al and Ca and a high concentration of K in the case of the chabazite-type zeolite. This composition differs from the zeolitic phase identifed with XRD where Ca is absent. However, chabazite with varying cations exists and an at least partial replacement of K for Ca is possible since the ionic radius of Ca (1.18 Å) is smaller than the one of K (1.33 Å).

Over time the amount of the chabazite-type zeolite increased at the expense of the aggregate of nanocrystals (Figure 3-30).

After 6.1 year-treatment the chabazite-type zeolite was the dominant phase. Additionally, prismatic crystals were observed (Figure 3-31 and 3-32) which are assumed to correspond to zeolite K-F, previously detected in the same sample with XRD. EDS microanalysis of the prismatic crystals revealed the presence of Si, Al and K which is in agreement with the composition of this zeolitic phase. It seems that zeolite K-F formed at the expense of the aggregate of nanocrystals, because its amount was further reduced.

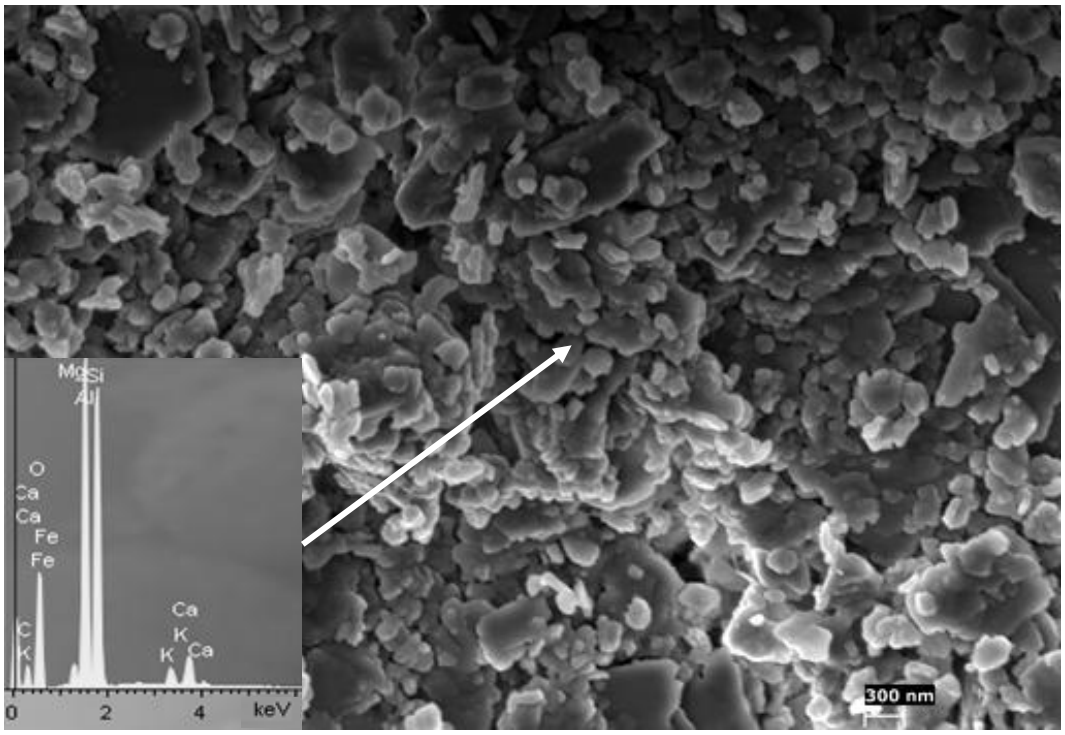

Figure 3-26. FESEM image of an aggregate of nanocrystals, possibly zeolite K-I, formed in kaolinite treated with 5 M KOH for 2 months (EDS in inset).

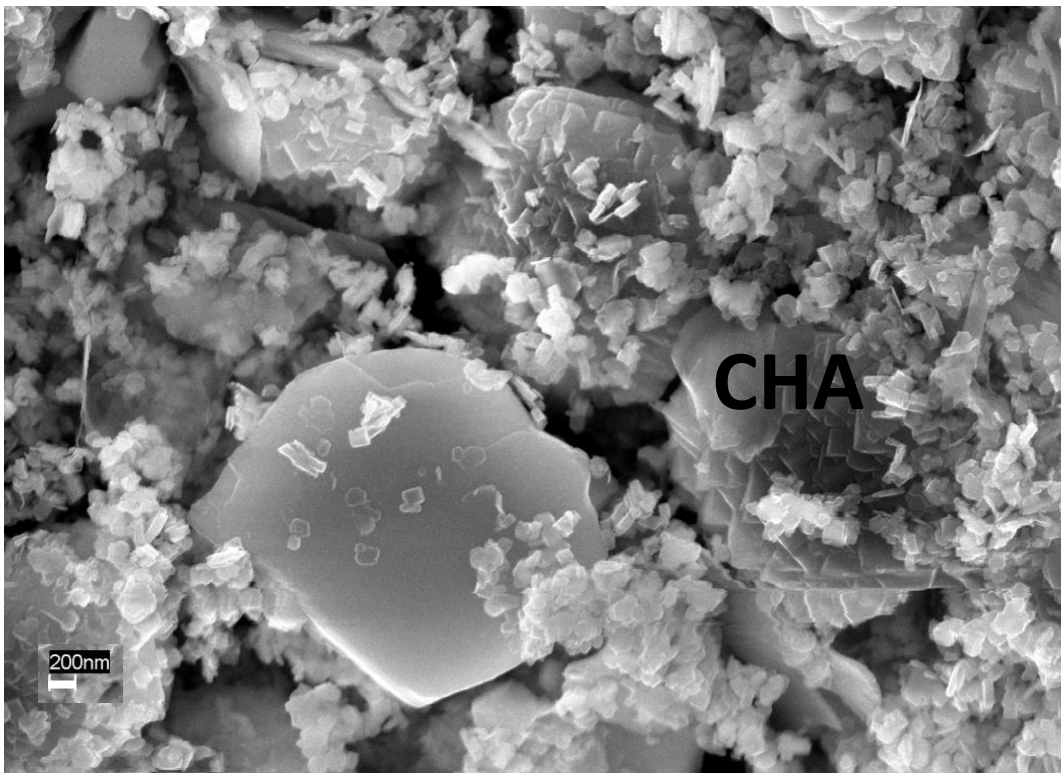

Figure 3-27. FESEM image, general view of kaolinite treated with 5 M KOH for 6 months, showing newly formed chabazite-type zeolites (CHA) in addition to the nanosized crystals.

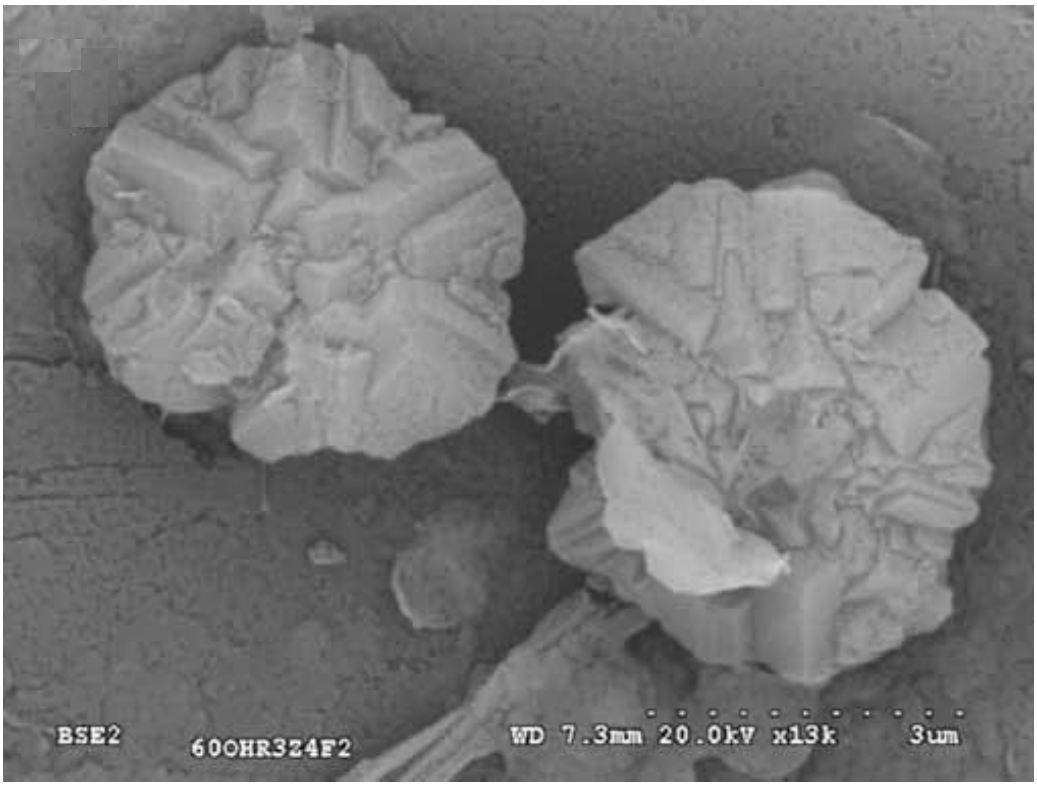

Figure 3-28. Example of polysynthetic twinning in chabazite (Fernández et al. 2010).

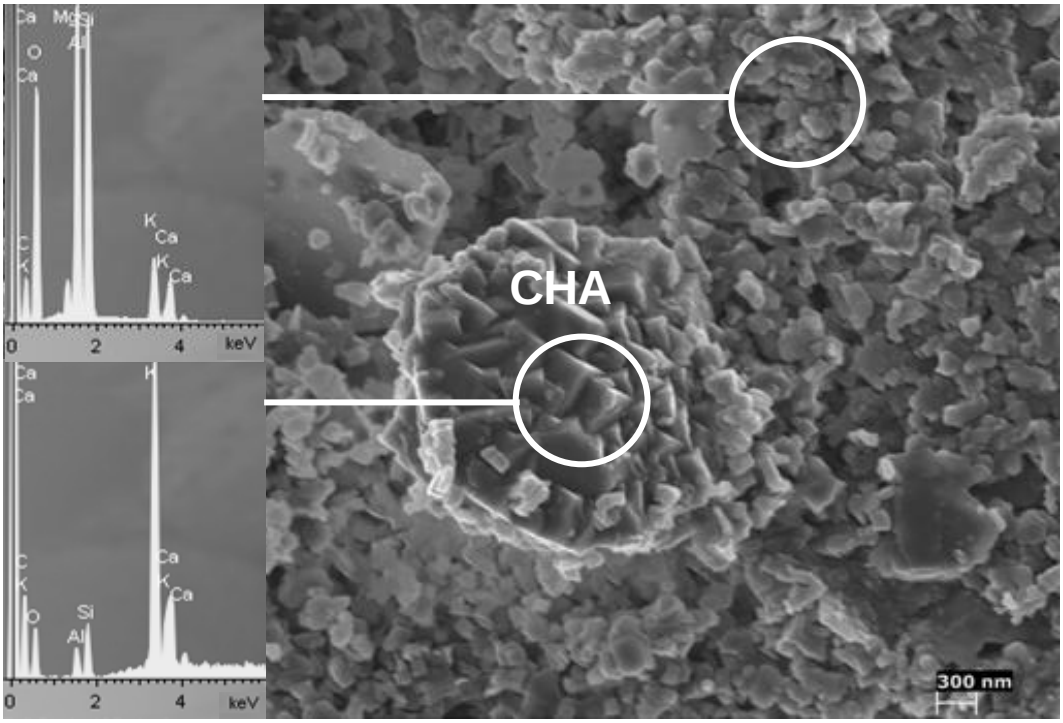

Figure 3-29. FESEM image of chabazite-type zeolite (CHA, EDS in inset) as well as an aggregate of nanocrystals (EDS in inset) in kaolinite treated with 5 M KOH for 1 year. Similar crystals have already been detected in the sample treated for 2 months.

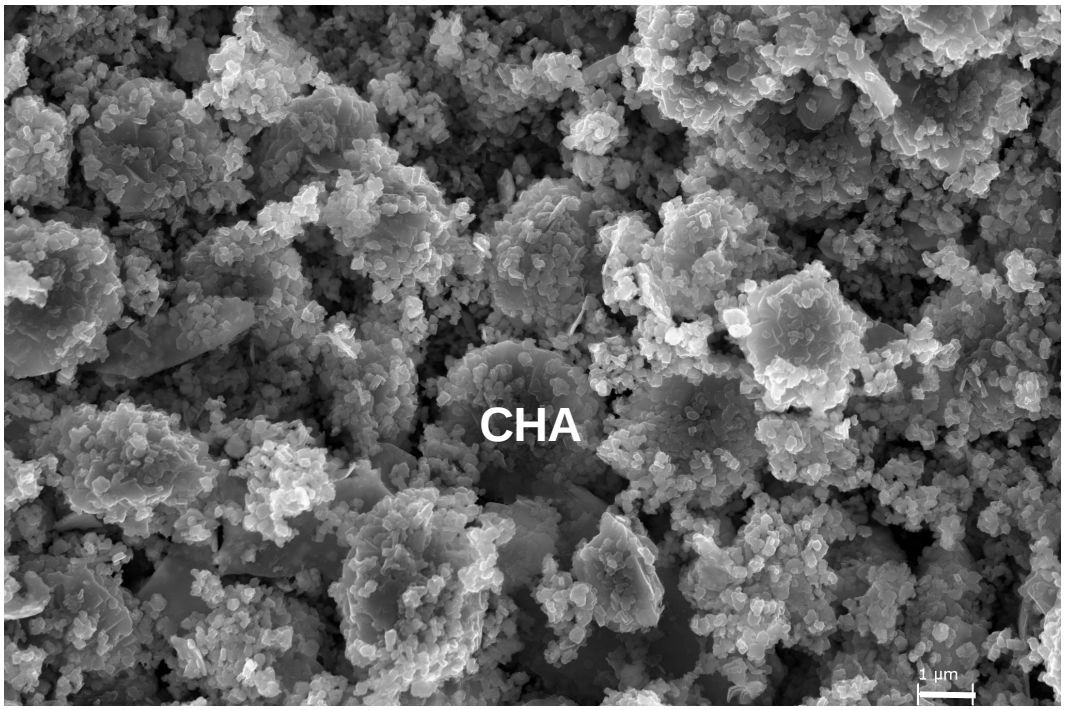

Figure 3-30. FESEM image of a kaolinite sample treated with 5 M KOH for 4.7 years. A large amount of chabazite-type zeolite (CHA) can be observed which seems to have crystallized at the expense of the nanocrystals.

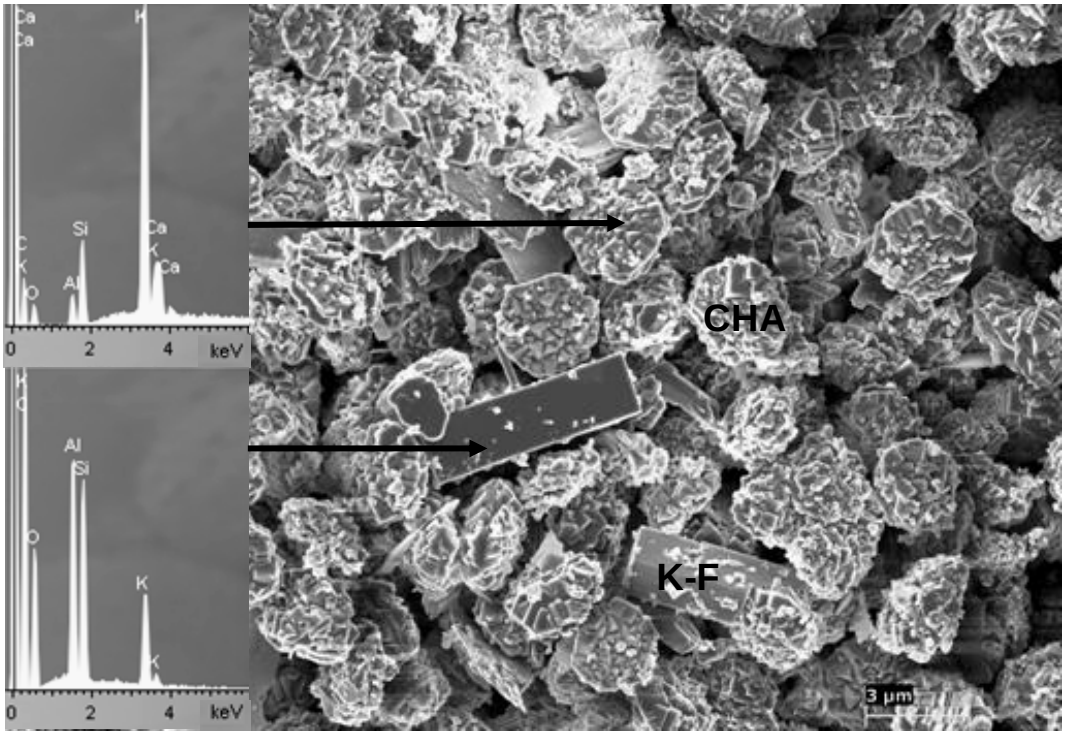

Figure 3-31. FESEM image of a kaolinite sample treated with 5 M KOH for 6.1 years. The chabazite-type zeolite (CHA, EDS in inset) is the dominant phase. A new prismatic phase (zeolite K-F, EDS in inset) appeared and the amount of nanocrystals decreased further.

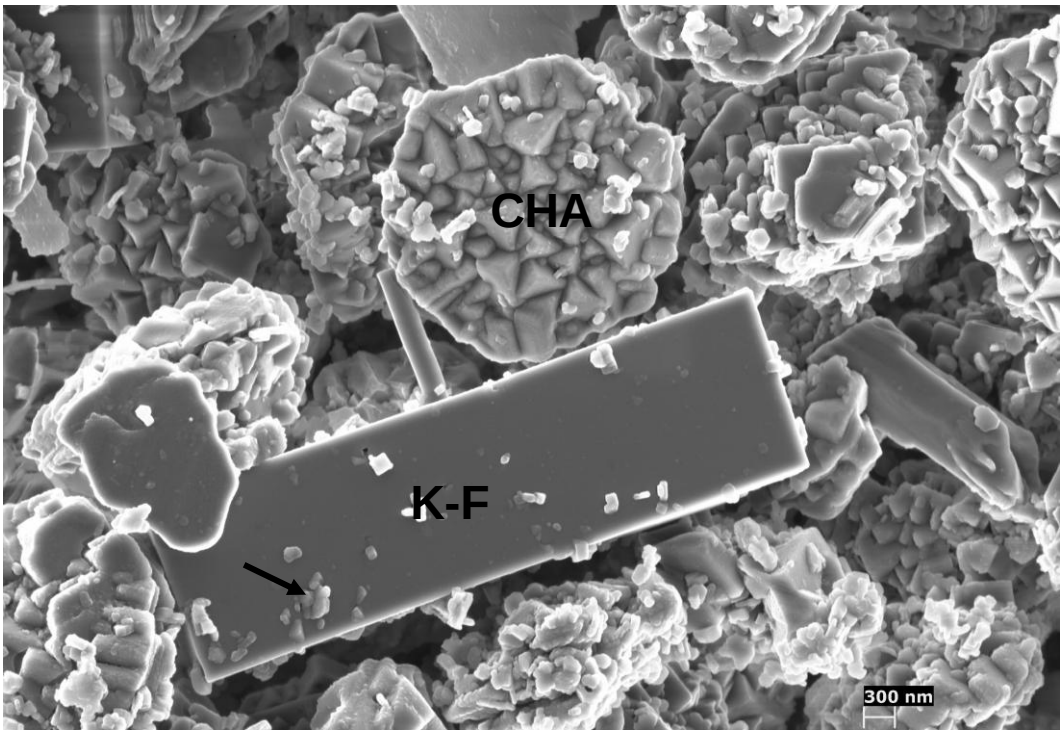

Figure 3-32. Detail of Figure 3-31. Apart from a chabazite-type zeolite (CHA) and a prismatic-shaped zeolite K-F, some nanosized particles (arrow) can still be observed in the sample.

3.1.3.3. TEM

TEM analysis of the kaolinite sample treated with 5 M KOH for 6 months revealed the presence of a chabazite-type zeolite and an aggregate of small, mainly hexagonal crystals (Figure 3-33). Halloysite was no longer detected. Structural formulae for the chabazite-type zeolite were calculated from TEM-AEM analyses but are not included here because they differed significantly from the formula of the chabazite identified with XRD which is $K_2Al_2SiO_6{\cdot}H_2O$. The inset in Figure 3-33 shows the qualitative composition of this phase. It contained Si, Al, K and Ca together with a trace amount of Mg. Fortunately, the SAED image (inset, Figure 3-33) allowed the unambiguous identification of the chabazite.

The small hexagonal crystals observed in the sample treated for 1 year might be mistaken for kaolinite. However, these crystals seemed thicker than the original kaolinite crystals, and were of quite homogeneous size around 100 nm. As previously mentioned, zeolite K-I crystallizes as small hexagonal plates (Barrer 1968). Evidence for the presence of zeolite K-I is given by the fact that kaolinite Bragg peaks experienced a significant intensity reduction in the XRD pattern of the sample treated for 1 year, whereas TEM (Figure 3-34) as well as FESEM (Figure 3-29) observations revealed the dominance of hexagonal nanocrystals in the kaolinite sample treated for 1 year. Thus, these

nanocrystals must correspond to the hexagonal crystals of zeolite K-I, unambiguously identified with XRD after 6 months of treatment.

The average structural formulae for the hexagonal crystals were calculated based on O_7 (Table 3-5) in order to facilitate comparison with the original kaolinite. It can be observed that the Si and the cation concentrations increased if compared to the original clay sample. Nevertheless, the K concentration was much lower than in the zeolite K-I identified using XRD which is $KAlSiO_4 \cdot 2H_2O$. TEM-SAED patterns (inset, Figure 3-34) did not contribute to an unambiguous identification of zeolite K-I either.

After 6.1 years of treatment, a larger number of zeolite K-F crystals was observed using TEM (Figure 3-35). Zeolite K-F seemed to have formed at the expense of zeolite K-I. A significant amount of the chabazite-type zeolite could still be observed at this point.

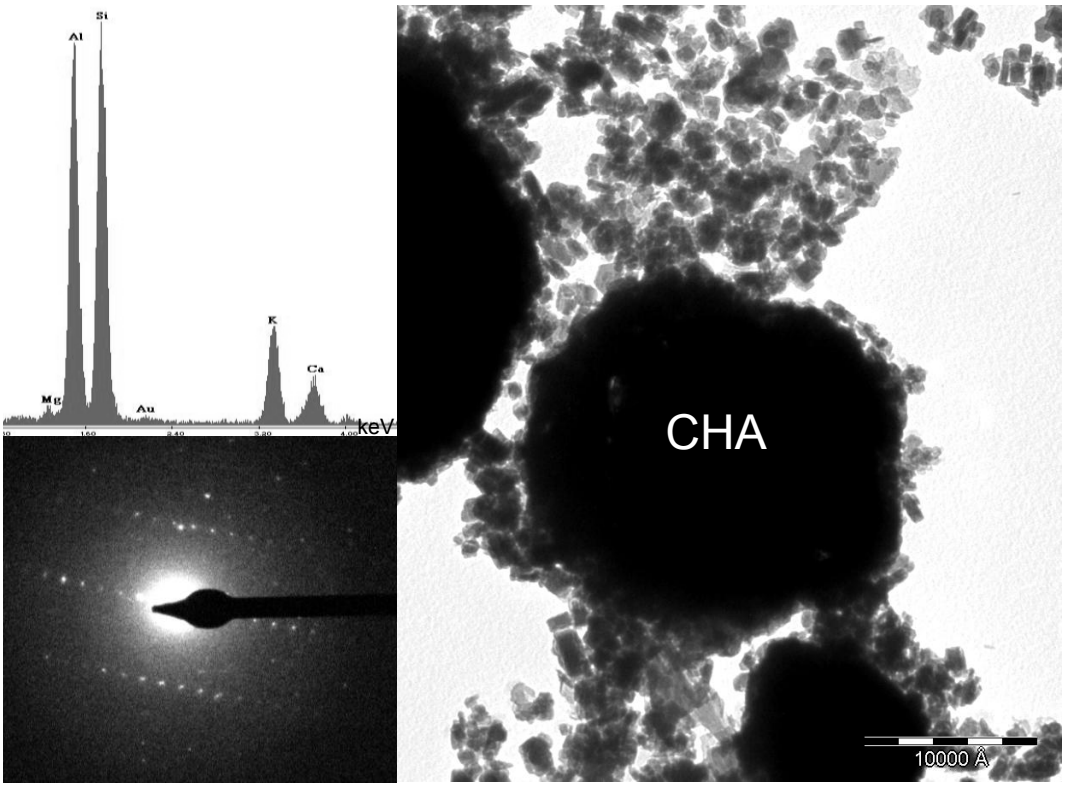

Figure 3-33. TEM image of kaolinite treated with 5 M KOH for 6 months. Besides the chabazite-type zeolite (CHA), an aggregate of small hexagonal crystals can be observed. Insets show TEM-AEM spectrum, and SAED along the [010] zone axis of the chabazite-type zeolite.

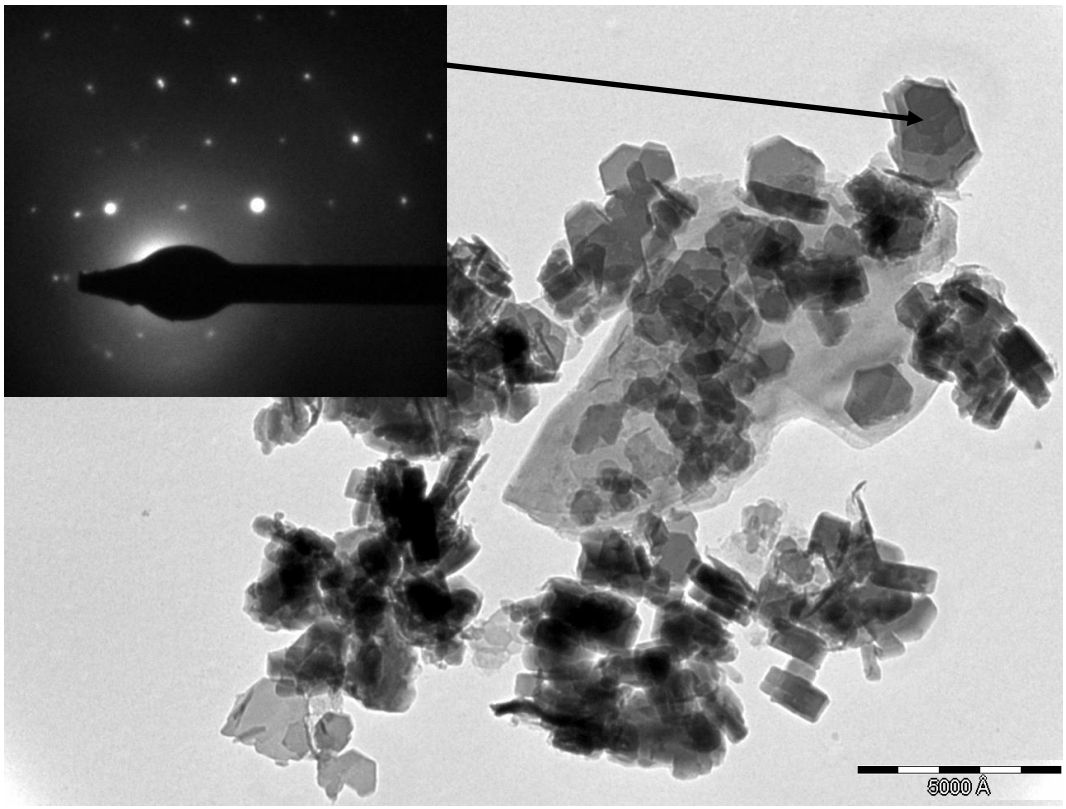

Figure 3-34. TEM image and SAED patterns of hexagonal crystals in kaolinite treated with 5 M KOH for 1 year. Inset shows SAED pattern of the hexagonal zeolite along the [00l] zone. TEM-AEM analyses of this phase are presented in Table 3-5.

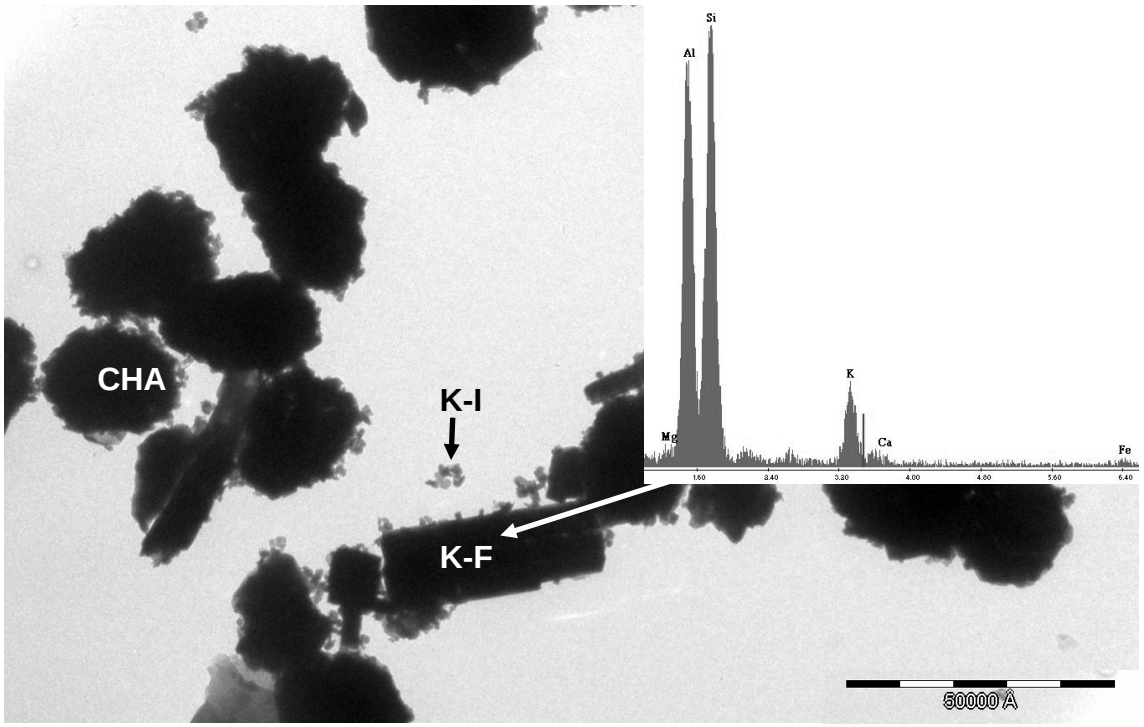

Figure 3-35. TEM image of kaolinite treated with 5 M KOH for 6.1 years. General aspect, showing zeolite K-F, K-I and a chabazite-type zeolite (CHA). The inset shows the EDS spectrum of zeolite K-F.

Table 3-5. Structural formulae of kaolinite and newly formed hexagonal crystals in kaolinite treated with 5 M KOH for 6 months and 1 year.

Structural formulae of kaolinite based on $O_5(OH)_2$							
Sample	Si	Al	Fe	Mg	K	Ca	Na
Untreated	2.07	1.94	0.01	0.00	0.00	0.00	*
average	±0.05	±0.03	±0.01				
Structural formulae of hexagonal crystals based on O_7							
1	1.89	1.75	0.03	0.19	0.46	0.15	*
2	1.96	1.76	0.02	0.15	0.36	0.06	*
3	2.01	1.80	0.01	0.10	0.21	0.07	*
4	2.06	1.72	0.04	0.09	0.20	0.05	*
6 months	1.98	1.76	0.03	0.13	0.31	0.08	*
average	±0.07	±0.03	±0.01	±0.05	±0.13	±0.05	
5	1.79	1.86	0.06	0.26	0.12	0.23	0.05
6	1.82	1.89	0.03	0.18	0.12	0.25	0
7	1.98	1.77	0.01	0.11	0.14	0.20	0
8	2.05	1.68	0.01	0.16	0.13	0.13	0.02
9	2.27	1.41	0.01	0.12	0.16	0.14	0
10	2.28	1.40	0.02	0.11	0.15	0.14	0
1 year	2.03	1.67	0.02	0.16	0.14	0.18	0.01
average	±0.21	±0.22	±0.02	±0.06	±0.02	±0.05	±0.02

* not analyzed

3.1.3.4. Nitrogen sorption

The surface area of kaolinite activated with 5 M KOH experienced a significant increase (Table 3-6) after 2-month treatment which coincided with the formation of nanosized crystals identified as zeolite K-I using XRD and TEM analysis. However, further treatment resulted in a reduction in surface area when a chabazite-type zeolite was detected which seemed to have formed at the expense of zeolite K-I after 6 months. Data by Ridha (2009) are in agreement with these findings showing a relatively low BET surface area of K-chabazite (17.82 m^2/g). Note that the surface area for K-chabazite reported by Ridha (2009) is not that different from the one observed here for the chabazite-dominated sample after 6.1 years of treatment (Table 3-6). The formation of zeolite K-F after 6.1 years did not seem to have influenced the surface area significantly.

The shape of the nitrogen sorption isotherm (type II) and the hysteresis loop (type H3) of kaolinite did not experience any significant changes upon alkaline activation using 5 M KOH (Figure 3-36).

Table 3-6. BET surface area of untreated kaolinite and kaolinite treated with 5 M KOH

Treatment time	Surface area (m^2/g)
0	23.79 ± 0.09
2 months	46.14 ± 0.17
6 months	25.43 ± 0.09
6.1 years	25.15 ± 0.13

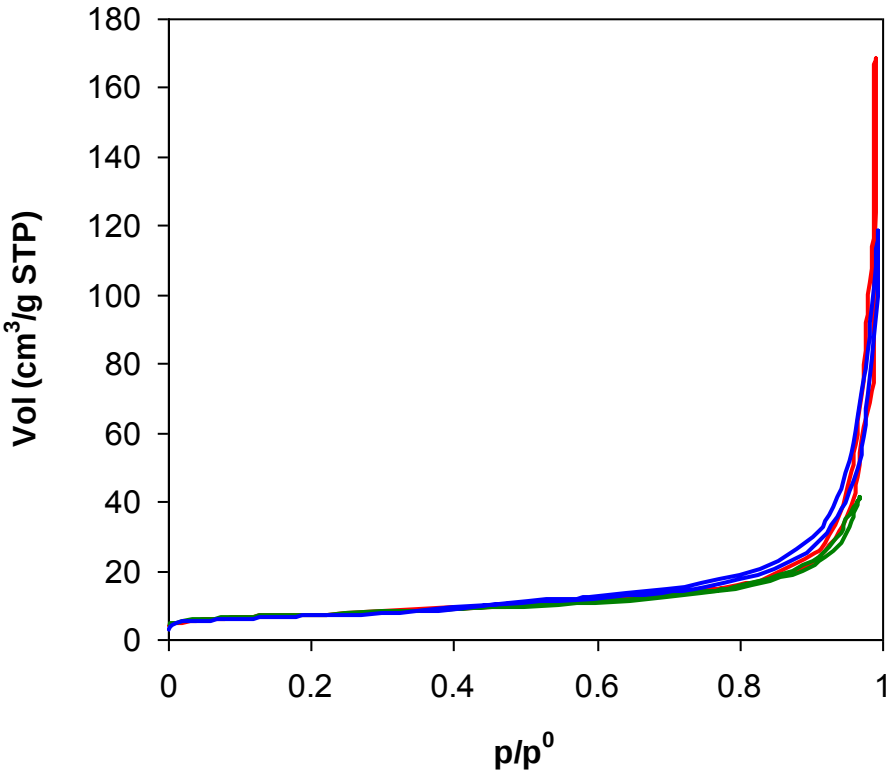

Figure 3-36. Nitrogen sorption isotherms of untreated kaolinite (blue), treated with 5 M KOH for 6 months (red) and 6.1 years (green).

3.2. Characterization of dioctahedral smecite (montmorillonite)

The following sections include the characterization of the untreated dioctahedral smectite and the study of its mineralogical evolution upon alkaline activation using 5 M NaOH and 5 M KOH.

3.2.1. Untreated montmorillonite

3.2.1.1. XRF

Results of X-ray fluorescence analysis of the < 2 μm fraction of the untreated smectite sample from Gabo de Gata was in good agreement with compositional data published for the same mineral (Table 3-7). The high concentration of P_2O_5 is due to the use of hexametaphosphate (Calgon) which was added as a dispersant. Note that published loss on ignition data (Caballero et al. 2005, Huertas et al. 2001) as well as that reported here are lower than the value obtained with TG (see below). The lower water content of the clay sample is due to drying during sample preparation.

The chemical analysis resulted in the following structural formula (without P_2O_5): $Na_{0.25}K_{0.09}Ca_{0.31}(Al_{1.20}Fe_{0.24}Mg_{0.46}Ti_{0.02})(Si_{3.81}Al_{0.19})O_{10}(OH)_2$

Table 3-7. XRF results of the starting material (wt %)

Material	SiO_2	Al_2O_3	Fe_2O_3	Na_2O	P_2O_5	TiO_2	MgO	K_2O	CaO	Loss on Ignition	Total
Smectite < 2 μm	57.42	17.73	4.83	1.91	1.71	0.19	4.64	1.11	2.16	7.30	99.00
Bentonite Serrata de Nijar*	62.14	18.95	4.47	2.35	0.00	0.00	3.27	0.78	1.80	6.40	100.16
Bentonite Serrata de Nijar**	58.92	19.48	3.48	2.28	0.06	0.27	4.83	1.21	2.51	7.09	100.13

* Caballero et al. (2005)

** Huertas et al. (2001)

3.2.1.2. XRD

Analyses of OA showed the presence of predominantly smectite. The d_{001} expanded from 14 Å to 16.6 Å upon EG treatment, to 24 Å upon DMSO treatment and collapsed to 10 Å upon deshydroxylation at 550 °C (Figure 3-37).

Huertas et al. (2001) reported XRD results of semiquantitative analysis of a clay sample from the same deposit which contained 96 % dioctahedral smectite, 1.5 % cristobalite, 1 % quartz, 1 % calcite and trace amounts of K-feldspar. According to Ramirez et al. (2002) the < 2 µm fraction is composed of a mixed-layer illite-smectite with about 10% non-swelling layers.

The crystallite size of the montmorillonite was 9 nm. This value is in agreement with published data (Bala et al. 2000).

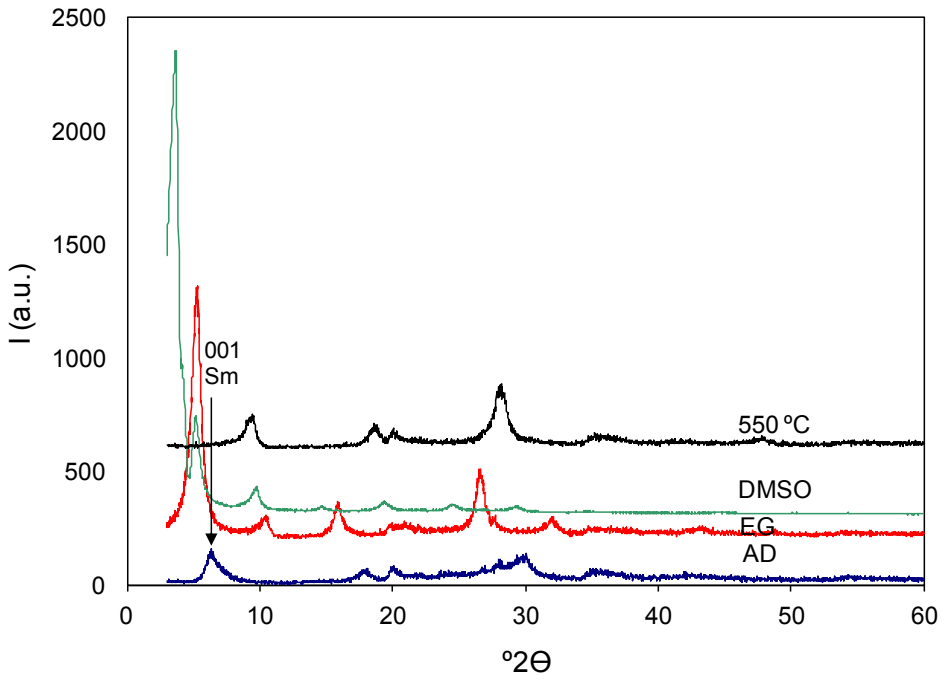

Figure 3-37: XRD patterns of montmorillonite (Sm = smectite, Cabo de Gata). Oriented aggregate air-dried (AD), treated with EG, DMSO and thermal treatment.

3.2.1.3. FESEM

The FESEM image (Figure 3-38) shows thin platelets with irregular outline which are typical for montmorillonite (Murray 2006). The microanalysis revealed the presence of Si, Al and Mg, the major elements composing montmorillonite, together with small amounts of Na, K, Ca and Fe. The qualitative composition is in good agreement with XRF data.

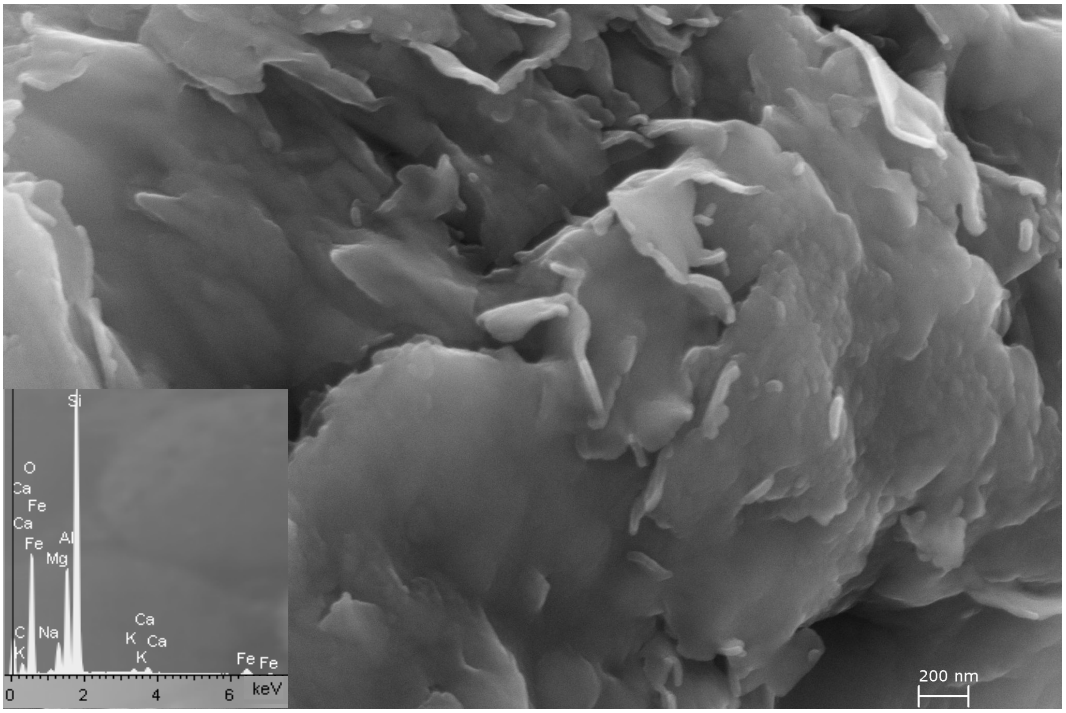

Figure 3-38. FESEM image and EDS spectrum of untreated montmorillonite (Cabo de Gata).

3.2.1.4. TEM

The representative TEM photomicrograph (Figure 3-39) of the untreated montmorillonite shows an aggregate of clay particles. Part of these particles had a flake-like structure. The structural formulae based on AEM data (Table 3-8) were calculated assuming that all Mg occupies octahedral sites. However, considering the dioctahedral character of montmorillonite, a small amount of the Mg might be actually present as interlayer cations. The obtained average structural formula based on TEM-AEM was in quite good agreement with XRF data.

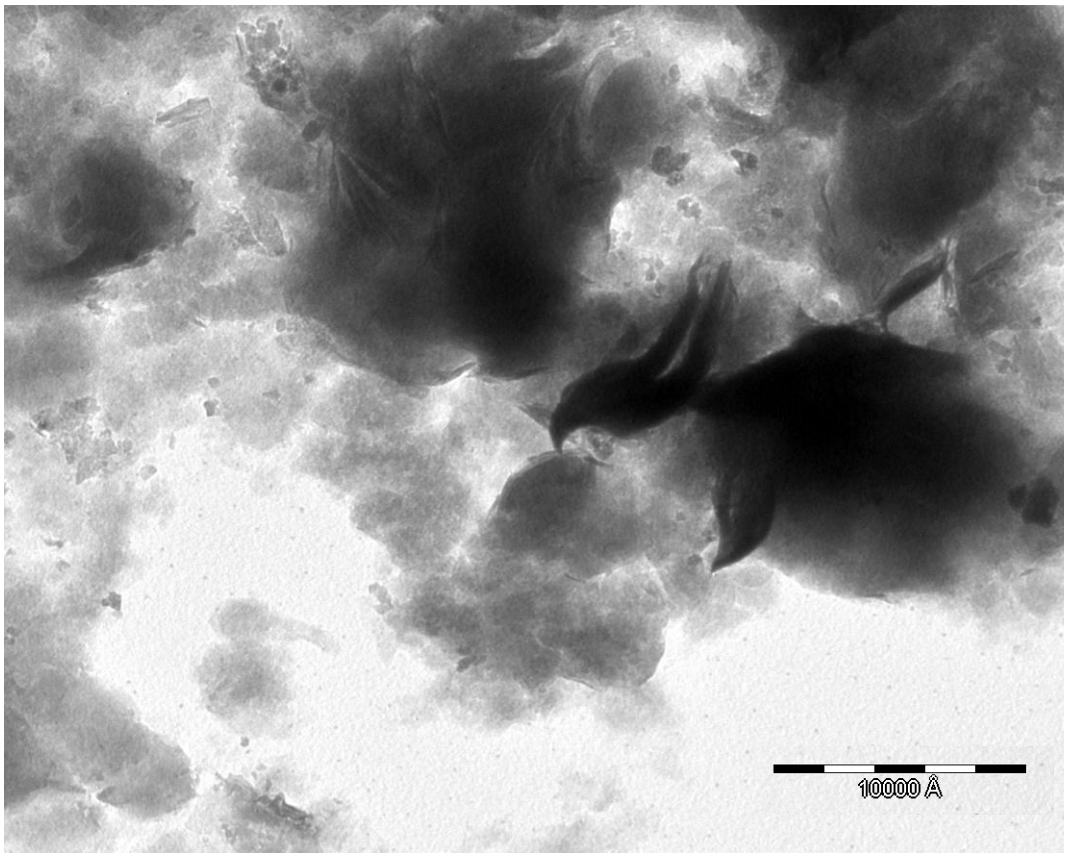

Figure 3-39. TEM image of untreated montmorillonite (Cabo de Gata).

Table 3-8. Structural formulae of untreated montmorillonite calculated from TEM-AEM data.

Structural formulae of montmorillonite based on $O_{10}(OH)_2$										
Analysis	Si	^{IV}Al	^{VI}Al	Mg	Fe	Σoct.cat.[1]	K	Ca	Na	Σint.cha.[2]
1	3.80	0.20	1.31	0.56	0.17	2.04	0.05	0.14	0.38	0.71
2	3.78	0.22	1.49	0.60	0.09	2.18	0.02	0.04	0.22	0.32
3	3.89	0.11	1.40	0.54	0.21	2.08	0.04	0.05	0.17	0.31
4	3.99	0.01	1.34	0.56	0.14	2.04	0	0.07	0.40	0.54
average	3.87 ± 0.10	0.14 ± 0.10	1.39 ± 0.08	0.57 ±0.03	0.15 ±0.05	2.09 ±0.07	0.03 ±0.02	0.08 ±0.05	0.29 ±0.11	0.48 ±0.19

[1] Sum of octahedral cations
[2] Sum of interlayer charge

3.2.1.5. Nitrogen sorption

The surface area of the untreated montmorillonite was 63.58 ± 0.45 m^2/g. Sanchez et al. (2006) reported a surface area of about 60 m^2/g for Febex bentonite (clay from the same deposit as the one used in this study). This value is within the range (45- 80 m^2/g) often reported for montmorillonite (Pernyeszi and Dekany 2003, Huang et al. 2004, Dogan et al. 2007). Rozalen et al. (2008) stated that smectites had a wider range between 30-120 m^2/g.

It has to be kept in mind that nitrogen might not have access to interlayer surfaces and the actual surface area could be higher than that calculated using the BET method. Newman (1987) stated that expandable interlayers would collapse during the pretreatment, consisting of evacuation and heating before N_2 sorption measurements are performed. Thus, the interlayer surface becomes inaccessible and nitrogen is only adsorbed on the external surface of montmorillonite crystals. Water, on the other hand, enters between the silicate layers resulting in higher surface area. The theoretical surface area of montmorillonite is 760 m^2/g (Greene-Kelly 1964) and includes the total area exposed when individual smectite sheets are fully delaminated. According to Yuang and Shen (2005), however, a complete delamination of smectite sheets is unlikely due to natural heterogeneities of the smectite. Fernandez et al. (2004) reported a total specific surface area of Febex bentonite of 725 ± 47 m^2/g, calculated based on water adsorption data.

The Nitrogen sorption isotherm of montmorillonite is of type II (Figure 3-40), which is typical for smectites (Barrer and MacLeod 1954, Valverde et al. 2000). This type of isotherm has been observed in the case of kaolinite and illite as well. However, the hysteresis loop of type H3 is much more pronounced than in the case of the latter two clay minerals. Generally, hysteresis is caused because pores of a specific size are filled at higher pressures and emptied at lower pressures. In pores with a diameter < 4 nm no hysteresis is observed (Groen et al. 2003). The same authors stated that the forced closure of the desorption branch at p/p^o around 0.35-0.45, which can be observed in Figure 3-40, is due to the collapse of the hemispherical meniscus during capillary evaporation. The meniscus collapses because the surface tension forces are larger than the tensile strength of the liquid. This phenomenon is, primarily, a result of the nature of the adsorptive. However, often, it has been erroneously related with the presence of a narrow distribution of pores centered ~ 4 nm.

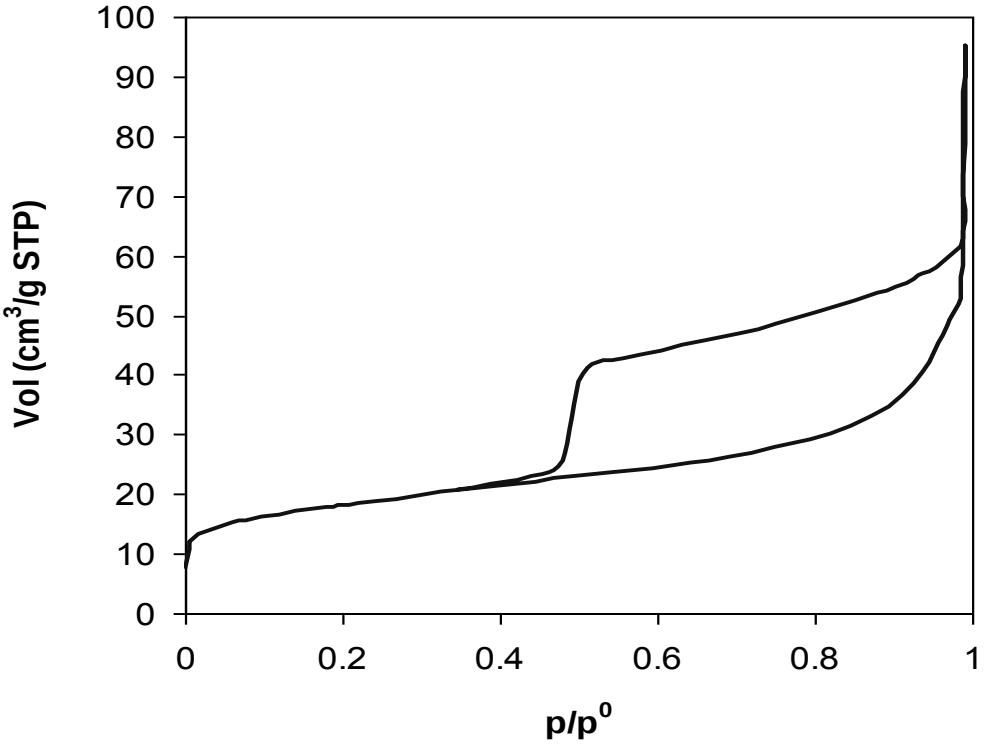

Figure 3-40. Nitrogen sorption isotherm of untreated montmorillonite.

3.2.1.6. Particle analysis

Montmorillonite showed a maximum at 130 nm (Figure 3-41) which corresponded to primary (individual) particles and has been detected in illite and kaolinite samples as well. The result is in agreement with published data by Pusch and Yong (2006), showing a maximum at 120 nm. The sample revealed a secondary maxiumum between 0.5 – 9 μm which is caused by clay particle aggregates.

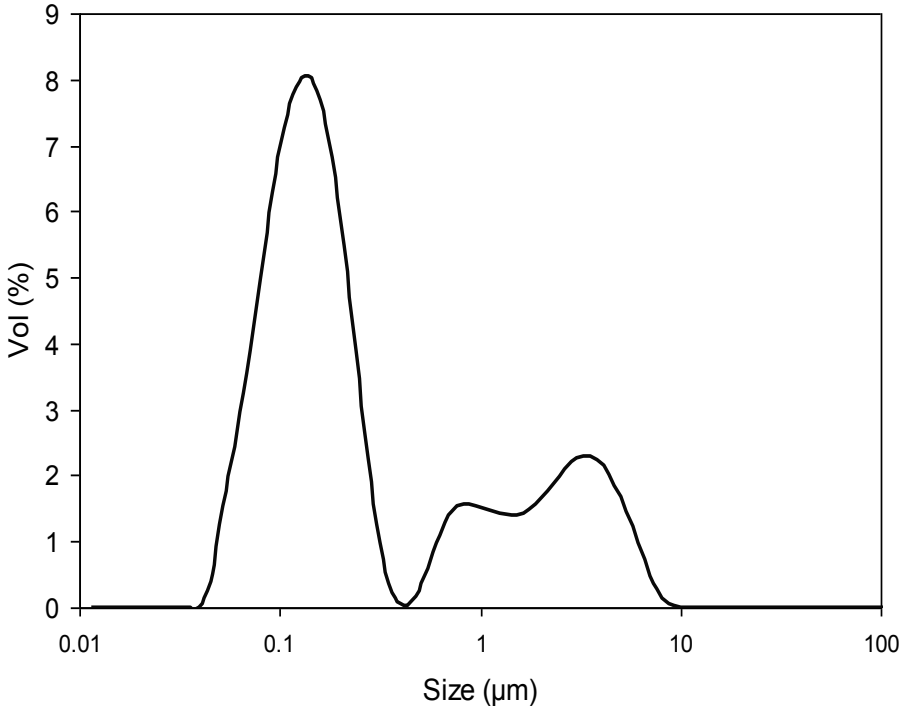

Figure 3-41. Particle size distribution of untreated montmorillonite.

3.2.1.7. TG

The thermogravimetric curve showed a loss of adsorbed water (external and interlayer water) of 17.5 % from about 30°C to 400 °C (Figure 3-42). At around 600 °C dehydroxylation of montmorillonite takes place (Newman and Brown 1987). The total weight loss amounted to 21.4 %, being about 3.3 % due to dehydroxylation. The thermogravimetric curve is typical for montmorillonite and similar data have been reported by Mielenz et al. (1955). Fernandez et al. (2006) reported a weight loss of 18 % for bentonite of the same deposit. A total weight loss between 16 – 22 % seems to be common for bentonites (Martin Vivaldi 1962).

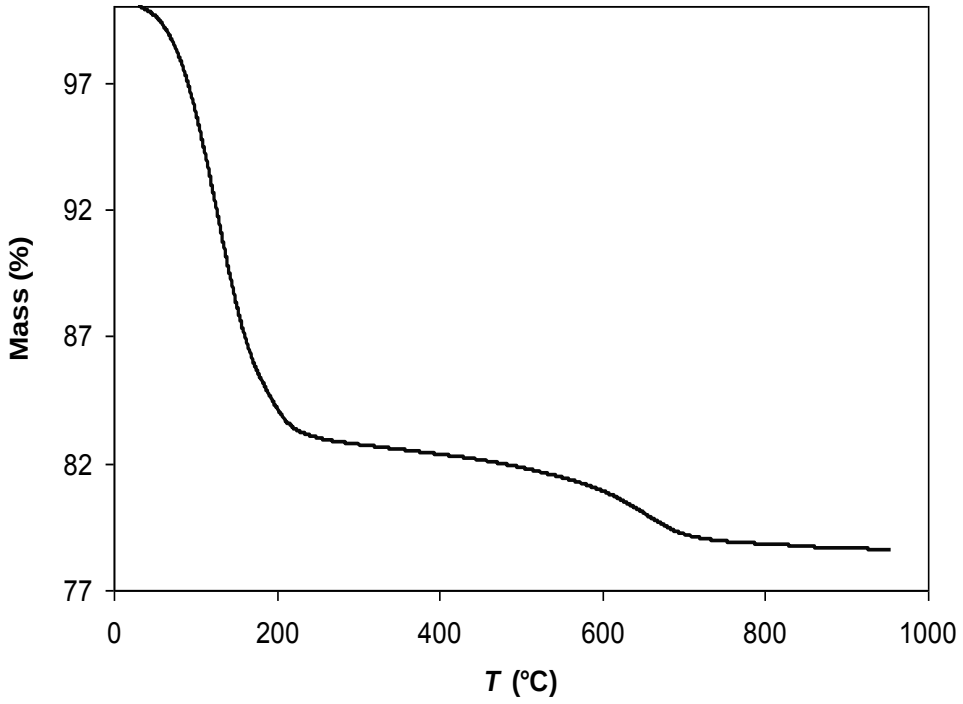

Figure 3-42. Thermogravimetric curve of untreated montmorillonite.

3.2.2. Montmorillonite treated with NaOH

3.2.2.1. XRD

XRD analyses (Figure 3-43) demonstrated that a new zeolitic phase appeared after 6-month treatment with 5 M NaOH. Bragg peaks matched those of a hydroxysodalite with the following formula: $Na_8[AlSiO_4]_6(OH)_2 \cdot nH_2O$ ($3 \leq n \leq 4$) (JPDF card no. 410009). This phase has been synthesized by Felsche et al. (1986) using kaolinite and 10-16 M NaOH at temperatures between 77-207 °C. Furthermore, an additional peak at 14.4 Å was observed which coincides with the 111 Bragg peak of a faujasite-type zeolite (zeolite X) with the following formula: $(Ca,Na)Al_2Si_{2.5}O_9 \cdot 6.4H_2O$, JPDF card no. 380232. Note that the same phases have been previously identified in the case of pure kaolinite treated with 5 M NaOH. At this point montmorillonite could still be identified in the sample, but Bragg peaks intensity seemed to be reduced. After 3.8 years the faujasite-type zeolite was clearly identified and the intensity of the hydroxysodalite Bragg peaks increased as well. Further treatment up to 5.3 years did not result in any significant mineralogical changes.

The <2 μm fraction of the sample treated for 5.8 years was separated using centrifugation. XRD analysis revealed the presence of smectite which expanded from 14 Å to ~17 Å upon EG treatment and collapsed to 10 Å upon heating (Figure 3-44).

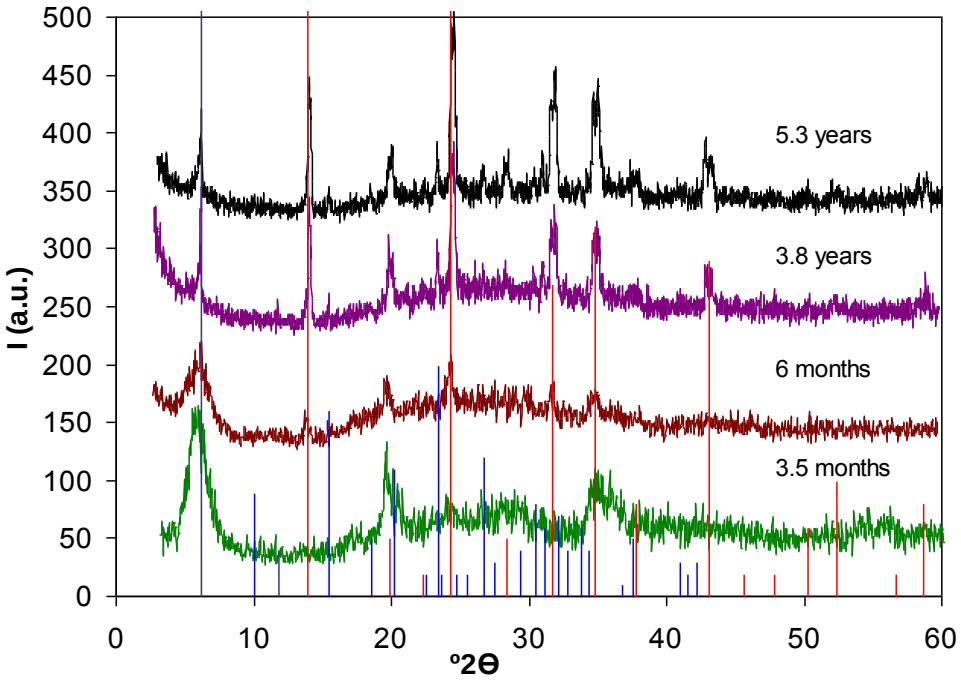

Figure 3-43: XRD patterns of montmorillonite treated with 5 M NaOH for different periods of time. Red line pattern: Hydroxysodalite (JPDF card no. 410009); Blue line pattern: Faujasite-type zeolite (JPDF card no. 380232).

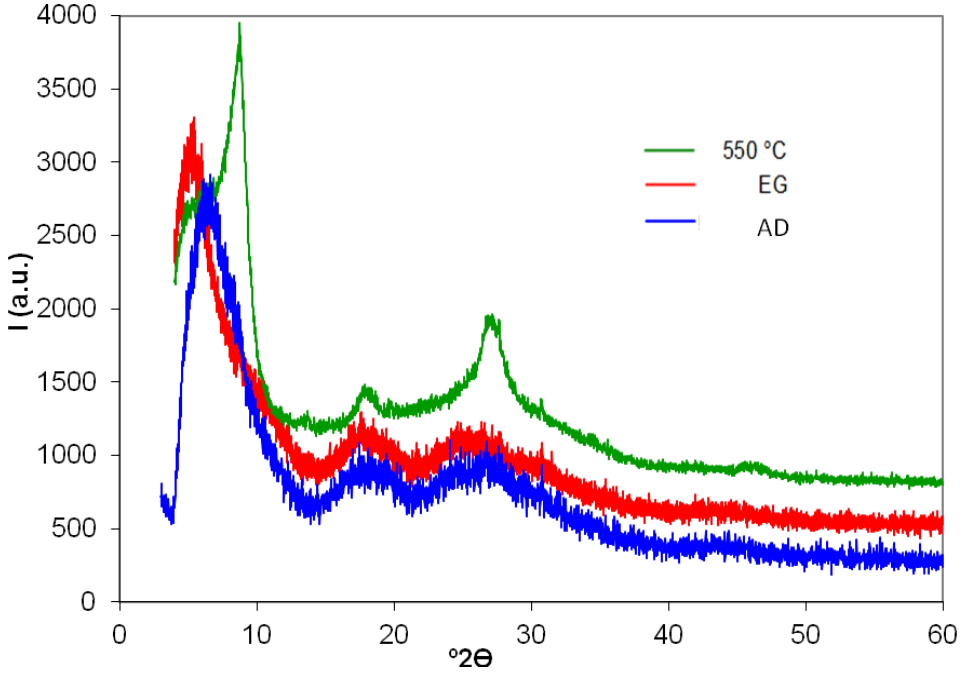

Figure 3-44. XRD patterns of oriented aggregates of the < 2 μm fraction of montmorillonite treated with 5 M NaOH for 5.8 years. Air-dried (AD), EG solvated and heat-treated at 550 °C.

3.2.2.2. FESEM

FESEM observations of montmorillonite treated with 5 M NaOH for 3.5 months (Figure 3-45) revealed the presence of a newly formed star-shaped phase with a cubic symmetry. However, the amount of this phase was small and the microanalysis showed a composition dominated by the composition of the untreated montmorillonite. Figure 3-46 shows crystals of identical morphology, identified as a sodalite-type zeolite by Cartlidge and Meier (1984).

After 6 months the amount of the zeolitic phase increased and the microanalysis showed a small increase in Na and Ca (Figure 4-47). These findings are in good agreement with XRD results, where hydroxysodalite was identified after 6 months of treatment. However, at this point the faujasite-type zeolite was not detected using FESEM.

In the sample treated for 3.8 years two newly formed phases with different morphologies, a star-shaped phase and an octahedral-shaped phase were clearly identified (Figure 4-48). EDS microanalysis proved that the star-shaped phase contained Al, Si and Na (Figure 4-49) which is consistent with the composition of hydroxylsodalite. Khajavi et al. 2007 have published SEM images of hydroxysodalite with a similar morphology (Figure 4-50) synthesized at 90 °C using sodium aluminate and sodium metasilicate dissolved in NaOH solution. The octahedral-shaped phase contained Al, Si and Ca (Figure 4-51), pointing to a faujasite-type zeolite with cubic symmetry.

After 5.3-year treatment a large portion of the clay minerals transformed into zeolitic phases (Figure 4-52). However, part of the sample still displayed a morphology similar to the original clay (Figure 5-53). This is consistent with XRD results pointing to the presence of expandable clay. The chemical composition of this clay experienced some change: the Mg concentration increased. The compositional changes identified using EDS microanalysis together with XRD results point to a saponitization of the montmorillonite at high pH which would result in the retention of the basic structure of 2:1 layers with substitution of Al by Mg in the octrahedral sheet. The formation of saponite from dioctahedral smectite at high pH has been reported previously, for example in the case of saponite from the Madrid Basin (Pozo Rodriguez and Casas Sainz de Aja 1992).

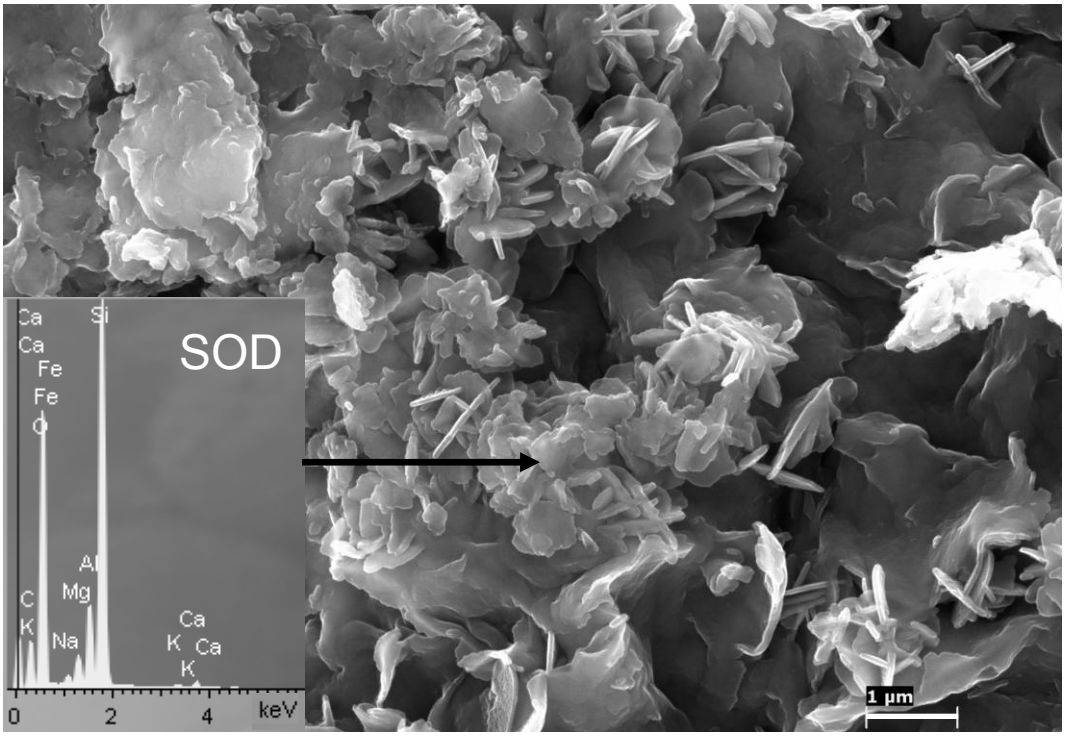

Figure 3-45. FESEM image of a montmorillonite sample treated with 5 M NaOH for 3.5 months. Besides unreacted clay particles, a newly formed star-shaped phase (hydroxysodalite, SOD) can be observed (EDS in inset).

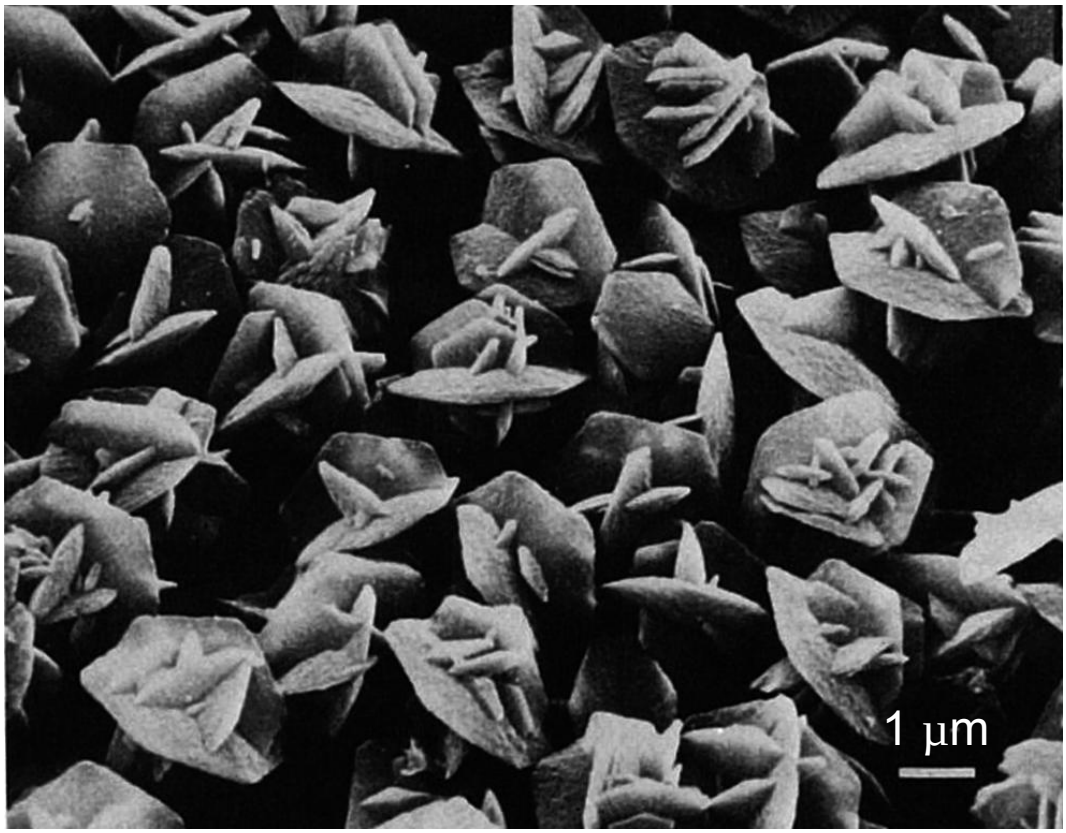

Figure 3-46. Sodalite-type zeolite of similar morphology as that observed here in the case of montmorillonite treated with 5 M NaOH (Cartlidge and Meier 1984).

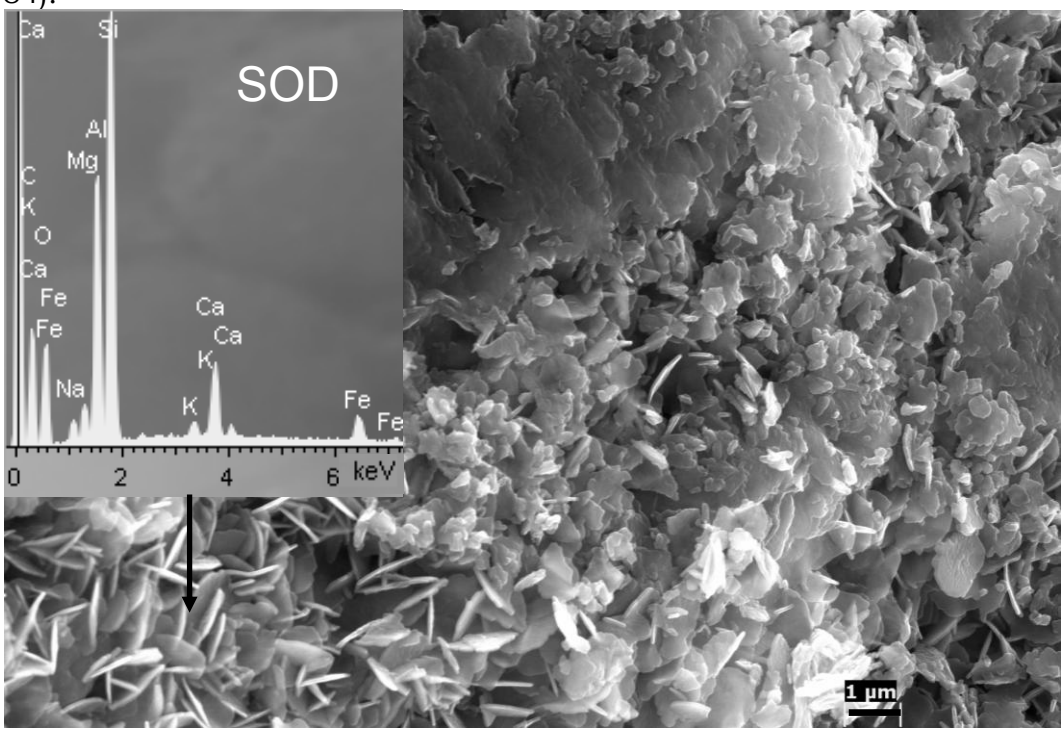

Figure 3-47. FESEM image of a montmorillonite sample treated with 5 M NaOH for 6 months. The amount of the newly formed star-shaped phase (hydroxysodalite, SOD) has augmented and its microanalysis (inset) reveals an increase in Ca and Na.

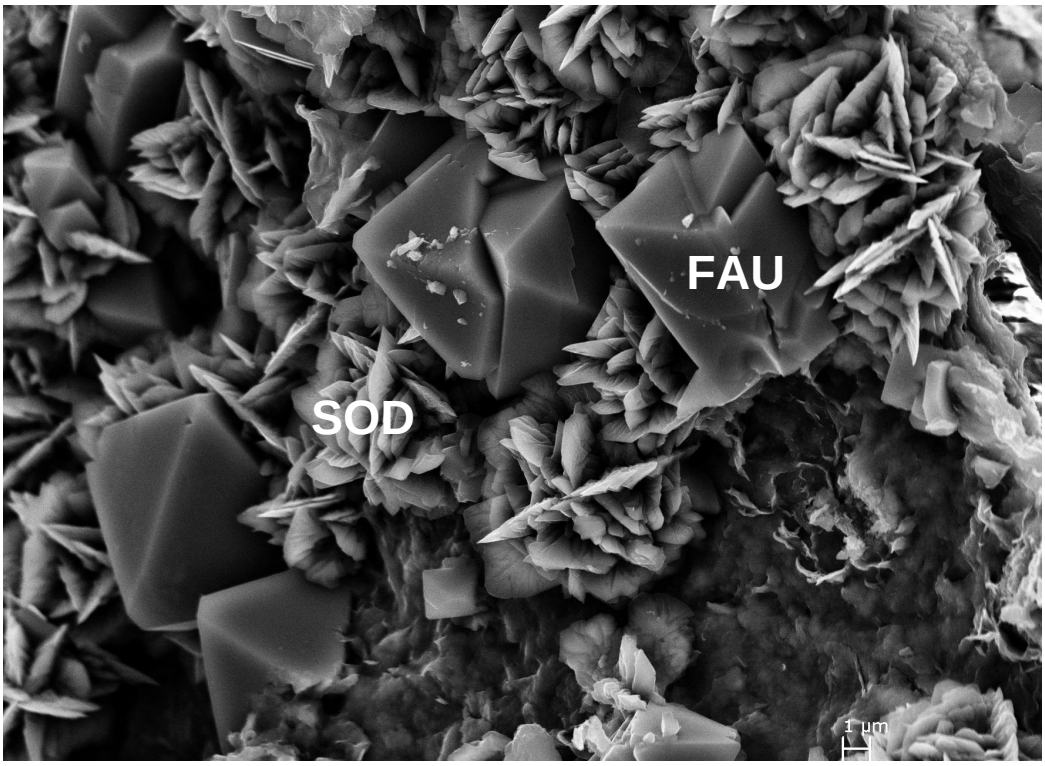

Figure 3-48. FESEM image of sodalite-type (SOD) and faujasite-type (FAU) zeolites formed in montmorillonite treated with 5 M NaOH for 3.8 years.

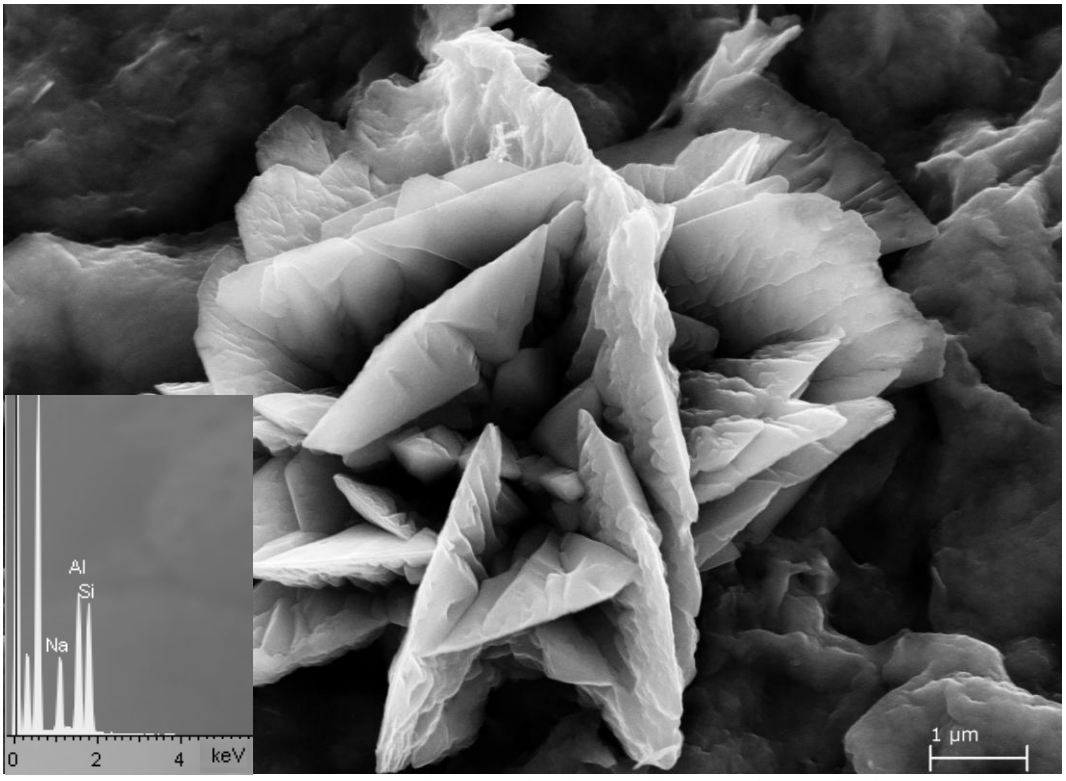

Figure 3-49. FESEM image of a newly formed star-shaped phase which was identified as hydroxysodalite in montmorillonite treated with 5 M NaOH for 3.8 years (EDS spectrum in inset).

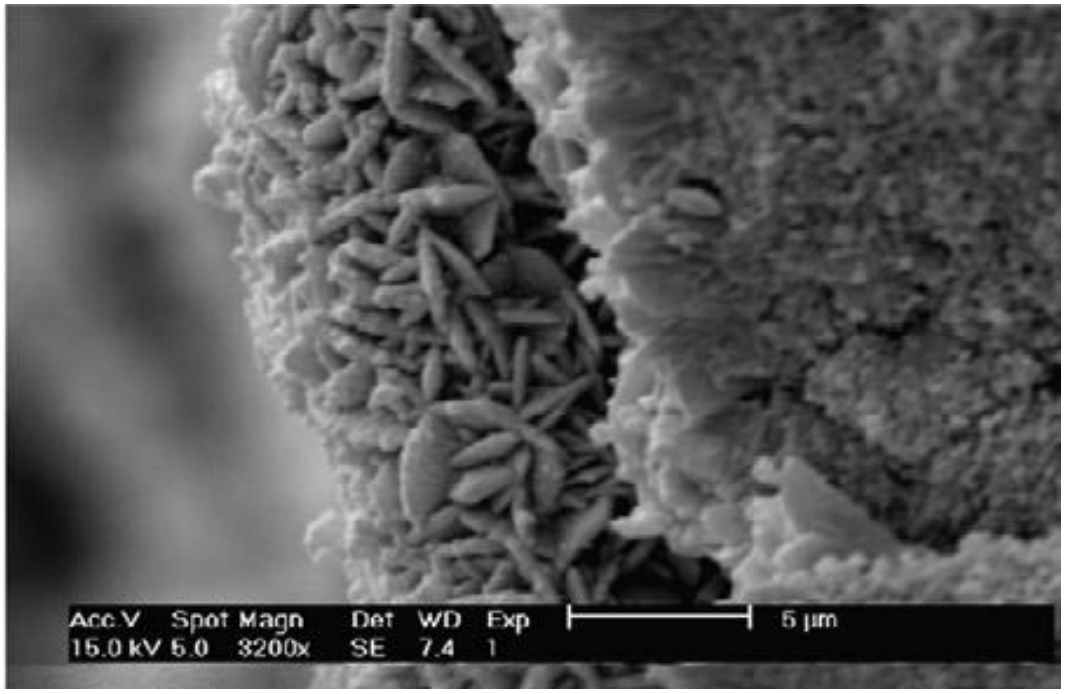

Figure 3-50. SEM image of a cross-section of a synthesized hydroxysodalite membrane, grown at T = 90 °C, 15 h (Khajavi et al. 2007).

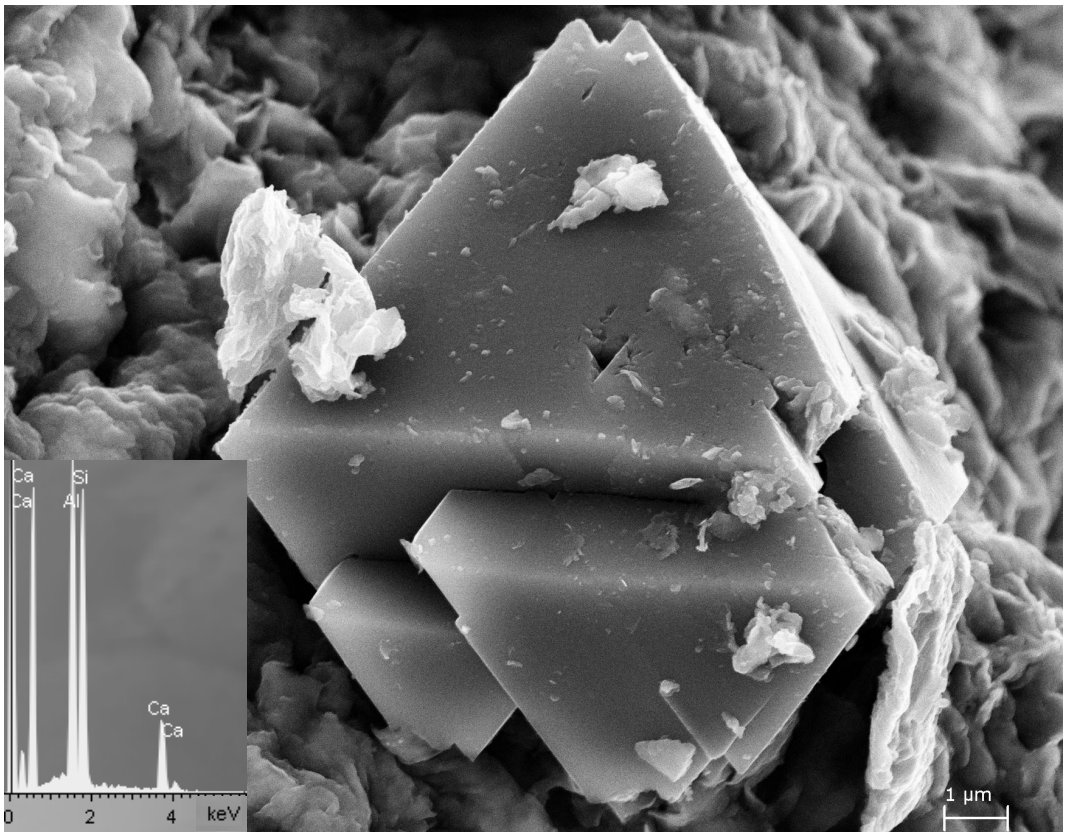

Figure 3-51. FESEM image of a newly formed octahedral faujasite-type zeolite in montmorillonite treated with 5 M NaOH for 3.8 years (EDS spectrum in inset).

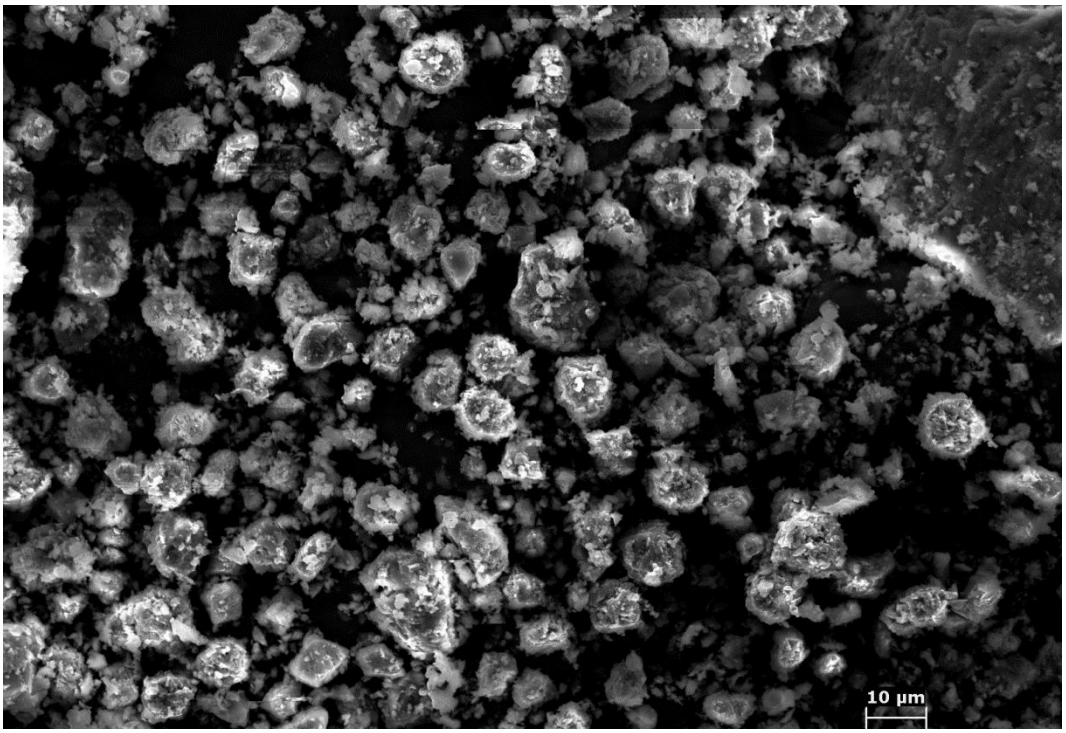

Figure 3-52. FESEM image of montmorillonite treated with 5 NaOH for 5.3 years. A large portion of the clay minerals transformed into zeolitic phases.

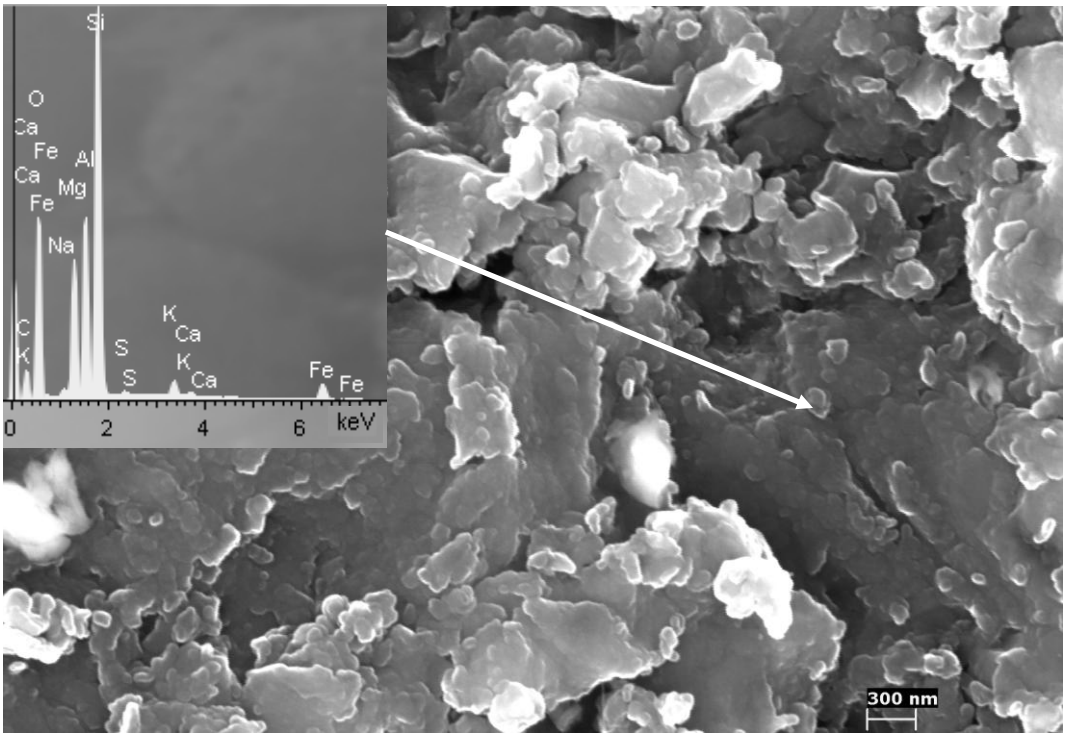

Figure 3-53. FESEM image of montmorillonite treated with 5 NaOH for 5.3 years. Parts of the sample conserved the original morphology of unreacted montmorillonite, but the chemical composition changed, the Mg concentration increased (see EDS spectrum in inset), pointing to saponitization.

3.2.2.3. TEM

The TEM image of montmorillonite treated with 5 M NaOH for 3.8 years did not reveal important morphological changes in the clay fraction (Figure 3-54). However, after 5.8 years of treatment the number of small clay particles of a few hundred nm seemed to have decreased significantly whereas the micron-sized particles remained unchanged (Figure 3-55). Note that TEM images and TEM-AEM data of zeolites formed during alkaline activation are not included here because they did not contribute to a more detailed characterization of these minerals.

Structural formulae based on TEM-AEM data for the < 2 μm fraction of montmorillonite treated with 5 M NaOH for 5.8 years showed a decrease in Si, whereas Mg and Fe, as well as the octahedral occupancy, increased (Table 3-9). It is assumed that the montmorillonite underwent a partial saponitization. However, the structural formulae calculated here revealed a much lower Mg concentration than commonly observed in saponites (Newman and Brown 1987). Furthermore, in some cases the interlayer charge was higher than expected for a saponite-type clay which might be due to impurities. The formation of a significant amount of interstratified chlorite-smectite is ruled out based on XRD results of EG solvated and heat-treated oriented aggregates. Based on XRD and MAS-NMR results, Sanchez et al. (2006) also identified saponite as a reaction product in the case of Febex bentonite treated with 0.1-0.5 M NaOH. The chemical composition reported by Sanchez et al. (2006) is quite similar to the one calculated for the montmorillonite treated with 5 M NaOH at room *T* for 5.8 years (Table 3-9).

Apart from the above described changes, other mineralogical phases were identified in the < 2 μm fraction. These phases revealed a decrease in Si as well as higher Al concentration and interlayer charge if compared to the original montmorillonite. The octahedral occupancy, in contrast, experienced little changes if compared with the original montmorillonite (Table 3-9). These results suggest that the montmorillonite experienced illitization. However, the dominant interlayer cation was Na. Thus, the newly formed phase should be closer to an interstratified smectite-paragonite. It might be argued that this mixed-layer phase could be a relic of the impurities in the original montmorillonite. However, structural formulae calculated from TEM-AEM analyses of the untreated montmorillonite (Table 3-8) are quite homogeneous and do not show any evidence of illitization. Sanchez et al. (2006) also suggested the presence of an illite/smectite interstratification in montmorillonite treated with 0.1-0.5 M NaOH additional to the Mg-smectite. In any case, the degree of illitization of montmorillonite observed in this study is assumed to be low, since swelling from 14 to ~17 Å upon EG solvation was still detectable with XRD in samples treated for 5.8 years.

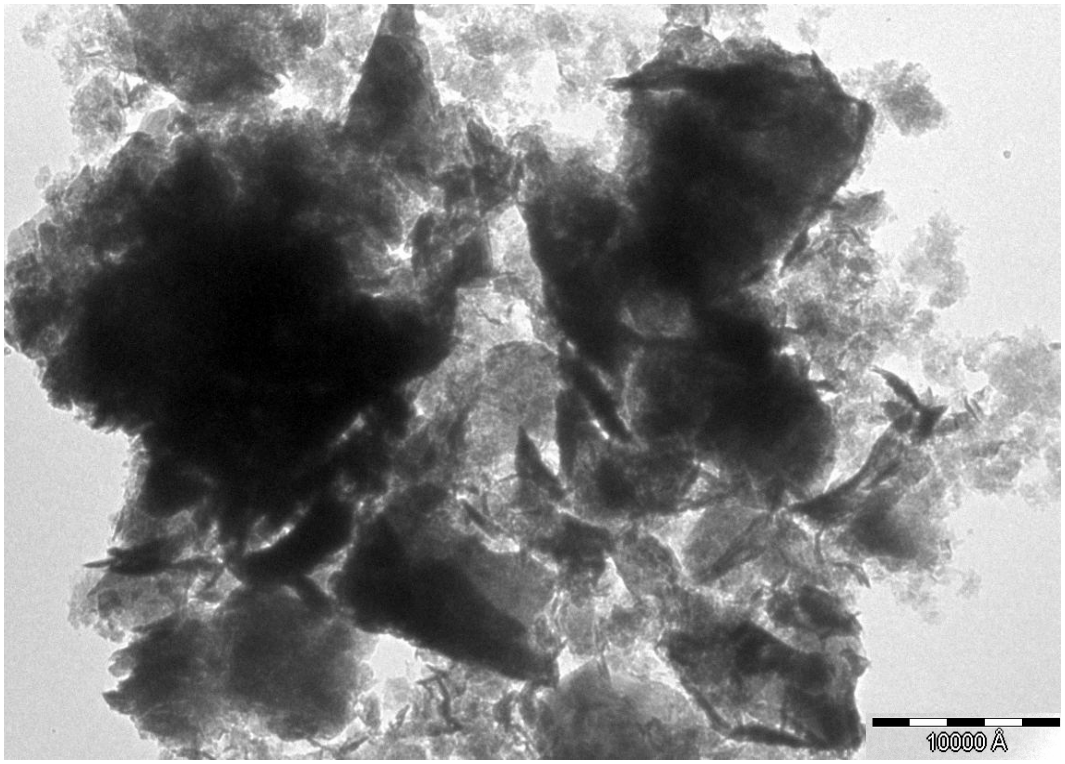

Figure 3-54. TEM image of montmorillonite treated with 5 M NaOH for 3.8 years. The clay fraction does not seem to have experienced important morphological changes.

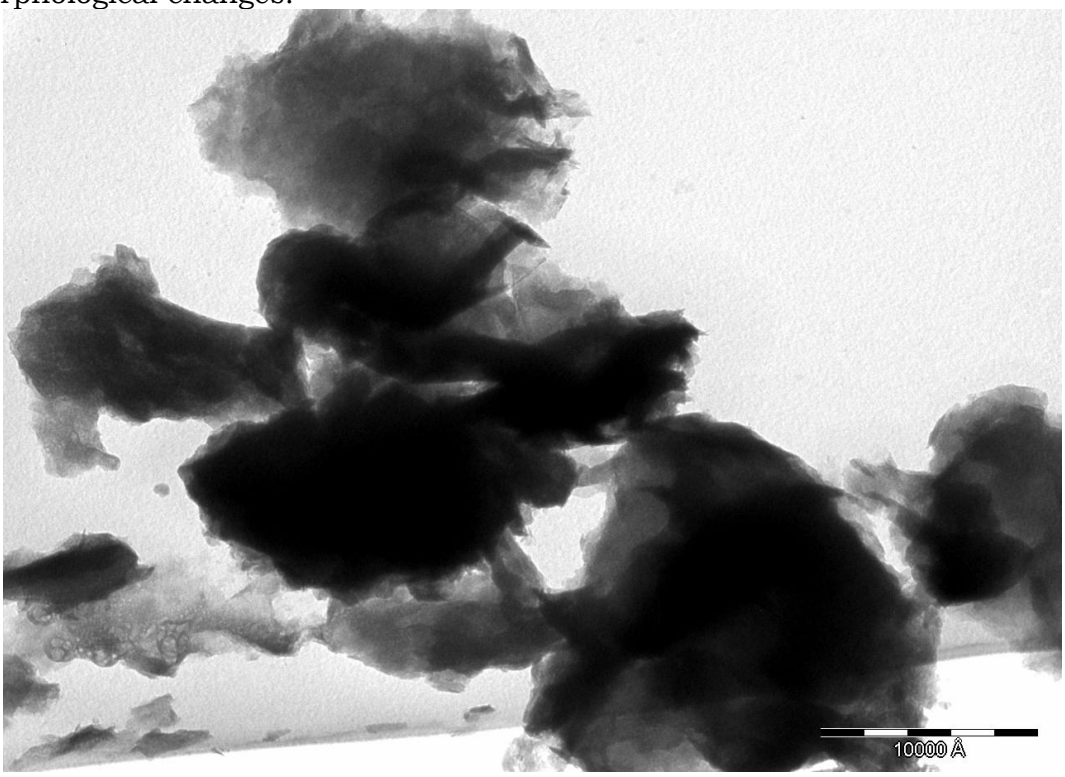

Figure 3-55. TEM image of the < 2 μm fraction of montmorillonite treated with 5 M NaOH for 5.8 years. The number of small clay particles of a few hundred nm seemed to have decreased significantly if compared to Figure 3-54. In contrast, the micron-size particles remained unchanged.

Table 3-9. Structural formulae of mineral phases of the < 2 μm fraction of montmorillonite treated with 5 M NaOH for 5.8 years calculated from TEM-AEM data (average structural formula of untreated montmorillonite is included)

Structural formulae of montmorillonite based on $O_{10}(OH)_2$										
	Si	^{IV}Al	^{VI}Al	Mg	Fe	Σoct.cat.[1]	K	Ca	Na	Σint.cha.[2]
Untreated	3.87	0.14	1.39	0.57	0.15	2.09	0.03	0.08	0.29	0.48
average	±0.10	±0.10	±0.08	±0.03	±0.05	±0.07	±0.02	±0.05	±0.11	±0.19
Saponitization										
1	3.64	0.36	0.82	1.04	0.31	2.17	0.06	0.24	0.51	1.05
2	3.56	0.44	0.74	1.04	0.31	2.09	0.18	0.28	0.63	1.37
3	3.62	0.38	0.98	1.25	0.16	2.39	0	0.18	0.20	0.56
4	3.62	0.38	1.00	1.15	0.25	2.40	0.11	0.09	0.20	0.49
5	3.57	0.43	0.80	1.46	0.23	2.49	0.04	0.14	0.23	0.55
6	3.44	0.56	1.06	0.98	0.34	2.38	0.14	0.13	0.17	0.57
7	3.32	0.68	0.72	1.14	0.46	2.32	0.17	0.17	0.61	1.12
Average	3.54	0.46	0.87	1.15	0.29	2.32	0.10	0.18	0.36	0.82
5.8 years	±0.12	±0.12	±0.14	±0.16	±0.09	±0.14	±0.07	±0.07	±0.21	±0.36
Bentonite*	3.63	0.37	0.71	1.14	0.42	2.27	0.14		0.55**	0.69
Illitization										
8	3.43	0.57	1.65	0.18	0.11	1.94	0.05	0.20	0.55	1.00
9	3.38	0.62	1.67	0.26	0.09	2.02	0.02	0.14	0.59	0.89
10	3.33	0.67	1.91	0.11	0.05	2.07	0.05	0.16	0.23	0.60
11	3.24	0.76	1.44	0.53	0.23	2.20	0.04	0.30	0.18	0.82
12	3.09	0.91	1.99	0.12	0.05	2.16	0	0.09	0.40	0.58
13	3.03	0.97	1.67	0.34	0.14	2.15	0	0.32	0.31	0.95
Average	3.25	0.75	1.72	0.26	0.11	2.09	0.02	0.20	0.38	0.81
5.8 years	±0.16	±0.16	±0.20	±0.16	±0.08	±0.10	±0.02	±0.09	±0.18	±0.18

[1] Sum of octahedral cations

[2] Sum of interlayer charge

* Sanchez et al. (2006), bentonite treated with 0.5 M NaOH at 200 °C for 540 days

** M^+

3.2.2.4. Nitrogen sorption

BET surface area results calculated from nitrogen adsorption data showed that montmorillonite treated with 5 M NaOH experienced a 30 % increase in surface area after 6 months (Table 3-10). After 5.3 years of alkaline activation the sample experienced a surface area increase of more than 100 % if compared with the original clay sample. This increase coincides with a extensive transformation of the samples into faujasite-type and sodalite-type zeolites, demonstrated using XRD and FESEM analyses. It is assumed that the faujasite-type zeolite is responsible for the surface area increase. The formation of the sodalite-type zeolite seemed to have counteracted this increase. The reported surface area of hydroxysodalite is only 22.8 m^2/g (Li et al. 2007). In kaolinite and Alhambra Formation soil samples where a transformation of faujasite into hydroxysodalite was observed, the surface area actually experienced a drastic decrease. In the case of the montmorillonite, clear evidence for transformation of faujasite into hydroxysodalite was not detected and both phases seemed to have formed simultameously.

The nitrogen sorption isotherm experienced some modification upon alkaline activation (Figure 3-56). After 6 months of treatment, the type H3 hysteresis loop was less pronounced. The shape is between the one observed in untreated montmorillonite and the one of untreated kaolinite/illite. This change indicates that an at least partial destruction/transformation of the montmorillonite had occured. However, even after 5.3 years of treatment with 5 M NaOH, the influence of the presence of smectite (evidenced using XRD, FESEM and TEM) on the shape of the loop was still observed. Note that according to Breck (1974) sorption isotherms of crystalline zeolites do not exhibit hysteresis because adsorption and desorption are completely reversible.

Table 3-10. BET surface area of untreated montmorillonite and montmorillonite treated with 5 M NaOH

Treatment time	Surface area (m^2/g)
0	63.58 ± 0.45
6 months	82.81 ± 0.43
5.3 years	141.39 ± 0.63

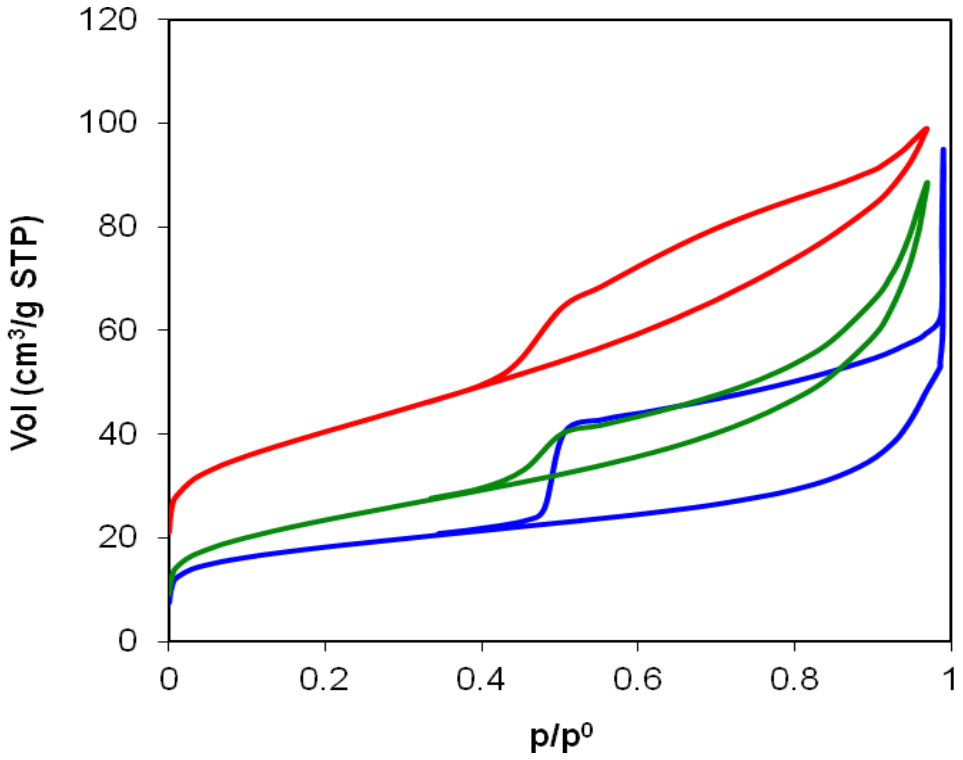

Figure 3-56. Nitrogen sorption isotherms of montmorillonite. Untreated (blue) and treated with 5 M NaOH for 6 months (green) and 5.3 years (red).

3.2.3. Montmorillonite treated with KOH

3.2.3.1. XRD

XRD analyses (Figure 3-57) demonstrated that the treatment with 5 M KOH did not cause any significant mineralogical changes after 6 months.

After 3.8-year treatment the formation of two zeolitic phases was observed. One of the new phases was similar to zeolite K-F with a tetragonal symmetry and the following formula: $KAlSiO_4 \cdot 1.5H_2O$ (JPDF card no. 380216). However, FESEM-EDS analysis and TEM-AEM analysis (see below) revealed that this phase contained Ca in addition to K. The Bragg peaks of the second phase corresponded to zeolite K-I with the following formula: $K_2Al_2SiO_8 \cdot 3.8H_2O$ (JPDF card no. 180988). Bauer and Velde (1999) also report the formation of zeolite K-I in smectite treated with 2-3 M NaOH at 80 °C.

Further treatment for up to 5.3 years did not result in the formation of any additional phases. The diffractogram of the < 2 μm fraction of the montmorillonite revealed that the broad peak of montmorillonite originally at 14 Å shifted to 10.9 Å after 6.3 years of alkaline activation. EG treatment of the oriented aggregates resulted in an expansion to ~11.6 Å (Figure 3-58). These results suggest that the montmorillonite has experienced a certain degree of illitization since unaltered montmorillonite normally expands to around 17 Å after EG treatment. Illitization of smectite at high pH conditions is a common process and has been described by many researchers (Eberl et al.,1993, Claret et al., 2002, and Drief et al., 2002).

Furthermore, it was observed that the Bragg peaks of zeolite K-I and K-F disappeared upon heat treatment at 550°C (Figure 3-58). Thermal stability of zeolites might vary significantly depending on their composition. Barrer (1982) stated that zeolite K-I decomposes at a temperature of around 168 °C, and Breck (1974) reported that structural changes in zeolite K-F would occur at temperatures ≥ 500 °C, a fact that is in agreement with the results of this study showing the disappearance of zeolite Bragg peaks after heat treatment at 550 °C.

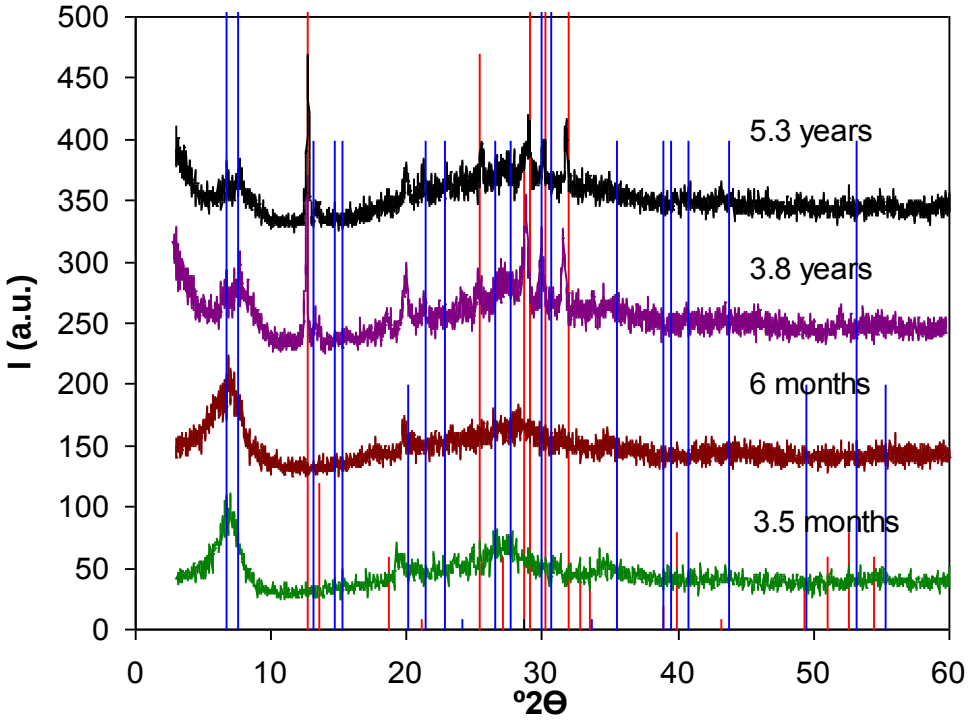

Figure 3-57: XRD patterns of montmorillonite treated with 5 M KOH for different periods of time. Red line pattern: Zeolite K-F (JPDF card no. 380216); Blue line pattern: Zeolite K-I (JPDF card no. 180988).

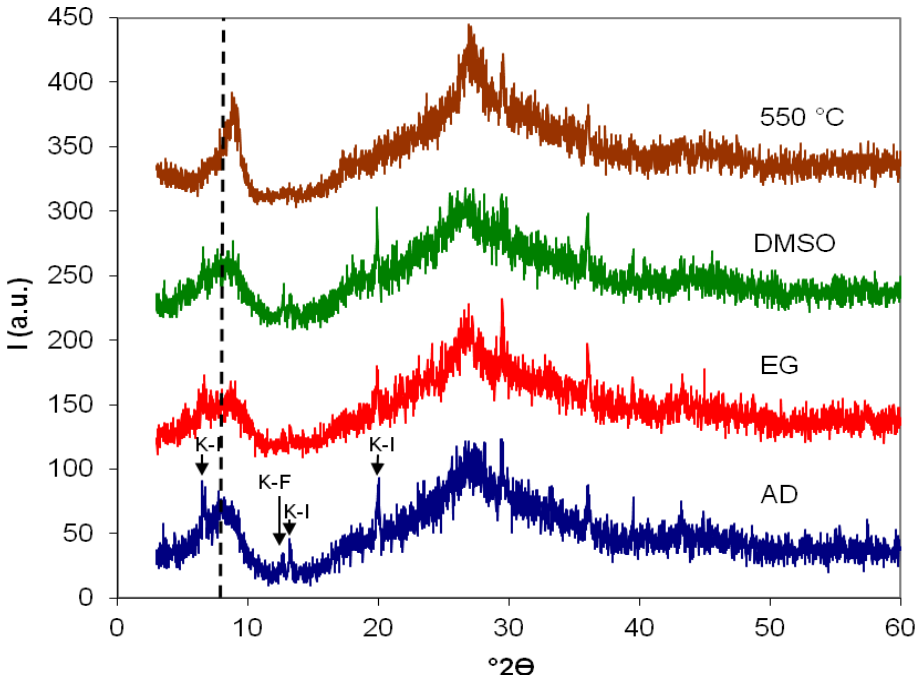

Figure 3-58. XRD patterns of the < 2 µm fraction of montmorillonite treated with 5 M KOH for 6.3 years. The 001 Bragg peak of montmorillonite, originally at 14 Å, has shifted to 10.9 Å during alkaline treatment (dashed line) and expanded to ~11.6 Å upon EG solvation (EG). OM air-dried (AD), DMSO solvated and treated at 550 °C. K-I = zeolite K-I, K-F = zeolite K-F.

3.2.3.2. FESEM

FESEM results are in agreement with XRD results in that morphological or compositional changes were not observed in the sample after 6-month treatment (Figure 3-59).

After 3.8 years of treatment two new zeolithic phases were detected (Figure 3-60). Large clusters of a cruciform-shaped zeolite together with a hexagonal crystal were observed. These phases were tentatively identified as zeolite K-F and K-I, respectively. The EDS microanalysis of the cruciform-shaped zeolite revealed the presence of Al, Si and small amounts of Mg, Na, K and Ca. Zeolite K-F with a comparable morphology (Figure 3-61) has been reported to form from kaolinite or metakaolinite treated with KOH (Barrer et al. 1968, Barrer and Mainwaring 1972, Belver et al. 2002).

After 5.3 years of treatment no additional phases were identified. However, the K concentration of zeolite K-F significantly increased, thus showing a composition closer to the zeolitic phase identified with XRD (Figure 3-62). Additionally, clusters of nanosized crystals were observed which might correspond to zeolite K-I. EDS-analysis revealed an increase in Al, K and Ca compared to the untreated montmorillonite. This composition is compatible with a zeolite (Figure 3-63). Note that the same type of nanosized crystals have been observed in the case of kaolinite treated with KOH.

Some of the clay particles showed morphologies very similar to the original clay (Figure 3-64).

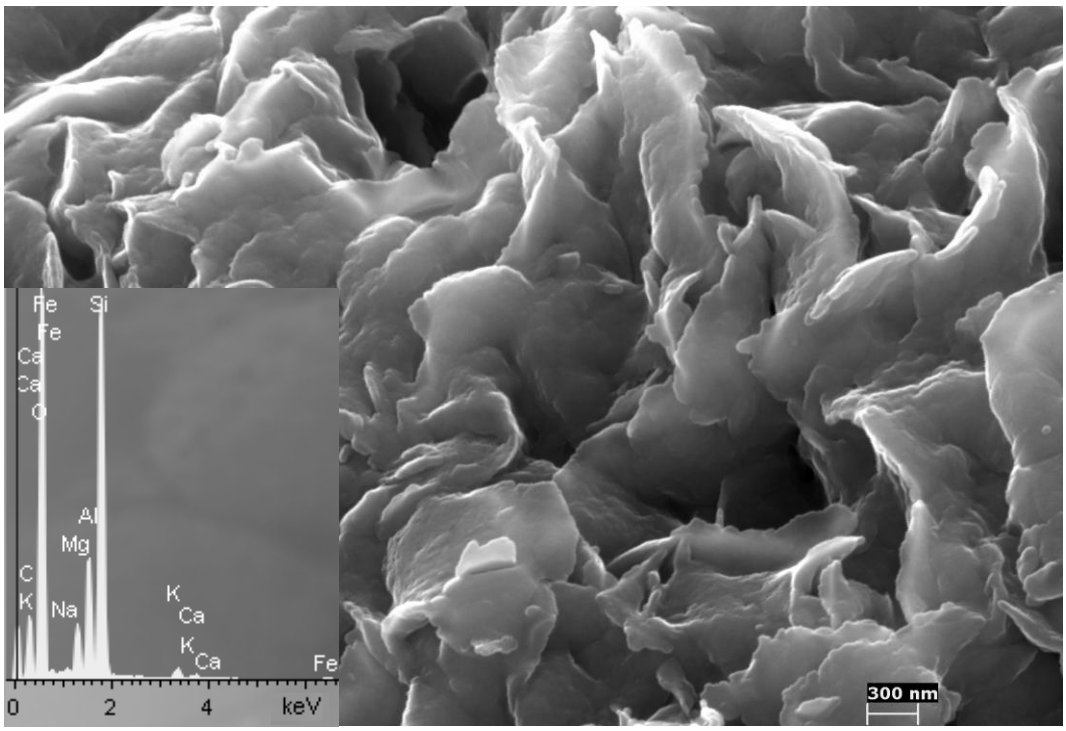

Figure 3-59. FESEM image of montmorillonite treated with 5 M KOH for 6 months. Morphological or compositional changes can not be observed (EDS in inset).

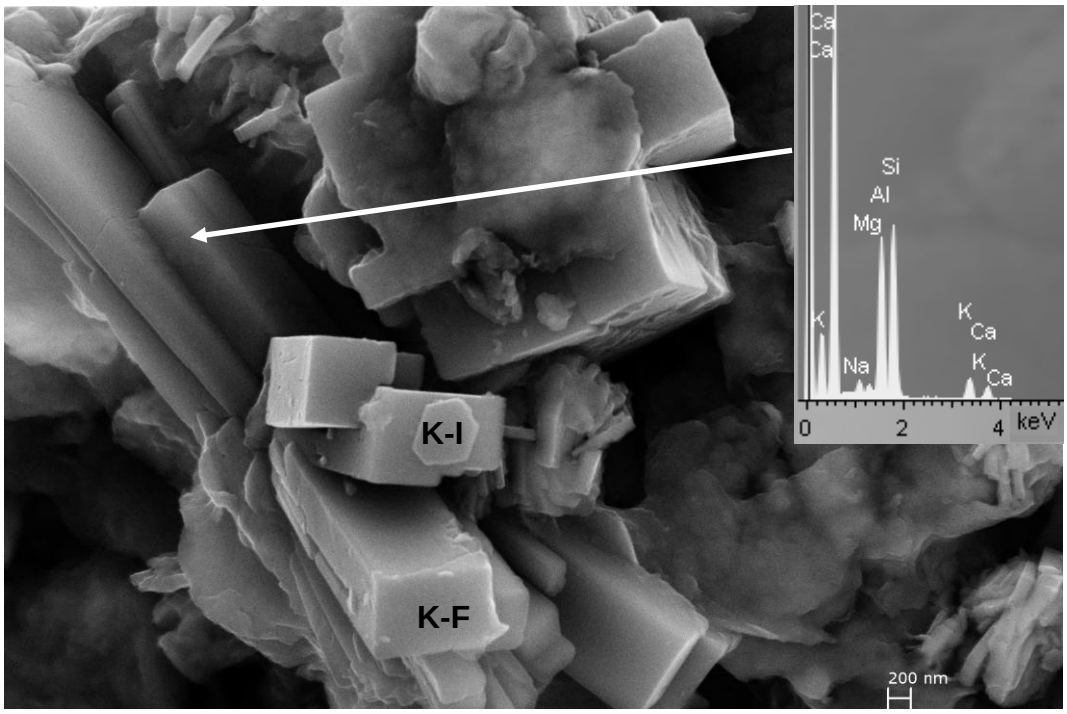

Figure 3-60. FESEM image of montmorillonite treated with 5 M KOH for 3.8 years. A new cruciform-shaped zeolitic phase, possibly zeolite K-F (EDS spectrum in inset), as well as a small hexagonal crystal which might correspond to zeolite K-I can be observed.

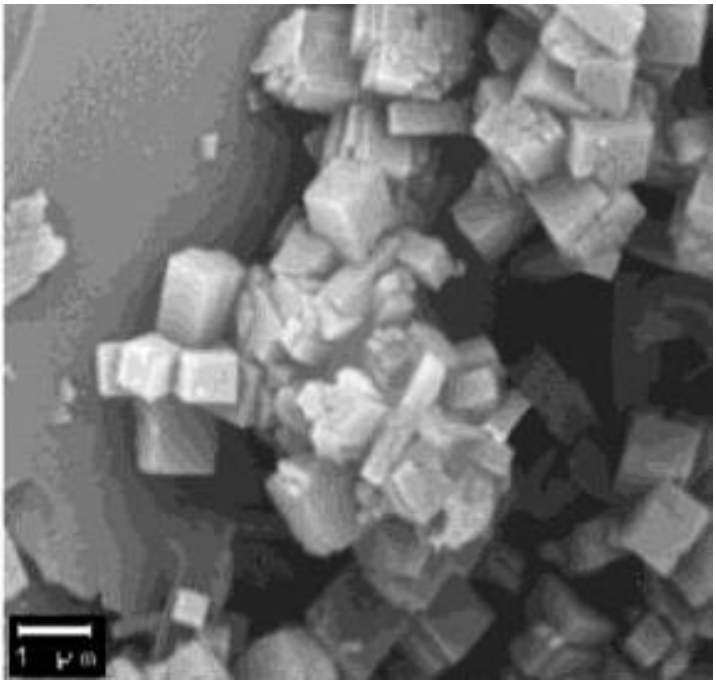

Figure 3-61. SEM image of zeolite K-F formed from metakaolinite treated with 5 M KOH (Belver et al. 2002).

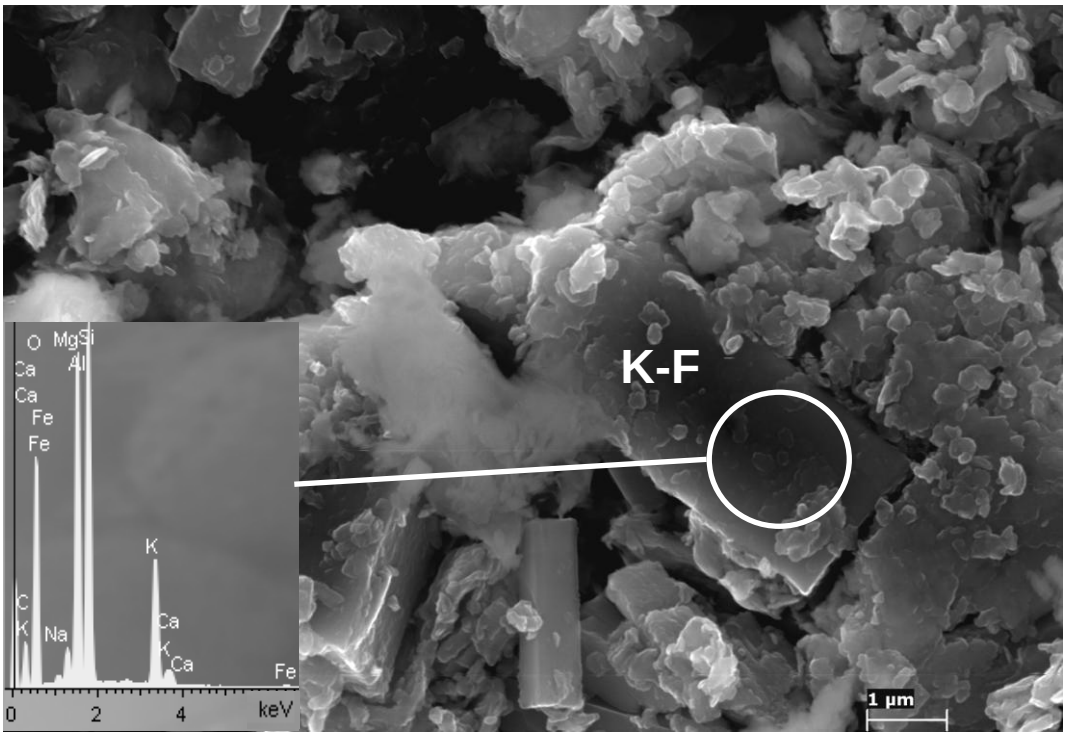

Figure 3-62. FESEM image of montmorillonite treated with 5 M KOH for 5.3 years. The EDS microanalysis (inset) now reveals a higher concentration of K in the zeolite K-F.

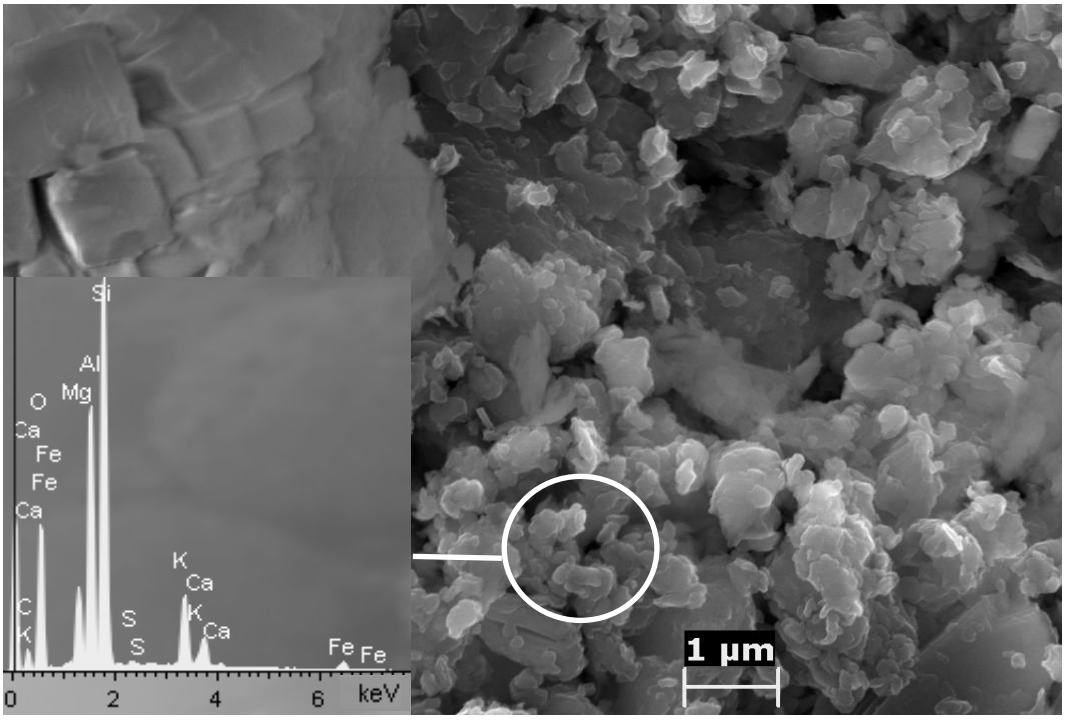

Figure 3-63. FESEM image of montmorillonite treated with 5 M KOH for 5.3 years. EDS microanalysis of the nanosized crystals, possibly zeolite K-I, reveals an increase in Al, K and Ca concentration if compared to the original montmorillonite.

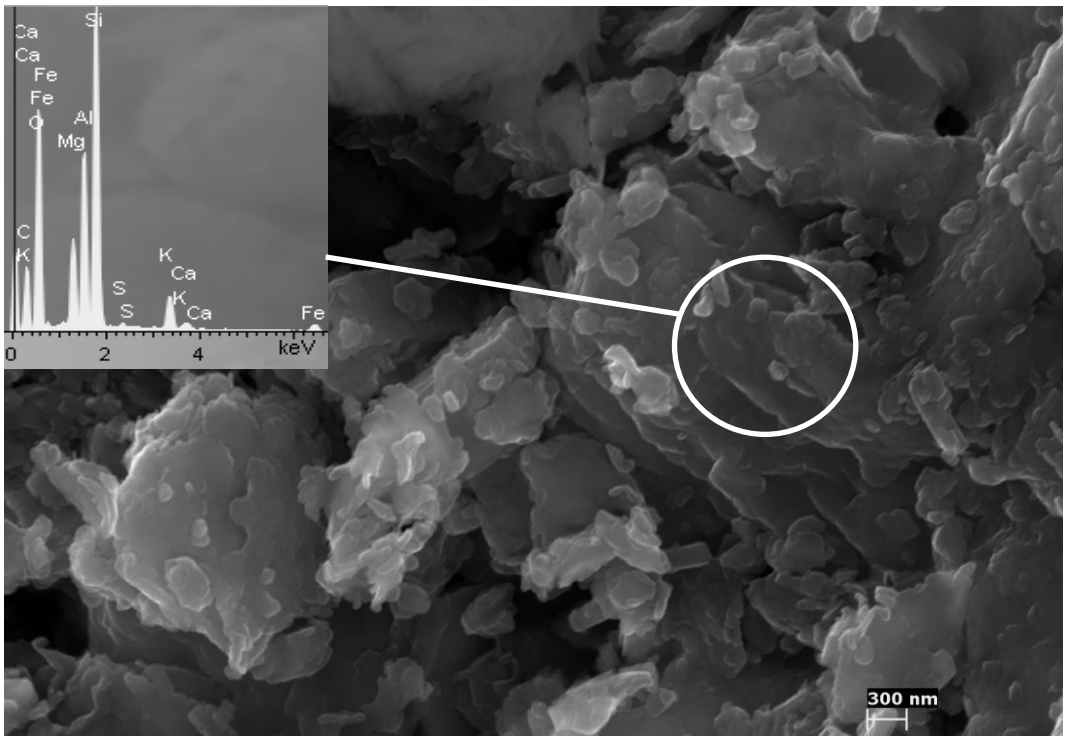

Figure 3-64. FESEM image of montmorillonite treated with 5 M KOH for 5.3 years. Some clay particles do not reveal significant morphological changes if compared to the original montmorillonite (EDS spectrum in inset).

3.2.3.3. TEM

After 6 months of treatment the morphology of the montmorillonite seemed unchanged (Figure 3-65). However, a star-shaped phase appeared which was unambiguously identified with TEM-SAED as $CaCO_3$ (Figure 3-66). Calcium carbonate with an identical morphology (Figure 3-67) has been reported by Jiao et al. (2009).

After 3.8-year treatment zeolite K-F and K-I were detected (Figure 3-68). These results confirm XRD and FESEM data. Due to the thickness of the zeolitic crystals, TEM-AEM results can only be considered qualitatively. Therefore, only representative EDS spectra are included here (insets, Figure 3-68 and 3-69). In general, TEM-AEM results are not in good agreement with published zeolite composition (Barrer et al. 1968).

TEM analysis of the clay sample treated for 6.3 years (Figure 3-70) showed an aggregate of nanosized gel-like particles with a high concentration of Si, Mg and Ca and poor in Al (inset, Figure 3-70). Note that a similar phase has been identified previously with FESEM (Figure 3-63). Additionally, clay particles with morphologies similar to the one of untreated montmorillonite were detected (Figure 3-71).

Table 3-11 shows structural formulae calculated from TEM-AEM data of the < 2 μm fraction of montmorillonite treated with 5 M KOH for 6.3 years. The chemical composition of these phases varies extremely. One group of

analyses showed an only slightly decreased Si concentration if compared with the composition of the original montmorillonite. Octahedral Al was partially replaced by Mg and the octahedral occupancy increased slightly. The interlayer charge increased as well due to an augmentation in K content. The compositional changes suggest a transformation into an illite-smectite interstratification. As previously stated, illitization of smectites treated with KOH is a common process. Ramirez et al. (2002) reported an increase in the percentage of illite in the illite-smectite interstratification after alkaline treatment of bentonite from Cabo de Gata in the presence of K^+ at a pH around 13. Eberl et al. (1993) also observed an important degree of illitization in Kinney and Wyoming montmorillonite treated with 3 M KOH at 35 °C. Results by Bauer and Berger (1998) and Bauer and Velde (1999) are in agreement with the above findings, detecting illite/smectite mixed-layer clays in smectite treated with 4 M KOH at 80 °C. Illitization would also explain the reduced expandability detected with XRD. The increased Mg concentration and the slight augmentation of octahedral cations might suggest a simultaneous formation of a chlorite-type clay mineral.

The development of chlorite or chlorite precursors during smectite-to-illite transformation is not an uncommon process and has been previously observed in the case of smectite treated with KOH solutions (Eberl et al. 1993, Pusch and Karnland 1996, Bauer and Velde 1999, Drief et al. 2002).

The second group of analyses (i.e., those showing an interlayer charge > 1.02) showed a very variable chemical composition, especially considering the Si concentration. However, some general trends could be identified: The Al content decreased and the Mg and Ca concentrations increased significantly during alkaline treatment. It is assumed that in many cases clay minerals were contaminated by carbonates containing Ca and Mg, amorphous Ca-Mg phases or zeolites. Note that traces of zeolites were detected in the diffractograms of the < 2 µm fraction (Figure 3-58). Calcium-rich impurities would also explain the increase in interlayer charge, in many cases much higher than permissible in a 2:1 clay.

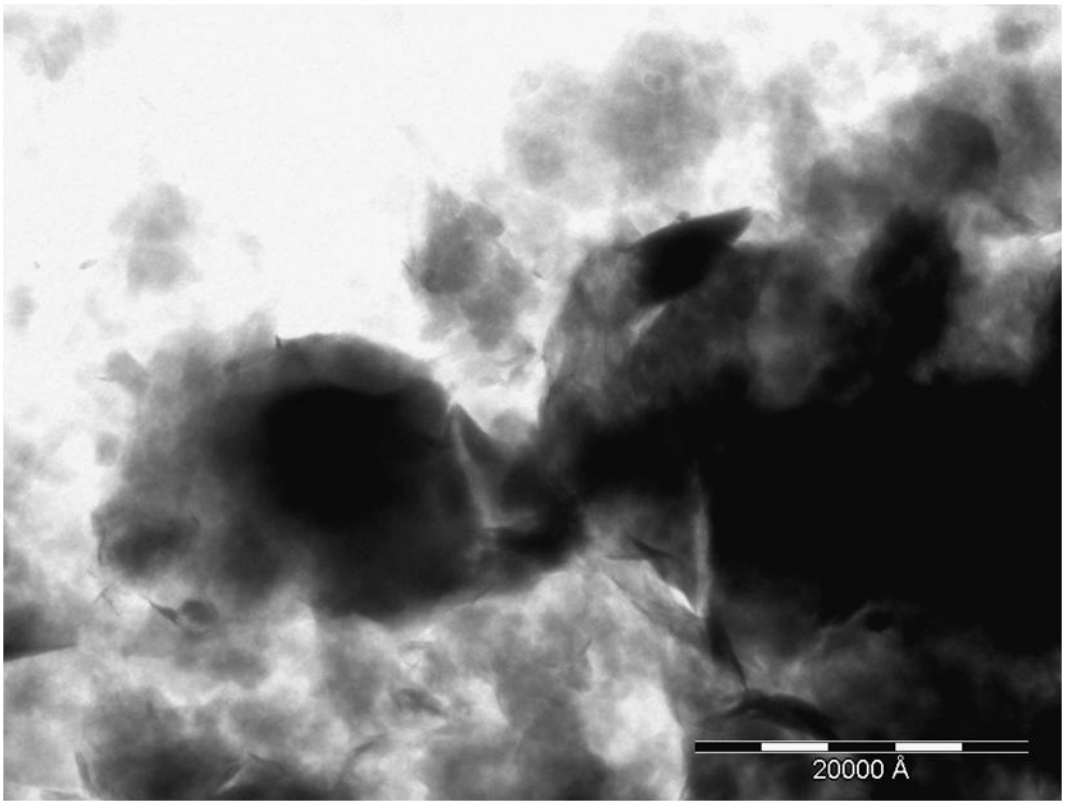

Figure 3-65. TEM image of montmorillonite treated with 5 M KOH for 6 months. Morphological changes cannot be detected.

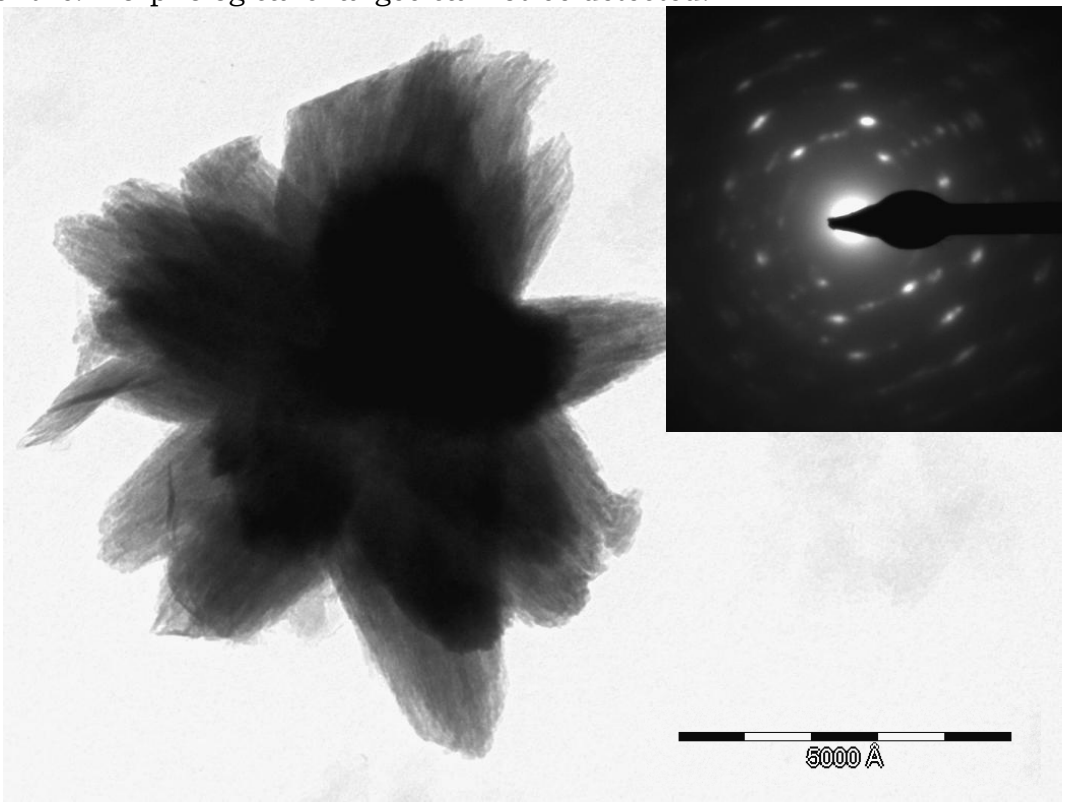

Figure 3-66. TEM image of montmorillonite treated with 5 M KOH for 6 months. Star-shaped calcium carbonate is detected. Inset shows SAED of calcite along the [42$\bar{1}$] zone axis.

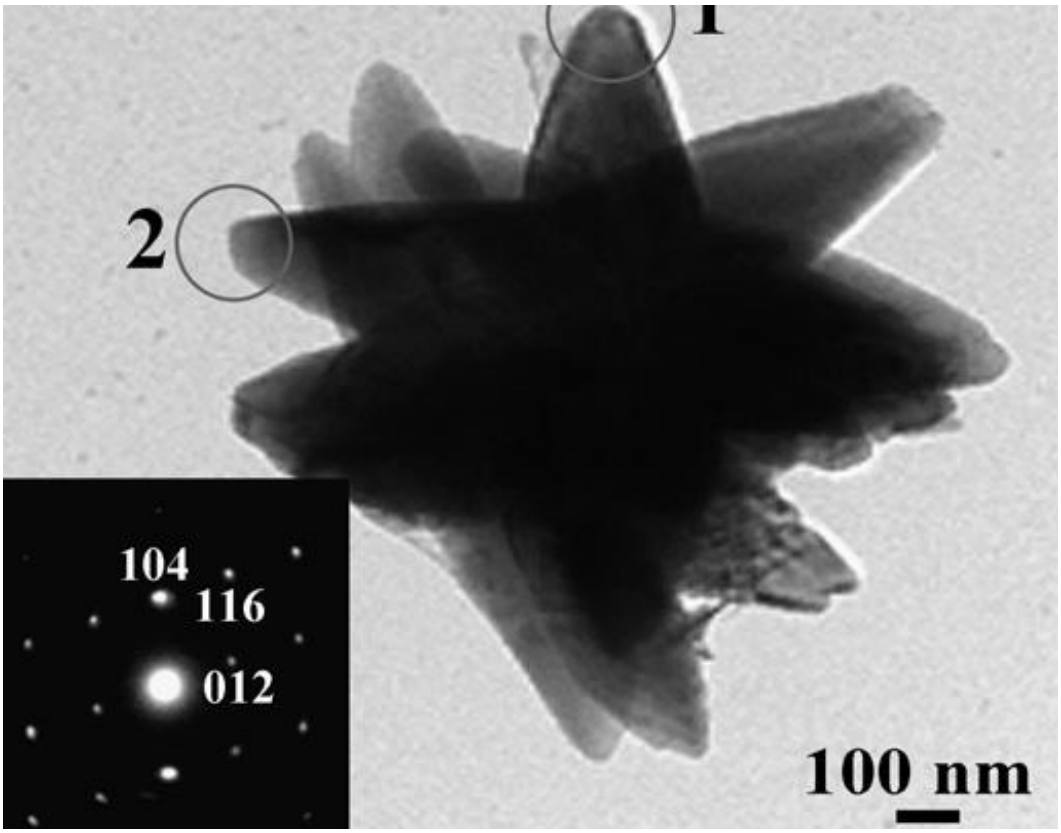

Figure 3-67. Calcium carbonate crystals with the same morphology as that shown in Figure 3-66 have been reported by Jiao et al. (2009).

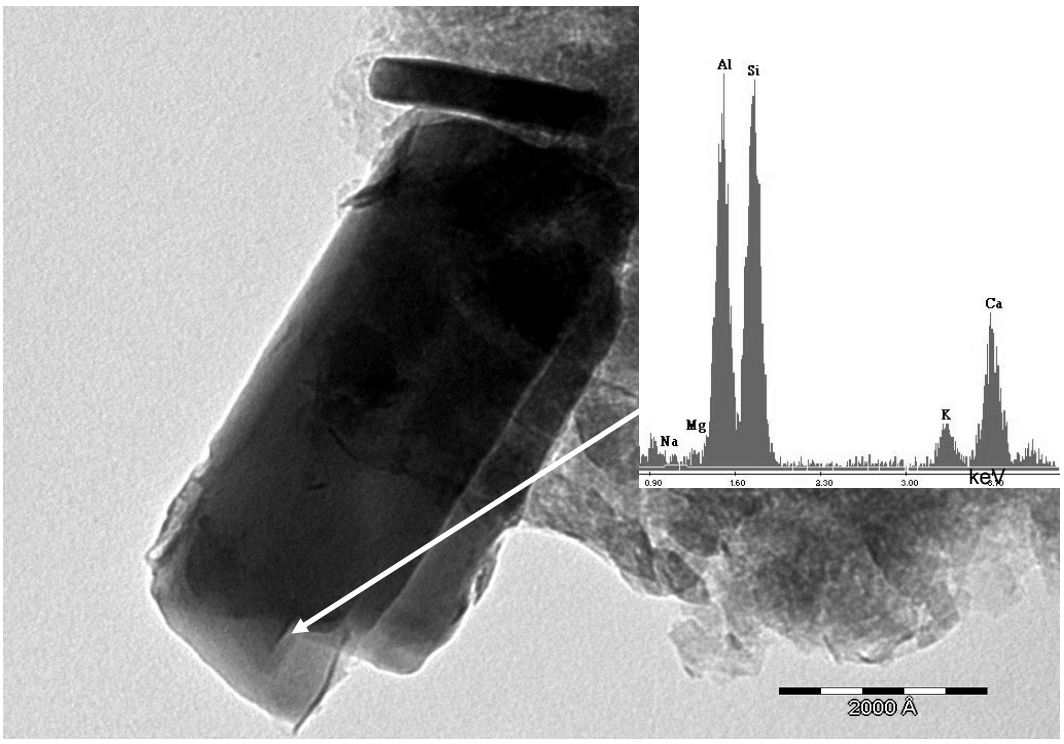

Figure 3-68. TEM image of montmorillonite treated with 5 M KOH for 3.8 years reveals the presence of zeolite K-F (EDS spectrum in inset).

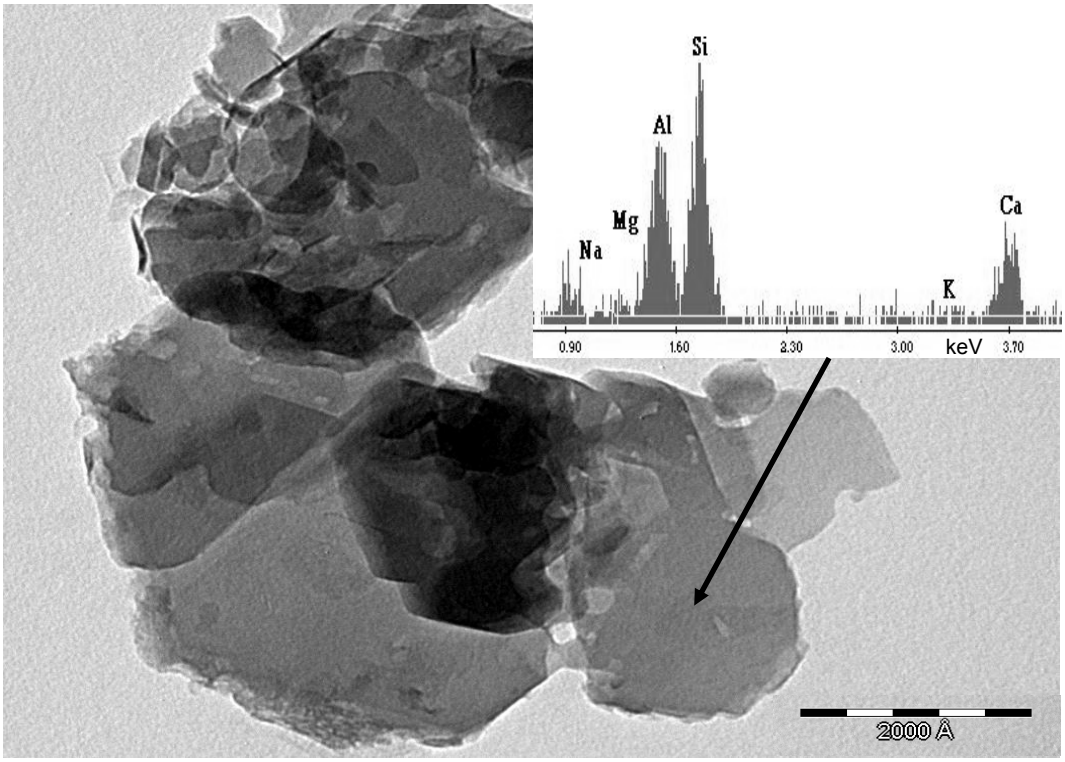

Figure 3-69. TEM image of montmorillonite treated with 5 M KOH for 3.8 years reveals the presence of hexagonal crystals, possibly zeolite K-I (EDS spectrum in inset).

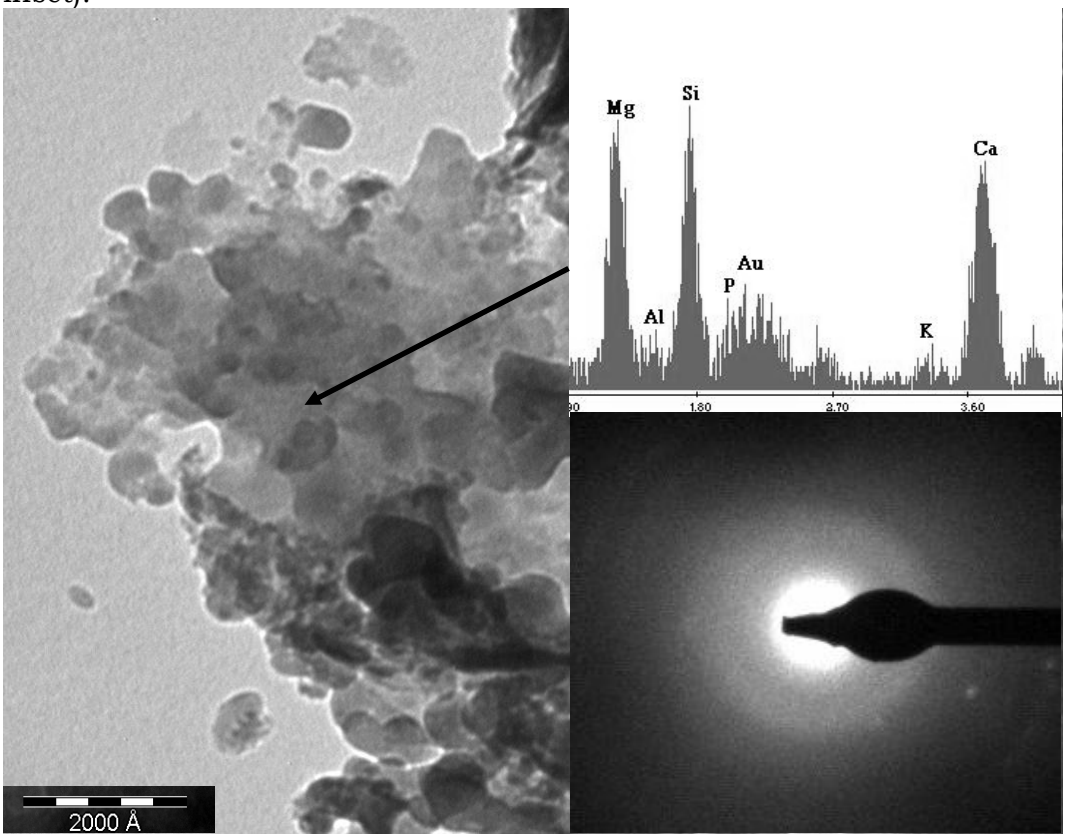

Figure 3-70. TEM image of montmorillonite (< 2 μm fraction) treated with 5 M KOH for 6.3 years. TEM-AEM results reveal the presence of Mg, Si, Ca and minor amounts of Al and K. The SAED pattern (inset) demonstrates the amorphous character of these nano-particles.

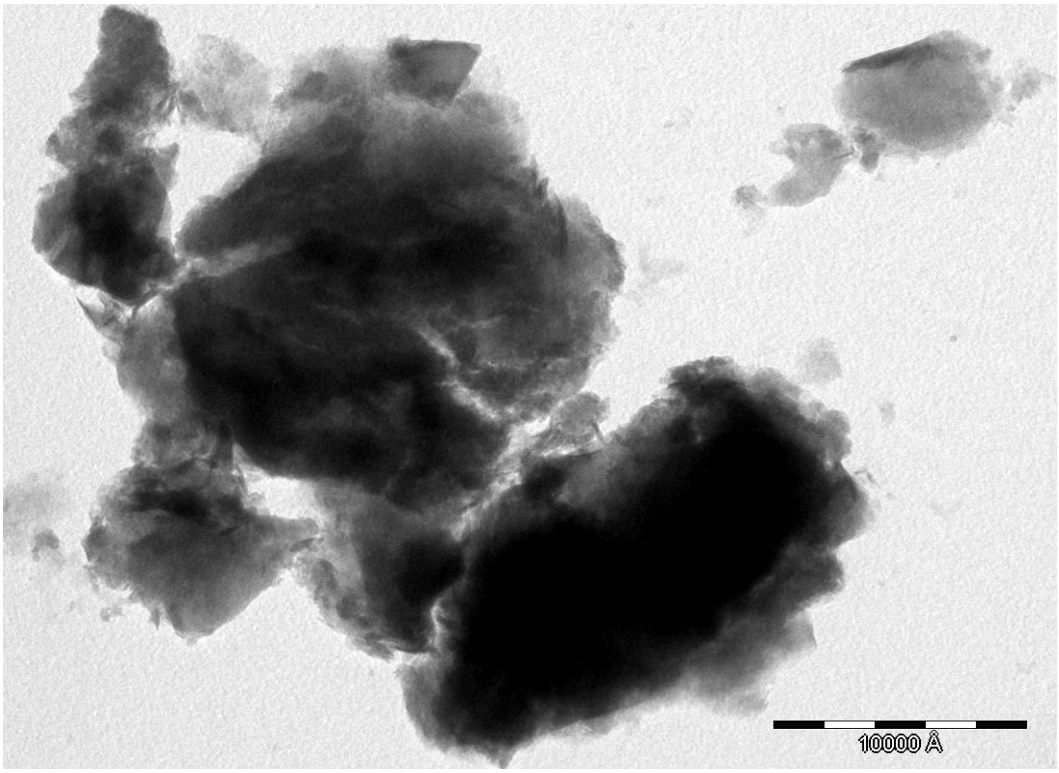

Figure 3-71. TEM image of montmorillonite (< 2 μm fraction) treated with 5 M KOH for 6.3 years. Clay particles have a similar morphology as the untreated montmorillonite.

Table 3-11. Structural formulae of the < 2 μm fraction of montmorillonite treated with 5 M KOH for 6.3 years calculated from TEM-AEM data (the average structural formula of untreated montmorillonite is included)

Structural formulae of montmorillonite based on $O_{10}(OH)_2$										
Analysis	Si	^{IV}Al	^{VI}Al	Mg	Fe	Σoct.cat.[1]	K	Ca	Na	Σint.cha.[2]
Average untreated	3.87 ±0.10	0.14 ±0.10	1.39 ±0.08	0.57 ±0.03	0.15 ±0.05	2.09 ±0.07	0.03 ±0.02	0.08 ±0.05	0.29 ±0.11	0.48 ±0.19
Interlayer charge < 1.02										
1	3.91	0.09	1.08	1.16	*0.10	2.34	0.22	0.17	0.15	0.71
2	3.84	0.16	1.10	1.07	*0.10	2.27	0.22	0.11	0.28	0.72
3	3.80	0.20	1.13	0.90	*0.10	2.13	0.40	0	0.62	1.02
4	3.79	0.21	1.39	0.59	0.11	2.09	0.18	0.07	0.30	0.62
5	3.78	0.22	0.92	1.00	0.20	2.12	0.23	0.18	0.32	0.91
Average 6.3 years	3.82 ±0.05	0.18 ±0.05	1.12 ±0.17	0.94 ±0.22	0.13 ±0.04	2.19 ±0.11	0.25 ±0.09	0.11 ±0.07	0.33 ±0.17	0.80 ±0.16
Interlayer charge > 1.02										
6	3.55	0.45	0.24	2.15	0.13	2.52	0.07	0.33	0.36	1.09
7	3.52	0.48	0.54	1.49	*0.10	2.13	0.19	0.38	0.09	1.04
8	4.01	0	0.70	1.22	*0.10	2.02	0.38	0.52	0	1.42
9	3.90	0.10	0.68	1.22	0.09	1.99	0.15	0.45	0.37	1.34
10	3.82	0.18	0.57	1.43	*0.10	2.10	0.25	0.54	0.29	1.62
11	3.66	0.34	0.46	1.79	0.04	2.29	0.11	0.40	0.38	1.29
12	3.64	0.36	0.80	1.30	*0.10	2.20	0.29	0.42	0.25	1.38
13	3.63	0.37	0.79	1.41	*0.10	2.30	0.39	0.41	0	1.21
14	3.51	0.49	0.80	1.42	*0.10	2.32	0.42	0.25	0.35	1.27
15	3.49	0.51	0.01	2.36	0.02	2.39	0.08	0.70	0.28	1.76
16	3.46	0.56	0.53	1.55	*0.10	2.18	0.41	0.53	0.35	1.82
17	3.44	0.56	0.05	2.16	*0.10	2.31	0.05	0.63	0.79	2.10
18	3.34	0.28	0	2.25	*0.10	2.35	0.08	0.50	0.25	1.33
19	3.21	0.79	0.50	1.59	0.22	2.31	0.26	0.52	0.28	1.58
20	3.06	0.94	0.06	2.24	0.02	2.32	0.25	0.71	0.61	2.28

[1] Sum of octahedral cations
[2] Sum of interlayer charge
* average value based on available data

3.2.3.4. Nitrogen sorption

BET surface area results calculated from nitrogen adsorption data showed that montmorillonite treated for 6 months with 5 M KOH did not experience changes in surface area (Table 3-12). This finding is in agreement with XRD and FESEM results which could not evidence any important mineralogical or morphological changes. However, after 5.3 years of alkaline activation the sample experienced a surface area increase of about 100 % compared with the original clay sample. At this point zeolitic phases, such as zeolite K-F and K-I could be detected with XRD and FESEM. Nevertheless, the reason for the surface area increase is not clear because mainly the external zeolite surface area is assumed to contribute to the samples total surface area (see section 4.3.2.).

The nitrogen sorption isotherm of the montmorillonite sample activated using KOH experienced similar modifications as the one treated with NaOH (Figure 3-72). The type H3 hysteresis loop was less pronounced than the one of the untreated montmorillonite, indicating the destruction of a significant amount of smectite. However, the influence of the presence of smectite (evidenced using XRD, FESEM and TEM) on the shape of the hysteresis loop of the sample treated for 5.3 years with 5 M KOH was still observed.

Table 3-12. BET surface area of untreated montmorillonite and montmorillonite treated with 5 M KOH.

Treatment time	Surface area (m^2/g)
0	63.58 ± 0.45
6 months	60.24 ± 0.33
5.3 years	123.22 ± 0.47

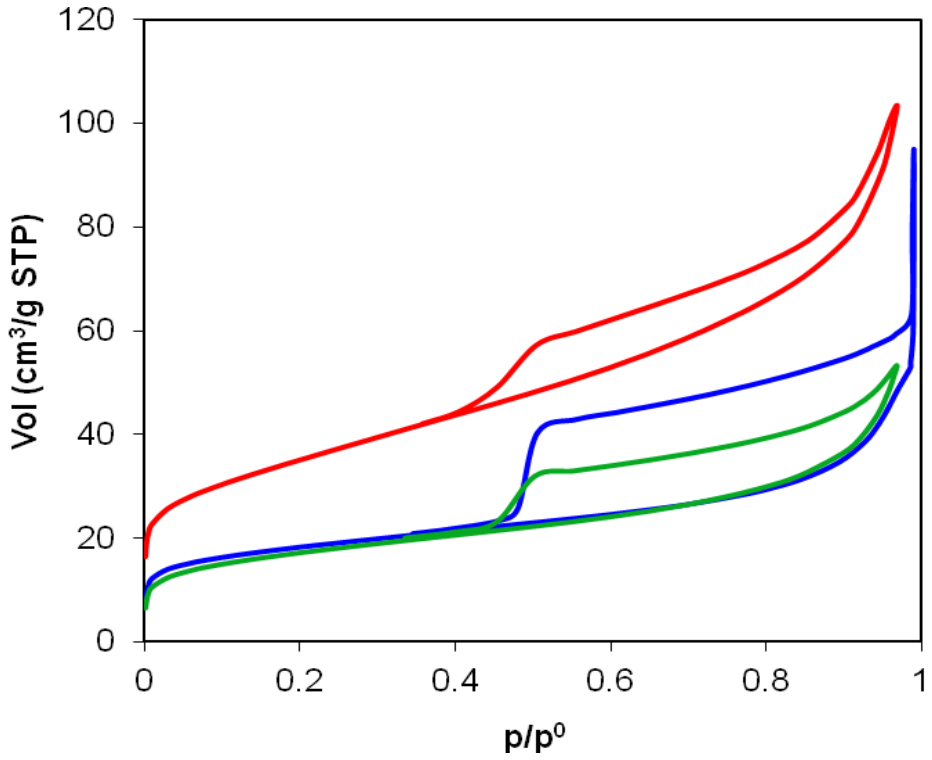

Figure 3-72. Nitrogen sorption isotherms of untreated montmorillonite (blue) and montmorillonite treated with 5 M KOH for 6 months (green) and 5.3 years (red).

3.3. Characterization of trioctahedral smectite (saponite)

The following sections include the characterization of the untreated saponite and the study of its mineralogical evolution upon alkaline activation using NaOH and KOH.

3.3.1. Untreated saponite

3.3.1.1. XRF

Table 3-13 shows XRF results of the < 2 μm fraction of untreated saponite. The composition of the trioctahedral smectite was in good agreement with published results for saponite from the same area, the Madrid basin (Suarez Barrios et al. 1996). The higher Na_2O and P_2O_5 concentrations were due to impurities caused by sodium hexametaphosphate (Calgon) added during sample preparation. These impurities result in slightly lower Si, Al and Mg concentracions.

The chemical analysis resulted in the following structural formula (not considering P_2O_5): $Na_{0.29}K_{0.05}Ca_{0.13}(Al_{0.06}Fe_{0.09}Mg_{2.60}Ti_{0.03})(Si_{3.68}Al_{0.32})O_{10}(OH)_2$

Table 3-13. XRF results of the starting material (wt %)

Material	SiO_2	Al_2O_3	Fe_2O_3	Na_2O	P_2O_5	MgO	K_2O	CaO	TiO_2	Loss on Ignition	Total
Trioctahedral smectite < 2 μm	45.81	4.05	1.55	1.89	2.97	21.67	0.49	0.76	0.23	20.00	99.42
Saponite Yuncillos < 2 μm*	49.45	4.72	1.29	0.07	-	24.34	0.44	0.78	0.20	18.31	99.6

* Suarez Barrios et al. (1996)

3.3.1.2. XRD

XRD analyses showed that this sample contained saponite and small amounts of illite (Figure 3-73). The presence of saponite is consistent with the appearance of a strong peak centered at 13 Å which shifted to 17 Å following EG treatment, to 19 Å following DMSO treatment and collapsed to 10 Å after heat treatment. Suarez Barrios et al. (1996) reported that the saponite from the same area contained a small amount of sepiolite which in our case was only observed using FESEM and TEM (Figure 3-75 and 3-82, see below). The XRD pattern matches fairly well that of a saponite with the following formula: $Ca_{0.2}Mg_3(SiAl)_4O_{10}(OH)_2 \cdot xH_2O$ (JPDF card no. 291491).

The crystallite size of the saponite was 5 nm. This value is in good agreement with published data (Vicente Valverde 2010).

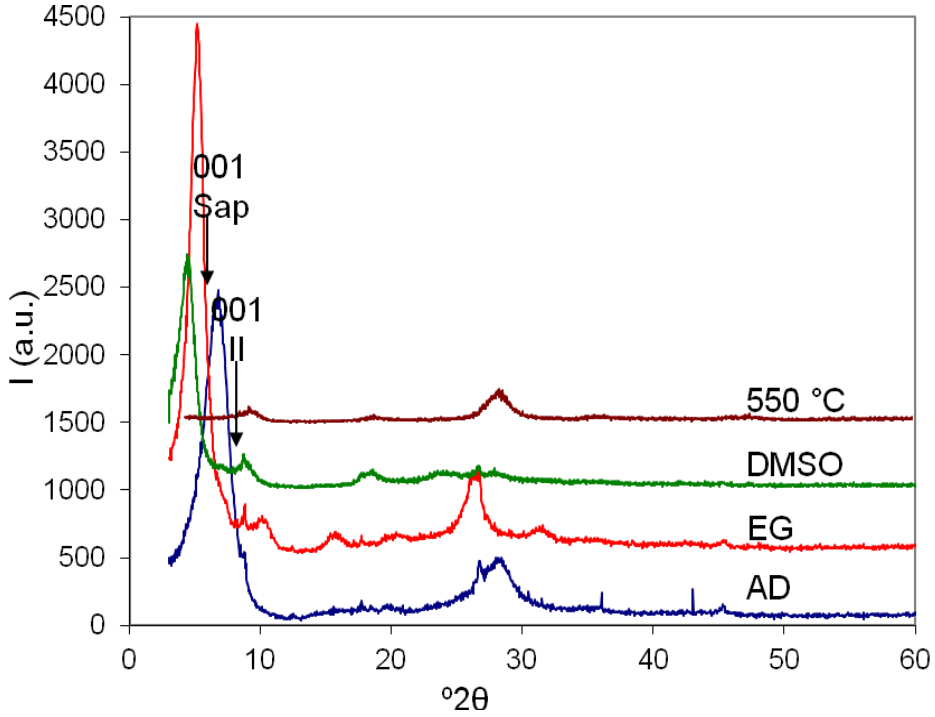

Figure 3-73: XRD of saponite. OA air-dried (AD), treated with EG, DMSO and heat treated. Sap = saponite, Il = illite.

3.3.1.3. FESEM

The FESEM image (Figure 3-74) shows the typical flake-like structure with irregular outline of saponite crystals (Deer et al. 1962, Wilson et al. 1968). The EDS analysis (inset, Figure 3-74) revealed large amounts of Si and Mg together with minor amounts of Al. These are the main elements of saponite.

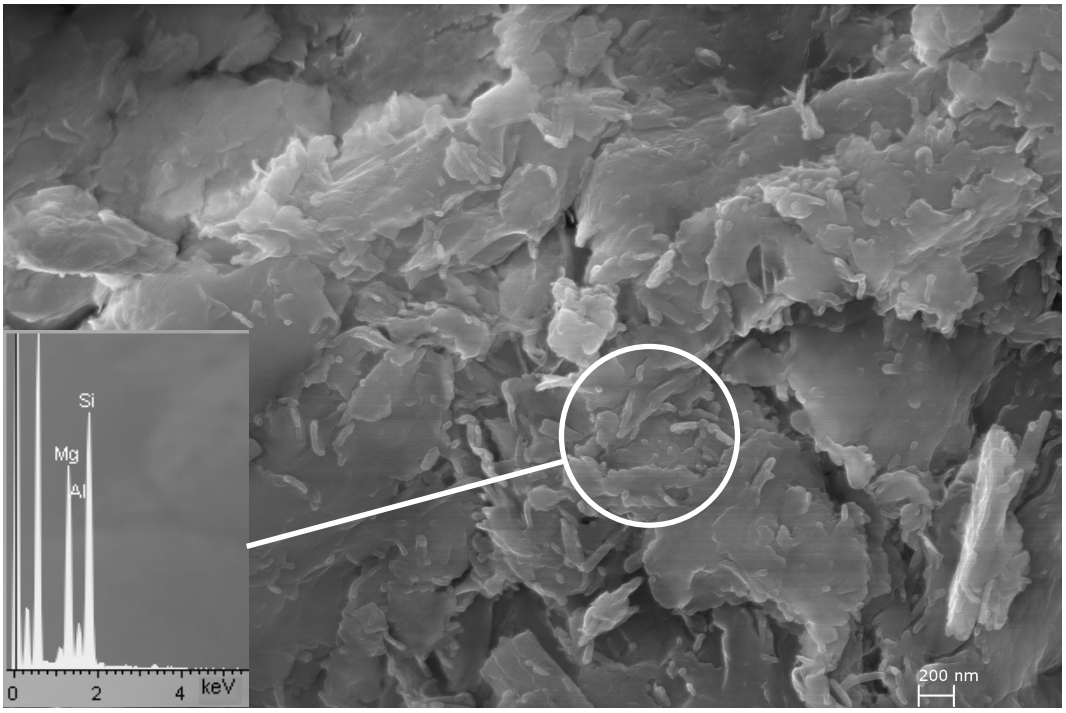

Figure 3-74. FESEM image and EDS spectrum of untreated saponite

3.3.1.4. TEM

TEM observations (Figure 3-75) revealed the presence of saponite particles together with sepiolite fibres in the untreated clay sample. AEM analyses (Table 3-14) showed that the tetrahedral layer of saponite only contains Si. This is not in agreement with the structural formula calculated from XRF data and, in general, saponite is assumed to have tetrahedral substitution. The discrepancy might be explained considering the presence of impurities such as illite and sepiolite. Especially, contamination due to the presence of sepiolite fibres might have resulted in an increase in tetrahedral Si in the case of the structural formula calculated based on TEM-AEM data. Note that the sum of the octahedral cations is < 3. Therefore, all Mg is assumed to be present in the octahedral layer and not as interlayer cations.

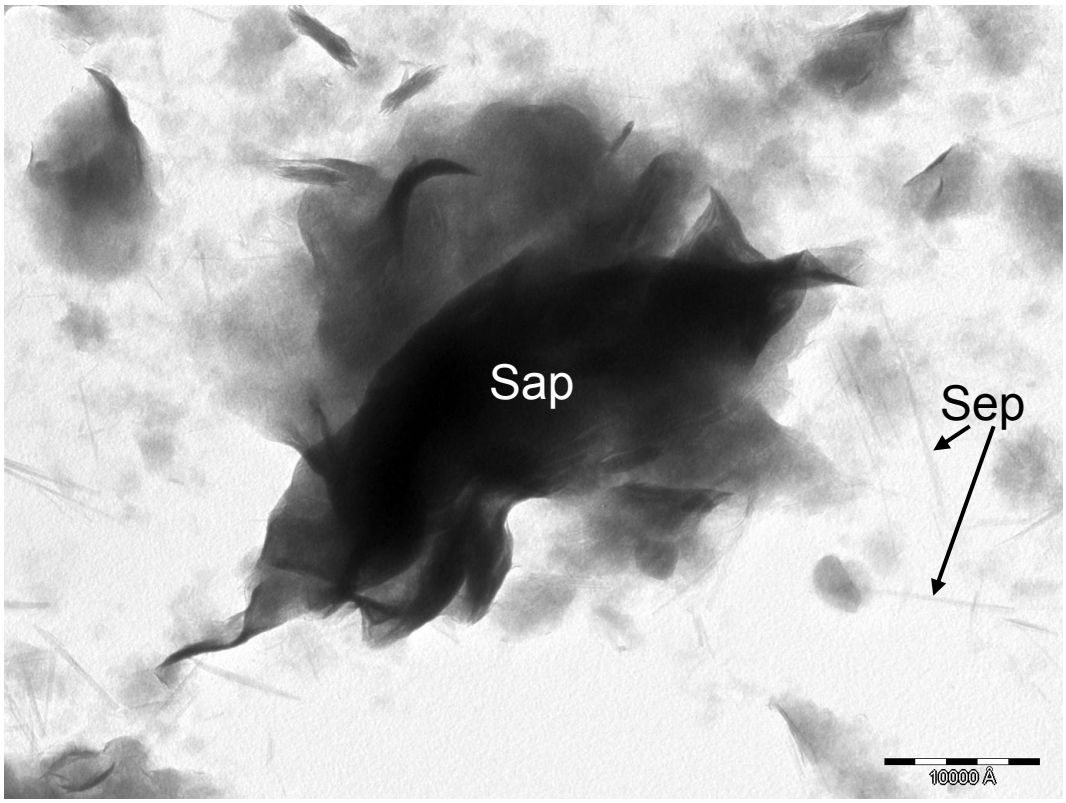

Figure 3-75. TEM image of untreated saponite. The sample contains saponite (Sap) and numerous sepiolite fibres (Sep).

Table 3-14. AEM analyses of untreated saponite and sepiolite

Structural formulae of saponite based on $O_{10}(OH)_2$										
Analysis	Si	^{IV}Al	^{VI}Al	Mg	Fe	Σoct.cat.[1]	K	Ca	Na	Σint.cha.[2]
1	3.97	0.03	0.49	2.19	0.04	2.72	0.06	0.02	*	**
2	4.07	0.00	0.34	2.26	0.07	2.67	0.00	0.00	*	**
3	3.98	0.02	0.33	2.48	0.00	2.81	0.02	0.02	*	**
4	3.98	0.02	0.37	2.35	0.06	2.78	0.02	0.02	*	**
5	4.05	0.00	0.41	2.21	0.07	2.69	0.00	0.00	*	**
6	4.13	0.00	0.32	2.25	0.02	2.59	0.00	0.00	*	**
7	4.04	0.00	0.34	2.39	0.02	2.75	0.00	0.00	*	**
average	4.03 ±0.06	0.01 ±0.01	0.37 ±0.06	2.30 ±0.11	0.04 ±0.03	2.72 ±0.07	0.01 ±0.02	0.01 ±0.01	*	**
Structural formulae of sepiolite based on $O_{15}(OH)_2$										
8	6.24	0.00	0.00	3.12	0.11	3.23	0.00	0.00	*	**
9	5.62	0.00	0.00	4.40	0.28	4.68	0.00	0.00	*	**

[1] Sum of octahedral cations
[2] Sum of interlayer charge
* not analyzed
** not calculated

3.3.1.5. Nitrogen sorption

The surface area of the untreated saponite was 143.75 ± 1.16 m^2/g, which is about 10 % lower than the value reported by Prieto et al. (1999) and Suarez Barrios et al. (1996). The reported values for saponite from the Yuncillos deposit, the same clay used in this study, were 161 and 165 m^2/g, respectively.

As in the case of the montmorillonite, the nitrogen sorption isotherm was of type II with a pronounced hysteresis loop of type H3 (Figure 3-76).

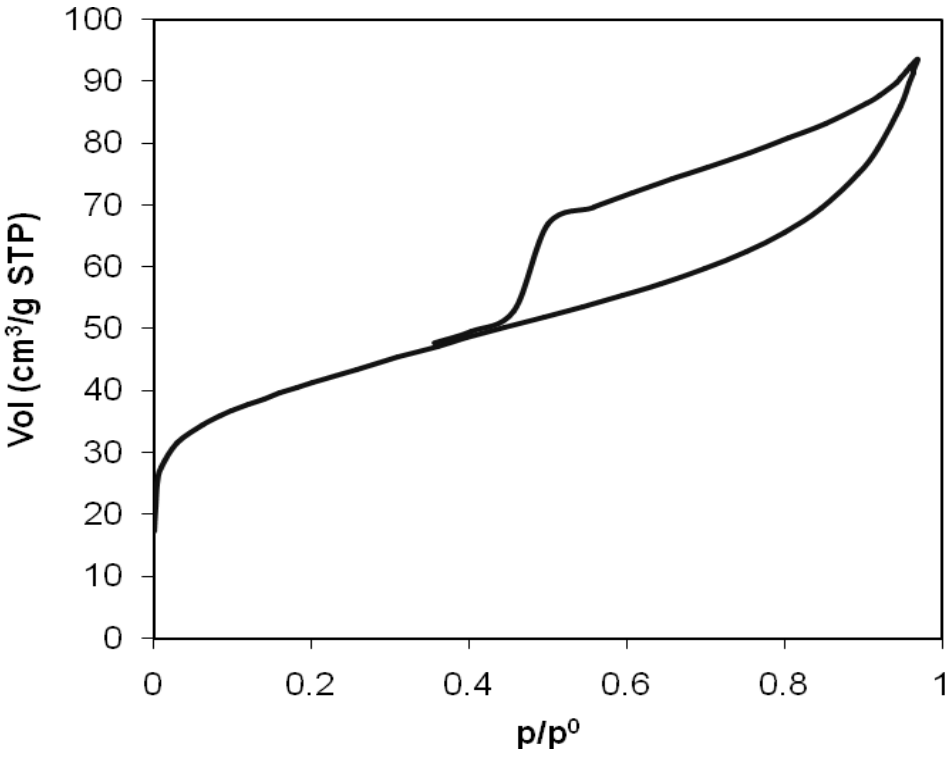

Figure 3-76. Nitrogen sorption isotherm of untreated saponite.

3.3.1.6. Particle size analysis

Saponite showed a particle size distribution quite similar to that of montmorillonite, having a primary maximum at 140 nm and a secondary maximum between 0.5 – 20 μm which is caused by clay particle aggregates (Figure 3-77).

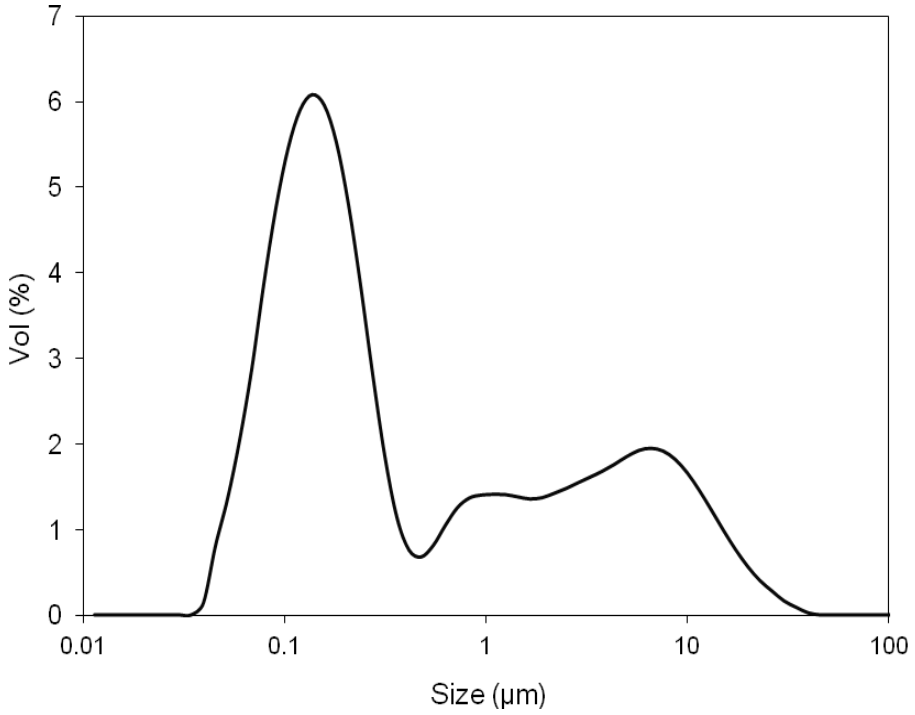

Figure 3-77. Particle size distribution of untreated saponite

3.3.1.7. TG

The thermogravimetric curve showed a rapid loss of adsorbed water of 15.5 % from 30°C to 300 °C (Figure 3-78). Between 300 °C and 750 °C weight loss was gradual and amounted to 1.8 %. Above 750 °C the dehydroxylation of the saponite began and ended at 890 °C. The high thermal stability of saponite and dehydroxylation temperatures around 800 °C have been mentioned by Kawano and Tomita (1991) and Cuevas et al. (2001). The total weight loss of the here tested sample amounted to 20 %, being about 1.8 % due to dehydroxylation. Suarez-Barrios et al. (1996) and Vicente et al. (2001) observed a very similar trend and a total weight loss between 18-19 % for samples from the same deposit.

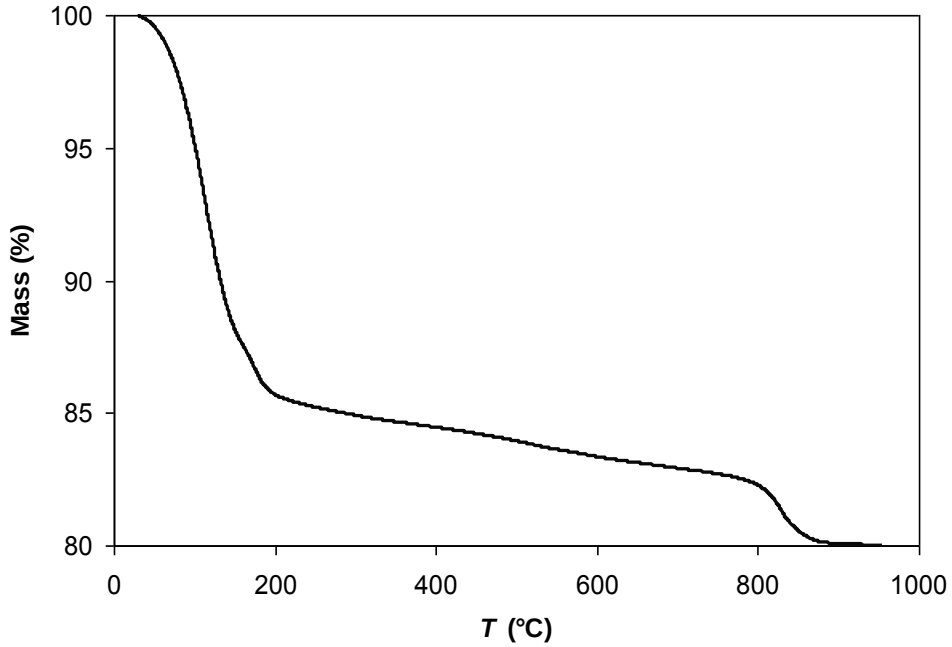

Figure 3-78. Thermogravimetric curve of untreated saponite.

3.3.2. Saponite treated with NaOH

3.3.2.1. XRD

XRD analyses of saponite (Figure 3-79) did not reveal significant mineralogical changes after 6 months of treatment using 5 M NaOH. Nevertheless, a peak at 3.04 Å was observed which corresponds to calcite.

1-year treatment still did not result in any modifications.

However, after 4.7 years of treatment the 001 Bragg peak of saponite shifted from 13 Å to 14.7 Å and additional peaks at 9.7, 7.4, 4.9, 3.7 and 2.9 Å appeared. This result suggests a transformation of the saponite into an interstratified saponite-chlorite. The above mentioned reflections of the newly formed phase were in quite good agreement with a corrensite with the following formula: $Mg_8Al_3Si_6O_{20}(OH)_{10}{\cdot}4H_2O$ (JPDF card no.130190). However, the 001 reflection of the corrensite, typically at ~ 29 Å (Abad et al. 2003, Hauff 1981), was absent, indicating that the sample lacked regularity. Note that the number of well defined 00*l* sub-orders was too small to calculate the coefficient of variation of the *d*(00*l*) values which would have given the degree of regularity (Bailey 1982). The randomly interstratified saponite-chlorite might be considered as a transition phase towards a regular corrensite (personal communication Nieto Garcia, F., 10.2.14). Corrensite, in turn, is often identified as an intermediate phase in the smectite-chlorite transformation (Beaufort et al. 1997, Brigatti and Poppi 1984, Bristow et al. 2009, Murakami et al. 1999).

Diffractograms of the sample treated with 5 M NaOH for 7.1 years (Figure 3-80) showed that after EG solvation, the Bragg peak at 14.7 Å shifted to 15.5 Å and not to 17 Å as in the case of the untreated saponite. Heat treatment at 550 °C caused a collapse of this Bragg peak to 12 Å. These results are further evidence that saponite has transformed into a saponite-chlorite interstratification. Actually, regular saponite-chlorite interstratifications (corrensite) reveal a very similar behaviour upon EG solvation and heating. The 002 Bragg peak of corrensite is reported to expand to about 15.5 Å and collapse to 12 Å, respectively (Hauff 1981, Beaufort and Meunier, 1994).

XRD analysis of the sample after prolonged alkaline activation neither allowed the identification of the poorly crystalline, gel-like phase detected with FESEM (see Figure 3-87) nor any crystalline zeolitic phases.

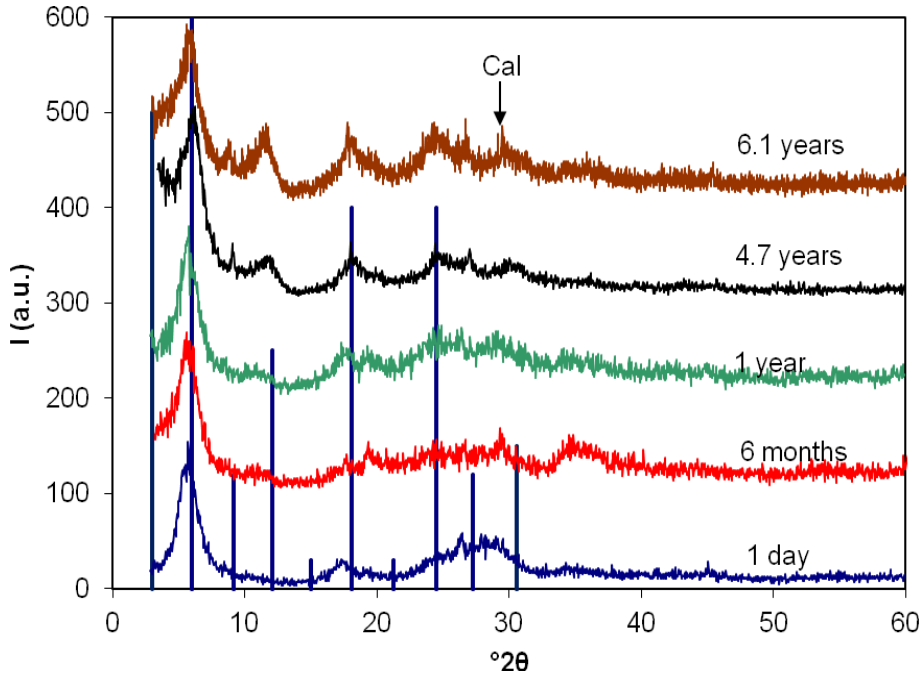

Figure 3-79: XRD patterns showing the mineralogical evolution of saponite treated with 5 M NaOH for different periods of time. Blue line pattern: Corrensite (JPDF card no. 130190), Cal = calcite.

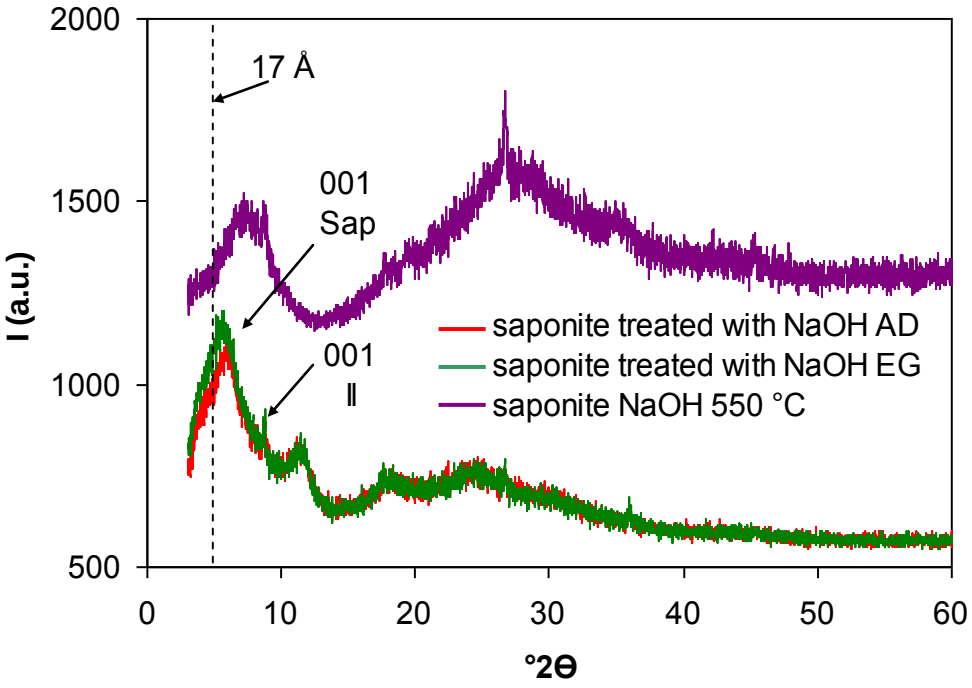

Figure 3-80. XRD patterns of OA of saponite treated with 5 M NaOH for 7.1 years. OA air-dried (AD), after EG solvation and heat-treated at 550 °C. Sap = saponite, Il = illite.

3.3.2.2. FESEM

FESEM analyses did not reveal any morphological changes of the clay mineral after 6 month-treatment with 5 M NaOH. However, some hexagonal plates formed (Figure 3-81) which are typical for portlandite ($Ca(OH)_2$) (Elert et al. 2002). It is assumed that the interlayer Ca^{2+} of saponite was exchanged with Na^+ from the alkaline activator and precipitated as portlandite at the high pH of the NaOH solution (pH ~ 13). Ca^{2+} of the tap water used during sample preparation might have been an additional source of Ca (personal communication, Nieto Garcia, F., 15.12.13).

1 year-treatment did not result in any appreciable morphological or compositional changes of the saponite (Figure 3-82).

After 4.7 years of treatment (Figure 3-83), crystals with a "sheaf of wheat"-like morphology were observed. The high concentrations of Ca and C shown by EDS microanalyses allowed their identification as calcite crystals. These findings are consistent with XRD results. A similar type of morphology has been previously documented for calcite crystals (Figure 3-84, Tracy et al. 1998) and can also be observed in the case of a calcite from Linares, Jaen (Figure 3-85).

Even after 6.1 years of treatment the morphology of saponite did not seem to have experimented important modifications (Figure 3-86). EDS microanalysis showed a very similar composition as the one of the original clay, only K experienced a small increase (inset, Figure 3-86). Furthermore, nanosized gel-like particles were observed in the sample activated for 6.1 years (Figure 3-87). EDS analysis showed the presence Na, Mg, Si and Ca and small concentrations of Al, Cl and K in these particles. Golden et al. (1985) detected the formation of an X-ray amorphous material after sepiolite had been treated with NaOH at 150 °C and Cuevas Rodriguez (1993) reported the formation of amorphous silica upon sepiolite dissolution. In this study sepiolite did not experience significant alteration upon NaOH treatment as evidenced by TEM (see Figure 3-88), thus, the source material for this gel-like phase could not be determined unambiguously. Due to the gel-character of this phase its identification was not possible using XRD. A well crystallized zeolitic phase was not observed in the saponite sample using FESEM.

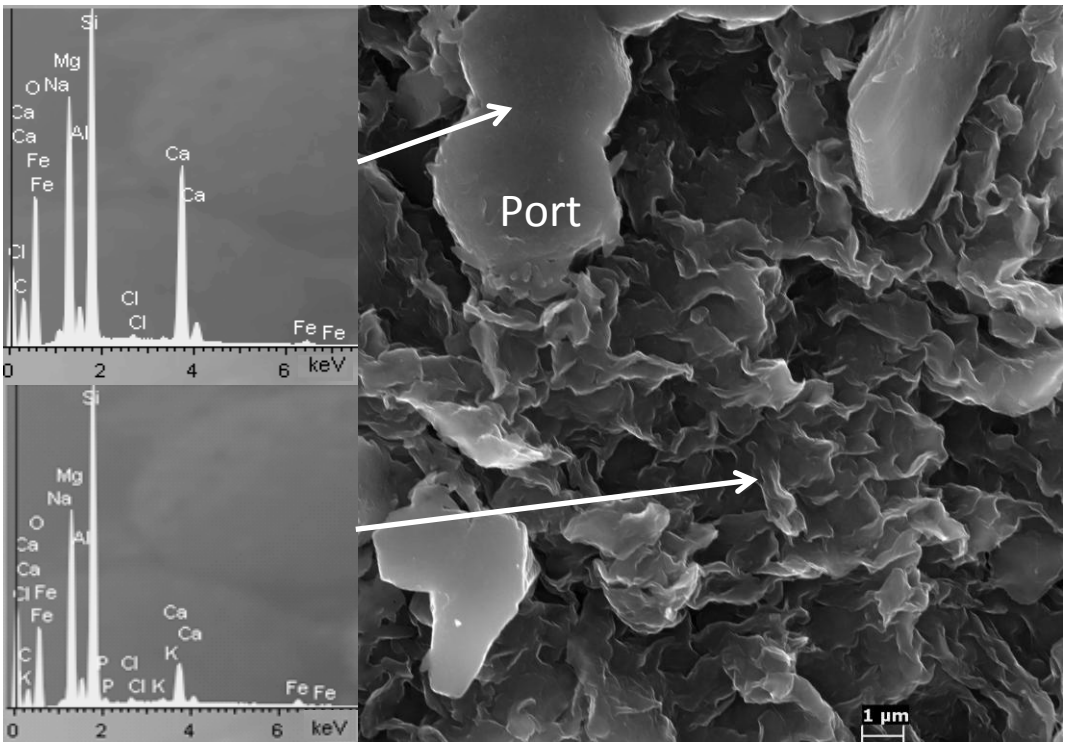

Figure 3-81. FESEM image of saponite treated with 5 M NaOH for 6 months. The hexagonal plates are tentatively identified as portlandite (Port) (EDS in insets).

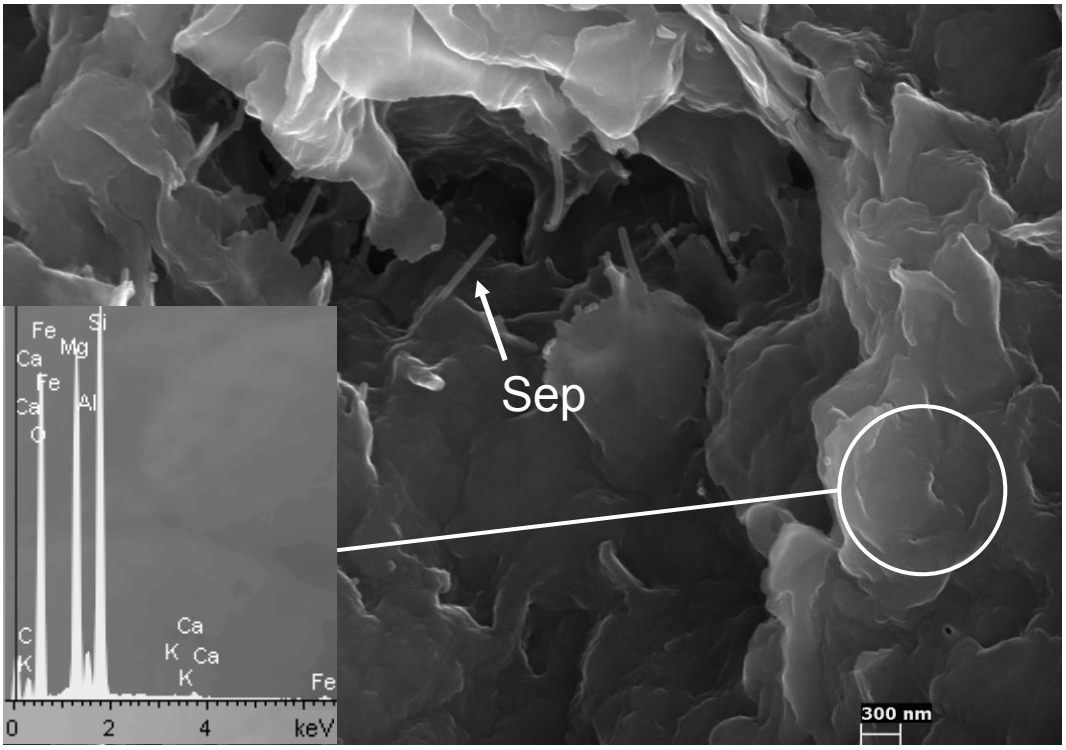

Figure 3-82. FESEM image of saponite treated with 5 M NaOH for one year. Morphological or compositional changes cannot be appreciated (EDS in inset). Fibrous clay, most likely sepiolite (Sep), can be observed.

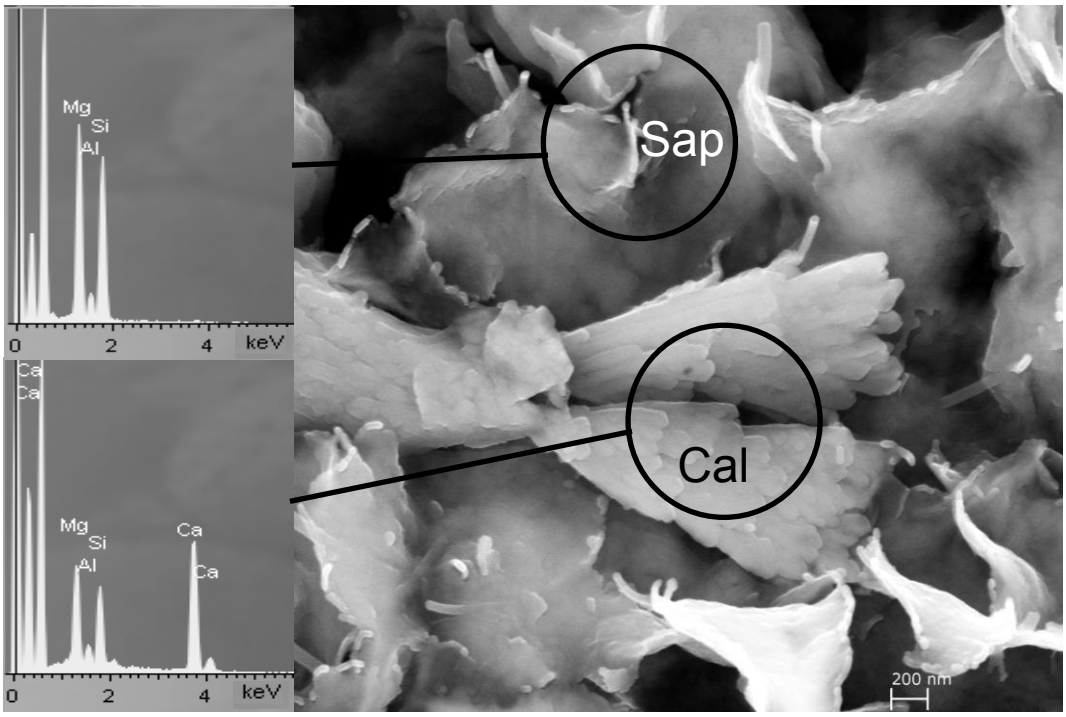

Figure 3-83. FESEM image of saponite treated with 5 M NaOH for 4.7 years. Unreacted saponite (Sap) and calcite crystals (Cal) with "sheaf of wheat" morphology are observed (EDS spectra in insets).

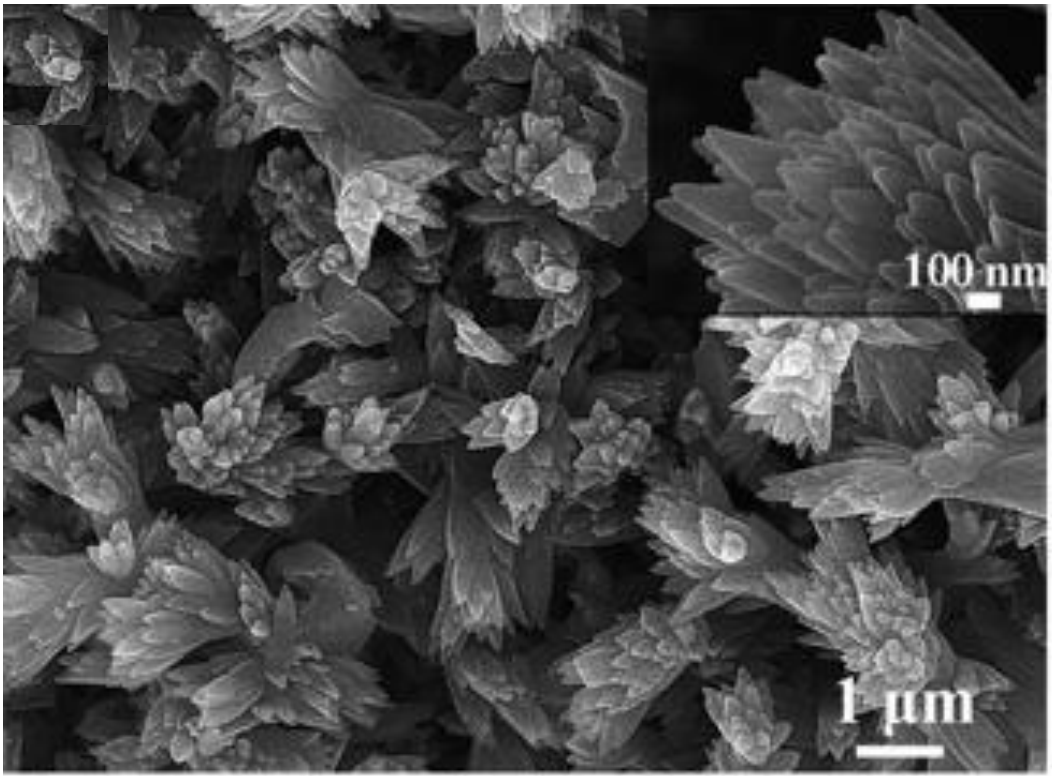

Figure 3-84. SEM images of $CaCO_3$ crystal of similar morphology as those observed in this study (Jiao et al. 2009).

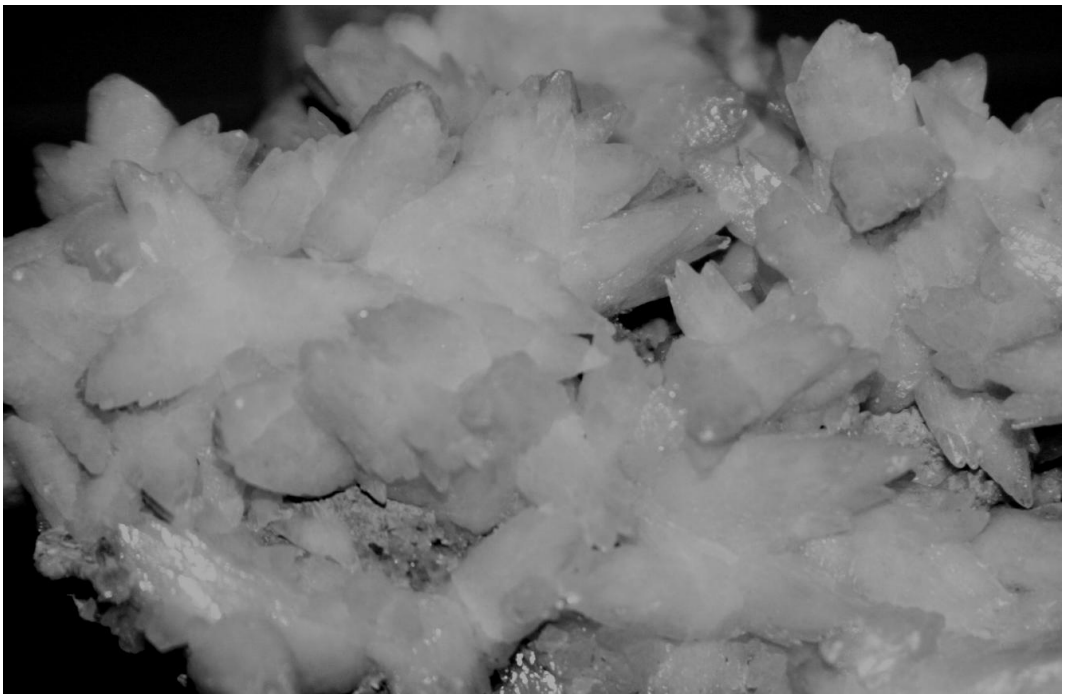

Figure 3-85. Calcite from Linares (Jaen, Spain) showing a similar morphology as that of calcite crystals observed in the saponite treated with 5 M NaOH for 4.7 years (Mineral collection, Department of Mineralogy and Petrology, University of Granada). Field of view: 60 mm.

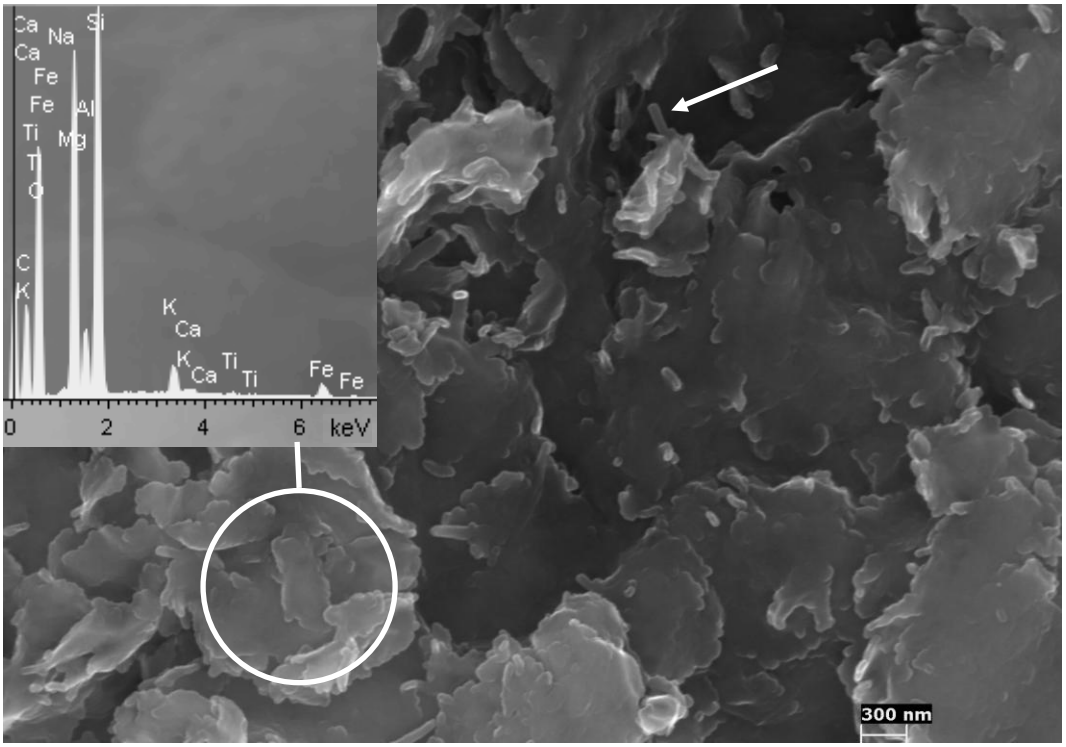

Figure 3-86. FESEM image of saponite treated with 5 M NaOH for 6.1 years. The saponite and sepiolite (arrow) crystals morphology seems unchanged. The slightly increased K content revealed by EDS microanalysis might be due to illite impurities.

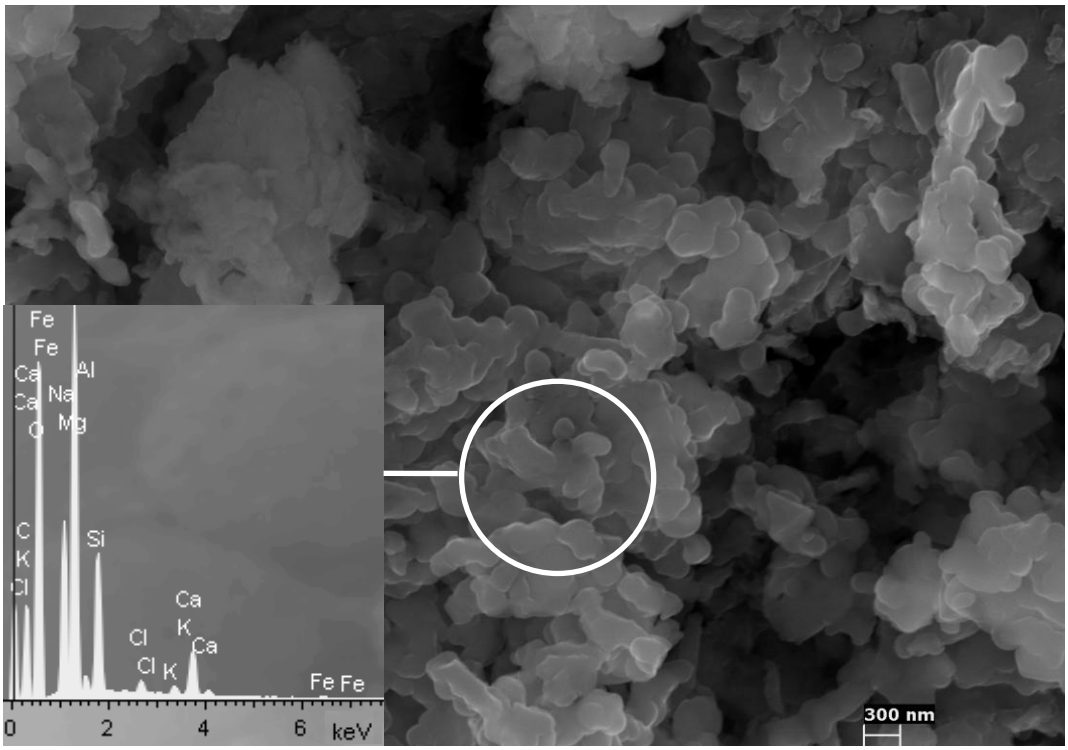

Figure 3-87. FESEM image of saponite treated with 5 M NaOH for 6.1 years. An aggregate of gel-like particles rich in Mg, Na and Si can be observed (EDS in inset).

3.3.2.3. TEM

TEM observations revealed no morphological changes in saponite treated with NaOH for 6.1 years (Figure 3-88). Sepiolite was also still present in the sample. Cuevas Rodriguez (1993), however, reported that illite and sepiolite present in trace amounts in saponite from the same area underwent severe degradation under hydrothermal conditions at 175 °C and neutral pH in the absence of K ions, while saponite remained basically unchanged. Here this tendency was not observed which might be due to the significantly lower treatment temperature (25 °C) of this study. Golden et al. (1985) detected a thinning of sepiolite fibers upon NaOH treatment evidenced by TEM analyses. We could not detect fiber thinning.

TEM-AEM analyses revealed gradual compositional changes in saponite upon alkaline treatment. Changes were already detected after 6 months of treatment. The structural formulae calculated based on TEM-AEM results indicated that the Si concentration decreased while Al, Fe and, especially, Mg increased (Table 3-15). Note that all structural formulae are calculated based on $O_{20}(OH)_{10}$, taking into account the structural formula of corrensite. Upon alkaline activation Al entered in the tetrahedral layer which was previously only occupied by Si. The octahedral layer experienced an important increase in Mg while the Al concentration decreased slightly. These results suggest that

saponite experienced a chloritization process and transformed into a random saponite-chlorite interstratification. Compared with published data for regular saponite-chlorite interstratification (Brigatti and Poppi 1984, Newman and Brown 1987), the Si concentration is still quite high after 6.1 years of treatment, indicating that the chloritization process might not be complete.

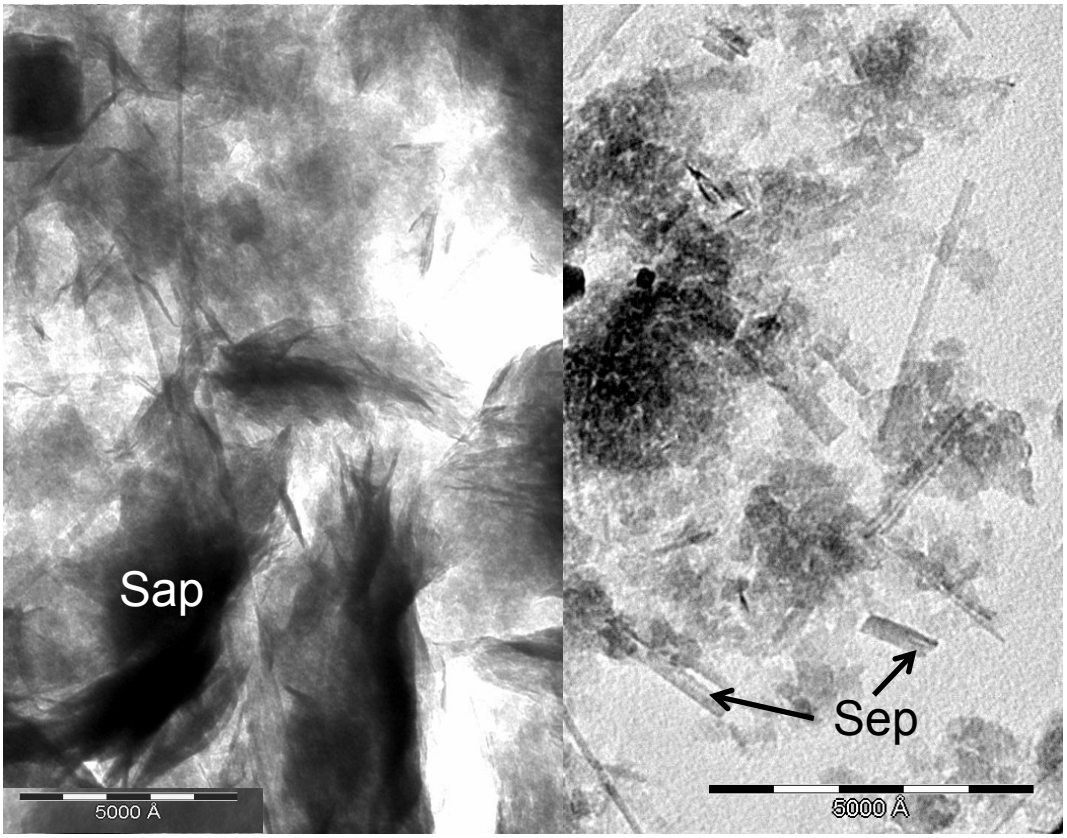

Figure 3-88. TEM images of saponite treated with 5 M NaOH for 6.1 years. Fibrous clay (sepiolite) can be detected. Sap = saponite, Sep = sepiolite.

Table 3-15. AEM analyses of saponite treated with 5 M NaOH for 6 months, 1 year and 6.1 years (for comparison the average structural formula of untreated saponite based on $O_{20}(OH)_{10}$ is included). The composition of the newly formed phase is close to corrensite ($Mg_8Al_3Si_6O_{20}(OH)_{10}\cdot 4H_2O$ JPDF card no.130190)

Structural formulae of saponite treated with 5 M NaOH for 6 months, 1 year and 6.1 years based on $O_{20}(OH)_{10}$										
Analysis	Si	^{IV}Al	^{VI}Al	Mg	Fe	Σoct.cat.[1]	K	Ca	Na	Σint.cha.[2]
Untreated saponite average	9.16 ±0.14	0.00	0.87 ±0.16	5.23 ±0.25	0.09 ±0.07	6.19 ±0.16	0.02 ±0.05	0.02 ±0.02	*	**
1	8.03	0.00	0.77	7.56	0.12	8.45	0.00	0.09	*	**
2	8.13	0.00	0.87	7.43	0.00	8.30	0.00	0.00	*	**
3	8.25	0.00	0.81	7.09	0.12	8.02	0.00	0.04	*	**
4	8.84	0.00	0.87	5.75	0.08	6.70	0.00	0.16	*	**
6 months average	8.31 ±0.36	0.00	0.83 ±0.05	6.96 ±0.83	0.08 ±0.06	7.87 ±0.80	0.00	0.07 ±0.07	*	**
5	7.97	0.03	0.86	7.51	0.08	8.45	0.04	0.09	*	**
6	8.09	0.00	0.99	7.02	0.12	8.13	0.08	0.13	*	**
7	7.56	0.44	0.59	8.05	0.17	8.81	0.09	0.04	*	**
1 year average	7.87 ±0.28	0.16 ±0.25	0.81 ±0.20	7.53 ±0.52	0.12 ±0.05	8.46 ±0.34	0.07 ±0.03	0.09 ±0.05	*	**
8	6.75	1.25	0.77	7.68	0.63	9.08	0.00	0.00	*	**
9	7.18	0.82	0.36	8.66	0.17	9.19	0.00	0.00	*	**
10	7.38	0.62	0.76	7.84	0.25	8.85	0.00	0.00	*	**
6.1 years average	7.10 ±0.32	0.90 ±0.32	0.63 ±0.23	8.06 ±0.53	0.35 ±0.25	9.04 ±0.17	0.00	0.00	*	**

[1] Sum of octahedral cations
[2] Sum of interlayer charge
* not analyzed
** not calculated

3.3.2.4. Nitrogen sorption

Nitrogen sorption data showed that saponite treated for 6.1 years with 5 M NaOH did not experience important changes in BET surface area (Table 3-16). The reason for the ~ 7 % increase in surface area of the sample treated for 6 months was unclear, and could be due to slight variations in sample preparation. Actually, a surface area decrease was expected in the case of the saponite sample treated with 5 M NaOH, transforming into a saponite-chlorite interstratification. This intermediate phase in the smectite-chlorite transformation, should have a lower surface area than the untreated saponite due to the contribution of chlorite. The reported surface area for a regular saponite-chlorite interstratification (corrensite) from the Source Clays Repository of the University of Missouri is 36 m^2/g (Siegel et al. 1989).

The nitrogen sorption isotherm of type II showed a somewhat steeper slope at higher partial pressure in the case of the sample treated for 6.1 years

if compared with the untreated sample, suggesting the presence of a higher amount of pores with a diameter > 4 nm, while the amount of micropores decreased slightly. In any case, as stated before, these modifications did not result in a significant change in surface area. The type H2 hysteresis loop remained unchanged (Figure 3-89).

Table 3-16. BET surface area of untreated saponite and saponite treated with 5 M NaOH.

Treatment time	Surface area (m^2/g)
0	143.75 ± 1.16
6 months	154.36 ± 0.72
6.1 years	144.77 ± 0.89

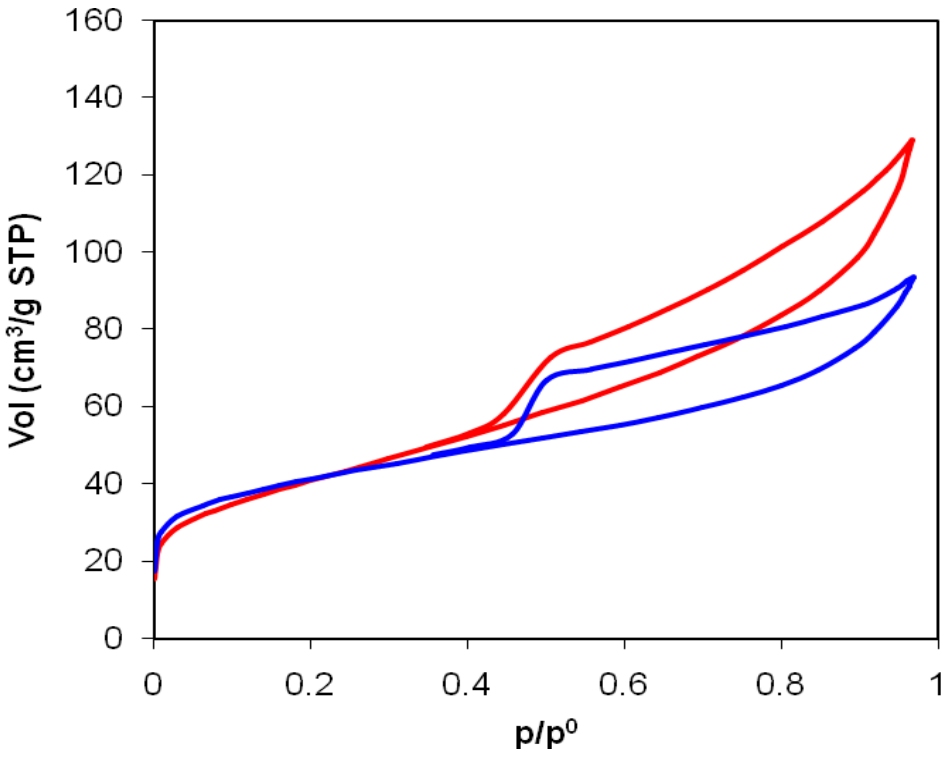

Figure 3-89. Nitrogen sorption isotherms of untreated saponite (blue) and saponite treated with 5 M NaOH for 6.1 years (red).

3.3.3. Saponite treated with KOH

3.3.3.1. XRD

XRD data revealed no significant mineralogical changes upon treatment of saponite with 5 M KOH, even after 6.1 years (Figure 3-90). Illite was still detected and its 001 Bragg peak intensity actually seemed to have increased slightly. Cuevas Rodriguez (1993) interpreted this phenomenon as a recrystallization process experienced by illite, leading to increased crystallinity. Zeolitic phases were not identified upon alkaline activation for 6.1 years.

The diffractograms of the sample treated with 5 M KOH for 7.1 years (Figure 3-91) showed that after EG solvation the 001 Bragg peak shifted from 13 Å to 14.3 Å and not to 17 Å as in the case of the untreated saponite. This result suggests that the treated saponite is less expandable. Additionally, monohydrocalcite ($CaCO_3 \cdot H_2O$, JPDF card no. 831922) was detected in the sample treated with 5 M KOH (Figure 3-91). Monohydrocalcite is a rare mineral which has been found in alkaline lakes. It has also been reported to be an intermediate carbonation product of CSH gels (Zhang et al. 2013a).

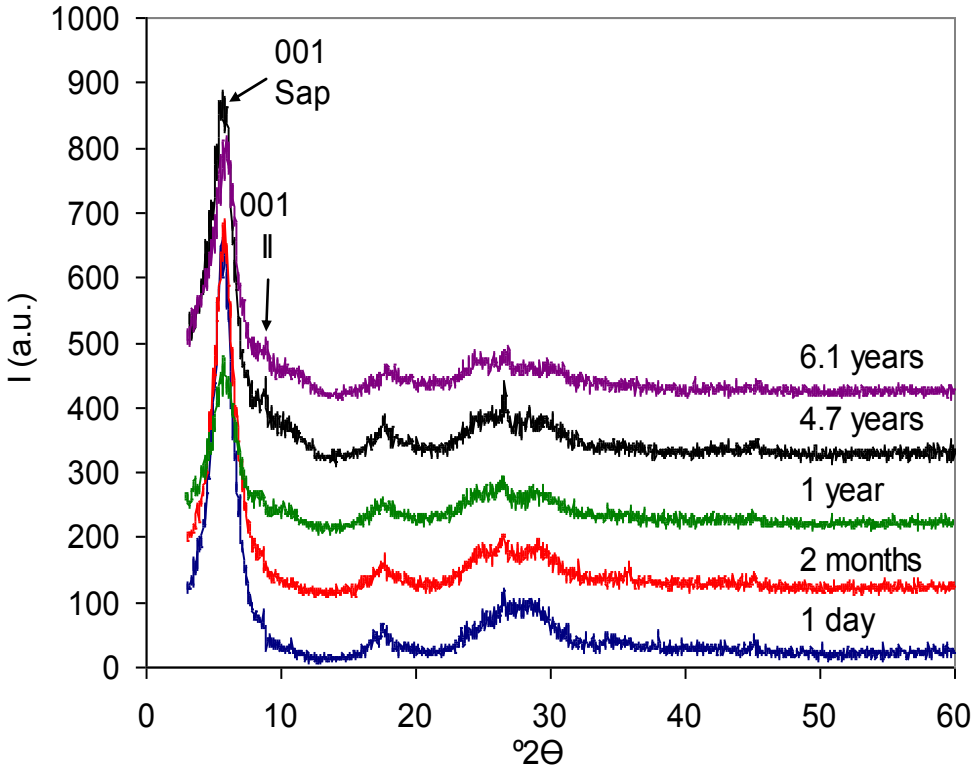

Figure 3-90: XRD patterns showing the mineralogical evolution of saponite treated with KOH for different periods of time. Sap = saponite, Il = illite.

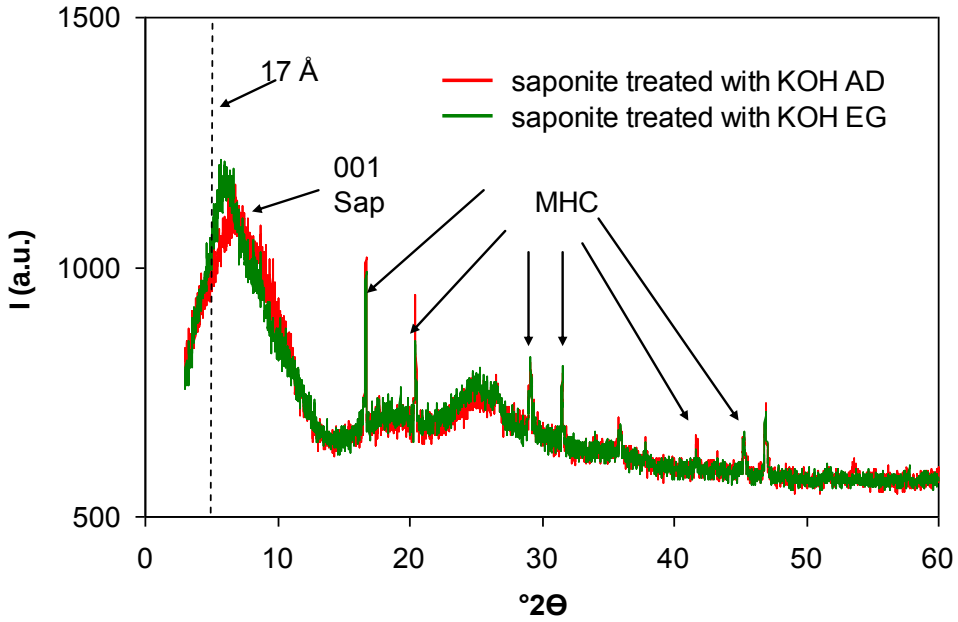

Figure 3-91: Diffractograms of saponite treated with 5 M KOH for 7.1 years. Samples solvated with EG and air-dried (AD). Additional peaks in the KOH treated sample correspond to monohydrocalcite (MHC, JPDF card no. 831922)

3.3.3.2. FESEM

FESEM analyses showed no morphological changes of the saponite after 6-months treatment. Sepiolite was still detected (Figure 3-92). As in the case of the sample treated with NaOH, Ca-rich crystals, presumedly portlandite, formed (inset, Figure 3-93). As mentioned previously, Ca^{2+} interlayer cations of the saponite and tap water used during sample preparation might have been sources for Ca^{2+}. Note that the same phenomenon has been reported by Taubald et al. (2000) in the case of Hammerschmiede smectite treated with an alkaline solution containing KOH at pH 13.22.

After 1-year treatment compositional changes of the saponite or any newly formed zeolitic phases could not be appreciated (Figure 3-94).

In samples treated for 4.7 years crystals with a "sheaf of wheat"-like morphology were observed (Figure 3-95). The high concentration of Ca and C evidenced by EDS microanalyses is compatible with the presence of monohydrocalcite, which has been identified with XRD. Liu et al. (2013) synthesized monohydrocalcite of similar dumbbell-like morphology. The Si concentration of saponite seems to have decreased slightly.

Further treatment up to 6.1 years resulted in the dissolution of sepiolite which could no longer be detected with this technique. A partial transformation of the sample into a gel-like structure was observed (insets, Figures 3-96 and 3-97). This gel-like phase showed an increased Al concentration. Due to the gel-character of this phase, its identification was not

possible using XRD. A well crystallized zeolitic phase was not observed in the saponite sample using FESEM.

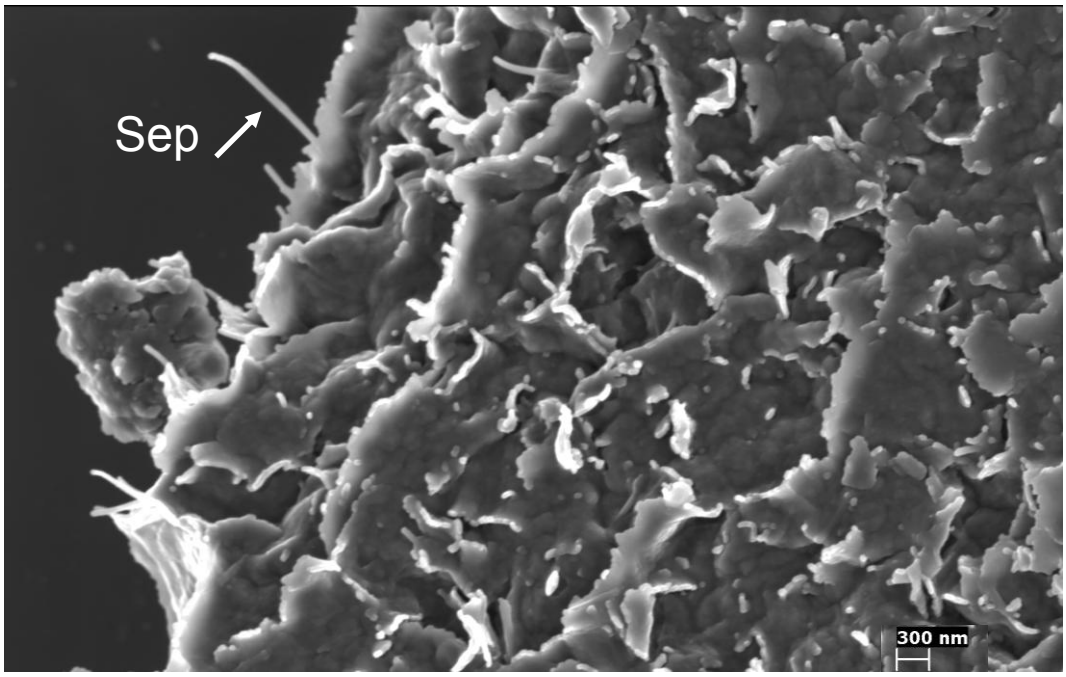

Figure 3-92. FESEM image of saponite treated with 5 M KOH for 6 months. Sepiolite fibres (Sep) can be observed.

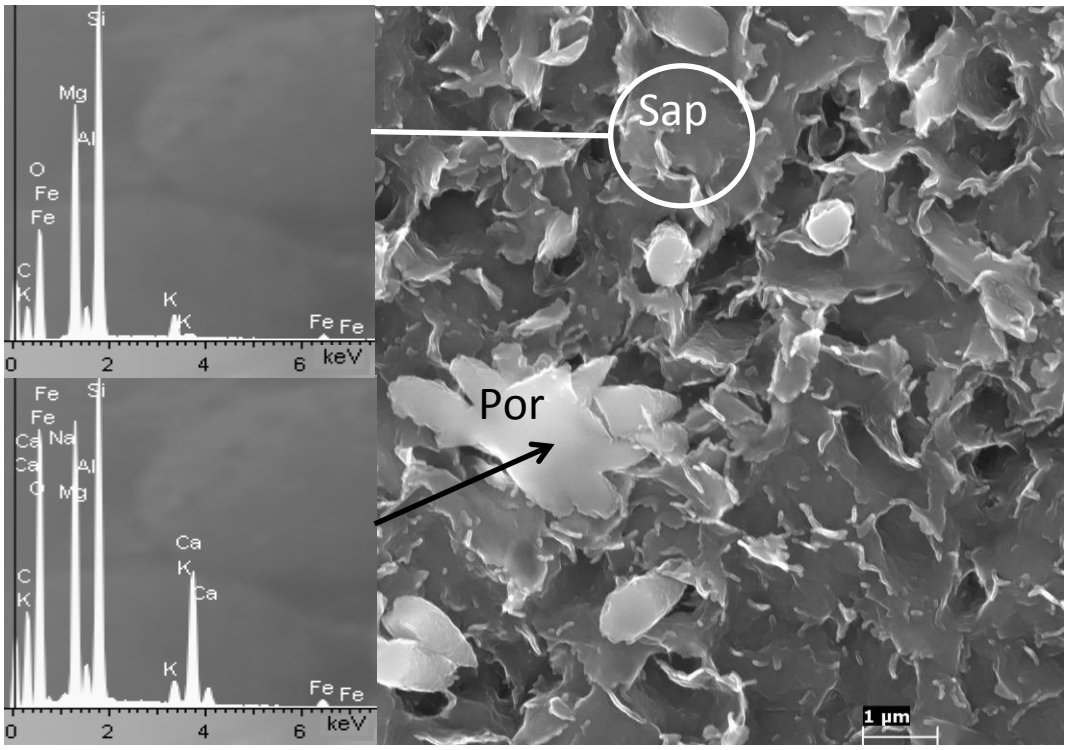

Figure 3-93. FESEM image of saponite treated with 5 M KOH for 6 months. The morphology of saponite (Sap) seems unchanged and, as in the case of samples treated with NaOH, large Ca-rich crystals, presumably portlandite (Port), can be observed (EDS in inset).

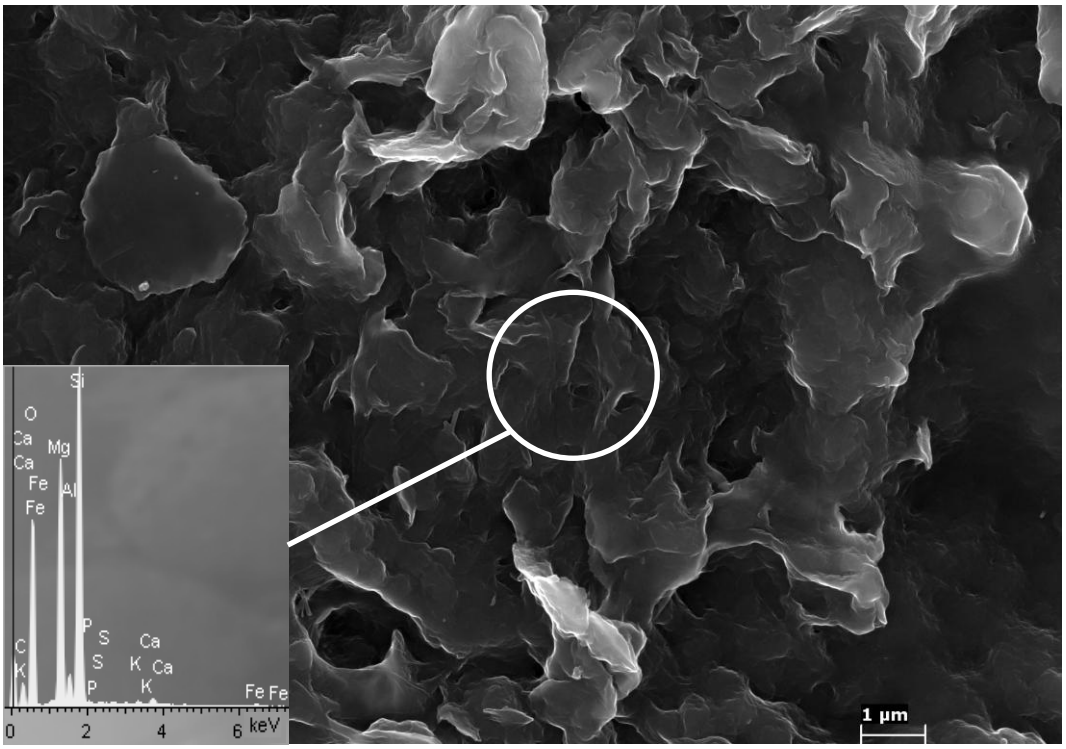

Figure 3-94. FESEM image of saponite treated with KOH for 1 year. The saponite does not show any chemical changes (EDS in inset) or newly formed zeolitic phases.

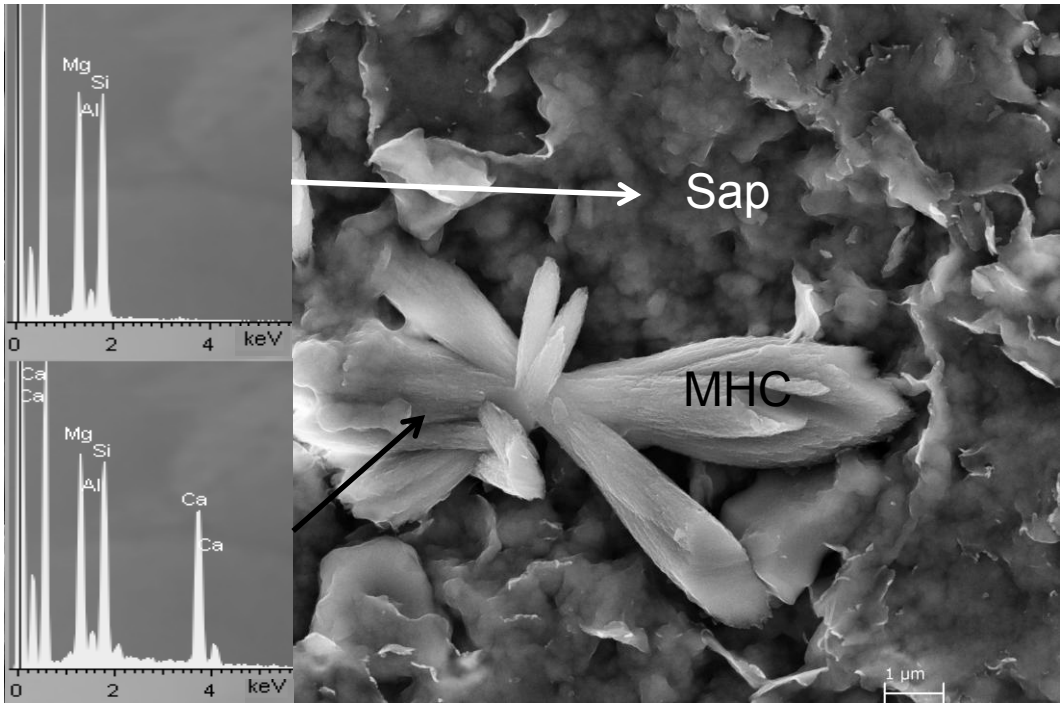

Figure 3-95. FESEM image of saponite treated with KOH for 4.7 years. Ca-rich crystals (EDS in inset) with "sheaf of wheat" morphology, possibly monohydrocalcite (MHC) are observed. The chemical composition of the saponite (Sap) seems to have experienced a slight decrease in Si (EDS in inset).

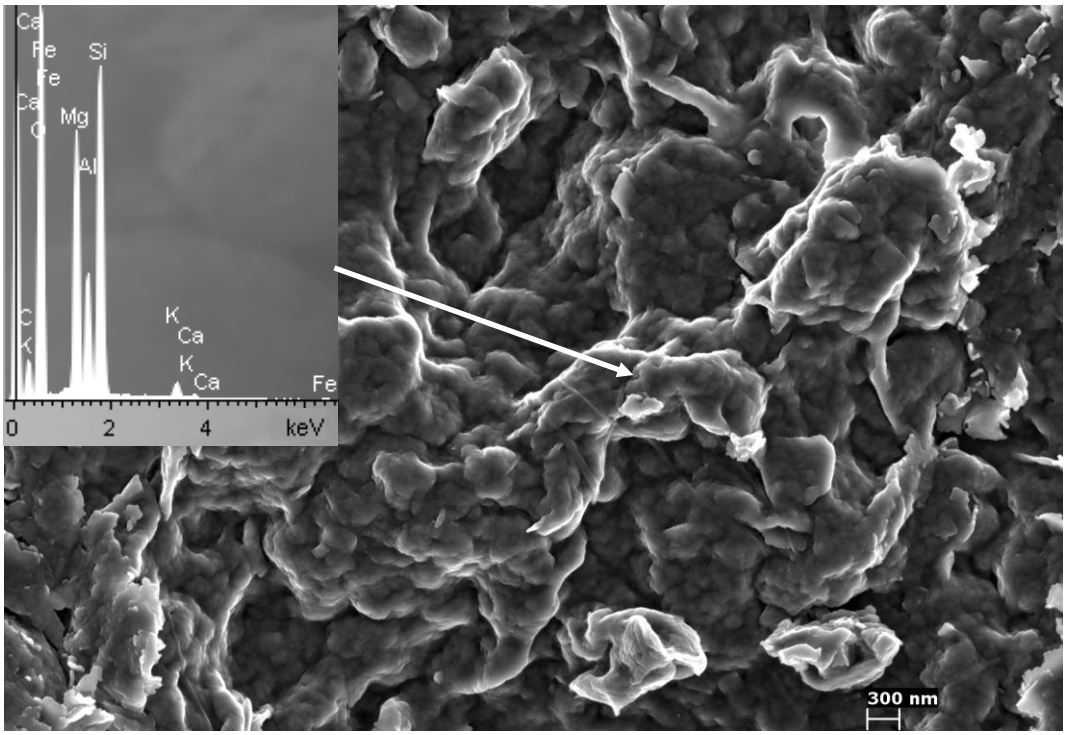

Figure 3-96. FESEM image of saponite treated with KOH for 6.1 years. General aspect of the sample. The Al concentration has increased (EDS in inset).

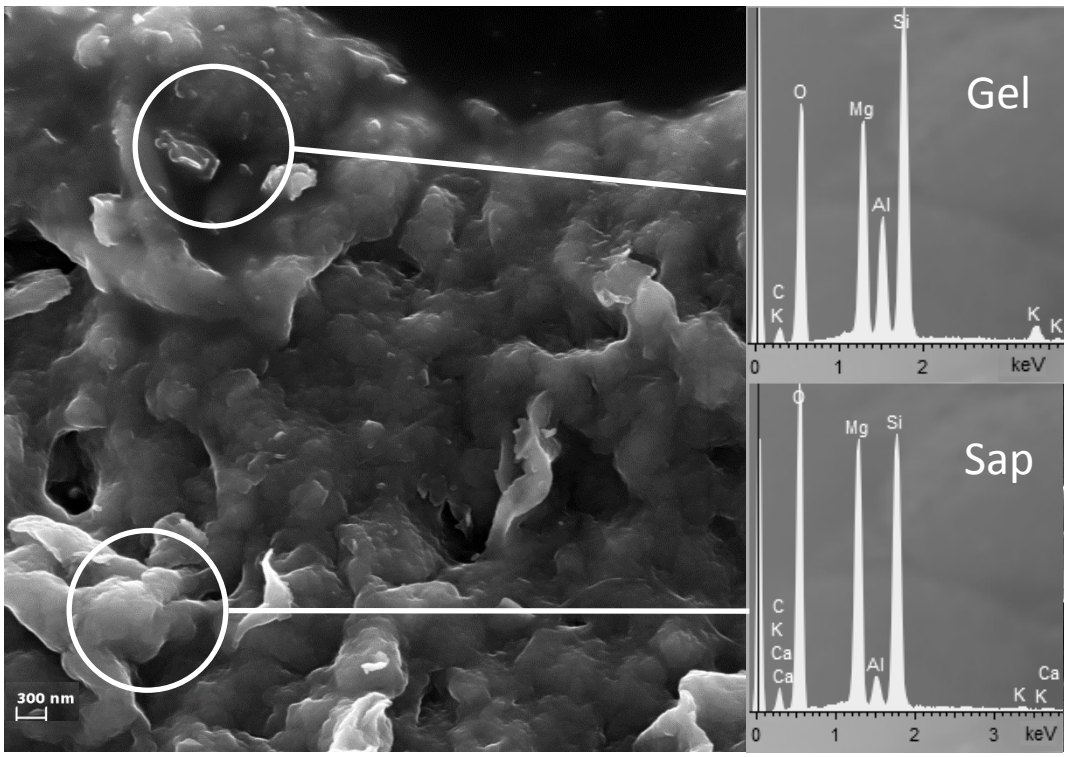

Figure 3-97. FESEM image of saponite (Sap) treated with KOH for 6.1 years. The sample is partially transformed into a gel-like structure. EDS microanalysis (inset) reveals the presence of Mg, Al and Si with a minor amount of K.

3.3.3.3. TEM

After 6-month treatment with 5 M KOH solution, some newly-formed phases showed extensive beam damage following TEM observation. Such damage resulted in amorphization. TEM-AEM data (not included here) allowed their identification as Ca and Mg hydroxides (Figure 3-98).

After 1-year treatment, morphological changes in the saponite could not be detected (Figure 3-99). The sepiolite fibers seemed to be unchanged as well.

However, after prolonged treatment for 6.1 years the amount of these fibers seems to have decreased, while saponite did not show any important morphological changes (Figure 3-100).

Nevertheless, TEM-AEM analyses evidenced important changes in the chemical composition of saponite (Table 3-17). After 1-year treatment the sample experienced a drastic reduction in Si. Al, that previously only occupied the octahedral layer, now compensated the lack of Si in the tetrahedral layer. The octahedral layer was now mainly occupied by Mg which experienced an important concentration increase. After 6.1-year treatment, the Si concentration was further reduced and the Mg concentration experienced a decrease as well to values below the original concentration of the untreated saponite. The composition of the interlayer cation did not show significant changes over the course of the treatment.

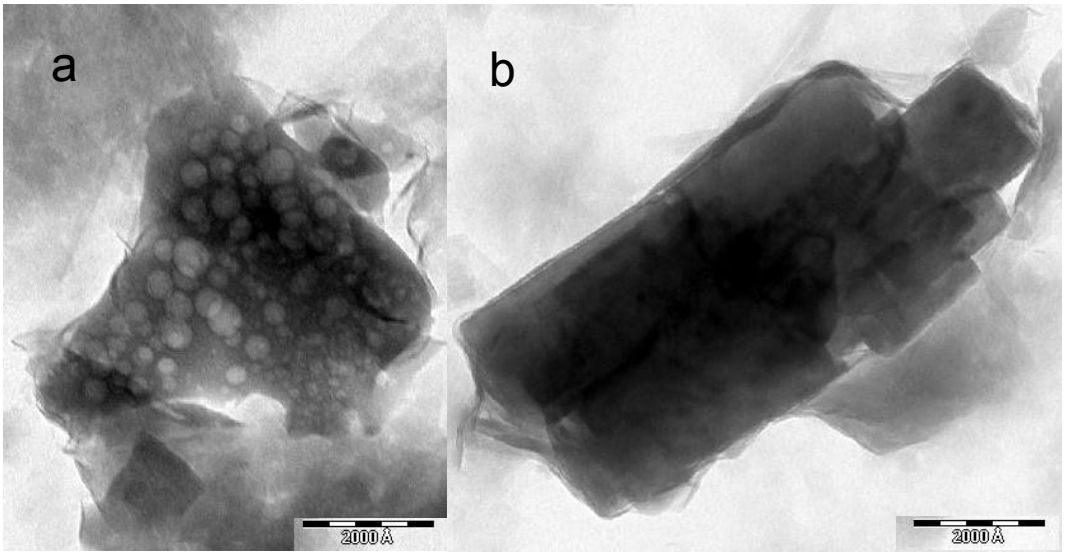

Figure 3-98. TEM image of saponite treated with 5 M KOH for 6 months. TEM-AEM data (not included) suggest the presence of $Mg(OH)_2$ (a) and $Ca(OH)_2$ (b).

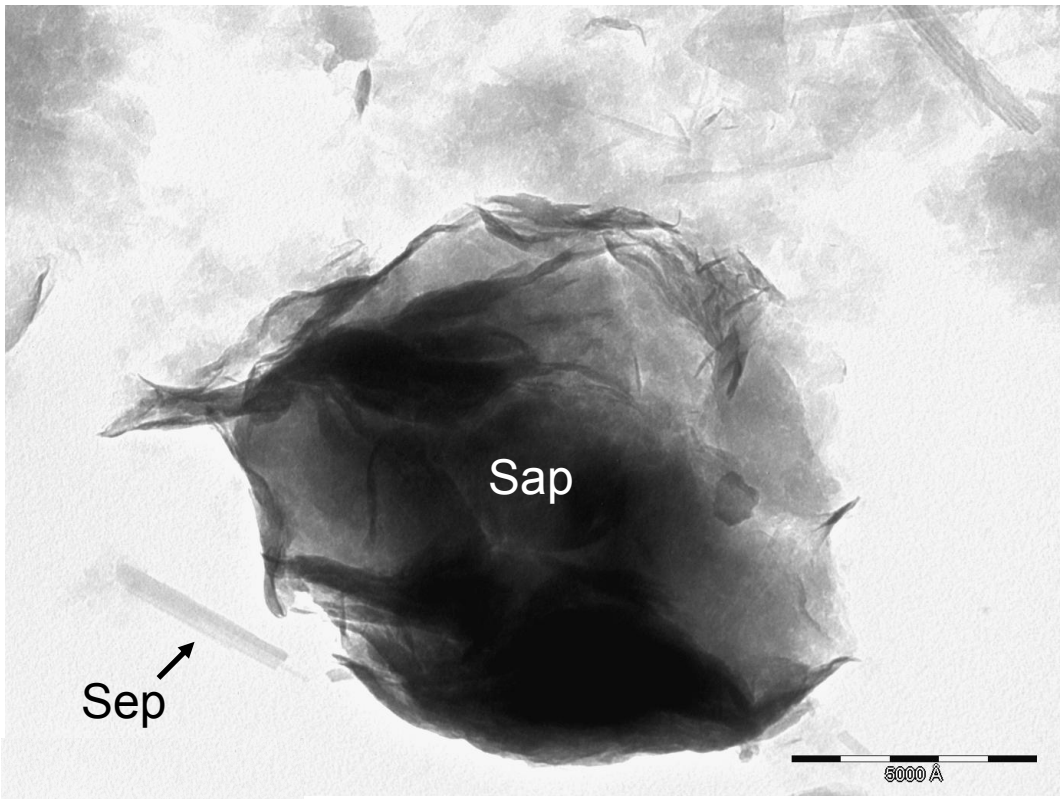

Figure 3-99. TEM image of saponite (Sap) treated with 5 M KOH for 1 year. Morphological changes can not be detected and sepiolite (Sep) is still observed.

Figure 3-100. TEM image of saponite treated with 5 M KOH for 6.1 years. The amount of sepiolite fibres has decreased, whereas the saponite morphology does not seem to have experienced any important changes.

Table 3-17. AEM analyses of saponite treated with 5 M KOH for 6 months, 1 year and 6.1 years (the average structural formula of untreated saponite is included)

Structural formulae of saponite treated with 5 M KOH based on $O_{10}(OH)_2$										
	Si	^{IV}Al	^{VI}Al	Mg	Fe	Σoct.cat.[1]	K	Ca	Na	Σint.cha.[2]
Untreated	4.03	0.01	0.37	2.30	0.04	2.72	0.01	0.01	*	**
average	±0.06	±0.01	±0.06	±0.11	±0.03	±0.07	±0.02	±0.01		
1	3.91	0.09	0.21	2.66	0.02	2.89	0.02	0.00	0.11	0.13
2	3.54	0.32	0.00	3.01	0.11	3.12	0.09	0.06	0.37	0.58
3	3.64	0.33	0.00	2.98	0.07	3.05	0.06	0.04	0.20	0.34
4	3.83	0.11	0.17	2.79	0.06	3.02	0.06	0.00	0.06	0.13
5	3.56	0.31	0.00	3.27	0.07	3.34	0.06	0.02	0.00	0.10
6 months	3.70	0.23	0.08	2.94	0.07	3.10	0.06	0.02	0.15	0.26
average	±0.17	±0.12	±0.11	±0.23	±0.03	±0.17	±0.02	±0.03	±0.14	±0.21
6	3.49	0.45	0.00	3.14	0.09	3.23	0.04	0.07	*	**
7	3.61	0.34	0.00	3.13	0.04	3.17	0.02	0.09	*	**
1 year	3.55	0.40	0.00	3.14	0.07	3.20	0.03	0.08	*	**
average	±0.09	±0.08	±0.00	±0.01	±0.04	±0.04	±0.01	±0.01		
8	2.58	0.31	0.00	2.23	0.04	2.27	0.01	0.03	0.16	0.23
9	2.70	0.28	0.00	2.01	0.04	2.05	0.01	0.04	0.16	0.25
10	2.69	0.29	0.00	2.01	0.04	2.05	0.05	0.03	0.15	0.26
11	2.71	0.27	0.00	2.02	0.04	2.06	0.01	0.03	0.12	0.19
6.1 years	2.67	0.29	0.00	2.07	0.04	2.11	0.02	0.03	0.15	0.23
average	±0.06	±0.02	±0.00	±0.11	±0.00	±0.11	±0.02	±0.01	±0.02	±0.03

[1] Sum of octahedral cations
[2] Sum of interlayer charge
* not analyzed
** not calculated

3.3.3.4. Nitrogen sorption

BET Surface area results calculated from nitrogen adsorption data showed that saponite treated for 6.1 years with 5 M KOH only experienced a minor decrease in surface area of less than 10 % (Table 3-18). The change might be due to the formation of a gel-like phase which caused an aggregation of the clay particles and blocked the access of nitrogen.

Neither the nitrogen sorption isotherm of type II, nor the type H3 hysteresis loop of saponite treated for 6.1 years experienced any significant changes (Figure 3-101).

Table 3-18. BET surface area of untreated and saponite treated with 5 M KOH.

Treatment time	Surface area (m^2/g)
0	143.75 ± 1.16
6 months	153.82 ± 0.73
6.1 years	136.81 ± 0.69

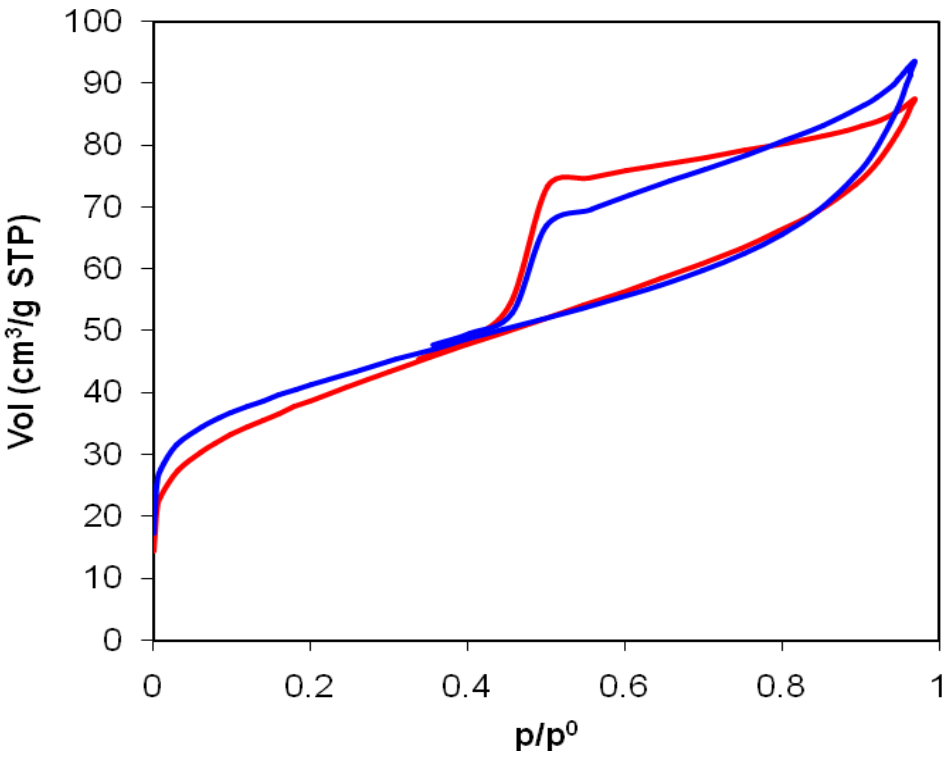

Figure 3-101. Nitrogen sorption isotherms of untreated saponite (blue) and saponite treated with 5 M KOH for 6.1 years (red).

3.4. Characterization of illite

The following sections include the characterization of the untreated illite and the study of its mineralogical evolution upon alkaline activation using NaOH and KOH.

3.4.1. Untreated illite

3.4.1.1. XRF

Due to the scarce amount of sample, XRF results for Beavers Bend State Park illite in Table 3-19 are based only on published data. This illite was proposed as a Clay Minerals Society source clay and its crystallography, composition and morphological features have been thoroughly studied (Mankin and Dodd 1961, Gaudette et al. 1966). Gaudette et al. (1966) give the following structural formulae based on chemical analysis: $K_{0.61}Na_{0.02}Ca_{0.01}(Al_{1.29}Fe^{+++}_{0.20}Fe^{++}_{0.19}Mg_{0.18}Ti_{0.04})(Si_{3.34}Al_{0.66})O_{10}(OH)_2$.

Table 3-19. XRF results of the starting material (wt %)

Mineral	SiO_2	Al_2O_3	Fe_2O_3	FeO	Na_2O	MgO	K_2O	CaO	Loss on Ignition
Illite *	49.85	23.68	6.60	1.87	0.34	1.86	6.64	0.12	6.8
Illite **	47	23.3	7.74	3.2	0.14	1.7	6.69	0.17	6.64

* Data published by Mankin and Dodd (1961)
** Data published by Gaudette et al. (1966)

3.4.1.2. XRD

The XRD pattern was in good agreement with JPDF card no. 020056, an illite with the following formulae $KAl_2Si_3AlO_{10}(OH)_2$. XRD analyses of OA showed illite as the main phase in the Beavers Bend sample. This is confirmed by the appearance of strong 00*l* reflections which do not change d-spacing upon treatment with EG or heating up to 550º C (Figure 3-102).

Semiquantitative analysis of the clay fraction (OA) revealed the illite content to be >90 % with a kaolinite/chlorite content < 5 %. Generally, it is accepted that Beavers Bend illite contains small amounts of chlorite (Gaudette et al. 1966, Chaudhuri et al. 1979). However, neither the treatment with DMSO, nor the thermal treatment gave unambiguous evidence of the presence of chlorite. The sharpness of the 001 Bragg peak showed that this illite is of a high crystallinity, having a crystallite size of 28 nm.

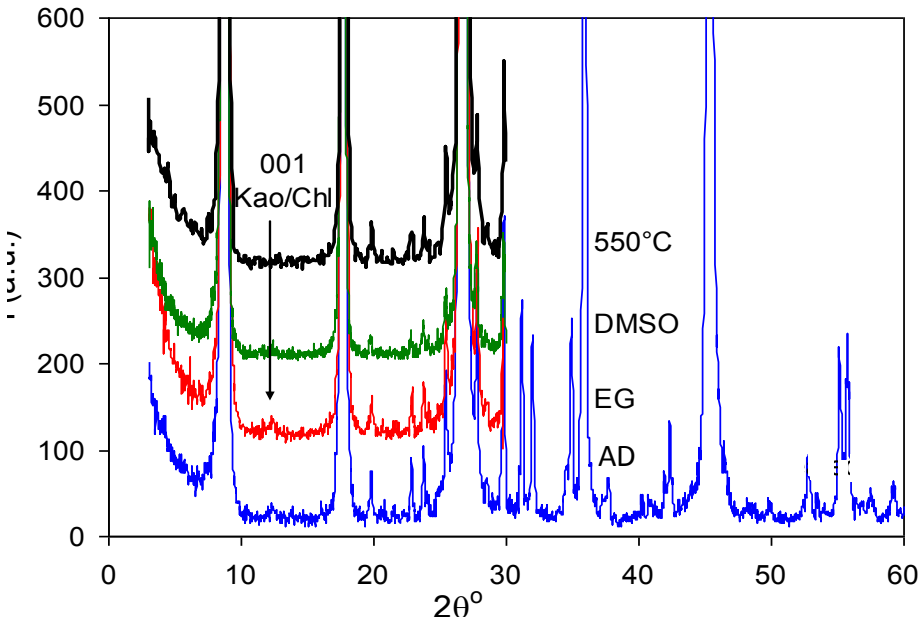

Figure 3-102. XRD patterns of illite. OA air-dried (AD), treated with EG, DMSO and heat treated at 550 °C. Kao = kaolinite, Chl = chlorite.

3.4.1.3. FESEM

The FESEM image (Figure 3-103) showed fine grained illite particles of irregular shape. The EDS spectrum revealed Si, Al and minor amounts of K, and Mg (inset, Figure 3-103). These elements are typical for illite and in agreement with XRF analysis. Trace amounts of Na and P, on the other hand, are impurities which were a result of the addition of sodium hexametaphosphate (Calgon) as a dispersant during the separation of the clay fraction. FESEM analyses further suggested the presence of a fibrous apatite-like phase (Figure 3-104). The EDS analysis showed high concentrations of Na, P and Ca additional to the elements of the original clay, thus, being evidence of a mixture of both phases (inset, Figure 3-104). A possible source for this phase is the sodium hexametaphosphate which might have scavenged Ca ions from the tap water during sample preparation. It is a known fact that phosphates have a great affinity for divalent ions such as Ca and Mg (Rolfe et al. 1960). Due to its low solubility, a calcium phosphate phase, possibly hydroxyapatite, precipitated.

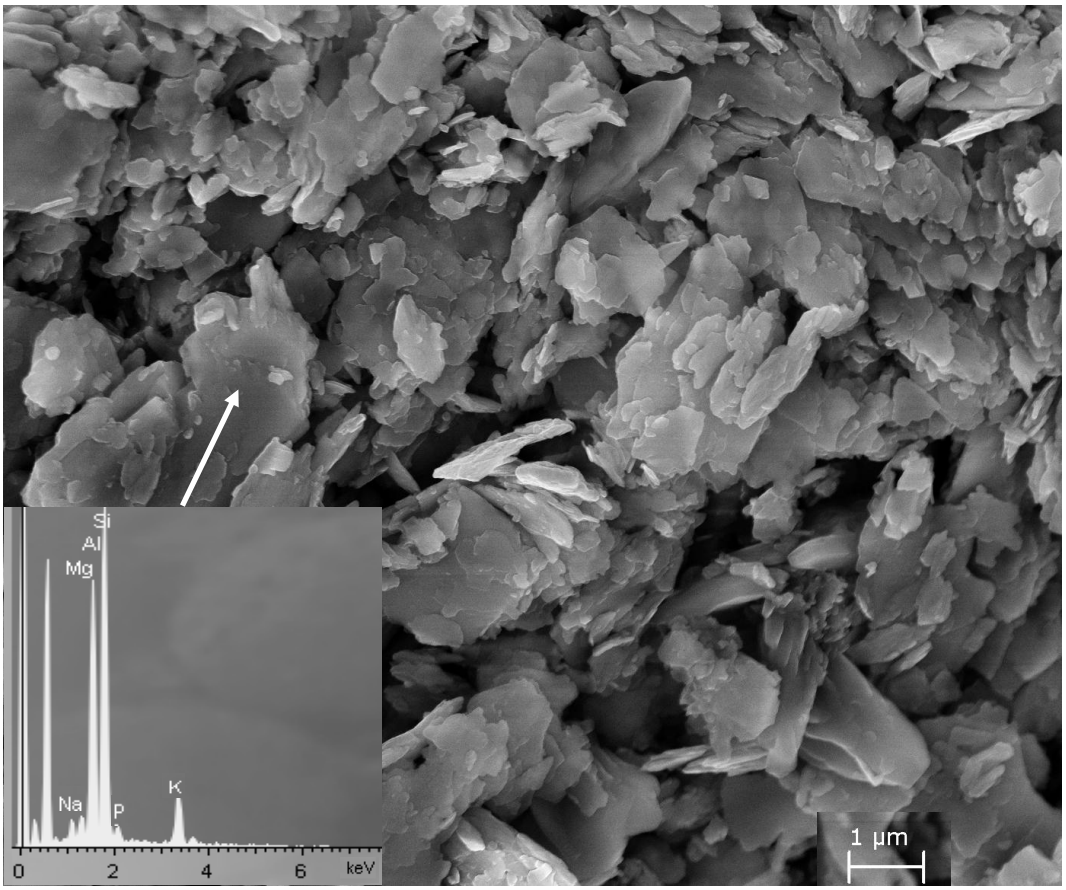

Figure 3-102. FESEM image and EDS spectrum of untreated illite

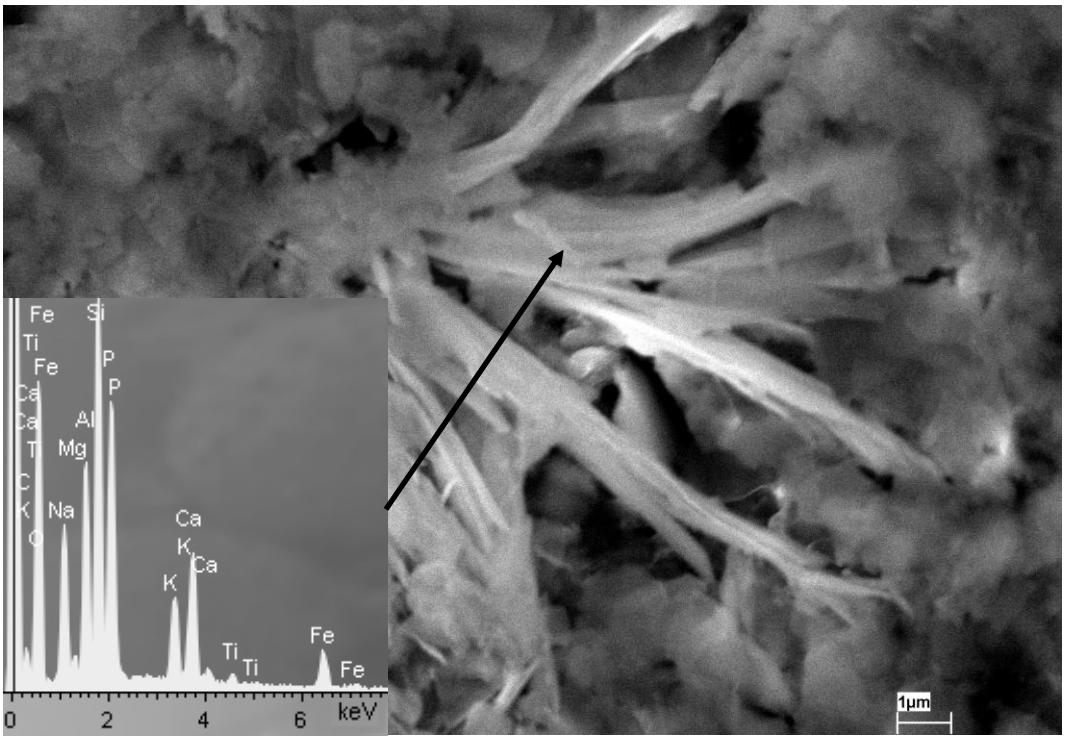

Figure 3-104. FESEM image of fibrous hydroxy-apatite in the untreated illite sample.

3.4.1.4. TEM

The TEM image of untreated illite (Figure 3-105) showed clay particles of 100 - 700 nm in size. The structural formulae of the untreated illite calculated from TEM-AEM results (Table 3-20) revealed a chemical composition typical for illite. However, the interlayer charge was high, in some cases higher than permissible. This number is also higher than the number in the structural formula given for this illite by Gaudette et al. (1966) which is based on bulk chemical analysis (see above). However, the bulk chemical analysis might include impurities such as kaolinite which would explain the lower interlayer charge in the case of data reported by Gaudette et al. (1966).

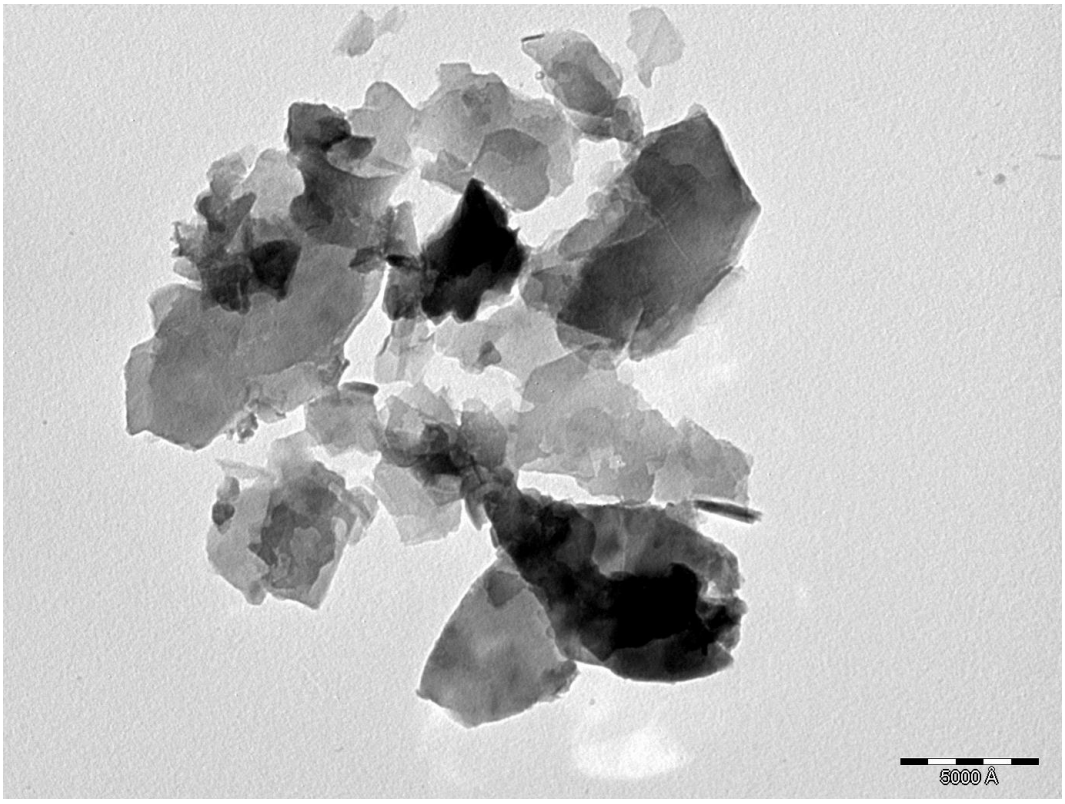

Figure 3-105. TEM image of untreated illite

Table 3-20. Structural formulae of untreated illite calculated from TEM-AEM data.

Structural formulae of illite based on $O_{10}(OH)_2$										
	Si	^{IV}Al	^{VI}Al	Mg	Fe	Σoct.cat.[1]	K	Ca	Na	Σint.cha.[2]
1	3.17	0.83	1.68	0.15	0.15	1.98	0.88	0.13	*	**1.14
2	3.31	0.69	1.69	0.22	0.15	2.07	0.67	0.08	*	**0.83
3	3.26	0.74	1.47	0.33	0.28	2.08	0.85	0.07	*	**0.99
4	3.12	0.88	1.62	0.26	0.15	2.03	1.02	0.06	*	**1.14
5	3.21	0.79	1.40	0.24	0.37	2.01	0.90	0.09	0.11	1.19
6	3.23	0.77	1.80	0.19	0.05	2.04	0.68	0.02	0.14	0.86
7	3.27	0.73	1.72	0.16	0.12	2.00	0.91	0.00	0.00	0.91
average	3.22 ±0.09	0.78 ±0.06	1.63 ±0.14	0.22 ±0.06	0.18 ±0.11	2.03 ±0.04	0.84 ±0.13	0.09 ±0.04	0.08 ±0.07	0.98 ±0.18

[1] Sum of octahedral cations
[2] Sum of interlayer charge
* not analyzed
** Na was not considered

3.4.1.5. Nitrogen sorption

The surface area of the untreated illite was 7.53 ± 0.17 m²/g. Murray and Lyons (1960) correlated surface area with the degree of crystallinity of the clay mineral, well-crystallized minerals showing a smaller surface area than poorly crystallized ones. The extremely low surface area of the illite from Beaver Bend State Park provides, thus, another evidence for the high crystallinity of this clay. Published surface area data of illite vary significantly and commonly range between 18-60 m²/g (Dogan et al. 2007, Macht et al. 2011, Beene et al. 1991). Occasionally, illite surface areas of more than 100 m²/g have been measured (Aylmore et al. 1970, Köhler et al. 2005).

The Nitrogen sorption isotherm was of type II which is common for non-porous adsorbent and identical to the one of the other clay minerals (Figure 3-106). A not very pronounced, type H3 hysteresis loop was observed, typical for aggregates of plate-like particles, giving rise to slit-shaped pores (Sing et al. 1985).

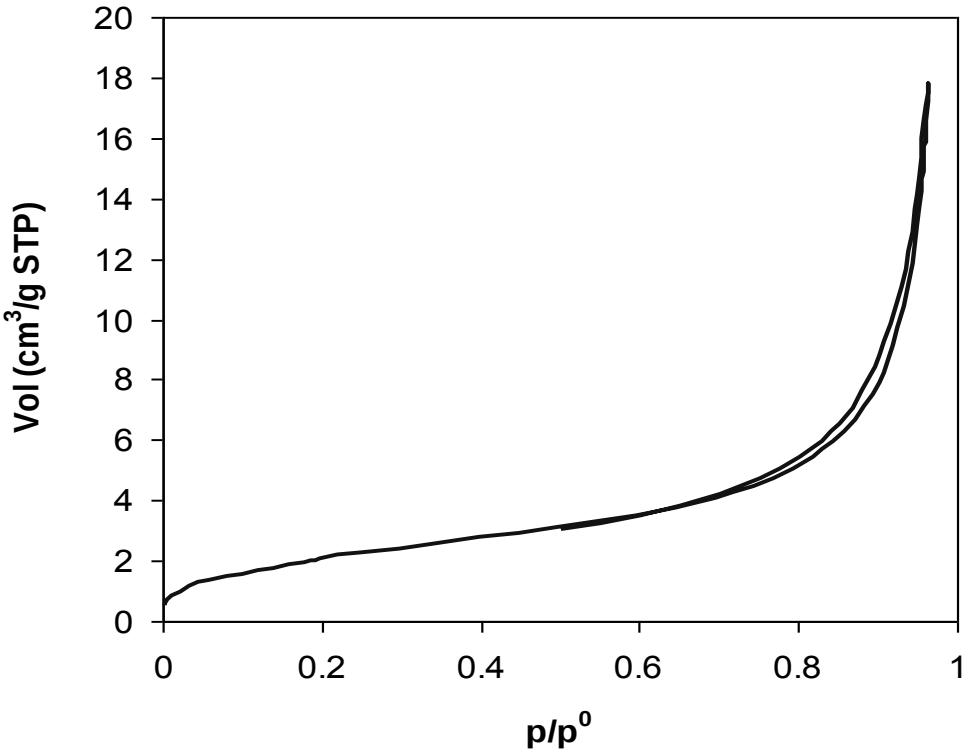

Figure 3-106. Nitrogen sorption isotherm of untreated illite

3.4.1.6. Particle size analysis

Particle size analysis revealed a maximum at 140 nm in the case of illite (Figure 3-107). A secondary maximum can be observed between 0.5-15 μm. Acording to Arnott (1965) the typical particle size-range of illite lies between 0.1-0.6 μm.

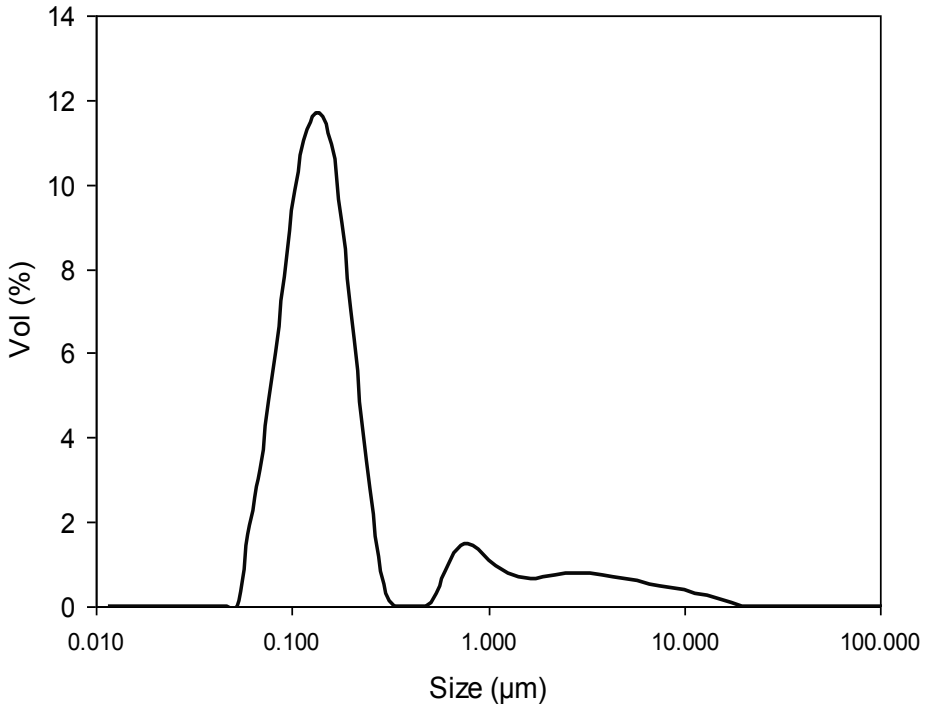

Figure 3-107. Particle size distribution of untreated illite.

3.4.1.7. TG

The thermogravimetric curve of illite (Figure 3-108) was less pronounced than in the case of smectite. It showed a continous weight loss of adsorbed water of 4.5 % beginning at 30 °C and ending at ~ 250 °C. Dehydroxylation started around this temperature, amounting to a total weight loss of 9.8 % at around 800 °C, 5.3 % being due to dehydroxylation.

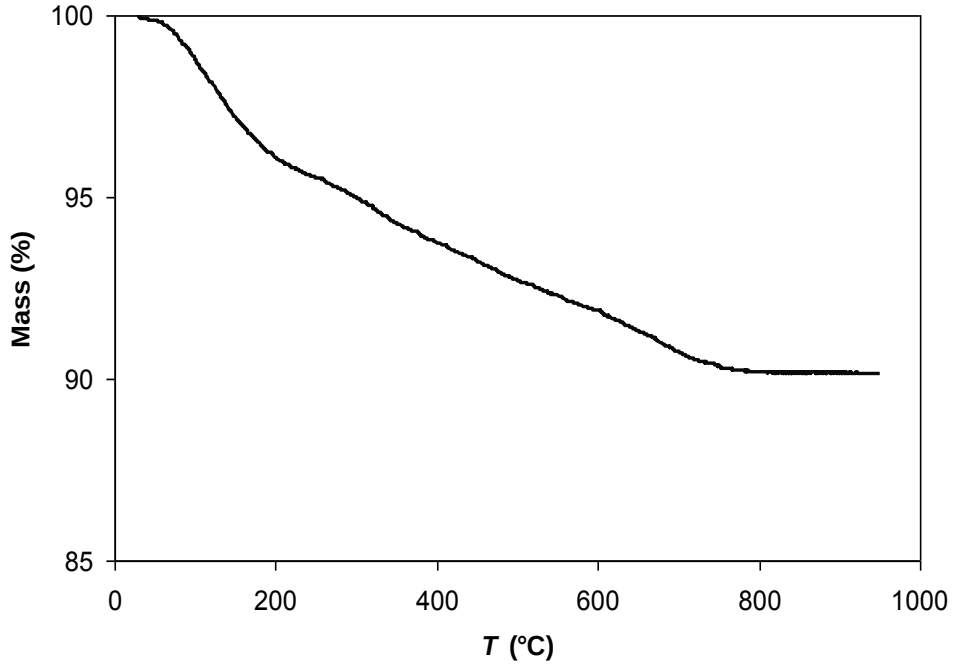

Figure 3-108. Thermogravimetric curve of untreated illite.

3.4.2. Illite treated with NaOH

3.4.2.1. XRD

XRD data revealed (Figure 3-109) an additional Bragg peak at 7.7 Å in samples treated for 8 months and 1 year which might suggest the presence of hydrotalcite (JPDF card no. 140191), a common reaction product in alkali-activated slags (Roy 1999, Ismail et al. 2013), or a sodium hydrogen phosphate hydrate (JPDF card no. 110359). In any case, it was not possible to determine the mineralogical phase unambiguously. Note that the same Bragg peak appeared in the sample treated with KOH (see below). Overall, the illite seemed unaltered after 1 year of alkaline activation using NaOH. EG solvation (Figure 3-110) confirmed that no crystallographic modifications (i.e. presence of expandable smectite layers) have occurred and that changes in element concentration detected with TEM (see below) were limited to variations in the chemical composition.

The fact that the crystallite size of illite did not change significantly upon alkaline activation (Table 3-21) is an additional proof that the clay mineral was not affected by the treatment. Further treatment for longer periods of time was not possible due to the limited amount of sample available.

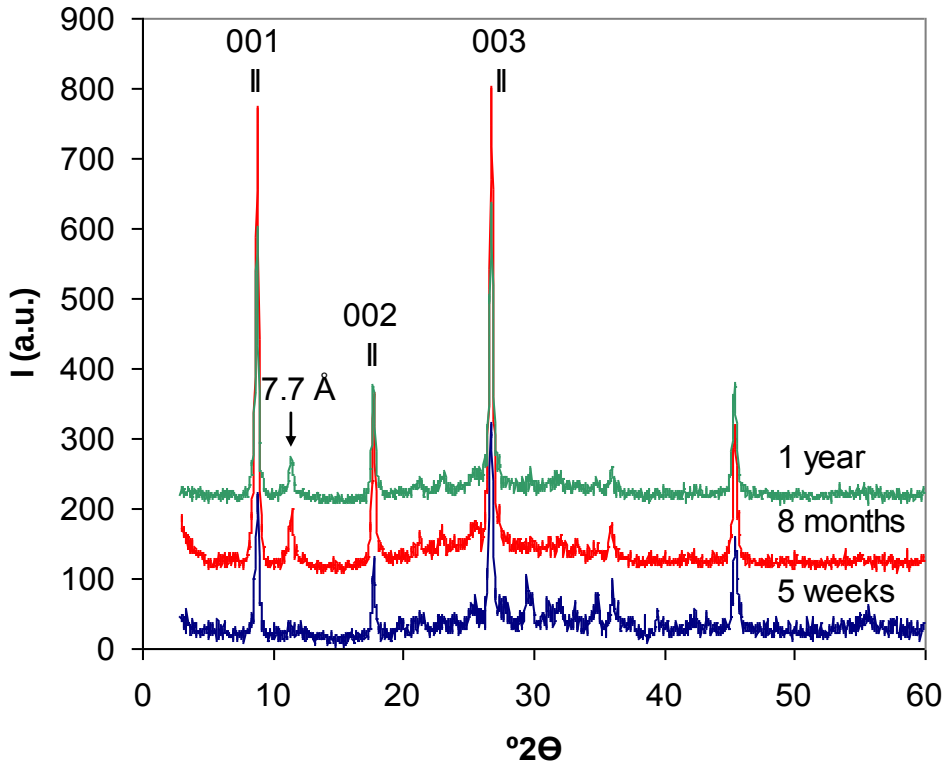

Figure 3-109. XRD patterns of illite treated with 5 M NaOH for different periods of time.

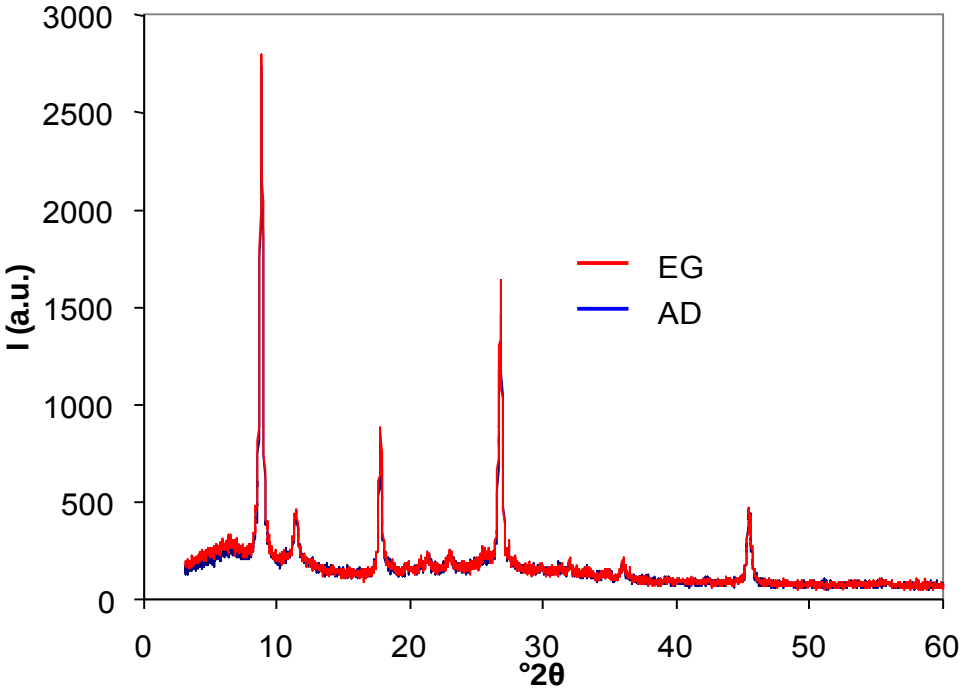

Figure 3-110. XRD of illite treated with 5 M NaOH for 1 year. OA air-dried (AD) and EG solvated.

Table 3-21: Crystallite size evolution upon alkaline activation using 5 M NaOH

Time	Crystallite size (nm)
untreated	31
5 weeks	29
8 months	34
1 year	33

3.4.2.2. FESEM

FESEM analysis did not evidence mineralogical or chemical changes of illite particles after 1 year of alkaline activation using NaOH. However, the fibrous apatite-like phase, previously identified as impurity in the untreated clay sample (Figure 3-111), dissolved upon alkaline treatment and recrystallized as nanosized spheres on the illite surface. Li et al. (1997) published SEM images of apatite formed on phosphorylated and precalcified bamboo (Figure 3-112) which had a similar morphology as the spheres formed on illite treated with NaOH.

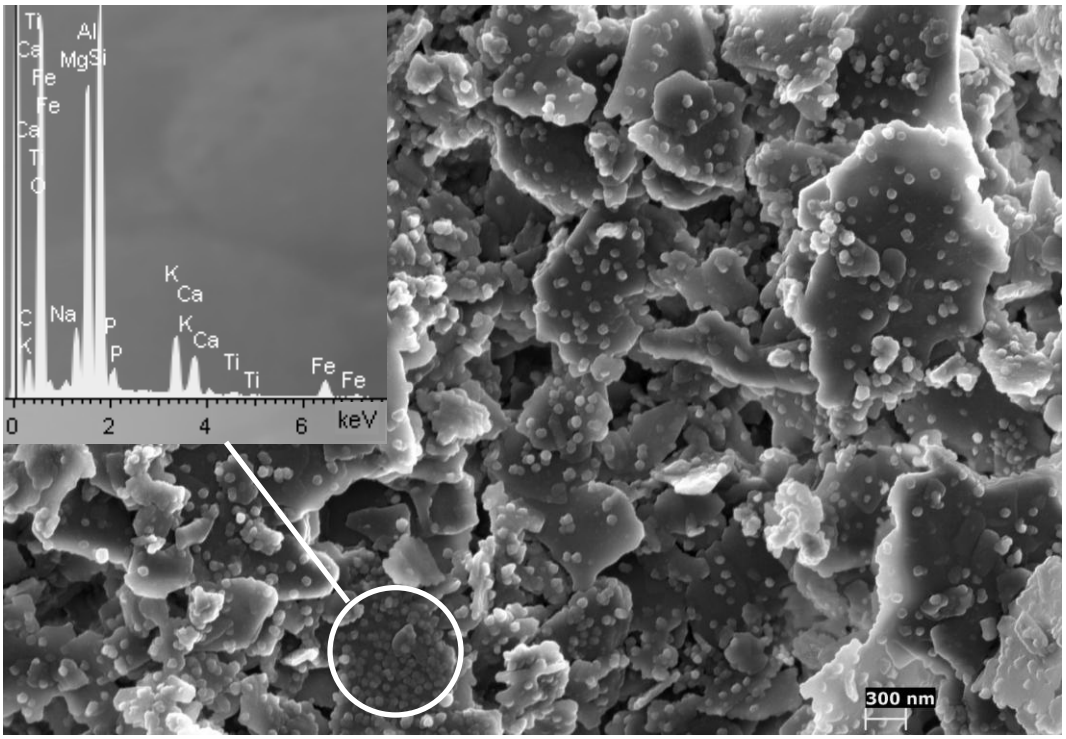

Figure 111. FESEM image of illite treated with 5 M NaOH for 1 year. A large amount of nanocrystals of an apatite-like phase precipitated on the surface of the illite particles (EDS in inset).

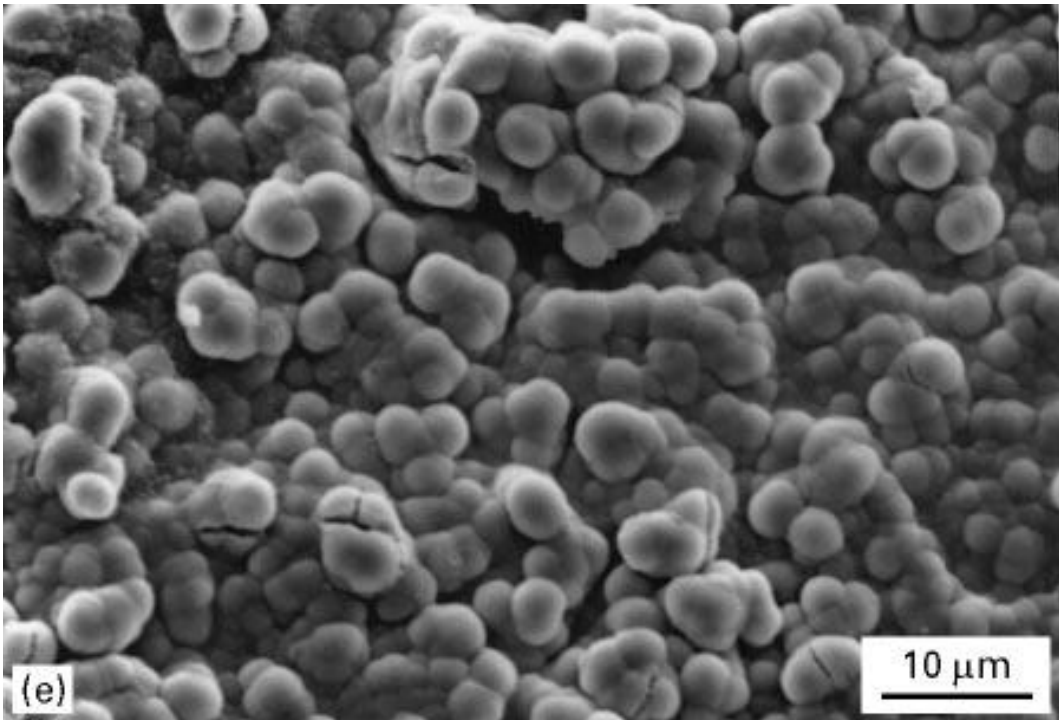

Figure 3-112. SEM image of apatite formed after $Ca(OH)_2$ treatment of NaOH-H_3PO_4 phosphorylated bamboo (Li et al. 1997).

3.4.2.3. TEM

The results of TEM-AEM analyses of the nanosized spheres of the sample treated for 1 year with 5 M NaOH were in agreement with the chemical composition of hydroxyapatite (inset, Figure 3-113). A quantitative analysis was not possible since P could not be quantified with this technique due to a lack of a suitable standard. No further changes were observed in this sample.

TEM-AEM analyses revealed a reduction in K^+ and to a lesser extent in Al and interlayer charge, whereas Si, Mg and Na increased slightly after 1 year of treatment with 5 M NaOH (Table 3-22). Compositional changes were very limited, but they might point to the initial degradation of illite and its transformation into smectitic clay. The transformation of illite into smectite or illite/smectite interstratification is a common weathering process observed in soils (Velde and Meunier 2006, Ross et al. 1987, Dabkowska-Naskret and Dlugosz 1996).

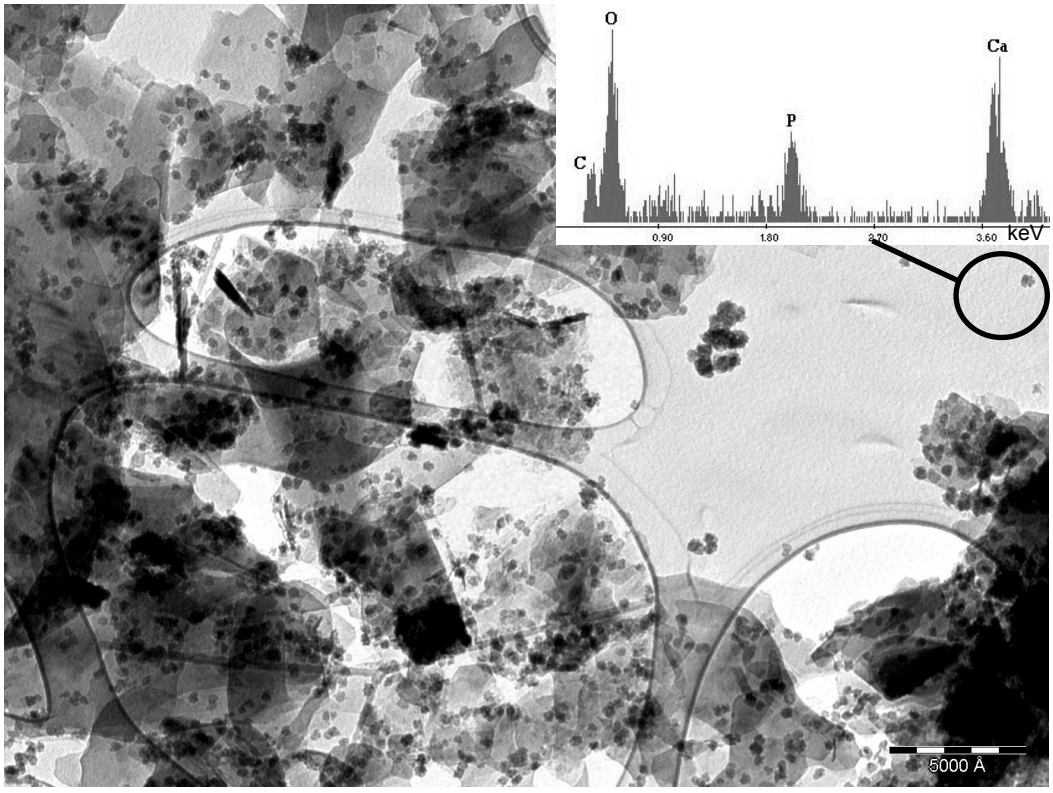

Figure 3-113. TEM-EDS analysis suggests the presence of hydroxyapatite (see EDS in inset) as nanosized spheres in the illite sample treated with 5M NaOH for 1 year.

Table 3-22. Structural formulae of untreated illite and illite treated with 5 M NaOH for 1 year calculated from TEM-AEM data

Structural formulae of illite based on $O_{10}(OH)_2$										
	Si	^{IV}Al	^{VI}Al	Mg	Fe	Σoct.cat.[1]	K	Ca	Na	Σint.cha.[2]
Untreated	3.22	0.78	1.63	0.22	0.18	2.03	0.84	0.09	0.08	1.01
average	±0.09	±0.06	±0.14	±0.06	±0.11	±0.04	±0.13	±0.04	±0.07	±0.15
1	3.29	0.71	1.55	0.32	0.19	2.06	0.65	0.07	0.21	1.00
2	3.35	0.65	1.54	0.32	0.16	2.02	0.65	0.07	0.20	0.99
3	3.25	0.75	1.62	0.44	0.09	2.15	0.46	0.07	0.16	0.76
1 year	3.30	0.70	1.57	0.36	0.12	2.08	0.57	0.07	0.19	0.92
average	±0.05	±0.05	±0.04	±0.07	±0.05	±0.07	±0.11	±0.00	±0.03	±0.14

[1] Sum of octahedral cations
[2] Sum of interlayer charge

3.4.2.4. Nitrogen sorption

The illite sample treated for one year with 5 M NaOH showed a ~ 3 times higher surface area than the untreated sample (Table 2-23). It is assumed that the increase in surface area is due to the formation of nanosized hydroxyapatite spheres. Published values for the surface area of synthesized hydroxyapatite powder range from 40-130 m^2/g (Liu et al. 1997, Bose and Saha 2003).

The shape of nitrogen sorption isotherm and the hysteresis loop of illite treated with 5 M NaOH for 1 year did not experience any changes if compared to the ones of the untreated sample (Figure 3-114).

Table 3-23. BET surface area of untreated illite and illite treated with 5 M NaOH.

Treatment time	Surface area (m^2/g)
0	7.52 ± 0.17
1 year	25.70 ± 0.49

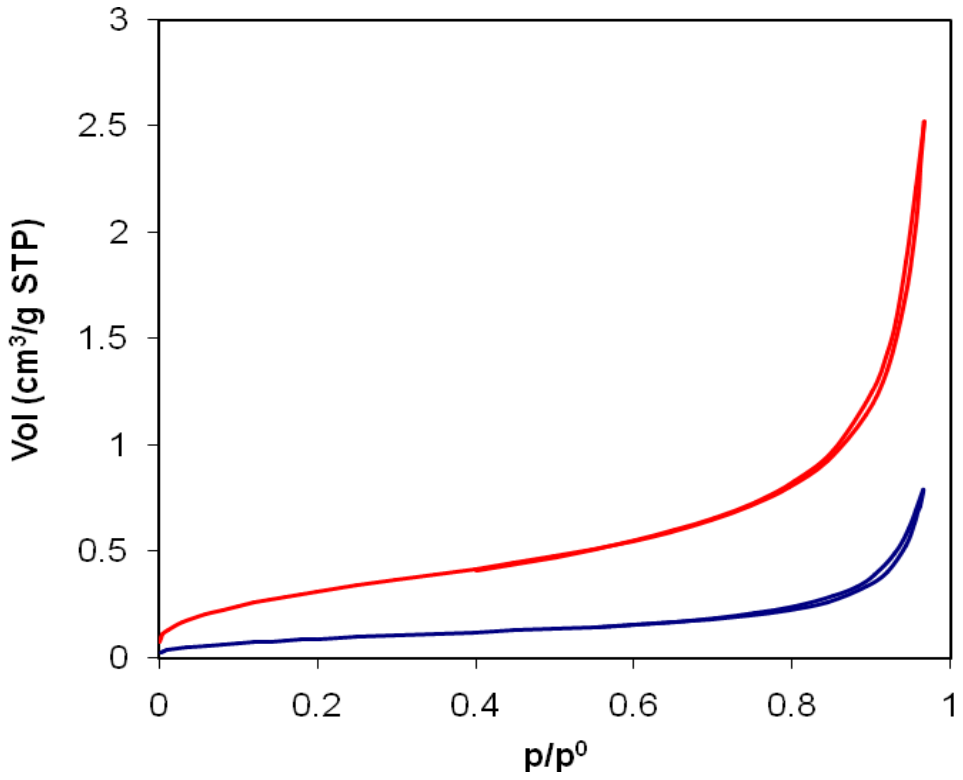

Figure 3-114. Nitrogen sorption isotherms of untreated illite (blue) and illite treated with 5 M NaOH for 1 year (red).

3.4.3. Illite treated with KOH

3.4.3.1. XRD

XRD patterns showed no significant mineralogical changes in the sample upon alkaline activation using KOH even after 4.5 years (Figure 3-115). As in the case of the sample treated with NaOH, an additional Bragg peak at 7.7 Å was observed, indicating the possible presence of either a sodium hydrogen phosphate hydrate (JPDF card no. 110359) or hydrotalcite (JPDF card no. 140191). The Bragg peak at 7.16 Å suggests the presence of chlorite in the sample treated for 4.5 years, because kaolinite would not have withstood the prolonged alkaline activation. It is likely that this mineral was present in the original clay and its survival provides evidence of the high stability of this Mg-clay mineral in alkaline environments. Berube et al. (1990) also reported the high stability of Mg-chlorite in saturated $Ca(OH)_2$ solution at pH 12.4. As in the case of the sample treated with NaOH, EG solvation did not reveal any modifications in the crystal structure of illite (Figure 3-116). The width of the 001 illite Bragg peak did not increase, indicating that layers of expandable clays have not formed.

The crystallite size of illite (Table 3-24) showed a slight increase upon alkaline activation using KOH which suggests a recrystallisation process (Ostwald ripening). Otherwise, the alkaline treatment did not seem to have affected this clay mineral.

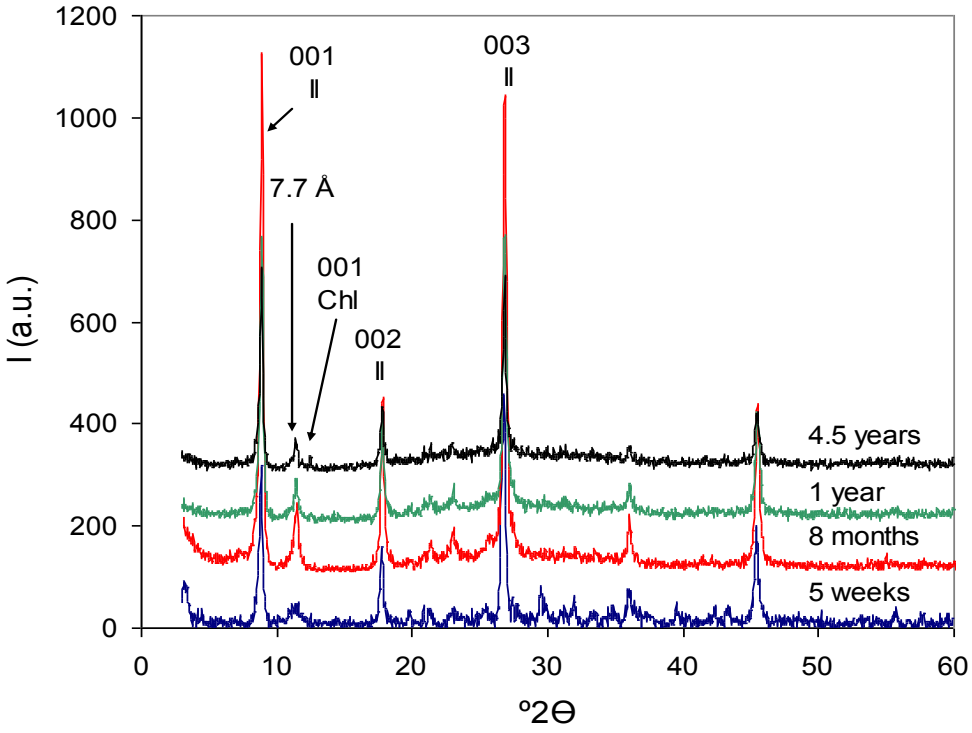

Figure 3-115. XRD patterns of illite treated with 5 M KOH for different periods of time. Il = illite, Chl = chlorite.

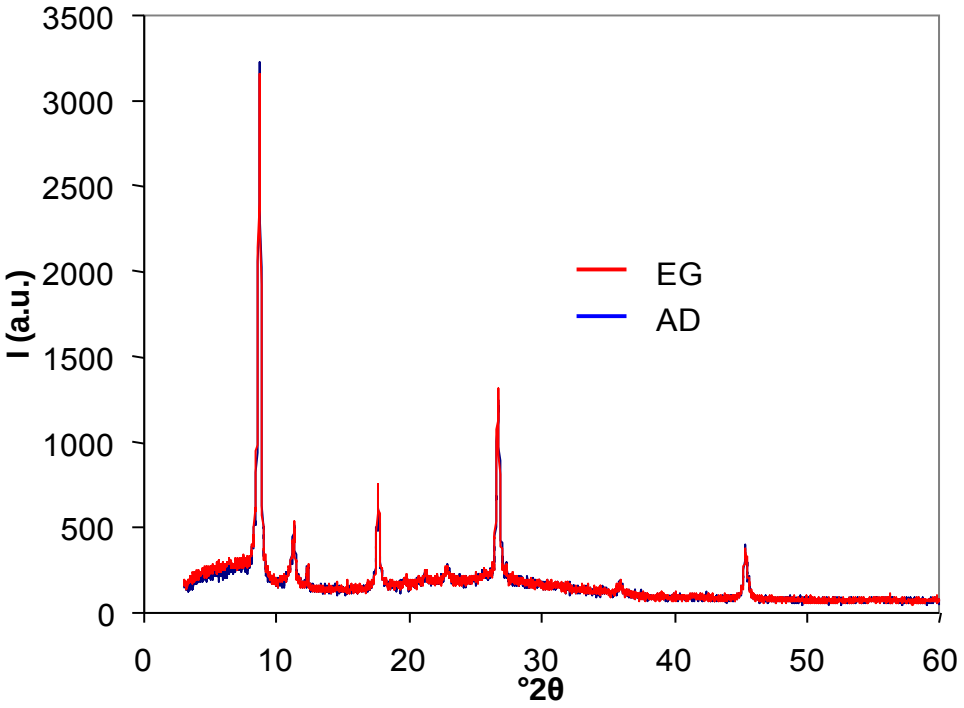

Figure 3-116. XRD patterns of illite treated with 5 M KOH for 4.5 years. OA air-dried (AD) and EG solvated.

Table 3-24: Crystallite size evolution upon alkaline activation using 5 M KOH

Time	Crystallite size (nm)
untreated	31
5 weeks	29
8 months	38
1 year	33
4.5 years	36

3.4.3.2. FESEM

FESEM analyses did not reveal any significant changes in the illite sample treated with KOH for 8 months (Figure 3-117).

However, after 1-year treatment a prismatic phase appeared which showed a morphological resemblance with zeolite K-F (Figure 3-118). A very similar zeolitic phase was previously identified in montmorillonite treated with KOH. EDS microanalysis results were compatible with a zeolitic phase (inset, Figure 3-118). Due to its scarcity it was not possible to identify this zeolite using XRD. After 4.5 years of treatment no additional changes were observed and the amount of the zeolitic phase did not seem to have increased (Figure 3-119). It is speculated that kaolinite which was present as an impurity in the original clay might be the main source material for this zeolitic phase, since illite as well as chlorite (see XRD data, Figure 3-115) seemed to remain unchanged. This would also explain why the number of zeolite K-F crystals did not increase over time, because all kaolinite might have transformed after 1 year.

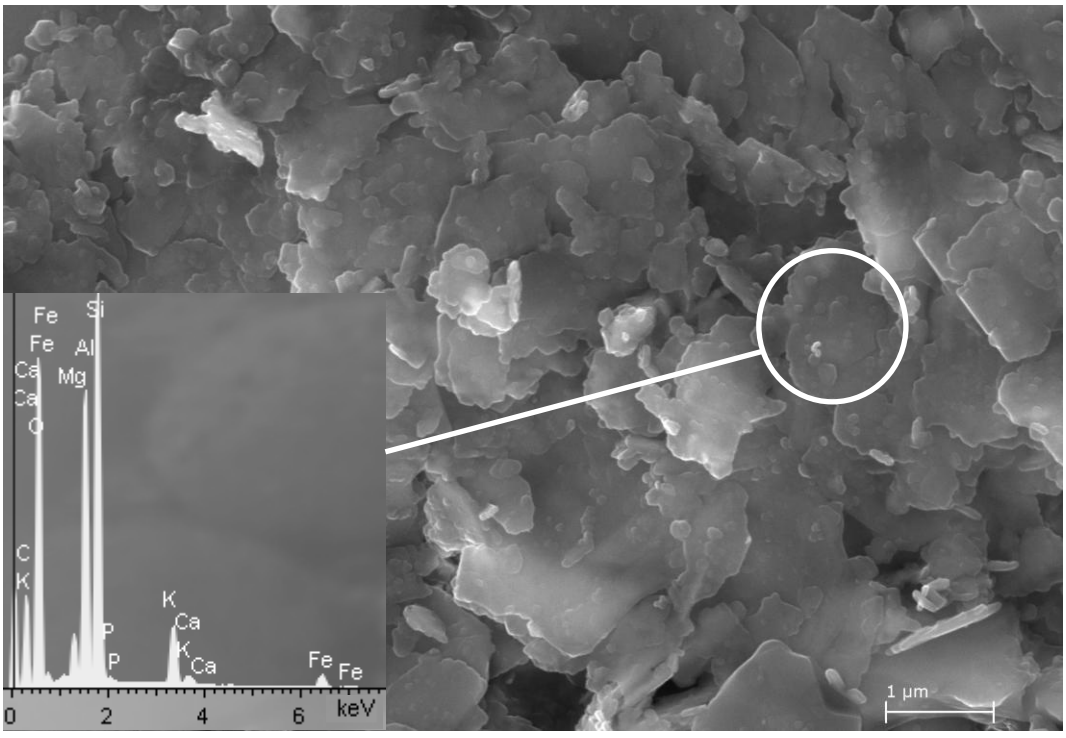

Figure 3-117. FESEM image of illite treated with 5M KOH treated for 8 months. No important changes were detected (EDS in inset).

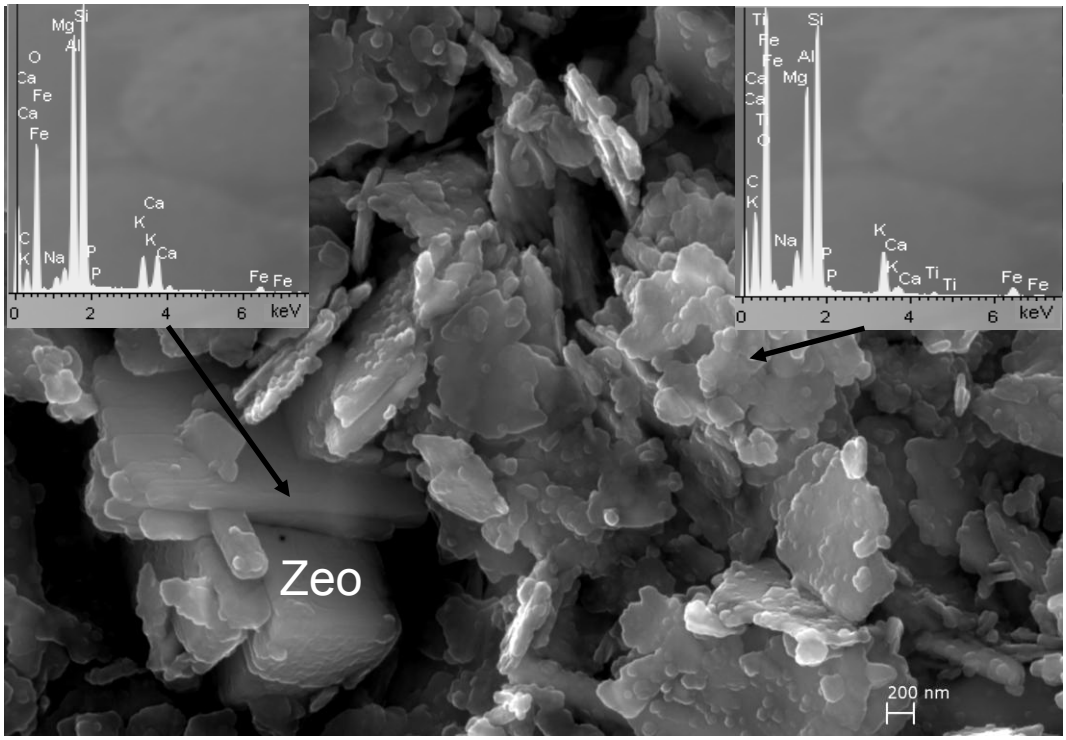

Figure 3-118. FESEM image of illite treated with 5M KOH for 1 year. A few bulky crystals of a newly formed phase, very likely a zeolitic phase (Zeo, EDS in inset, upper left), were observed, having a higher concentration of Al and Ca than the original clay (EDS in inset, upper right).

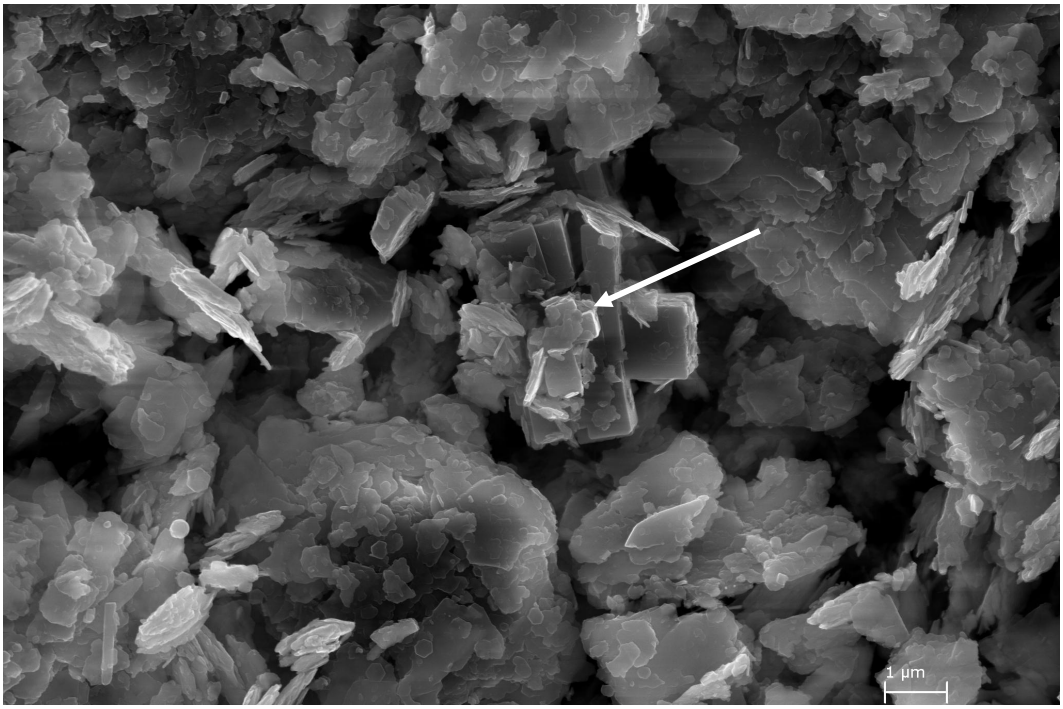

Figure 3-119. FESEM image of illite treated with 5 M KOH for 4.5 years. Unreacted illite and a cruciform-shaped zeolitic phase (arrow) can be observed.

3.4.3.3. TEM

TEM observations (Figure 3-120) did not reveal any important morphological changes upon alkaline treatment. However, TEM-AEM analyses (Table 3-25) showed a slight increase in Si and a decrease in interlayer charge due to a reduction in K, which might hint the beginning of illite degradation and its transformation into a smectitic clay mineral. Transformation of illite into smectite or illite/smectite interstratification is a common weathering process in soils, however, it is generally related to K deficient environments (Velde and Meunier 2008). Some hexagonal crystals were observed which might correspond to zeolite K-I. Furthermore, a small amount of nanosized, sphere-shaped crystals was detected. These crystals are identical to the one observed in the illite sample treated with 5 M NaOH which were identified as hydroxyapatite. The amount of these nanosized crystals is smaller than in the sample treated with NaOH, possibly because part of the Ca is incorporated into the zeolitic phase and not available for hydroxyapatite crystallization.

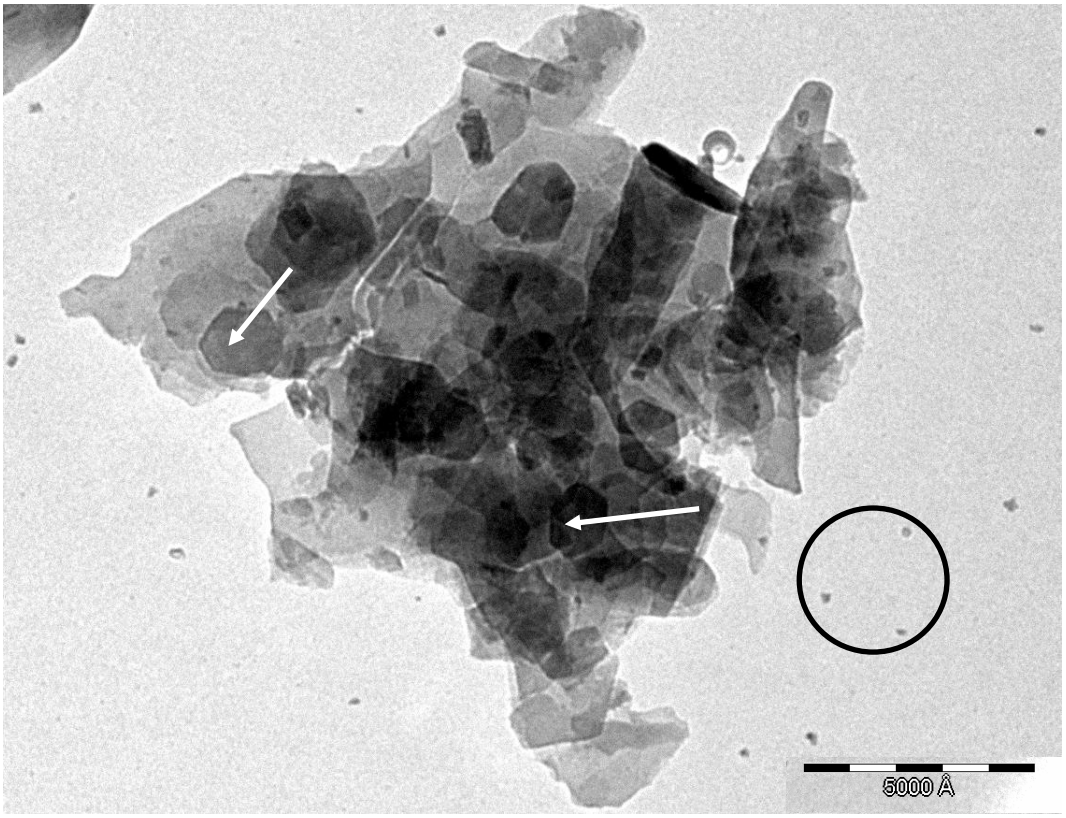

Figure 3-120. TEM image of illite treated with 5 M KOH for 4.5 years. Some hexagonal crystals (arrows) can be observed. These crystals might correspond to zeolite K-I. Small sphere-shaped crystals (circle) might correspond to hydroxyapatite.

Table 3-25. Structural formulae of untreated illite and illite treated with 5 M KOH for 4.5 years calculated from TEM-AEM data

Structural formulae of illite based on $O_{10}(OH)_2$										
	Si	^{IV}Al	^{VI}Al	Mg	Fe	Σoct.cat.[1]	K	Ca	Na	Σint.cha.[2]
Untreated average	3.22 ±0.09	0.78 ±0.06	1.63 ±0.14	0.22 ±0.06	0.18 ±0.11	2.03 ±0.04	0.84 ±0.13	0.09 ±0.04	0.08 ±0.07	1.01 ±0.15
1	3.37	0.63	1.76	0.16	0.19	2.11	0.53	0.04	0.12	0.73
2	3.27	0.73	1.64	0.27	0.19	2.10	0.65	0.02	0.12	0.81
3	3.40	0.60	1.57	0.21	0.26	2.04	0.74	0.00	0.07	0.81
4.5 years average	3.35 ±0.07	0.65 ±0.07	1.66 ±0.10	0.21 ±0.06	0.21 ±0.04	2.08 ±0.04	0.64 ±0.10	0.02 ±0.02	0.10 ±0.02	0.78 ±0.05

[1] Sum of octahedral cations
[2] Sum of interlayer charge

3.4.3.4. Nitrogen sorption

The illite sample treated for one year with 5 M KOH showed an about 3 times higher surface area than the untreated sample (Table 3-26). The surface area increase might be explained considering the formation of zeolitic phases, possibly zeolite K-F and K-I. However, the contribution of these phases to the surface area increase is uncertain, because their average pore size is below the detection limit of this analytical technique. Thus, mainly the zeolites outer surface will contribute to a detectable surface area increase (see discussion, section 4.3.2.). Furthermore, the formation of nanosized hydroxyapatite might have contributed to a certain surface area increase as well.

The shape of nitrogen sorption isotherm and the hysteresis loop of illite treated with 5 M KOH for 1 year did not experience any important modifications if compared to the one of the untreated sample (Figure 3-121).

Table 3-26. BET surface area of untreated and illite treated with 5 M KOH.

Treatment time	Surface area (m^2/g)
0	7.53 ± 0.17
1 year	22.99 ± 0.44

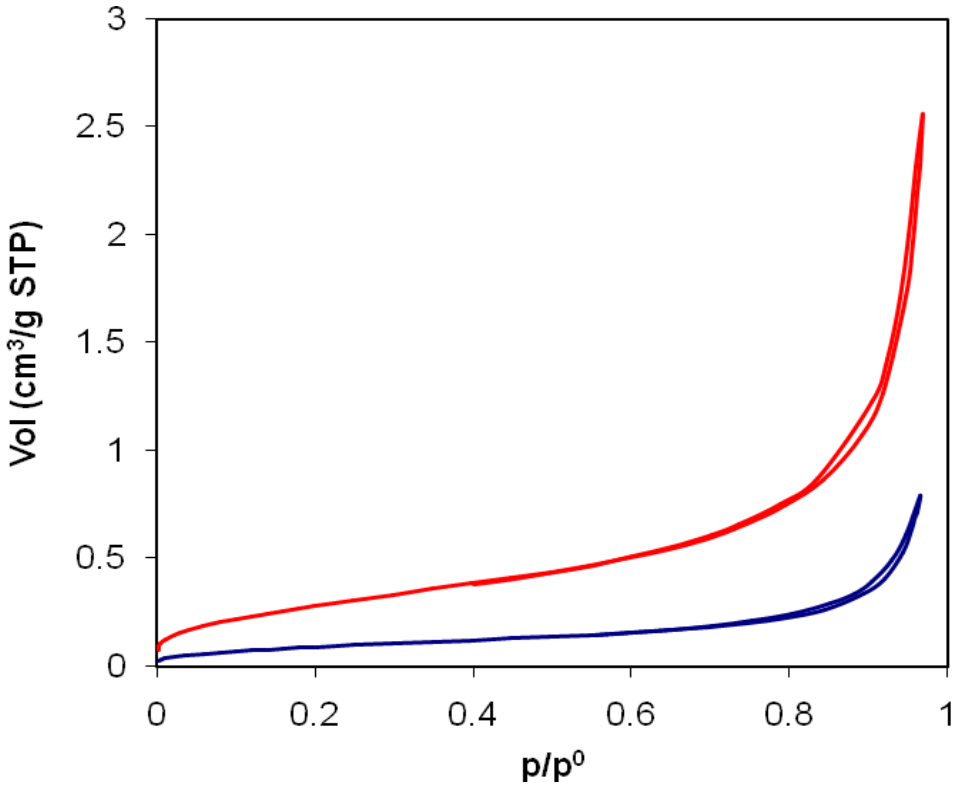

Figure 3-121. Nitrogen sorption isotherms of untreated illite (blue) and illite treated with 5 M KOH for 1 year (red).

3.5. Alhambra Formation soil

In the following sections results regarding the mineralogical characteristics of the Alhambra Formation soil before and after alkaline activation using $Ca(OH)_2$, NaOH and KOH solutions are presented.

3.5.1. Untreated Alhambra Formation soil

3.5.1.1. XRF

X-ray fluorescence analysis (Table 3-27) of the < 2 μm of the untreated sample showed a high silica and aluminium content. This is not surprising because the material contains mainly phyllosilicates and, possibly trace amounts of quartz and feldspars. The relative high K_2O concentration is a result of the elevated illite amount which was confirmed by X-ray diffraction (Figure 3-122). A small contribution to the K_2O concentration might be due to the presence of traces of K-feldspars. Na, Ca and Mg concentrations were relatively low, but sufficient to be correlated with the presence of paragonite, smectite and, possibly, trace amounts of albite. The iron oxide content was high. The excess in Fe can be explained considering the presence of iron oxihydroxides which are responsible for the red colour of the Alhambra Formation soil.

Table 3-27. XRF results of starting materials (wt %).

Mineral	SiO_2	Al_2O_3	Fe_2O_3	Na_2O	P_2O_5	TiO_2	MgO	K_2O	CaO	Loss on Ignition	Total
Alhambra Formation < 2 μm	38.8	25.9	16.17	0.52	0.55	0.71	1.01	3.43	0.74	12.25	100.08

3.5.1.2. XRD

Semi-quantitative powder XRD of the whole sample showed (Figure 3-122) that the earth from the Alhambra Formation was composed of quartz (65 %) and phyllosilicates (30 %), with small amounts of feldspars (5 %), calcite/ dolomite (< 5 %) and iron oxihydroxides (possibly goethite, hematite, lepidocrocite and ferrihydrite). Martin-Garcia et al. (1998) report a comparable mineralogical composition based on semi-quantitative XRD results.

XRD analysis of OA (Figure 3-123) showed that the clay fraction includes about 45 % illite (d_{001}= 9.98 Å), 30 % kaolinite (d_{001}= 7.14 Å), 15 % smectites (d_{001}= 12.5-14 Å) with minor amounts (< 10 %) of paragonite (d_{001}= 9.60 Å) and chlorite (3.53 Å). In addition to these phases, Martin-Garcia et al. (1998) detected small amounts of interstratified illite/smectite minerals in Alhambra Formation soil. However, in our case, the presence of mixed-layer illite/smectite could not be confirmed unambiguously using the method described by Moore and Reynolds (1997). The absence of well defined Bragg peaks of iron oxide and/or hydroxide reflects the low crystallinity or the X-ray amorphous character of these phases. The crystallite sizes of illite and kaolinite were 15 and 16 nm, respectively.

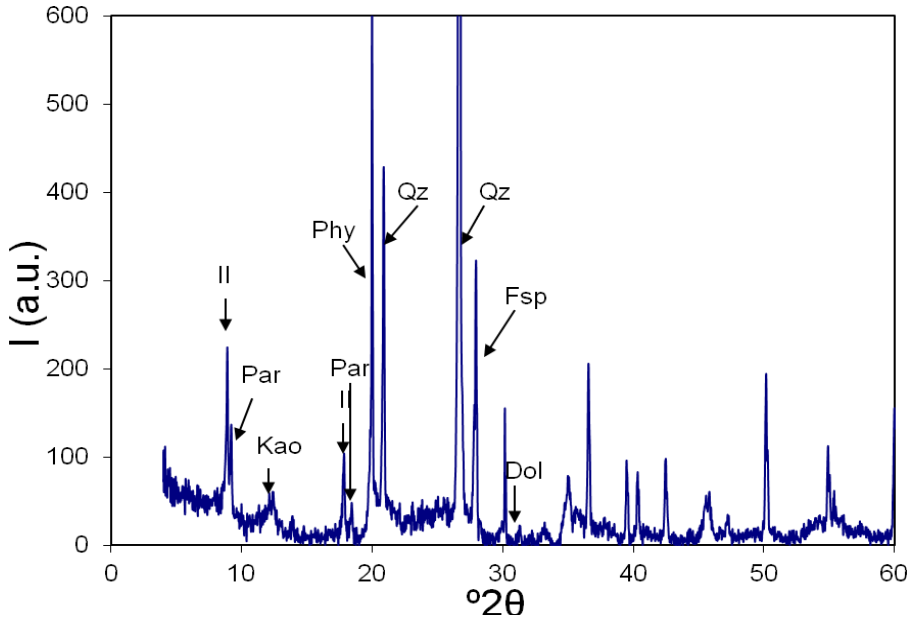

Figure 3-122. XRD pattern of untreated Alhambra Formation soil (whole sample). Il = Illite, Par = paragonite, Kao = Kaolinite, Phy = phyllosilicates, Qz = quartz, Fsp = feldspar, Dol = dolomite.

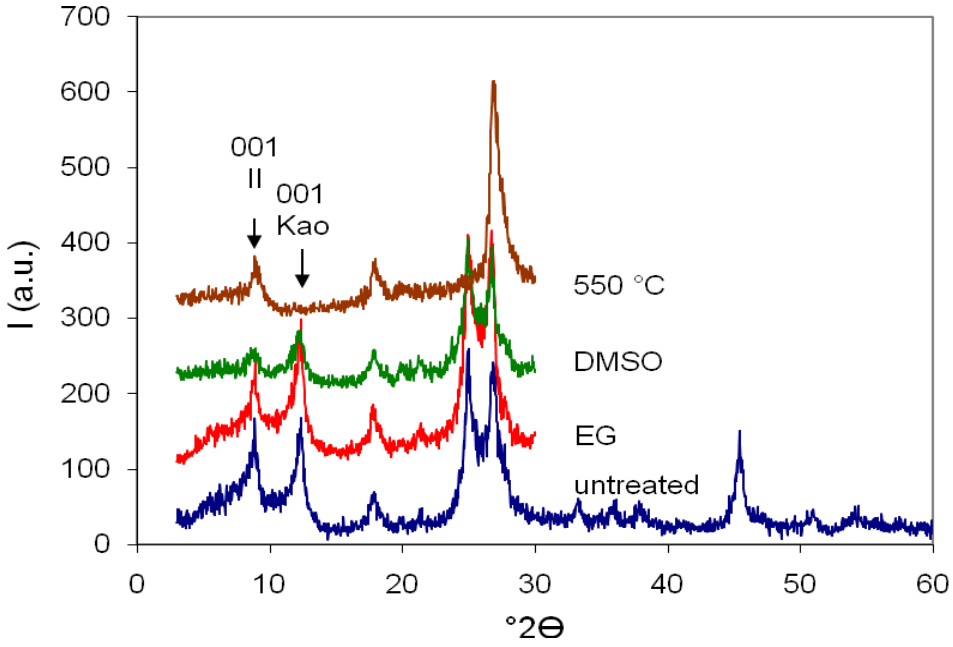

Figure 3-123. XRD patterns of the < 2 µm fraction of untreated Alhambra Formation clay (OA). Il = Illite, Kao = Kaolinite.

3.5.1.3. FESEM

FESEM observations (Figure 3-124) showed the typical laminar structure of phyllosilicates of micrometric/submicrometric size.

EDS microanalyses (inset, Figure 3-124) indicated that Si and Al were generally the major elements, together with smaller amounts of K, Na, Mg and Fe, the latter probably due to iron oxides/hydroxides or illite/smectite. The EDS microanalysis is compatible with the presence of clay minerals like illite (Si, Al, K), kaolinite (Al, Si) and smectite (Si, Al, Na, K, Mg, Fe). These results are in agreement with XRF and XRD results.

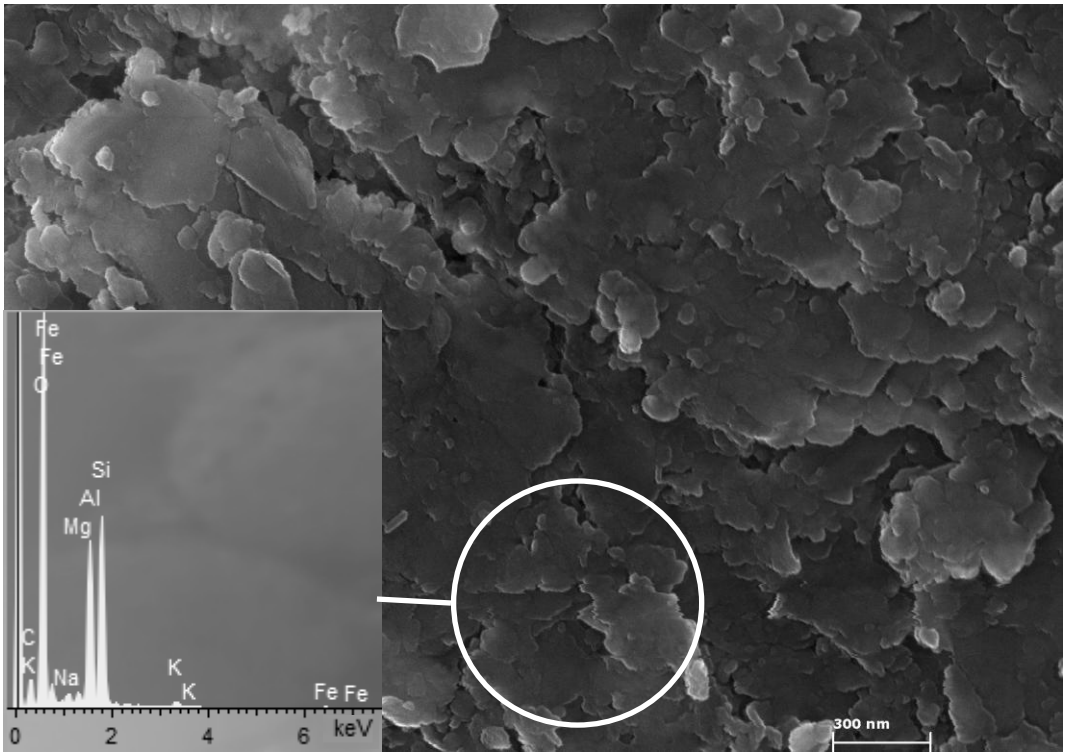

Figure 3-124. FESEM image of the < 2 μm fraction of the untreated Alhambra Formation soil. EDS microanalysis (inset) shows an "average" chemical composition of clay particles compatible with illite/smectite.

3.5.1.4. TEM

The results of TEM analyses were in agreement with XRD and FESEM results regarding the mineralogy of the Alhambra Formation clay. Smectites (Figure 3-125a), kaolinite (Figure 3-125b), illite (Figure 3-125c) and paragonite (Figure 3-125d) were observed. Small amounts of goethite and rutile were also identified.

TEM-AEM microanalysis allowed the calculation of the structural formulae of the main clay minerals in the Alhambra Formation soil (Table 3-28).

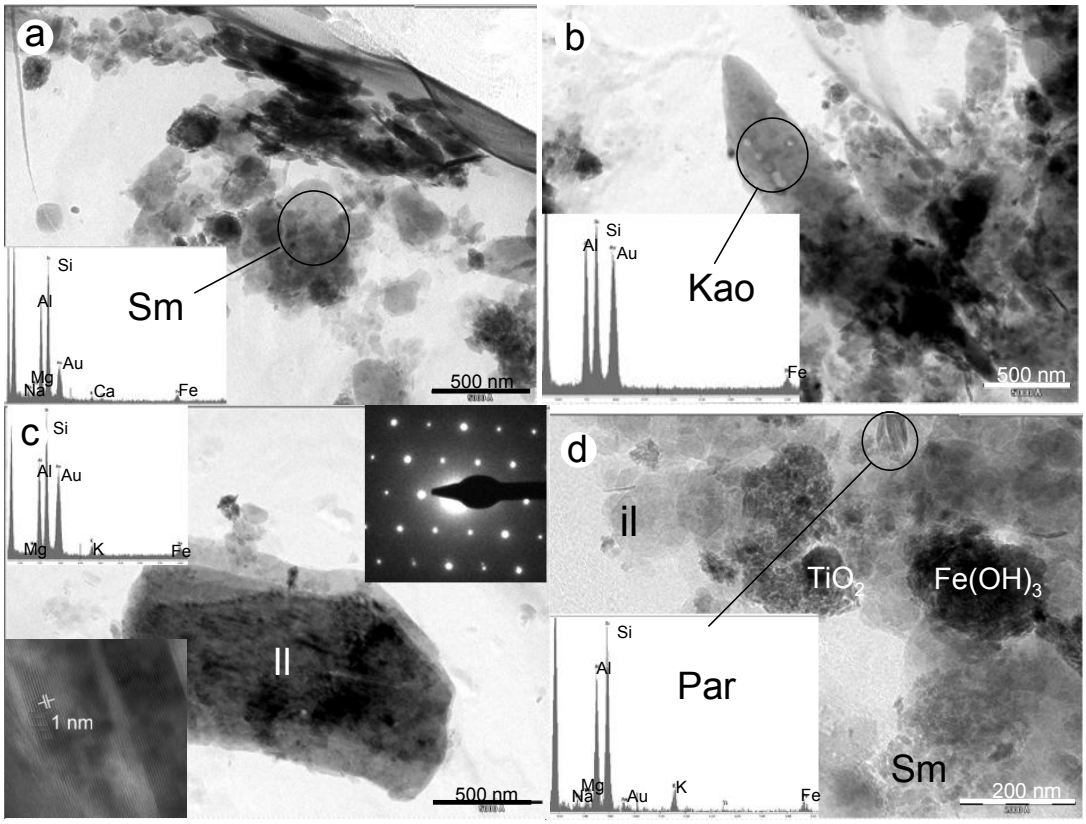

Figure 3-125. TEM images (Elert et al. 2008) of untreated Alhambra Formation soil (circle indicates the spot where microanalysis was performed). a) Smectite (Sm) is identified by EDS (inset). b) Kaolinite (Kao) is identified by EDS (inset). c) Illite (Il) is identified by SAED along the [001] zone axis (inset, upper-right corner), EDS (inset, upper-left) and TEM high-resolution lattice-fringe image showing d_{001} = 1 nm (inset, lower-left). d) Paragonite (Par) is identified by EDS (inset), together with Il, Sm, goethite ($Fe(OH)_3$) and rutile (TiO_2).

Table 3-28. Structural formulae of phyllosilicates of the Alhambra Formation soil (< 2 µm fraction) calculated from TEM-AEM data.

Structural formulae of illite based on $O_{10}(OH)_2$										
	Si	^{IV}Al	^{VI}Al	Mg	Fe	Σoct.cat.[1]	K	Ca	Na	Σint.cha.[2]
1	3.01	0.99	1.52	0.17	0.57	2.27	0.57	-	-	0.57
2	3.02	0.98	1.79	0.08	0.36	2.24	0.33	-	-	0.33
3	3.27	0.74	1.84	0.29	0.04	2.17	0.48	-	-	0.48
4	3.13	0.86	1.93	0.15	0.14	2.22	0.42	-	-	0.42
average	3.11 ± 0.12	0.89 ± 0.12	1.77 ± 0.18	0.17 ± 0.09	0.28 ± 0.24	2.23 ± 0.04	0.45 ± 0.10	-	-	0.45 ± 0.10
Structural formulae of smectite based on $O_{10}(OH)_2$										
1	3.60	0.40	1.60	0.17	0.02	2.03	0.13	0.06	-	0.25
2	3.60	0.40	1.57	0.24	-	1.98	0.39	-	0.16	0.55
3	3.83	0.17	1.82	0.12	-	2.06	0.05	-	0.13	0.18
4	3.68	0.32	1.48	0.24	-	2.14	0.29	-	-	0.29
5	3.56	0.44	1.52	0.63	-	2.34	0.14	-	-	0.14
average	3.65 ± 0.11	0.35 ± 0.11	1.60 ± 0.13	0.28 ± 0.20	0.00 ± 0.01	2.11 ± 0.14	0.20 ± 0.14	0.01 ± 0.03	0.06 ± 0.08	0.28 ± 0.16
Structural formulae of paragonite based on $O_{10}(OH)_2$										
1	3.17	0.83	1.89	0.12	-	2.10	0.07	-	0.63	0.70
2	3.33	0.67	1.76	0.21	-	2.11	0.07	0.05	0.44	0.61
average	3.25 ± 0.11	0.75 ± 0.11	1.83 ± 0.09	0.17 ± 0.06	-	2.11 ± 0.01	0.07 ±0.00	0.03 ± 0.04	0.54 ± 0.13	0.66 ± 0.06
Structural formulae of kaolinite based on $10_5(OH)_2$										
	Si	Al	Mg	Fe						
1	2.02	1.75	-	0.23						
2	2.09	1.78	-	0.11						
3	2.15	1.65	0.14	0.06						
4	2.23	1.60	0.07	0.06						
5	2.08	1.78	0.11	0.06						
6	2.10	1.59	0.10	0.24						
7	1.99	1.94	-	0.06						
average	2.09 ± 0.08	1.73 ± 0.12	0.06 ± 0.06	0.12 ± 0.08						

[1] Sum of octahedral cations
[2] Sum of interlayer charge
- below detection limit

3.5.1.5. Nitrogen sorption

The BET surface area of the < 2 μm fraction of the untreated Alhambra Formation soil was 70.78 ± 0.28 m^2/g. This value seems reasonable since this soil is composed of a mixture of clay minerals including illite, kaolinite and smectite.

The nitrogen sorption isotherm was of type II (Figure 3-126), which is also observed in the pure clays. However, the type H3 hysteresis loop was more pronounced than the one observed in the case of illite and kaolinite, reflecting the presence of smectitic clay minerals. This result is consistent with the fact that the Alhambra Formation soil contains a mixture of expandable and non-expandable clay minerals.

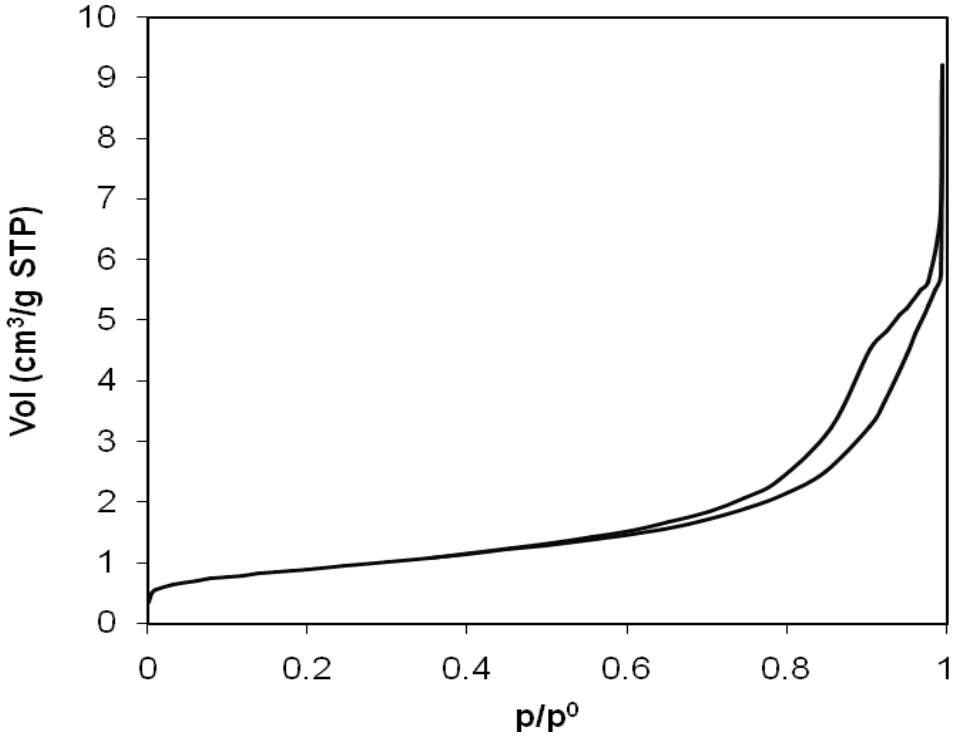

Figure 3-126. Nitrogen sorption isotherm of the < 2 μm fraction of the untreated Alhambra Formation soil.

3.5.1.6. Particle size analysis

Particle size analysis revealed a maximum at 140 nm and a secondary maximum between 0.5-15 μm in the case of the Alhambra Formation soil (Figure 3-127). The particle size distribution is very similar to the one of pure illite, which is not surprising because illite is the dominant clay mineral in this soil.

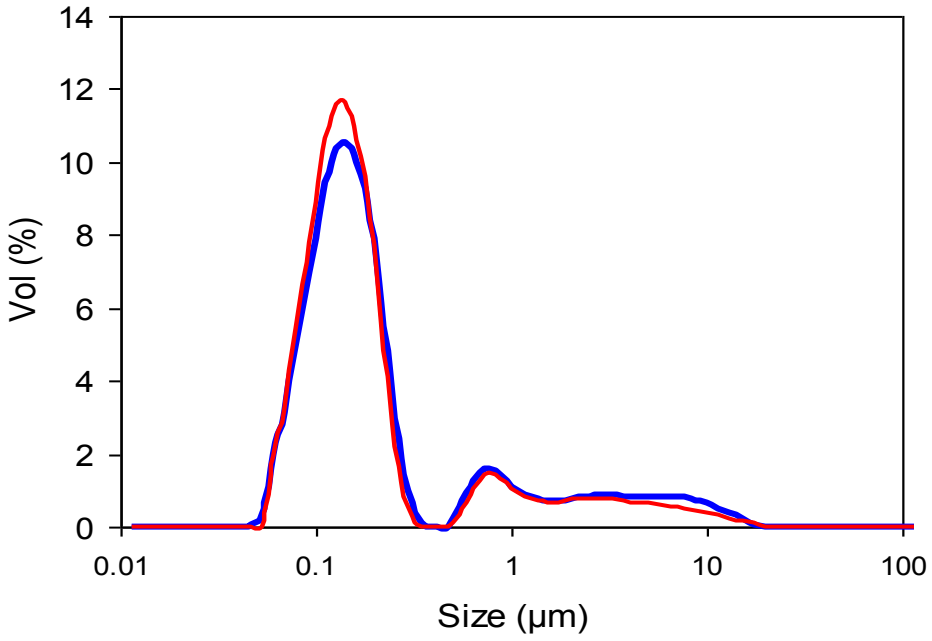

Figure 3-127. Particle size distribution of untreated Alhambra Formation soil (blue). The particle size distribution curve of pure illite (red) is included for comparison.

3.5.1.7. TG

The thermogravimetric curve showed a loss of adsorbed water of 6 % from about 30°C to 400 °C (Figure 3-128). At around 500 °C dehydroxylation of the Alhambra Formation soil started. The total weight loss amounted to 12.1 %, being about 6.1 % due to dehydroxylation. The shape of the thermogravimetric curve is very similar to the one of pure illite until ~ 500 °C was reached. At this point weight loss due to dehydroxylation was higher than observed in pure illite. The higher weight loss can be explained considering the presence of kaolinite which has a larger number of structural hydroxyl groups per unit than 2:1 clays.

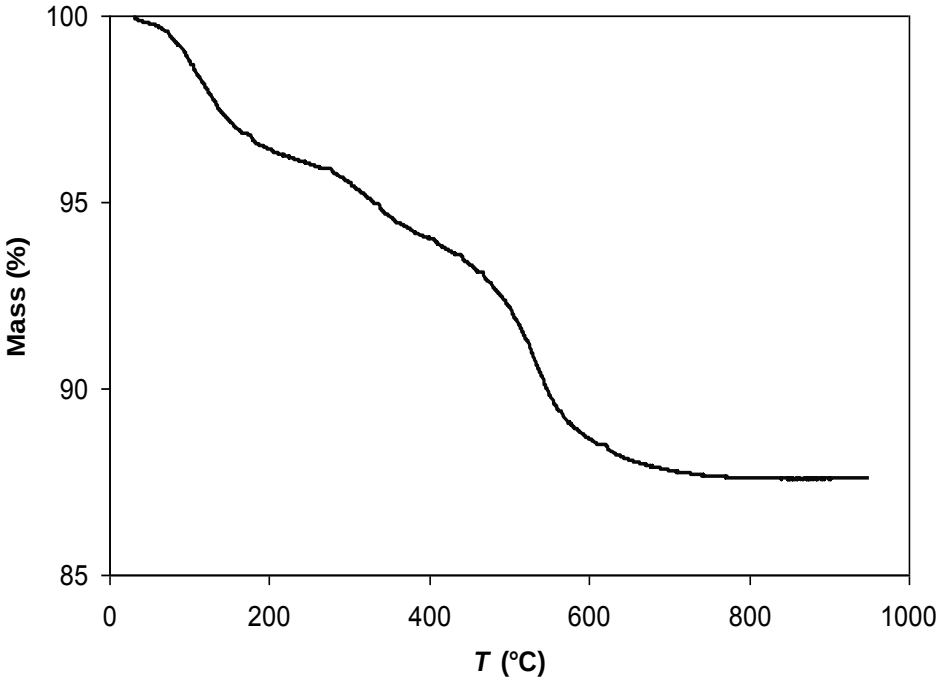

Figure 3-128. Thermogravimetric curve of untreated Alhambra Formation soil.

3.5.2. Alhambra Formation soil treated with $Ca(OH)_2$

In this section results of the study of the mineralogical evolution of the < 2 μm of the Alhambra Formation soil treated with saturated $Ca(OH)_2$ solution are presented. The mineralogical and textural evolution were studied using XRD, FESEM, TEM and nitrogen sorption.

3.5.2.1. XRD

XRD analyses revealed that the attack with saturated $Ca(OH)_2$ solution caused only limited changes in the mineralogy of the clay sample (Figure 3-129). The 12.5-14 Å broad Bragg peak seemed to have experienced a reduction, suggesting that smectites might have been destroyed partially. However, the diffractogram of the EG solvated oriented aggregate of the Alhambra Formation clay fraction treated for 1 year with $Ca(OH)_2$ clearly showed the presence of expandable clays (Figure 3-130). Other clay minerals, such as kaolinite and illite, did not experience any significant changes and newly formed phases could not be detected after one-year treatment using this technique.

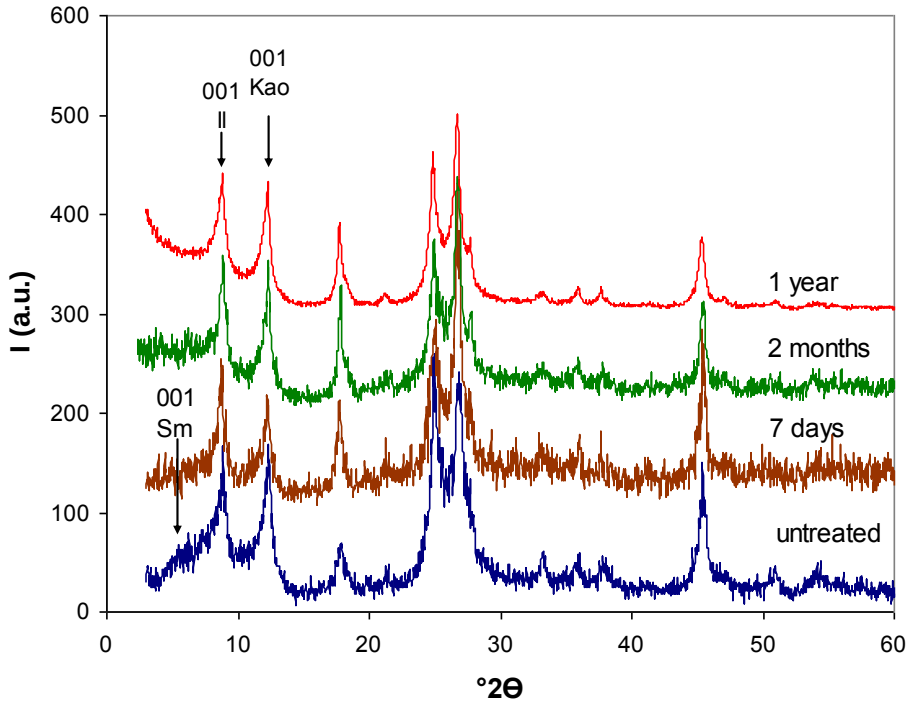

Figure 3-129. XRD patterns of Alhambra Formation soil treated with $Ca(OH)_2$ for different periods of time.

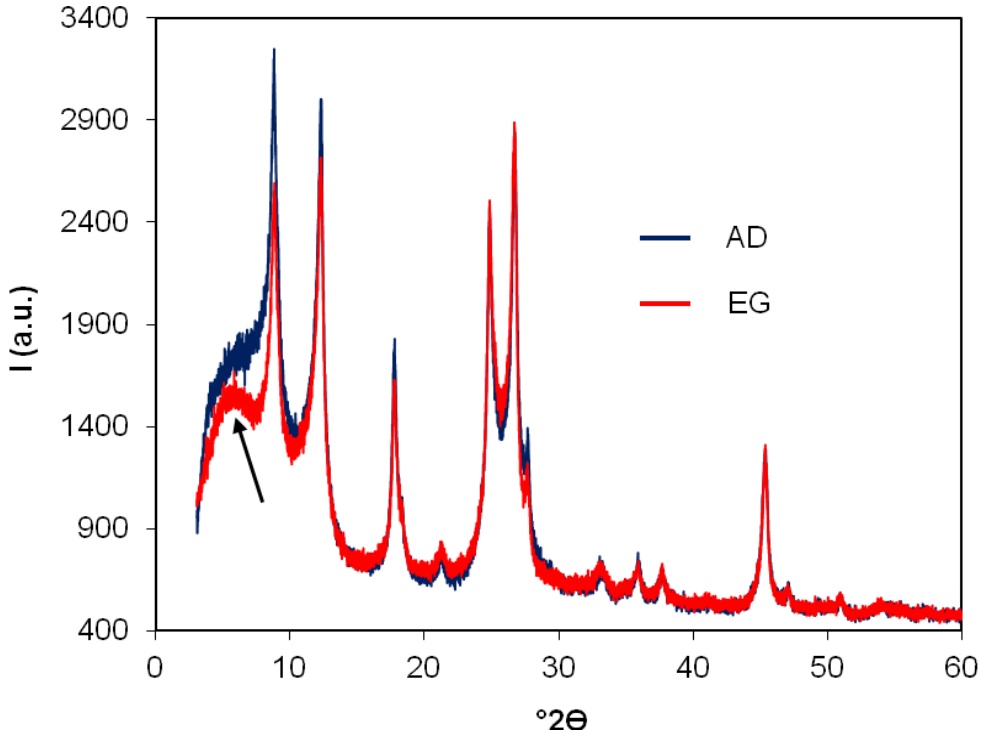

Figure 3-130. XRD patterns of Alhambra Formation soil treated with $Ca(OH)_2$ for 1 year. OA air-dried (AD). EG solvation reveals the presence of expandable clay (arrow).

3.5.2.2. FESEM

FESEM analyses confirmed that $Ca(OH)_2$ produced little morphological or chemical changes in Alhambra Formation soil. Besides aggregates of planar-shaped original phyllosilicates, a scarce amount of a granular or flake-like phase, possibly Ca-silicate-hydrate (CSH) type I was detected (Figure 3-131). Diamond et al. (1964) described CSH type I as a poorly crystalline phase with "snowflake" morphology. Note that the EDS microanalysis (inset, Figure 3-131) was dominated by the underlying clay, possibly illite. CSH or CASH phases commonly form upon alkaline activation with $Ca(OH)_2$. They have been reported in the case of various starting materials including Opalinus clay, bentonite, biotite, muscovite and feldspars (Liebig und Althaus 1997, Gaucher and Blanc 2006). Berube et al. (1990) observed CSH phases of very similar morphology in the case of chert treated with saturated $Ca(OH)_2$ (Figure 3-132). Figure 3-133 shows aggregates with a chemical composition (inset a, Figure 3-133) compatible with calcium carbonate. Furthermore, an aggregate of nanosized crystals, possibly zeolite precursor gel particles, was detected (3-134). However, a crystalline zeolitic phase was not observed. Results by Berube et al. (1990) are in agreement with these findings. The authors treated a wide verity of minerals including biotite, chlorite, illite and metabentonite with saturated $Ca(OH)_2$ solution at 23 °C for 265 days and observed only very limited alteration of the clay minerals and the formation of reticular phases, possibly CSH.

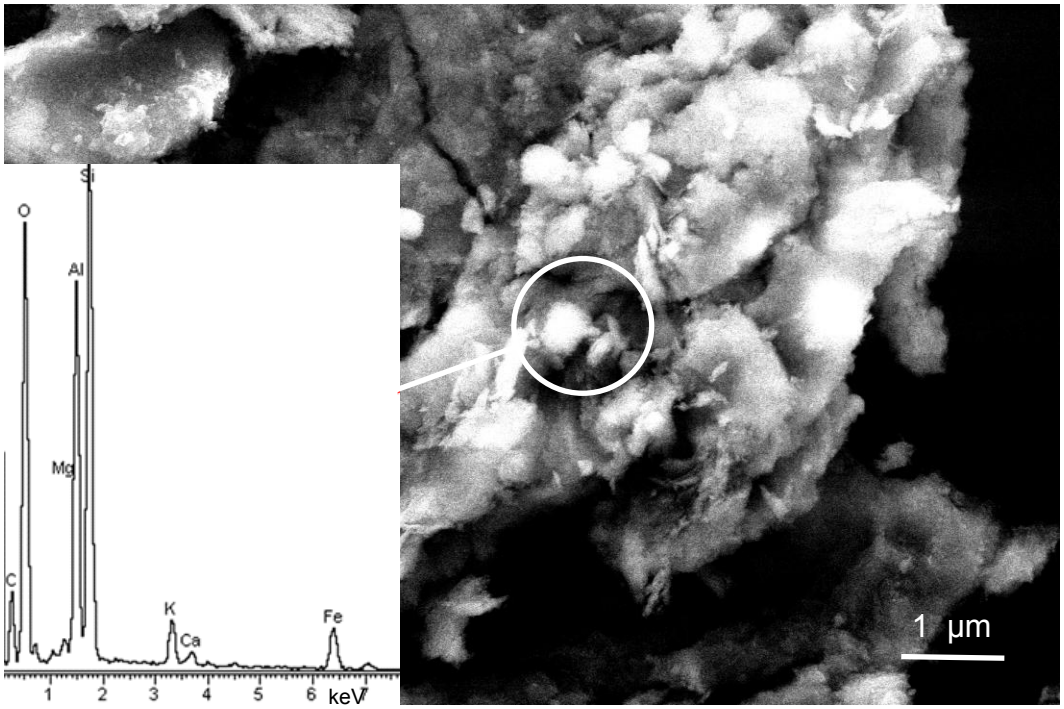

Figure 3-131: FESEM image of Alhambra Formation soil treated for 1 year with $Ca(OH)_2$. The inset shows the EDS spectrum and the circle indicates the spot where the analysis of the newly formed phase, probably CSH (I), was performed. The EDS analysis is dominated by the unreacted underlying clay.

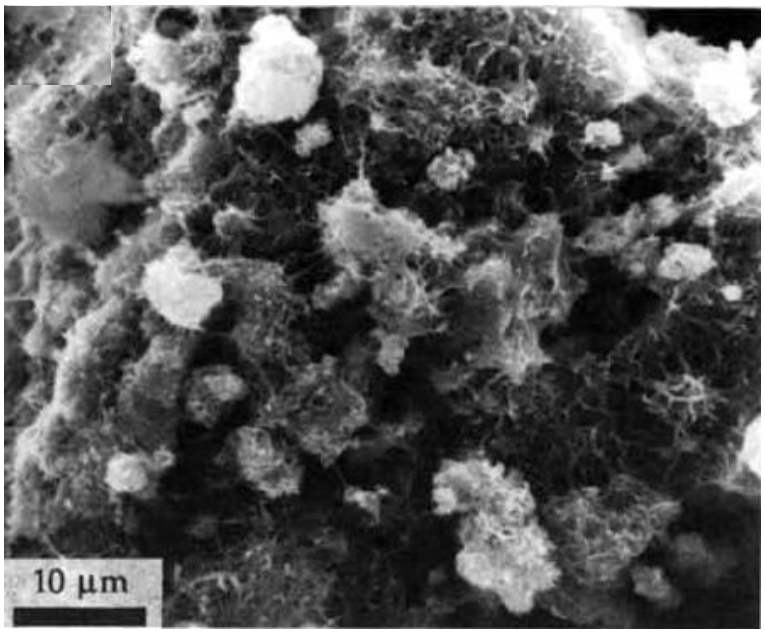

Figure 3-132. SEM image of chert after lime treatment, showing reticular C-S-H (Berube et al. 1990).

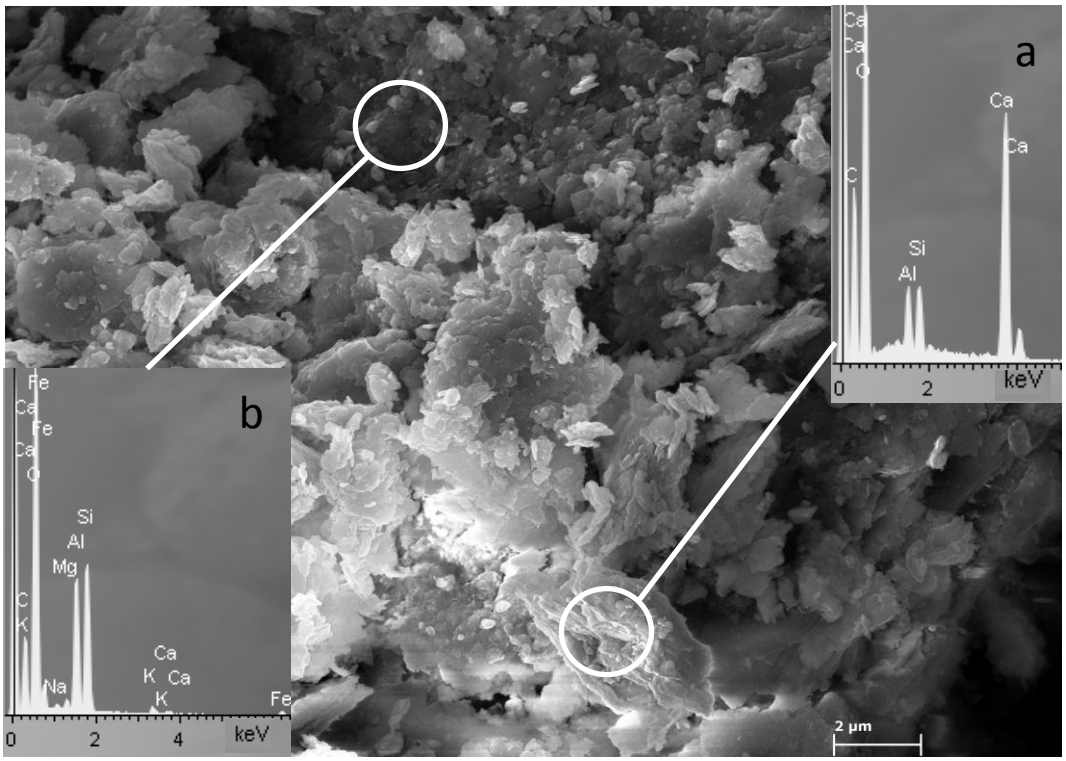

Figure 3-133. FESEM image of Alhambra Formation soil treated with saturated $Ca(OH)_2$ for 1 year. Ca-carbonate (inset a) and unaltered clay minerals (inset b) can be observed.

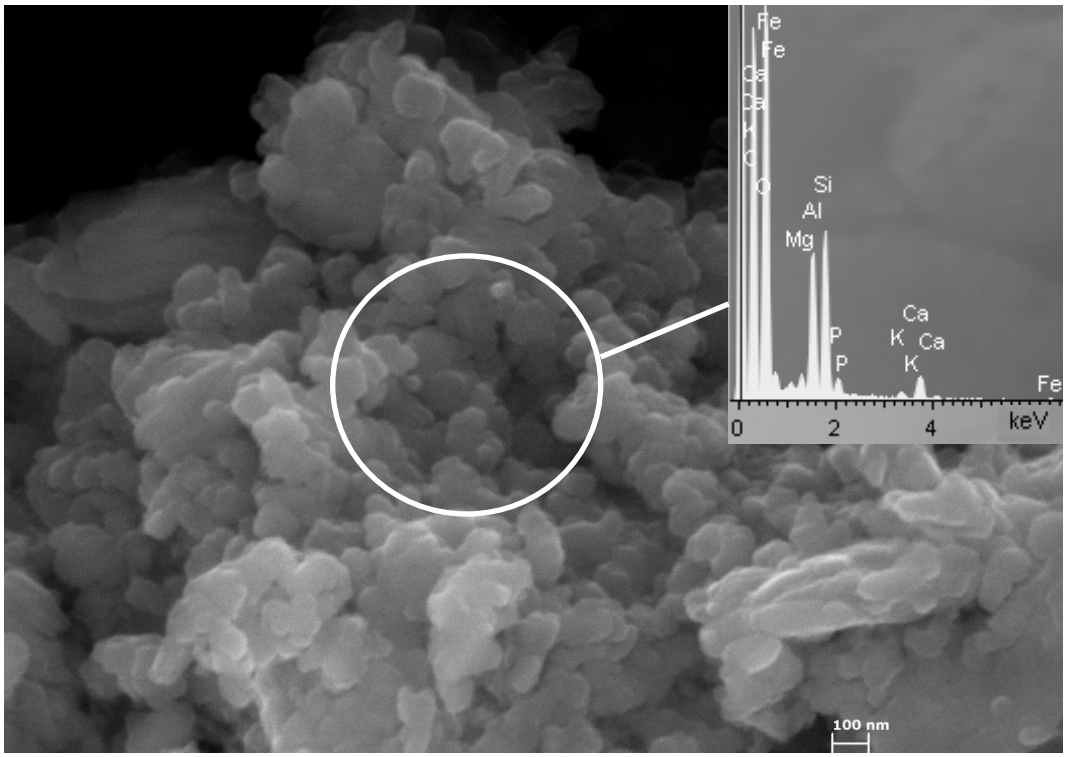

Figure 3-134: FESEM image of Alhambra Formation soil treated for 1 year with $Ca(OH)_2$. The inset shows the EDS spectrum and the circle indicates the spot where the analysis of the newly formed phase, possibly zeolite precursor gel particles, was performed.

3.5.2.3. TEM

TEM analyses could not confirm the presence of granular or flake-like calcium silicate hydrates (CSH). Furthermore, clay minerals did not seem to have experienced any significant changes during 1-year treatment using saturated $Ca(OH)_2$ solution (Figure 3-135).

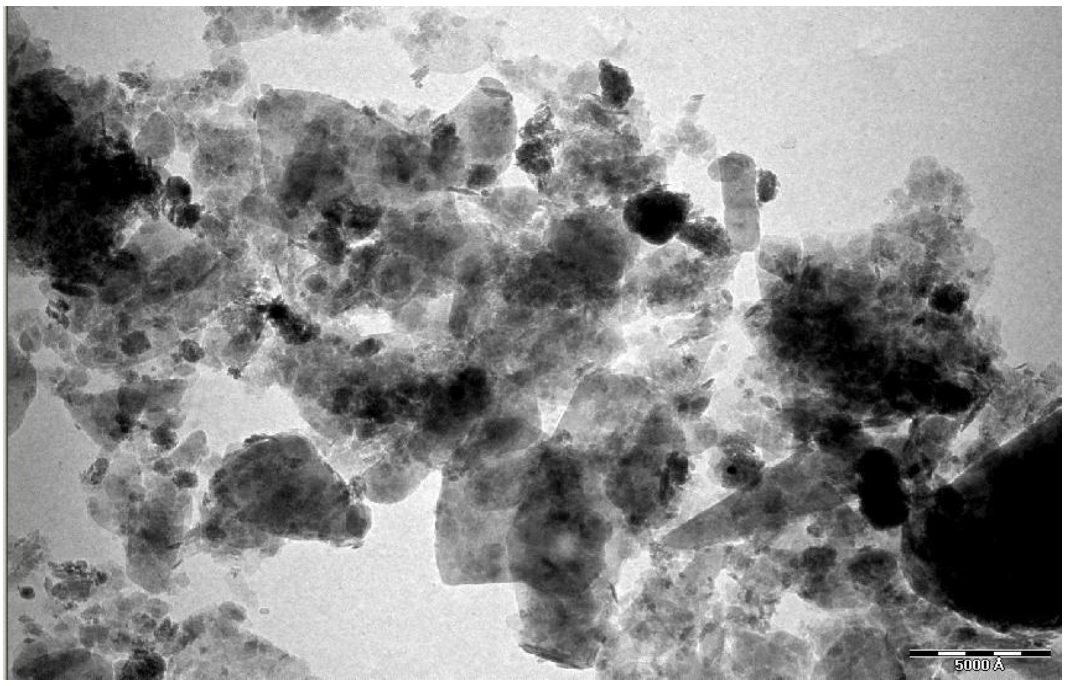

Figure 3-135: TEM image of Alhambra Formation soil treated with $Ca(OH)_2$ for one year.

3.5.2.4. Nitrogen sorption

The BET surface area of Alhambra Formation soil treated with $Ca(OH)_2$ for one year (76.35 ± 0.83 m^2/g) did not experience any significant change if compared with the one of the untreated soil (70.78 ± 0.28 m^2/g). A significant surface area decrease as a result of the destruction of smectite was not observed. However, the formation of CSH might have counteracted a surface area decrease to a certain extent. In any case, the amount of CSH formed must have been rather small since it would have been expected to produce an important increase in surface area. Surface areas of poorly crystalline CSH phases are reported to be in the range of 135-380 m^2/g (Diamond et al. 1964).

The nitrogen sorption isotherm of type II and the hysteresis loop of type H3 showed only minor changes (Figure 3-136), suggesting that expandable clays were still present. The destruction of smectites should have resulted in a less pronounced hysteresis loop, closer to the one observed in kaolinite and illite. Nitrogen sorption data, thus, provide additional evidence that the clay minerals in the sample treated with $Ca(OH)_2$ did not suffer important textural or mineralogical changes.

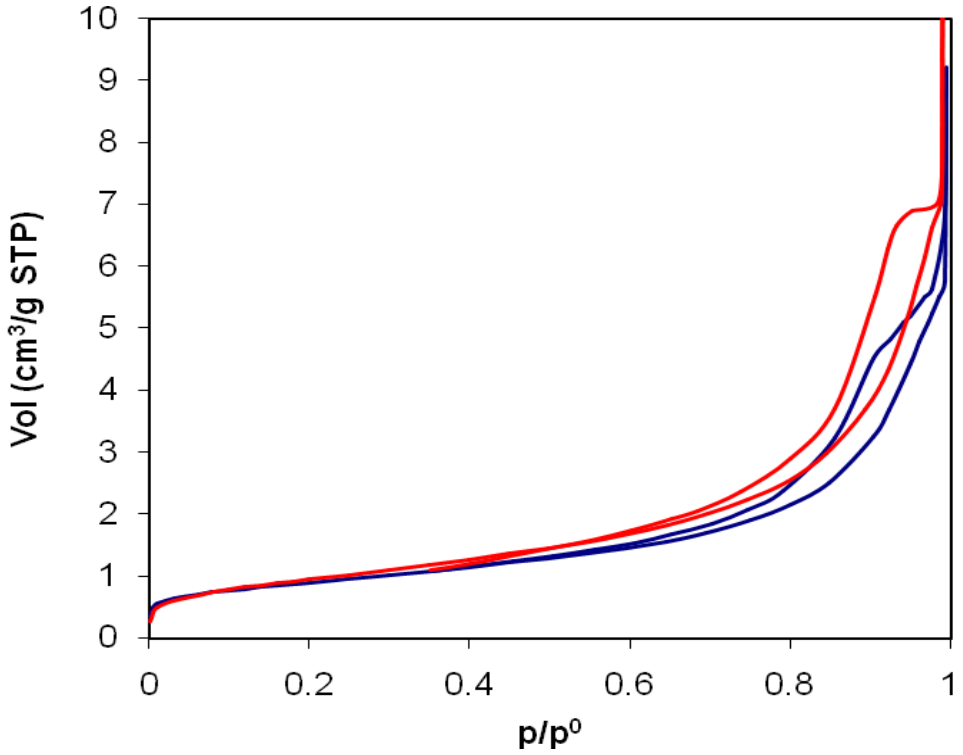

Figure 3-136. Nitrogen adsorption isotherms of Alhambra Formation soil. Untreated (blue) and after treatment with $Ca(OH)_2$ for 1 year (red).

3.5.3. Alhambra Formation soil treated with NaOH

In this section results of the study of the mineralogical evolution of the < 2 μm fraction of the Alhambra Formation soil treated with 0.4 M NaOH and 5 M NaOH are presented. The mineralogical evolution was studied using XRD, FESEM, TEM and nitrogen sorption.

3.5.3.1. XRD

Smectites were the only clay phase which seemed to have been attacked in the sample of the Alhambra Formation soil treated with 0.4 M NaOH solution (Figure 3-137). The Bragg peak intensity of illite and kaolinite did not experience any significant reduction. Furthermore, it was not possible to detect any other changes in the clay mineralogy or the formation of new phases using XRD.

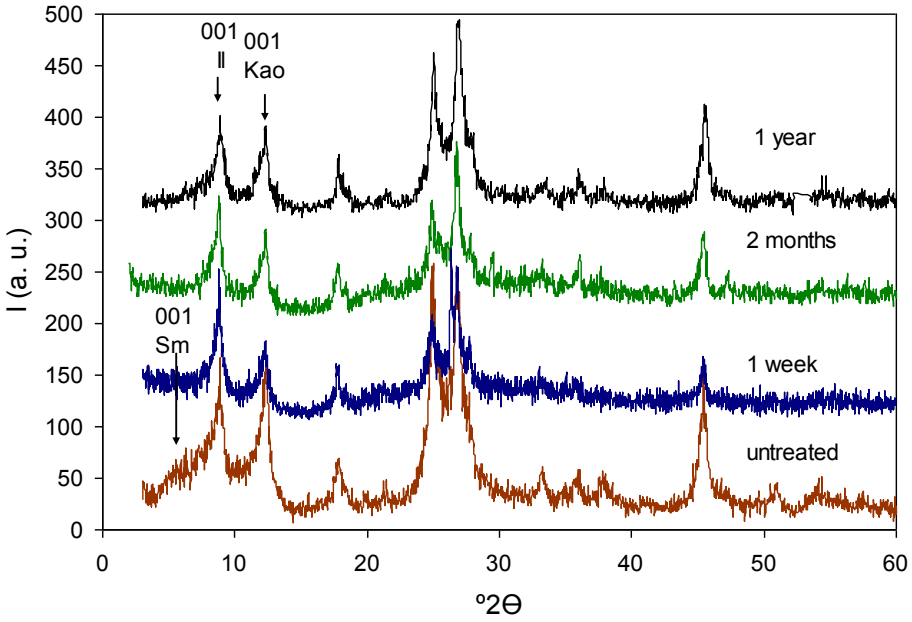

Figure 3-137. XRD patterns of Alhambra Formation clays (OA) treated with 0.4 M NaOH solution for different periods of time.

In the case of the Alhambra Formation soil treated with 5 M NaOH solution XRD results showed more clearly the mineralogical evolution upon alkaline activation than in the case of the sample treated with 0.4 M NaOH. Changes included the dissolution of clay minerals and the formation of new phases. After 6 months a faujasite-type zeolite (zeolite X) with the following formula: $Na_2Al_2Si_{2.5}O_9 \cdot 6.2H_2O$ (JPDF card no. 380237) was identified (Figure 3-138). At this point the intensity of the 001 Bragg peaks of illite and kaolinite was reduced.

After 1-year treatment kaolinite was no longer detectable and the intensity of the faujasite-type zeolite Bragg peak had increased.

Further treatment up to 6 years caused the appearance of an additional sodalite-type zeolite (Figure 3-139) with the following formula: $Na_{2.16}Al_2Si_{1.68}O_{7.44}$ ·H_2O (JPDF card no. 311271). The intensity of the illite Bragg peak at 10 Å (d_{001}) was significantly reduced but the peak could still be observed even after 7.5 years of alkaline activation. The intensity of the faujasite-type zeolite Bragg peaks seemed to have decreased after 7.5 years of treatment. Note that the zeolitic phases formed upon alkaline activation of Alhambra Formation soil were identical to the ones formed in pure kaolinite and montmorillonite treated with NaOH.

The XRD pattern of the EG solvated sample treated for 7.5 years showed that expandable clays were no longer present (Figure 3-140).

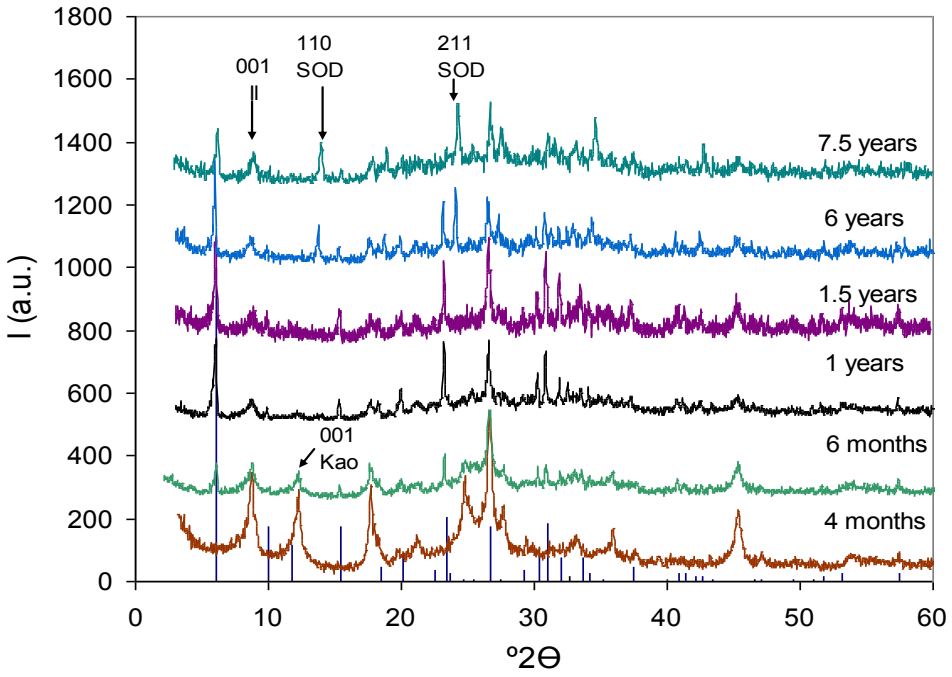

Figure 3-138. XRD patterns of Alhambra Formation clays (OA) treated with 5 M NaOH solution for different periods of time. Blue line pattern: Faujasite-type zeolite (JPDF card no. 380237). Il = illite, Kao = kaolinite, SOD = hydroxysodalite.

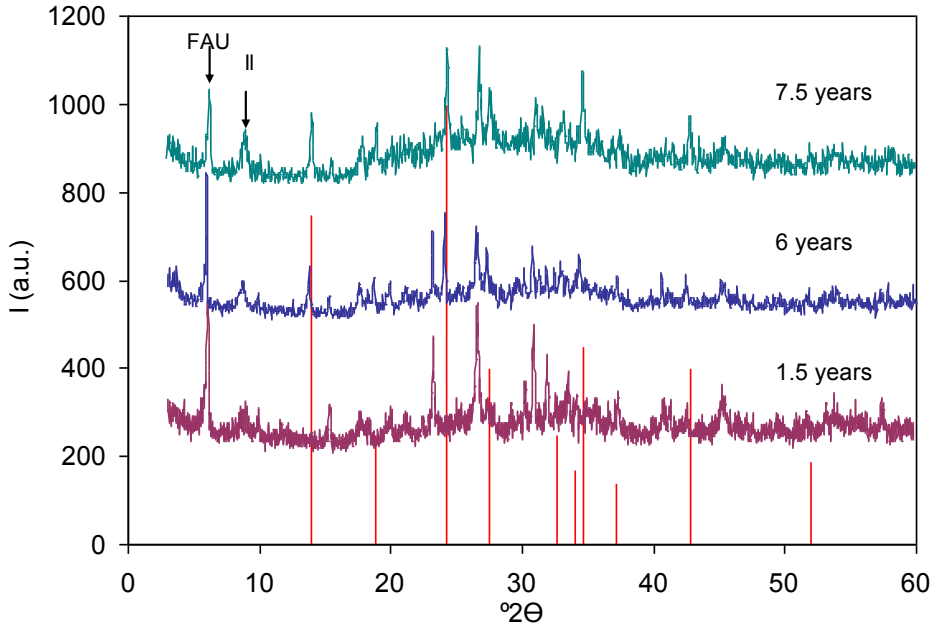

Figure 3-139. XRD patterns of Alhambra Formation clays (OA) treated with 5M NaOH solution for different periods of time. Red line pattern: sodalite- type zeolite (JPDF card no.311271). FAU = faujasite, Il = illite.

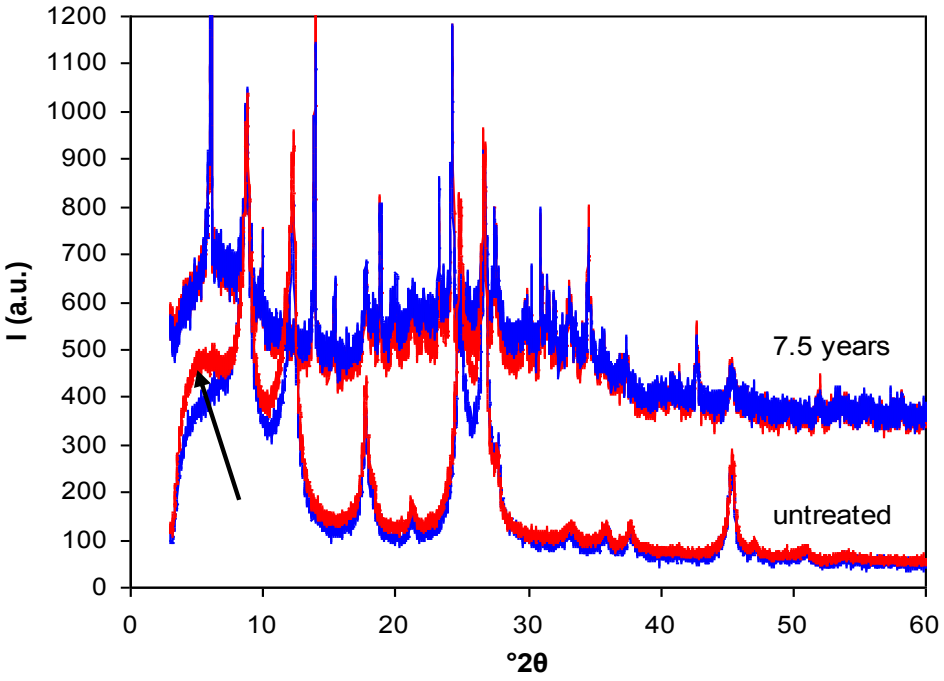

Figure 3-140. XRD patterns of OA (blue = air-dried, red = EG solvated) of untreated Alhambra Formation soil (arrow indicates presence of expandable clay minerals) and soil treated with 5 M NaOH for 7.5 years.

3.5.3.2. FESEM

FESEM analysis of the Alhambra Formation clay treated with 0.4 M NaOH for 2 months did not reveal any morphological changes and microanalysis only showed a slight increase in Na (inset, Figure 3-141).

After 1 year the sample revealed a poorly crystalline, porous structure (Figure 3-142). This structure might be a zeolite precursor, indicating the early stage of zeolite formation. Note that this phase was not observed using NaOH solution of higher concentrations. Microanalysis (inset, Figure 3-142) showed the presence of Al, Si, K, Fe and a high concentration of Na which agrees with the composition of a zeolite mixed with clay minerals such as illite and kaolinite. Additionally, clusters of newly formed nanocrystals together with large prismatic crystals were observed (Figure 3-143). EDS microanalysis revealed a high concentration of Na (inset, Figure 3-144) which suggests that the prismatic-shaped crystals were Na_2CO_3. Sodium carbonate crystals might form when excess alkalis (NaOH) react with atmospheric CO_2.

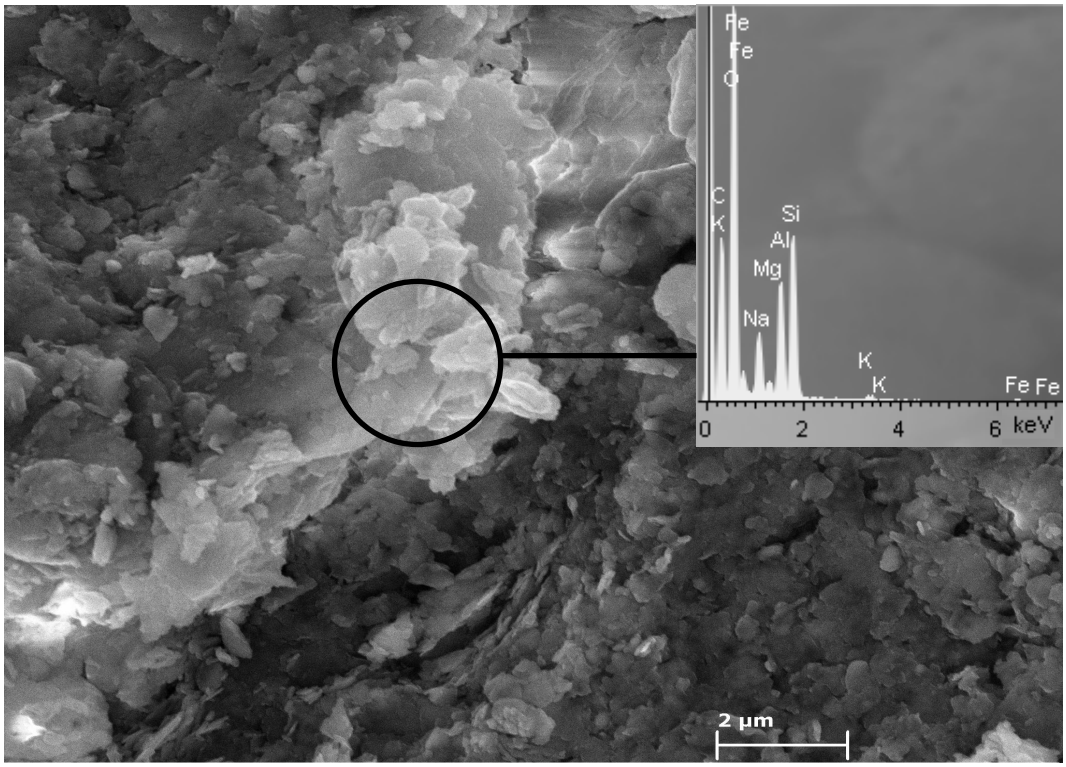

Figure 3-141. FESEM image of Alhambra Formation clay treated with 0.4 M NaOH for 2 months. EDS analysis (inset) shows a slight increase in Na. However, morphological changes can not be observed.

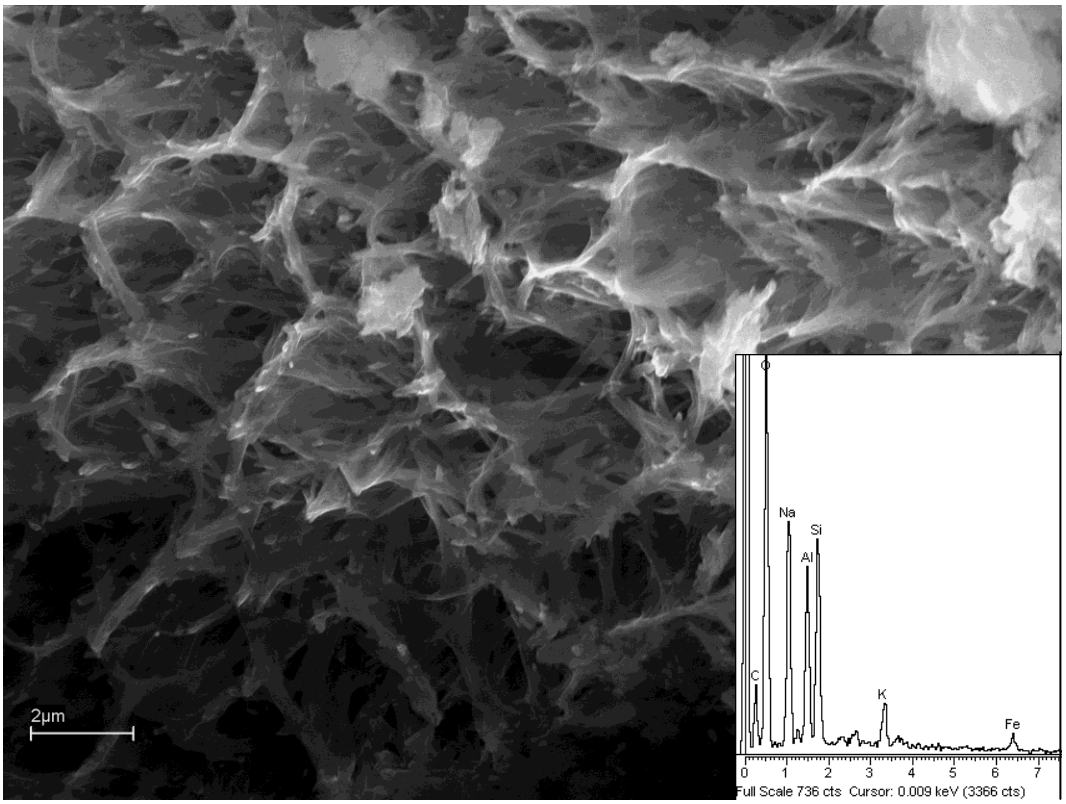

Figure 3-142. FESEM image of Alhambra Formation clay treated with 0.4 M NaOH for 1 year. A porous, poorly crystalline structure, which might resemble a zeolite precursor, can be observed (EDS in inset).

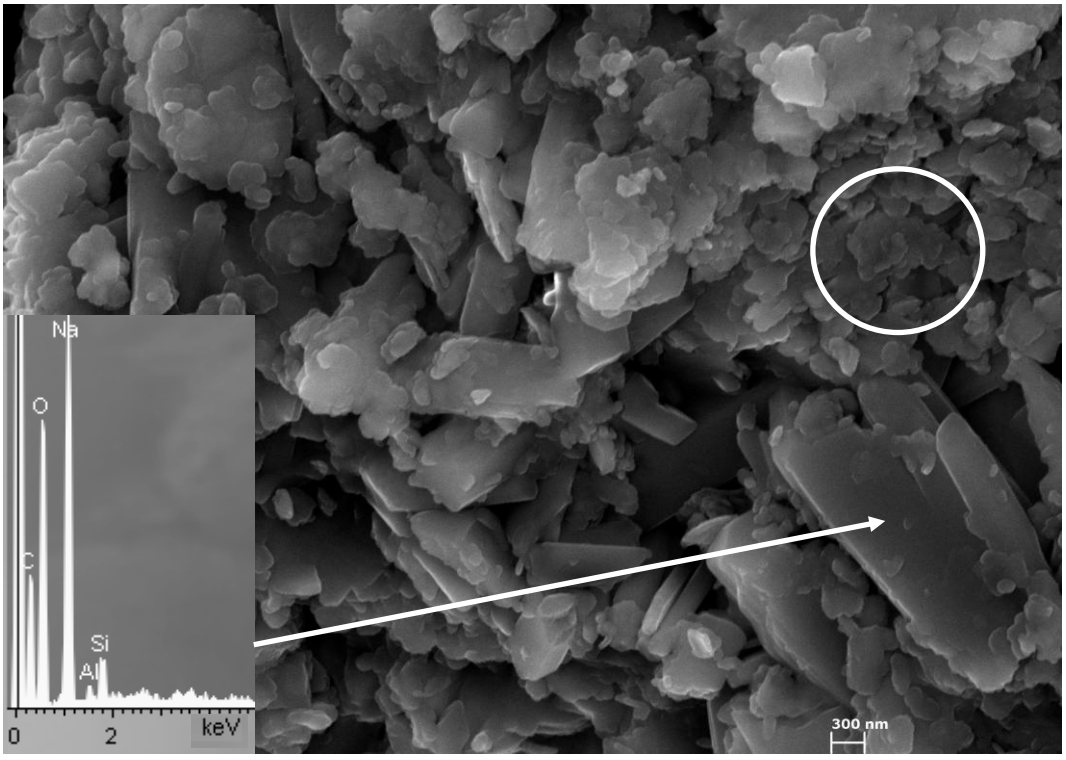

Figure 3-143. Figure X. FESEM image of Alhambra Formation clay treated with 0.4 M NaOH for 1 year. Clusters of $NaCO_3$ crystals (EDS in inset) together with newly formed nano-crystals (circle), can be observed.

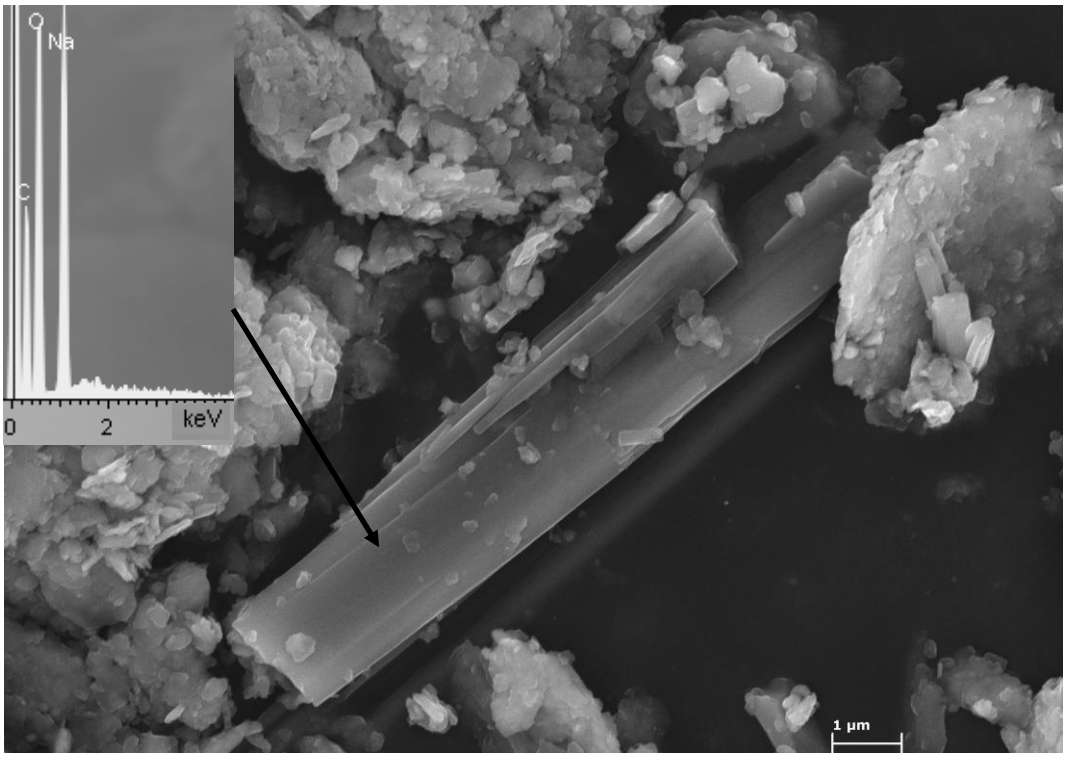

Figure 3-144. FESEM image of Alhambra Formation clay treated with 0.4 M NaOH for 1 year. A prismatic Na_2CO_3 (EDS in inset) crystal can be observed.

FESEM analysis of the Alhambra Formation clay treated with 5 M NaOH for 2 months did not reveal any morphological changes (Figure 3-145). However, EDS microanalysis suggested a slight increase in Mg if compared to the original clay sample. The increase in Mg might be interpreted as an indication for a saponatization process which has also been detected in the case of pure montmorillonite treated with 5 M NaOH.

The sample treated for 6 months showed faujasite-type zeolite crystals with increased Ca concentration and unreacted clay minerals (Figure 3-146).

After 1-year treatment a considerable amount of a faujasite-type zeolite (Figure 3-147) was detected. Additionally, some star-shaped crystals of about 1 µm were also observed. Morphological characteristics and EDS microanalysis results point to a sodalite-type zeolite. However, the amount of this sodalite-type zeolite was small and could not be detected using XRD at this point.

Further treatment up to 7.5 years did not produce any additional phases. The amount of the sodalite-type zeolite (Figure 3-148) increased at the expense of the faujasite-type zeolite. This is in agreement with XRD data which allowed the detection of hydroxysodalite in samples treated for 6 years with 5 M NaOH. The transformation into the sodalite-type zeolite was accompanied by a significant increase in Na concentration. The sodalite crystals formed compact aggregates of about 4 µm after 7.5 years of treatment. Furthermore,

Alhambra Formation soil treated for 7.5 years still contained clay particles which showed a very similar morphology and suffered only minor chemical changes if compared to the untreated clay sample (Figure 3-149).

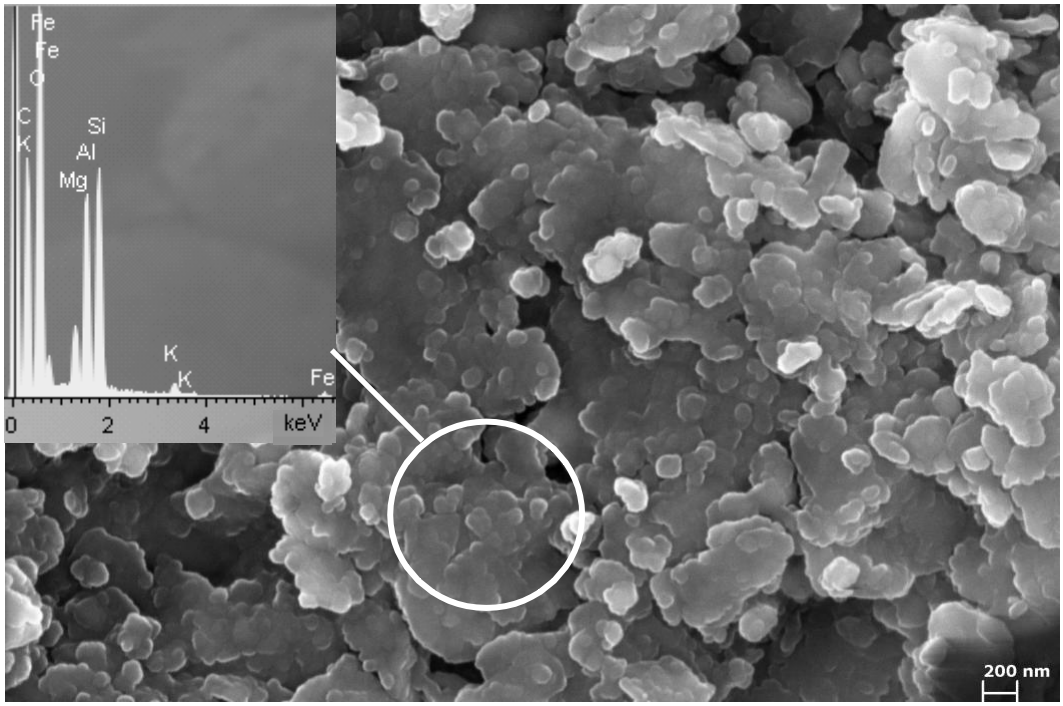

Figure 3-145. FESEM image of Alhambra Formation soil treated with 5 M NaOH for 2 months. No significant morphological changes are detected. However, EDS microanalysis (inset) shows a slight increase in Mg concentration.

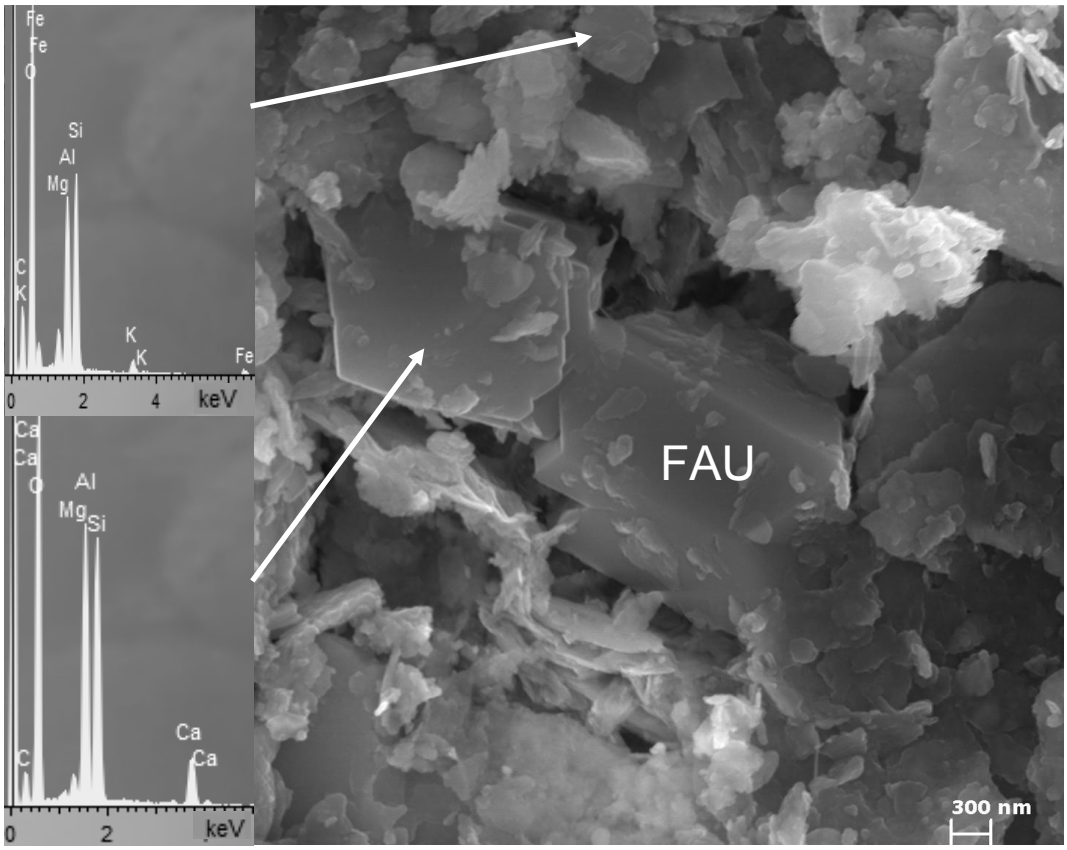

Figure 3-146. FESEM image of Alhambra Formation soil treated with 5 M NaOH for 6 months. Unreacted clay minerals (EDS in upper inset) and a faujasite-type zeolite (FAU) with an elevated Ca concentration (EDS in lower inset) can be observed.

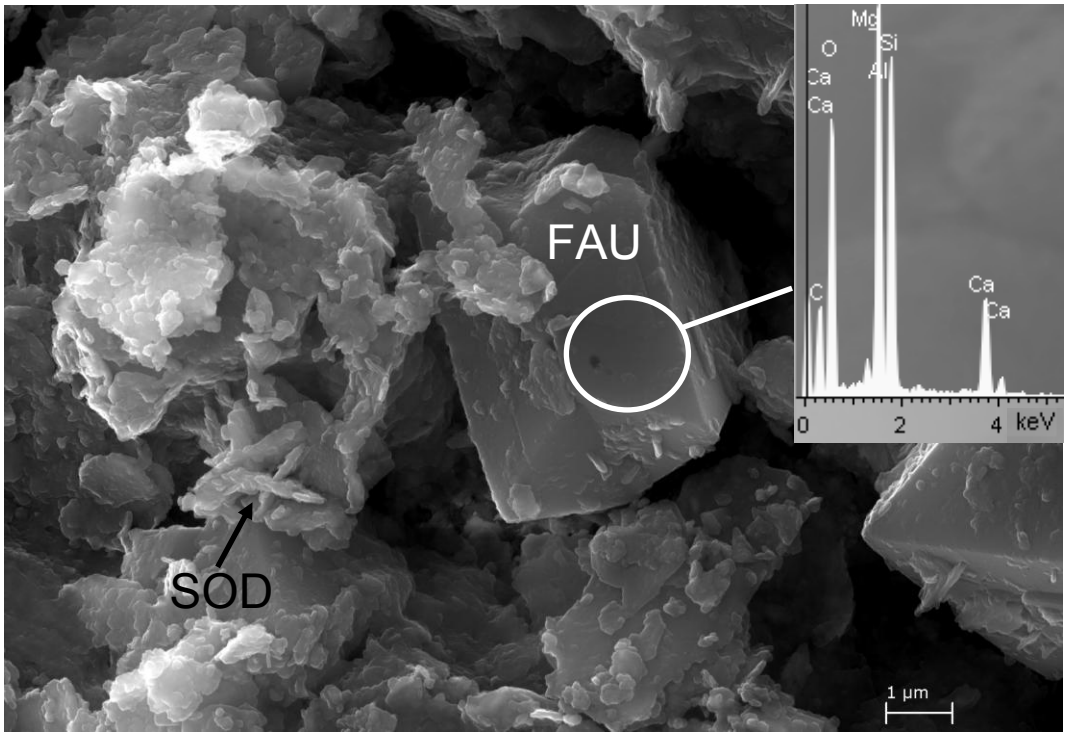

Figure 3-147. FESEM image of Alhambra Formation soil treated with 5 M NaOH for 1 year. A faujasite-type zeolite (FAU, EDS in inset) as well as a sodalite-type zeolite (SOD, red arrow) can be observed.

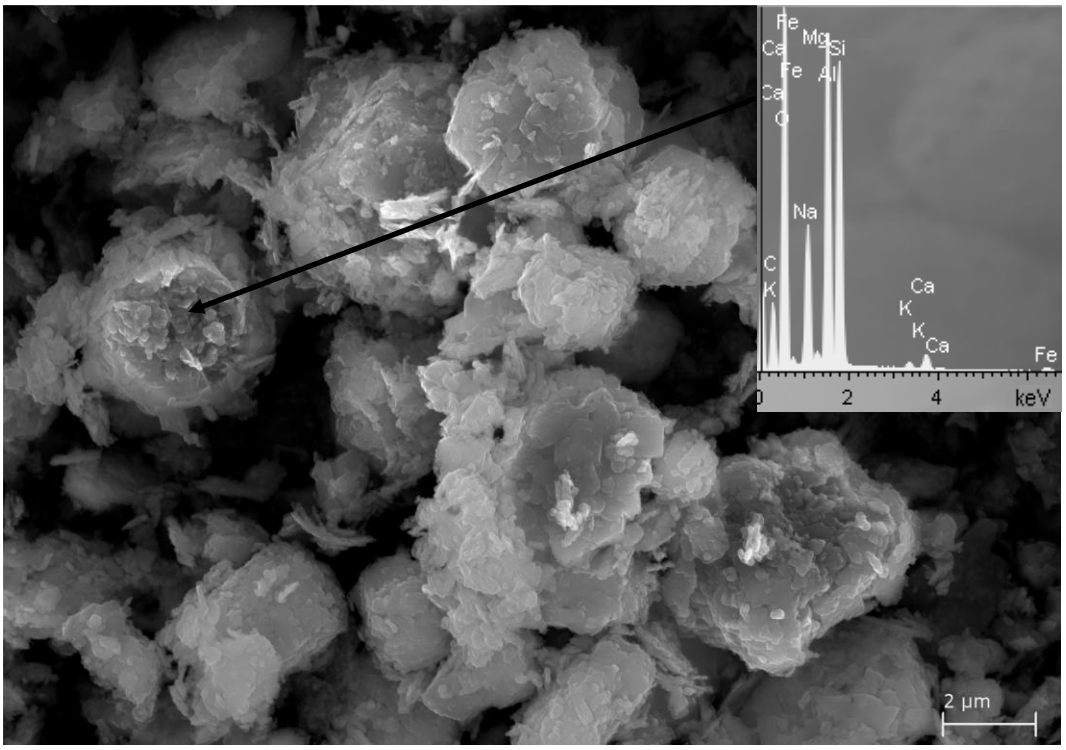

Figure 3-148. The FESEM image shows the general aspect of Alhambra Formation soil treated with 5 M NaOH for 7.5 years. The newly formed zeolitic phases seem to represent different stages of faujasite-sodalite transformation. EDS (inset) reveals an elevated Na concentration.

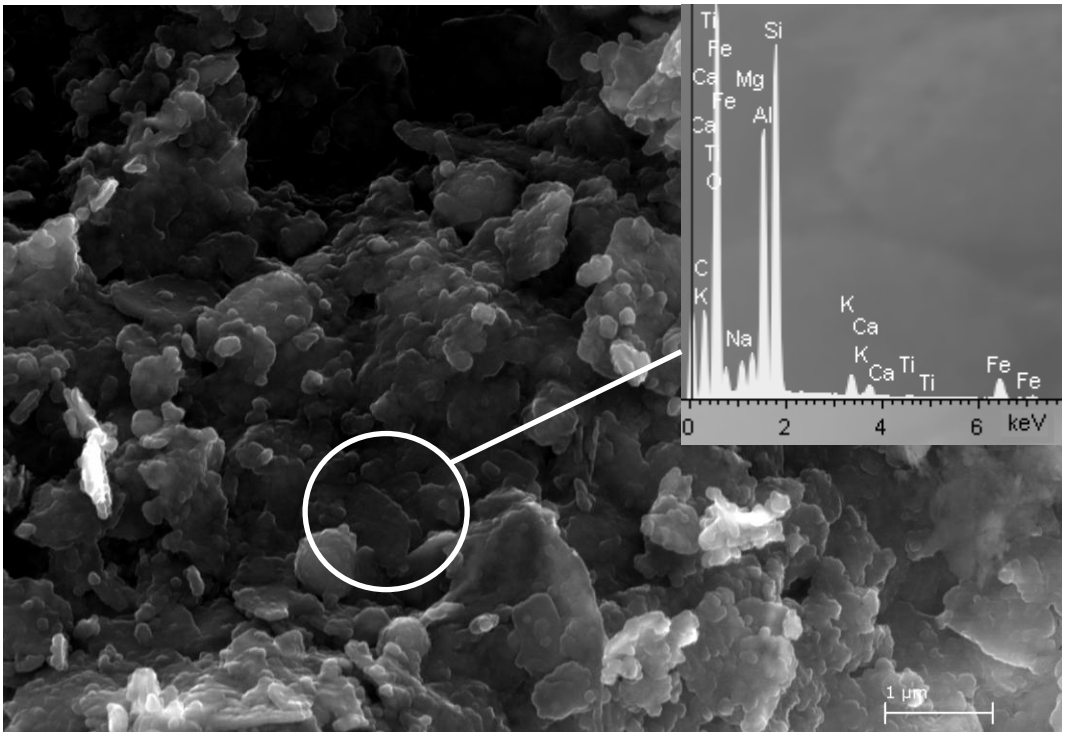

Figure 3-149. FESEM image of Alhambra Formation soil treated with 5 M NaOH for 7.5 years. Parts of the sample retain their original morphology and show only minor chemical changes (EDS in inset).

3.5.3.3. TEM

Figure 3-150 shows a fibrous phase formed in Alhambra Formation soil treated with 0.4 M NaOH for 1 year. SAED and TEM-AEM (Table 3-29) analyses were in fairly good agreement with a foshagite phase (McMurdie and Flint 1943). This fibrous calcium silicate hydrate (CSH) has the following formula: $Ca_5Si_3O_{11}{\cdot}3H_2O$ (JPDF card 030929). The micrometric fibers consisted of an oriented aggregate of nanoparticles which formed a picket fence (Figure 3-151). Figure 3-152 shows an aggregate of fibrous calcium silicate hydrate crystals. Note that the amount of this phase must have been relatively small since it was not detected with XRD or FESEM. Calcium silicate hydrates are common reaction products formed during alkaline treatment of clays, the source of calcium often being the exchangeable calcium of the unaltered montmorillonite. In our case, the tap water used during sample preparation might have been an additional source. Ramirez et al. (2002), Claret et al. (2002) and Sanchez et al. (2006) also reported the formation of CSH in the case of montmorillonite treated with 0.1-0.5 M NaOH. However, the CSH phase detected by these authors had an amorphous, gel-like character.

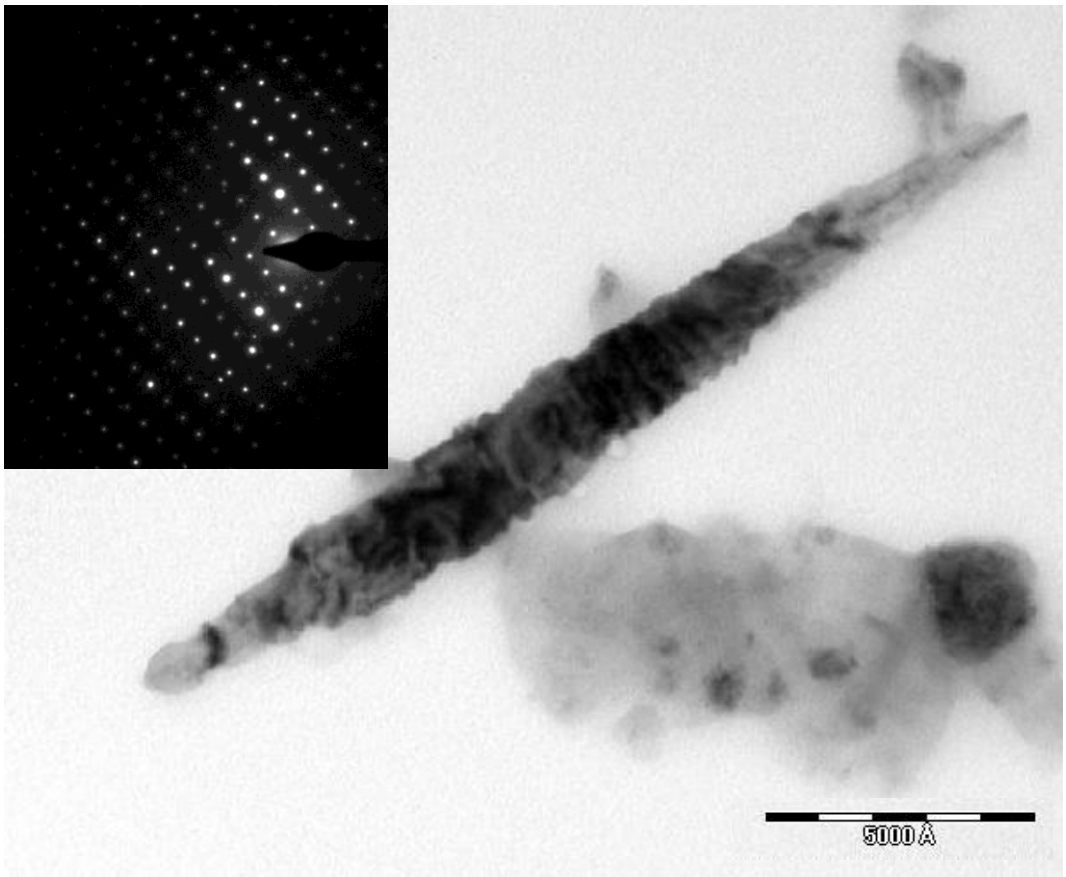

Figure 3-150. TEM image and SAED (inset) of a newly formed fibrous phase, possibly a calcium silicate hydrate, in Alhambra Formation soil treated with 0.4 M NaOH for 1 year. The crystal is made up of an oriented aggregate of nano-crystals which diffract as a single crystal.

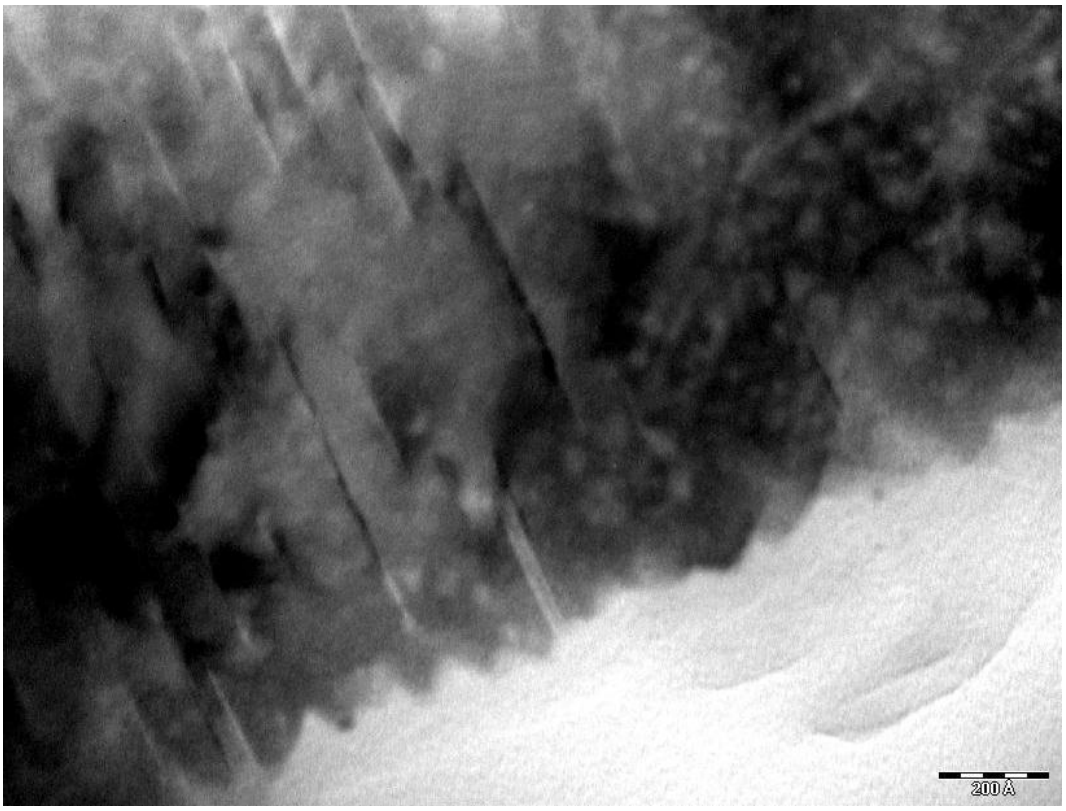

Figure 3-151. TEM image. Detail of the newly formed fibrous phase, presumably calcium silicate hydrate in Alhambra Formation soil treated with 0.4 M NaOH for 1 year.

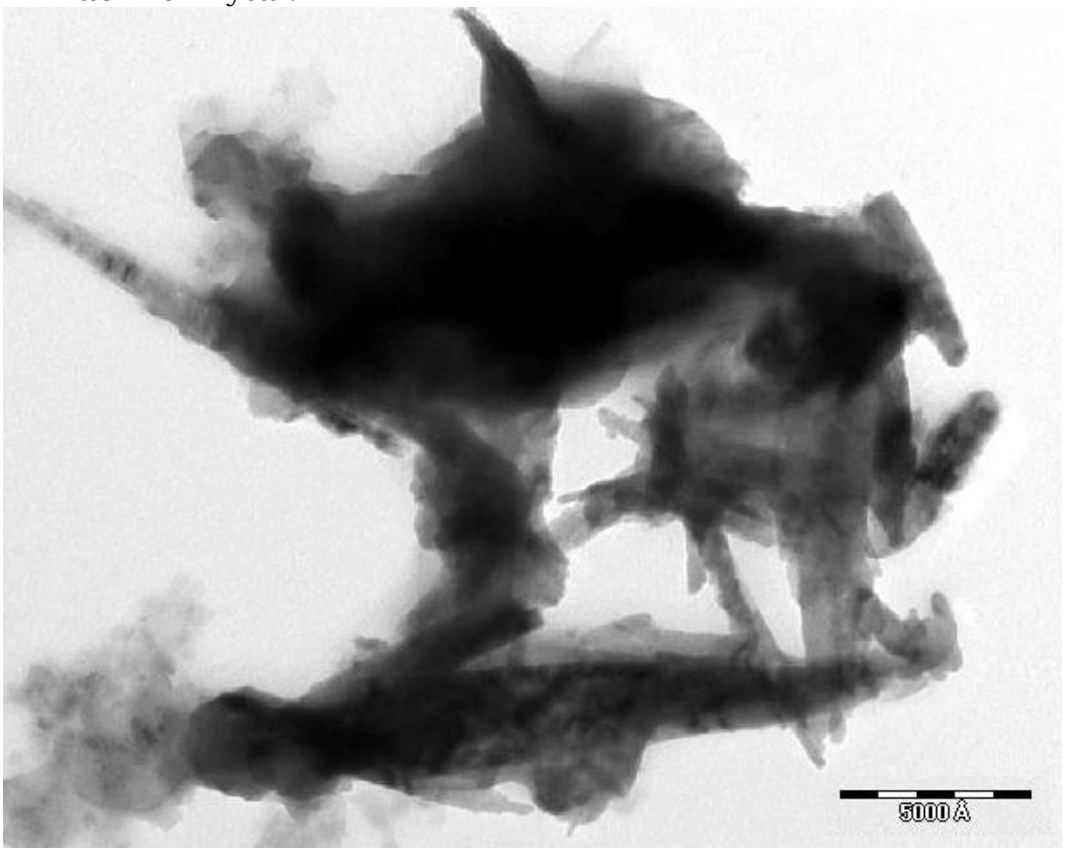

Figure 3-152. Tem image of an aggregate of fibrous calcium silicate hydrate in Alhambra Formation soil treated with 0.4 M NaOH for 1 year.

Table 3-29. Structural formulae calculated from TEM-AEM data of newly formed calcium silicate hydrate in Alhambra formation soil treated with 0.4 M NaOH for 1 year

Structural formulae of CSH based on O_{11}							
	Si	Al	Mg	Fe	K	Ca	Na
1	2.25	0.1	0.45	0.00	0.00	5.9	0.00
2	2.33	0.09	0.35	0.00	0.00	5.86	0.00
3	2.51	0.06	0.29	0.18	0.00	5.38	0.00
4	2.14	0.08	0.60	0.04	0.00	5.95	0.00
Average	2.31 ± 0.31	0.08 ± 0.03	0.42 ± 0.27	0.06 ± 0.17	0.00	5.77 ± 0.53	0.00

TEM analysis of the Alhambra Formation soil treated with 5 M NaOH for 1 year revealed a phase with a close resemblance to a sodalite-type zeolite (Figure 3-153). However, the zeolitic phase was mixed with clay minerals. It was, thus, not surprising that TEM-AEM data (Table 3-30) were not in agreement with the chemical composition of the sodalite-type zeolite identified previously with XRD, which has the following formula: $Na_{2.16}Al_2Si_{1.68}O_{7.44} \cdot H_2O$ (JPDF card no. 311271). Actually, the zeolitic phase showed a concentration of Si and Al quite similar to the one of smectite in untreated Alhambra Formation soil. However, if compared with the unreacted smectite in the Alhambra Formation soil, the interlayer charge, namely Ca^{2+} and Na^{+}, had increased. Nevertheless, the Na concentration was still lower than expected for a sodalite-type zeolite.

Figure 3-154 shows a sodalite-type phase after the Alhambra Formation soil had been treated for 6.2 years with 5 M NaOH. The TEM-AEM analysis revealed the presence of Si and Al together with Na, Mg, K and Fe. It is assumed that the relatively high concentrations of K and Fe are due to impurities such as illite and iron oxihydroxides.

TEM-AEM analysis (Table 3-31) of the < 2 μm fraction of the Alhambra Formation soil showed a composition compatible with an illitic clay mineral, however, quite rich in Mg. Compared to the illite of the untreated Alhambra Formation soil, the Mg and Fe content as well as the interlayer charge increased substantially. Considering XRD data which showed a reduction in the clays swelling capacity and nitrogen sorption data which revealed a modification of the hysteresis loop, pointing to the destruction of swelling clays, it is assumed that the smectites of the <2 μm fraction of the Alhambra Formation soil underwent an important degree of illitization. TEM-AEM analysis did not provide evidence for saponitization.

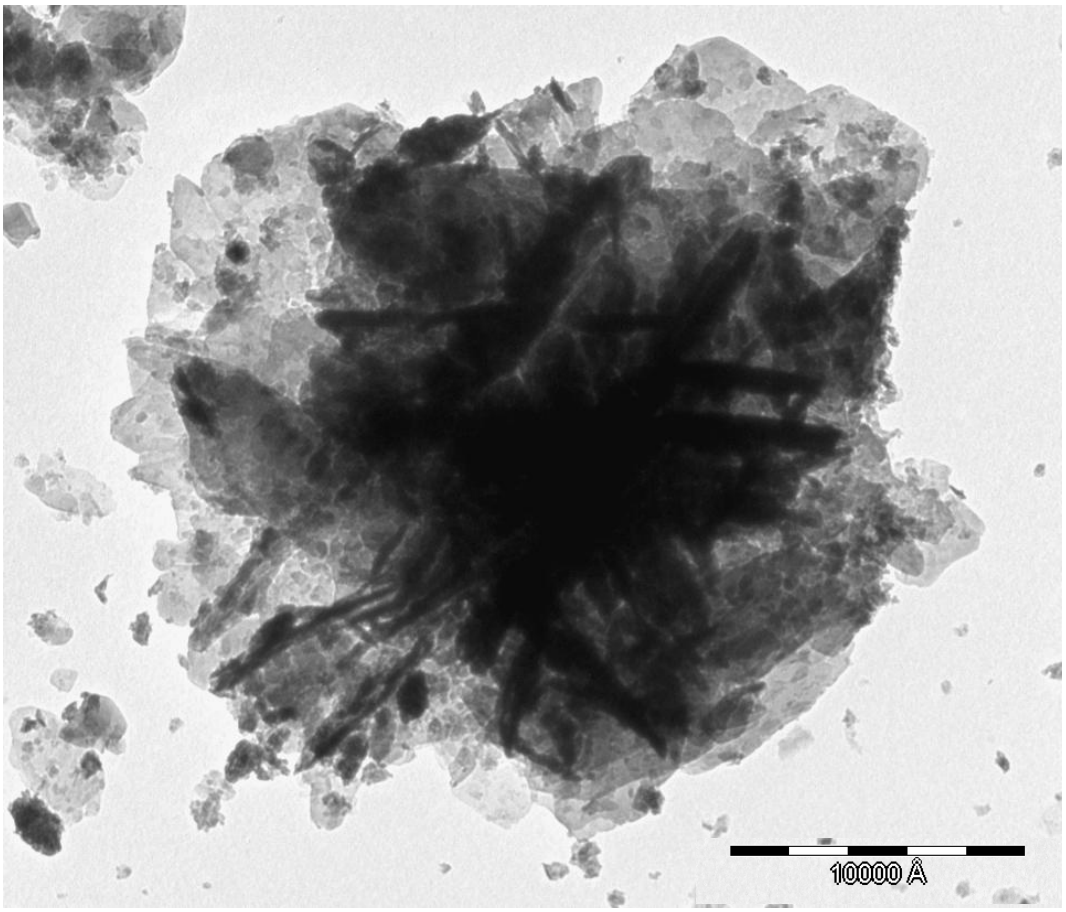

Figure 3-153. TEM image of Alhambra Formation soil treated with 5 M NaOH for 1 year. The morphology of the newly formed phase is compatible with a sodalite/cancrinite-type zeolite.

Table 3-30. Structural formulae calculated from TEM-AEM data of sodalite-type zeolite in Alhambra formation soil treated with 5 M NaOH for 1 year. For comparison the structural formula of untreated smectite (Alhambra Formation) is included, calculated based on $O_{7.44}$

Structural formulae of a sodalite-type zeolite based on $O_{7.44}$							
Analysis	Si	Al	Mg	Fe	K	Ca	Na
1	2.86	1.17	0.12	0.01	0.00	0.14	0.49
2	2.70	1.37	0.10	0.10	0.00	0.16	0.30
3	2.55	1.39	0.11	0.26	0.00	0.16	0.46
average	2.70 ± 0.16	1.31 ± 0.12	0.11 ± 0.01	0.12 ± 0.13	0.00	0.15 ± 0.01	0.42 ± 0.10
Untreated smectite	2.47	1.32	0.19	0.00	0.14	0.01	0.04

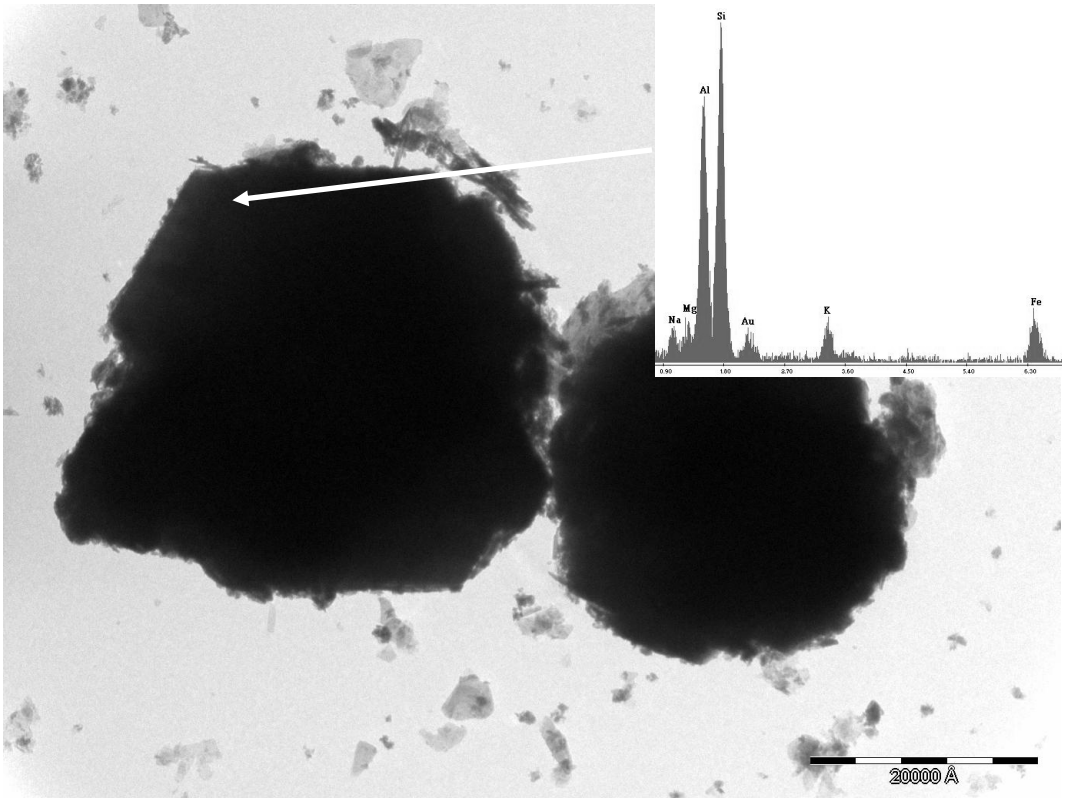

Figure 3-154. TEM image of sodalite-type zeolite formed in Alhambra Formation soil treated with 5 M NaOH for 6.2 years. TEM-AEM analysis (EDS in inset) shows the presence of Na, Mg, K and Fe together with Al and Si.

Table 3-31. TEM-AEM analysis of the < 2 μm fraction of the Alhambra Formation soil treated with 5 M NaOH for 7.5 years

Structural formulae of clay minerals based on $O_{10}(OH)_2$										
Analysis	Si	^{IV}Al	^{VI}Al	Mg	Fe	Σoct.cat.[1]	K	Ca	Na	Σint.cha.[2]
untreated illite average	3.11 ± 0.12	0.89 ± 0.12	1.77 ± 0.18	0.17 ± 0.09	0.28 ± 0.24	2.23 ± 0.04	0.45 ± 0.10	0.00	0.00	0.45 ± 0.10
untreated smectite average	3.65 ± 0.11	0.35 ± 0.11	1.60 ± 0.13	0.28 ± 0.20	0 ± 0.01	2.11 ± 0.14	0.20 ± 0.14	0.01 ± 0.03	0.06 ± 0.08	0.28 ± 0.16
1	2.92	1.08	1.32	0.49	0.55	2.36	0.62	0	0.16	0.78
2	3.08	0.92	1.57	0.26	0.24	2.07	0.80	0.06	0.20	1.12
3	3.07	0.93	1.30	0.50	0.36	2.16	0.71	0.09	0.24	1.13
4	3.18	0.82	1.44	0.49	0.25	2.18	0.55	0.04	0.31	0.94
5	2.99	1.01	1.35	0.44	0.57	2.36	0.40	0.04	0.18	0.66
6	3.30	0.70	1.29	0.40	0.51	2.20	0.44	0.06	0.21	0.77
Average 7.5 years	3.09 ±0.14	0.91 ±0.14	1.38 ±0.11	0.43 ±0.09	0.41 ±0.15	2.22 ±0.12	0.59 ±0.16	0.05 ±0.03	0.22 ±0.05	0.90 ±0.20

[1] Sum of octahedral cations

[2] Sum of interlayer charge

3.5.3.4. Nitrogen sorption

BET surface area, calculated from nitrogen sorption data, revealed a significant decrease in surface area of the Alhambra Formation soil treated with 0.4 M NaOH for 1 year (Table 3-32). This decrease is assumed to be caused by a partial destruction of smectites. This decrease confirmed that no significant amounts of CSH phases or zeolites, i.e., faujasite, had formed in this sample, because these phases would have caused an increase in surface area or at least counteracted the decrease induced by the smectite destruction.

The shape of the nitrogen isotherm and the hysteresis loop did not experience any significant changes if compared with the untreated soil sample (Figure 3-155), indicating that an important portion of smectites were still present after 1-year treatment.

Table 3-32. BET surface area of Alhambra Formation soil treated with NaOH for different periods of time

Treatment time	Surface area (m^2/g)	
	0.4 M NaOH	5 M NaOH
0	70.78 ± 0.28	70.78 ± 0.28
6 months	*	144.99 ± 1.79
1 year	43.90 ± 0.79	244.38 ± 5.27
7.5 years	*	109.87 ± 1.88

*not determined

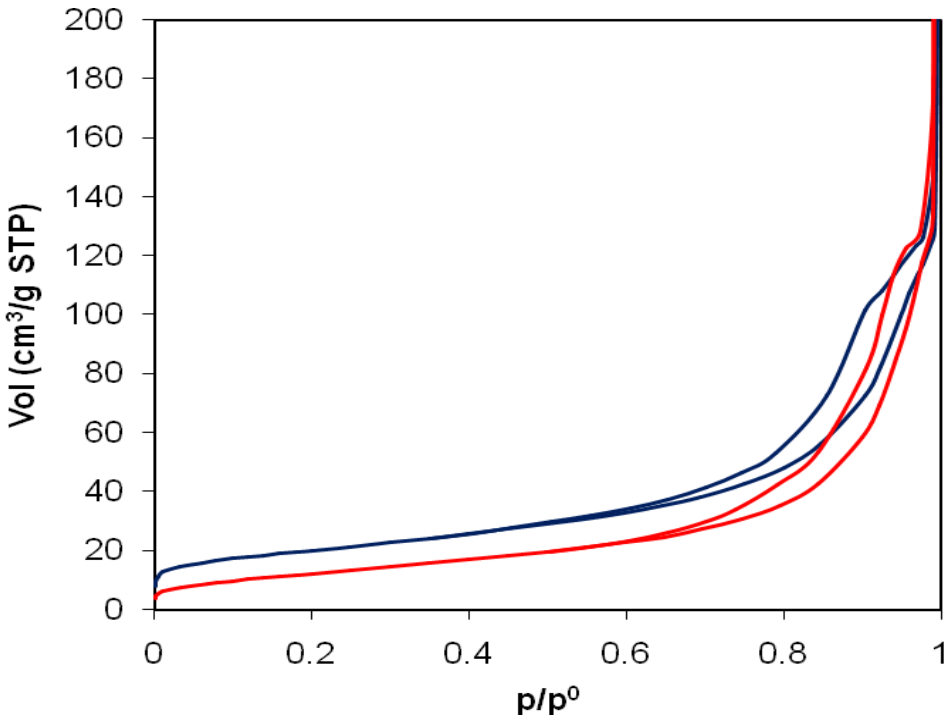

Figure 3-155. Nitrogen sorption isotherms of untreated Alhambra soil (blue) and soil treated with 0.4 M NaOH for 1 year (red).

In contrast, the surface area of the Alhambra Formation soil treated with 5 M NaOH for 6 months experienced an important increase (Table 3-32). This increase coincided with the formation of a faujasite-type zeolite. After 1 year of treatment the surface area further increased as a result of continuing faujasite formation. However, after 7.5 years the sample experienced a significant decrease in surface area as a result of the formation of a large amount of a sodalite-type zeolite additional to the faujasite-type zeolite. The BET surface area of sodalite-type zeolite is reported to be only 22.8 m^2/g (Li et al. 2007).

The nitrogen sorption isotherm of the sample treated with 5 M NaOH (Figure 3-156) had a significantly less pronounced hysteresis loop after 6 months. After one year of treatment, the shape of the hysteresis loop was identical to the one observed for the pure illite and kaolinite, suggesting the destruction of smectites. A more prolonged treatment of up to 7.5 years did not result in further modifications of the nitrogen isotherm.

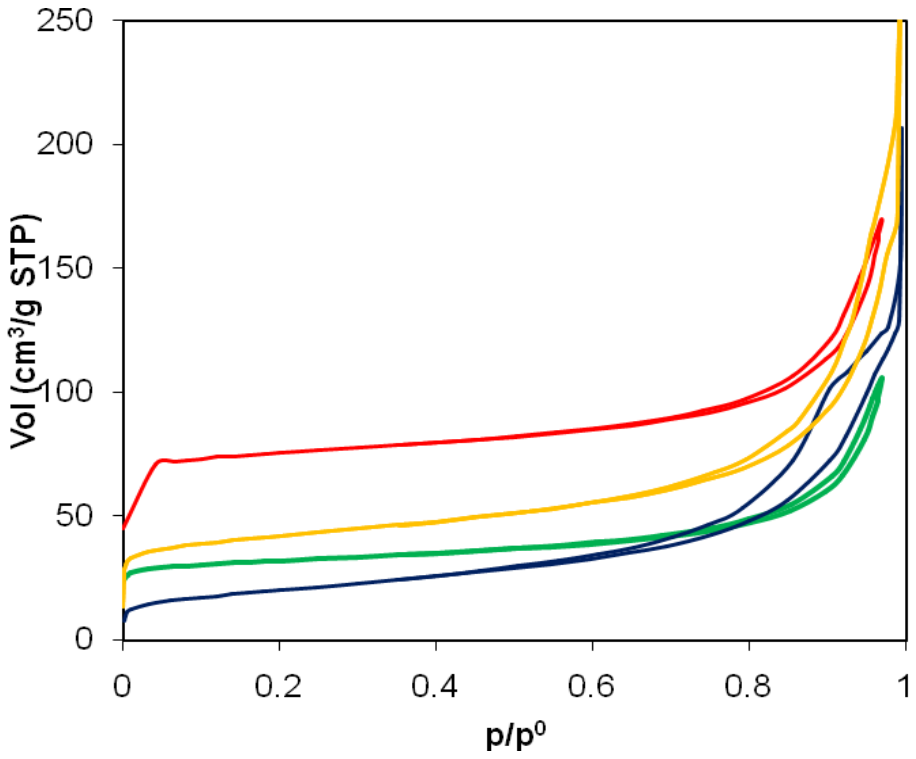

Figure 3-156. Nitrogen sorption isotherms of untreated Alhambra Formation soil. Untreated (blue), treated with 5 M NaOH for 6 months (yellow), 1 year (red) and for 7.5 years (green).

3.5.4. Alhambra Formation soil treated with KOH

In this section results regarding the mineralogical evolution of the Alhambra Formation soil treated with 0.4 M KOH and 5 M KOH are reported. The samples were studied using XRD, FESEM, TEM and nitrogen sorption.

3.5.4.1. XRD

As in the case of the sample treated with NaOH, smectite was the clay mineral which was primarily attacked in the sample of the Alhambra Formation soil treated using 0.4 M KOH solution (Figure 3-157).

After one year of alkaline activation the intensity of the 001 illite and kaolinite Bragg peak decreased and an additional peak at 4.44 Å was observed which might correspond to the 003 reflection of zeolite K-I ($K_2Al_2Si_2O_8 \cdot 3.8H_2O$, JPDF card no. 180988). The formation of K-I zeolites upon activation of kaolinite with KOH has been described by Barrer et al. (1968), Belver et al. (2002) and Bauer et al. (1998). Note that the same phase has been detected in Alhambra Formation soil treated with 5 M KOH for 4 months (see below).

Furthermore, due to an imperfect seal of the storage bottle, air had accidentally accessed during treatment and caused the carbonation of the sample. Thus, after one year of treatment kalicinite ($KHCO_3$, JPDF card no. 120292) was observed.

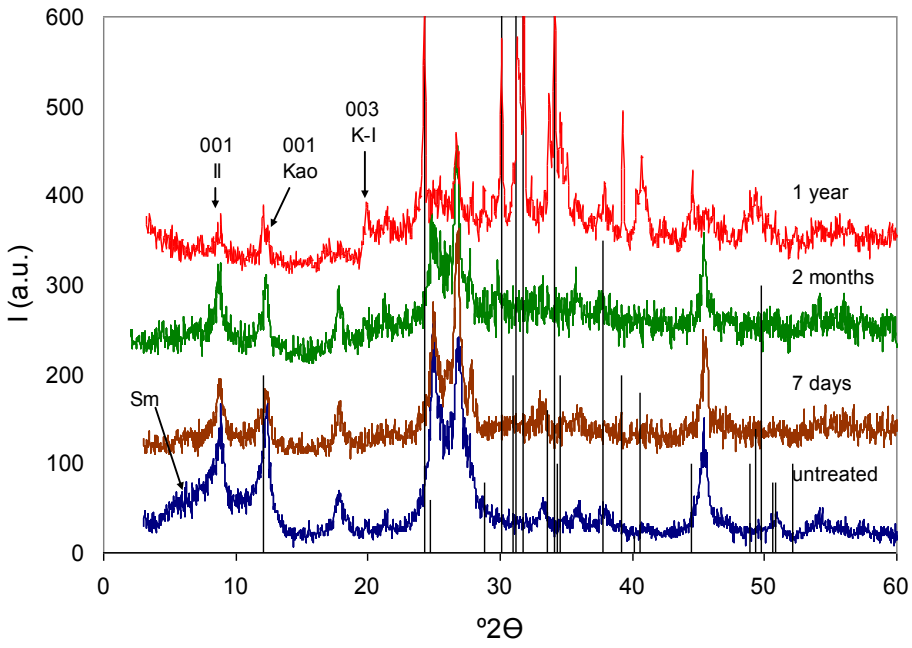

Figure 3-157. XRD patterns of Alhambra Formation clays (OA) treated with 0.4 M KOH solution for different periods of time. Black line pattern: kalicinite (JPDF card no.120292), Il = illite, Kao = kaolinite, Sm = smectite, K-I = zeolite K-I.

In Alhambra Formation soil treated with 5 KOH solution (Figure 3-158) the formation of zeolite K-I (JPDF card no.180988) was observed in the sample treated for 4 months. The intensity of kaolinite was significantly reduced after 6 months of treatment.

After 1 year of alkaline activation with 5 M KOH, an additional peak at 9.3 Å was detected which might correspond to the 003 Bragg peak of a chabazite-type zeolite ($K_2Al_2SiO_6 \cdot H_2O$, JPDF card no. 120194). At this point, the 001 Bragg peak of kaolinite disappeared completely. Note that zeolite K-I and the chabazite-type zeolite have also been detected in the case of pure kaolinite treated with 5 M KOH.

After 6 years of treatment the intensity of the 001 Bragg peak of illite seemed to have increased, possibly due to a recrystallization process in the presence of K^+ which involved Ostwald ripening. Indeed, the crystallite size of illite increased by about 35 % (Table 3-33).

Further treatment did not result in any significant mineralogical changes. The hump between 20 and 40 °2θ and the severe background noise in the case of the sample treated for 7.5 years was due to the thinness of the clay layer of the OA, rather than to any amorphous phases other than the underlying glass slide.

XRD patterns of the EG solvated sample treated for 7.5 years revealed that expandable clays were no longer present (Figure 3-159).

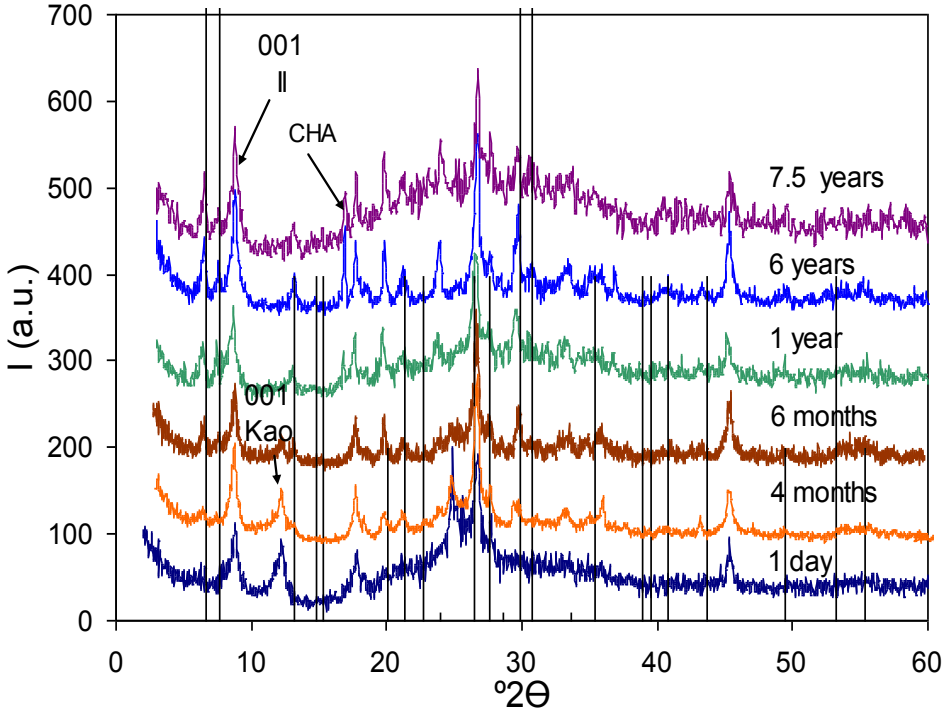

Figure 3-158. XRD patterns of Alhambra Formation clays (OA) treated with 5 M KOH solution for different periods of time. Black line pattern: Zeolite K-I (JPDF card no.180988), Il = illite, Kao = kaolinite, CHA = chabazite.

Table 3-33. Crystallite size (nm) of illite from Alhambra Formation soil treated with 5 M KOH for different periods of time.

Treatment time	Crystallite size (nm)
0 day	15
6 months	16
1 year	18
1.5 years	18
6 years	21
7.5 years	23

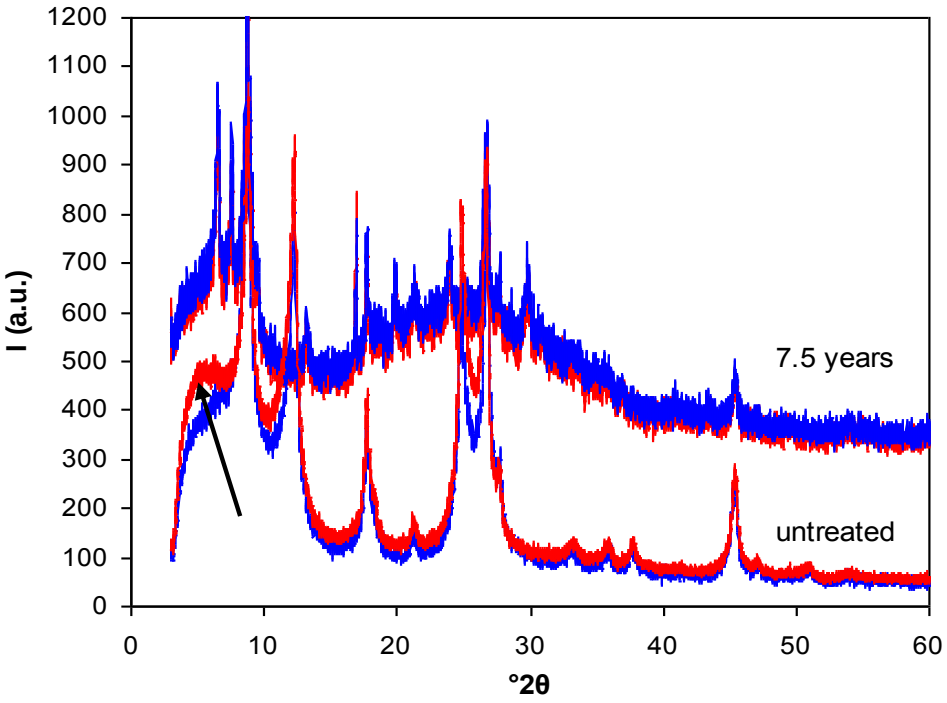

Figure 3-159. XRD patterns of oriented aggregates (blue = air-dried, red = EG solvated) of untreated Alhambra Formation soil (presenting expandable clay, arrow) and treated with 5 M KOH for 7.5 years.

3.5.4.2. FESEM

The FESEM image (Figure 3-160) of the sample treated with 0.4 M KOH for 2 months showed an aggregate of nanosized crystals. The morphology and the increased K concentration of these crystals points to zeolite K-I.

After one year of treatment an important part of the sample was covered with rounded crystals with a very high K concentration (Figure 3-161) which might correspond to kalicinite. Note that this phase was detected with XRD.

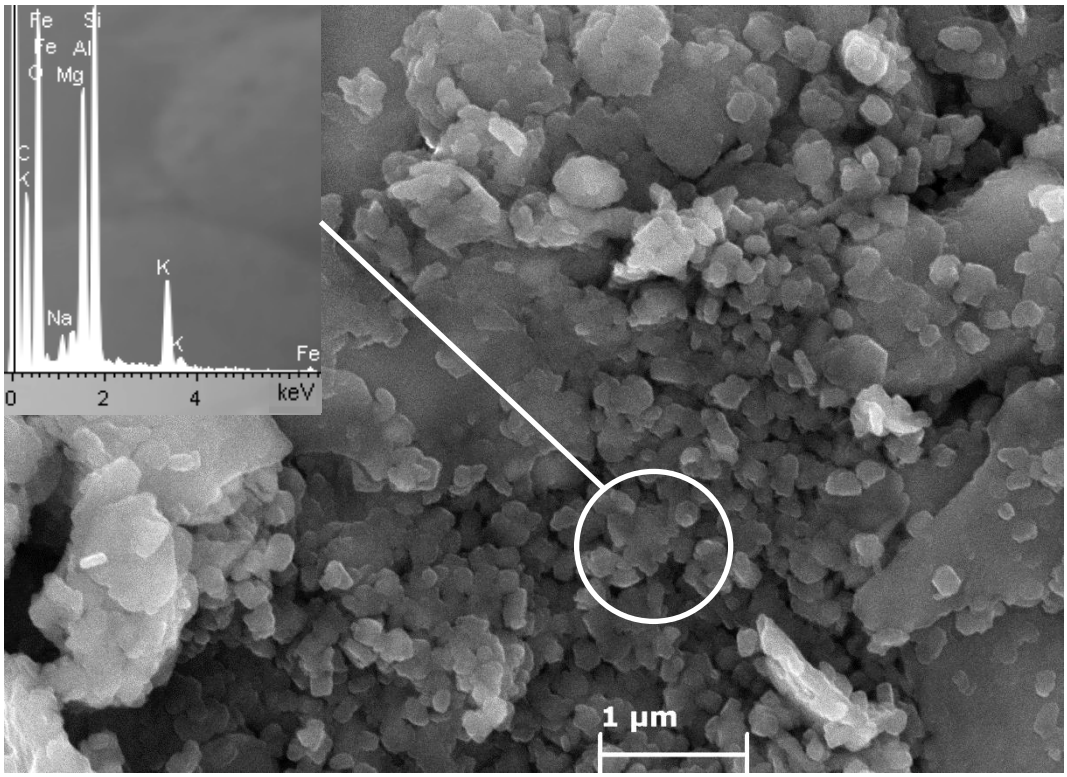

Figure 3-160. FESEM image of the Alhambra Formation soil treated with 0.4 M KOH for 2 months. Nanosized crystals (possible zeolite K-I, EDS in inset) can be observed.

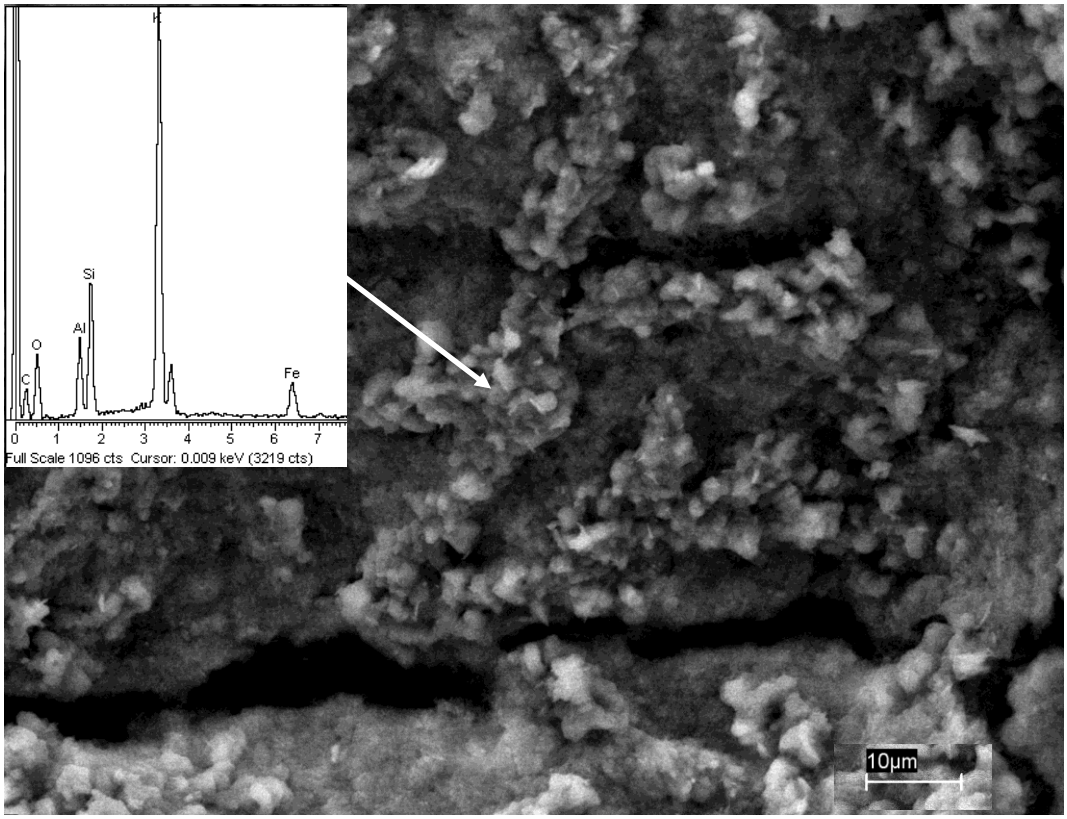

Figure 3-161. FESEM image of the Alhambra Formation soil treated with 0.4 M KOH for 1 year. An important part of the sample is covered with small, sphere-shaped particles, having a very high K concentration (inset). These particles might correspond to kalicinite.

The FESEM image of the Alhambra Formation soil treated with 5 M KOH for 6 months showed a large amount of small crystals with increased K and Ca concentration (Figure 3-162). These crystals are assumed to correspond to zeolite K-I, previously identified with XRD.

After one year of treatment, crystals with a morphology identical to a chabazite-type zeolite were observed (Figure 3-163) which is also in agreement with XRD results.

In the sample treated for 7.5 years prism-shaped crystals were detected (Figure 3-164). Based on morphology they might be identified as zeolite K-F, even though, they were not detected with XRD. Note that both, the chabazite-type zeolite and zeolite K-F have been observed together with zeolite K-I in pure kaolinite treated with 5 M KOH. After prolonged alkaline treatment large parts of the sample have transformed into an aggregated of nanosized particles (Figure 3-165), which were observed together with the chabazite-type zeolite (Figure 3-166).

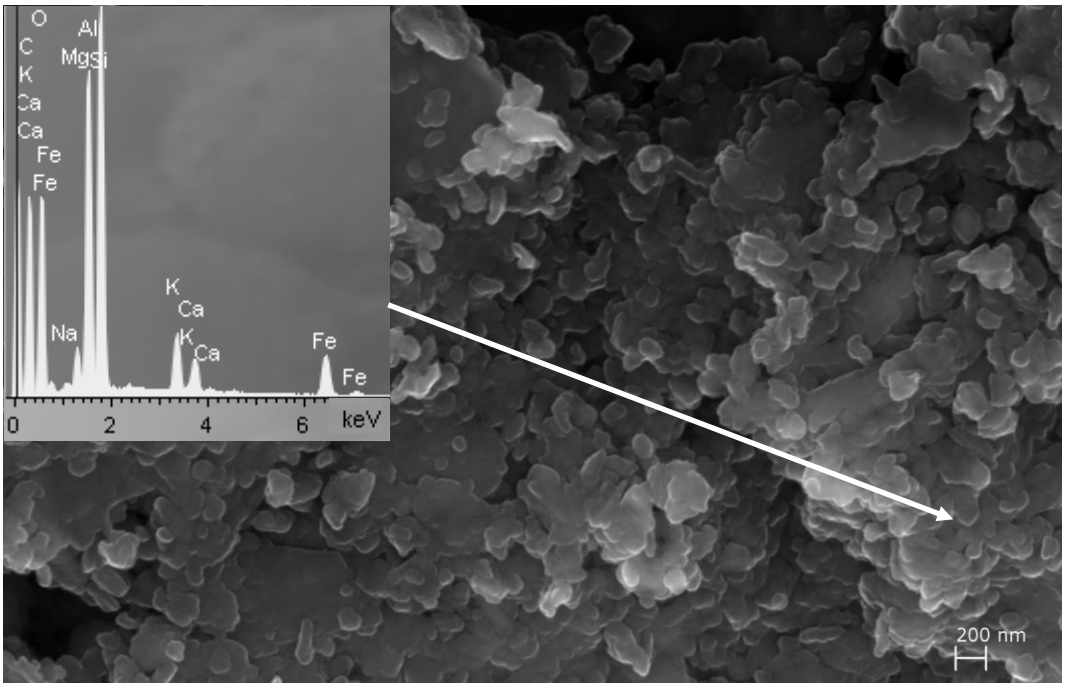

Figure 3-162. FESEM image of Alhambra Formation soil treated with 5 M KOH for 6 months. Aggregates of nanosized crystals with increased Ca and K concentration were observed (EDS in inset).

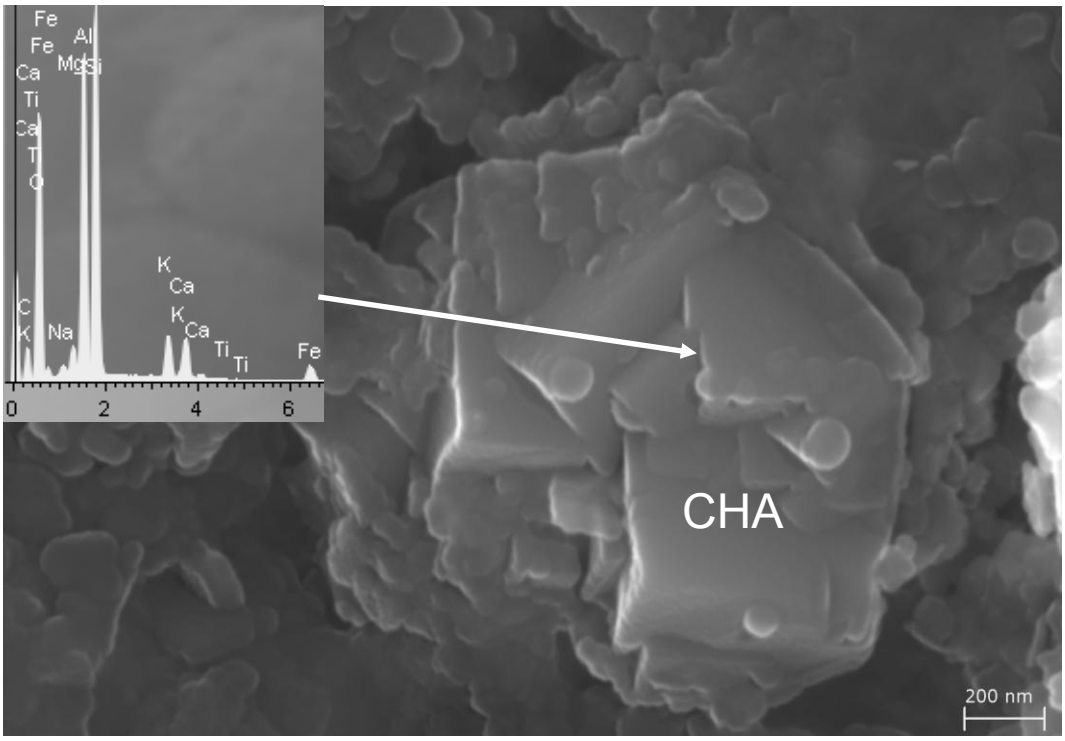

Figure 3-163. FESEM image of Alhambra Formation soil treated with 5 M KOH for 1 year. A chabazite-type zeolite (CHA) was detected (EDS in inset).

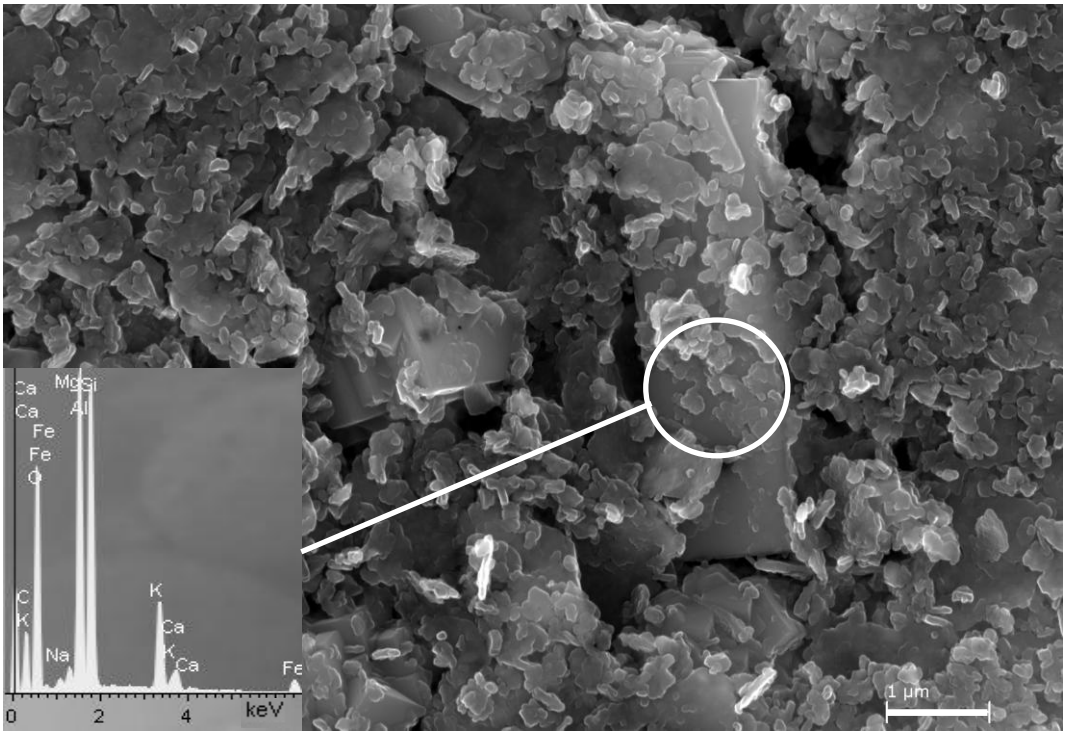

Figure 3-164. FESEM image of Alhambra Formation soil treated with 5 M KOH for 7.5 years. A prism-shaped crystal with morphology similar to zeolite K-F was observed (EDS in inset).

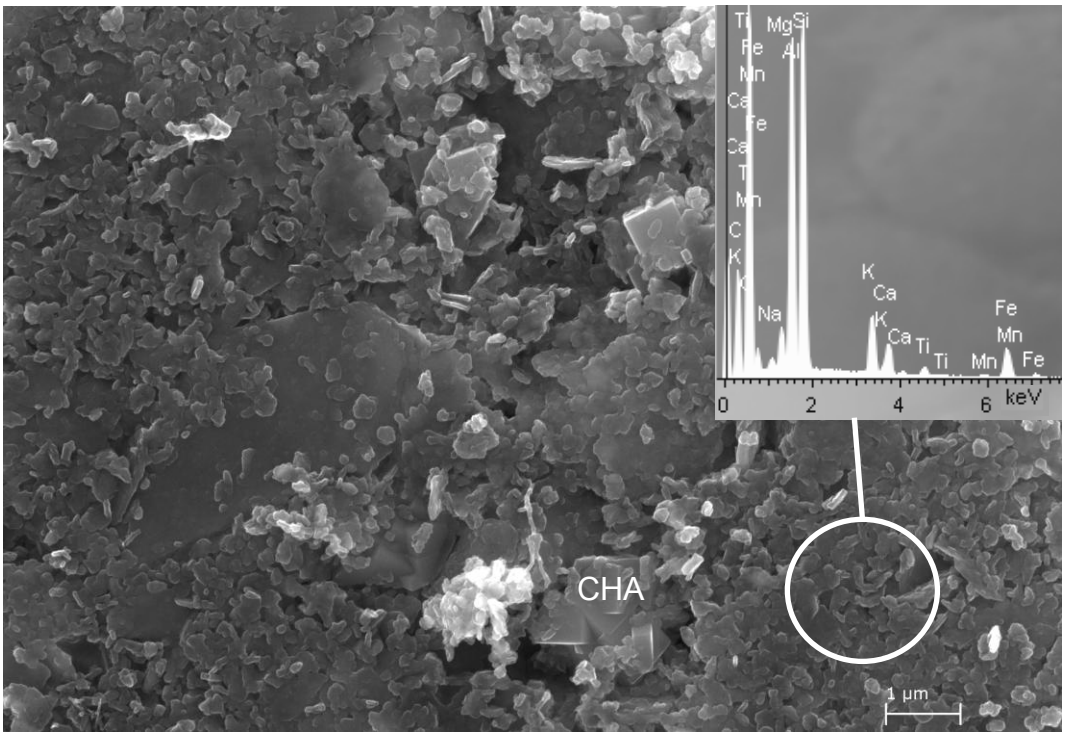

Figure 3-165. FESEM image of Alhambra Formation soil treated with 5 M KOH for 7.5 years. Large parts of the sample were comprised of an aggregate of nanosized particles (EDS in inset).

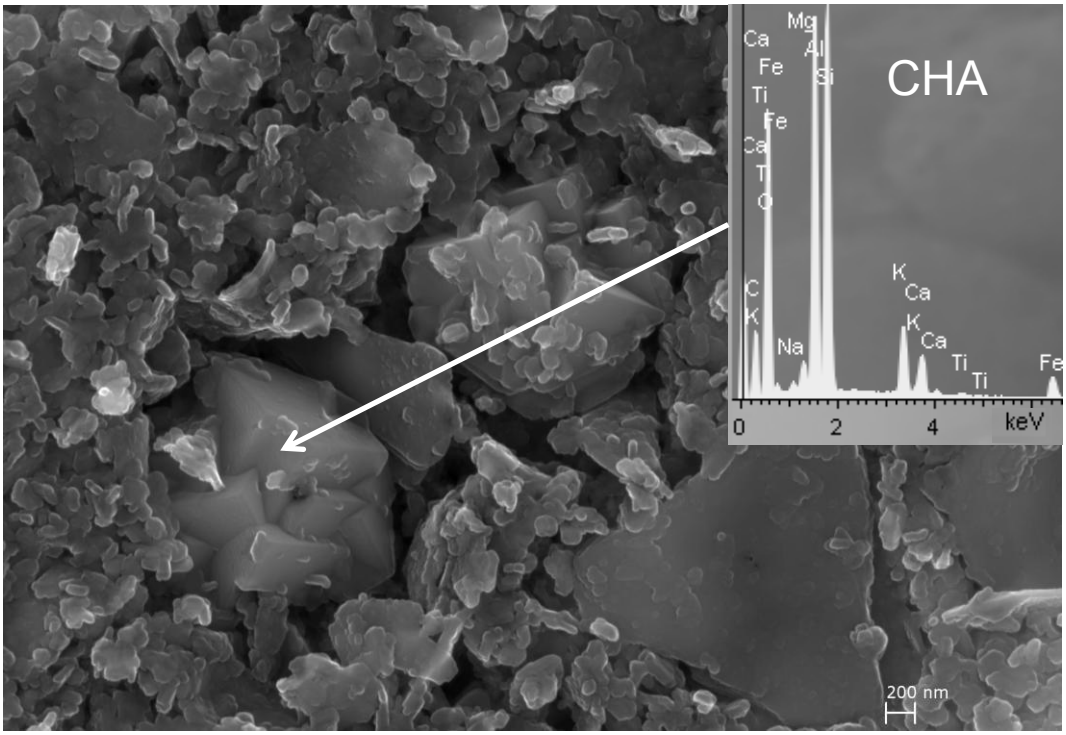

Figure 166. FESEM image of Alhambra Formation soil treated with 5 M KOH for 7.5 years. Chabazite-type crystals were observed (EDS in inset).

3.5.4.3. TEM

TEM analysis of the Alhambra Formation soil treated with 0.4 M KOH for 1 year did not reveal significant changes in the clay morphology (Figure 3-167).

However, TEM-AEM data of smectite particles showed a decrease in Si and an increase in Fe, K as well as in the total interlayer charge (Table 3-34). The obtained structural formulae are compatible with different stages of smectite illitization. Unfortunately, it cannot be established unambiguously whether illitization is provoked by alkaline activation or interstratified illite/smectite was already present in the original clay. However, nitrogen sorption data (see below) point to a destruction/transformation of expandable clays.

Furthermore, a sphere-shaped phase was detected which contains mainly Si. The SAED pattern confirmed the amorphous character of this phase (inset, Figure 3-168). The presence of this amorphous phase suggests that silica has been released following attack and dissolution of clay minerals.
As mentioned earlier, the sample suffered carbonation due to an imperfect seal, leading to the formation of kalicinite. TEM-AEM analysis (inset, Figure 3-169) revealed the presence of potassium carbonate which showed amorphization due to e-beam irradiation.

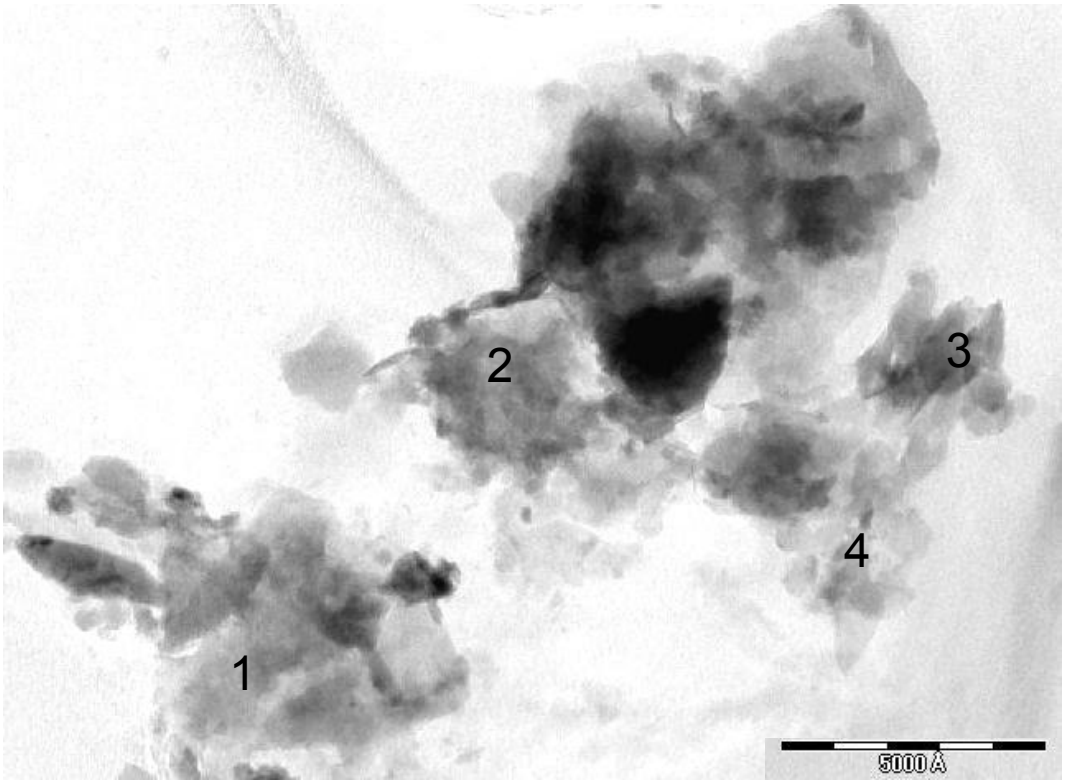

Figure 3-167. TEM image of Alhambra Formation soil treated with 0.4 M KOH for 1 year. Numbers indicate the spots where TEM-AEM analyses were performed and correspond to data in Table 3-34.

Table 3-34. Structural formulae calculated from TEM-AEM data of clay minerals from the Alhambra Formation soil treated with 0.4 M KOH for 1 year (the average formulae of smectite of untreated Alhambra Formation soil is included for comparison).

Structural formulae of clay minerals based on $O_{10}(OH)_2$										
	Si	^{IV}Al	^{VI}Al	Mg	Fe	Σoct.cat.[1]	K	Ca	Na	Σint.cha.[2]
untreated smectite average	3.65	0.35	1.60	0.28	0	2.11	0.20	0.01	0.06	0.28
1	3.50	0.50	1.43	0.30	0.37	2.10	0.46	0	0.22	0.68
2	3.59	0.41	1.74	0.12	0.23	2.09	0.33	0	0.09	0.42
3	3.41	0.59	1.53	0.25	0.30	2.08	0.57	0	0.18	0.75
4	3.25	0.75	1.28	0.19	0.64	2.11	0.72	0	0.23	0.95
5	3.57	0.43	1.62	0.14	0.30	2.06	0.24	0.10	0.11	0.53
treated average	3.46 ± 0.14	0.54 ± 0.14	1.52 ± 0.18	0.20 ± 0.08	0.37 ± 0.16	2.09 ± 0.02	0.46 ± 0.19	0.02 ± 0.05	0.17 ± 0.06	0.67 ±0.21

[1] sum of octahedral cation

[2] sum of interlayer charge

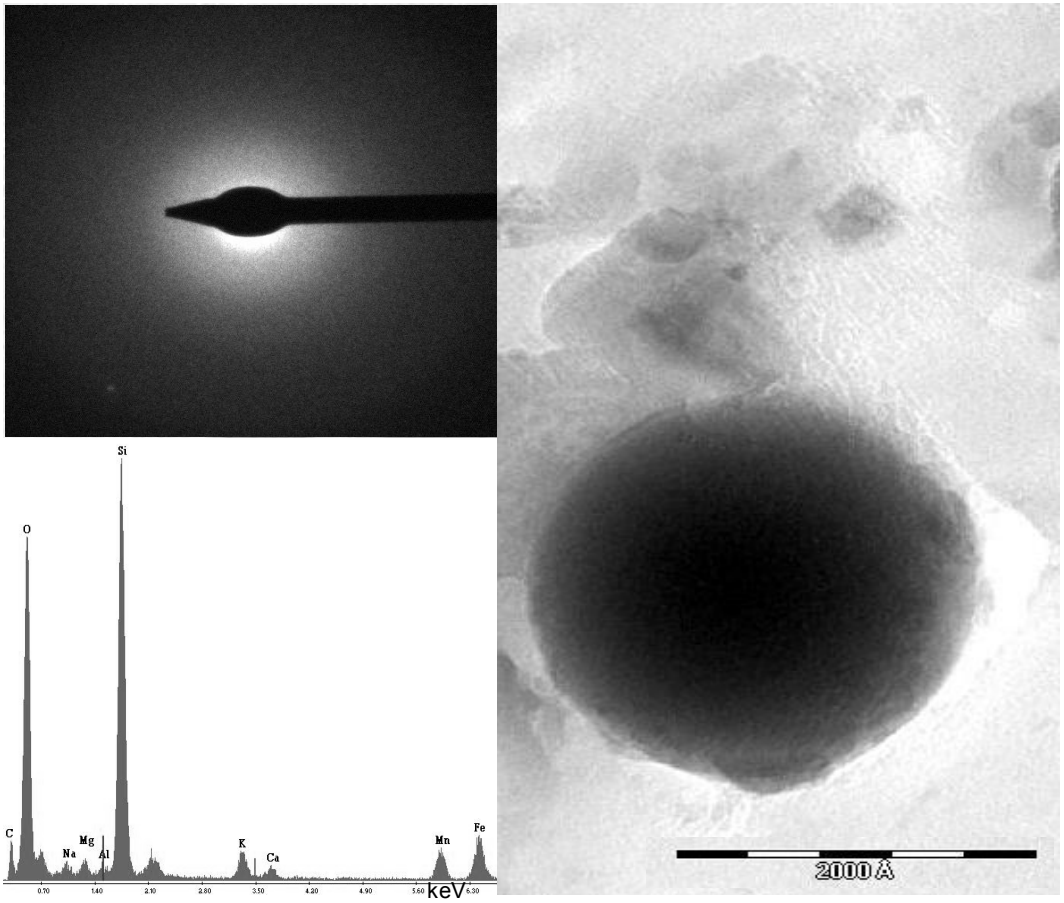

Figure 3-168. TEM image of Alhambra Formation soil treated with 0.4 M KOH for 1 year. SAED (inset) reveals the amorphous character of the newly formed sphere-shaped phase which according to TEM-AEM analysis is mainly composed of Si (EDS in inset).

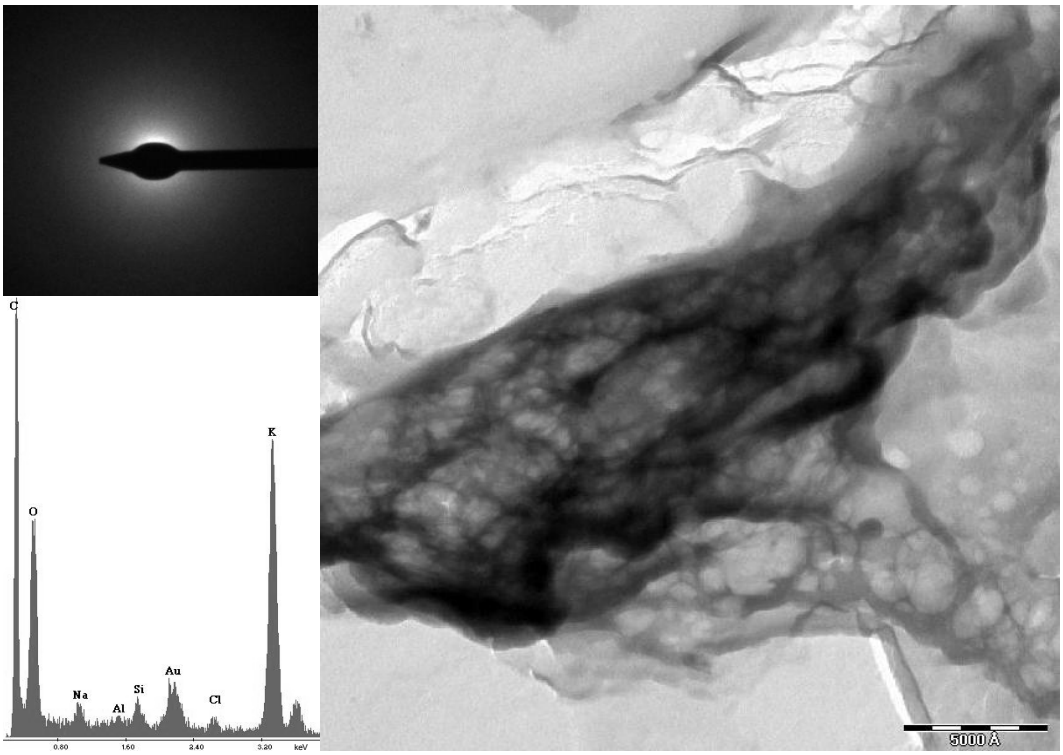

Figure 3-169. TEM image of Alhambra Formation soil treated with 0.4 M KOH for 1 year. SAED (inset) revealed the amorphous character of a newly formed phase which according to TEM-AEM analysis (lower inset) had a composition compatible with potassium carbonate. Amorphization due to e-beam irradiation led to the globular texture observed in the TEM image.

The TEM image (Figure 3-170) of the sample treated with 5 M KOH for 6 months showed newly formed prismatic and hexagonal crystals. Based on morphological characteristics these crystals are assumed to be zeolite K-F and K-I, respectively. The hexagonal-shaped crystals might be mistaken for kaolinite. However, they were quite abundant and were not observed in the untreated soil. Unfortunately, SAED did not allow an unambiguous differentiation from kaolinite. Structural formulae of the hexagonal crystals based on TEM-AEM results are presented in Table 3-35. Chemical composition differed from the structural formula given in JPDF card no. 180988, which is $K_2Al_2Si_2O_8 \cdot 3.8H_2O$. Results showed an excess in Si and a lack in Al and K. Furthermore, other cations such as Mg, Ca and Na were present.

After 1-year treatment an additional zeolitic phase was identified (Figure 3-171). Based on morphology this phase was identified as a chabazite-type zeolite. The chemical composition (inset, Figure 3-161), however, differed significantly from the one reported in JPDF card no. 120194, which is $K_2Al_2SiO_6 \cdot H_2O$,

Table 3-36 shows the structural formulae of the < 2 μm fraction treated for 7.5 years with 5 M NaOH based on TEM-AEM data. In some cases the chemical composition was similar to that of illite of the untreated Alhambra

Formation soil. However, the K concentration as well as the interlayer charge had increased. Admittedly, a larger number of analyses would be required for a more definitive interpretation of the transformation undergone by the remaining < 2 μm fraction. However, considering XRD and nitrogen sorption data, it can be assumed that smectites originally present in Alhambra Formation soil underwent illitization. In contrast, the original illite did not seem to have experienced any degradation in the presence of K, but rather some stabilization. This finding confirms XRD results which indicated recrystallization in the case of illite.

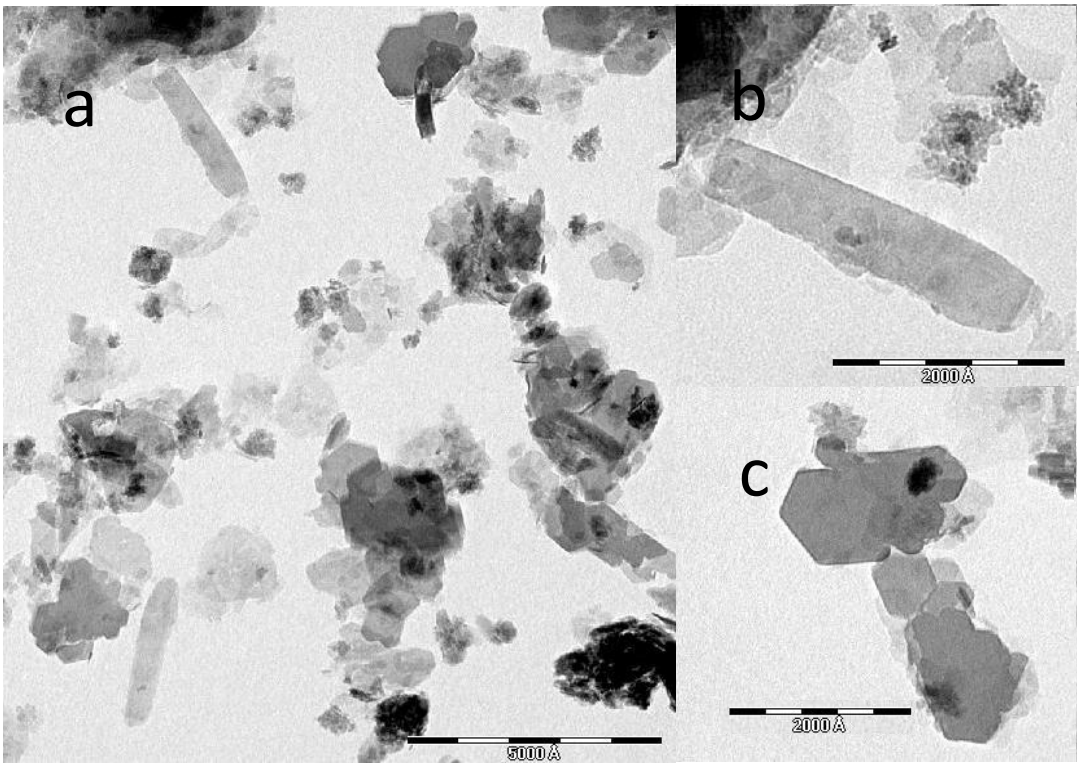

Figure 3-170. TEM image of Alhambra Formation soil treated with 5 M KOH for 6 months (a). Newly formed prismatic (b) and hexagonal (c) crystals, possibly zeolites, can be observed.

Table 3-35. Structural formulae calculated from TEM-AEM data of hexagonal crystals in Alhambra formation soil treated with 5 M KOH for 6 months.

Structural formulae of hexagonal crystals based on O_8							
	Si	Al	Mg	Fe	K	Ca	Na
1	2.50	1.70	0.13	0.03	0.08	0.22	0.06
2	2.33	1.84	0.15	0.04	0.10	0.31	0.06
3	2.64	1.43	0.11	0.03	0.13	0.37	0
4	2.55	1.62	0.08	0	0.09	0.32	0.06
5	2.61	1.46	0.20	0	0.19	0.24	0.11
6 months Average	2.53 ± 0.12	1.61 ± 0.17	0.13 ± 0.05	0.02 ± 0.02	0.12 ± 0.04	0.29 ± 0.06	0.06 ± 0.04

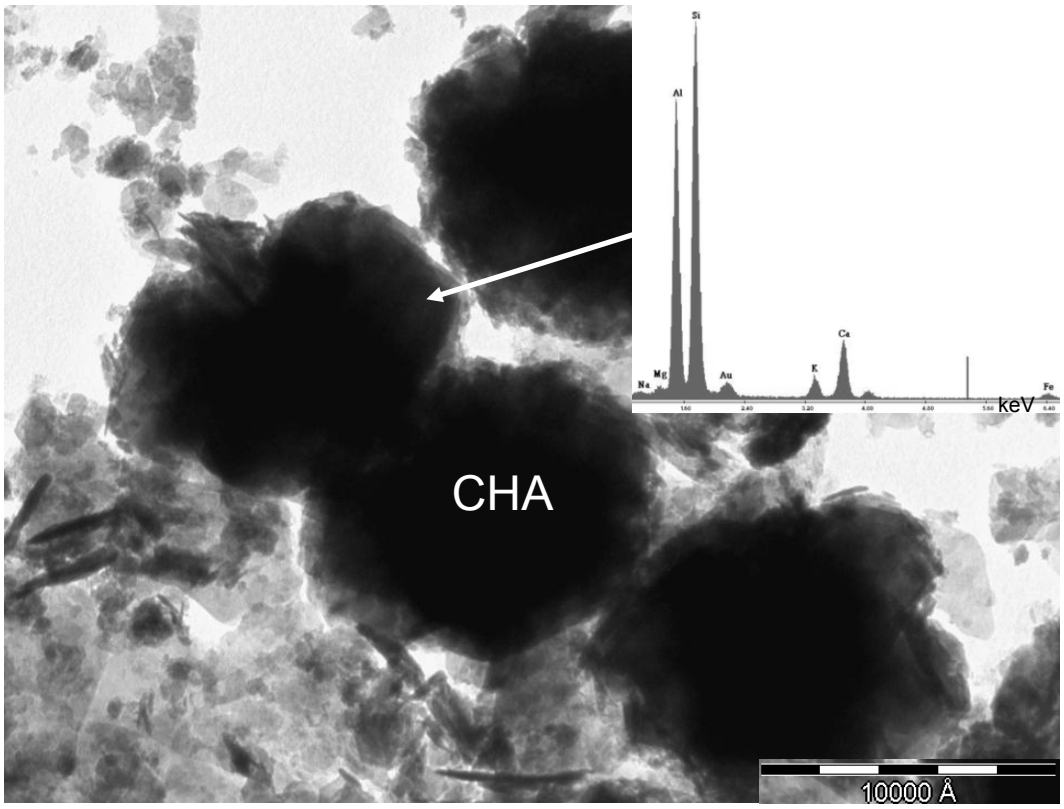

Figure 3-171. TEM image of Alhambra Formation soil treated with 5 M KOH for 1 year. A newly formed phase, possibly a chabazite-type zeolite, can be observed (EDS in inset).

Table 3-36. TEM-AEM analysis of the < 2 μm fraction of the Alhambra Formation soil treated with 5 M KOH for 7.5 years.

Structural formulae of clay minerals based on $O_{10}(OH)_2$										
Analysis	Si	^{IV}Al	^{VI}Al	Mg	Fe	Σoct.cat.[1]	K	Ca	Na	Σint.cha.[2]
untreated illite average	3.11 ± 0.12	0.89 ± 0.12	1.77 ± 0.18	0.17 ± 0.09	0.28 ± 0.24	2.23 ± 0.04	0.45 ± 0.10	0.00	0.00	0.45 ± 0.10
untreated smectite average	3.65 ± 0.11	0.35 ± 0.11	1.60 ± 0.13	0.28 ± 0.20	0 ± 0.01	2.11 ± 0.14	0.20 ± 0.14	0.01 ± 0.03	0.06 ± 0.08	0.28 ± 0.16
1	3.00	1.00	1.08	0.44	0.75	2.27	0.75	0.10	0.08	1.03
2	3.19	0.81	1.70	0.18	0.25	2.13	0.68	0.04	0.00	0.76
3	3.07	0.93	1.68	0.25	0.18	2.11	0.74	0.00	0.22	0.96
4	4.01	0.00	1.43	0.35	0.15	1.93	0.31	0.00	0.28	0.59

[1] Sum of octahedral cations
[2] Sum of interlayer charge

3.5.4.4. Nitrogen sorption

The surface area of the soil sample treated with 0.4 M KOH for 1 year showed a significant decrease of about 70 % which is consistent with the destruction of smectites (Table 3-37). The amount of newly formed nanosized particles, possibly zeolite K-I, must have been very small and did not counteract the surface area decrease induced by the destruction of smectite.

The nitrogen sorption isotherm showed a clear modification with a less pronounced hysteresis loop (Figure 3-172). The shape of the hysteresis loop is very close to the one observed in illite and kaolinite, indicating asignificant destruction of expandable clays. Note that pure smectites have a very pronounced hysteresis loop. The modification of the hysteresis loop was more significant in the sample treated with 0.4 M KOH than in the one treated with 0.4 M NaOH, suggesting that the KOH treatment was more effective in destroying smectites. This is also in agreement with the lower surface area observed in the case of the sample treated with KOH if compared to the sample treated with NaOH, and can be explained by the higher pH maintained during alkaline activation.

Table 3-37. BET surface area of Alhambra Formation soil treated with KOH for different periods of time.

Treatment time	Surface area (m^2/g)	
	0.4 M KOH	5 M KOH
0	70.78 ± 0.28	70.78 ± 0.28
6 months	*	76.87 ± 0.25
1 year	21.44 ± 0.53	65.14 ± 0.21
> 6 years	*	60.99 ± 0.19

* not determined

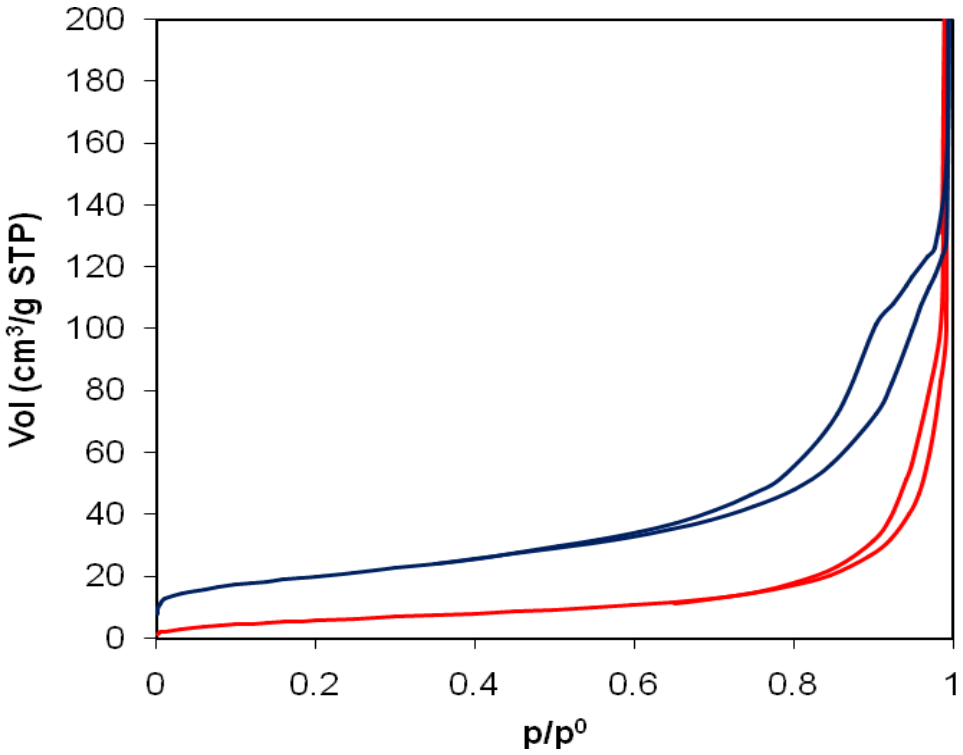

Figure 3-172. Nitrogen sorption isotherms of untreated Alhambra Formation soil (blue) and soil treated with 0.4 M KOH for 1 year (red).

The surface area of the soil sample treated with 5 M KOH showed a slight increase after 6 months. The destruction of expandable clays might have caused a certain decrease. However, the formation of hexagonal nanocrystals (zeolite K-I) seemed to have led to an increase which was also observed in the case of pure kaolinite and montmorillonite. Thus, the formation of zeolite K-I counteracted the reduction caused by the destruction of smectites.

Nevertheless, after 1-year treatment a reduction in surface area was observed (Table 3-37). This decrease was caused by the formation of K-chabazite, observed using FESEM. Note that the BET surface area of this zeolite is reported to be only 17.82 m^2/g (Ridha 2009).

The shape of the isotherm after 1-year treatment, was similar to the one of kaolinite and illite and suggests the destruction of smectite (Figure 3-173).

After 6.2 years of treatment the surface area experienced a further decrease, because the number of chabazite crystals had increased. The shape of the nitrogen isotherm did not show any additional modification.

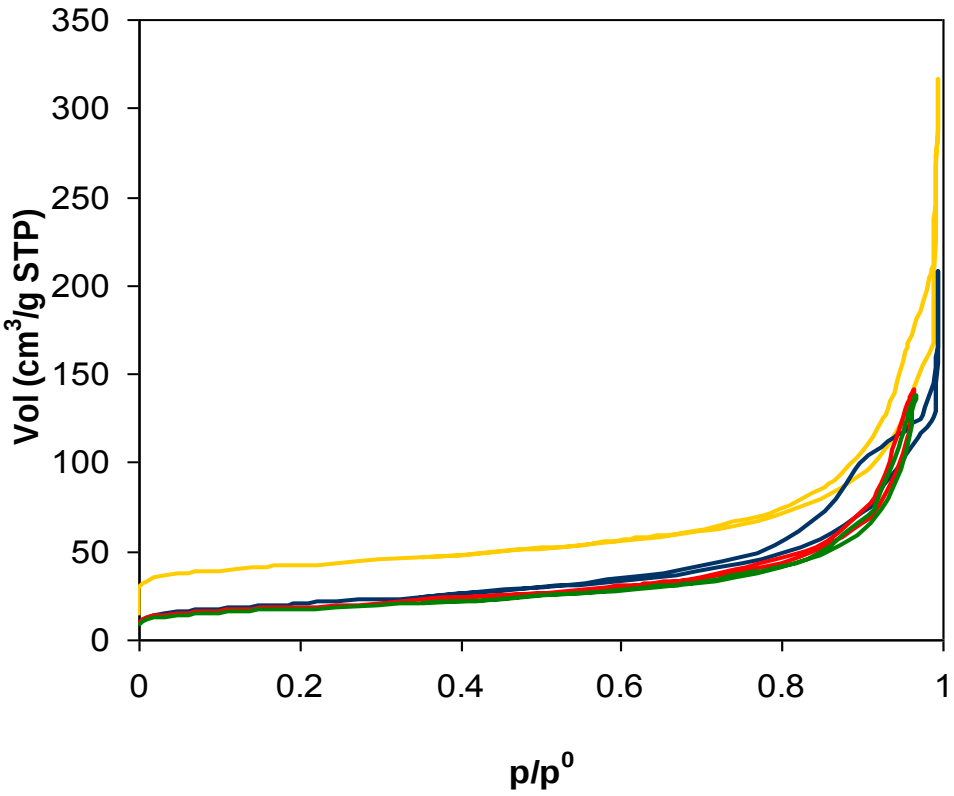

Figure 3-173. Nitrogen sorption isotherms of untreated Alhambra Formation soil. Untreated (blue), and treated with 5 M KOH for 6 months (yellow), 1 year (red) and 7.5 years (green).

3.6. pH evolution upon alkaline activation

In the following section the results regarding the pH decrease upon alkaline activation of the Alhambra Formation clays using solutions of different concentrations are presented. The influence of organic matter (OM) on the pH evolution is also considered.

Test results using 0.4 M NaOH or 0.4 M KOH solutions as well as saturated $Ca(OH)_2$ solution revealed an important decrease in pH upon alkaline activation of Alhambra Formation soil (Figure 3-174). This was especially true for NaOH and $Ca(OH)_2$ solutions. The decrease in pH during alkaline treatment of clays seems to be a common phenomenon and has been reported for example by Chermark (1992 and 1993) in the case of Opalinus shale treated with NaOH or KOH.

Figure 3-175 shows that the pH decrease upon alkaline activation was less significant when 5 M NaOH or 5 M KOH were used if compared with 0.4 M NaOH or 0.4 M KOH. Comparison of data for 5 M NaOH and 5 M KOH revealed that the pH drop was more pronounced when NaOH was used. Furthermore, comparison of pH data for Alhambra Formation soil with and without OM (Figure 3-176) revealed that the pH reduction was initially faster in the case of the soil treated with H_2O_2 to remove OM, but both samples reached a similar value after almost 2 years of treatment. Relating decrease in pH with reactivity, this would suggest an initially more extensive reaction between phyllosilicates and the alkaline activator in the case of the sample without OM. This observation is in agreement with XRD and FESEM results (see section 3.7).

In general, the pH value stabilized over time and in some cases even increased slightly (Figure 3-176). This might be explained by the fact that OH^- is released upon zeolite formation and might counteract the OH^- decrease upon mineral dissolution. Gaucher and Blanc (2006) stated that 2 moles of OH^- are released upon precipitation of 1 mole of analcime. In the case of saturated $Ca(OH)_2$ solution and 0.4 M NaOH solution, the more drastic reduction might be explained by mineral dissolution and the formation of CSH phases which have been detected in both cases. Gaucher and Blanc (2006) reported that the precipitation of 1 mole of tobermorite consumes 4 moles of OH^-. Note that in the case of both samples formation of crystalline zeolites was not detected.

Interestingly, the measured pH was systematically higher for 5 M KOH than for 5 M NaOH solutions. pH measurements of very concentrated strong bases are known to be rather complicated (Lechert 2001) and actually gave values above the theoretical maximum of pH 14 in the case of 5 M KOH (Figures 3-175 and 3-176). In order to verify whether the difference in pH was due to an analytical error or impurities of the reagent, acid-base titration was

performed to confirm the concentration of 0.1 M NaOH and 0.1 M KOH solutions which had a pH of 12.6 and 13.5, respectively. Titration results confirmed the concentration of both solutions and revealed that the pH was higher in 0.1 M KOH than in 0.1 M NaOH solution. Chermak (1992, 1993) seemed to have been aware of the above described phenomenon. The author used 0.008 M KOH and 0.01 M NaOH solutions to obtain solutions with a pH of 11.88. The difference in pH of alkaline solutions of identical ionic strength might be explained by ion pairing taking place in concentrated ionic solutions, where a temporary union between a cation and an anion into a single entity can be observed due to interionic attraction of these ions in close proximity (www.bas.bg/cleps/poemes/.../ionic_ solutions.pdf, accessed 4.11.2013). Ion pairing might be more pronounced in the case of Na^+, because of its higher charge density (ionic radius of Na^+ = 0.97 Å) if compared to K^+ (ionic radius = 1.33 Å). Duxson et al. (2005b) also recognized the greater basicity of KOH if compared to equimolar NaOH solutions and concluded that KOH solutions had a higher pH and promoted faster aluminosilicate dissolution due to the greater amount of free hydroxide.

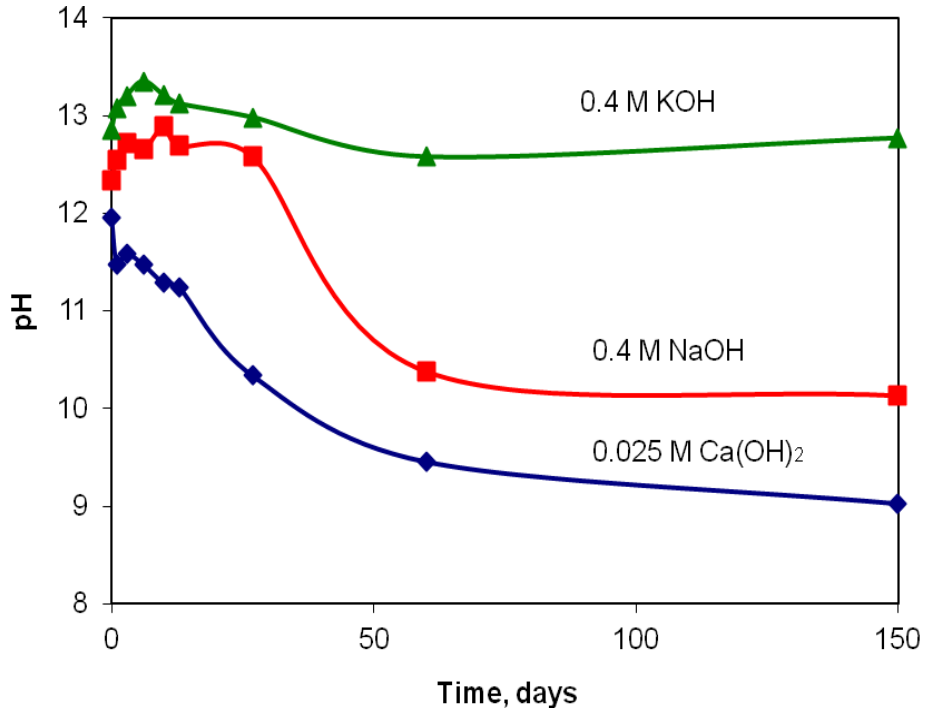

Figure 3-174. pH evolution of Alhambra Formation soil treated with different alkaline solutions.

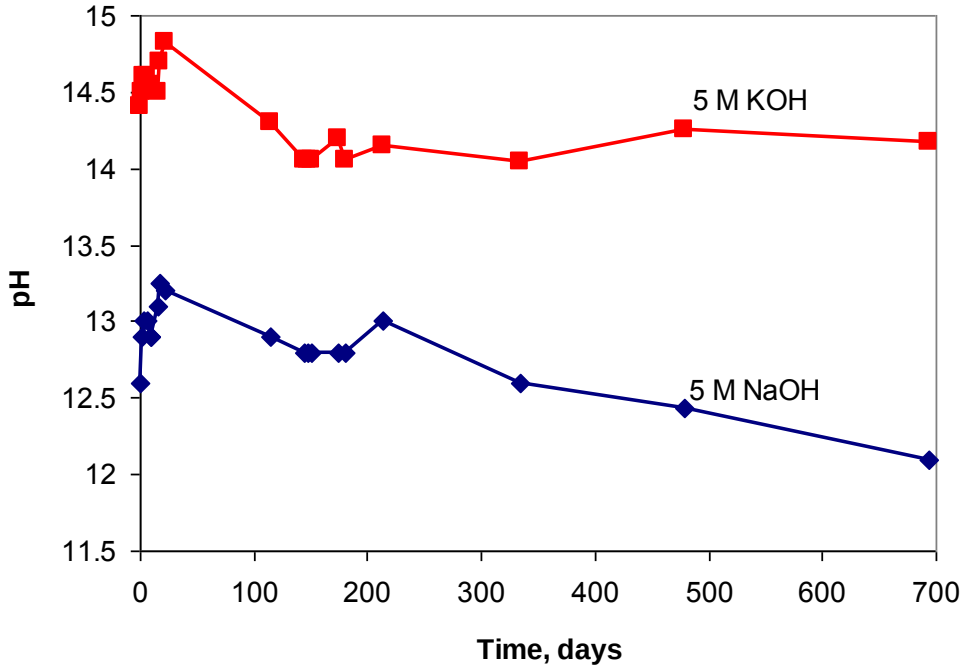

Figure 3-175. pH evolution of Alhambra Formation soil with OM treated with 5 M NaOH and 5 M KOH.

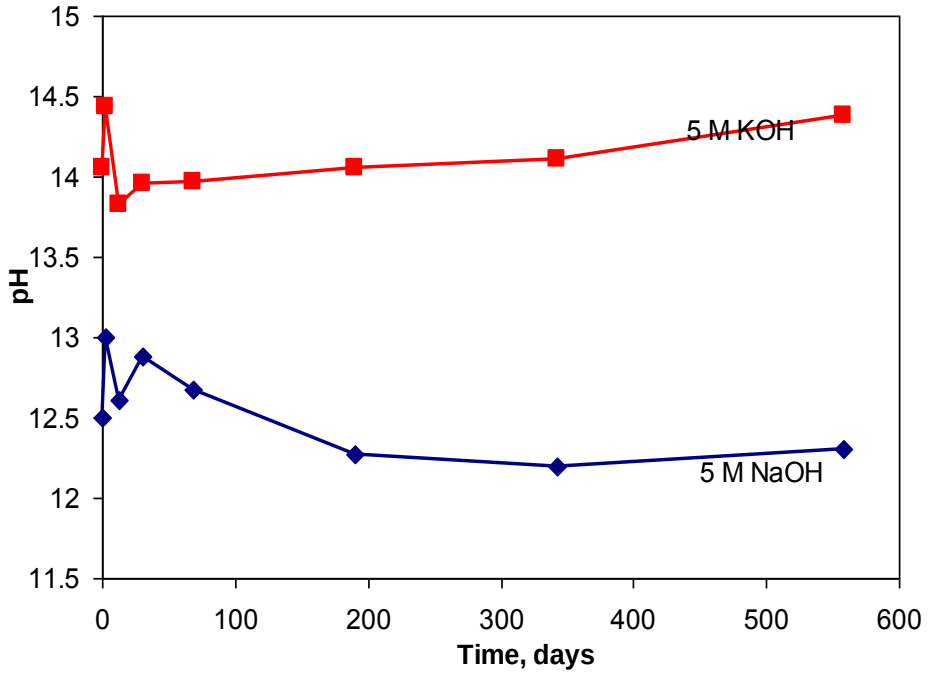

Figure 3-176. pH evolution of Alhambra Formation soil without OM treated with 5 M NaOH and 5 M KOH.

3.7. Influence of organic matter on the reactivity of Alhambra Formation soil

It is known that organic matter (OM) is stabilized through the formation of organo-mineral complexes (Allison 1973). Leinweber et al. (1999) found that OM in vertisols was characterized by strong organic-mineral bonds to swelling clay minerals which are believed to contribute to its stability. The researchers determined that most of the OM (70-91 %) in vertisols was associated with the clay-size fraction which they attributed to the large specific surface area, especially of swelling clays. The findings by Leinweber and co-workers are in agreement with results by Mayer (1994), stating that the greatest reduction in bioavailability of organic molecules has been observed with minerals such as expandable clays and allophanic materials. According to Saidy et al. (2013) hydrous iron oxides are also very effective in the sorption and stabilization of OM. However, their sorption capacity decreases with increasing pH and their contribution to OM sorption under the highly alkaline conditions in this study is uncertain.

OM in soils and sediments has been widely characterized (Hedges and Oades 1997) and a significant amount of research has been performed on the stabilization of OM through the formation of organo-mineral complexes. However, little attention has been paid to the fact that the presence of OM might, to a significant degree, influence reactions between clay minerals and pore waters (Lunt 1980, Claret et al. 2002). Wattel-Koekkoek (2002) stated that the sorption of OM would render the clay surface hydrophobic, resulting in its passivation. Thus, OM may inhibit clay dissolution in high-pH alkali-rich solutions (e.g., solutions generated by water-induced concrete alteration). Reduced reactivity modifies clay stability and its transformation into new phases, an important consideration not only in the case of earthen architecture conservation, but also when clay is used as backfill material for nuclear waste disposal or waste water barrier (Wilson et al. 2006).

Here the possible effect of OM on the reactivity of clays treated with alkaline solutions was studied. One batch of Alhambra Formation soil was treated with H_2O_2 in order to remove OM prior to alkaline activation using 5 M NaOH or 5 M KOH. The mineralogical evolution over time of soil with and without OM was studied with different analytical techniques including XRD, FESEM, nitrogen sorption and TG/ evolved gas analysis (FTIR). Prior to that, the OM content of the < 2 μm fraction of the Alhambra Formation soil was quantified using TG and elemental analysis.

3.7.1. Determination of the organic matter content of the Alhambra Formation soil

In order to remove the OM of the < 2 µm fraction of the Alhambra Formation soil, one batch was subjected to H_2O_2 treatment prior to alkaline activation. Effervescence upon H_2O_2 attack was a clear indicator for the presence of OM. TG analysis coupled with evolved gas analysis, as well as elemental analysis were performed on clay samples before and after H_2O_2 treatment to verify the effectiveness of the H_2O_2 treatment and to determine the amount of OM in the soil.

3.7.1.1. TG

The major weight loss observed in the treated and untreated soil samples can be attributed to adsorbed and structural water of the clays. Note that the sample with OM showed a more pronounced weight loss between 300-500 °C, the temperature range commonly associated with the thermal decomposition of OM (Figure 3-177). The difference in weight loss between the untreated sample and the sample treated with H_2O_2 was 1.1 wt%, which is attributed to the OM content. The obtained value is in agreement with published data by Martin-Garcia et al. (1998) for the Alhambra Formation soil. Note that most soils have an OM content of 0.5-5 wt% (Saride et al. 2013).

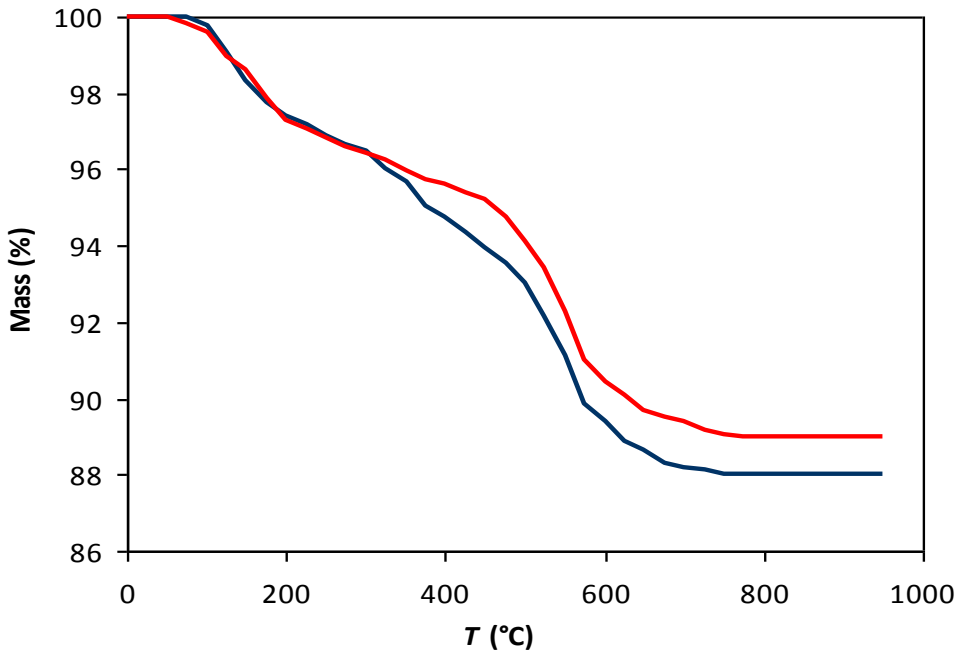

Figure 3-177. Thermogravimetric curve of untreated Alhambra Formation soil with OM (blue) and without OM (red).

The evolved gas analysis was performed using air as a carrier gas, considering a temperature range between 230 ºC and 500 ºC which is commonly associated with the oxidative thermal decomposition of OM. The presence of CO gas is an indicator for incomplete combustion, typical for the existence of OM. The spectrum of the untreated clay sample (Figure 3-178a) revealed the presence of CO additional to CO_2, whereas the spectrum of the clay treated with H_2O_2 did not show any detectable amounts of CO (Figure 3-178b). These findings suggest that the H_2O_2-treatment had been effective in destroying the major part of the OM (organic carbon). Plante et al.(2005) reported that it was possible to remove about 87 % of the initial organic C from clay samples by hydrogen peroxide treatment. According to the authors, the remaining C corresponds to black carbon, a term used to describe the C which withstands strong chemical or thermal oxidation and is considered inert. Black carbon includes graphitic and pre-graphitic phases such as charcoal, graphite, soot and coal (Schumacher 2002). Graphitic and pre-graphitic phases are very common in soils, for example in schists and phyllites (Rodriguez-Gallego, M., personal communication 15.10.2013). Martin (2000) reported the presence of micaschists in the conglomerate of the Alhambra Formation. The schists originate from the Sierra Nevada reliefs and include a significant amount of graphite.

Note that the initial treatment of the clay fraction with acetic acid eliminated any carbonates (inorganic carbon) that could have had interfered in the TG results. In any case, the decomposition of carbonates occurs at T >500 °C at a heating rate > 2 °C/min (Rodriguez-Navarro et al. 2009, 2012) and only CO_2 is released during their thermal decomposition.

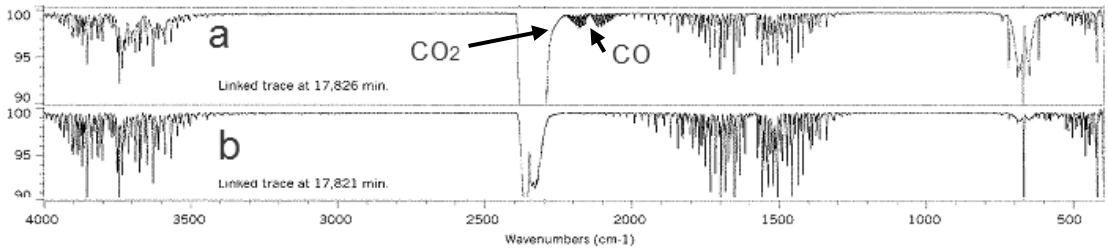

Figure 3-178. Evolved gas FTIR spectra of Alhambra Formation soil a) with OM and b) without OM. The spectra were taken at 356 ºC.

3.7.1.2. Elemental analysis

Organic carbon, nitrogen and hydrogen were quantified by means of elemental analysis (Table 3-38). The difference in carbon content between the untreated clay sample and the sample treated with H_2O_2 was about 0.66 wt% which is attributed to the organic carbon content. Assuming that organic carbon constitutes about 58 % of the OM content (Schumacher 2002), the OM content would amount to 1.14 wt%. The value calculated from TG data and the results of elemental analysis are, thus, in good agreement.

The sample treated with H_2O_2 showed a carbon content of 0.25 wt% which is assumed to correspond to black carbon. Note that elemental analysis yields the total content of both, elemental and organic carbon, while TG only quantifies the organic carbon which can be oxidised and evolved as CO or CO_2 gases. Elemental carbon includes the above mentioned graphitic and pre-graphitic phases.

Table 3-38. Elemental analysis results of samples heated up to 1020 °C.

Sample	wt%		
	Nitrogen	Carbon	Hydrogen
Clay, untreated	0.21	0.91	1.36
Clay treated with H_2O_2	0.09	0.25	1.33

3.7.2. Effect of OM on the reactivity of Alhambra Formation soil treated with 5 M NaOH

Possible differences in the mineralogical evolution of Alhambra Formation soil upon alkaline activition induced by the presence or absence of OM were studied using XRD, FESEM and nitrogen sorption.

3.7.2.1. XRD

XRD patterns revealed that OM adsorbed on the clay particles surface clearly modifies the minerals reactivity towards alkaline activation. The mineralogical evolution was faster and changes were more pronounced in the case of the soil samples treated with 5 M NaOH where the OM was removed prior to alkaline treatment. However, the zeolitic phases formed upon alkaline activation were the same.

After 6 months of alkaline activation with NaOH a new zeolitic phase, a faujasite-type zeolite (Figure 3-179) with the following formulae: $Na_2Al_2Si_{2.5}O_9 \cdot 6.2H_2O$ (JPDF card no. 380237), was identified in the Alhambra Formation soil with and without OM. However, the 111 Bragg peak intensity was significantly higher in the sample without OM. Furthermore, the Bragg peak intensity of illite was reduced and only traces of kaolinite could be detected in this sample, whereas the reduction in Bragg peak intensity of illite and kaolinite was less pronounced in the sample with OM.

After one year of treatment XRD data revealed nearly identical patterns in the case of Alhambra Formation soil samples with and without OM treated with 5 M NaOH. In both cases the faujasite-type zeolite was detected (Figure 3-180). However, the XRD pattern of the sample without OM showed small additional peaks at 6.4 and 3.7 Å, which corresponded to a sodalite-type zeolite with the following formula: $Na_{2.16}Al_2Si_{1.68}O_{7.44} \cdot H_2O$ (JPDF card no. 311271).

After prolonged alkaline activation, the sodalite-type zeolite was observed in both samples. The amount of this phase increased over time at the expense of the faujasite-type zeolite and became the dominant phase. In the case of the sample without OM the faujasite-type zeolite had disappeared after > 6 years of treatment, while it was still detectable in the case of the sample with OM (Figure 3-181).

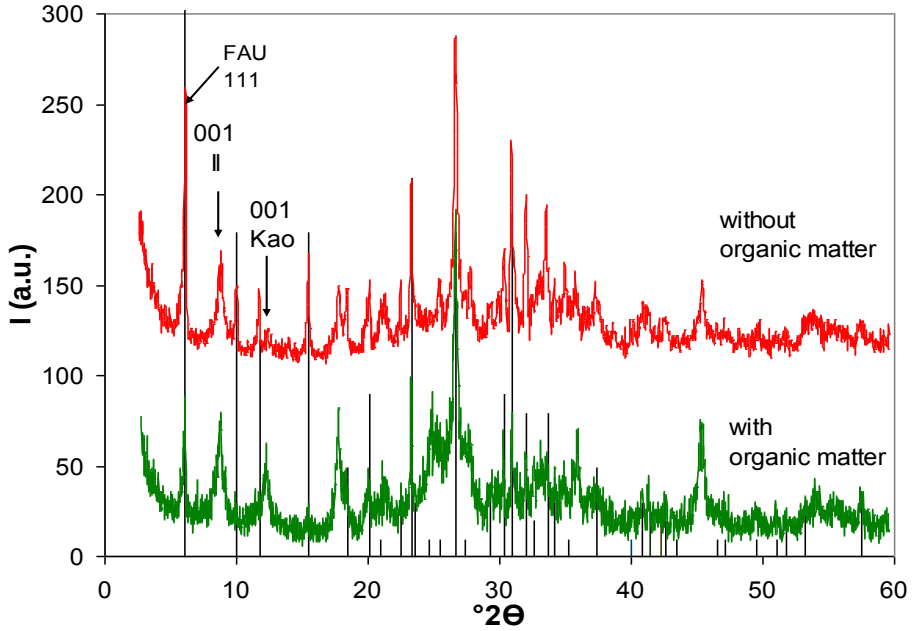

Figure 3-179. XRD patterns of Alhambra Formation clays (OA) treated with 5M NaOH solution for 6 months. Black line pattern: Faujasite-type zeolite (JPDF card no. 380237).

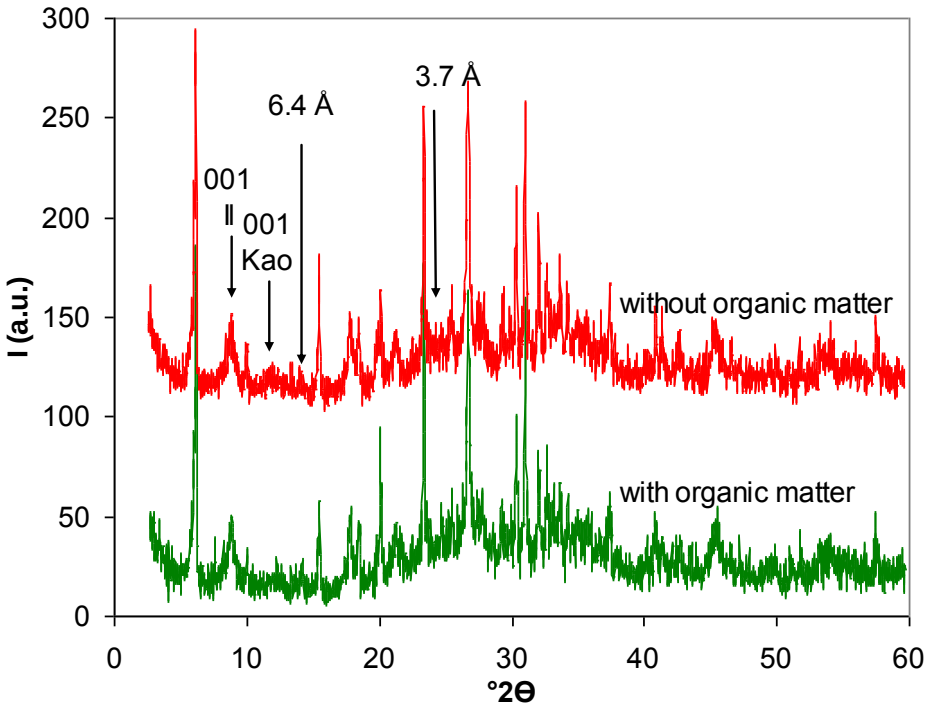

Figure 3-180. XRD patterns of Alhambra Formation clays (OA) treated with 5M NaOH solution for 1 year. Both diagrams are nearly identical.

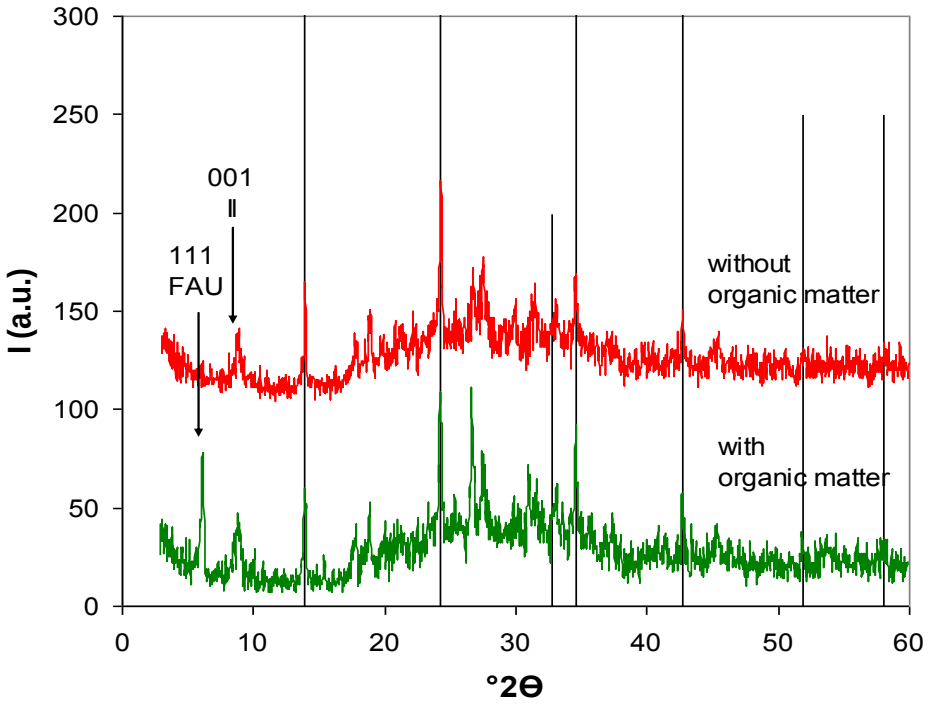

Figure 3-181. XRD patterns of Alhambra Formation clays (OA) treated with 5M NaOH solution for >6 years. Black line pattern: Sodalite-type zeolite (JPDF card no. 311271). The faujasite-type zeolite can no longer be detected in the sample without OM.

3.7.2.2. FESEM

FESEM observations confirmed differences in the mineralogical evolution of the Alhambra Formation soil treated with 5 M NaOH depending on the presence or absence of OM.

In the clay sample containing OM treated for 6 months a small amount of faujasite-type zeolite was observed together with a large portion of unreacted clay (Figure 3-182). The crystal size of the faujasite was about 2 μm. The sample without OM, on the other hand, showed a large number of zeolites of two distinct morphologies which are thought to correspond to a) the faujasite-type zeolite; and b) crystals showing distinct degrees of transformation into a sodalite-type zeolite (Figure 3-183). Furthermore, the crystal size of the faujasite-type zeolite was about twice the size of the faujasite crystals observed in the sample with OM. During the faujasite-to-sodalite transformation, the Ca concentration seemed to decrease while the Na concentration increased slightly as evidenced by EDS microanalysis (Insets, Figure 3-183).

Both samples showed similar textural features after 1 year of treatment (Figure 3-184 and 3-185). Faujasite-type zeolite crystals, which seemed to have increased in size, together with some sodalite-type zeolites were observed. However, the amount of the sodalite-type zeolite was too small to be detected with XRD in the case of the sample with OM. In the case of the sample without OM, XRD allowed the detection of the sodalite-type zeolite. Note that the polycrystalline aggregates of the sodalite-type zeolite crystals had increased in size to ~ 4-5 μm in the sample without OM (Figure 3-186).

Even after more than 6-year treatment, differences between the sample with and without OM were detected. The former presented a somewhat delayed evolution. Whereas, the sample with OM treated for 7.5 years still contained faujasite-type zeolite (Figure 3-187) apart from the sodalite-type zeolite (Figure 3-188), the one without OM only contained the sodalite-type zeolite (Figure 3-189). In both samples, the sodalite-type zeolite now showed compact aggregates with about 5 μm diameter, very similar to hydroxysodalite crystal aggregates observed in pure kaolinite treated with 5 M NaOH for 6.1 years.

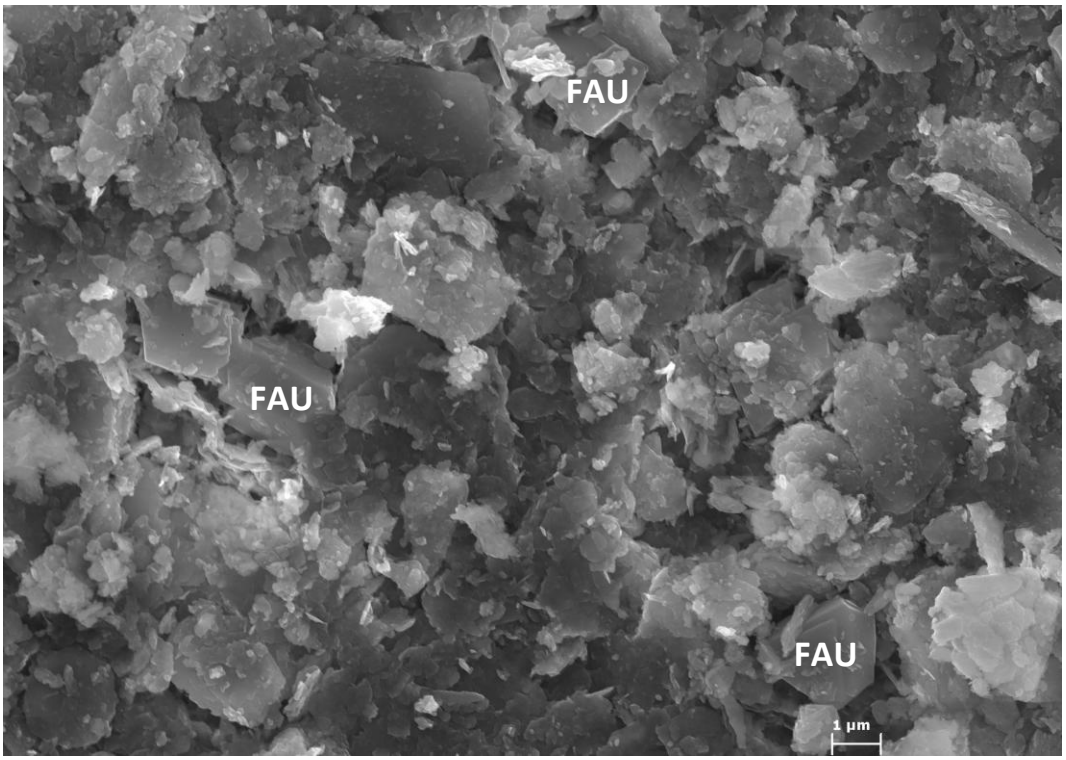

Figure 3-182. FESEM image of Alhambra Formation soil with OM treated with 5 M NaOH for 6 months. In addition to a large amount of unreacted clay, a faujasite-type zeolite (FAU) but no sodalite-type zeolite can be observed.

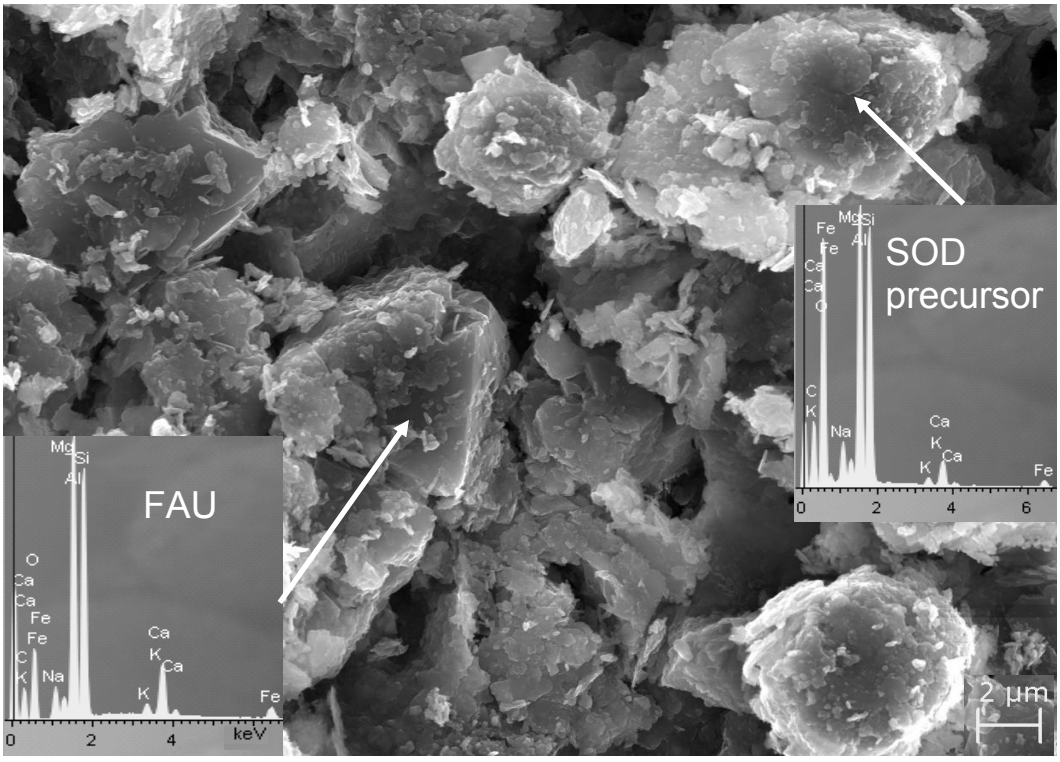

Figure 3-183. FESEM image of Alhambra Formation soil without OM treated with 5 M NaOH for 6 months. Crystals of faujasite-type zeolite (FAU) can be observed which seem to show distinct degrees of transformation into a sodalite-type zeolite (arrows, EDS spectra in insets).

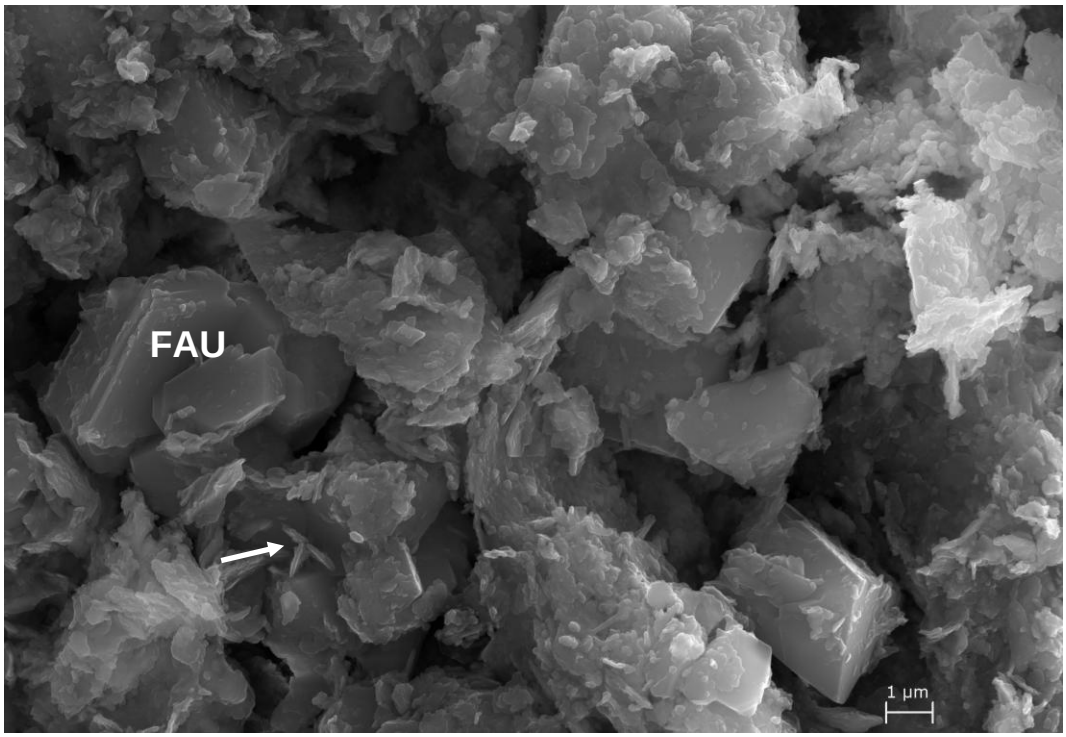

Figure 3-184. FESEM image of Alhambra Formation soil with OM treated with 5 M NaOH for 1 year. Faujasite- (FAU) and sodalite-type zeolites (SOD, red arrow) can be observed.

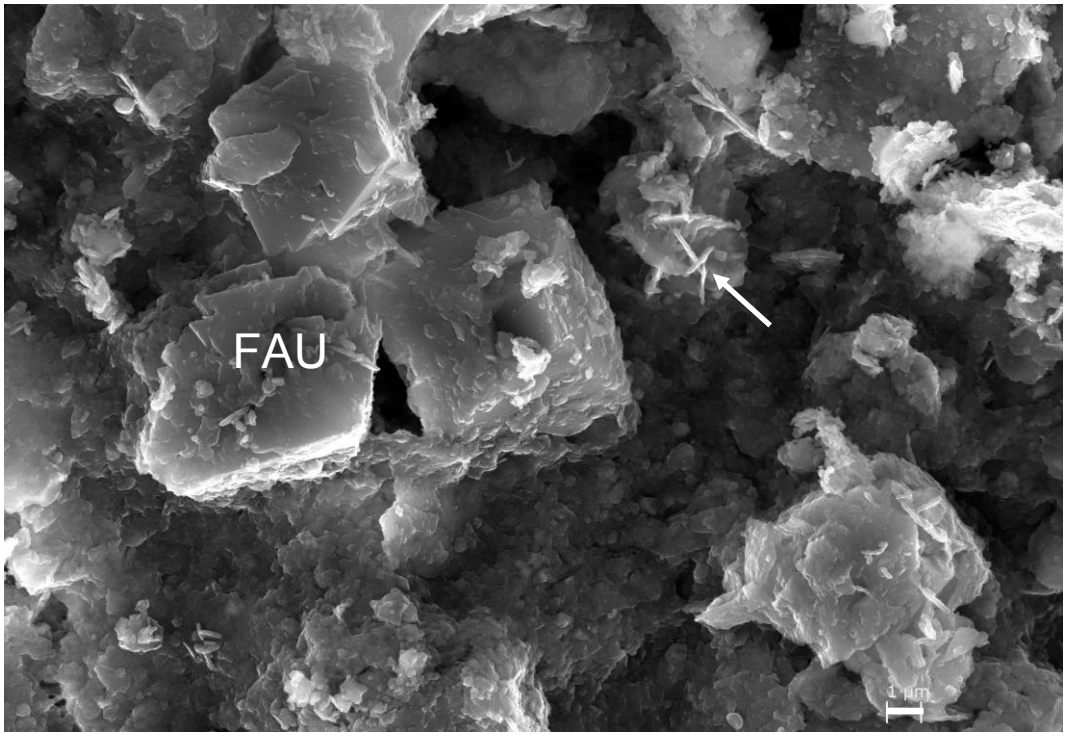

Figure 3-185. FESEM image of Alhambra Formation soil without OM treated with 5 M NaOH for 1 year. Faujasite- (FAU) and sodalite-type zeolites (SOD, red arrow) can be observed.

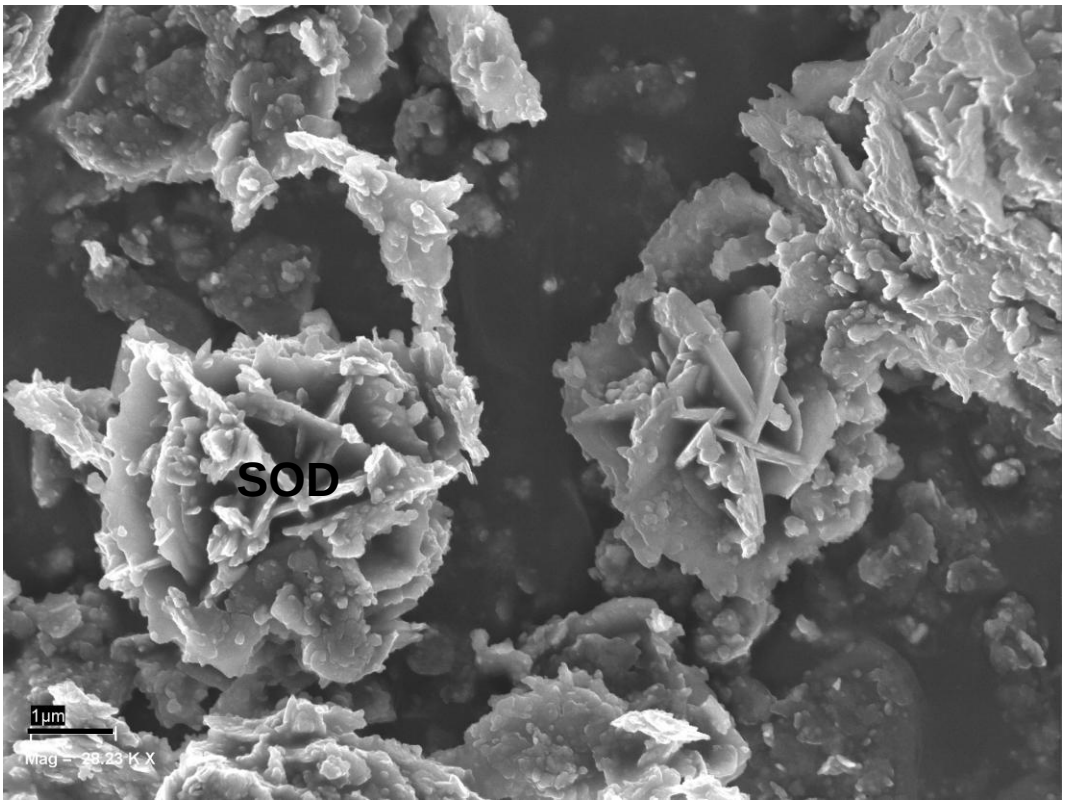

Figure 3-186. FESEM image of Alhambra Formation soil without OM treated with 5 M NaOH for 1 year. Sodalite-type zeolites (SOD) can be observed.

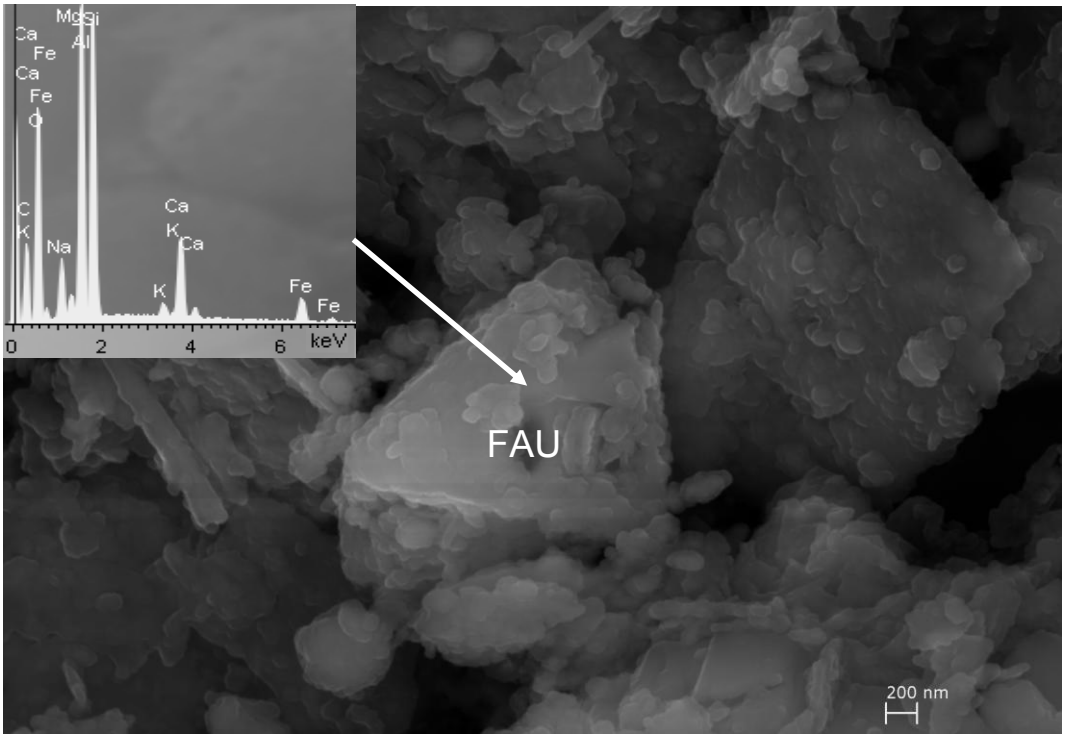

Figure 3-187. FESEM image of Alhambra Formation soil with OM treated with 5 M NaOH for 7.5 years. The sample still contains faujasite-type zeolite (EDS in inset).

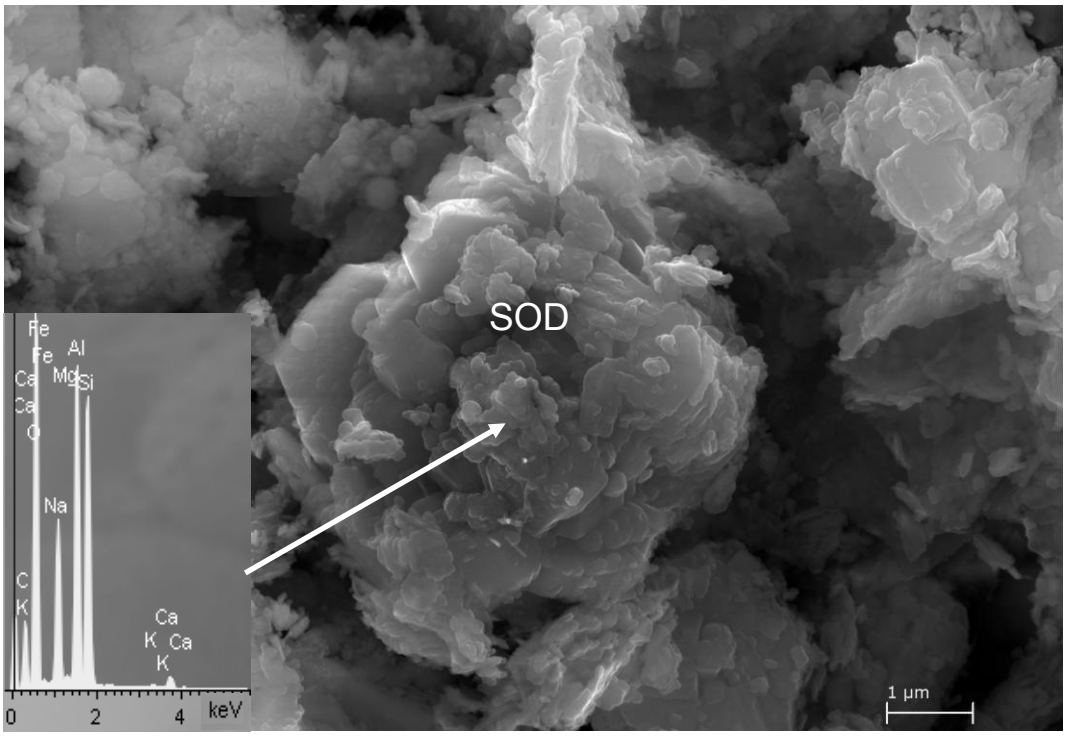

Figure 3-188. FESEM image of Alhambra Formation soil with OM treated with 5 M NaOH for 7.5 years. The image shows a sodalite-type zeolite (EDS in inset).

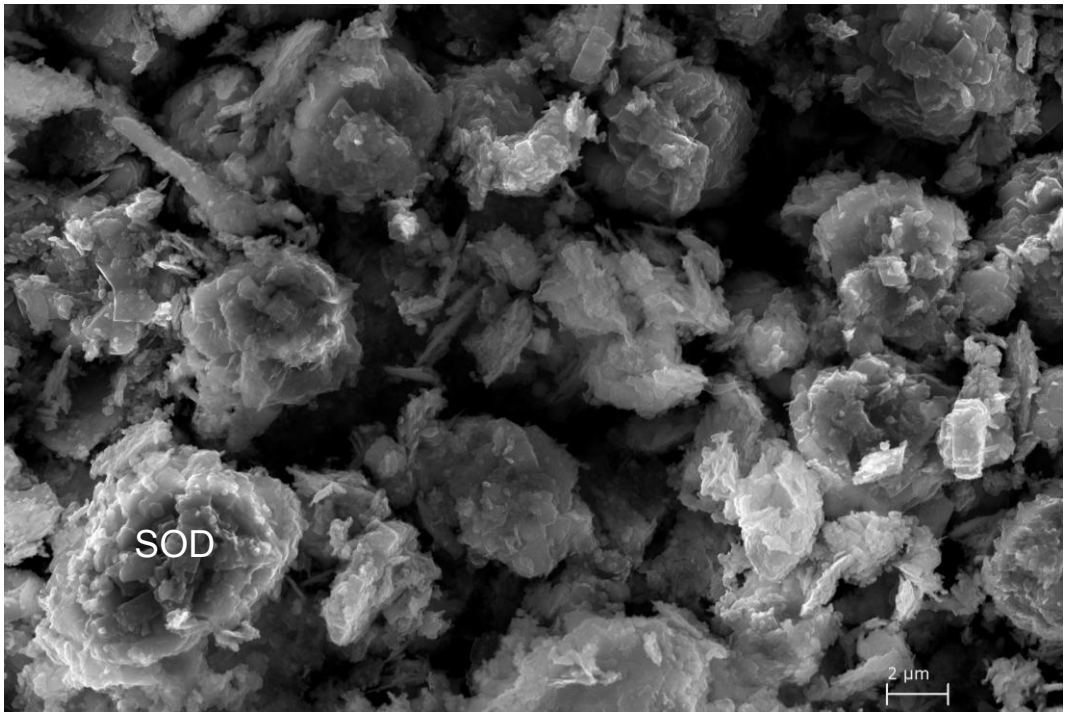

Figure 3-189. FESEM image of Alhambra Formation soil without OM treated with 5 M NaOH for 6.2 years. Only sodalite-type zeolites (SOD) can be observed.

3.7.2.3. Nitrogen sorption

BET surface area (Table 3-39) calculated from nitrogen adsorption data revealed a slightly higher surface area of the untreated sample without OM if compared to the one with OM. It is assumed that adsorption of OM reduces the electrostatic repulsion of clay particles and, thus, facilitates aggregation. This would result in a lower surface area in the case of the soil with OM. Zhang et al. (2013b) came to a similar conclusion regarding reduced surface area of clay minerals in the presence of OM, OM acting as an aggregation agent for clay particles. Apart from particle aggregation, Kaiser and Guggenheim (2003) and Tombacz et al. (1998) attributed the reduction in specific surface area to the clogging of micropores by adsorbed OM. In any case, the nitrogen sorption isotherms of the samples with and without OM revealed no significant differences (Figure 3-190).

A significant increase in surface area of the Alhambra Formation soil treated with 5 M NaOH for 6 months was detected in both samples. However, the increase was more pronounced in the case of the sample without OM (215.05 ± 4.06 m^2/g) than in the case of the one with OM (144.99 ± 1.79). This increase coincides with the formation of a faujasite-type zeolite which was more extensive in the sample without OM. Compared with the untreated soil sample, the hysteresis loop of the treated sample with OM, and especially of the treated sample without OM, was less pronounced, indicating that expandable clay minerals were partially destroyed (Figure 3-191).

After 1-year treatment, surface area data were practically identical in the samples with and without OM. This is in agreement with XRD and FESEM results, showing an important degree of transformation in both cases. The nitrogen sorption isotherm (Figure 3-192) showed an identical shape for both samples. Furthermore, the shape of the hysteresis loop was similar to the one observed in pure kaolinite and illite, suggesting the destruction of smectite.

After prolonged treatment (> 6 years) both samples experienced a decrease in surface area which was especially severe in the case of the sample without OM (Table 3-39). This decrease is thought to be due to the transformation of the faujasite-type zeolite into the sodalite-type zeolite, because the reported surface area of sodalite-type zeolite (22.8 m^2/g, Li et al. 2007) is significantly lower than the one of the faujasite-type zeolite (400 m^2/g, Sutarno and Arryanto 2007). These results are consistent with XRD and FESEM results, suggesting that some faujasite-type zeolite was still present in the sample with OM, whereas the sodalite-type zeolite was the dominant phase in the sample without OM. The shape of the nitrogen sorption isotherm did not experience any further modification and was very similar for both samples (Figure 3-193).

Table 3-39. BET surface area of Alhambra Formation soil with and without OM and treated with 5 M NaOH for different periods of time.

Treatment time	Surface area (m^2/g)	
	With OM	Without OM
0	70.78 ± 0.28	82.52 ± 0.52
6 months	144.99 ± 1.79	215.05 ± 4.06
1 year	244.38 ± 5.27	245.96 ± 5.47
> 6 years	109.87 ± 1.88	31.49 ± 0.27

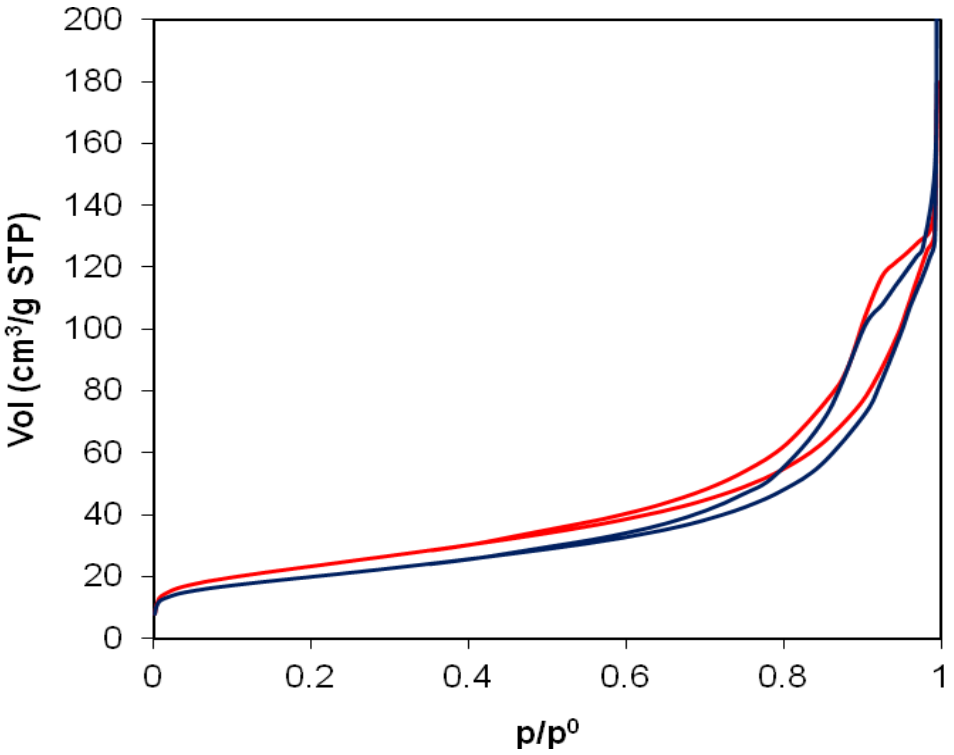

Figure 3-190. Nitrogen sorption isotherms of untreated Alhambra Formation soil with (blue) and without (red) OM.

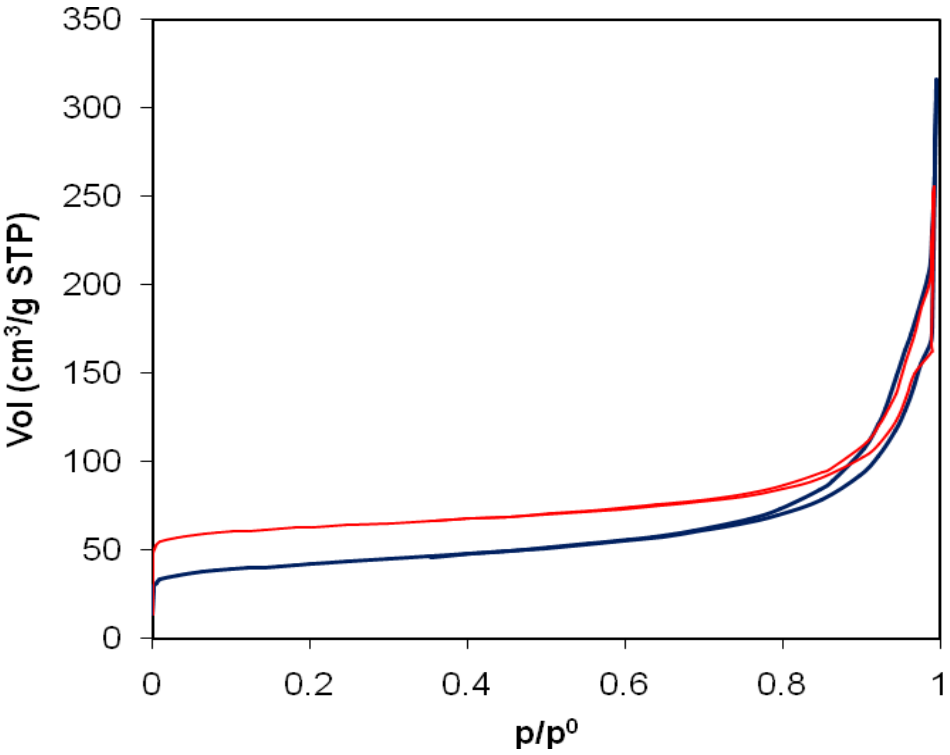

Figure 3-191. Nitrogen sorption isotherms of Alhambra Formation soil with (blue) and without (red) OM treated for 6 months with 5 M NaOH.

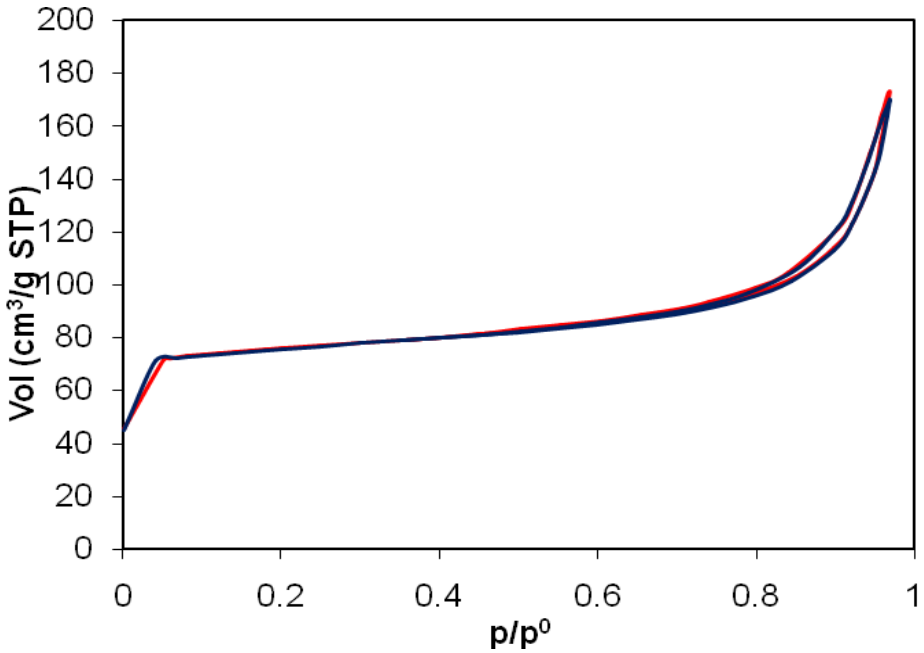

Figure 3-192. Nitrogen sorption isotherms of Alhambra Formation soil with (blue) and without (red) OM treated for 1 year with 5 M NaOH.

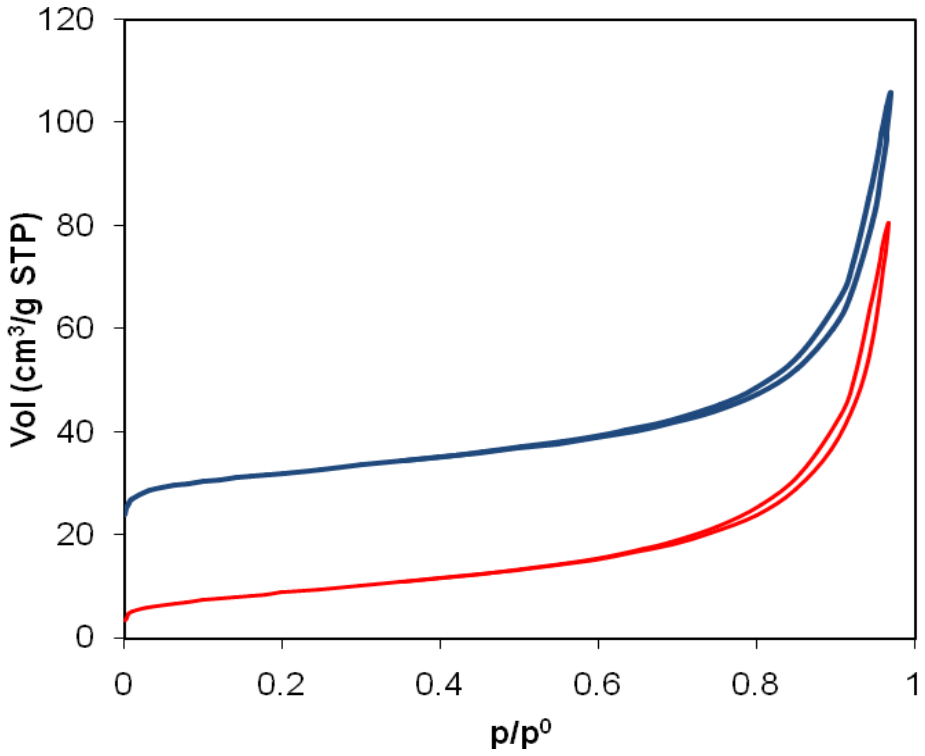

Figure 3-193. Nitrogen sorption isotherms of Alhambra Formation soil with (blue) and without (red) OM treated for >6 years with 5 M NaOH.

3.7.3. Effect of OM content on the reactivity of Alhambra Formation soil treated with 5 M KOH

Possible differences in the mineralogical evolution of Alhambra Formation soil upon treatment with 5 M KOH caused by the presence or absence of OM were studied using XRD, FESEM and nitrogen sorption.

3.7.3.1. XRD

The mineralogical evolution of the sample treated with 5 M KOH without OM was somewhat faster than the one of the sample with OM during the first 6 months. The XRD diagrams of both samples showed the presence of zeolite K-I (JPDF card no. 180988). However, in the sample without OM the decrease of the 001 kaolinite Bragg peak was more pronounced, and an additional peak at 5.2 Å was observed which corresponds to the 003 Bragg peak of a chabazite-type zeolite (JPDF card no. 120194) (Figure 3-194).

After 1 year of treatment the XRD patterns of both samples were very similar and the 003 reflection of the chabazite-type zeolite was detected in the sample with OM as well. Kaolinite could no longer be detected in either of the samples (Figure 3-195). No additional diffraction patterns are included here because further treatment did not result in important changes.

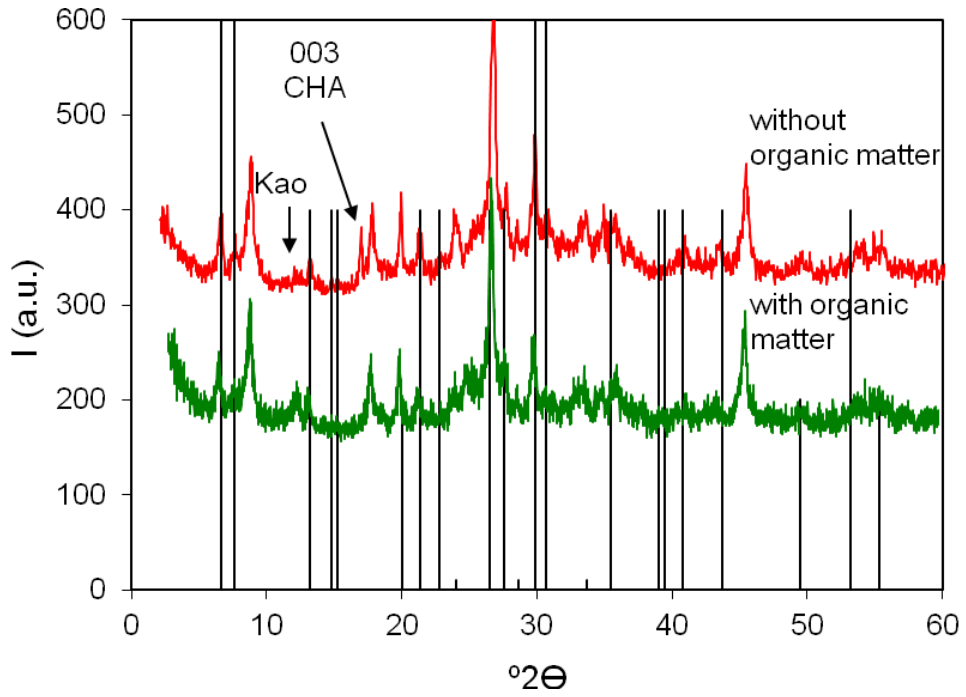

Figure 3-194. XRD patterns of Alhambra Formation clays (OA) treated with 5M KOH solution for 6 months. Black line pattern: Zeolite K-I (JPDF card no. 180988). The chabazite (CHA) 003 Bragg peak at 5.2 Å can be observed in the sample without OM. Kao = kaolinite.

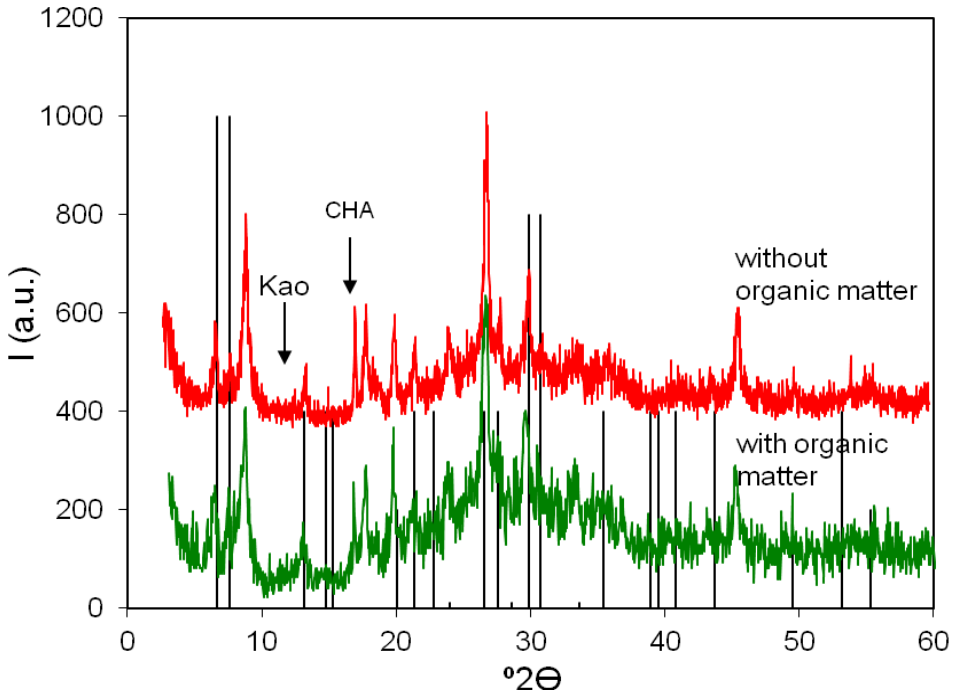

Figure 3-195. XRD patterns of Alhambra Formation clays (OA) treated with 5M KOH solution for 1 year. Black line pattern: Zeolite K-I (JPDF card no. 180988). The chabazite (CHA) Bragg peak at 5.2 Å can be now observed in both samples. Kao = kaolinite.

3.7.3.2. FESEM

FESEM analyses did not reveal important differences between the samples with and without OM. After 6 months of treatment large amounts of nanosized crystals, possibly zeolite K-I were detected (Figure 3-196 and 3-197). In both samples a number of crystals with chabazite-type morphology additional to nanosized crystals were observed after 1 year of treatment (Figure 3-198 and 3-199). Further treatment did not induce additional changes which would have allowed a distinction between the samples` mineralogical evolution.

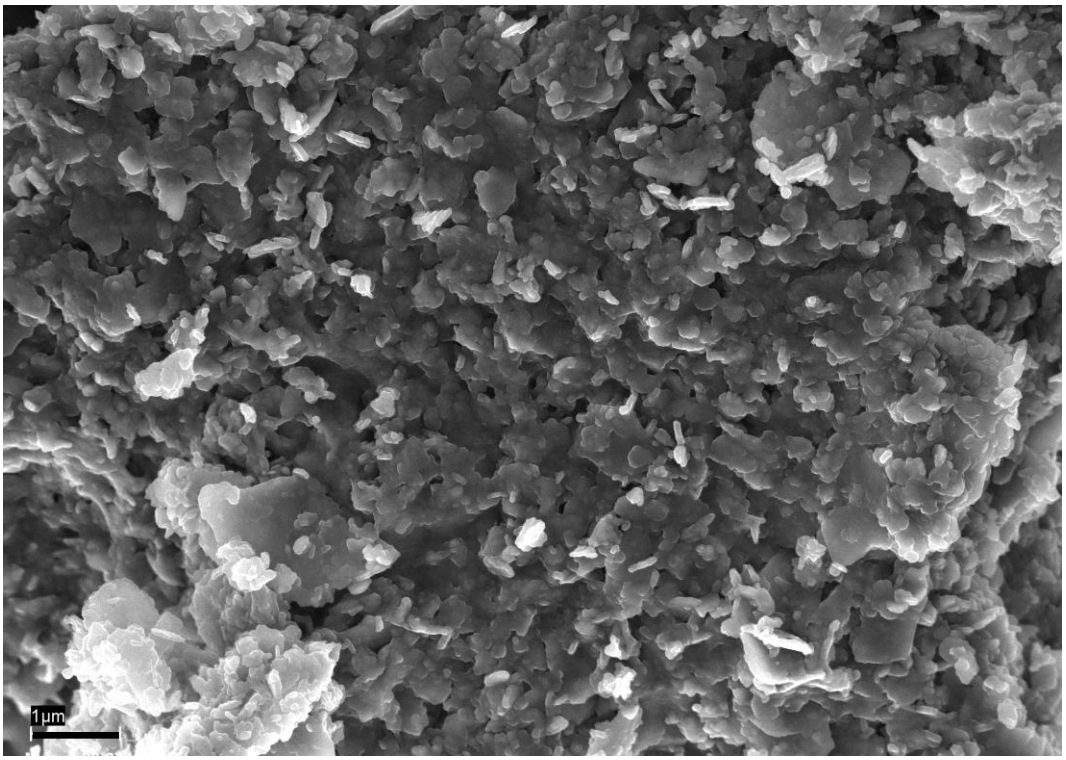

Figure 3-196. FESEM image of Alhambra Formation soil with OM treated with 5 M KOH for 6 months.

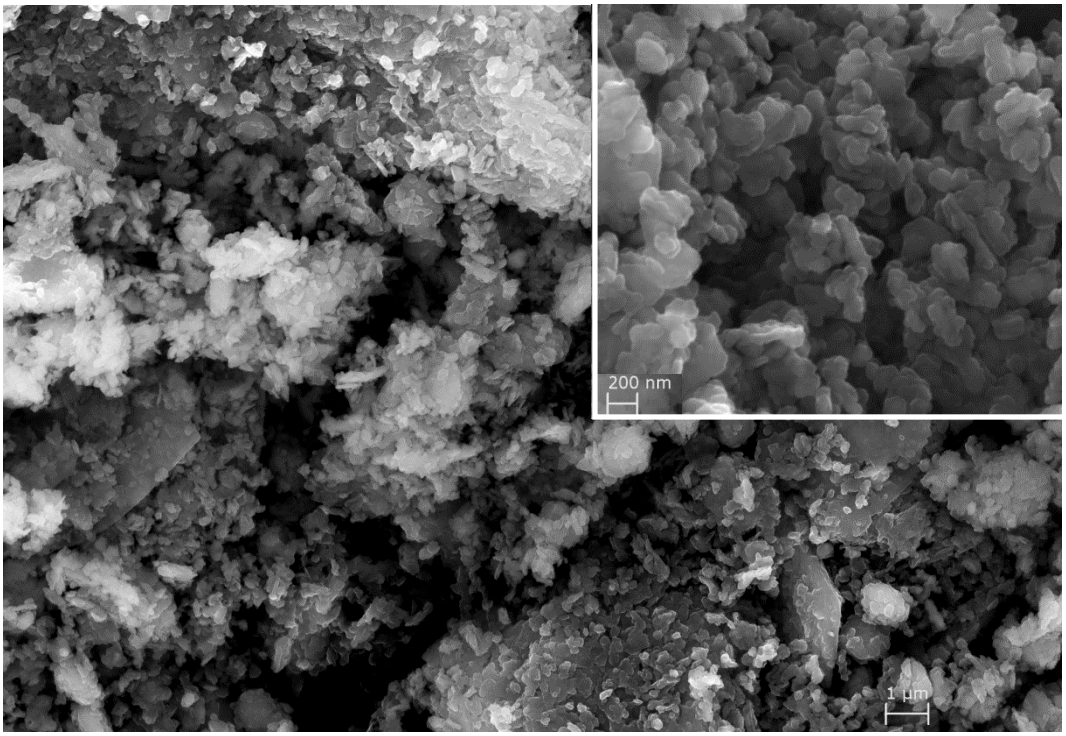

Figure 3-197. FESEM image of Alhambra Formation soil without OM treated with 5 M KOH for 6 months. Inset shows a detail of the nanosized crystals, possibly zeolite K-I.

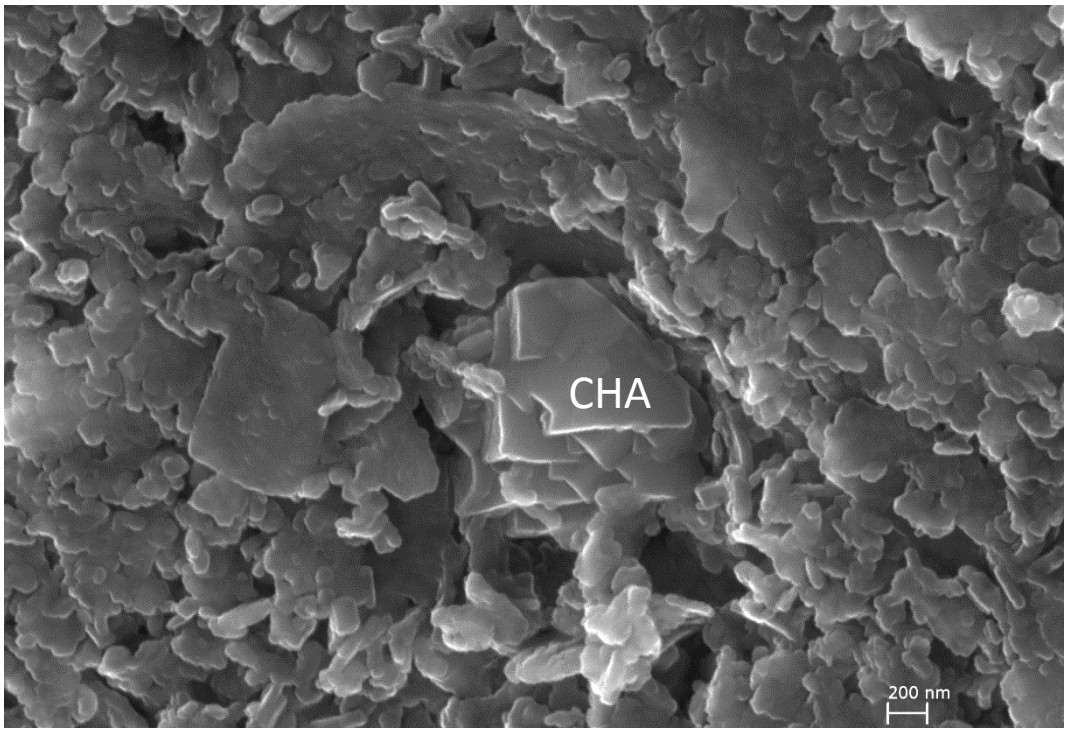

Figure 3-198. FESEM image of Alhambra Formation soil with OM treated with 5 M KOH for 1 year. Chabazite (CHA) crystals are observed.

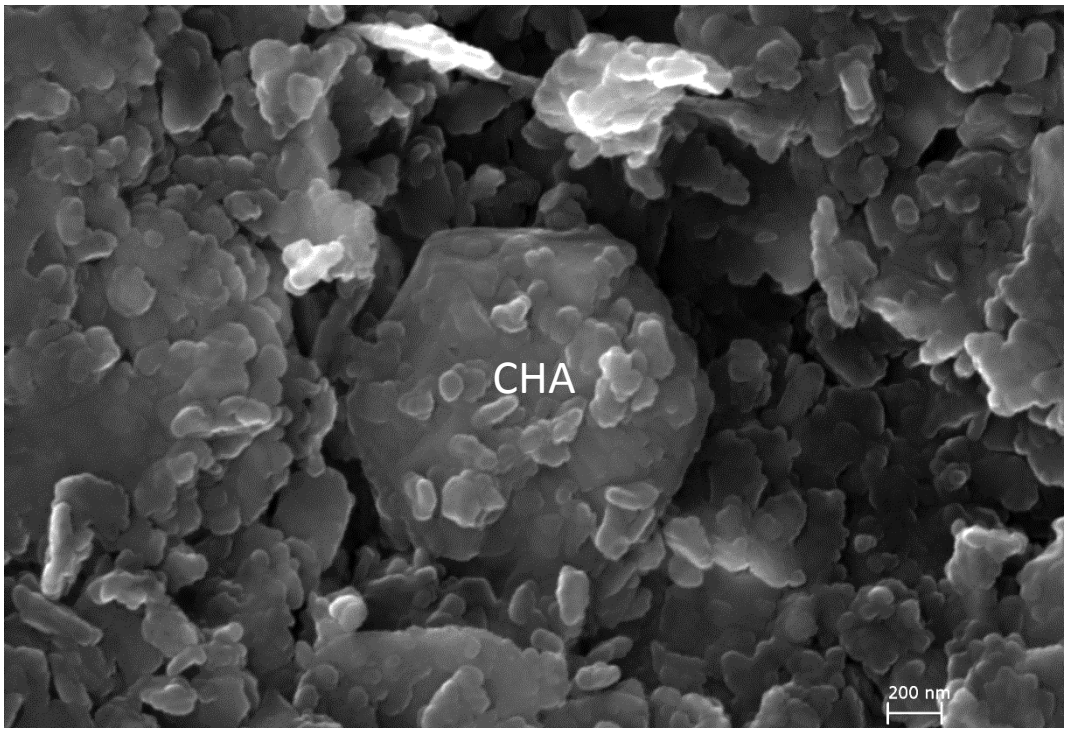

Figure 3-199. FESEM image of Alhambra Formation soil treated without OM treated with 5 M KOH for 1 year. Chabazite (CHA) crystals are observed.

3.7.3.3. Nitrogen sorption

The BET surface area evolution was quite different for the samples with and without OM treated with 5 M KOH (Table 3-40). While the sample with OM experienced a surface area decrease of about 15 % over time, the sample without OM showed an important increase, especially after 1 year of treatment. The reason for the drastic increase in surface area after 1 year of KOH treatment is unclear. It is speculated that the amount of nanosized zeolite K-I crystals was much larger in the sample without OM if compared to the one with OM. The chabazite-type zeolite, on the other hand, has a reported surface area of 17.82 m^2/g (Ridha, 2009) and will not contribute to any significant increase.

The shape of the nitrogen sorption isotherms of both samples was very similar over the course of the alkaline treatment. After 6 months the hysteresis loop of both samples was less pronounced than the one of the untreated soil, indicating that part of the expandable clay minerals were destroyed (Figure 3-200). The influence of the presence of expandable clays on the shape of the hysteresis loop seemed less pronounced in the case of the sample without OM, indicating a more advanced destruction of smectite if compared with the sample containing OM.

After 1-year treatment, however, the hysteresis loop had a similar shape in both samples. The shape of the hysteresis loop (Figure 3-201), was identical to the one observed in pure kaolinite and illite, suggesting the destruction of smectite. Further treatment did not induce any changes in the shape of the isotherms (Figure 3-202).

Table 3-40. BET surface area of Alhambra Formation soil with and without OM and treated with 5 M KOH for different periods of time

Treatment time	Surface area (m^2/g)	
	With OM	Without OM
0	70.78 ± 0.28	82.52 ± 0.52
6 months	76.87 ± 0.25	85.92 ± 0.25
1 year	65.14 ± 0.21	142.77 ± 0.58
> 6 years	60.99 ± 0.19	87.38 ± 0.70

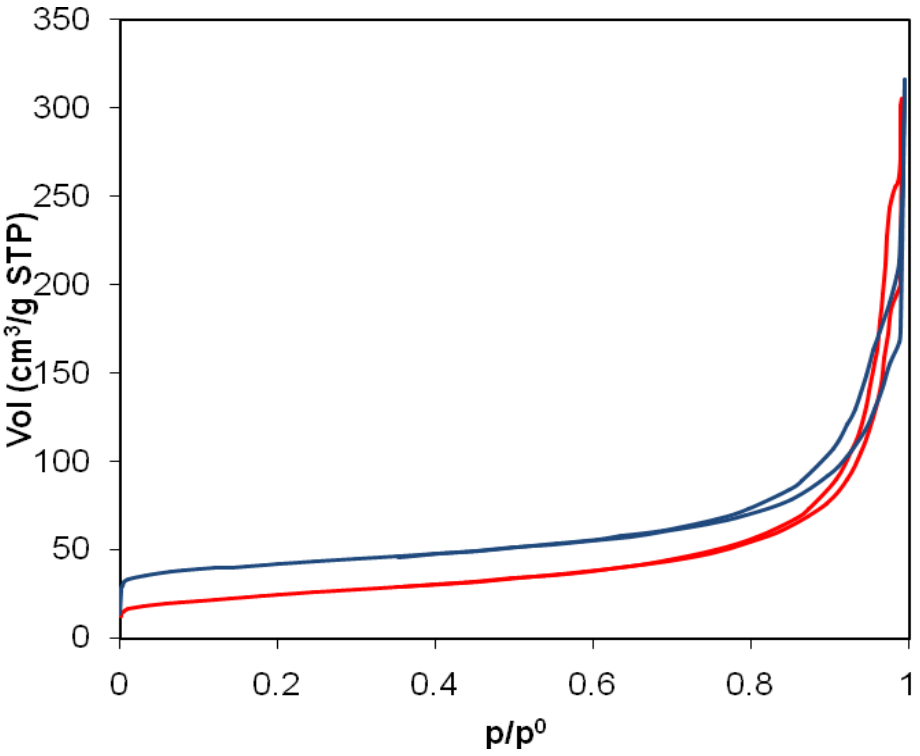

Figure 3-200. Nitrogen sorption isotherms of Alhambra Formation soil with (blue) and without (red) OM treated for 6 months with 5 M KOH.

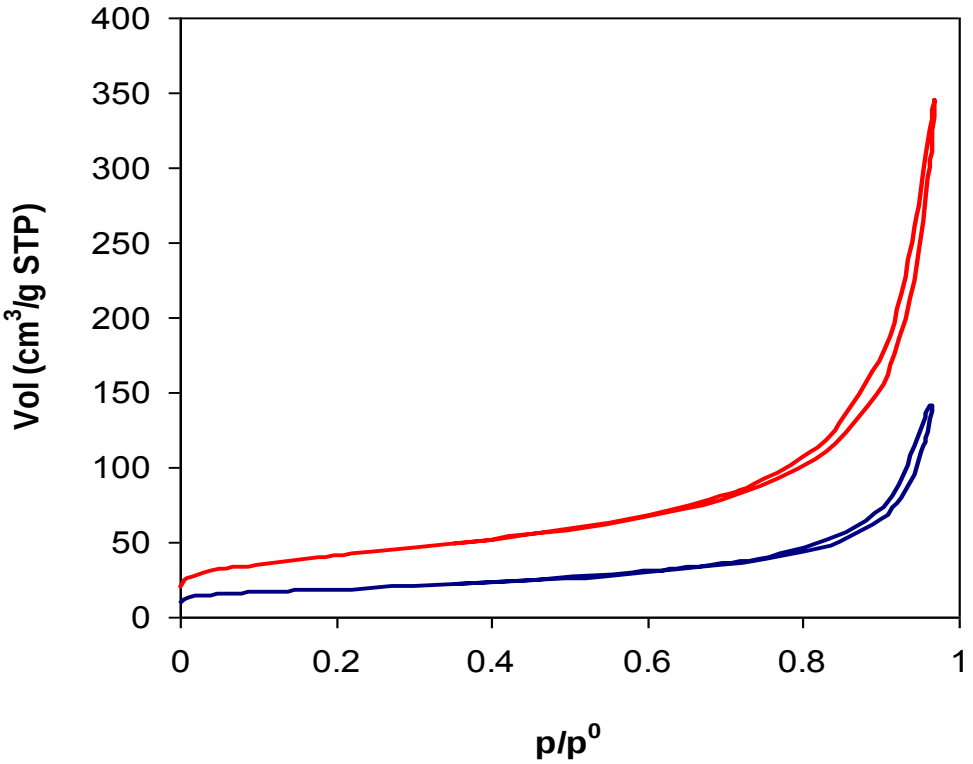

Figure 3-201. Nitrogen sorption isotherms of Alhambra Formation soil with (blue) and without (red) OM treated for 1 year with 5 M KOH.

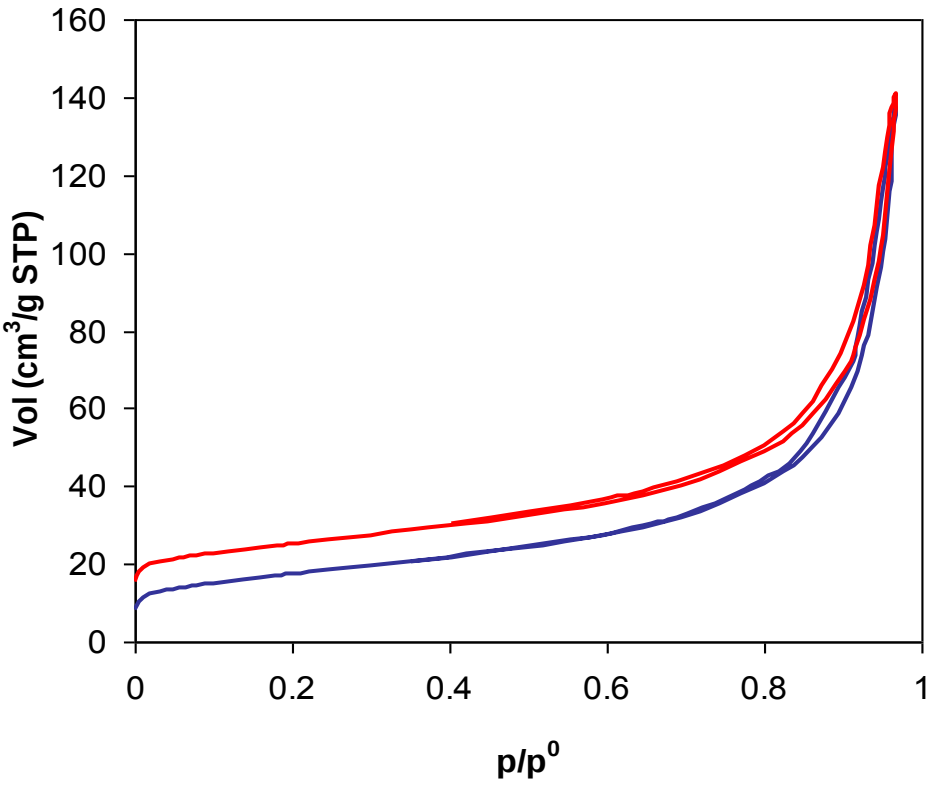

Figure 3-202. Nitrogen sorption isotherms of Alhambra Formation soil with (blue) and without (red) OM treated for > 6 years with 5 M KOH.

3.7.4. TG/ evolved gas analysis (FTIR) of soil samples treated with 5 M NaOH and 5 M KOH

As previously stated, TG/evolved gas analysis (FTIR) results showed that H_2O_2 was effective in destroying OM. In fact, evolved gas spectra showed no CO and very small amounts of CO_2 in the samples treated with H_2O_2 prior to NaOH or KOH activation (Figure 3-203b and d, Figure 3-204b and d). In contrast, evolved gas FTIR spectra of samples with OM and treated for 6 months with either 5 M NaOH or 5 M KOH (Figure 3-203a and 3-204a) showed a significant CO content. This is in agreement with XRD and FESEM results, showing a slower dissolution of clay minerals and delayed formation of zeolitic phases after 6-month treatment. After 1-year alkaline treatment, the OM content was significantly reduced in the samples treated with 5 M NaOH and 5 M KOH. At this point XRD and FESEM showed an identical mineralogical evolution in samples with and without OM. KOH seems to be slightly more effective in destroying OM. In the evolved gas spectrum (Figure 3-204c) only trace amounts of CO were detected after 1 year of alkaline treatment with KOH. It is assumed that the higher pH of the KOH solution if compared with the pH of the NaOH solution is responsible for the greater effectiveness of the former in destroying OM (compare Figures 3-203c and 3-204c).

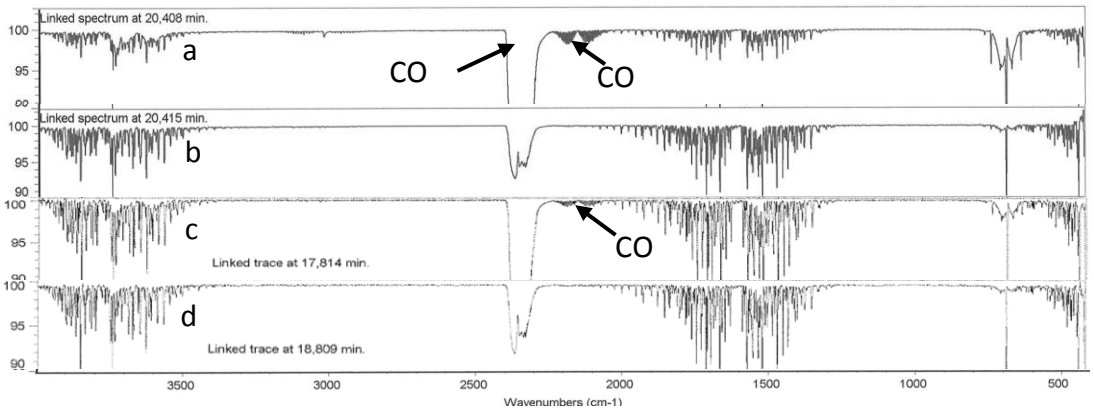

Figure 3-203. Evolved gas FTIR spectra taken between 356-408 °C of Alhambra Formation soil treated with 5 M NaOH for a) 6 months with OM, b) 6 months without OM (H_2O_2 treatment), c) 1 year with OM and d) 1 year without OM (H_2O_2 treatment).

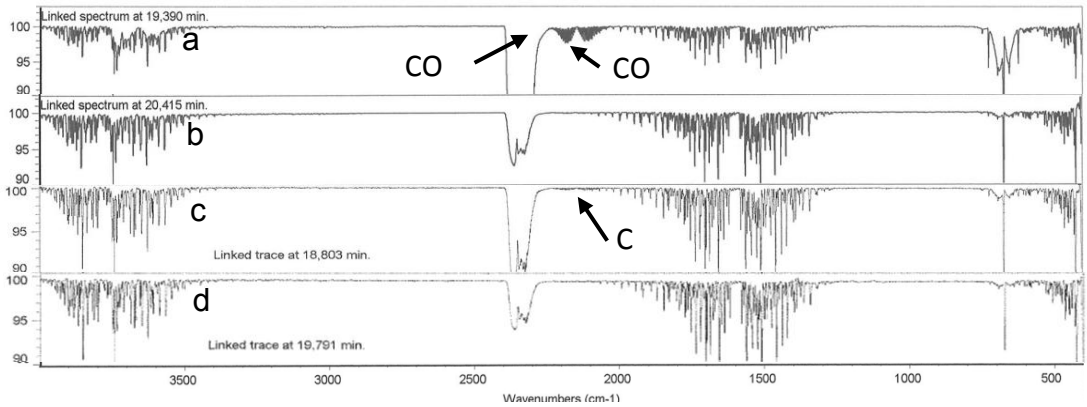

Figure 3-204. Evolved gas FTIR spectra taken between 376-408 °C of Alhambra Formation soil treated with 5 M KOH for a) 6 months with OM, b) 6 months without OM (H_2O_2 treatment), c) 1 year with OM and d) 1 year without OM (H_2O_2 treatment).

To further elucidate the relation between the pH of the alkaline solution and its effectiveness for OM destruction, evolved gas FTIR spectra of samples with OM treated with a) $Ca(OH)_2$, b) 0.4 M NaOH and c) 0.4 M KOH solution are included (Figure 3-205). The comparatively large amount of CO in the spectrum of the sample treated with saturated $Ca(OH)_2$ solution, indicates that this solution was least effective in destroying OM. The low efficiency is thought to be due to the rapid pH decrease which was around pH 9 after 50 days of treatment. In addition, the strong chemical affinity of humic acid with calcium might lead to the formation of insoluble calcium humic acid (Saride et al. 2013). Thus, the presence of OM in soils might inhibit pozzolanic reactions between the stabilizer and the soil when lime is used. Saride et al. (2013) stated that a pH of 10 would be sufficient to initiate pozzolanic reactions in soils with low OM content, while organic-rich soils require a higher pH "to cater the OM first and then form pozzolanic compounds".

The 0.4 M KOH solution, on the other hand, was more effective in destroying OM and only traces of CO were detected in the spectrum. Note that the pH remained above 12 after 50 days of treatment. The 0.4 M NaOH solution showed an intermediate effectiveness and had a pH of around 10 after 50 days.

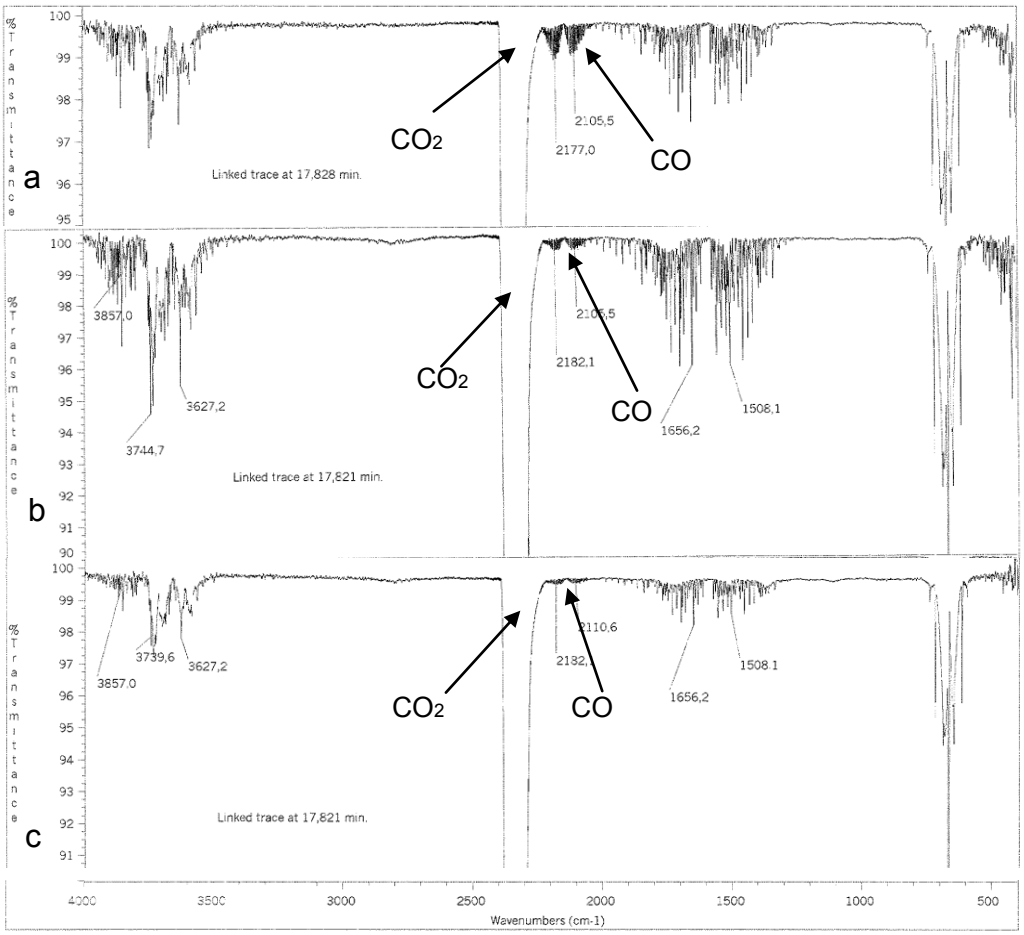

Figure 3-205. Evolved gas FTIR spectra of Alhambra Formation soil with OM after one year of alkaline activation using a) saturated $Ca(OH)_2$, b) 0.4 M NaOH and c) 0.4 M KOH solutions. The spectra were taken at 356 ºC.

3.8. Adobe blocks treated with alkaline solutions

The following sections include the chemical and mineralogical characterization of the < 1 mm fraction of the Alhambra Formation soil which was used for the preparation of adobe test blocks. Furthermore, the evaluation of the penetration of the alkaline solutions was examined. Finally, the influence of the alkaline treatment on the adobe blocks` mineralogical, textural, hydric and mechanical properties were studied. The following analytical techniques and test methods were applied: XRD, FESEM, mercury intrusion porosimetry, hydric, compressive strength and drilling resistance testing as well as color measurements.

3.8.1. Characterization of the < 1 mm fraction of the Alhambra Formation

3.8.1.1. XRF

The chemical composition of the < 1 mm fraction of the Alhambra Formation was determined using XRF (Table 3-41). For comparison the chemical analysis of the < 2 µm is included. Compared with the < 2 µm fraction it becomes evident that the SiO_2 concentration increased due to the higher amount of quartz. The concentration of iron compounds, on the other hand, was lower in the < 1 mm fraction than in the < 2 µm, indicating that iron oxihydroxides are mainly associated with the clay fraction.

Table 3-41. XRF results of starting materials (weight %)

Material	SiO_2	Al_2O_3	Fe_2O_3	Na_2O	MnO	P_2O_5	TiO_2	MgO	K_2O	CaO	Loss on Ignition	Total
Alhambra Formation < 1 mm	49.1	23.3	8.85	0.54	0.05	0.12	0.86	0.95	2.76	0.91	12.25	99.69
Alhambra Formation < 2 µm	38.8	25.9	16.17	0.52	0.00	0.55	0.71	1.01	3.43	0.74	12.25	100.08

3.8.1.2. XRD

Semi-quantitative powder XRD of the < 1 mm fraction of the Alhambra Formation soil showed that the sample was composed of quartz (55 %) and phyllosilicates (45 %), with small amounts of feldspars (< 5 %), calcite/dolomite (< 5 %) and iron oxihydroxides. Compared to the XRD results of the whole sample (see section 3.6.1.), the quartz content decreased by 10 %, whereas the phyllosilicate content increased by 15 %. This seems reasonable because clay minerals are associated with the finer fractions.

3.8.2. Penetration depth of alkaline solutions in adobe blocks

The penetration capacity of consolidants is of great importance and many consolidation treatments have failed due to the limited penetration of the consolidant. Especially in the case of synthetic organic polymers, it has been observed that reverse migration occurs upon solvent evaporation, causing the formation of thin superficial layers without any long-lasting consolidation effect (Chiari, 1990). In a comparative laboratory study (Romero Jimenez 2013) the effectiveness of ethyl silicate for the consolidation of adobe was evaluated. This consolidant was chosen because it is considered as one of the most appropriate materials for adobe consolidation, as it produces a silica gel binder which is compatible with silicate minerals in earthen material, adding strong bonds between clay particles (Chiari, 1990, Selwitz et al. 1990).

However, we found that the penetration of the consolidant in adobe blocks was limited to about 3 mm and did not improve sufficiently the resistance towards the action of water. Only the outer superficial layer of the block remained intact, but the core disintegrated completely after 4 hours of immersion in water (Figure 3-206). Apparently, ethyl silicate only consolidated the outer surface of the adobe block but did not hinder the penetration of water, thus, facilitating the disintegration of the unconsolidated core.

Figure 3-206. Adobe block treated with ethyl silicate and immersed in water for 4 hours (Romero Jimenez 2013).

In order to determine the penetration depth of alkaline solutions a pH indicator (alizarin red) was applied on treated adobe blocks. Adobe blocks were immersed for 20 minutes in alkaline solution and stored in a plastic bag for 24 h to avoid drying. Afterwards, the treated test blocks were split in half and stained with the pH indicator. The penetration depth was about 1 cm (Figure 3-207).

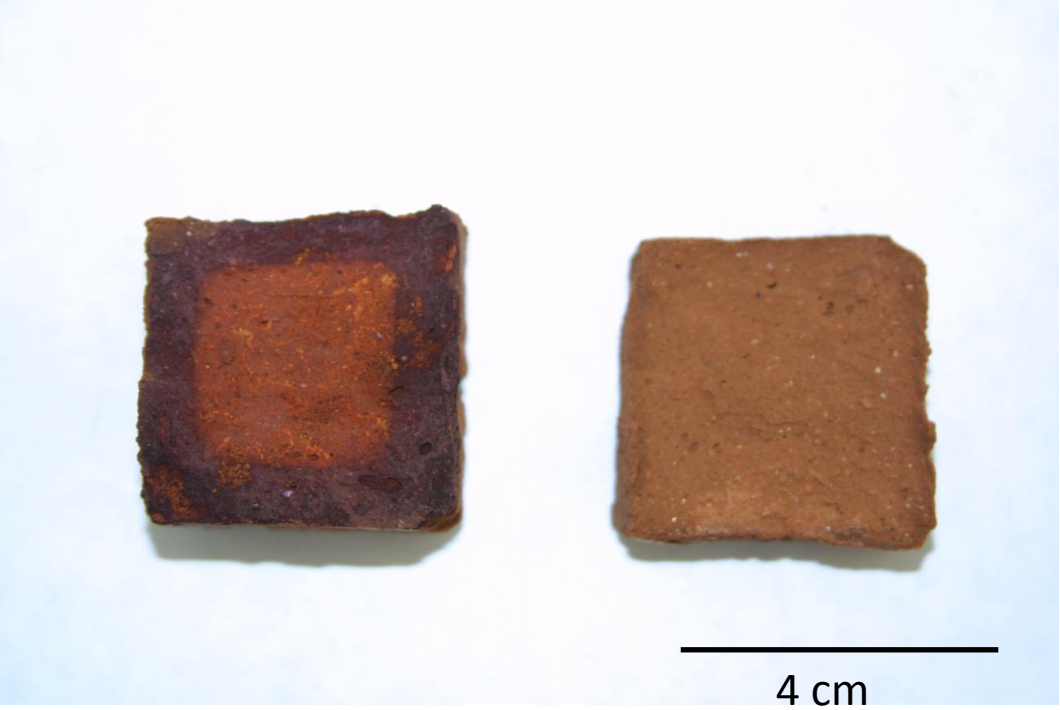

Figure 3-207. Adobe block (4x4x4 cm) immersed in 5M NaOH for 20 minutes and stored in a plastic bag for 24 hours to prevent drying. The block was split in half and stained with alizarin red. The penetration depth was ~1 cm.

The penetration depth of the alkaline solution in adobe blocks was again determined after the blocks had been stored for 50 days in a plastic bag at 85 % RH. As can be seen in Figure 3-208, the alkaline activator had penetrated the entire sample, including the core of the adobe block. Using pH indicator paper the pH was determined to be around 12 in the case of the samples treated with KOH and NaOH (not shown here). The sample treated with $Ca(OH)_2$ (Figure 3-209) did not experience a visible colour change upon application of alizarin red. It should be noted that the indicator`s transition range lies between pH 10.1-12. Indeed, pH indicator paper showed a pH 7-8 in the case of the sample treated with saturated $Ca(OH)_2$ solution.

Figure 3-208: Untreated adobe block (left) and adobe block treated with 5M KOH and stored in a plastic bag for 50 days (right). Both samples were split in half and stained with alizarin red to show the penetration depth of the alkaline solution. It can be observed that the 5 M KOH solution penetrated the entire adobe block because the application of the pH indicator resulted in a homogeneous deep red coloration.

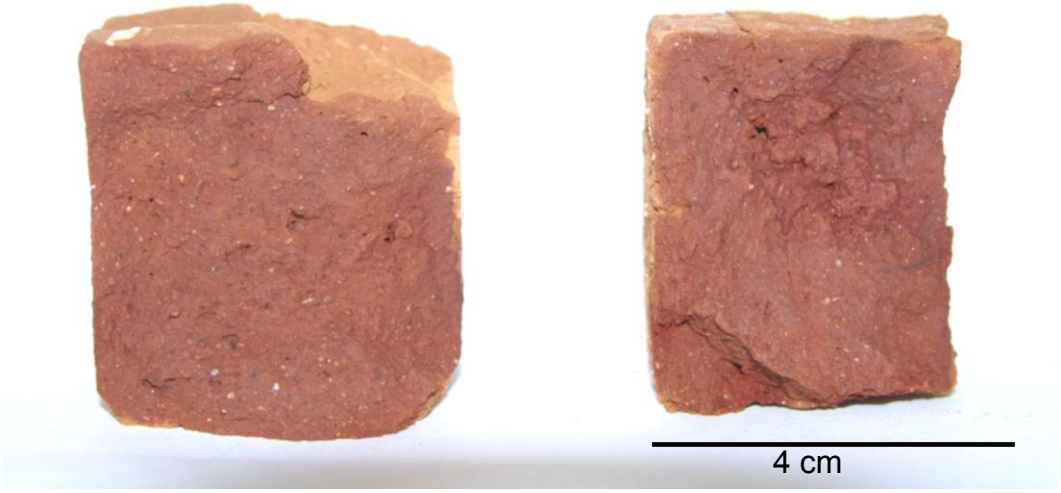

Figure 3-209: Untreated adobe block (left) and adobe block treated with saturated $Ca(OH)_2$ solution and stored in a plastic bag for 50 days (right). Both samples were split in half and stained with alizarin red to show the penetration depth of the alkaline activator. No color change could be observed.

3.8.3. XRD analyses of adobe blocks treated with alkaline solutions

XRD results showed the presence of quartz, clay (illite) and feldspar as the dominant phases of the Alhambra Formation soil but did not reveal significant mineralogical changes after the sample had been treated with $Ca(OH)_2$ (Figure 3-210). The sample treated with NaOH (Figure 3-211) showed additional peaks at 9.6 Å and 4.85 Å which also appeared in the sample treated with KOH (Figure 3-212) and corresponded to the 001 and 002 Bragg peak of paragonite. Furthermore, the intensity of the peak at 3.53 Å had increased in the diffraction pattern of the sample treated with NaOH (surface). This peak corresponds to the 104 Bragg of chlorite. In the diffraction pattern of the sample treated with KOH (surface) the intensity of the peak at 4.04 Å had increased. This peak might correspond to albite. Additionally, an increase in the peak intensity at 2.89 Å was detected in the KOH treated sample which corresponds to the 104 reflection of dolomite.

Overall, these changes in intensity are an indication that the mineral distribution is not perfectly homogeneous within the tested adobe blocks. These results also suggest that the alkaline treatment, either did not induce any significant mineralogical changes in the clay minerals or the effects were limited to the formation of amorphous or poorly crystalline phases such as zeolite precursors.

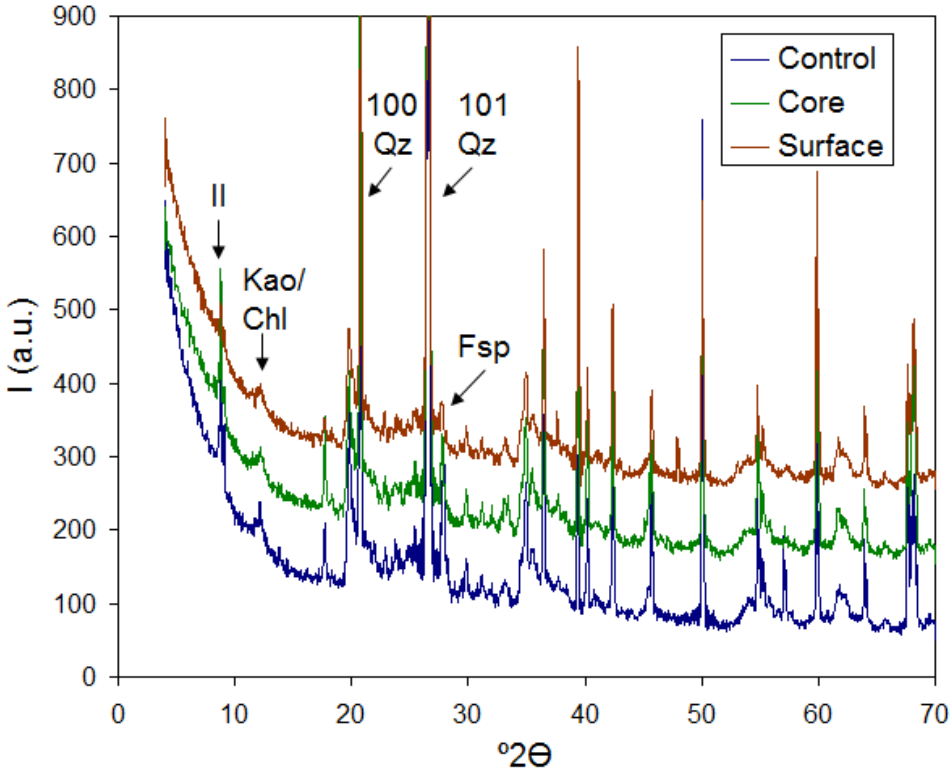

Figure 3-210. XRD patterns of adobe blocks untreated (control) and treated with $Ca(OH)_2$. Il = illite, Kao = kaolinite, Chl = chlorite, Qz = Quartz, Fsp = feldspar.

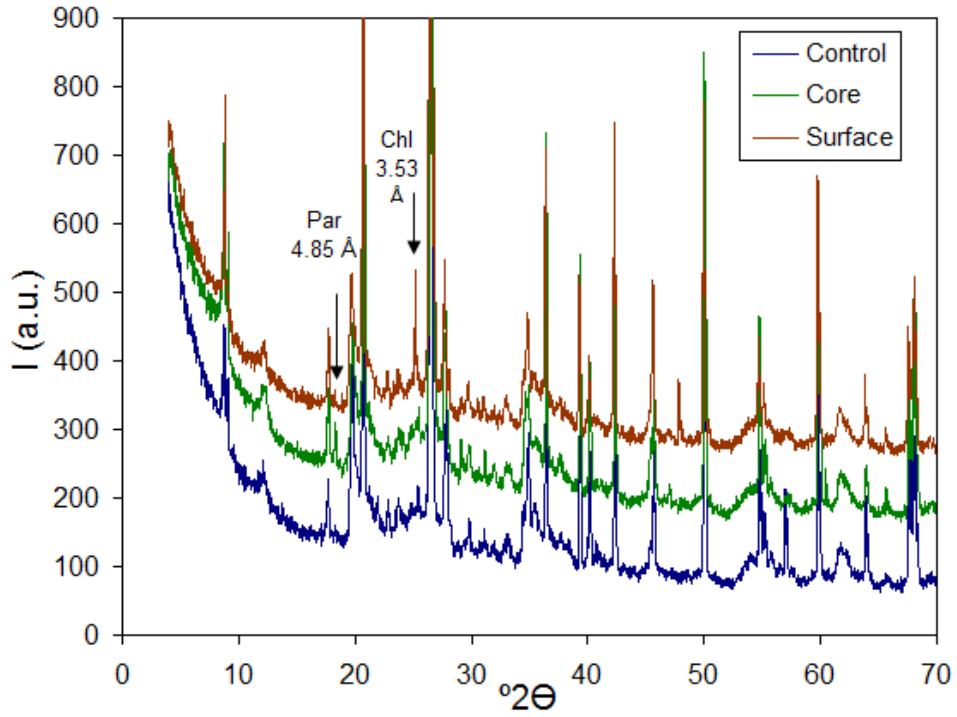

Figure 3-211. XRD patterns of adobe blocks untreated (control) and treated with NaOH. Par = paragonite, Chl = chlorite.

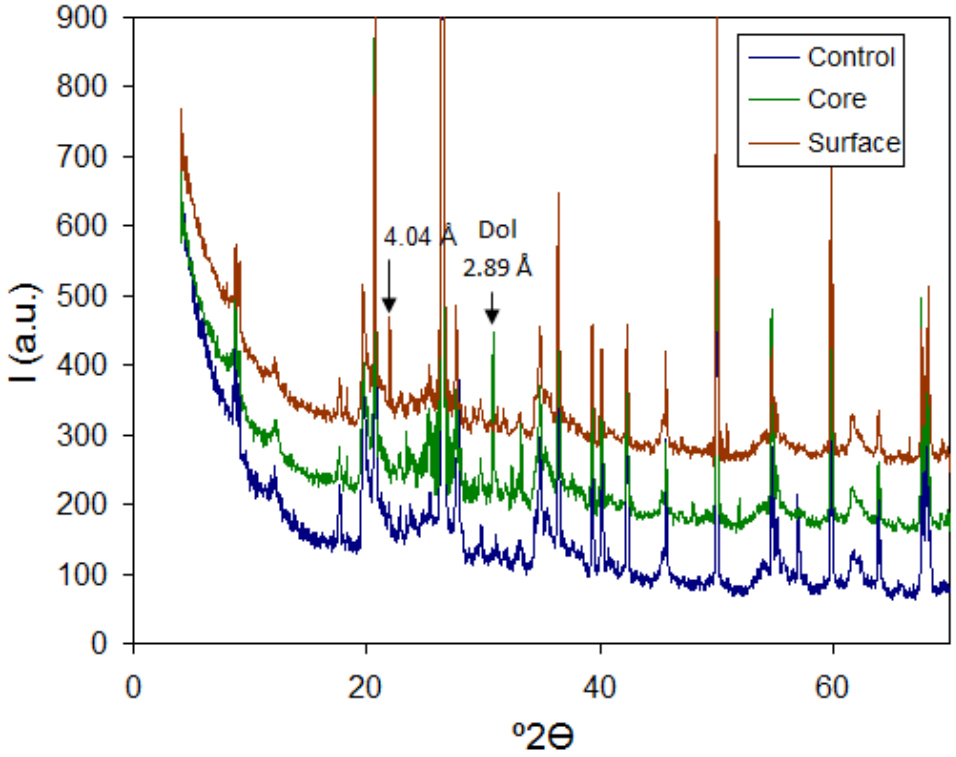

Figure 3-212. XRD patterns of adobe blocks untreated (control) and treated with KOH. Dol = dolomite.

3.8.4. FESEM analyses of adobe blocks treated with alkaline solutions

FESEM images showed no clear evidence of clay transformation due to the activation with alkaline solutions after 50-days treatment. Using EDS microanalysis (Figure 3-213), Ca was detected in the sample treated with $Ca(OH)_2$. Otherwise, the composition did not differ greatly from the one of the untreated Alhambra Formation soil and no newly formed phases were identified. Results by Karnland et al. (2007) are consistent with these findings, showing no significant mineralogical changes in Wyoming bentonites treated with saturated $Ca(OH)_2$ solution for more than 100 days at room temperature.

In the case of the sample treated with NaOH a small amount of a gel-like phase was observed which contained a high concentration of sodium (Figure 3-214). This new phase might be interpreted as a zeolite precursor. A similar phase has been detected as a reaction product in alkali-activated fly-ash (Kovalchuk et al., 2008). Due to its amorphous character its identification with XRD was not possible.

EDS analysis of the sample treated with KOH (Figure 3-215) revealed an increased K concentration in a gel-like phase. The formation of potassium hydroxide associated with this gel-like phase can not be ruled out.

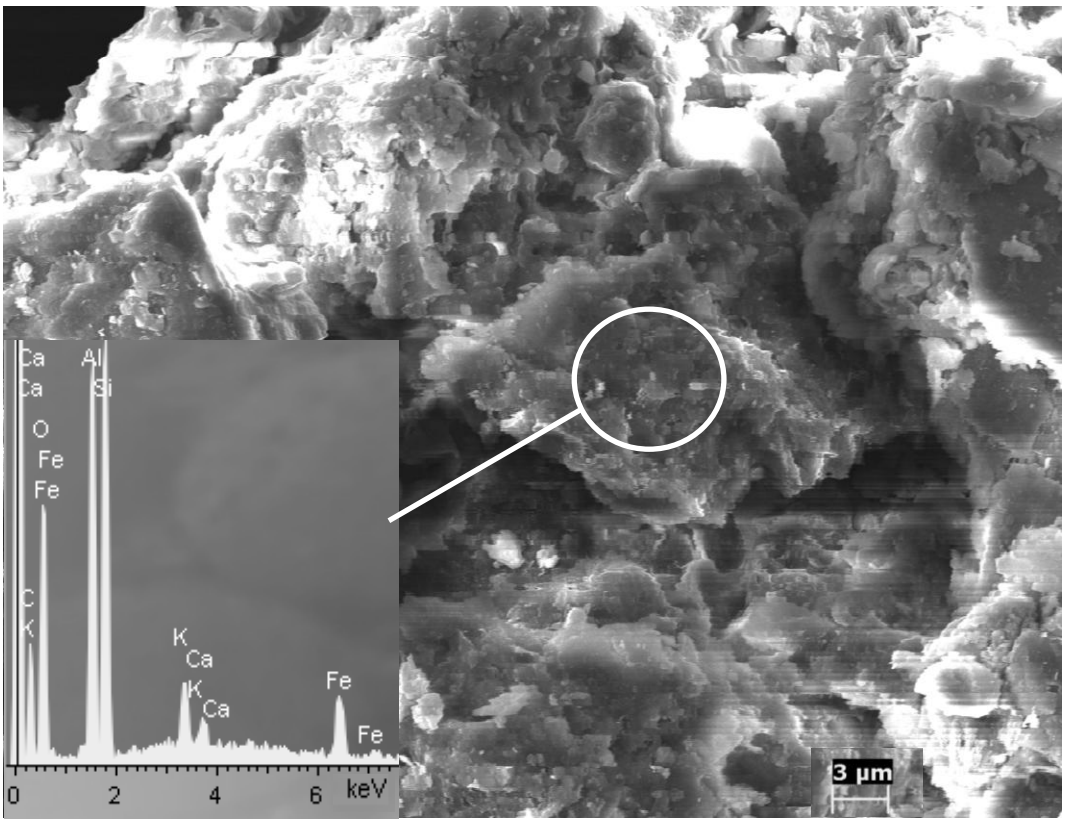

Figure 3-213. Adobe block treated with $Ca(OH)_2$. The circle indicates the spot where the EDS microanalysis (inset) was performed.

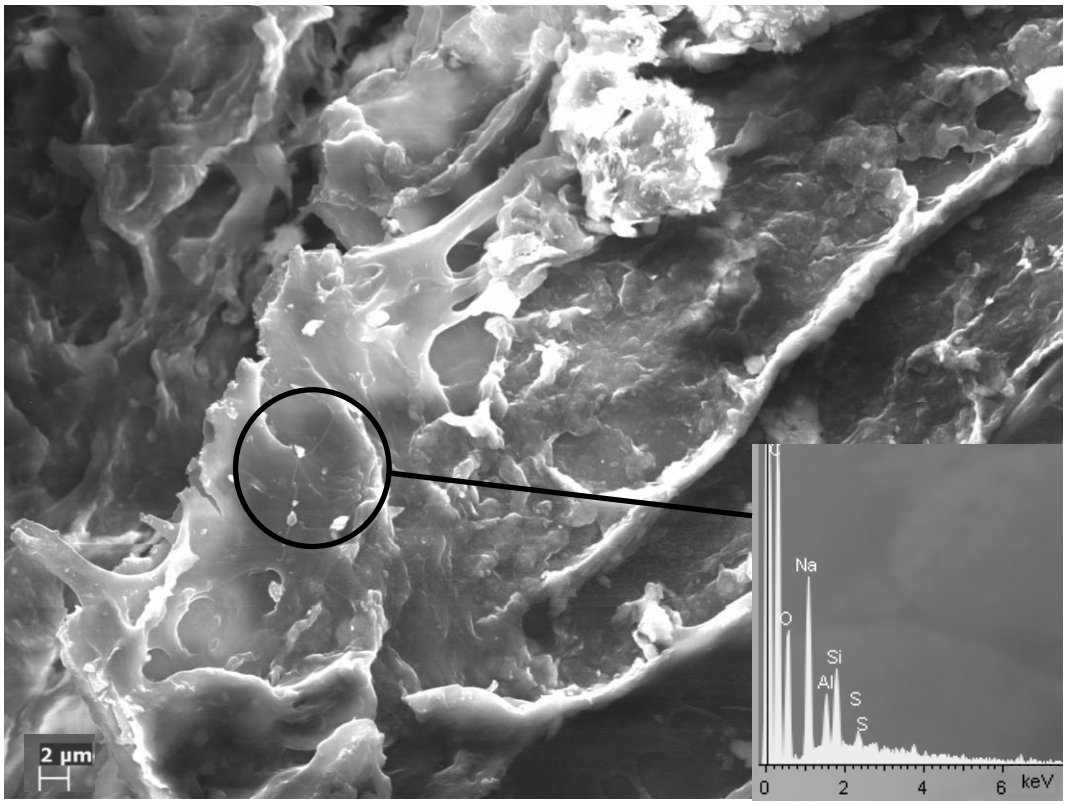

Figure 3-214. Adobe block treated with NaOH. The circle indicates the spot where the EDS microanalysis (inset) was performed.

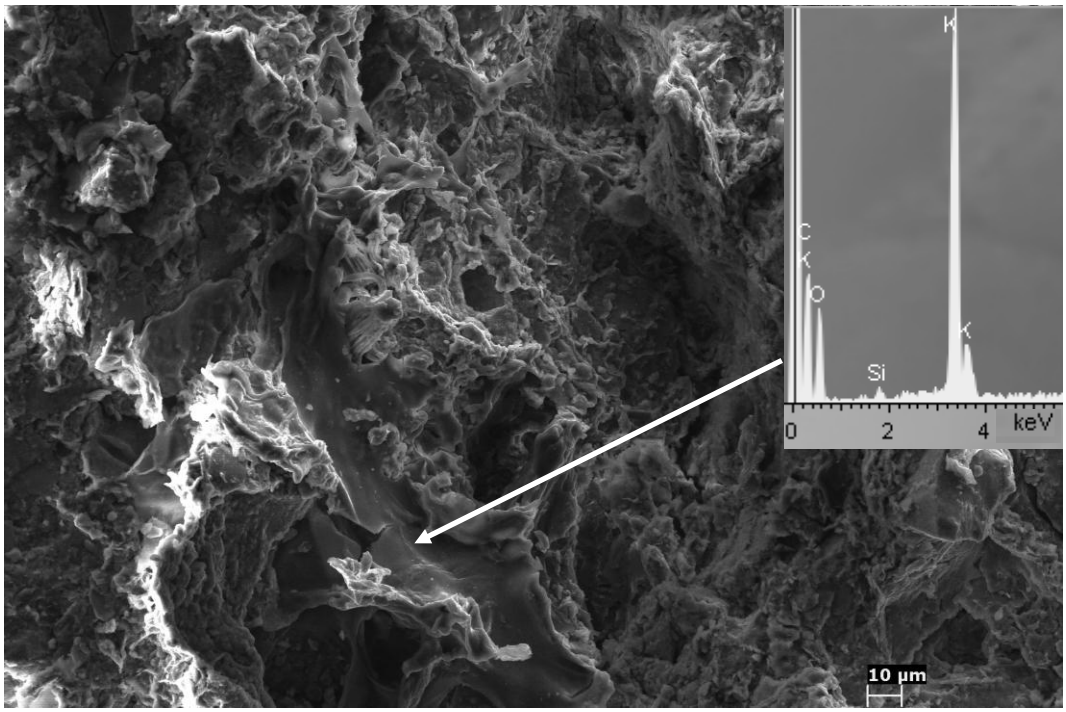

Figure 3-215. Adobe block treated with KOH. A gel-like phase, possibly potassium hydroxide can be observed (EDS in inset).

3.8.5. Porosimetry of untreated and treated adobe blocks

The porosity and the pore size distribution of the adobe blocks were determined using mercury intrusion porosimetry. The untreated adobe sample (control) revealed a porosity of 24.7 % (Table 3-42) which is similar to the porosity values reported for adobe by Ahmadi (2008) which were between 24.7-27.3 %.

The untreated sample (control) showed a maximum around 1 μm pore diameter. Abundant pores were also observed for sizes below 0.1 μm and a small amount of pores had sizes larger than 10 μm. In general, the observed pore size distribution corresponds to intergranular porosity among the sand particles with a limited contribution of smaller size pores, possibly associated with clay aggregates (Figure 3-216 and 3-217).

All treated samples experienced an increase in porosity. This increase was associated with crack development due to the swelling and shrinkage of clay during immersion and subsequent drying which resulted in an increase in the coarser pore fraction (7-200 μm). In general, the water treatment as well as the treatment with the alkaline solutions did not cause significant changes in the pore size distribution and the volume of pores < 1 μm.

The increase in porosity due to coarser pores was slightly less pronounced in the sample treated with KOH compared with all other treated samples (Figure 3-216, Table 3-42). However, it should be noted that porosity measurements for different samples treated with the same alkaline solution varied considerably, complicating a more detailed interpretation of the results.

Table 3-42. Porosity of untreated (Control) and treated adobe blocks (immersed in water, treated with $Ca(OH)_2$, NaOH and KOH)

Sample	Porosity (%)
Control	24.7 ± 0.7
Water	27.2 ± 1.3
$Ca(OH)_2$	27.8 ± 0.9
NaOH	28.7 ± 0.4
KOH	26.5 ± 1.2

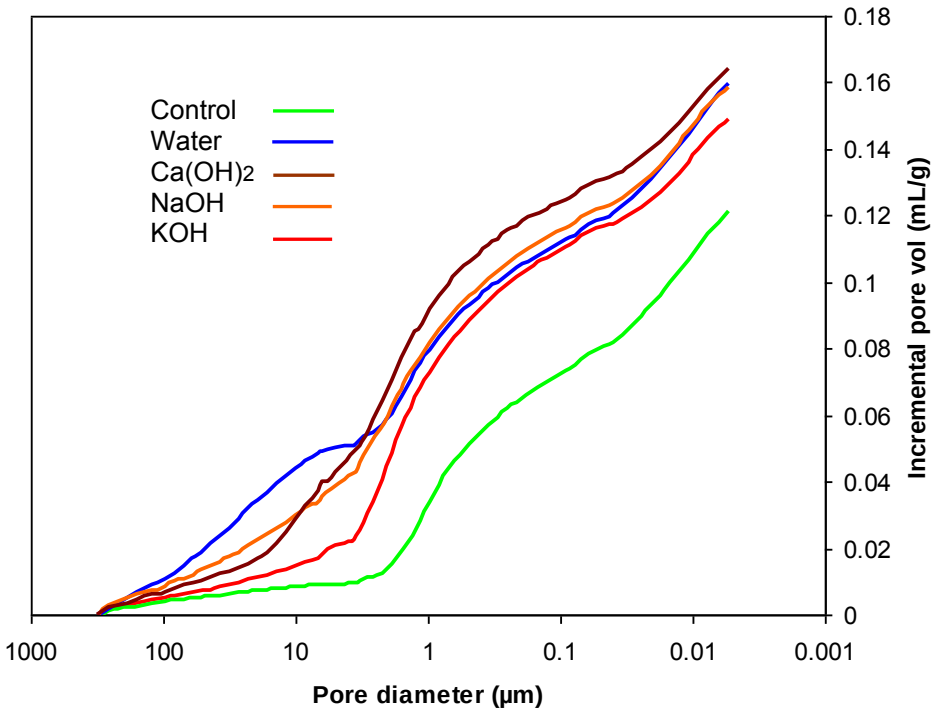

Figure 3-216. Incremental pore volume of untreated (Control) and treated adobe blocks (immersed in water, treated with $Ca(OH)_2$, NaOH and KOH).

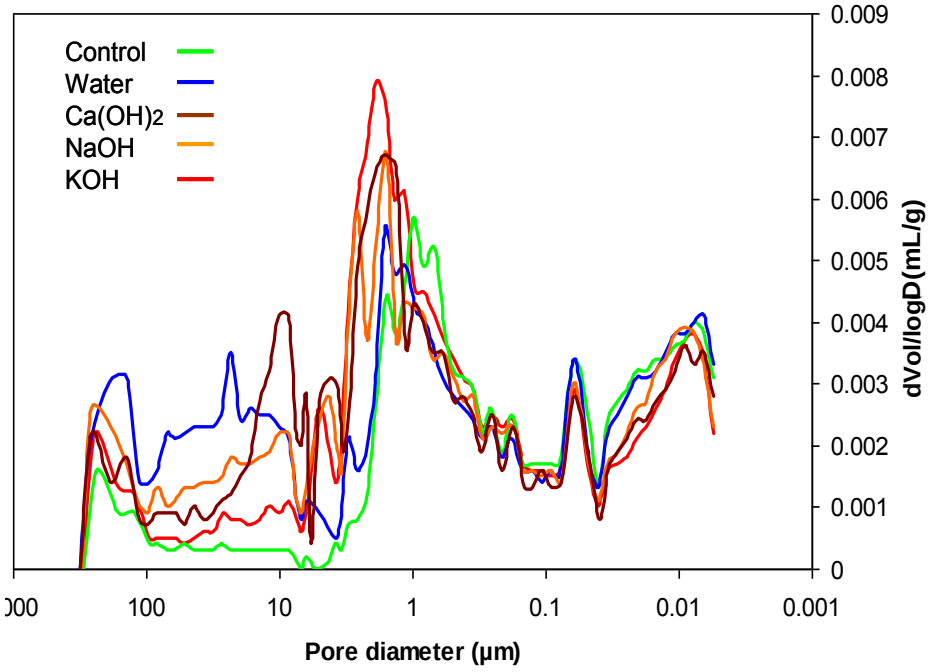

Figure 3-217. Pore size distribution of untreated (Control) and treated adobe blocks (immersed in water, treated with $Ca(OH)_2$, NaOH and KOH).

3.8.6. Water behaviour of adobe blocks

To evaluate the hydric properties of the samples, the free water absorption capacity (A_b) of untreated and treated adobe blocks was determined. Indirectly, this test provided valuable information on the water resistance of adobe test blocks. The experiment was performed in duplicate in order to validate the test results.

The weight loss due to a partial disintegration of the samples upon treatment was considered in the calculation of the free water absorption (Table 3-43). As can be seen in Figure 3-218, all 4 samples absorbed a similar amount of water during the first 4 minutes of the experiment. After this first phase, both, the untreated sample and the sample treated with $Ca(OH)_2$, showed a very similar behaviour. They absorbed a larger amount of water during the first 30 minutes of the experiment than the samples treated with NaOH and KOH. The higher water absorption rate was caused by the formation of fissures. At this point a progressive disintegration of the untreated sample and the sample treated with $Ca(OH)_2$ was observed (Figure 3-219, Table 3-43). Ren and Kagi (1995) reported a similar behaviour for untreated adobe blocks immersed in water which disintegrated completely after 2.5 hours. Results by Karnland et al. (2007) are also in agreement with our findings. The authors did not detect any reduction in the swelling pressure of Wyoming bentonite treated with saturated $Ca(OH)_2$ solutions. It can be concluded that the treatment using $Ca(OH)_2$ did not improve the water resistance of the adobe block. Samples treated with NaOH and KOH showed a better resistance towards the action of water and experienced only little material loss after 2.5 h (Table 3-44). However, the samples did not reach a steady absorption rate due to the formation of fissures over time which allowed for a larger amount of water to be absorbed. In the case of the sample treated with NaOH the formation of fissures was evidenced by a sudden increase in the absorption rate after 150 min. Weight gain continued until the disintegration of the samples took place during the first 24 hours of the experiment (Figure 2-220). The sample treated with KOH, on the other hand, disintegrated after 48 hours of immersion in water.

It can be concluded that the experiment did not allow the determination of reliable data regarding the water absorption characteristics of the adobe blocks since the results were masked by the formation of fissures which allowed a larger amount of water to be absorbed than would be expected by the intrinsic characteristics of the material. However, the results clearly showed differences in the resistance towards the action of water. The treatment with NaOH, and especially the one using KOH, improved the water resistance of the adobe blocks significantly.

Table 3-43: Water absorption rate of untreated and treated adobe test blocks. Note that the water absorption rate is calculated from the initial linear section of the free water absorption curve, plotted against the square root of time.

Sample	Water absorption rate ($1/min^{-1/2}$)
untreated	1.75
$Ca(OH)_2$	1.98
NaOH	1.26
KOH	1.23

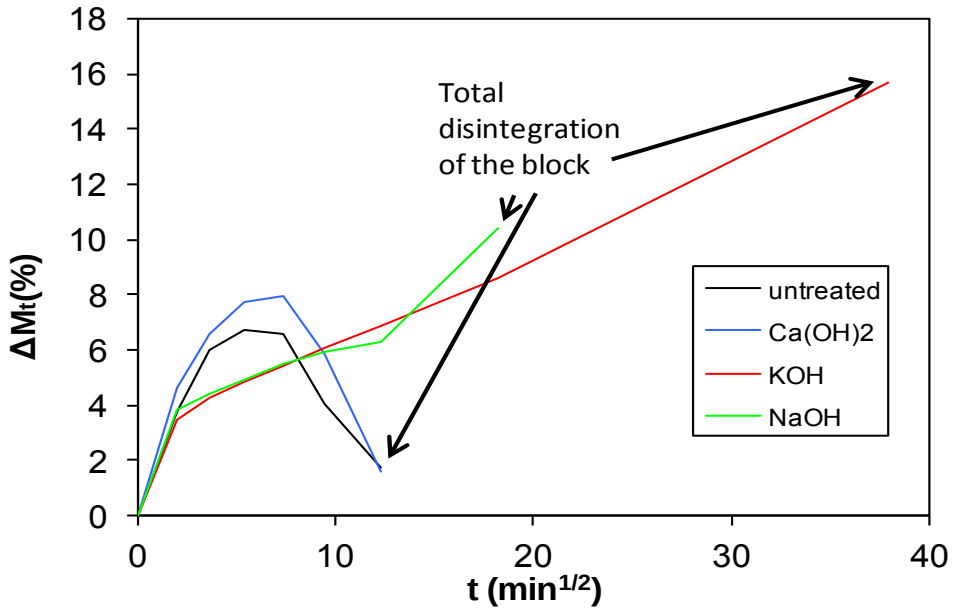

Table 3-218: Free water absorption of untreated and treated adobe blocks versus time. Note that the sudden break of the curves indicates the total disintegration of the sample.

Table 3-44: Material loss of untreated and treated adobe test blocks upon immersion in water for 2.5 h.

Sample	Material loss (wt%)
untreated	86.0
$Ca(OH)_2$	91.0
NaOH	1.0
KOH	0.7

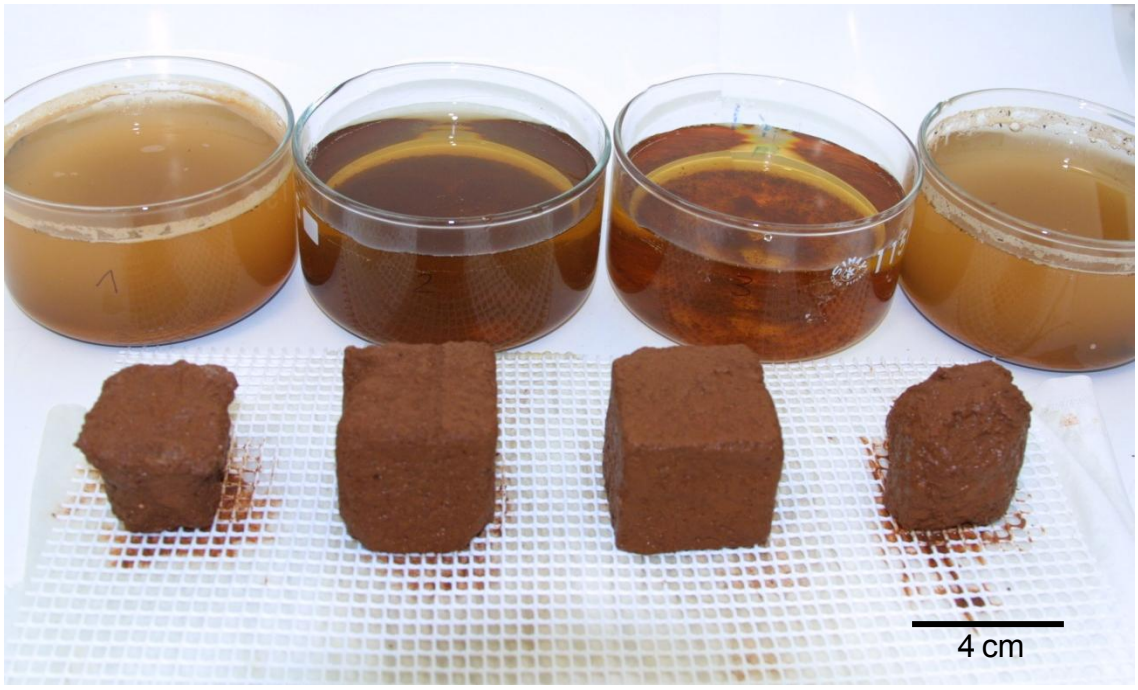

Figure 3-219: Samples (left to right, untreated, treated with NaOH, KOH and $Ca(OH)_2$) after immersion in water for 1 hour.

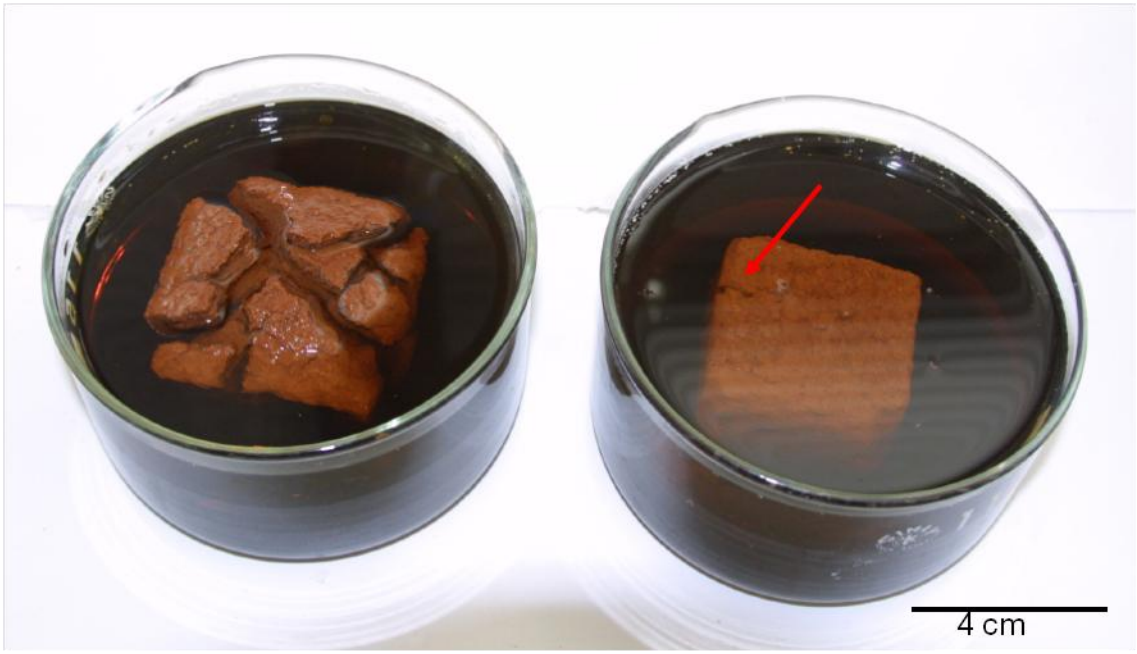

Figure 3-220: Samples treated with NaOH (left) and KOH (right) immersed in water for 48 hours. The formation of fissures led to a complete disintegration of the sample treated with NaOH. The block treated with KOH showed the beginning of crack formation (arrow).

The improved water resistance might be caused by different phenomena: a) clay mineral dissolution and the transformation into zeolite precursor gel with cementating properties; b) cation exchange in the case of

KOH, because K^+ shows a reluctance to fully hydrate which reduces the swelling tendency of K^+ saturated clays (Boek et al. 1995); c) flocculation induced by the high Na^+ or K^+ concentration in 5 M NaOH or 5 M KOH solutions (van Olphen 1987).

In order to determine the cause of the improved water resistance, adobe blocks were treated with 4.65 M (saturated) KCl solution following the same protocol as in the case of the alkaline solution. Whereas cation exchange or flocculation would be facilitated by a treatment with KCl, mineral dissolution and transformation are not expected to occur due to the neutral pH of the KCl solution. Figure 3-221 shows the untreated adobe block and blocks treated with 5 M KOH and 4.65 KCl after immersion in water for 2 h. Evidence is provided that cation exchange or flocculation were not the main cause for the improved water resistance because the block treated with 4.65 M KCl experienced significant material loss. In contrast, the block treated with 5 M KOH remained basically unchanged, indicating that the dissolution of clay minerals and the formation of amorphous phases (zeolitic precursors) was responsible for the improved water resistance (Table 3-45). Admittedly, material loss after water immersion was slightly lower in the case of the block treated with KCl if compared to the untreated adobe block. Thus, cation exchange or flocculation might have induced a certain improvement regarding water resistance.

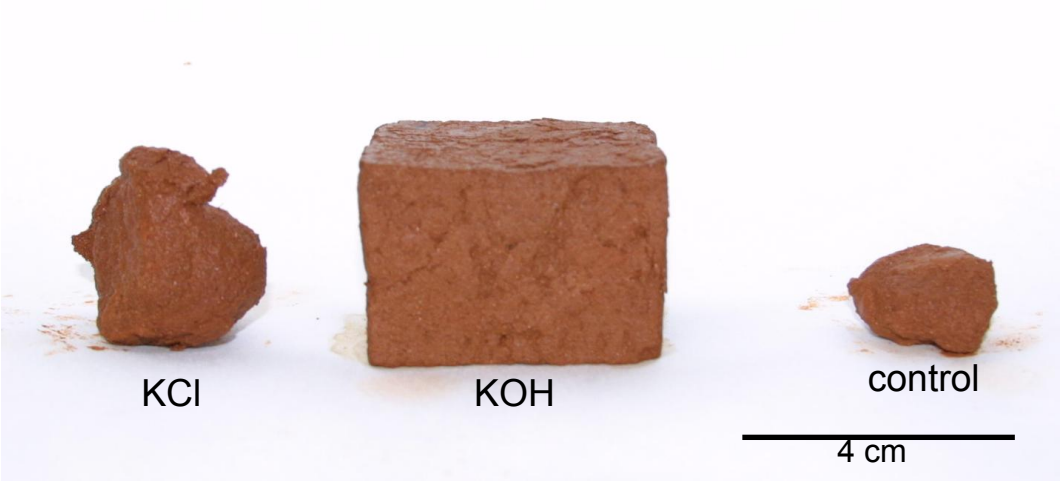

Figure 3-221. Untreated adobe block (control) and blocks treated with 4.65 M KCl (saturated KCl solution at 20 °) and 5 M KOH after immersion in water for 2 hours.

Table 3-45. Material loss of adobe blocks after immersion in water for 2 hours.

Treatment	Material loss (wt%)
4.65 M KCl	74
5 M KOH	0.1
Water	90

3.8.7. Compressive strength and drilling resistance measurement system (DRMS) analyses of adobe blocks

The compressive strength measurements (Table 3-46) indicated that the treatment with $Ca(OH)_2$ seemed to have weakened the adobe block if compared with the untreated sample. Its compressive strength was reduced by ~ 21%. The NaOH treatment did not improve significantly the compressive strength of the adobe block, whereas the KOH treatment led to a compressive strength increase of ~ 24%. Due to limitations regarding the number of samples, the compressive strength testing could only be performed using one adobe block per treatment. Thus, results should be regarded as preliminary. Figure 3-222 shows the adobe blocks before and after compressive strength testing. The variations in compressive strength of the samples treated with different alkaline solution might be explained by the fracturing experienced during the activation treatment. Fracturing might have been more pronounced in the case of the sample treated with $Ca(OH)_2$ (Figure 3-222). Furthermore, the treatment with KOH conferred additional strength to the adobe block which is thought to be associated with the formation of amorphous phases, having cementing properties. However, this effect should have been detected in the case of the NaOH treated adobe block as well.

Overall, it was found that the compressive strength of all tested adobe blocks, including the untreated control, is well above the published minimum requirements. According to the "Uniform Building code" and the "New Mexico State Adobe Code" the minimum compressive strength for adobe bricks is 2 MPa (McHenry 1981). Houben and Guillaud (1994) state the minimum compressive strength for adobe blocks to be 2.5 MPa.

In general, the obtained compressive strength of adobe blocks fabricated with Alhambra Formation soil is somewhat higher than published data. Piattoni et al. (2011) found the compressive strength of adobe bricks made from soil with 22.4 % clay content to be 5.15 MPa, which is more than 30 % lower than the compressive strength of the Alhambra Formation adobe. However, many aspects such as sample size, composition of the raw material and manufacturing parameters can influence the mechanical properties of adobe blocks and may result in variations in the measured compressive strength values.

Table 3-46. Compressive strength of adobe blocks before and after alkaline activation.

Sample	Compressive Strength (MPa)
Untreated	8.13
$Ca(OH)_2$ treatment	6.41
NaOH treatment	8.45
KOH treatment	10.06

Figure 3-222. Adobe blocks before (above) and after (below) compressive strength testing (left to right: untreated, treated with $Ca(OH)_2$, NaOH and KOH). Note that the yellow layer is sulphur which is used to parallel the samples surfaces.

As mentioned before, compressive strength testing was performed on a limited number of samples and should only be regarded as preliminary. Therefore, additional drilling resistance measurements were carried out to further elucidate the effect of alkaline activation on the adobes` mechanical strength. Drilling resistance was determined using a Drilling Resistance Measurement System (DRMS) which allows the continuous measurement of the force necessary to drill a hole in the adobe block under constant operating conditions. This technique is considered very promising for the evaluation of consolidation treatments, especially in soft, porous materials (Tiano et al. 2000). Table 3-47 summarizes the drilling resistance results of untreated and treated adobe blocks. Admittedly, variations in drilling resistance of about 15% were observed in different adobe blocks treated with the same alkaline solution. However, some general tendencies were identified. The test results revealed that the $Ca(OH)_2$ treatment did not increase drilling resistance

significantly, whereas samples treated with NaOH and KOH experienced a more pronounced increase in resistance.

As in the case of the water resistance test, the drilling resistance of the adobe block treated with 4.65 M KCl was compared to that of a block treated with 5 M KOH and an untreated block (Table 3-48). Results clearly show that the KCl treatment did not improve drilling resistance significantly. The KOH treatment, in contrast, resulted in an ~ 40 % increase in resistance. This finding indicates that mechanical resistance is predominately improved by the interaction of clay minerals with the alkaline solution which includes dissolution of aluminosilicates and the formation of amorphous phases at high pH. Generally, drilling resistance measurements are found to show good linear correlation with uniaxial compressive strength data (Pamplona et al. 2007). However, as mentioned previously, our compressive strength test results were not conclusive.

Table 3-47. Average drilling resistance of adobe blocks before and after alkaline activation (based on a minimum of 10 drill tests per sample).

Sample	Drilling Resistance (N)
Untreated	4.36 ± 0.48
Water treatment	5.11 ± 0.38
$Ca(OH)_2$ treatment	4.66 ± 0.50
NaOH treatment	7.29 ± 0.57
KOH treatment	6.92 ± 0.78

Table 3-48. Average drilling resistance of adobe blocks* before and after treatment (based on a minimum of 10 drill tests per sample).

Sample	Drilling Resistance (N)
Untreated	4.84 ± 0.64
KCl treatment	5.17 ± 0.23
KOH treatment	7.83 ± 0.32

* Note that minor differences in drilling resistance results in Table 3-47 and 3-48 are due to the use of different batches of adobe blocks.

3.8.8. Color change of adobe blocks

Color measurements of untreated adobe bricks and bricks subjected to alkaline activation were performed in order to determine possible color changes upon treatment. According to Sasse and Snethlage (1996) changes in color are acceptable when ΔE is ≤ 5.

Table 3-49 shows the average color measurement results of the untreated adobe sample and samples treated with the different alkaline solutions. For each sample 5 measurements were performed. Lightness L* did not change significantly in the case of samples treated with KOH and NaOH. However, the chromatic coordinates a* and b* changed, indicating a change towards a more reddish/yellowish color in the treated samples. In the case of $Ca(OH)_2$ the treatment resulted in an important darkening of the sample, but the color coordinates changed less than in the former samples (Figure 3-223, Table 3-50).

Considering calculated ΔE values it is evident that KOH and NaOH caused a colour change which was only slightly above the acceptable limit. Samples treated with $Ca(OH)_2$, on the other hand, experienced a more severe colour change.

Table 3-49: Average color measurement results of untreated and treated adobe blocks.

Parameter	untreated	KOH	NaOH	$Ca(OH)_2$
L*	41.77 ± 1.32	41.22 ± 0.65	40.97 ± 0.75	33.22 ± 0.62
a*	16.11 ± 0.51	19.23 ± 0.38	19.90 ± 0.35	17.56 ± 0.38
b*	21.19 ± 0.36	25.19 ± 0.39	25.44 ± 0.85	19.77 ± 0.33

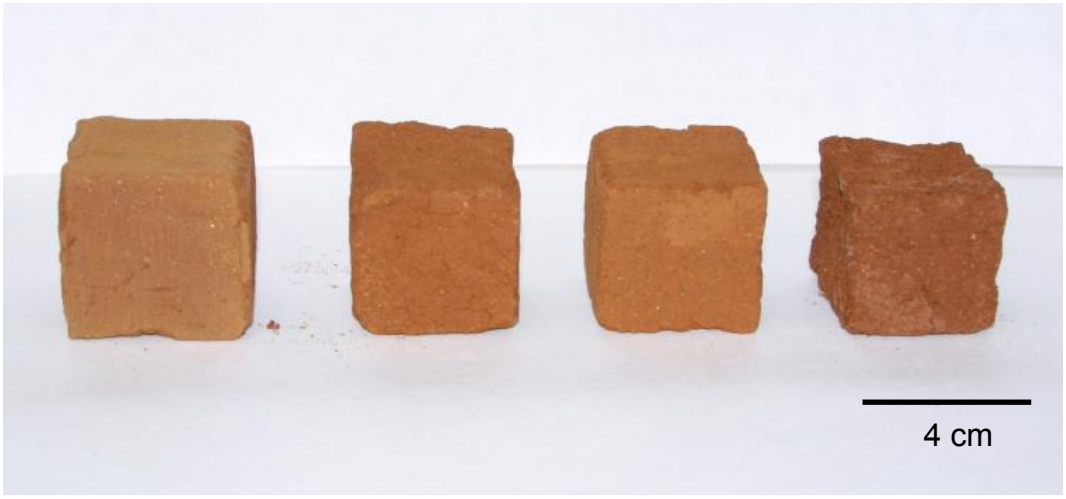

Figure 3-223: Color change of adobe blocks upon alkaline activation (from left to right, untreated, NaOH, KOH and $Ca(OH)_2$.

Table 3-50: Average colour change ΔE of treated samples.

Sample	Average ΔE	Standard deviation
KOH	5.14	± 0.55
NaOH	5.81	± 0.72
$CaOH)_2$	10.25	± 0.81

3.9. Salt crystallization test

During the treatment of soils with alkaline solutions, unreacted alkalis might react with atmospheric CO_2 to form carbonates. Actually, in this study the formation of carbonates was observed in various cases, namely $CaCO_3$, $CaCO_3 \cdot H_2O$, Na_2CO_3 and $KHCO_3$ (Figure 3-224, Table 3-51). Hos et al. (2002) have detected sodium carbonates with identical morphology in the case of aluminosilicates synthesized using alkaline silicate solution. The formation of sodium carbonates has also been observed in the case of inorganic polymers synthesized from metakaolin, sodium silicates and NaOH (Barbosa et al. (2000).

Calcium carbonates will not cause deterioration and might even improve mechanical properties of the soil. Especially the "sheaf of wheat"-shape crystals detected in treated saponite might interlock into the soil structure and lead to an increase in mechanical strength. Note that the addition of lime has a long tradition in soil stabilization (Houben and Guillaud 1994). Sodium carbonate and potassium carbonate, on the other hand, are soluble salts which may produce serious damage during cycles of crystallization in building stones and other porous building materials (Goudie and Viles 1997).

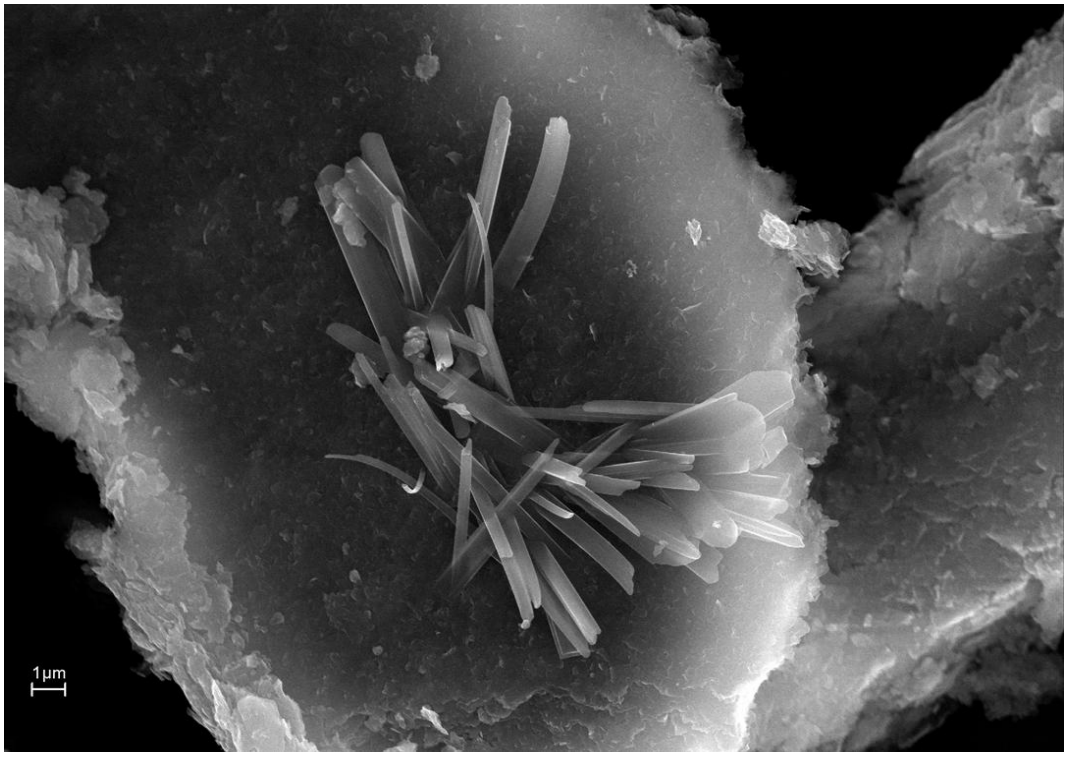

Figure 3-224. FESEM image of Alhambra Formation soil treated with 0.4 M NaOH for 1 year. Fibrous sodium carbonate crystals can be observed.

Table 3-51. Carbonates formed upon alkaline treatment of clays

Mineral	Solution	Salt
Montmorillonite	5 M KOH	$CaCO_3$
Saponite	5 M NaOH	$CaCO_3$
Saponite	5 M KOH	$CaCO_3 \cdot H_2O$
Alhambra Formation soil	0.4 M NaOH	Na_2CO_3
Alhambra Formation soil	0.4 M KOH	$KHCO_3$

3.9.1. Evaluation of salt damage

In order to evaluate the damaging character of sodium and potassium carbonates, a salt crystallization study was performed using calcarenite from Santa Pudia, Granada. Stone prisms were partially immersed in different salt solutions such as Na_2SO_4, Na_2CO_3, K_2CO_3 and $KHCO_3$. Na_2SO_4 is one of the most widely used salts in durability tests of building materials and has been proven to be extremely destructive (Rodriguez-Navarro and Doehne 1999). In this study it was included as a reference. As previously mentioned, porous stone prisms were used in this test because adobe blocks would not have withstood immersion in aqueous salt solution.

As expected, severe damage occurred in the case of the stone prism placed in saturated Na_2SO_4 solution and extensive salt efflorescence as well as incipient damage was visible after 8 days of testing. The remaining calcarenite prisms showed only very limited efflorescence and negligible damage (Figure 3-225).

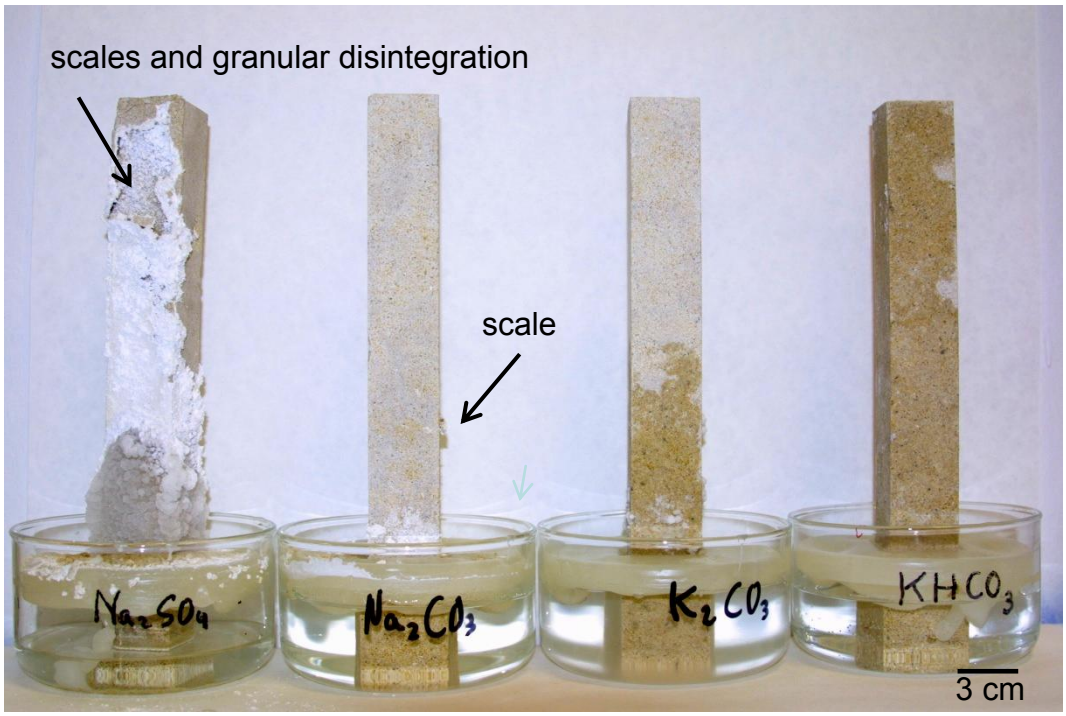

Figure 3-225. Aspect of calcarenite blocks being partially immersed in salt solutions for 8 days.

After 7 weeks the Na_2SO_4 salt solution had evaporated completely and massive efflorescence and severe damage, including scaling, had occurred (Figure 3-226). In the case of the saturated Na_2CO_3 solution less efflorescence was detected and some damage occurred due to subflorescence crystallization which induced fracturing and scaling. Saturated K_2CO_3 and $KHCO_3$ solutions did not cause any damage to the stone after 7 weeks and little efflorescence was detected on the surface. At this point only a very small amount of K_2CO_3 solution had evaporated. The low evaporation rate of the K_2CO_3 solution can be explained considering its equilibrium RH which is very close to the ambient RH (Table 3-52).

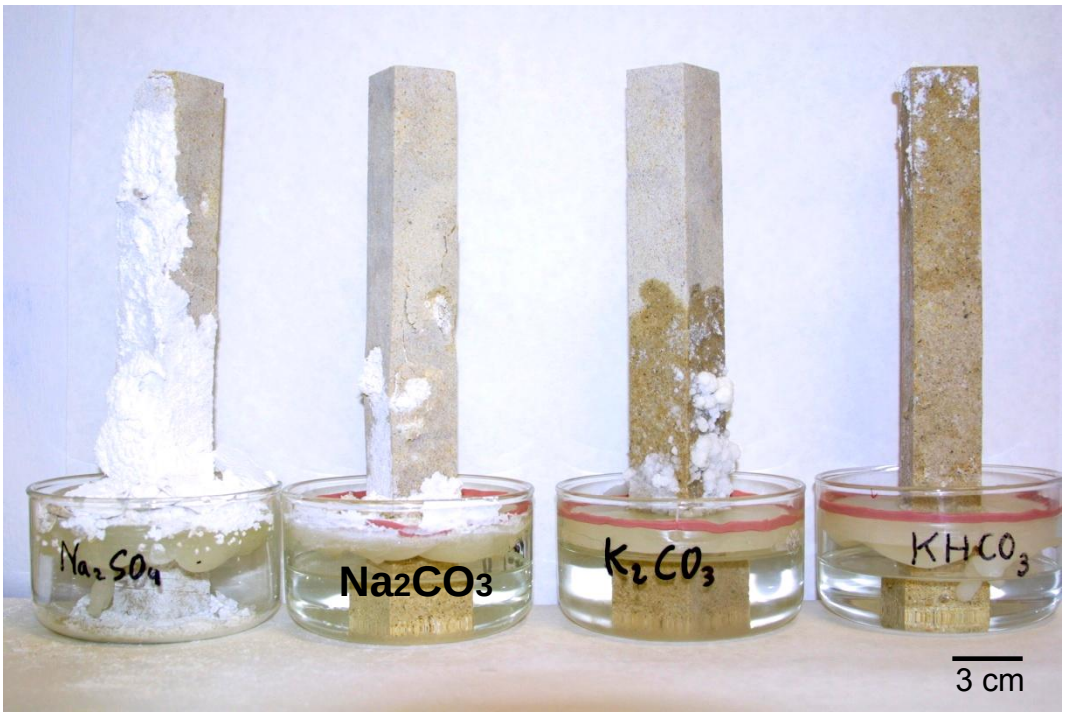

Figure 3-226. Aspect of calcarenite blocks subjected to evaporative crystallization following immersion in salt solutions for 7 weeks.

Table 3-52. Equilibrium RH (%) of the salt solutions.

	Na_2SO_4	Na_2CO_3	K_2CO_3	$KHCO_3$
Equilibrium RH, %	93*	92*	43*	92**

* O`Brien 1948

** Laboratory result

Figure 3-227 shows the calcarenite blocks after 7.5 months. The aspect of the block immersed in Na_2SO_4 did not change any further. However, the sample treated with Na_2CO_3 showed severe damage including scaling and fracturing which affected the whole stone block. Note that efflorescence was very limited in the case of Na_2CO_3, suggesting that in-pore crystallization of

this salt was dominant. Samples treated with K_2CO_3 and $KHCO_3$ revealed an increased amount of efflorescence and in the case of $KHCO_3$ very limited damage was detected in zones with flaws that were already present in the untreated stone (Figure 3-228). Note that at this point, a large quantity of the K_2CO_3 solution still remained in the crystallization dish.

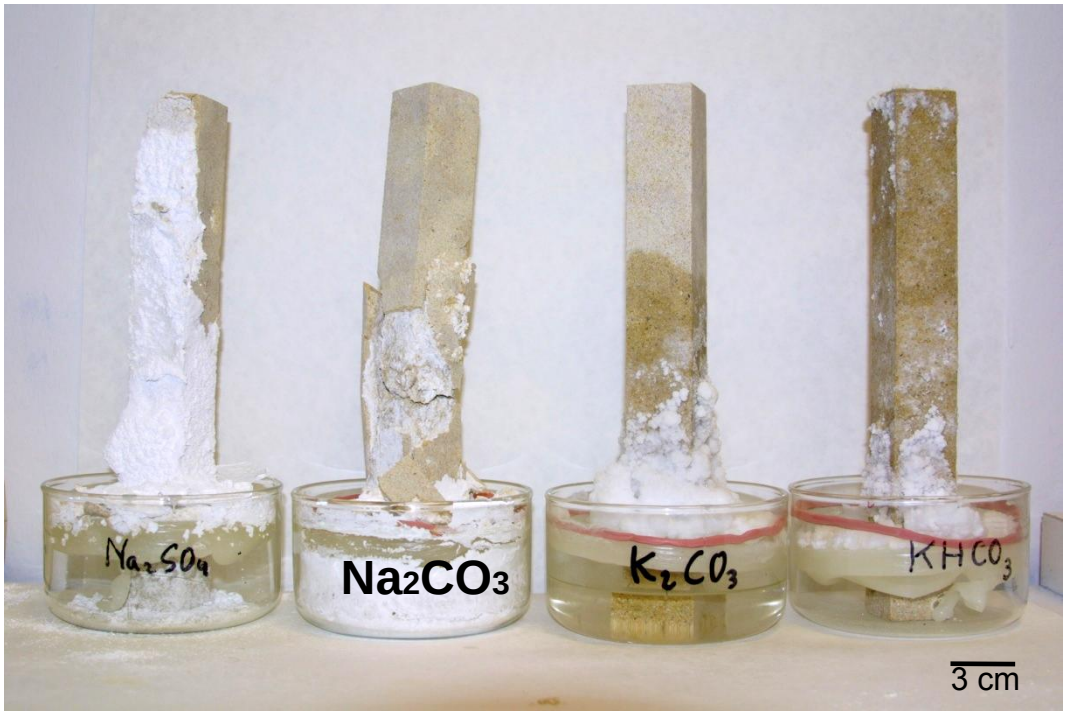

Figure 3-227. Aspect of calcarenite blocks after 7.5 months.

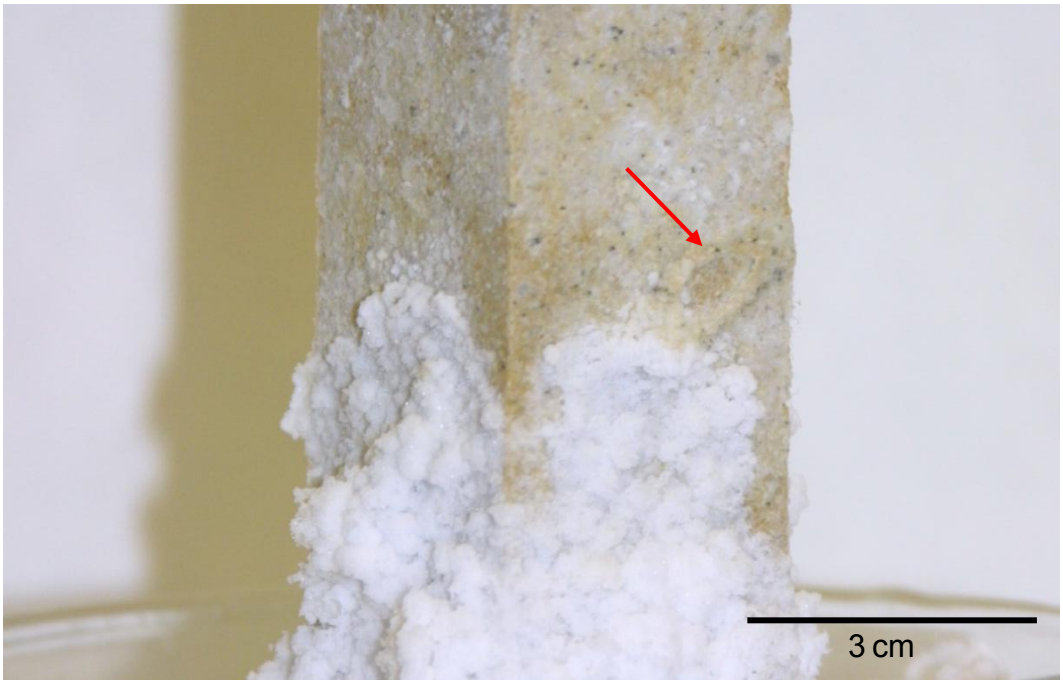

Figure 3-228. Calcarenite block treated with $KHCO_3$. Minor damage in zones with flaws can be observed (arrow).

In order to verify the damage caused by the different salt solutions, stone weight loss after completion of the test was determined. Efflorescence and loose stone material were removed (Figure 3-229). The now exposed surface of the calcarenite block previously immersed in K_2CO_3 revealed crack development (Figure 3-230).

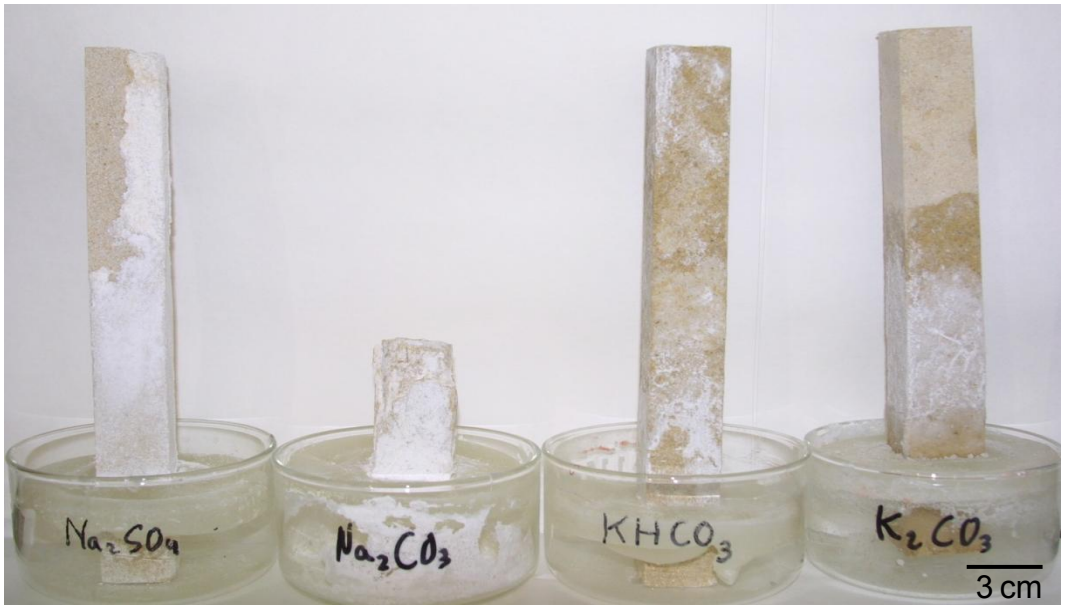

Figure 3-229. Aspect of calcarenite blocks after the removal of efflorescence and loose stone pieces.

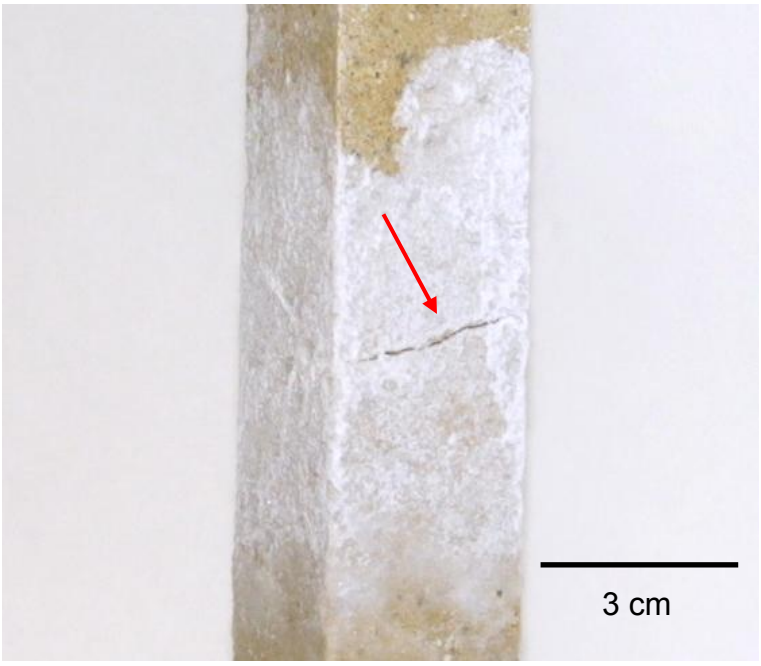

Figure 3-230. Calcarenite treated with K_2CO_3. After the removal of efflorescence, crack development (arrow) was discovered.

The material loss due to the actions of the salts is summarized in Table 3-53. Material loss was most significant in the case of Na_2CO_3. Note that Na_2SO_4 caused important damage, even thought, weight loss data does not seem to indicate this, being nearly 25 times lower than in the case of Na_2CO_3. Samples treated with K_2CO_3 and $KHCO_3$ did not experience any material loss.

Table 3-53. Material loss, salt retained in the stone prisms and salt efflorescence (wt %).

	Na_2SO_4	Na_2CO_3	K_2CO_3*	$KHCO_3$
Material loss**	2.3	57.2	0	0
Salt retained	1.1	55.7	17.8	37.9
Efflorescence	98.9	44.3	28.2	62.1

* only 46 wt% K_2CO_3 solutions evaporated
** with respect to the initial weight of the stone prisms

Figure 3-231 shows the evaporation curves of the different salt solutions. For an equal porous support and equal environmental conditions, evaporation is not only influenced by viscosity, surface tension and vapor pressure of the solution (Rodriguez-Navarro and Doehne 1999), but also by the amount of salt retained in the stone which blocks the stone pores and reduces the evaporation rate. Evaporation was fastest in the case of Na_2SO_4, where hardly any salt was retained in the stone prism. Evaporation rates of Na_2CO_3 and $KHCO_3$ were significantly lower, although, these salts have a nearly identical equilibrium RH as Na_2SO_4. However, larger amounts of Na_2CO_3 and $KHCO_3$ were retained in the stone prisms, resulting in reduced evaporation rates. The lowest evaporation rate was observed in the case of K_2CO_3. K_2CO_3 is a deliquescent salt with a significantly lower equilibrium RH compared to the other salt solutions. After more than 1 year test duration only 46 wt% K_2CO_3 solutions had evaporated.

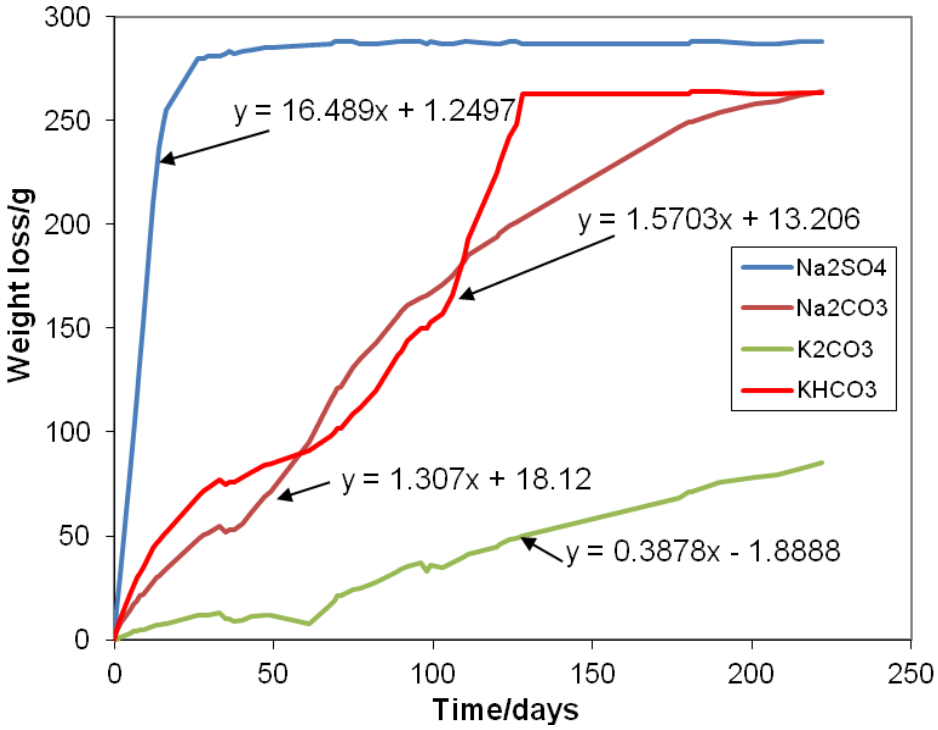

Figure 3-231. Evaporation rates of the different salt solutions (rates based on slope of the initial linear section of the curve).

The difference in damage potential of the various salts can be explained by the location of the crystallization front and, more importantly, the supersaturation reached at the point of crystallization. While hardly any damage was detected in the case of $KHCO_3$, severe damage occurred in the case of Na_2CO_3 and Na_2SO_4 where the salt crystallization provoked scaling and/or fracturing. The behavior of Na_2CO_3 and Na_2SO_4 is typical for salts which form metastable hydrated phases that transform into less soluble stable hydrated phases (Table 3-54). Schiro et al. (2012) observed severe damage when Na_2SO_4 heptahydrate transformed into mirabilite via a dissolution/precipitation mechanism. The solubility difference between stable and metastable hydrates enables the build-up of a high supersaturation and the generation of high crystallization pressure which is higher than the tensile strength of the stone and, thus, creates important damage.

$KHCO_3$, on the other hand, precipitated within the stone prism without causing mayor damage. This is thought to be due to the fact that this salt crystallized at lower supersaturation levels because there is no metastable phase with a higher solubility which would allow the generation of sufficient supersaturation with respect to the stable phase. In order to produce a high crystallization pressure, and thus, generate damage, the existence of

metastable phases with different degrees of hydration is required as explained by Schiro et al. (2012). The salts fulfilling this requirement are Na_2SO_4 and Na_2CO_3. In fact these salts have highly hydrated phases with extremely high molar volumes. In addition to the high supersaturation the systems can reach via dissolution of metastable phases, the high molar volumes of decahydrates ensures that a significant fraction of the pore volume will be filled with salt in order to effectively transmit crystallization pressure (Schiro et al. 2012). In the case of K_2CO_3 it could be argued that a high supersaturation and damage could also be generated due to the existence of two hydrated phases in addition to the anhydrous one. However, the highest hydrate only includes two water molecules and the solubility difference between hydrates is relatively small. The associated lower molar volume and limited supersaturation are responsibility for the reduced damage observed upon K_2CO_3 crystallization.

Table 3-54. Molar mass, molar volume and mass density of salts and their hydrated forms (Weast 1979).

Salt	Name	Mol. wt g/mol	Mol. vol. cm^3/mol*	Density g/cm^3	Solubility at 25 °C $g/100cm^3$
Na_2SO_4	Thenardite	142.04	53.00	2.68	***107.05
$Na_2SO_4 \cdot 7H_2O$	Heptahydrate	268.15	175.26	1.53**	***105.84
$Na_2SO_4 \cdot 10H_2O$	Mirabilite	322.19	220.68	1.46	***60.87
Na_2CO_3	Trona	105.99	41.89	2.53	21.50
$Na_2CO_3 \cdot 1H_2O$	Thermonatrite	124.00	55.11	2.25	33.00
$Na_2CO_3 \cdot 7H_2O$		232.10	153.71	1.51	16.90
$Na_2CO_3 \cdot 10H_2O$		286.14	198.71	1.44	****(20 °C) 21.70
K_2CO_3	Potash	138.21	56.88	2.43	****(20 °C) 112.00
$K_2CO_3 \cdot 1.5H_2O$		165.24	81.00	2.04	129.40
$K_2CO_3 \cdot 2H_2O$		174.24	85.41	2.04	146.90
$KHCO_3$	Kalicinite	100.12	46.14	2.17	22.40

* calculated from molar mass and mass density data
** Gans 1978
*** calculated from Steiger and Asmussen (2008)
**** http://www.chemicalbook.com

4. Discussion

The present study revealed differences in the clay minerals response towards the alkaline treatments. Different factors influence this response, such as structure and composition as well as reactive surface area of clay minerals, pH and chemistry of the alkaline solution, and the presence of organic matter (OM). Below these factors will be examined, also considering their influence on the newly formed mineralogical phases. Furthermore, the viability of alkaline treatments as an alternative consolidation treatment will be analyzed. Aspects influencing the practical application of alkaline activation for the consolidation of earthen architecture will be discussed, including possible adverse effects, such as salt formation.

4.1. Chemical and structural properties of clay minerals and their influence on reactivity

The results of this study showed that illite experienced a significantly lower degree of alteration than smectites and kaolinite in long-term experiments using 5 M NaOH or 5 M KOH. Note that experiments were performed in batch reactors and no attempt has been made to determine dissolution rates, since these are influenced by solution composition and its evolution over time. Here, the evaluation of the reactivity of clay minerals has been exclusively based on qualitative observations of the mineralogical evolution upon alkaline activation.

Carroll and Starkey (1971) presented data based on batch reactor experiments which are in agreement with our findings, showing that 2.8 M NaOH attacked kaolinite and montmorillonite more strongly than illite (Table 4-1).

Table 4-1. Analysis of supernatants of the reaction of 1 g of clay minerals with 50 ml of 2.8 M NaOH for 10 days at 25 °C (Carroll and Starkey 1971).

Mineral	SiO_2 (ppm)	Al_2O_3 (ppm)
Illite, Fithian, Illinois	160	180
Montmorillonite, Wyoming	580	200
Kaolinite, Bath, South Carolina	1120	580
Kaolinite, Waynesboro, Virginia	2200	2000

Experimental results by Jozefaciuk and Bowanko (2002) also revealed a lower reactivity of illite if compared to bentonite and kaolinite, considering the percentage of solid dissolved in batch reactor experiments using 5 M NaOH at

room *T*. The wt% of dissolved solid after 2 weeks of treatment were 7.23 wt% for bentonite, 7.11 wt% for kaolinite and only 3.62 wt% for illite. Marshal et al. (2004) came to a similar conclusion treating Hanford Sediments with simulated tank waste solutions containing 2.8 M NaOH. Compared to chlorite, smectite and kaolinite, illite appeared to be more resistant against the treatment.

Variations in clay reactivity can be explained by structural and chemical differences of the clay minerals. According to Schoonheydt and Johnston (2006) surface properties of clay minerals depend on their chemical composition, the nature of the surface atoms, the extent and type of defect sites, the layer charge and the type of exchangeable cations.

In the following sections the general mechanisms responsible for clay mineral dissolution are discussed, considering the surface complexation model proposed by Stumm (1997). The influence of pH on clay mineral dissolution will also be examined. Subsequently, a more detailed analysis of the reactivity of the different clay minerals, namely dioctahedral 1:1 and 2:1 as well as trioctahedral 2:1 clays is included.

4.1.1. Dissolution of clay minerals

A significant amount of research has been dedicated to mineral dissolution, including clay minerals, at low or near neutral pH which corresponds to the pH range of natural weathering conditions (White and Brantley 1995). In recent years, the use of clay as barrier material in contact with concrete in man-made repositories has caused an increased interest in the dissolution and transformation of clay minerals in an alkaline environment (Bauer et al. 1998). This is especially true for smectites (Claret et al. 2002, Bauer and Velde 1999, Rozalen et al. 2008).

General agreement exists that the contribution of the tetrahedral surface to the clay minerals reactivity is limited and hydroxyl groups exposed on the outer periphery of the mineral are the most reactive surface functional groups in clays (Sposito 1984). Surface hydroxyl groups can be either found on the gibbsite basal plane, for example in the case of kaolinite, or at the edge plane perpendicular to the basal plane, located at broken edges, steps and defect sites. The former hydroxyl groups are coordinated to pairs of Al^{3+} and their charge is not pH dependent. The latter hydroxyl groups are coordinated to a single Al^{3+} or Si^{4+} cation and their charge is pH dependent. The single coordinated hydroxyl groups are considered the most reactive sites and are common to all clay minerals.

The point of zero charge is the pH value where the net surface charge of the clay is zero. Below this value, increased protonation of >AlOH will induce a

positive surface charge. The contribution to the positive surface charge as a result of protonation of >SiOH will only be significant at a very low pH < 2 (Duval et al. 2002, Rayss and Sudolski 2002). Above the point of zero charge, the surface will have an increasingly negative charge because deprotonation of >SiOH and >AlOH occurs (Figure 4-1). According to Rozalen et al. (2009a) >SiOH and >AlOH groups will be completely deprotonated at a pH ~12 in the case of montmorillonite at 0.01M ionic strength (Figure 4-2).

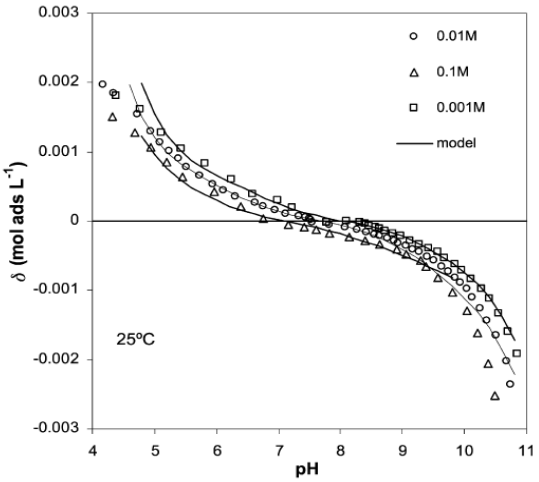

Figure 4-1. Surface charge of montmorillonite as a function of pH and ionic strength of KNO_3 solution (Rozalen et al. 2009a).

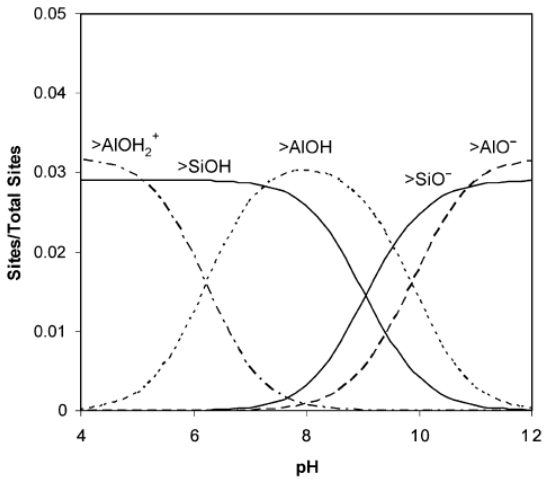

Figure 4-2. Distribution of montmorillonite surface species as a function of pH at 0.01 M KNO_3 ionic strength (Rozalen et al. 2009a).

In the surface complexation model, Stumm (1997) considered the charged surface complexes to be the precursors to the activated complexes which are released into solution. The detachment of surface metal species occurs by weakening of metal-oxygen bonds at the mineral surface through bond polarization by the charged surface complexes (Zinder et al. 1986). The authors (1986) further reported that the polarization and weakening of metal-oxygen bonds can be caused by protons and/or ligands. General agreement exists that dissolution rates are proportional to the concentration of negatively charged surface sites at high pH (Brady and Walther 1989, Stumm 1997).

4.1.2. Influence of pH on the dissolution and transformation of clay minerals

The synthesis of aluminous zeolites is commonly performed at high pH, where OH^- is used to solubilize silicate and aluminate species (Davis and Lobo 1991). Cundy and Cox (2005) described the OH^- groups as a mineraliser which acts as a catalyst, not only converting the starting materials into a mobile form

(dissolution process), but also conveying chemical reactivity in order for silicate and aluminate anions to form new chemical bonds and generate the zeolite framework. Note that the main metal species in solution at high alkaline conditions are expected to be $Al(OH)_4^-$ (Gaucher and Blanc 2006) as well as $H_2SiO_4^{2-}$ and $H_3SiO_4^-$ (Lechert 2001). Cundy and Cox (2005) further stated that the OH^- groups need to de-complex during or after framework formation in the case of zeolites, enabling the existence of the new structure as a stable solid phase.

Obviously, at lower pH, the OH^- concentration decreases and the dissolution rates of aluminosilicates is reduced. It has been shown experimentally that the dissolution rates of clay minerals decrease with increasing pH at acid conditions, minimize at near neutral pH and increase with increasing pH at basic conditions (Figure 4-3).

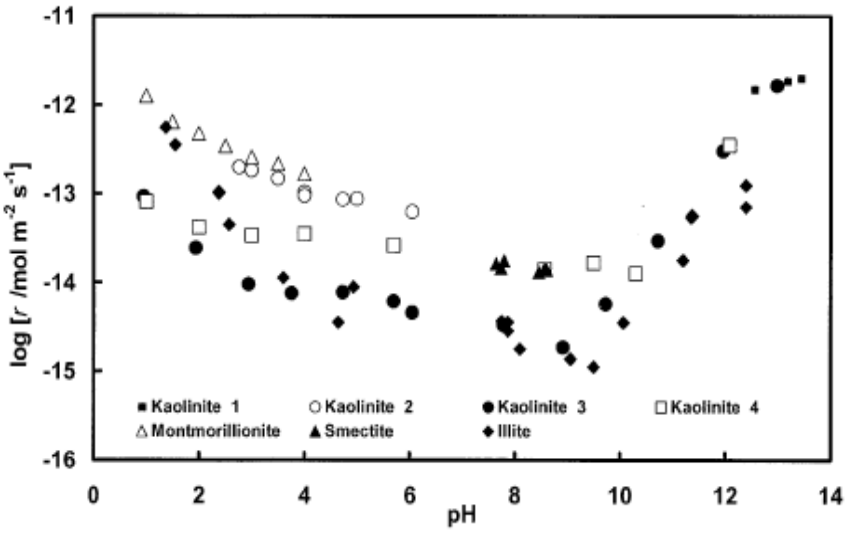

Figure 4-3. Comparison of apparent clay mineral dissolution rates summarized by Köhler et al. (2003).

Our results indicate that a certain threshold pH must be maintained during the treatment in order to promote an appreciable degree of mineral transformation. Saturated $Ca(OH)_2$ solution as well as 0.4 M NaOH solution, which experienced a rapid decrease to pH ≤ 10 within 60 days in this study, did not result in extensive mineralogical modification after 1 year of treatment. Considering our results as well as data on surface speciation (Figure 4-2) and on the dissolution rates of clay minerals (Figure 4-3), it becomes evident that a pH well above 10 is required to promote significant mineral dissolution and transformation into new phases. According to Huertas et al. (2009) only limited alteration of bentonite can be expected at a pH below 11. Gaucher and Blanc (2006) summarized dissolution rate data of montmorillonite which

showed a first acceleration inflection at pH ~11 and a second, more pronounced one at pH ~13. Bell (1996) was also aware of the pH dependence of mineral dissolution and pozzolanic reactions and claimed that in the case of soil stabilization with lime a pH ~ 12.4 (pH of saturated $Ca(OH)_2$ solution) should be maintained to achieve maximum reactivity. Further evidence of the importance of a sufficiently high pH for effective mineral transformation is provided by experimental results by Ramirez et al. (2005). The authors did not observe any mineralogical changes in Callovo-Oxfordian clay treated with NaOH or KOH solutions at pH 10. In contrast, treatments at pH 12 resulted in a decrease of the smectite and smectite-rich illite/smectite interstratification peak intensity in XRD patterns. The same experiments performed at pH 14 caused a complete destruction of smectite and smectite-rich illite/smectite interstratification. Obviously, dissolution rates also depend on *T* (Rozalen et al. 2009b, Figure 4-4) and similar dissolution rates can be achieved at lower pH if *T* is increased.

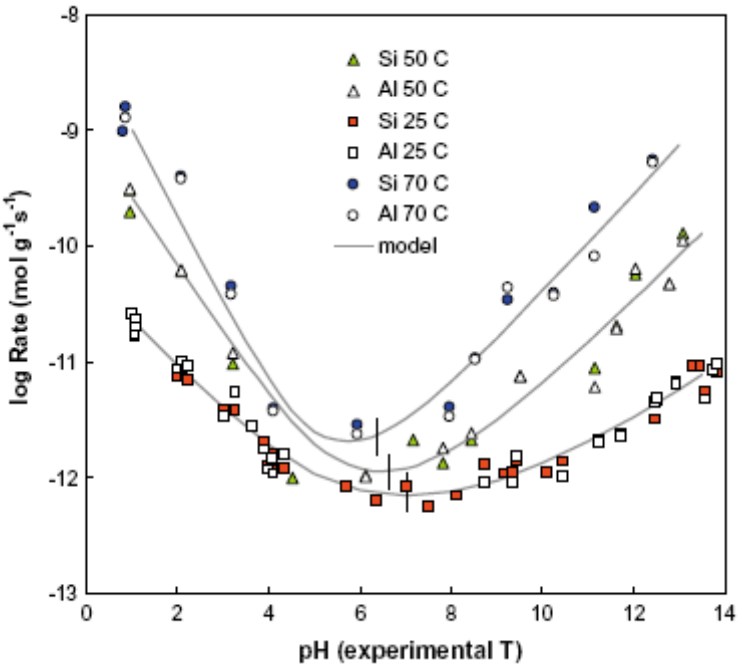

Figure 4-4. Experimental dissolution rates versus pH derived from Si and Al concentration of montmorillonite at 25, 50 and 70 °C. Small vertical lines indicate the corresponding neutral pH at each *T* (pH 7 at 25 °C, pH 6.63 at 50 °C and pH 6.4 at 70 °C) (Rozalen et al. 2009b).

The importance of alkalinity is also illustrated by experimental data reported by Barrer (1982), showing the pH dependence of induction times and zeolite yield in the case of mordenite. The induction time increased with decreasing pH and the yield was very low when zeolite synthesis was performed at a pH < 11.5 (Figure 4-5).

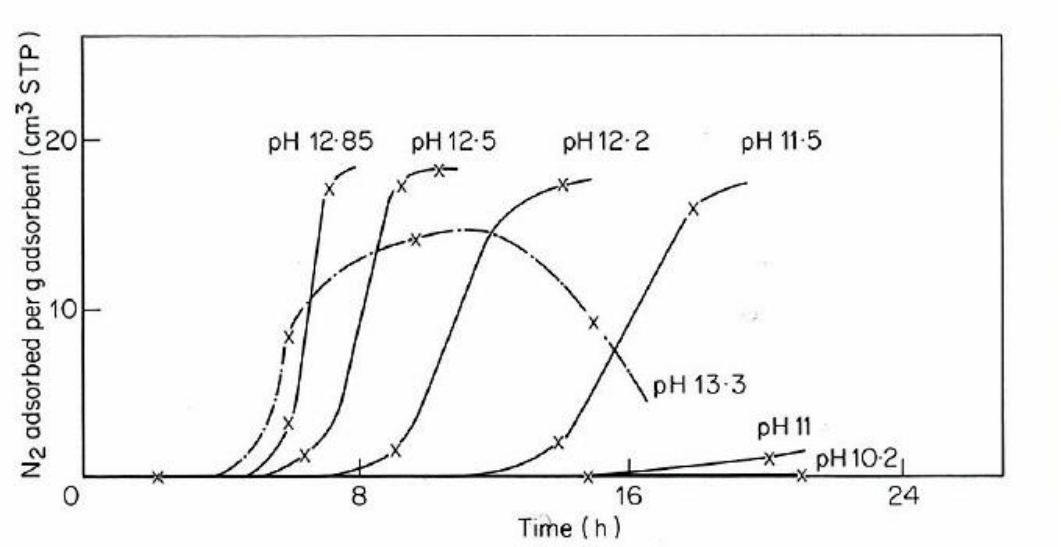

Figure 4-5. Influence of pH on zeolite yield (mordenite) versus time (300 °C synthesis *T*). Yield was calculated based on BET data. Note that mordenite transformed into other species at pH 13.3 (Barrer 1982).

As mentioned previously, experimental results of this study demonstrated an important decrease in pH during treatment, especially when a saturated $Ca(OH)_2$ solution was used. $Ca(OH)_2$ has a very limited solubility in water. Thus, the resulting OH^- concentration is low and the buffering capacity of the clay minerals results in a fast decrease in pH to < 10. These findings are in agreement with test results by Fernandez et al. (2006 and 2010). The authors observed no important mineralogical changes when saturated $Ca(OH)_2$ solution was percolated through cylindrical bentonite columns at *T* between 25-120 °C. Due to the buffering effect of the bentonite, the final pH reached was never above pH 9.5. Similar results were observed when bentonite was treated with saturated $Ca(OH)_2$ solution in batch reactors (Fernandez et al. 2010). Ramirez et al. (2002) also reported a reduction in pH during alkaline treatment of bentonite in batch reactors. A fast reduction in pH was also detected during the reaction of 0.1 M NaOH solutions with Opalinus Shale (Chermak 1993, Figure 4-6). The researcher found that the decrease in pH depended on the Opalinus Shale/NaOH ratio. Larger amounts of Opalinus Shale added to the same amount of NaOH solution resulted in a faster and more significant decrease in pH.

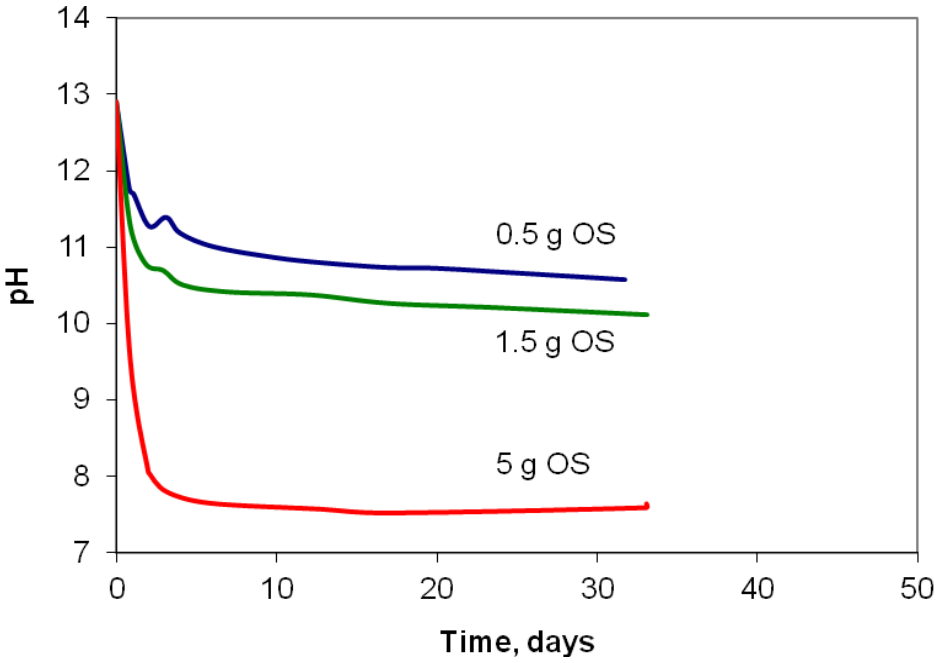

Figure 4-6. pH evolution of Opalinus Shale (OS) treated with 0.1 M NaOH at 200 °C (Data from Chermak 1993).

The decrease in pH can be explained by the hydrolysis of clay minerals in basic medium which exerts a buffering effect (Sanchez et al. 2006). Berube et al. (1990) showed in a computer simulation that the pH decrease in saturated lime solution was directly related to the amount of dissolved minerals. Gaucher and Blanc (2006) gave the following dissolution reaction for montmorillonite in an alkaline medium:

$Na_{0.33}Mg_{0.33}Al_{1.67}Si_4O_{10}(OH)_2+4.68OH^-+2H_2O \leftrightarrow$

$0.33Na^++0.33Mg^{2+}+1.67Al(OH)_4^-+4HSiO_3^-$

According to this reaction one mole of montmorillonite will consume 4.68 moles of OH^-. The pH reduction might not only be caused by the buffering effects of clays, but also by the formation of certain mineral phases such as CSH (Gaucher and Blanc 2006). The caused pH decrease has important implication on the efficiency of the alkaline treatment. It becomes obvious that alkaline solutions of sufficiently high concentrations are required to supply the necessary OH^- in order to counteract the clays buffering effect.

The influence of ionic strengths of alkaline solutions on the dissolution of different clay minerals can be deduced from data (Table 4-2) presented by Jozefaciuk and Bowanko (2002). The amount of dissolved solid increased 10 times or more, depending on the clay mineral, when the NaOH concentration was increased from 0.1 M to 5 M. Note that Jozefaciuk and Bowanko (2002) observed a significant amount of dissolved solid in the case of illite treated

with 5 M NaOH for 2 weeks. This result seems contrary to the findings reported here regarding the reactivity of the Beaver Bend illite. However, it has to be kept in mind that the dissolution rate depends on the illite crystallinity (a key data not provided by Jozefaciuk and Bowanko 2002). Furthermore, the findings reported here are based on long-term experiments. The dissolution rates in short-term experiments are often higher because they are governed by an initial fast dissolution of fine-grained materials, highly strained areas or defect sites (Huertas et al. 1999). Jozefaciuk and Bowanko (2002) actually stated that they frequently observed a sharpening of the basal reflections which they attributed to the dissolution of amorphous mineral particles. According to the same authors short-term alkali treatments are frequently applied previous to XRD analysis to clean the mineral surfaces of silicon oxides.

Table 4-2. Amount of dissolved solid (wt%) after alkaline treatment with NaOH at room *T* for 2 weeks (Jozefaciuk and Bowanko 2002).

Mineral	0.1 M NaOH	1 M NaOH	5 M NaOH
Bentonite	0.77	2.55	7.23
Kaolinite	0.42	1.47	7.11
Illite	0.23	0.54	3.62

4.1.3. Reactivity of dioctahedral 1:1 clay

Our experimental results revealed extensive dissolution and transformation of kaolinite. XRD data showed that the kaolinite 001 Bragg peak intensity suffered a significant reduction after 6 months of treatment with 5 M NaOH or 5 M KOH. Furthermore, the presence of large amounts of newly formed zeolitic phases were observed with FESEM. Note that kaolinite treated with 5 M NaOH for 6 months experienced a surface area increase of as much as 13 times if compared to the untreated sample which was attributed to the formation of a faujasite-type zeolite. Detected changes in surface area in samples treated with 5 M KOH were less significant because the newly formed zeolites had a pore size below the detection limit of the analytical technique (see section 4.3.2.). After 1-year alkaline activation the intensity of the 001 kaolinite Bragg peak further decreased, suggesting that only a small fraction of kaolinite was left in the samples treated with 5 M NaOH or 5 M KOH. The kaolinite in the Alhambra formation soil showed an even faster dissolution, and the 001 Bragg peak disappeared completely after 1-year treatment with 5 M NaOH or 5 M KOH. The faster dissolution in the case of the kaolinite in the Alhambra Formation soil is a result of its lower crystallinity if compared to the

pure kaolinite tested here. Average crystallite sizes were 36 nm in pure kaolinite and 16 nm in kaolinite of the Alhambra Formation soil.

The observed high reactivity can be explained considering the structural characteristics of kaolinite. Its unit cell is made up of a tetrahedral sheet which is bound through shared oxygen to an octahedral sheet. Unit cells are linked in the c direction by hydrogen bonding between hydroxyl sites on the gibbsite basal plane and the electronegative oxygens of the silicon tetrahedral sheet (Brady et al. 1996). The hydrogen bonding results in a strong connection of the unit cells, inhibiting intracrystalline swelling in kaolinites. Isomorphic substitution is unimportant and the cation exchange capacity and surface area are low compared with other clay minerals.

Nonetheless, the fast dissolution of kaolinite can be explained considering the contribution of the >AlOH groups on the gibbsite basal plane (Xie and Walther 1992, Huertas et al. 1999) in addition to the reactive sites on edge planes which are the reactive sites responsible for mineral dissolution in the case of 2:1 clays. However, Ganor et al. (2003) stated that the basal plane hydroxyl groups coordinated to pairs of Al^{3+} were less reactive than > AlOH groups on edge surfaces coordinated to a single Al^{3+}. Significant reactions on the Si-tetrahedral side of kaolinite are not expected to take place. According to Schoonheydt and Johnston (2006) under ambient conditions the least reactive surface found on clay minerals is the neutral siloxane surface of 2:1 phyllosilicates where no isomorphous substitution has occurred, and the Si-tetrahedral side of the 1:1 kaolinite group. These surfaces are hydrophobic and interact only weakly with water molecules.

Experimental results by Bauer und Berger (1998) also gave evidence for the high reactivity of kaolinite. The authors found that kaolinite showed a one to two orders of magnitude higher dissolution rate than smectites and stated that structural differences would account for the different behaviour of the two clays. Bauer and Berger (1998) assumed that the Al sites were more reactive than the Si sites and that the dissolution of the octahedral layer in kaolinites caused a partial hydrolysis of Si and eventually the dissolution of the tetrahedral sheet. The higher reactivity of Al sites can be explained considering the lower bond strength of Al-O (512 kJ mol^{-1}) if compared to the bond strength of Si-O (798.7 kJ mol^{-1}). Bauer and Berger (1998) further reported that hydrolysis of the octahedral and tetrahedral layers proceeded as parallel reactions in kaolinites and as serial reactions in smectite. The rate limiting step was the dissolution of the octahedral layer in kaolinites and the dissolution of the tetrahedral layer in smectites.

4.1.4. Reactivity of dioctahedral 2:1 clay minerals

As a result of the low crystallinity of the original montmorillonite (Cabo de Gata) and the fact that Bragg peaks of newly formed zeolitic phases in samples treated with 5 M NaOH and 5 M KOH coincide with the clay`s 001 Bragg peak, XRD patterns did not allow an unambiguous evaluation of the degree of montmorillonite dissolution. However, the intensity of the 001 montmorillonite Bragg peak seemed to be reduced after 6-month treatment with 5 M NaOH. Fortunately, nitrogen sorption data provided clear evidence for alteration in the case of the pure montmorillonite. Significant modifications in the shape of the hysteresis loop of the nitrogen sorption curves were observed which suggested an at least partial destruction of montmorillonite after 6 months of treatment with 5 M NaOH or 5 M KOH (see Figure 3-56 and 3-72). In the case of the Alhambra Formation soil (Figure 4-7), the pronounced hysteresis loop of the original sample (green) was significantly reduced after the treatment with KOH or NaOH (not included here) for 1 year. The shape of the hysteresis loop (yellow) became identical to the one observed for pure kaolinite samples (blue), indicating the destruction of smectite.

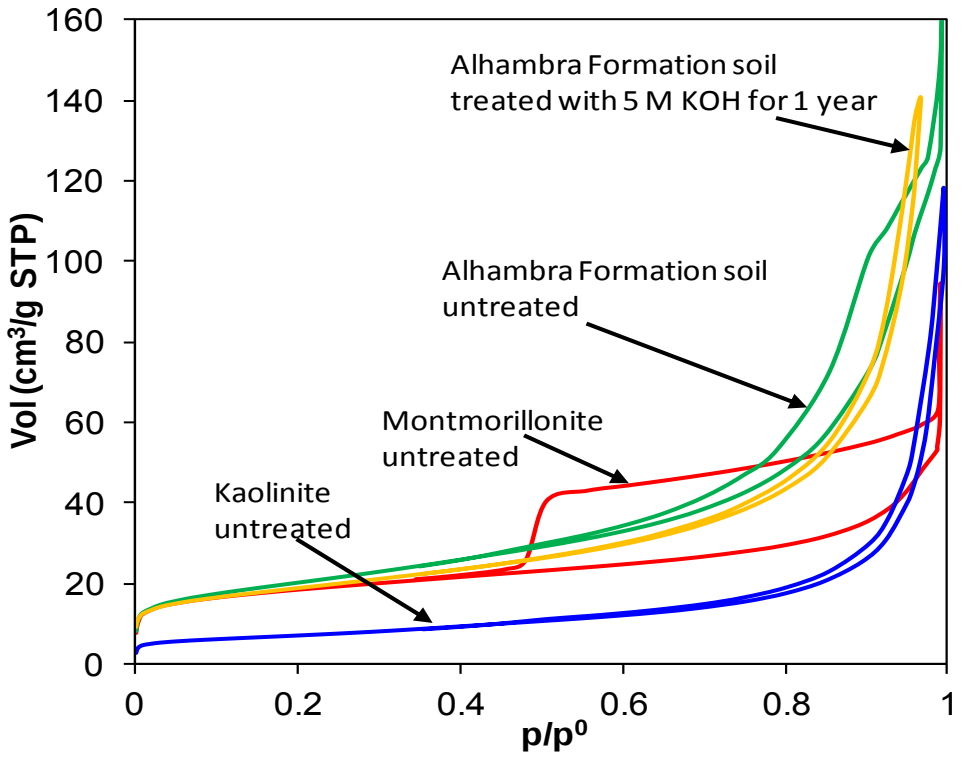

Figure 4-7. Modification of the nitrogen sorption isotherm (yellow) of Alhambra Formation soil treated with 5 M KOH for 1 year, indicating the destruction of smectites. Isotherms of untreated kaolinite (blue), montmorillonite (red) and Alhambra Formation soil (green) are included for comparison.

Pure illite (Beaver Bend State Park) treated with 5 M NaOH or 5 M KOH for 1 year, on the other hand, only experienced very small changes in the chemical composition as revealed by TEM-AEM data. These changes might be interpreted as an incipient transformation of the illite into smectitic clay minerals. XRD data of the same samples revealed that the effect of the alkaline treatment was limited to compositional changes and did not result in changes in peak position and/or width. Actually, the average crystallite size of illite increased over time upon alkaline activation using 5 M KOH, possibly due to a recrystallization process in the presence of K^+ which involved Ostwald ripening. Ostwald ripening is characterized by the dissolution of small particles and the growth of larger ones in order to minimize surface free energy, obeying the Gibbs-Thomson law (Inoue et al. 1988). The average crystallite size of untreated pure illite was 28 nm and 15 nm in the case of the illite in the Alhambra Formation soil. After prolonged alkaline treatment for more than 4 years, the average crystallite size was 36 and 23 nm, respectively.

As mentioned previously, some bulky crystals, most likely a zeolitic phase, were observed in the pure illite sample treated with 5 M KOH for 1 year. However, the amount of these crystals was too small to be detected with XRD. Furthermore, the number of crystals did not increase over time, suggesting that kaolinite present as impurity in the original illite sample was the source material for these zeolites.

In contrast, the illite in the Alhambra Formation soil experienced important dissolution upon treatment with 5 M NaOH. After 6 months of alkaline activation, the intensity of 001 illite Bragg peak was significantly reduced. Dissolution in the case of the illite of the Alhambra Formation soil can be explained by its significantly lower crystallinity if compared to the Beaver Bend illite (see above). An unambiguous analysis of the changes in the chemical composition of the illite in the Alhambra Formation soil upon alkaline activation was not possible, because illitization of the original smectitic minerals had occured.

Results by Barrer et al. (1968) support the findings of this study, suggesting a relative low reactivity of illitic clays in the presence of K. The authors reported that mica present as an impurity in kaolinite was unreactive in 1.8 – 4.1 M KOH solutions. Further evidence for a lower reactivity of illite is provided by experimental results by Ramirez et al. (2005) which showed that smectite and smectite-rich interstratifications disappeared, whereas illite and illite-rich interstratifications remained basically unaltered when treated with NaOH or KOH solution at pH 14 and 60 °C for 168 h.

Montmorillonite and illite are both dioctahedral 2:1 clay minerals composed of two tetrahedral layers, sandwiching an octahedral layer. Both minerals show a strong anisotropic behaviour regarding their response to

dissolution reactions. As mentioned previously, general agreement exist that the contribution of the tetrahedral surface to the clay minerals reactivity is limited and that hydroxyl groups located at broken edges, steps and defect sites are the most reactive surface sites in 2:1 clays (Sposito 1984, Schoonheydt and Johnston 2006). Proof for the preferential dissolution along the {110} faces of 2:1 clays has been provided by atomic force microscopy (AFM) studies by Kuwahara (2006, 2008) who showed that basal surfaces were unreactive within the experimental duration in the case of smectite and muscovite. Yokoyamo et al. (2005) came to a similar conclusion, studying the dissolution of montmorillonite under alkaline conditions using AFM. Samson et al. (2005) used FESEM to demonstrate that biotite also dissolved faster on edge surfaces than on basal surfaces at high pH and room *T*.

Based on structural consideration both clay minerals, montmorillonite and illite, will follow a similar dissolution mechanism under alkaline conditions. Nevertheless, differences regarding their reactivity can be explained by compositional variations. Illite has generally a significantly higher net negative charge if compared with montmorillonite. Higher net charge, usually reduces the swelling ability (Norrish 1954). Slade et al. (1991) indicated that increasing net charge causes an increase in interlayer cation concentration which could result in a greater water up-take. However, opposing electrostatic forces increase more rapidly at higher net charge and swelling will be less. The lower negative charge of montmorillonites will, thus, result in a higher swelling capacity, offering a larger surface for interaction with the alkaline solution.

Whereas the layer charge of an ideal illite is caused by substitution of Si^{4+} for Al^{3+} in the tetrahedral sheet and is generally compensated by K^{+} in the interlayer, the charge of montmorillonite is generally due to substitution of Al^{3+} for Mg^{2+} in the octahedral sheet and is predominantly compensated by Na^{+} in the interlayer (Newman and Brown 1987, Table 4-3).

Table 4-3. Idealized structural formulae and layer charge (equivalents $mole^{-1}$) of clays (adapted from Thomas 1998).

Mineral	Idealized Formula	Tetrahedral Charge	Octahedral Charge	Layer Charge
Kaolinite	$Si_4Al_4O_{10}(OH)_8$	0	0	0
Montmor.	$Na_{0.66}Si_8(Al_{3.34}Mg_{0.66})O_{20}(OH)_4$	0	-0.66	-0.66
Saponite	$(Na, Mg, Ca)_{0.66}(Si_{7.34}Al_{0.66})$ $Mg_6O_{20}(OH)_4$	-0.66	0	-0.66
Muscovite	$K_2(Si_6Al_2)Al_4O_{20}(OH)_4$	-2.00	0	-2.00

According to Sposito (1984) isomorphic substitution occurring in the tetrahedral sheet will result in a more localized charge, facilitating the formation of an inner-sphere complex. In the so-called inner-sphere complex no solvent (water) molecule is interposed between the surface functional group (the ditrigonal cavity) and the cation it binds.

Due to the charge distribution and the similarity of the ionic radius of K^+ (0.138 nm) and the diameter of the ditrigonal cavity of the siloxane surface (0.26 nm), a very stable surface complex forms in the case of illite. Newman and Brown (1987) calculated the maximum layer charge at which muscovite or illite with different cations would remain expandable. The authors concluded that muscovite or illite with interlayer Na would still expand at a layer charge at which the same clays with interlayer K would no longer do so.

In the case of dioctahedral smectites, the isomorphic substitution in the octahedral sheet creates a less localized charge, generally resulting in an outer-sphere complex where a water molecule is interposed between the surface functional group and the cation it binds, primarily Na^+ in the case of montmorillonite (Sposito 1984). Note that Na^+ has a smaller ionic radius and a higher ionic potential than K^+, resulting in significantly higher hydration energy for Na^+ (405 kJ/mol) if compared to K^+ (321 kJ/mol). The higher hydration energy of Na^+ indicates that more energy is needed for the dehydration of Na than of K (Aiello et al. 1991). Thus, Na will more likely be present in a hydrated state in the clay interlayer, forming an outer-sphere complex. Usually, an outer-sphere complex is less stable than an inner-sphere complex because it involves only electrostatic bonding mechanisms whereas the later involves covalent bonding or a combination of covalent and electrostatic bonding (Sposito 1984). The effect of the formation of inner-sphere complexes on clay stability is well documented by the example of Na-beidellite. Hensen and Schmit (2002) showed that Na-beidellite, having only tetrahedral substitution, experienced limited swelling, because Na cations are strongly bonded to the clay surface and do not hydrate easily beyond the one-layer hydrate. Na-montmorillonite, on the other hand, has predominantly octahedral substitution and swells readily as a result of the hydration of interlayer cations (Norrish 1954). In the case of illite water seems to be mostly adsorbed on the particle surface and only small amounts of water may be inter-layered within the illite sheets (Deer et al.(1962). Pashley and Quirk (1984), however, stated that swelling in illites is limited to swelling between crystal platelets, i.e. osmotic swelling.

The above described chemical differences not only modify the swelling behaviour of 2:1 clays, but also influence physical properties such as crystallinity. The higher bond stability of individual illite units results in higher crystallinity. The crystallite size of the Beaver Bend illite used here was

determined to be 28 nm, whereas the crystallite size of montmorillonite from Cabo de Gata was only 9 nm. It is a well known fact that crystallinity has a direct influence on mineral dissolution. Follett et al. (1965) reported that 78.6 % of SiO_2 was extracted using 0.5 M NaOH in the case of an allophane, whereas the amount of extracted SiO_2 was only 6.0 and 10.2 % in the case of illite and montmorillonite, respectively.

4.1.5. Reactivity of trioctahedral 2:1 clay

XRD and FESEM revealed no alteration of saponite after 1-year treatment with 5 M NaOH or 5 M KOH. However, TEM-AEM data showed modifications in the chemical composition after 6 months of alkaline activation which continued over time. In the case of the sample treated with 5 M NaOH a randomly interstratified saponite-chlorite formed which was identified with XRD after 4.7-year alkaline treatment. The sample treated with 5 M KOH experienced a similar chemical alteration after 1 year, i.e., the Si concentration decreased and the Mg concentration increased. However, more prolonged treatment resulted in a decrease in Mg in the sample treated with KOH, whereas the Mg concentration continued to increase in the sample treated with NaOH. FESEM-EDS analysis revealed that the KOH treatment resulted in the formation of a gel-like phase which contained Al, Si and Mg and could not be identified with XRD. Both alkaline treatments resulted in a certain decrease in expandability of the clay mineral.

As all minerals of the smectite group, saponite is an expandable 2:1 clay with a high surface area. However, compositional characteristics seem to be responsible for its relative stability. The net negative charge of saponite, a clay mineral with trioctahedral character, usually derives from Al^{3+} substitution of Si^{4+} in the tretrahedral layer which is partially compensated by substitution of Mg^{2+} for trivalent cations in the octahedral layer. However, octahedral occupancy might be less than 3 per $O_{10}(OH)_2$. Thus, the charge density of saponite is generally in the range of 0.4-0.6 per $O_{10}(OH)_2$, which is typical for a mineral of the smectite group (Newman and Brown 1987, Table 4-3). The negative layer charge is principally compensated by incorporation of Ca^{2+} and Mg^{2+} in the interlayer, although, Na^{+} might also be present (Newman and Brown 1987).

Becerro et al. (2009) reported a higher stability of trioctahedral smectites, namely saponite, hectorite and laponite if compared to dioctahedral smectites such as montmorillonite and beidellite when treated with alkaline solutions at 300 °C. The authors suggested that the full occupation of the octahedral sheet by mainly Mg^{2+} (i.e., forming a brucite layer) would be decisive for the higher stability of the former group of clays under alkaline

attack. Pokrovsky and Schott (2004) demonstrated that dissolution rates of brucite were drastically reduced as pH increased (Figure 4-8). Using acid/base titration the same authors determined the point of zero charge of brucite to be ~ 11 pH. According to the same authors the concentration of deprotonated >MgOH groups was only significant at pH > 12 (Figure 4-9). Considering that the dissolution rates are proportional to the concentration of negatively charged surface sites (i.e., deprotonated $>MgO^-$ and $>AlO^-$ sites) at high pH (Brady and Walther 1989, Stumm 1997), it can be expected that the dissolution of brucite layers will occur at lower rates than the dissolution of gibbsite layers.

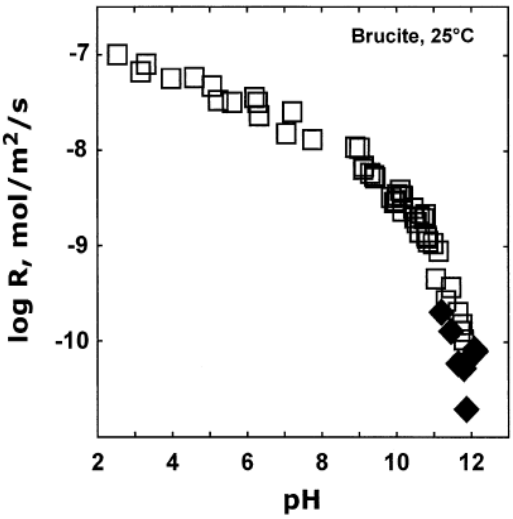

4-8. Brucite steady-state dissolution rates as a function of pH in 0.01 M NaCl (Pokrovsky and Schott 2004).

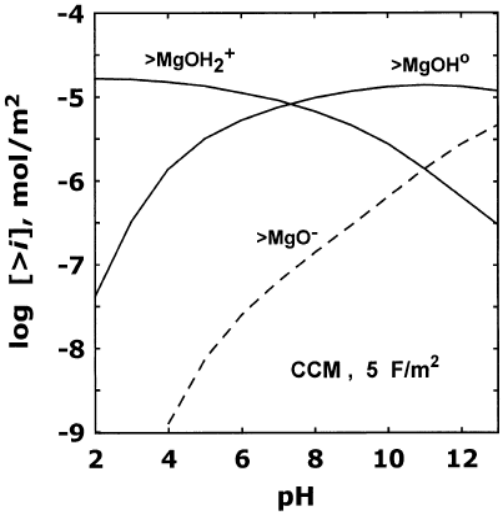

Figure 4-9. Calculated surface speciation of brucite in 0.01 M NaCl (Pokrovsky and Schott 2004).

Another evidence for the stability of the trioctahedral smectite at high pH is given by the fact that one of the reaction products of Febex bentonite at pH > 13 was saponite (Sanchez et al. 2006, Ramirez et al. 2002). Under natural conditions, the formation of saponite from dioctahedral smectite at high pH has also been observed, for example in the case of saponite from the Madrid Basin (Pozo Rodriguez and Casas Sainz de Aja 1992). Bristow et al. (2009) acknowledged the importance of a high pH (~9 or higher) for the formation of trioctahedral smectites at appreciable rates. Our research also showed that dioctahedral smectite underwent compositional changes at pH > 13 which are compatible with saponization.

In conclusion, or experimental results showed that illite was the least reactive clay mineral, especially in the presence of K^+. Montmorillonite and especially kaolinite revealed significant alteration after 6 months of alkaline treatment with both NaOH and KOH solutions. Comparing di- and

trioctahedral smectites, it was evident that modifications of the later were limited to chemical changes during alkaline treatment for up to 1 year. Thus, indicating a higher stability of the saponitic clay. Test results further indicate that the crystallinity of clay minerals has an important influence on the clays reactivity which was especially evident in the case of the highly crystalline illite from Beavers Bend State Park which hardly showed any alteration.

4.2. Mineralogical evolution of clay minerals upon alkaline activation

According to Fernandez et al. (2006) the main short-term reaction processes during alkaline activation of clays is dominated by ion exchange, whereas dissolution-precipitation of mineral phases would govern long-term reactions. The most common minerals formed through dissolution-precipitation reactions include zeolites, CSH or CASH phases, clay minerals and feldspars (Gaucher and Blanc 2006). The following sections include an overview of the newly formed phases observed in this study upon alkaline activation of the various clays minerals. Aspects related to formation mechanisms and phase evolution are discussed.

4.2.1. Zeolites

Considering the mineralogical evolution of pure clays and the Alhambra Formation soil treated with 5 M NaOH or 5 M KOH, certain tendencies can be drawn (Table 4-4 and 4-5). Zeolites are the dominant newly formed phases detected upon alkaline activation of kaolinite, montmorillonite and Alhambra Formation soil. However, zeolite formation was not detected in the case of saponite and to a very limited degree in illite. The use of saturated $Ca(OH)_2$ solution did not result in zeolite formation. According to Fernandez et al. (2010) zeolite formation is not favoured in $Ca(OH)_2$ systems which seems to be related to the low solubility of $Ca(OH)_2$ and the resulting low OH^- concentration.

Table 4-4. Summary of zeolitic phases detected in clays treated with 5 M NaOH. Zeolites are listed in the order of their detection with XRD and FESEM. Dominant cations detected with FESEM-EDS are included.

Clay Mineral	Zeolites
Kaolinite	Faujasite, Ca+Na Hydrox.sodalite, Na
Montmorillonite	Hydrox.sodalite, Na Faujasite, Ca
Saponite	-
Illite	-
Alhambra Formation soil	Faujasite, Ca Hydrox.sodalite, Na+(Ca)

- not observed

Table 4-5. Summary of zeolitic phases detected in clays treated with 5 M KOH. Zeolites are listed in the order of their detection with XRD and FESEM. Dominant cations detected with FESEM-EDS are included.

Clay Mineral	Zeolites
Kaolinite	Zeolite K-I, K Chabazite, K+(Ca) Zeolite K-F, K
Montmorillonite	Zeolite K-I, K+(Ca) Zeolite K-F, K+(Ca)
Saponite	-
Illite	(Zeolite K-F ?)
Alhambra Formation soil	Zeolite K-I, K+(Ca) Chabazite, K+(Ca) Zeolite K-F, K+(Ca)

- not observed

Zeolites are tectosilicates. They are microporous, crystalline, hydrated aluminunosilicates and consist of a framework of Si and Al tetrahedra, linked together by sharing all four oxygen ions. The negative charge introduced by the presence of Al^{3+} is compensated by extraframework cations. Zeolites are characterized by their capability to lose and gain water reversibly and to exchange constituent cations without major structural changes (Mumpton 1977).

Natural zeolites commonly exhibit low Si/Al ratios (Barrer 1982). The same applies for the first examples of zeolites synthesized in the laboratory which include zeolite P (gismondine-type zeolite), Q, A and X (faujasite-type zeolite) (Cundy and Cox 2005). Typical cations in natural and synthetic low-silica zeolites are Na^+, K^+, Ca^{2+} and Ba^{2+} ions. The alkali and earth-alkali metal cations act as structure-directing agents (Davis and Lobo 1991, Moliner 2012). The type of zeolite formed does not only depend on the dominant cation in the synthesis solution, but also on the synthesis *T*, the concentration of the hydroxide solution (Barth-Wirsching and Höller 1989), the pH (Lechert 2001) and the Si/Al ratio of the substrate (Sig Ko and Seung Ahn 2004).

Zeolite synthesis is commonly performed at $T \geq 60$ °C because the induction time for zeolite formation decreases drastically when *T* is increased (Barrer 1982). Thus, an important outcome of our research is the finding, that important amounts of zeolites formed in the case of kaolinite, montmorillonite and Alhambra Formation soil, alkaline activated at room *T*. Admittedly, zeolite formation took much longer (i.e., 2-6 months depending on clay mineral and activation solution) than under common zeolite synthesis conditions.

According to Barrer (1982), the zeolite mordenite, for example, precipitated within 1-10 days at *T* between 100-200 °C.

The experimental results summarized in Table 4-4 and 4-5 indicate that the cation of the mineralizing solution, either Na^+ or K^+, determines the type of zeolite formed. Barrer (1982) discussed the structure-directing role of cations and concluded that sodic environments favour the formation of faujasite and sodalite hydrates, whereas chabazite forms in potassic environments. Edingtonite-type zeolites (zeolite K-F) crystallize in a variety of cation environments, including potassic environments. Barrer´s results are in agreement with our findings. In the case of kaolinite, montmorillonite and the Alhambra Formation soil, faujasite and hydroxy sodalite formed when NaOH was used for activation. The treatment with KOH, on the other hand, resulted in the formation of zeolite K-I and K-F, as well as chabazite in kaolinite and Alhambra Formation soil. In montmorillonite, only zeolites K-I and K-F were detected. The reason why the chabazite zeolite was not observed in the case of montmorillonite is not clear.

Occasionally, a retardation/acceleration effect of different cations on zeolite nucleation is mentioned (Aiello et al. 1991). Generally, a retardation effect of K^+ is observed, whereas Na^+ facilitates zeolite nucleation. In this study only in the case of montmorillonite a slower transformation was observed in the sample treated with 5 M KOH compared to 5 M NaOH. In all other samples, zeolites usually formed after similar treatment periods when NaOH or KOH solution were used. In the case of the Alhambra Formation soil, zeolite formation was already detected after 4 months when 5 M KOH was used versus 6 months when treated with 5 M NaOH. Admittedly, smaller time intervals between sampling and a quantitative analysis of newly formed phases would have given more conclusive information regarding the effect of cations on zeolite formation.

The fact that identical zeolites formed from different starting materials suggests that certain variations in the composition, especially in the Si/Al ratio, of the starting material are permissible, at least in the case of the zeolites synthesized here. Barth-Wirsching and Höller (1989) reported identical results under highly alkaline conditions, but found that the Si/Al ratio of the same zeolite type varied with varying Si/Al ratios of the starting materials. Vigil de Villa et al. (2001) stated that the influence of the mineral substrata composition was only important when dilute alkaline solutions (< 0.1 M) were used. In contrast, the nature of the zeolites formed in concentrated alkaline solutions (> 0.1 M) did not depend on the substrata.

Our results further show that zeolites such as faujasite and chabazite contain calcium which was released into the alkaline solution from the starting clays upon cation exchange. In addition, the tap water used during

sample preparation might have been an additional source for calcium. Barrer (1982) reported that the cations present in zeolites would depend on the cations in the mineralizing solution and might even change after zeolite formation if the cation composition of the ambient solution changes. However, some zeolites show a strong affinity for a certain cation (Smart and Moore 2005). Cation selectivity varies for different zeolites (Flanigan and Mumpton 1977). Barrer et al. (1969) reported a higher thermodynamic affinity for Ca^{2+} than for Na^{+} in zeolite X. This statement is in agreement with our findings showing Ca as the main cation in the faujasite-type zeolite synthesized with 5 M NaOH solution. Note that zeolite X is a synthetic analogue of faujasite. The same might be true for chabazite (Shibue 1981). Another well known example is the selectivity for Ca^{2+} of zeolite A which is the reason for its use as ion-exchange agent in detergents, where it is added as a water softener (Barrer 1982, Figure 4-10).

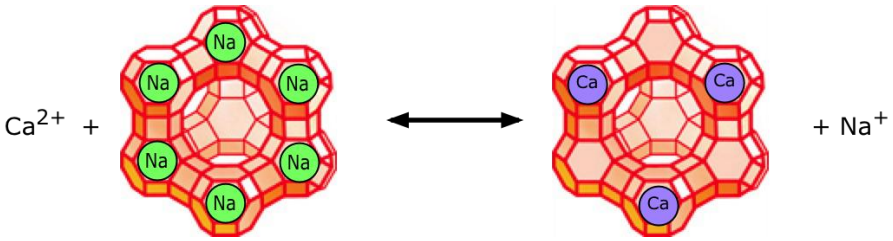

Figure 4-10. Ca ions in water displace Na ions, which are released into water (www.chem1.com, 25.9.12).

The order of appearance of the different zeolite types observed in this study generally followed an identical path in most tested clay minerals. In the case of kaolinite and Alhambra Formation soil treated with NaOH, a faujasite-type zeolite was first detected, followed by a sodalite-type zeolite. The less stable faujasite transformed into hydroxysodalite, the latter being the dominant phase after prolonged treatment for more than 6 years. In the case of kaolinite treated with 5 M NaOH, the faujasite-type zeolite disappeared completely and only hydroxysodalite was observed after 6.1 years of treatment. These results are in agreement with findings by Bosnar et al. (2004), who reported a spontaneous transformation of less stable zeolites such as A, X, Y into more stable ones like hydroxysodalite or zeolite P in a crystallizing system of high alkalinity. Transformation of zeolite Na-X (faujasite-type zeolite) into denser hydroxysodalite has also been reported by Novembre et al. (2004). According to Cundy and Cox (2005) the growth of the hydroxysodalite crystals is the rate-limiting step in this transformation process.

In the case of kaolinite, montmorillonite and Alhambra Formation soil samples treated with 5 M KOH, zeolite K-I was the first one to be detected, followed by a chabazite-type zeolite and/or zeolite K-F. In the case of the montmorillonite sample, the chabazite-type zeolite was not observed. The reason for the absence of this type of zeolite is unclear, especially, since

Fernandez et al. (2010) detected it as a reaction product in Febex bentonite treated with K^+ containing, highly alkaline solutions. In the kaolinite sample, zeolite K-F seems to have formed at the expense of zeolite K-I, which is known to be unstable (Breck 1974). Experimental results by Bauer et al. (1998) also provided evidence for the metastable character of zeolite K-I. Their SEM observations revealed that the hexagonal K-I zeolite formed the substrate for the nucleation of prismatic phillipsite crystals. Note that phillipsite is commonly sythesized from kaolinite using KOH (Barrer 1982).

Davis and Lobo (1992) explained that zeolite synthesis follows the Ostwald´s law of successive reactions (Ostwald´s Step Rule). Since synthetic zeolites are generally considered thermodynamically metastable, the first phase produced is consumed and replaced by a more stable second phase. Transformation might go on until the most stable phase is formed. However, conversion might be slow if the energy barrier for the transformation to a more thermodynamically stable phase is high.

Apart from transformation processes, coarsening of zeolite crystals during alkaline activation has been observed here. For instance, faujasite crystals formed in the case of Alhambra Formation soil treated with 5 M NaOH for 6 months doubled their size after 1-year treatment. Crystal coarsening is often related to Ostwald ripening, where smaller particles dissolve and larger one grow in order to reduce total surface free energy and increase stability. However, the effect of Ostwald ripening on zeolite crystal coarsening is controversial (Cundy and Cox 2005). Whether Ostwald ripening is responsible for the size increase in the case of the zeolite crystals formed here is not clear. XRD evidenced that clay minerals, which could have served as an alumina and silica source for further growth of existing crystals were still present in the alkaline solution after 1 year of treatment.

In the case of the saponite tested in this study, it is speculated that the low Al concentration inhibited zeolite crystallization. The synthesis of high-silica zeolites (Si/Al > 5) is generally achieved by the use of organic cations such as alkylammonium which act as mineralizers and structure-directing agents, or by the addition of zeolite seeds. Commonly, reaction *T* is higher than in the case of low-silica zeolites (Barrer 1982, Davis and Lobo 1991, Moliner 2012). Furthermore, the required reaction time becomes longer with increasing Si-content of the starting material (Barth-Wirsching and Höller, 1989). Kovalchuk et al. (2008) present data on the activation of fly-ash with NaOH which showed that zeolites did not form at a Si/Al ratio above 3.5. The authors claim that zeolite crystallization in high-silica systems requires intense curing conditions, i.e. long curing time and/or high *T*.

Additionally, the high Mg concentration in the case of saponite, might also inhibit zeolite formation. Breck (1974) reported on experimental

simulation of the action of sea water on basalt. In the presence of Mg, montmorillonite was the main product, whereas an analcime-type zeolite formed in the absence of Mg.

The lack of significant zeolite formation in the case of the illite tested here can be explained by the low dissolution rate of the mineral under the treatment conditions of this study. Higher temperatures might have been necessary to promote appreciable mineral dissolution. Apart from small compositional changes detected with TEM-AEM, illite remained basically unaltered as revealed by XRD.

As a general rule, the formation of zeolites will be benefical for the stabilization of soils in earthen architecture because zeolites do not expand when in contact with water (Mumpton 1977). Furthermore, the formation of zeolites is expected to result in improved mechanical properties of clays and soils. Slaty et al. (2013) obtained a cement clinker replacement with a compressive strength of up to 23 MPa based on kaolinite activated with NaOH at 80 °C for 24 h. The authors related the high compressive strength of this material to the formation of zeolites and feldspatoids including phillipsite, natrolite and hydroxysodalite which fill pore spaces and bind the matrix. Furthermore, Roy (1999) suggested that the high durability of pozzolanic Roman cement mortars could be related to the presence of zeolites, such as analcime.

4.2.2. Non-zeolitic phases

Additional to zeolite formation, transformation of clay minerals into other phases of higher stability under highly alkaline conditions has been observed here.

As previously mentioned, the first modification clay minerals will undergo in solutions with high Na^+, K^+ or Ca^{2+} concentrations is cation exchange (Gaucher and Blanc 2006, Taubald et al. 2000, Bell 1996). Especially in the case of smectites, the clay swelling capacity might be reduced significantly if Na^+ is exchanged for K^+ (Anderson et al. 2010). Our research provided evidence for cation exchange in the case of saponite. In saponite samples portlandite formed upon exchange of Ca^{2+} for Na^+ or K^+ during alkaline treatment with the corresponding NaOH or KOH solutions.

The second phase of alteration under highly alkaline conditions is characterized by dissolution-precipitation processes, leading to the transformation of clay minerals (Bauer and Velde 1999, Drief et al. 2002).

The diffractograms of kaolinite treated with 5 M NaOH or 5 M KOH showed the predominance of zeolitic phases and a complete destruction of the clay after prolonged treatment. In contrast, the analysis of montmorillonite

and Alhambra Formation soil revealed the persistence of clay minerals. These, however, generally had a lower swelling capacity than the original clays. TEM-AEM analysis of the clay fractions of the treated montmorillonite and Alhambra Formation soil samples indicated an important degree of illitization of the smectitic clay minerals. Illitization is a common process under alkaline conditions and numerous investigations have been dedicated to the transformation of dioctahedral smectites into interstratified illite/smectite minerals (Inoue et al.1988, Eberl et al. 1993). During illitization, the substitution of Si for Al leads to an increase in tetrahedral layer charge which is compensated by cations. At a certain layer charge, which varies with different interlayer cations, the electrostatic forces will eventually overcome the cation hydration forces and lead to an interlayer collapse accompanied by a loss in swelling capacity (Karnland and Birgersson 2006). Additional to the illitization, the montmorillonite treated with 5 M NaOH also showed a certain degree of transformation into a saponitic clay mineral. Saponitization of montmorillonite has been previously reported in the case of Febex bentonite at a pH > 13 (Sanchez et al. 2006, Ramirez et al. 2002). A reduction in swelling capacity has generally been observed upon illitization. Saponization, in contrast, is not expected to alter clay swelling and is, thus, not beneficial to the stabilization of earthen architecture. Saponite generally showed a higher stability under highly alkaline conditions and its transformation into chlorite-type minerals might require an alkaline treatment over very long periods of time. XRD data of saponitic clay demonstrated a transformation into a random saponite-chlorite interstratification after alkaline activation for more than 1 year. In any case, the observed transformation into the above mentioned interstratification did not reduce the clays swelling capacity significantly and, thus, is not expected to improve the clays water resistance.

In a few samples, namely in the Alhambra Formation soil treated with $Ca(OH)_2$ or with 0.4 M NaOH, calcium silicate hydrate (CSH) phases have been identified. In the case of the Alhambra Formation soil treated with 0.4 M NaOH, the source of Ca must have been the clay minerals, in particular smectite, since calcite and dolomite were eliminated by an acetic acid attack during sample preparation. Berube et al. (1990) reported that in systems with high Si concentrations, CSH phases precipitate even if the calcium concentration is low. CSH phases observed in this study formed preferential when alkaline solutions of lower ionic strength were used which stabilized at a pH ≤ 10 after 60 days. In experiments where clay samples were treated with 5 M NaOH and 5 M KOH solutions (pH ≥ 12), Ca was generally associated with the formation of zeolites or alkaline earth metal hydroxides which later carbonated. Yip et al. (2005) came to a similar conclusion, stating that crystalline CSH might not be formed in very high pH environments.

Gaucher and Blanc (2006) summarized synthesis conditions of CSH phases and found that these phases normally formed when saturated $Ca(OH)_2$ solution or ~ 0.5 M alkaline solutions containing Ca, Na and K were used for the activation of clays, feldspars or quartz. CSH phases are the main products formed during the setting of Portland cement (Richardson 2008). They can be expected to contribute to the stabilization of soils and improve mechanical strength of earthen structures due to their cementing properties (Berube et al. 1990). According to Bell (1996) CSH and CASH (calcium aluminosilicate hydrate) would strengthen soil by binding adjacent soil particles together. The same is true for calcite detected in the case of saponite treated with 5 M NaOH and 5 M KOH. The cementing effect of calcium carbonate is comparable to that taking place during carbonation of lime mortars (Cazalla et al. 2000).

Furthermore, our research showed that a gel-like Ca-Mg silicate formed in the montmorillonite sample treated with 5 M KOH. This phase might also improve mechanical strength. Van Jaarsveld and van Deventer (1999) reported an increase in strength due to the formation of a similar phase in alkaline cements prepared using fly-ash activated with NaOH.

4.3. Surface area measurements of untreated and alkaline activated clay minerals

In the following sections the usefulness of surface area measurements for the evaluation of clay reactivity as well as for the study of the clay minerals evolution upon alkaline activation will be discussed.

4.3.1. Surface area measurements versus Particle size analyses of untreated clay minerals

Surface area is one of the most common parameters used to determine soil reactivity. However, our results suggest that the reactivity of pure clays was governed by structural and chemical characteristics rather than by surface area. Kaolinite and montmorillonite both revealed a high reactivity, but the BET surface area of kaolinite was less than half of that of montmorillonite. Choi et al. (2005) reported similar findings regarding the relationship between specific surface area and dissolution rates of clay minerals under alkaline conditions. According to the authors, kaolinite showed higher Si release even though it had a lower specific surface area than montmorillonite and illite treated under comparable conditions. Thus, surface area measurements seem only useful to evaluate the reactivity of soils of similar composition or of clays which dissolve following the same pathway in highly alkaline environments.

In general, BET surface area values here were in agreement with published data. The very low surface area of only 7.53 m^2/g of the illite from Beavers Bend State Park can be explained by the high cristallinity of this clay which has been acknowledged previously (Gaudette et al. 1966).

Generally, surface area will increase with decreasing particle size. However, particle size analyses revealed a very similar size of the primary maximum for all clays tested here (Figure 4-11). Pusch and Young (2006) recognized the insignificant differences in particle size between smectites and illites in the ultrafine size range and explained the higher surface area of montmorillonite if compared with illite considering the different length-to-thickness aspect ratio of both clays. Whereas, in illite it is commonly 5-25, it is at least 250 for montmorillonite. This leads to a 10-50 times larger surface area of montmorillonite. The larger surface area will certainly contribute to a higher reactivity of montmorillonite if compared to illite. The greater thickness of illite particles can be explained by the higher layer charge and the presence of K^+ as the main interlayer cation which confers stability to the clay crystal. In contrast, low charged Na-smectites are easily delaminated (Laird 2006).

Particle size analyses showed that saponite and montmorillonite had a much higher tendency to form micrometer-sized (1-50 μm) aggregates than

illite and kaolinite. Aggregation can render part of the smectite surface inaccessible to nitrogen. This tendency explains why measured, "apparent" surface areas of smectites are often lower than expected.

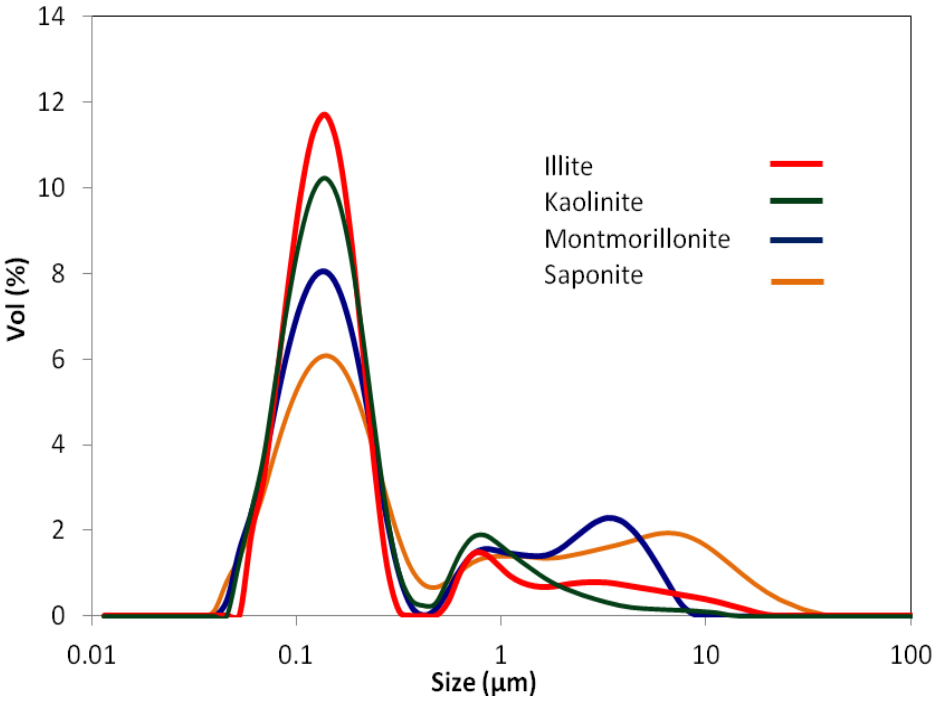

Figure 4-11. Particle size distribution of tested pure clay minerals.

4.3.2. Surface area evolution upon zeolite formation

It was hoped that BET surface area data would be useful to estimate the degree of transformation of clay minerals. Zeolites are very porous materials and their formation should lead to an increase of the samples surface area upon alkaline activation. However, this study showed that surface area measurements using nitrogen were not suitable to determine the degree of zeolite formation in the case of the tested clays. Actually, a surface area decrease was observed as a result of the transformation of less stable zeolites into zeolites of higher stability.

The pore size distribution of zeolites is fairly narrow (Mumpton 1977). Zeolites are microporous with a pore width below 1.5 nm (Thommes 2007). The detection limit of pore size distribution measurements using nitrogen is 0.5 nm according to Groen et al. (2003). In the case of clays treated here with 5 M NaOH, faujasite and hydroxysodalite were the detected zeolitic phases. The reported pore sizes for faujasite and hydroxysodalite are 0.8 and < 0.26 nm, respectively (Table 4-6). It is, thus, not surprising that only the formation

of faujasite led to a measureable surface area increase (Table 4-7), because the pore size of hydroxysodalite was below the detection limit of this technique. No increase in surface area of treated clays was detected upon formation of this zeolite (Table 4-7), even though, the porosity of hydroxysodalite is reported to be 35% (Table 4-6, Breck 1974). According to Sherry (1968) faujasite-type zeolites have the biggest cavities and cavity entrances of any known zeolites. The largest cavities of these zeolites might have a diameter of 12 Å. Thus, faujasite-type zeolites enable N_2 adsorption and contribute to a significant BET surface area increase as observed here.

Table 4-6. Pore size and porosity of zeolites according to Breck (1974).

Zeolite	Pore size (nm)	Porosity, %
Faujasite	0.8	47
Hydroxysodalite	< 0.26	35
Zeolite K-I	0.26	39
Chabazite	0.4	47
Zeolite K-F	0.26	31

Table 4-7. BET surface area (m^2/g) of untreated and treated clay minerals. Newly formed phases upon treatment with 5 M NaOH or 5 M KOH detected with XRD are included.

	Kaolinite		Montmorill.		Saponite		Illite		Alhambra Formation soil	
Untreated	23.79		63.58		143.75		7.53		70.78	
Treatment	NaOH	KOH	NaOH	KOH	NaOH	KOH	NaOH	KOH	NaOH	KOH
2 months		46.14 K-I								
6 months	273.33 FAU/ SOD	25.43 K-I/ CHA	82.81 SOD/ FAU	60.24 none	154.36 none	153.82 none			144.99 FAU	76.87 K-I
1 year	320.92 FAU/ SOD						25.69 H-Apa	22.99 (K-F)	244.38 FAU	65.14 K-I/ CHA
≥3.8 years	16.77 SOD	25.15 CHA/ K-F	141.39 FAU/ SOD	123.22 K-I/ K-F	144.77 S/C	136.81 -			109.87 FAU/ SOD	60.99 K-I/ CHA

Legend: FAU = faujasite, SOD = hydroxysodalite, K-I = zeolite K-I, CHA = chabazite, K-F = zeolite K-F, Sme = smectite, S/C = saponite-chlorite interstratification, H-Apa = hydroxyapatite, - = not determined.

In the case of clays treated here with 5 M KOH a surface area increase was detected which is associated with the formation of zeolite K-I. Zeolite K-I consists of hexagonal nanocrystals. It is thought that the measured surface area increase is mainly due to the contribution of the external surface of the nanosized crystals, because the diameter of the zeolite pores is below the detection limit of this technique (Table 4-6). The formation of chabazite generally resulted in a surface area decrease. Considering the pore sizes of chabazite (Table 4-6), it becomes clear that it falls below the detection limit of nitrogen sorption. Thus, only the zeolites external surfaces will be contributing to the samples total surface area. Given that an inverse relationship between surface area and crystal size exists, the increase in the amount of larger crystals will reduce the overall surface area. The reported BET surface area of K-chabazite is actually only 17.82 m^2/g (Ridha 2009).

The above shows a general problem connected with the use of nitrogen sorption for the determination of the surface area of microporous materials. Janssen and VanOorschot (1989) as well as Thommes (2007) acknowledged that nitrogen adsorption might not give reliable quantitative results in the case of microporous materials. These authors advocated the use of argon. Even though, the kinetic diameters of nitrogen (0.36 nm) and argon (0.34 nm) are quite similar, argon exhibits weaker interactions with most absorbents. Alternatively, CO_2 (kinetic diameter = 0.33 nm) might be used for surface area measurements (Thommes 2007). The same author suggested that BET surface area should be regarded as "apparent" surface area in the case of microporous solids with pores of molecular dimensions such as zeolites or carbon molecular sieves.

4.3.3. Surface area evolution upon formation of non-zeolitic phases

In the case of the tested illite sample treated with 5 M NaOH, the formation of apatite is assumed to be responsible for the detected surface area increase. Published values for surface areas of synthesized hydroxyapatite powder range from 31-43 m^2/g (Liu et al. 1997). Bose and Saha (2003) reported the synthesis of hydroxyapatite nanopowders with needle shape and spherical morphology and a BET surface area of up to 130 m^2/g.

The here tested saponite, on the other hand, showed no variation upon transformation into a random saponite-chlorite interstratification when treated with 5 M NaOH. Actually, a certain decrease in surface area due to the formation of this interstratification was expected. Note that the reported surface area for a regular saponite-chlorite interstratification (corrensite) is 36 m^2/g (Siegel et al. 1990). Our experimental result, thus, suggests that the degree of chloritization might still be quite low.

The saponite treated with 5 M KOH suffered a slight surface area decrease of less than 10 % which might have been caused by the formation of a gel-like phase which led to pore clogging. In the case of the saponite sample treated with KOH an unambiguous identification of the newly formed phase was not possible. This fact complicated the interpretation of the surface area data and revealed the main drawback of this method for the evaluation of the mineralogical evolution. Without a detailed identification of all mineralogical phases present in a sample, BET surface area measurements results might be misleading and result in an underestimation of the degree of transformation.

However, nitrogen sorption data provided evidence for the presence or absence of expandable clays. It was observed that the shape of the hysteresis loop of the nitrogen sorption isotherm experienced a clear modification, being less pronounced after the destruction of smectites. In order to make use of this technique for the identification of expandable clays in soil samples its sensitivity would have to be determined against soil samples with a known proportion of expandable clays.

4.4. Influence of organic matter (OM) on reactivity of soils

Our experimental results demonstrated that mineral dissolution and transformation upon alkaline activation with 5 M NaOH or 5 M KOH was delayed as a result of the presence of OM in the Alhambra Formation soil.

Typically, soil OM includes plant and animal residues at various stages of decomposition, cells and tissues of soil organisms, and substances synthesized by the soil population. It can be divided into non-humic substances such as carbohydrates, lipids and amino acids and humic substances. Conventionally, humic substances are divided according to their solubility characteristics:

1. Humic acid is not soluble under acidic conditions but is soluble in alkali.
2. Fulvic acid is soluble in acid and alkali.
3. Humin is not soluble in acid and alkali.

According to Cornejo and Hermosin (1996) humic substances and polysaccarides are the main components of soil OM which interact with the soil inorganic components, forming organo-mineral complexes.

The fact that part of the humic substances are insoluble under alkaline conditions are consistent with our findings, showing the presence of traces of OM even after 1 year of alkaline treatment with 5 M NaOH or 5 M KOH. The long-lasting passivation of the clay surface by OM might limit the efficiency of the alkaline treatment significantly and, in some cases, make it even unsuitable. Data by Claret et al. (2002) support these findings. Using scanning transmission X-ray microscopy, the authors demonstrated that the most reactive sites at the particle edges of illitic and smectitic clays were still protected by OM after 1-year treatment with highly alkaline solutions at 60 °C. However, the extractability of OM with alkaline treatments might depend on structural and compositional properties of clay minerals. Results by Wattel-Koekkoek (2002) showed that extraction of OM was facilitated by a lower CEC, for example in clays such as kaolinite which have a lesser ability to bind OM. Denef and Six (2005) found that illite led to stronger organic bonds when compared to kaolinite clay. Smectite is also considered as a more effective protector against microbial degradation of OM than kaolinite (Zech at al. 1997).

Originally, OM was thought to be adsorbed in a monolayer covering the entire clay mineral surface. However, this assumption was revised (Mayer 1994, 1999, Ransom et al. 1997). Newer findings showed that OM adsorption takes primarily place at reactive surface sites. Experimental data by Kubicki et al. (1997), who used salicylic acid as a humic acid analogue, supported the above theory showing that organo-mineral surface complexes were predominantly formed on the edges of illite grains. Kaiser and Guggenheim (2003) studied the relation between specific surface area of minerals and

different loading of OM. The authors suggested that OM sorption took place at specific reactive sites such as aluminol groups at illite edges or at single coordinated OH groups in iron oxyhydroxides. Studying continental margin sediments Ransom et al. (1997) found that OM was primarily associated with clay minerals, forming accumulations at edge-to-face junctions of clay particle.

Generally, it is assumed that sorption of dissolved organic carbon (DOC) is positively related to the specific surface area and CEC of clays. Data (Table 4-8) presented by Saidy et al. (2013) support this idea, showing that the DOC sorption capacity was greater for smectite than for illite and kaolinite. However, when the DOC sorption capacity was expressed on a surface area basis, the order of increasing sorption capacity changed: illite < smectite < kaolinite. The change in the order of sorption capacity seems to be related to structural differences of the clay minerals. The higher sorption capacity in the case of kaolinite can be explained considering the presence of >AlOH groups on the octahedral sheet that offer additional reactive sites for DOC sorption (Saidy et al. 2013). In contrast, DOC sorption mainly takes place at the reactive sites on the clay edge surface in the case of illite and smectite. Mayer (1999) concluded that, even though the mineral surface is only partially covered with OM, the mineral reactivity is still reduced because the reactive sites are the ones passivated by OM.

Table 4-8. Cation exchange capacity (CEC), surface area (SSA) and DOC sorption capacity (Q_{max}) of clays (Saidy et al. 2013).

Mineral	CEC (cmol/kg)	SSA(m^2/g)	Q_{max}(mg/g)	Q_{max}(mg/m^2)
Smectite	86.9	169.80	38.67	0.233
Illite	23.0	108.00	13.00	0.124
Kaolinite	8.9	6.01	2.82	0.464

The fact that the reactive sites of clay minerals were covered by OM which was difficult to remove even under extremely high alkaline conditions (i.e. prolonged treatment with 5 M NaOH or 5 M KOH) explains the delayed mineralogical evolution observed in the case of Alhambra Formation soil containing about 1 % OM. Experimental results of this study showed that clay minerals protected by OM experienced a significantly slower dissolution upon alkaline treatment using 5 M NaOH or 5 M KOH. This was particularly true for the kaolinite in the Alhambra Formation soil. Furthermore, the formation of new zeolitic phases was much faster in the absence of OM in the case of the Alhambra Formation soil samples treated with 5 M NaOH or 5 M KOH.

To the authors knowledge direct evidence for the retardation effect of OM on clay dissolution and transformation is limited in published scientific literature. As mentioned earlier, Claret et al. (2002) observed a low reactivity of illite, smectite and a randomly interstratified mixed layered mineral treated with highly alkaline solutions at 60 °C for 1 year which they blamed on the OM present in the soil from the Callovo-Oxfordian Formation. Chin and Mills (1991) studied the effect of organic ligands on kaolinite dissolution under acid conditions. They concluded that humic acid, which is insoluble under acid conditions, inhibited dissolution due to its high affinity for the kaolinite surface (82 % of added humic acid was adsorbed by the clay mineral). The authors further assumed that humic materials were bond to surface Al sites, resulting in a passivation of the clay surface. Additional evidence for the stabilizing effect of OM on clays was brought upon by a study performed by Ossa Ossa et al. (2013). The authors observed a delayed or even inhibited illitization of smectites in black shales of the Francevillian basin, Gabon. According to the authors the organo-mineral complexation might modify clay surface properties by preventing cation exchange during diagenesis.

The results of this study and published data clearly show that the soils OM content is an important parameter to be considered in the practical application of alkaline treatments for the consolidation of earthen structures.

4.5. Improved water resistance of treated adobe blocks

Our experimental results of adobe blocks prepared using Alhambra Formation soil and treated with alkaline solutions evidenced that NaOH and KOH reduced the water absorption rate and improved the water resistance. Both phenomena are thought to be the result of a reduction in the clays swelling capacity. The treatment with $Ca(OH)_2$, on the other hand, did not lead to an improved water behaviour.

As previously stated, the immediate effect of alkaline activation of clays is the exchange of cations for the dominant cations in the alkaline solution (Fernandez et al. 2006). Exchange of Na^+ for Ca^{2+} and, especially, K^+ will result in reduced intracrystalline swelling in the case of smectites (Anderson et al. 2010, Hensen and Smit 2002). Using Monte Carlo simulations, Boek et al. (1995) found that K^+ ions were reluctant to fully hydrate. Instead, once bonded to the clay surface, they screened the negatively charged surfaces more effectively than Na^+. Na^+ ions, on the other hand, were able to hydrate and became detached from the clay surface, forcing the clay layers apart in a series of discrete steps. According to Liu and Lu (2006) swelling in K-montmorillonite would not proceed beyond the double-layer hydrate (~ 15 Å). In summary, the replacement of interlayer cations for K^+ upon KOH treatment might reduce the swelling capacity of clays and result in a greater water resistance of earthen structures.

In the case of the NaOH treatment, cation exchange will not improve the adobe water behaviour (Anderson et al. 2010). However, highly concentrated alkaline solution might induce flocculation which results in decreased osmotic and intracrystalline swelling, depending on the electrolyte concentration (Karnland et al. 2007). Moway et al. (1979) explained that the presence of an electrolyte facilitates the flocculation of colloidal clay particles, resulting in an aggregation of particles and surface area decrease. Due to the decrease in surface area less water will be absorbed by the clay and swelling will be reduced. Van Olphen (1987) studied the effect of electrolytes on the flocculation behaviour of colloidal systems and concluded that two competing particle interaction forces exist: an electrical double layer repulsion force and an attractive van der Waals´force. The electrolyte has practically no effect on the van der Waals´attraction forces. However, the range of electrical double layer repulsion decreases with increasing electrolyte concentration, facilitating flocculation. Amorim et al. (2007) presented data of the effect of 0.1-1 M NaCl, KCl and $CaCl_2$ solutions on clay swelling. Generally, clay swelling decreased with increasing Na^+, K^+ and Ca^{2+} concentration. The authors observed that compared with NaCl, lower concentrations of KCl, and especially $CaCl_2$ were required to inhibit osmotic swelling (Figure 4-12). Alkaline solutions of higher ionic strength might even reduce intracrystalline clay swelling. According to

Lagaly (2006), 5 M NaCl would restrict smectite interlayer expansion to water bilayers (~ 15 Å), whereas 5 M KCl would result in a monolayer hydrate (~ 12.5 Å). Karnland (1997) suggested that a total loss of swelling pressure would be achieved with 6.1 M NaCl solution.

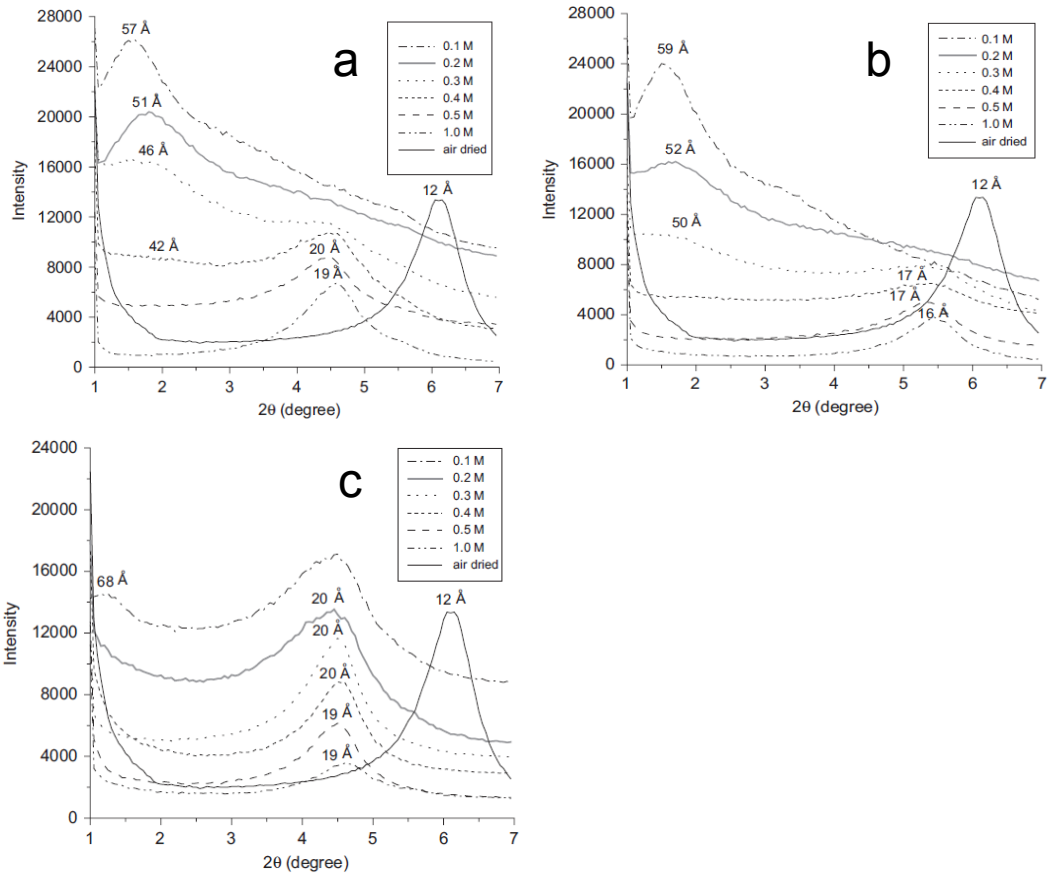

Figure 4-12. X-ray patterns of Na-bentonite in a) NaCl, b) KCL and c) $CaCl_2$ solutions Amorim et al. (2007).

The above described effects might, in part, be responsible for the here observed improved water behaviour of adobe blocks treated with 5 M NaOH or 5 M KOH.

In order to establish the main cause of the observed improved water resistance, adobe blocks were treated with concentrated KOH and KCl solutions. The experiment revealed a significantly higher water resistance of the adobe block treated with KOH if compared to the one treated with KCl. The former block hardly suffered any material loss upon immersion in water, whereas the material loss of the block treated with KCl was almost 75 % after 2 h of immersion. An untreated adobe block, included as control, suffered an even greater material loss of 90 %. These results suggest that the dissolution of clay minerals and the formation of amorphous phases (i.e. zeolite precursors) at high pH upon KOH treatment were responsible for the improved

water resistance. On the contrary, the effect of the KCl treatment, i.e., cation exchange or flocculation, seemed to have been of minor importance. Note that the material loss of the KCl-treated adobe block was only 15 % lower than the one of the untreated block. Results by Karnland et al. (2007) support these findings, showing a continued reduction in swelling pressures which amounted to 60 % when Wyoming bentonite was treated with 1 M NaOH. When 1 M NaCl was used the swelling pressure decreased instantly. However, the total reduction was only 25 % (Figure 4-13). The authors explained this behaviour with a reversible osmotic effect in the case of NaCl, whereas a permanent reduction was achieved using NaOH due to an instant osmotic effect, and a continuous mineral dissolution accompanied by beidellitization. However, the authors did not consider the formation of amorphous phases with cementing properties.

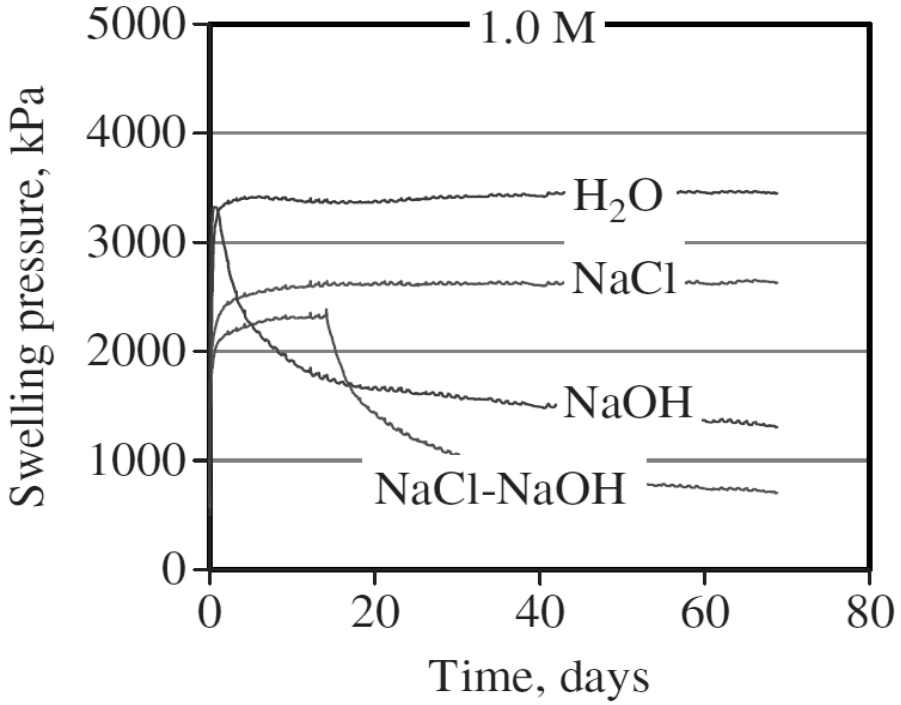

Figure 4-13. Swelling pressure response of Wyoming bentonite saturated with 1 M NaCl, 1 M NaOH and water (Karnland et al. 2007).

Our experimental results also showed that saturated $Ca(OH)_2$ solution did not have any positive effect on the water resistance of the treated adobe blocks. Calcium exchange of interlayer cations should result in flocculation because the closely held, divalent ions reduce the range of electrical double layer repulsion. This will allow clay particles to approach each other to form face-to-face aggregates after overcoming repulsion forces (Rolfe et al. 1960, Abdullah et al. 1999). Admittedly, the ionic strength of the saturated $Ca(OH)_2$ solution (0.025 M) used in this study is about one order of magnitude lower

than the ionic strength of the $CaCl_2$ solution reported to be effective in reducing clay swelling, which was 0.2 M (Amorim et al. 2007). Results presented by Karnland et al. (2007) are in agreement with our findings, showing that the swelling pressure of Wyoming bentonite was not significantly reduced upon treatment with saturated $Ca(OH)_2$ solution.

Our research also revealed that the treatment with saturated $Ca(OH)_2$ did not lead to significant clay mineral dissolution or formation of large amounts of phases with cementing properties. Both phenomena being crucial for the improved water resistance observed in the case of NaOH and KOH treatments.

4.6. Improved mechanical strength of treated adobe blocks

The observed increase in mechanical strength of adobe blocks treated with NaOH and KOH suggests that some mineralogical modifications took place which not only modified the swelling behaviour but also improved the mechanical properties. The $Ca(OH)_2$ treatment, on the other hand, did not result in any strength increase.

Furthermore, the drilling resistance of blocks treated with concentrated KOH solution was systematically higher than the one of the blocks treated with KCl solution. This result shows that the strength increase must have been principally connected to the formation of amorphous phases with cementing properties at high pH upon KOH treatment. Cation exchange or the osmotic effect of strong electrolytes, on the other hand, had an only minor effect, if any at all.

In this study amorphous phases, possibly zeolitic precursors, where detected in the case of adobe blocks treated with 5 M NaOH and cured for 50 days at room *T*. Zeolites, on the other hand, were not observed in alkaline activated adobe blocks. This is not surprising, because zeolites were only observed in powdered Alhambra Formation soil samples after a 4-month treatment with 5 M KOH and a 6-month treatment with 5 M NaOH. Criado et al. (2005) acknowledged the fact that the formation of well crystallised zeolites would require very long periods of time, whereas amorphous zeolite precursors are expected to form at ambient conditions within a short reaction time. It is concluded that mineralogical transformations were limited to the dissolution of clay minerals and the formation of amorphous phases. As a result of their amorphous character, these phases could not be detected with XRD in adobe blocks prepared from Alhambra Formation soil.

Such amorphous phases (zeolite precursors) are reported to improve the mechanical strength in alkali-activated cements (Xu and Van Deventer 2000). Amorphous zeolite precursors act as binding material in alkali-activated cements based on a wide variety of starting materials including fly-ash, furnace slag and clays. The concentrations of alkaline solutions used for the preparation of alkali-activated cements are similar to the ones employed here, i.e. 2-10 M alkaline solutions. However, these solutions are mixed directly with the aluminosilicates to be activated. Furthermore, compared to the conditions in this study, curing *T* is normally higher and reaction times are substantially shorter in the case of alkaline cements, resulting in amorphous to semi-crystalline matrices (Xu and Van Deventer 2000). Increasing curing *T* (up to a certain threshold *T*) generally leads to an increase in mechanical strength (Fernandez-Jimenez et al. 2008). For example, alkali-activated cements prepared using a mixture of kaolinite and fly-ash with KOH as an activator and cured at 30 °C for 24 h resulted in materials with a high mechanical

strength of up to 20 MPa (Van Jaarsveld et al. 2002). Duxson et al. (2005a) reported an even higher compressive strength of around 60 MPa for cements prepared from alkaline activated metakaolin cured for 20 h at 40 °C.

To our knowledge published data on mechanical strength development upon alkaline activation of a clay mineral at room *T* are very scarce. Davidovits (1994) found that the compressive strength of alkali-activated cement based on kaolinite treated with NaOH increased from 1 MPa to 8 MPa at 25 °C after 15 days of curing. Furthermore, the obtained cement was water resistant (Davidovits 1994, Davidovits and Boutterin (1982). The findings by Davidovits are consistent with the experimental results here, showing that alkaline activation can be performed at room *T* in a reasonable period of time.

The here observed improvements in water and mechanical resistance can be clearly related to the interaction between the alkaline activator and the aluminosilicates in the treated adobe blocks. The fact that we did not observe crystalline zeolitic phases in treated adobe blocks, indicates that the formation of amorphous zeolitic precursors should be sufficient in promoting improvements in water and mechanical resistance. A few researchers even question whether the formation of crystalline zeolitic phases is desirable for achieving improved mechanical strength. Grutzeck et al. (2004) suggested that the formation of zeolites, depending on their morphology, might disrupt the alkali-activated cement matrix. They mentioned the case of analcime which crystallizes in large cubes. Fernandez-Jimenez et al. (2008) came to a similar conclusion, observing higher mechanical strength in alkali-activated cements with higher amorphous gel/zeolite ratio.

4.7. Salt formation upon alkaline treatment of clays

As mentioned earlier, during the treatment of soils with alkaline solutions, unreacted alkali might react with atmospheric CO_2 to form carbonates such as Na_2CO_3, K_2CO_3 and $KHCO_3$. These carbonates are highly soluble and potentially harmful to earthen structures.

A significant amount of research has been dedicated to the analysis of the damaging effect of salt weathering on historic architecture, archaeological sites and civil engineering works (roads, dams and building foundations). Scientists have tried to rank the damaging potential of various salts. Available data on the damaging potential of salts generally rank Na_2SO_4 as the most harmful salt. However, in some studies Na_2CO_3 was considered as the most destructive salt (Goudie and Viles 1997). Differences in ranking might depend on variables such as environmental conditions, i.e. *T* and RH (Rodriguez-Navarro and Doehne 1999), or substrate characteristics, i.e. total porosity and pore size distribution. Data on the damaging potential of K_2CO_3 are very scarce and $KHCO_3$ has not been included in salt crystallization tests to the authors' knowledge (see extensive review by Goudie and Viles 1997).

Our laboratory study of the damaging effect of various salts revealed that Na_2SO_4 and Na_2CO_3 crystallization caused severe damage to the porous material tested. In the case of Na_2SO_4, massive efflorescence and material loss due to scaling was observed. Na_2CO_3, on the other hand, produced subflorescence which resulted in fracturing as well as severe scaling. The damaging effect of K_2CO_3 was less pronounced and included efflorescence and the formation of minor fractures. In the case of $KHCO_3$ some efflorescence was observed without any detectable deterioration.

A higher damaging potential of Na_2CO_3 compared to K_2CO_2 has also been recognized in conservation treatments using sodium and potassium silicates for the consolidation of earthen architecture (Oliver 2008). The application of alkaline silicates can result in the formation of important amounts of sodium and potassium carbonates upon reaction with atmospheric CO_2 (Arnold and Zehnder 1990). The use of sodium silicates as a consolidant has actually been questioned because of the formation of damaging subflorescence under unfavorable conditions (Kühn 1981). In contrast, K_2CO_3 was often considered to be harmless because it would not crystallize due to its highly hygroscopic/deliquescent nature (Arnold and Zehnder 1990). However, the same authors warn that K_2CO_3 might react with different earth alkali salts to form potassium sulphates, nitrates and chlorides with high damaging potential. The same applies for Na_2CO_3.

As mentioned previously, the formation of $CaCO_3$, $CaCO_3{\cdot}H_2O$, Na_2CO_3 and $KHCO_3$ has been detected during alkaline activation of the here tested clays. $KHCO_3$, $CaCO_3$ and $CaCO_3{\cdot}H_2O$ are not expected to produce any

significant damage and might be even beneficial in the case of the latter two. Na_2CO_3, on the other hand, has been proven to be deleterious in the here performed salt crystallization tests, suggesting that the use of KOH is preferable for the consolidation of earthen structures.

Carbonate formation is a common phenomenon under highly alkaline conditions. Criado et al. (2005) described the tendency of highly alkaline systems to reduce their pH through neutralization. A common neutralization process is the carbonation of lime mortar. In the case of alkaline activation, excess of metal alkali hydroxide can react with atmospheric CO_2 which results in the formation of carbonates and in a reduction of the pH. Carbonation requires water and is, thus, favoured by high RH. However, complete water saturation in the case of porous materials hinders carbonation because diffusion of CO_2 becomes difficult. In porous building materials the carbonation process proceeds from the outside inward (Elert et al. 2002). Porefilling caused by the precipitation of carbonates will hinder the access of CO_2 and eventually slows down carbonation over time.

During the application of the alkaline consolidation treatment to earthen structures, conditions are favourable for carbonation to occur. Whether the amount of precipitated carbonates during alkaline activation is large enough to create damage in earthen structures is not known. In any case, the risk of the formation of damaging carbonates can be reduced by the addition of $Ca(OH)_2$ to the alkaline activation solution. Upon carbonation the formation of the less soluble $CaCO_3$ would be favoured instead of highly soluble Na_2CO_3 or K_2CO_3. See Table 4-9 for solubility data of carbonates.

Additional to the damaging effect of carbonates, the subsequent reduction in pH might hinder the transformation of clay minerals during the alkaline treatment. See Table 4-9 for the pH of various carbonates in solution. Criado et al. (2005) also reported a reduced rate of alkaline aluminosilicate gel formation due to the formation of sodium bicarbonate and the subsequent pH reduction during alkaline activation of fly ash using NaOH.

Table 4-9. pH and solubility of various carbonates.

Carbonate	pH (0.01 N solutions)	Solubility (g/100ml at 20 °C)
Na_2CO_3	11.6	21.5
K_2CO_3	11.5	112
$KHCO_3$	8.2	33.7
$CaCO_3$	(saturated solution) 9.4	0.0014 (25 °C)

4.8. Dispersion of clay minerals during sample preparation - pitfall

During sample preparation sodium hexametaphosphate (calgon) was used as a dispersant. The dispersant action of phosphates can be attributed to the sequestration of divalent cations (Rolfe et al. 1960).

XRF and TEM data of several clay samples of this study, namely montmorillonite, saponite and illite, revealed the presence of phosphate, a residue after the treatment with sodium hexametaphosphate. Phosphate adsorption on clay minerals is assumed to be a rapid process which is completed within 24 h. At pH 7-8, montmorillonite and illite showed significantly higher adsorption capacities for phosphate than kaolinite (Table 4-10, Edzwald et al. 1976). General agreement exist that phosphate adsorption decreases with increasing pH (Edzwald et al. 1976, Lake and MacIntyre 1977).

Table 4-10. Phosphate adsorption capacity (mg P/g) of clay minerals (Edzwald et al. 1976).

Mineral	Adsorption capacity at pH 7-8
kaolinite	0.091
montmorillonite	0.746
illite	2.51

Golubev et al. (2006) studied the effect of various ligands on smectite dissolution at pH 6-6.5 and reported an inhibiting action of phosphates. However, at higher pH the inhibiting action should be reduced due to the lower amount of phosphates adsorbed.

In this study, the effect of the sodium hexametaphosphate on the clays reactivity has not been examined in detail. In any case, the passivating effect of phosphate on the transformation of kaolinite is negligible, because the phosphate adsorption capacity of this clay mineral seems to be small (Edzwald et al. 1976). In the case of the illite in this study, an insoluble calcium phosphate (apatite) formed, the calcium source being the tap water used during sample preparation. A significant interference of apatite formation with clay dissolution is not expected, since apatite precipitated as non-passivating nanocrystals. Phosphate might have had an inhibiting effect on smectite dissolution in this study. However, pure montmorillonite and smectites in the Alhambra Formation soil showed extensive transformation and a possible passivating effect of phosphates, if any, seems to be negligible and transitory.

In any case, in order to prevent any possible interactions, the use of phosphates should be avoided in future studies and an alternative dispersion method should be employed.

4.9. Practical application

In the following section some aspects concerning the practical application of alkaline treatments for the consolidation of earthen architecture will be discussed.

4.9.1. Study of the adobe/soil characteristics prior to the consolidation treatment

The determination of the soil/adobe composition prior to the consolidation treatment is of eminent importance. First of all, the use of alkaline solutions might not be indicated in the case of adobe/soils with extremely high organic matter content, because reactions between clay minerals and alkaline activator are substantially retarded. Furthermore, soils dominated by certain clay minerals such as saponite might not experience important improvement upon treatment. Transformation into clay minerals which still present relatively high swelling capacity (i.e. corrensite) in the case of saponite, might prevent an improvement in water and mechanical resistance.

4.9.2. Application of the consolidation treatment

The application of alkaline solutions in situ can be done by brushing or spraying. Several applications might be necessary and the earthen structure should be covered with an impermeable plastic in between treatments to reduce water evaporation and increase penetration. If possible the treatment should be performed during the season with highest precipitation to further reduce the risk of early drying. However, *T* is also an important factor since mineral dissolution and transformation will be faster at higher *T*. Bell (1996) stated that pozzolanic reactions would be significantly retarded at *T* around 4 °C and might even cease at lower *T*. After dormant periods, the pozzolanic reaction potential can be regained when *T* increases. The same should be true for excess alkalis which remained in the earthen structure after drying. During the rainy season, moisture supply will result in the rehydration/dissolution of such alkalis, facilitating further reaction between alkaline activator and clay minerals. Admittedly, part of the excess alkalis might have carbonated over time. Carbonation reaction proceeds from the outside inward (Elert et al. 2002), thus, only the outer surface may experience carbonation. Moorehead (1986) claimed that carbonation times become impractical in the case of lime mortars when the diffusion distance of CO_2 to the reaction site is more than 5 mm in dense compacts and 25 mm in porous compacts. It is, therefore, reasonable to assume that alkalis deeper in the structure might be still available for further reaction with clay minerals.

5. Conclusions

The application of alkaline solutions for the consolidation of earthen structures can be regarded as a valuable alternative to conventional consolidation treatments. The experimental results of this study have clearly shown that clay minerals can be transformed into cementing materials using alkaline solutions at room *T*. These cementing materials included zeolite precursors, zeolites, CSH phases and calcite. Additionally, some clay minerals experienced transformation into mixed-layer clays.

The response towards alkaline activation was not the same for the different clay minerals tested here. Kaolinite and dioctahedral smectite dissolved and transformed readily. Saponite experienced a slower transformation into a corrensite-type mineral which still showed expansion. The highly crystalline illite tested here, on the other hand, only suffered minor chemical modifications.

The different response of clay minerals can be related to structural and compositional characteristics. Kaolinite, a 1:1 clay, showed extensive dissolution because >AlOH groups on the gibbsite layer additional to the hydroxyl groups at broken edges, steps and defect sites contributed to the clay´s overall reactivity. In contrast, the contribution of the basal layer to the reactivity of 2:1 clay minerals is limited and dissolution takes mainly place at the edge surfaces. The lower reactivity of illite if compared with montmorillonite, both diactahedral 2:1 clays, can be explained considering compositional differences. Illite has a much higher net charge due to isomorphic substitution in the tetrahedral layer which is compensated by K^+. In montmorillonite, on the other hand, layer charge is mainly caused by octahedral substitution and is compensated by Na^+. The compositional differences result in a more stable structure in the case of illite which commonly has a higher crystallinity and lower specific surface area than montmorillonite and does not experience intracrystalline swelling. Montmorillonite, in contrast swells readily in polar solvents and offers a much larger surface area for reaction. Saponite, being an expandable clay, showed lower reactivity under alkaline conditions. This is thought to be due to the presence of mainly Mg in its octahedral layer. Furthermore, isomorphic substitution commonly occurs in the tetrahedral layer and is compensated by Ca^{2+} or Mg^{2+} which might add to the clay´s stability.

Whereas extensive zeolite formation was observed in kaolinite and montmorillonite, no zeolites were detected in the case of saponite which is thought to be due to the low Al and high Mg content of this clay mineral. In illite samples treated with KOH, some zeolites were detected. However, these are thought to have formed from kaolinite which was present as an impurity.

The clay minerals of the Alhambra Formation soil, a mixture of kaolinite, smectite, illite and paragonite, generally showed a similar transformation path as observed for the pure clays. However, kaolinite experienced a faster dissolution in the case of the Alhambra Formation soil, because the crystallinity of this kaolinite was lower than the one of the pure clay.

Apart from the mineral composition, the soil organic matter content might have an important influence on the successfulness of the alkaline treatment. Our results indicate that mineral dissolution and transformation was delayed as a result of the presence of organic matter. The organic matter content was 1 wt% in the case of the Alhambra Formation soil studied here.

The different response of the various clay minerals as well as the influence of organic matter on the efficiency of the treatment shed light on an important aspect to be considered prior to the application of any consolidation treatment. A detailed study of the earthen materials mineral composition and organic matter content is necessary. For example, a high concentration of saponitic clays or an elevated organic matter content may render this treatment inefficient.

This study further revealed that using saturated $Ca(OH)_2$ solution, it was not possible to maintain a high enough pH in order to promote adequate mineral dissolution and transformation. Highly concentrated NaOH and KOH solutions, in contrast, resulted in extensive transformation in the case of the majority of clay minerals tested here. In general it can be concluded that a sufficiently high pH well above 10 has to be maintained during the treatment to ensure adequate mineral dissolution and transformation.

The structure directing role of the different cations was evident during alkaline activation. When NaOH was used a faujasite-type zeolite as well as a hydroxy-sodalite formed independent of the clay mineral used as the starting material. In the case of KOH, zeolite K-I together with zeolite K-F and/or a chabazite-type zeolite were observed.

As indicated above, both, NaOH and KOH solutions were effective in producing mineralogical changes. However, salt crystallization tests evidenced that sodium carbonates, which have been observed to form during the alkaline treatment with NaOH, have a much higher damaging potential than potassium carbonate and/or bicarbonate. The later phases were observed to form as a byproduct of the KOH treatment. Considering these results, it can be concluded that KOH solutions are preferable for the use in conservation treatments. Furthermore, an addition of $Ca(OH)_2$ to the alkaline solution is advisable to promote the precipitation of $CaCO_3$ and reduce the risk of the formation of harmful, more soluble carbonates.

In situ treatments of adobe test blocks with highly alkaline solutions showed that an improvement in water resistance was achieved. A comparative study using concentrated KCl confirmed that the observed improved resistance was due to clay mineral dissolution and transformation into amorphous phases with cementing properties at high pH. Cationic exchange or the osmotic effect exerted by highly concentrated electrolytes, on the other hand, seemed to have played a negligible role in this improvement. The mineralogical and morphological study of the treated adobe test blocks led us to the conclusion that amorphous phases, possibly zeolite precursors that formed after 50 days of curing, served as cementing material and improved mechanical strength. Crystalline zeolitic phases were not observed in the treated adobe test blocks. It is believed that the formation of zeolites, which would require longer treatment durations, is not necessary in order to achieve an increase in strength.

After a thorough examination of the experimental results, some aspects were identified which might be worth investigating further.

In this study, adobe test blocks were only treated with highly alkaline solutions, i.e., 5 M KOH and 5 M NaOH. Tests should be performed to evaluate whether less concentrated solutions would also be effective in improving the water resistance and mechanical strength of earthen materials. In this way the risk of carbonate formation due to excess alkali as well as treatment cost would be reduced. Furthermore, the treatment would be less invasive from an environmental point of view. Evidently, the required alkaline solution concentration will depend on the soils clay content and the composition of the clay minerals.

The last point leads to another aspect which would be important to examine: The influence of the clay composition on the effectiveness of the alkaline treatment. It would be interesting to include adobe blocks prepared from soils with elevated smectite or organic matter content in a future study, in order to evaluate whether the treatment would be effective under such adverse conditions.

Another aspect to be considered is the possibility of preparing restoration mortars using a mixture of soil and an alkaline solution. These mortars might be a valuable alternative to conventional mortars prepared using Portland cement mixtures and could be used for capping or general protection of vertical walls of earthen structures.

Finally, the positive outcome of the laboratory results should be confirmed by an in situ study in the field. For this purpose adobe test walls or, ideally, historic earthen structures could be treated with alkaline solutions and their performance monitored over long periods of time.

7. Bibliography

Abad, I, Jimenez-Millan, J.J., Molina, J.M., Nieto, F., Vera, J.A., Anomalous reverse zoning of saponite and corrensite caused by contact metamorphism and hydrothermal alteration of marly rocks associated with subvolcanic bodies, *Clays and Clay Minerals* **51** (2003) 543–554.

Abdullah, W.S., Alshibli, K.A., Al-Zou`bi, M.S. Influence of pore water chemistry on the swelling behaviour of compacted clays, *Applied Clay Science* **15** (1999) 447-462.

Ahmadi, S., *Adobe conservation: Evaluation of silicone and acrylic consolidants*, MA Thesis, Queen's University, Kingston, Ontario, Canada, (2008).

Aiello, R., Crea, F., Alfonso, N., Subotic, B., Testa, F., Influence of cations on the physicochemical and structural properties of aluminosilicate gel precursors. Part1. Chemical and thermal properties, *Zeolites* **11** (1991) 767-775.

Allison, F.E., 1973, Chapter 9 - The interaction of organic matter with clays, *Developments in Soil Science – Soil Organic Matter and Its Role in Crop Production*, (1973) Elsevier, Amsterdam, 162-177.

Amorin, C.L.G., Lopes, R.T., Barroso, R.C., Queiroz, J.C., Alves, D.B., Perez, C.A., Schelin, H.R., Effect of clay-water interactions on clay swelling by X-ray diffraction, *Nuclear Instruments and Methods in Physics Reseach* **A 580** (2007) 768-770.

Anderson, R.L., Tatcliffe, I., Greenwell, H.C., Williams, P.A., Cliffe, S., Coveney, P.V., Clay swelling - A challenge in the oilfield, *Earth-Science Review* **98** (2010) 201-216.

Armbrust, D.V. and Dickerson, J.D., Temporary wind erosion control: cost and effectiveness of 34 commercial materials, *Journal of Soil Water Conservation* **26** (1971) 154-157.

Arnold, A., Zehnder, K., Salt weathering on monuments, *Advanced Workshop "Analytical methodologies for the investigation of damaged stones"*, Zezza, F. (ed.), Pavia, Italy, 14-21 Sept. 1990, 31-58.

Arnott, R.J., Particle sizes of clay minerals by small-angle X-ray scattering, *American Mineralogist* **50** (1965) 1563-1575

Ashurst, J., Ashurst, N., *Mortars, plasters and renders*, English Heritage Technical Handbook Vol.3, Gower Technical Press, England, (1988) 85pp.

Aylmore, L.A.G., Sills, I.D., Quirk, J.P., Surface area of homoionic illite and montmorillonite clay minerals as measured by sorption of nitrogen and carbon dioxide, *Clays and Clay Minerals* **18** (1970) 91-96.

Azanon, J.M., Azor, A., Booth Rea, G., Martin Rosales, W., de Justo Aplanes, J.L., Torcal, F., Espinar, M., Las fallas del recinto de la Alhambra, *Geogaceta* **34** (2003) 159-162.

Baily, S.W., Nomenclature for regular interstratifications, *Clay Minerals* **17** (1982) 243-248.

Bain, J.A., Morgan, D.J., The role of thermal analysis in the evaluation of impure clay deposits as mineral raw materials, *Clay Minerals* **8** (1969) 171-192.

Bala, P., Samantaray, B.K., Srivastava, S.K., Synthesis and characterization of Na-montmorillonite-alkylammonium intercalation compounds, *Materials Research Bulletin* **35** (2000) 1717-1724.

Barbosa, V.F.F., MacKenzie, K.J.D., Synthesis and thermal behaviour of potassium sialate geopolymers, *Materials letters* **57** (2003) 1477-1482.

Barbosa, V.F.F., MacKenzie, K.J.D., Thaumaturgo, C., Synthesis and characterization of materials based on inorganic polymers of alumina and silica: sodium polysialate polymers, *International Journal of Inorganic Materials* **2** (2000) 309-317.

Barrer, R.M., *Hydrothermal Chemistry of Zeolites*, Academic Press, London (1982) 360pp.

Barrer, R.M., Cole, J.F., Sticher, H., Chemistry of soil minerals. Part V. Low temperature hydrothermal transformations of kaolinite, *Journal of the Chemical Society (A)* (1968) 2475-2485.

Barrer, R.M., Davies, J.A., Rees, L.V.C., Comparison of the ion exchange properties of zeolites X and Y, *Journal of Inorganic and Nuclear Chemistry* **31** (1969) 2599-2609.

Barrer, R.M., MacLeod, D.M., Intercalation and sorption by montmorillonite, *Transaction of the Faraday Society* **50** (1954) 980-989.

Barrer, R.M., Mainwaring, D.E., Chemistry of Soil Minerals. Part XIII. Reactions of metakaolinite with single and mixed bases, *Journal of the Chemical Society (Dalton Transactions)* (1972) 2534-2546.

Barth-Wirsching, U., Höller, H., Experimental studies on zeolite formation conditions, *European Journal of Mineralogy* **1** (1989) 489-509.

Bauer, A., Berger, G., Kaolinite and smectite dissolution rate in high molar KOH solutions at 35° and 80° C, *Applied Geochemistry* **13** (1998) 905-916.

Bauer, A., Velde, B., Berger,G., Kaolinite transformation in high molar KOH solutions, *Applied Geochemistry* **13** (1998) 619-629.

Bauer, A., Velde, B., Smectite transformation in high molar KOH solutions, *Clay Minerals* **34** (1999) 259-273.

Beaufort, D., Baronnet, A., Lanson, B., Meunier, A., Corrensite : A single phase or a mixed-layer phyllosilicate in the saponite-to-chlorite conversion series ? A case study of Sancerre-Couy deep drill hole (France), *American Mineralogist* **82** (1997) 109-124.

Beaufort, D., Meunier, A., Saponite, corrensite and chlorite-saponite mixed-layers in Sancerre-Couy deep drill-hole (France), *Clay Minerals* **29** (1994) 47-61.

Becerro, A., Mantovani, M., Escudero, A., Mineralogical stability of phyllosilicates in hyperalkaline fluids: Influence of layer nature, octahedral occupation and presence of tetrahedral Al, *American Mineralogist* **94** (2009) 1187-1197.

Beene, G.M., Bryant, R., Wiliams, D.J.A., Electrochemical properties of illites, *Journal of Colloid and Interface Science* **147** (1991) 358-369.

Bell, F.G., Lime stabilization of clay minerals and soils, *Engineering Geology* **42** (1996) 223-237.

Belver, C., Bañares Muñoz, M.A., Vicente, M.A., Chemical activation of a kaolinite under acid and alkaline conditions, *Chemistry of Materials* **14** (2002) 2033-2043.

Benavente, D., Garcia del Cura, M.A., Garcia-Guinea, J., Sanchez-Moral, S., Ordonez, S., Role of pore structure in salt crystallization in unsaturated porous stone, *Journal of Crystal Growth* **260** (2004) 532-544.

Bereznitski, Y., Jaroniec, M., Maurice, P., Desorption characterization of two Clay Minerals Society standard kaolinites, *Journal of Colloid and Interface Science* **205** (1998) 528-530.

Berube, M.A., Chaquette, M., Locat, J., Effects of lime on common soil and rock forming minerals, *Applied Clay Science* **5** (1990) 145-163.

Boardman, D.J., Glendinning, S., Rogers, C.D.F., Development of stabilisation and solidification in lime-clay mixes, *Geotechnique* **50** (2001) 533-543.

Boek, E.S., Coveney, P.V., Skipper, N.T., Monte Carlo molecular modeling studies of hydrated Li-, Na- and K-smectites: Understanding the role of potassium as a clay swelling inhibitor, *Journal of the American Chemical Society* **117** (1995) 12608-12617.

Bose, S., Saha, S.K., Synthesis and characterisation of hydroxyapatite nanopowders by emulsion technique, *Chemistry of Materials* **15** (2003) 4464-4469.

Bosnar, S., Antonic-Jelic, T., Bronic, J., Krznaric, I., Subotic, B., Influence of anions on the kinetics of zeolite A crystallization: a population balance analysis, *Journal of Crystal Growth* **267** (2004) 270-282.

Boynton, R.S., Lime and Limestone in *Encyclopedia of Chemical Technology*, 3rd edn., Wiley, New York (1984) 343-382.

Brady, P.V., Cygan, R.T., Nagy, K.L., Molecular controls on kaolinite surface charge, *Journal of Colloid and Interface Science* **183** (1996) 356-364.

Brady, P.V., Walther, J.V., Controls on silicate dissolution rates in neutral and basic pH solutions at 25 °C, *Geochimica et Cosmochimica Acta* **53** (1989) 2823-2830.

Breck, D.W., *Zeolite molecular sieves – Structure, chemistry and use*, John Wiley and Sons, Inc., New York (1974) 771pp.

Brigatti, M.F., Poppi, L., Chrystal chemistry of corrensite: A review, *Clays and Clay Minerals* **32** (1984) 391-399.

Bristow, T.F., Kennedy, M.J., Derkowski, A., Droser, M.L., Jiang, G., Creaser, R.A., Mineralogical constraints on the paleoenvironments of the Ediacaran Doushantuo Formation, *Proceedings of the National Academy of Science* **106** (2009) 13190-13195.

Brown, P.W. and Clifton, J.R. Adobe I: The properties of adobe, *Studies in Conservation*, **23** (1978) 139-146.

Brown, W.W., Robbins, C.R., Clifton, J.R., Adobe II: Factors affecting the durability of Adobe structures, *Studies in Conservation* **24** (1979) 23-39

Brunauer, S., Emmett, P.H., Teller, E., Adsorption of gases in multimolecular layers, *Journal of the American Chemical Society* **60** (1938) 309-319.

Burton, G., Vapour glycolation, *American Mineralogy* **40** (1955) 124-126

Caballero, E., Jimenez de Cisneros, C., Huertas, F.J., Huertas, F., Pozzuoli, A., Linares, J., Bentonitas from Cabo de Gata, Almeria, Spain: a mineralogical and geochemical overview, *Clay minerals* **40** (2005) 463-480.

Cartlidge, S., Meier, W.M., Solid state transformations of synthetic CHA- and EAB-type zeolites in sodium form, *Zeolites* **4** (1984) 218-225.

Carroll, D., Starkey, H.C., Reactivity of clay minerals with acids and alkalines, *Clays and Clay Minerals* **19** (1971) 321-333.

Cazalla O., Rodriguez-Navarro C., Sebastian E., Cultrone, G., and de la Torre M. J., Aging of lime putty: Effects on traditional lime mortars carbonation, *Journal of the American Ceramic Society* **83** (2000) 1070-1076.

Celis, R., Cornejo, J., Hermosin, M.C., Surface fractal dimensions of synthetic clay-hydrous iron oxide associations from nitrogen adsorption isotherms and mercury porosity, *Clay minerals* **31** (1996) 355-363

Celis, R., Cornejo, J., Hermosin, M.C., Textural properties of synthetic clay-ferrihydrate associations, *Clay Minerals* **33** (1998) 395-407.

Chaudhuri, S., Brookins, D.G., The rb-Sr systematics in acid-leached clay minerals, *Chemical Geology* **24** (1979) 231-242.

Chermak, J.A., Low temperature experimental investigation of the effect of high pH NaOH solutions on the Opalinus Shale, Switzerland, *Clays and Clay Minerals* **40** (1992) 650-658.

Chermak, J.A., Low temperature experimental investigation of the effect of high pH KOH solutions on the Opalinus Shale, Switzerland, *Clays and Clay Minerals* **41** (1993) 365-372.

Chiari, G., Chemical surface treatments and capping techniques of earthen structures: A long-term evaluation, *Proceedings of the 6th International Conference on the Conservation of Earthen Architecture: Adobe 90 preprints*: October 14-19, 1990, Las Cruces, New Mexico. Grimstad, K. (ed.), The Getty Conservation Institute, Marina del Rey, California, 267-273.

Chin, P.-K.F., Mills, G.L., Kinetics and mechanisms of kaolinite dissolution: effects of organic ligands, *Chemical Geology* **90** (1991) 307-317.

Choi, S., Amistadi, M.K., Chorover, J., Clay weathering and contaminant dynamics in a caustic aqueous system. I. Wet chemistry and aging effects, *Geochimica et Cosmoquimica Acta* **69** (2005) 4425-4436.

Claret, F., Bauer, A., Schäfer, T., Griffault, L., Lanson, B., Experimental investigation of the interaction of clays with high-pH solutions: A case study from the Callavo-Oxfordian formation, Muese-Haute Marne Underground Laboratory (France), *Clays and Clay Minerals* **50** (2002) 633-646.

Coffman, R., Selwitz, C., Agnew, N., The Getty adobe research project at Fort Selden II. A study of the interaction of chemical consolidants with adobe and adobe constituents, *Proceedings of the 6th International Conference on the Conservation of Earthen Architecture: Adobe 90 preprints*: October 14-19, 1990, Las Cruces, New Mexico. Grimstad, K. (ed.), The Getty Conservation Institute, Marina del Rey, California, 250-254.

Coles, C.A., Young, R.N., Aspects of kaolinite characterization and retention of Pb and Cd, *Applied Clay Science* **22** (2002) 39-45.

Conde-Pumpido, R., Ferron, J.J., Campillo, G., Influence of granulometric factors on the rheology of kaolins of Galicia, Spain, *Applied Clay Science* **3** (1988) 177-185.

Cornejo, J., Hermosin, M.C., Interaction of humic substances and soil clays, Chapter 15, *Humic substances in terrestrial ecosystems*, Piccolo, A. (ed.), Elsevier Science (1996) 595-624.

Criado, M., Palomo, A., Fernández-Jiménez, A., Alkali activation of fly ashes. Part 1: Effect of curing conditions on the carbonation of the reaction products, *Fuel* **84** (2005) 2048-2054.

Cruciani, G., Zeolites upon heating: Factors governing their thermal stability and structural changes, *Journal of Physics and Chemistry of Solids* **67** (2006) 1973-1994.

Cuevas Rodriguez, J., Comportamiento hidrotermal de las arcillas saponiticas de la cuenca de Madrid, *Estudios Geológicos* **49** (1993) 137-146.

Cuevas, J., Garralon, A., Ramirez, S., Leguey, S., Hydrothermal alteration of a saponitic bentonite: Mineral reactivity and evolution of surface properties, *Clay Minerals* **36** (2001) 61-74.

Cultrone, G., Estudio mineralógico-petrográfico y físico-mecánico de ladrillos macizos para su aplicación en intervenciones del Patrimonio Histórico, Tesis Doctoral, Universidad de Granada (2001) 292pp.

Cundy, C.S., Cox, P.A., The hydrothermal synthesis of zeolites: Precursors, intermediates and reaction mechanism, *Microporous and Mesoporous Materials* **82** (2005) 1-78.

Dabkowska-Nasret, H., Dlugosz, J., Occurence and characteristics of layer silicates in alluvial soils from the Lower Wisla river valley, Poland, *Applied Clay Science* **11** (1996) 77-83.

Davidovits, J., Boutterin, C., *Procédé de fabrication d´objets pour le bâtiment a partir de sols et argiles latéritiques*, French Patent 2,528,822 (1982).

Davidovits, J., Geopolymers: Man-made rock geosynthesis and the resulting development of very early high strength cement, *Journal of Materials education* **16** 2&3 (1994) 91-139.

Davis, M.E., Lobo, R.F., Zeolite and Molecular Sieve Synthesis, *Chemistry of Materials* **4** (1992) 756-768.

Deer, W.A., Howie, R.A., Zussman, J., *Rock-forming Minerals*, Vol. 3 Sheet Silicates, Longmans, London (1962) 270pp.

de la Torre, M.J.; Sebastián E., Rodríguez, J., A study of the wall material in the Alhambra (Granada, Spain), *Cement and Concrete Research* **26** 6 (1996) 825-839.

de la Villa, R.V., Cuevas, J., Ramirez, S., Leguey, S., Zeolite formation during the alkaline reaction of bentonite, *European Journal of Mineralogy* **13** (2001) 635-644.

Jimenez Delgado, M.C., Cañas Guerrero, I. Earth building in Spain, *Construction and Building Materials* **20** (2006) 679-690.

Denef, K., Six, J., Clay mineralogy determines the importance of biological versus abiotic processes for macroaggregate formation and stabilization, *European Journal of Soil Science* **56** (2005) 469-470.

Deng, Y., Harsh, J.B., Flury, M., Young, J.S., Boyle, J.S., Mineral formation during simulated leaks of Hanford waste tanks, *Applied Geochemistry* **21** (2006) 1392-1409.

Diamond, S., White, J.L., Dolch, W.L., Transformation of clay minerals by calcium hydroxide attack, *International Series of Monographs on Earth Sciences, Vol.10, Clays and Clay Minerals*, Ingerson, E. (ed.), (A Pergamon Press Book) The Macmillan Company, New York 1964, 359-379.

Doehne, E., Price, C.A., *Stone Conservation - An overview of current research*, The Getty Conservation Institute, Los Angeles ISBN 9781606060469 (2010) 158pp.

Dogan, M., Dogan, A.U., Yesilyurt, F.I., Alaygut, D., Buckner, I., Wurster, D.E., Baseline studies of the Clay Minerals Society Special Clays: Specific surface area by the Brunauer Emmett Teller (BET) method, *Clays and Clay Minerals* **55** (2007) 534-541.

Drief, A., Nieto, F., Sanchez-Navas, A., Experimental clay-mineral formation from a subvolcanic rock by interaction with 1 M NaOH solution at room temperature, *Clays and Clay minerals* **49** (2001) 92-106.

Drief, A., Martinez-Ruiz, F., Nieto, F., Velilla Sanchez, N., Transmission Electron Microscopy evidence for experimental illitization of smectite in K-enriched seawater solution at 50°C and basic pH, *Clays and Clay Minerals* **50** (2002) 746-756.

Duval, Y., Mielczarski, J.A., Pokrovsky, O.S., Mielczarski, E., Ehrhardt, J.J., Evidence of the existence of three types of species at the quartz-aqueous solution interface at pH 0-10: XPS surface group quantification and surface complexation modelling, *Journal of Physical Chemistry B* **106** (2002) 2937-2945.

Duxson, P., Provis, J.L., Lukey, G.C., Mallicoat, S.W., Kriven, W.M., van Deventer, J.S.L., Understanding the relationship between geopolymer composition, microstructure and mechanical properties, *Colloids and Surfaces* A **269** (2005a) 47-58.

Duxson, P., Lukey, G.C., Separovic, F., van Deventer, J.S.J., Effect of alkali cations on aluminum incorporation in geopolymeric gels, *Industrial and Engineering Chemistry Research* **44** (2005b) 832-839.

Eades, J.L., Grim, R.E., Reaction of hydrated lime with pure clay minerals in soil stabilization, *Highways Research Board Bulletin* **262** (1960) 51-63

Eades, J.L., Nichols (Jr.), F.P., Grim, R.E., Formation of new minerals with lime stabilization as proven by field experiments in Virginia, *Highways Research Board Bulletin* **335** (1962) 31-39.

Eberl, D.D., Velde, B., McCormick, T., Synthesis of illite-smectite from smectite at earth surface temperature and high pH, *Clay Minerals* **28** (1993) 49-60.

Edzwald, J.K., Toensing, D. C., and Leung, M. C., Phosphate adsorption reactions with clay minerals, *Environmental Science and Technology* **10** (1976) 485-490.

Elert, K., Rodriguez-Navarro, C., Sebastiabn Pardo, E., Hansen, E., Cazalla, O., Lime mortars for the conservation of historic buildings, *Studies in Conservation* 47 (2002) 62-75.

Elert, K., Sebastian, E., Valverde, I., Rodriguez-Navarro, C., Alkaline treatment of clay minerals from the Alhambra Formation: Implications for the conservation of earthen architecture, *Applied Clay Science* **39** (2008) 122-132.

Felsche, J., Luger, S., Baerlocher, Ch., Crystal structures of the hydro-sodalite $Na_6[ALSiO_4]_6 \cdot 8H_2O$ and of the anhydrous sodalite $Na_6[ALSiO_4]_6$, *Zeolites* **6** (1986) 367-372

Fernandez, A.M., Baeyens, B., Bradbury, M., Rivas, P., Analysis of the porewater chemical composition of a Spanish compacted bentonite used in an engineered barrier, *Physics and Chemistry of the Earth* **29** (2004) 105-118.

Fernandez, R., Cuevas, J., Sanchez, L., Vigil de la Villa, R., Leguey, S., Reactivity of the cement-bentonite interface with alkaline solution using transport cells, *Applied Geochemistry* **21** (2006) 977-992.

Fernandez, R., Rodriguez, M., Vigil de la Vega, R., Cuevas, J., Geochemical constraints on the stability of zeolites and C–S–H in the high pH reaction of bentonite, *Geochimica et Cosmochimica Acta* **74** (2010) 890-906.

Fernandez-Jimenez, A., Monzo, M., Vicent, M., Barba, A., Palomo, A., Alkaline activation of metakaolin-fly ash mixtures: Obtain of Zeoceramics and Zeocements, *Microporous an Mesoporous Materials*, **108** (2008) 41-49.

Flanigen, E.M., Mumpton, F.A., Commercial properties of natural zeolites, *Mineralogy and Geology of Natural Zeolites*, Mineralogical Society of America Short Course Notes **4** 1977, 165-175.

Follet, E.A.C., McHardy, W.J., Mitchell, B.D., Smith, B.F.L., Chemical dissolution techniques in the study of soil clays: Part I, *Clay Minerals* **6** (1965) 23-34.

Font, F., Hidalgo., P., La tapia en España. Técnicas actuales y ejemplos, *Informes de la Construcción* **63** (2011) 21-34.

Foster, M.D., The relation between composition and swelling in clays, *Clay and Clay Minerals* **3** (1955) 205-219.

Franco, F., Perez-Maqueda, L.A., Perez-Rodriguez, J.L., The effect of ultrasound on the particle size and structural disorder of a well-ordered kaolinite, *Journal of Colloid and Interface Science* **274** (2004) 107-117.

Ganor, J., Cama, J., Metz, V., Surface protonation data of kaolinite – reevaluation based on dissolution experiments, *Journal of Colloid and Interface Science* **264** (2003) 67-75.

Gans, W., Thermodynamic stability of sodium sulphate heptahydrate, *Zeitschrift für Physikalische Chemie, Neue Folge*, **111** (1978) 38-46.

Gaucher, E.C., Blanc, P., Cement/clay interactions-a review : Experiments, natural analogues, and modeling, *Waste Management* **26** (2006) 776-788.

Gaudette, H.E., Eades, J.L., Grim, R.E., The nature of illite, *Clays and Clay Minerals 13* (1966) 33-48.

Golden, D.C., Dixon, J.B., Shadfan, H., Kippenberger, L.A., Palygorskite and sepiolite alteration to smectite under alkaline conditions, *Clays and clay minerals* **33** (1985) 44-50.

Goldman, L.J., Greenfield, L.I., Damle, A.S., Kingsbury, G.L., Northheim, C.M., Truesdale, R.S., *Clay liners for waste management facilities – design, construction and evaluation*, EPA Contract No. 68-01-7310, US Environmental Protection Agency, Ohio, USA (1990).

Golubev, S.V., Effect of pH and organic ligands on the kinetics of smectite dissolution at 25 °C, *Geochimica et Cosmochimica Acta* **70** (2006) 4436-4451.

Gonzalez Garcia, F., Sánchez Camazano, M., Differentiation of kaolinite from chlorite by treatment with dimethylsulfoxide, *Clay Minerals* **7** (1968) 447-450

Goudie, A., Viles, H., *Salt weathering hazards*, John Wiley & Sons New York, ISBN 0-471-95842-5, 1997, 241pp.

Greene-Kelly, R., The specific surface areas of montmorillonites, *Clay Minerals B*ulletin **5** (1964) 392-400.

Grim, R.E., *Clay Mineralogy*, Mac Graw-Hill, New York 1968, 596pp.

Groen, J.C., Pfeffer, L.A.A., Perez-Ramirez, J., Pore size determination in modified micro- and mesoporous materials. Pitfalls and limitations in gas adsorption data analysis, *Microporous and Mesoporous Materials* **60** (2003) 1-17.

Grutzeck, M., Kwan, S., DiCola, M., Zeolite formation in alkali-activated cementitious systems, *Cement and Concrete Research* **34** (2004) 949-955.

Hauff, P., *Corrensite: Mineralogical ambiguities and geologic significance*, Geological Survey, Open-File Report 81-850, US Department of the Interior (1981) 45pp.

He, C., Osbaeck, B., Makovicky, E., Pozzolanic reactions of six principal clay minerals: Activation, reactivity assessments and technological effects, *Cement and Concrete Research* **25** (1995) 1691-1702.

Heathcote, K.A., Durability of earthwall buildings, *Construction and Building Materials* **9** (1995) 185-189.

Hedges, J.I., Oades, J.M., Comparative organic geochemistries of soils and marine sediments, *Organic Geochemistry* **27** (1997) 319-361.

Hensen, E.J.M., Smit, B., Why clays swell, *Journal of Physical Chemistry B* **106** (2002) 12664-12667.

Hos, J.P., McCormick, P.G., Byrne, L.T., Investigation of a synthetic aluminosilicate inorganic polymer, *Journal of Materials Science* **37** (2002) 2311-2316.

Houben, H. and Guillaud, H., *Earth construction: a comprehensive guide*. CRA Terre-EAG, Intermediate Technology Publication, London (1994) 362 pp.

Huang, F-C. Lee, J.-F., Lee, C.-K., Chao, H.-P. Effects of cation Exchange on the pore and surface structure and adsorption characteristics of montmorillonite, *Colloids and Surfaces A: Physcochem. Eng. Aspects* **239** (2004) 41-47.

Huertas, F.J., Chou, L., Wollast, R., Mechanism of kaolinite dissolution at room temperature and pressure: Part II. Kinetic study, *Geochimica et Cosmochimica Acta* **63** (1999) 3261-3275.

Huertas, F.J., Carretero, P., Delgado, J., Linares, J., Samper, J., An experimental study on the ion-exchange behaviour of the smectite of Cabo de Gata (Almeria, Spain): FEBEX bentonite, *Journal of Colloid and Interface Science* **239** (2001) 409-416.

Huertas, F.J., Hidalgo, A., Rozalen, M.L., Pellicione, S., Domingo, C., Garcia Gonzalez, C.A., Andrade, C., Alonso, C., Interaction of bentonite with supercritically carbonated concrete, *Applied Clay Science* **42** (2009) 488-496.

Inoue, A., Velde, B., Meunier, A., Touchard, G., Mechanism of illite formation during smectite-to-illite conversion in a hydrothermal system, *American Mineralogist* **73** (1988) 1325-1334.

Ismail, I., Bernal, S.A., Provis, J.L., Hamdan, S., van Deventer, J.S.J., Drying-induced changes in the structure of alkali-activated pastes, *Journal of Material Science* **48** (2013) 3566-3577.

Janssen, M.J.G., van Oorschot, The characterization of zeolites by gas adsorption, *Zeolites: Facts, Figures, Future*, Jacobs, P.A., van Santen, R.A. (eds.) Elsevier, Amsterdam (1989) 633-642.

Jiao, J., Liu, X., Gao, W., Wang, C., Feng, H., Zhao, X., Chen, L., Two-step synthesis of flowerlike calcium carbonate/bipolymer composite materials, *CrystEngComm* **11** (2009) 1886-1891.

Jozefaciuk, G., Bowanko, G., Effect of acid and alkali treatments on surface areas and adsorption energies of selected minerals, *Clays and Clay Minerals* **50** (2002) 771-783.

Kaiser, K., Guggenberger, G., Mineral surfaces and soil matter, *European Journal of Soil Science* **54** (2003) 219-236.

Karnland, O., *Bentonite swelling pressure in strong NaCl solutions*, SKB Technical Report 97-31, Sweden (1997) 30pp.

Karnland, O., Birgersson, M., *Montmorillonite stability*, Technical Report TR-06-11, SKB, Sweden (2006) 39pp.

Karnland, O., Olsson, S., Nilsson, U., Sellin, P., Experimental determined swelling pressures and geochemical interactions of compacted Wyoming bentonite with highly alkaline solutions, *Physics and Chemistry of the Earth* **32** (2007) 275-286.

Kawano, M., Tomita, K., Dehydration and rehydration of saponite and vermiculite, *Clays and Clay Minerals* **39** (1991) 174-183.

Khajavi, S., Kapteijn, F., Jansen, J.C., Synthesis of thin defect-free hydroxyl sodalite membranes: New candidate for activated water permeation, *Journal of Membrane Science* **299** (2007) 63-72.

Kinuthia, J.M., Wild, S., Jones, G.I., Effects of monovalent and divalent metal sulphates on consistency and compactation of lime-stabilised kaolinite, *Applied Clay Science* **14** (1999) 27-45.

Köhler, S.J., Bosbach, D., Oelkers, E.H., Do clay mineral dissolution rates reach steady state ? *Geochimica et Cosmochimica* Acta **69** (2005) 1997-2006.

Kovalchuk, G., Fernandez-Jimenez, A., Palomo, A., Activacion alcalina de cenizas volantes. Relacion entre el desarrollo mecanico resistente y la composicion quimica de la ceniza, *Materiales de Construccion* **58** (2008) 35-52.

Kubicki, J.D., Itoh, M.J., Schroeter, L.M., Apitz, S.E., Bonding Mechanisms of Salicylic Acid Adsorbed onto Illite Clay: An ATR−FTIR and Molecular Orbital Study, *Environmental Science and Technology*, **31** (1997) 1151-1156.

Kühn, H., *Erhaltung und Pflege von Kunstwerken und Antiquitäten 2*, Keysersche Verlagsbuchhandlung, München, ISBN 3874050750 (1981) 424pp.

Kuila, U., Prasad, M., Specific surface area and pore-size distribution in clays and shales, *Geophysical Prospecting* **61** (2013) 341-362.

Kuwahara, Y., In situ AFM study of smectite dissolution under alkaline conditions at room temperature, *American Mineralogist*, **91** (2006) 1142-1149.

Kuwahara, Y., In situ observations of muscovite dissolution under alkaline conditions at 25-50 ºC by AFM with an air/fluid heater system, *American Mineralogist*, **93** (2008) 1028-1033.

Lagaly, G., Chapter 5 - Colloid Clay Science, *Handbook of Clay Science*, Bergaya, F., Theng, B.K.G., Lagaly, G., (eds.), Elsevier Ltd. (2006) 141-245.

Laird, D.A., Influence of layer charge on swelling of smectites, *Applied Clay Science* **34** (2006) 74-87.

Lake, C.A., MacIntyre, W.G., *Phosphate and tripolyphosphate adsorption by clay minerals and Estuarine sediments*, Project A-072-VA, Bulletin 109, Virginia Water Resources Research Center/Virginia Polytechnic Institute and State University, Virginia (1977) 45pp.

Lechert, H., The pH-value and its importance for the crystallization of zeolites, *Verified synthesis of zeolitic materials*, Robson, H. (ed.) Elsevier Science B.V. (2001) 33-38.

Lecomte, I., Liegeois, M., Rulmont, A., Cloots, R., Maseri, F., Synthesis and characterization of a new inorganic polymeric composites based on kaolin or white clay and on ground-granulated blast furnace slag, *Journal of Material Research* **18** (2003) 2571-2579.

Lee, W.K.W., van Deventer, J.S.J., The effects of inorganic salt contamination on the strength and durability of geopolymers, *Colloids and Surfaces A: Physiochem. Eng. Aspects* **211** (2002) 115-126.

Lee; W.K.W., van Deventer, J.S.J., The interface between natural siliceous aggregates and geopolymers, *Cement and Concrete Research* **34** (2004) 195-206.

Leinweber P., Schulten, H.R., Jancke, H., New evidence for the molecular composition of soil organic matter in Vertisols, *Soil Science* **164** (1999) 857-870.

Liebig, E., Althaus, E., Kaolinit and Montmorillonit als puzzolanische Komponenten in Kalkmörteln – unbehandelt und nach thermischer Aktivierung, *Cement, Kalk und Gips International* **50** 5 (1997) 282-290.

Li, S., Liu, Q., Wijn, J., Wolke, J., Zhou, B., Groot, K., In-vitrio apatite formation on phosphorylated bamboo, *Journal of Materials Science: Materials in Medicine* **8** (1997) 543-549.

Li, D., Yao, J., Wang, H., Hao, N., Zhao, D., Ratinac, K.R., Ringer, S.P., Organic-functionalized sodalite nanocrystals and their dispersion in solvents, *Microporous and Mesoporous Materials* **106** (2007) 262-267.

Liu, H.S., Chin, T.S., Lai, L.S., Chiu, S.Y., Hung, K.H., Chang, C.S., Lui, M.T., Hydroxyapatite synthesized by a simplified hydrothermal method, *Ceramics International* **23** (1997) 19-25.

Liu, R., Liu, F., Zhao, S., Su, Y., Wang, D., Shen, Q., Crystallization and oriented attachment of monohydrocalcite and its crystalline phase transformation, *CrystEngComm.* **15** (2013) 509-515.

Liu, X.D., Lu, X.C., A thermodynamic understanding of clay-swelling inhibition by potassium ions, *Angewandte Chemie International Edition* **45** (2006) 6300-6303.

Lorimer, G.W., Cliff, G., Analytical electron microscopy of minerals, *Electron Microscopy in Mineralogy*, Wenk H.R. (ed.), Springer-Verlag, New York, (1976) 506-519.

Lunt, M.G., Stabilised soil blocks for building, *Building Research Establishment, Overseas Building Notes*, No. 184 (1980) 127-144.

Macht, F., Eusterhues, K., Pronk, G.J., Totsche, K.U., Specific surface area of clay minerals: Comparison between atomic force microscopy measurements and bulk-gas (N_2) and liquid (EGME) adsorption methods, *Applied Clay Science* **53** (2011) 20-26.

Madsen, F.T., Müller-Vonmoos, M., The swelling behaviour of clays, *Applied Clay Science* **4** (1989) 143-156.

Mankin, C.J., Dodd, C.G., Proposed reference illite from the Ouachita Mountains of Southeastern Oklahoma, *Clays and Clay Minerals*, Proc. 10th Natl. Conf., Austin, Texas, 1961, Swineford, A. and Franks, P.C. (eds.) Pergamon Press, New York, 372-379.

Marshal, K., Harsh, J.B., Flury, M., Felmy, A.R., Zhao, H., Colloid formation in Hanford sediments reacted with simulated tank waste, *Environmental Science and Technology* **38** (2004) 5750-5756.

Martin Ramos, J.D. *Using Xpowder: A software package for powder X-ray diffraction analysis*. www.xpowder.com, D.L.GR 1001/04, ISBN 84-609-1497-6, Spain (2004) 105pp.

Martin-Garcia, J.M., Delgado, G., Parraga, J.F., Bech, J., Delgado, R., Mineral formation in micaceous Mediterranean red soils of Sierra Nevada, Granada, Spain, *European Journal of Soil Science* **49** (1998) 253-268.

Martin, J.M., Geologia e historia del oro de Granada, *Boletin Geologico y Minero* 111-3 (2000) 47-60.

Martin Vivaldi, J.L., The bentonites of Cabo de Gata (Southeast Spain) and of Guelaya Volcanic Province (North Marocco), *Clays and Clay Minerals* **11** (1962) 327-357.

Matero, F. and Bass, A., Orphans of the storm: The preservation of architectural plasters in earthen ruins, *Cultural Resources Management* **17** (1994) 21-26.

Mayer, L.M., Relationships between mineral surfaces and organic carbon concentrations in soils and sediments, *Chemical Geology* **114** (1994) 347-363.

Mayer, L.M., Extent of coverage of mineral surfaces by organic matter in marine sediments, *Geochimica et Cosmochimica Acta* **63** (1999) 207-215.

McHenry, P.G., *Appropriate building codes and specifications for adobe construction* (Document 13351), US The National Science Foundation, Appropiate Technology International (ATI), Office of Foreign Disaster Assistance (OFDA), Sept. 1981, New Mexico, US, 425-450.

McMurdie, H.F., Flint, E.P., X-ray patterns of hydrated calcium silicates, *Journal of Research of the National Bureau of Standards* **31** (1943) 225-228.

Merchan, N., Bañares-Muñoz, M.A., Vicente, M.A., Intercalation compounds between ethyl-2oxocyclopentanecarboxylate and saponite, *Journal of Inclusion Phenomena and Molecular Recognition in Chemistry* **31** (1998) 219-230.

Merlino, S., Bonaccorsi, E. and Armbruster, T., Tobermorites: Their real structure and order-disorder (OD) character, *American Mineralogist* **84** (1999) 1613-1621.

Mertens, G., Snellings, R., Van Balen, K., Bicer-Simsir, B., Verlooy, P., Elsen, J., Pozzolanic reactions of common natural zeolites with lime and parameters affecting their reactivity, *Cement and Concrete Research* **39** (2009) 233–240.

Mielenz, R.C., Schieltz, N.C., King, M.E., Thermogravimetric analysis of clay and clay-like minerals, *Clays and Clay Mineral* **2** (1954) 285-314.

Mohamed, A.M.O., The role of clay minerals in marly soils on its stability, *Engineering Geology* **57** (2000) 193-203.

Moliner, M., Direct synthesis of functional zeolitic materials, *International Scholarly Research Network Materials Science* **2012** (2012) 24pp.

Moore, D., M., Reynolds, R.C., *X-ray diffraction and the identification and analysis of clay minerals*, Oxford University Press, (1989) 322p.

Moorehead, D.R., Cementation by the carbonation of hydrated lime, *Cement and Concrete Research* **16** (1986) 700-708.

Mowafy, Y.M., Bauer, G.E. and Sakeb, F.H, Treatment of expansive soils: A laboratory study, *Transportation Research Record* **1032** (1979) 34-39.

Mumpton, F.A., Chapter VIII, Using zeolites in agriculture, *Innovative biological technologies for lesser developed countries*, Congress of the US, Office of Technology Assessment, Washington D.C. (1985) 127-157.

Murakami, T., Sato, T., Inoue, A., HRTEM evidence for the process and mechanism of saponite-to-chlorite conversion through corrensite, *American Mineralogist* **84** (1999) 1080-1087.

Murray, H.H., Lyons, S.C., Further correlations of kaolinite crystallinity with chemical and physical properties, *Clays and Clay Minerals* **8** (1960) 11-17.

Murray, H.H., Chapter 2 Structure and Composition of the Clay Minerals and their Physical and Chemical Properties, *Developments in Clay Science* **2** (2006) 7–31.

Newman, A.C.D., The interaction of water with clay mineral surfaces, *Chemistry of clays and clay minerals, Mineralogical Society Monograph No.6*, A.C.D. Newman (ed.) Longman Scientific & Technical, London (1987) 237-274.

Newman, A.C.D., Brown, G., The chemical constitution of clay, *Chemistry of clays and clay minerals, Mineralogical Society Monograph No.6*, A.C.D. Newman (ed.) Longman Scientific & Technical, London (1987) 1-128.

Norrish, K., The swelling of montmorillonite, *Discussion of the Faraday Society* **18** (1954) 120-134.

Novembre, D., Di Sabatino, B., Gimeno, D., Garcia-Valles, M., Martinez-Manent, S., Synthesis of Na-X zeolites from tripolaceous deposits(Crotone, Italy) and volcanic zeolitised rocks (Vico volcano,Italy), *Microporous and Mesoporous Materials* **75** (2004) 1-11.

Oliver, A., Conservation of nondecorated earthen materials, *Terra a literature review - An overview of research in earthen architecture conservation*, Avrami, E., Guillaud, H., Hardy, M. (eds.) J. Paul Getty Trust, Los Angeles (2008) 159 pp.

Ontiveros Ortega E., Sebastián Pardo E., Valverde Espinosa I., Deterioration in XI-XIV century Arab ramparts (Granada, Spain). *Materials and Structures* **32** (1999) 45-51.

Ossa Ossa, F., El Albani, A., Hofmann, A., Bekker, A., Gauthier-Lafaye, F., Pambo, F., Meunier, A., Fontaine, C., Boulvais, P., Pierson-Wickmann, A.C., Cavalazzi, B., Macchiarelli, R., Exceptional preservation of expandable clay minerals in the ca. 2.1 Ga black shales of the Francevillian basin, Gabon and its implication for atmospheric accumulation, *Chemical Geology* **362** (2013) 181-192.

Palomo, A., Glasser, F.P., Chemically-bonded cementitious materials based on metakaolin, *British Ceramic Transactions* **91** (1992) 107-112.

Palomo, A., Blanco-Varela, M.T., Granizo, M.L., Puertas, F., Vazquez, T., Grutzeck, M.W., Chemical stability of cementitious materials based on metakaolin, *Cement and Concrete Research* **29** (1999) 997-1004.

Palumbo G., Ginell W. S., Rodríguez-Navarro C. *Earthen architecture research survey: Analysis report*. Getty Conservation Institute, Los Angeles 1999.

Pamplona, M., Kocher, M., Snethlage, R., Aires Barros, L., Drilling resistance: overview and outlook. *Zeitschrift der Deutschen Gesellschaft für Geowissenschaften* **158** (2007) 665-676.

Pardo, P., Huertas, F.J., Kojdecki, M.A., Bastida, J., Crystallite size evolution in hydrothermal formation of kaolinite, *Zeitschrift für Kristallographie Proceedings* **1** (2011) 63-68.

Pashley, R.M., Quirk, J.P., The effect of cation valency on DLVO and hydration forces between macroscopic sheets of moscovite mica in relation to clay swelling, *Colloids and Surfaces* **9** (1984) 1-17.

Pernyesszi, T., Dekany, I., Surface fractal and structural properties of layered clay minerals monitored by small-angle X-ray scattering and low-temperature nitrogen adsorption experiments, *Colloid and Polymer Science* **281** (2003) 73-78.

Piattoni, Q., Quagliarini, E., Lenci, S., Experimental analysis and modelling of the mechanical behaviour of earthen bricks, *Construction and Building Materials* **25** (2011) 2067-2075.

Plante, A.F., Pernes, M., Chenu, C., Changes in clay-associated organic matter quality in a C depletion sequence as measured by differential thermal analyses, *Geoderma* **129** (2005) 186-199.

Pokrovsky, O.S., Schott, J., Experimental study of brucite dissolution and precipitation in aqueous solution: Surface speciation and chemical affinity control, *Geochimica et Cosmochimica Acta* **68** (2004) 31-45.

Pozo Rodríguez, M., Casas Sainz de Aja, J., Mineralogia y sedimentologia del yacimiento de saponita de Yuncos (Toledo), *Estudios Geologicas* **48** (1992) 47-65.

Prieto, O., Vicente, M.A., Bañares-Muñoz, A., Study of the porous solids obtained by acid treatment of a high surface area saponite, *Journal of Porous Materials* **6** (1999) 335-334.

Prokofev, V. Y., Gordina, N.E., Efremov, A.M., Synthesis of type A zeolite from mechanoactivated metakaolin mixtures, *Journal of Materials Science* **48** (2013) 6276-6285.

Provis, J.L., Lukey, G.C., van Deventer, J.S.J., Do geopolymers actually contain nanocrystalline zeolites? A reexamination of existing results, *Chemistry of Materials* **17** (2005) 3075-3085.

Pusch, R., Karnland, O., Physico/chemical stability of smectite clays, *Engineering Geology* **41** (1996) 73-85.

Pusch, R. Yong, R.N., *Microstructure of smectite clays and engineering performance*, Taylor and Francis, New York (2006).

Rahier, H., Van Mele, B., Biesemans, M., Wastiels, J., Wu, X., Low-temperature synthesized aluminosilicate glasses, Part I. Low-temperature reaction stoichiometry and structure of a model, *Journal of Materials Science* **31** (1996) 71-79.

Rajasekaran, G., Murali, K., Srinivasaraghavan, R., Fabric and mineralogical studies on lime treated marine clays, *Ocean Engineering*. **24** 3 (1997) 227-234.

Ramirez, S., Cuevas, J., Vigil, R., Leguey, S., Hydrothermal alteration of "La Serrata" bentonite (Ameria, Spain) by alkaline solutions, *Applied Clay Science* **21** (2002) 257-269.

Ramirez, S., Vieillard, P., Bouchet, A., Cassagnabere, A., Meunir, A., Jacquot, E., Alteration of the Callovo-Oxfordian clay from Meuse-Haute Marne underground laboratory (France) by alkaline solution. I. A XRD and CEC study, *Applied Geochemistry* **20** (2005) 89-99.

Ransom, B., Bennett, R.H., Baerwald, R., Shea, K., TEM study of in situ organic matter on continental margins: Occurrence and the "monolayer" hypothesis, *Marine Geology* **138** (1997) 1-9.

Rayss, J., Sudolski, G., Ion adsorption in the porous sol-gel silica layer in the fibre optic pH sensor, *Sensors and Actuators B* **87** (2002) 397-405.

Rees, C.A., Provis, J.L., Lukey, G.C., van Deventer, J.S.J., The mechanism of geopolymer gel formation investigated through seeded nucleation, *Colloids and Surfaces A; Physiochem. Eng. Aspects* **318** (2008) 97-105.

Ren, K.B., Kagi, D.A., Upgrading the Durability of Mud Bricks by Impregnation, *Building and Environment* **30** 3 (1995) 433-440.

Richardson, I.G., The calcium silicate hydrates, *Cement and Concrete Research* **38** (2008) 137-158.

Ridha, F.N., *The Thermodynamic study of nitrogen and carbon dioxide adsorption on alkali-exchanged chabazite zeolites*, Doctoral Thesis, Monash University, Australia (2009).

Rios Reyes, C.A., Wiliams, C., Castellanos Alarcon, O.M., Nucleation and growth process of sodalite and cancrinite from kaolinite-rich clay under low-temperature hydrothermal conditions, *Materials Research* **16** (2013) 424-438.

Rodriguez-Navarro, C., Hansen, E., Sebastian, E., Ginell, W.S., The role of clays in the decay of ancient Egyptian limestone sculptures, *Journal of the American Institute for Conservation* **36** (1997) 151-163.

Rodriguez-Navarro, C., Sebastian, E., Doehne, E., Ginell, W.S., The role of sepiolite-palygorskite in the decay of ancient Egyptian limestone sculptures, *Clays and Clay Minerals* **46** (1998) 414-422.

Rodriguez-Navarro, C., Doehne, E., Salt weathering: Influence of evaporation rate, supersaturation and crystallization pattern, *Earth Surface Processes and Landform* **24** (1999) 191-209.

Rodriguez-Navarro, C, Ruiz-Agudo, E., Luque, A., Rodriguez-Navarro, A.B., Ortega-Huertas, M., Thermal decomposition of calcite: Mechanisms of formation and textural evolution of CaO nanocrystals, *American Mineralogist* **94** (2009) 578-593.

Rodriguez-Navarro, C., Kudlacz, K., Ruiz-Agudo, E., The mechanism of termal decomposition of dolomite: New insights from 2D-XRD and TEM analises, *American Mineralogist* **97** (2012) 38-51.

Rogers, C.D.F., Glendinning, S., Improvement of clay soils in situ using lime piles in the UK, *Engineering Geology* **47** (1997) 243-257.

Rolfe, B.N., Miller, R.F., McQueen, I.S., Dispersion characteristics of montmorillonite, kaolinite, and illite clays in waters of varying quality, and their control with phosphate dispersants, *Geological Survey Professional Paper 334-G*, US Government Printing Office, Washington (1960) 229-271.

Romero Jimenez, J.J., *Estudio de un consolidante: Silicato de litio en adobe*, Trabajo Fin de Máster en Ciencia y Tecnología en Patrimonio Arquitectónico, Universidad de Granada (2013) 40pp.

Ross, G.J., Wang, C., Hill, R.G., Mineralogical variability of the clay in a map delineation of Brandon soil, *Canadian Journal of Soil Science* **67** (1987) 83-93.

Rowles, M., O´Connor, B., Chemical optimization of the compressive strength of aluminosilicate geopolymers synthesized by sodium silicate activation of metakaolinite, *Journal of Materials Chemistry* **13** (2003) 1161-1165.

Roy, D.M., Alkali-activated cements. Opportunities and challenges, *Cement and Concrete Research* **29** (1999) 249-254.

Rozalen, M.L., Huertas, F.J., Brady, P.V., Cama, J., Garcia-Palma, S., Linares, J., Experimental study of the effect of pH on the kinetics of montmorillonite dissolution at 25 °C, *Geochimica et Cosmochimica Acta* **72** (2008) 4224-4253.

Rozalen, M., Brady, P.V., Huertas, F.J., Surface chemistry of K-montmorillonite: Ionic strength, temperature dependence and dissolution kinetics, *Journal of Colloid and Interface Science* **333** (2009a) 474-484.

Rozalen, M., Huertas F.J., Brady, P.V., Experimental study of the effect of pH and temperature on the kinetics of montmorillonite dissolution, *Geochimica et Cosmochimica Acta* **73** (2009b) 3752-3766.

Ruiz-Agudo, E., Mees, F., Jacobs, P., Rodriguez-Navarro, C., The role of saline solution properties on porous limestone salt weathering by magnesium and sodium sulfates, *Environmental Geology* **52** (2007) 269-281.

Saidy, A.R., Smernik, R.J., Baldock, J.A., Kaiser, K., Sanderman, J., The sorption of organic carbon onto differing clay minerals in the presence and absence of hydrous iron oxide, *Goderma* **209-210** (2013) 15-21.

Samson, S.D., Nagy, K.L., Cotton, W.B., Transient and quasi-steady-state dissolution of biotite at 22-25ºC in high pH, sodium, nitrate, and aluminate solutions, *Geochimica et Cosmochimica Acta* **69** (2005) 399-413.

Sanchez, L., Cuevas, J., Ramirez, S., Ruiz de Leon, D., Fernandez, R., Vigil dela Villa, R., Leguey, S., Reaction kinetics of FEBEX bentonite in hyperalkaline conditions resembling the cement-bentonite interface, *Applied Clay Science* **33** (2006) 125-141.

Sanders, R.L., Washton, N.M., Mueller, K.T., Measurement of the reactive surface area of clay minerals using solid-state NMR studies of a probe molecule, *Journal of Physical Chemistry C* **114** (2010) 5491-5498.

Saride, S., Puppala, A.J., Chikyala, S.R., Swell-shrink and strength behaviors of lime and cement stabilized expansive organic clays, *Applied Clay Science* **85** (2013) 39-45.

Sasse, H.R., Snethlage, R., Methods for the evaluation of stone consolidation treatments, *Saving our architectural heritage. The conservation of historic stone structures*, Baer, N.S., Snethlage, R. (eds.) John Wiley & Sons Ltd., Chichester (1997) 223-243.

Schiro, M., Ruiz-Agudo, E., Rodriguez Navarro, C., Damage mechanisms of porous materials due to in-pore salt crystallization, *Physical Review Letter* **109** (2012) 265503.

Schoonheydt, R.A., Johnston, C.F., Chapter 5. Surface and interface chemistry of clay minerals, *Handbook of Clay Science*, Bergaya, F., Theng, B.K.G., Lagaly, G., (eds.), Elsevier, Oxford (2006) 139-172.

Schumacher, B.A., *Methods for the determination of total organic carbon/TOC) in soils and sediments*, US Environmental Protection Agency, Las Vegas (2002) 23pp.

Sebastián Pardo, E.M., *Proyecto Docente*, Universidad de Granada (2003) 279pp.

Sebastián Pardo, E.M., Rodriguez Gallego,M., Perez Lorente, F., Mineralogia y genesis de la haloisita de Haro (La Rioja), *Boletin Sociedad Española de Mineralogia* **7** (1983)133-138.

Sebastian, E., Cultrone, G., (2010), Chapter 2, Technology of Rammed-Earth Constructions ("Tapial") in Andalusia (Spain): Their Restoration and

Conservation, *Materials, Technologies and Practice in Historic Heritage Structures*, Bostenaru Dan, M. et al. (eds.), ISBN: 978-90-481-2683-5, Springer Science.

Selwitz, C., Coffman, R., Agnew, N., The Getty adobe research project at Fort Selden III: An evaluation of the application of chemical consolidants to test walls, *Proceedings of the 6th International Conference on the Conservation of Earthen Architecture: Adobe 90 preprints*: October 14-19, 1990, Las Cruces, New Mexico. Grimstad, K. (ed.), The Getty Conservation Institute, Marina del Rey, California, 255-260.

Sherry, H.S., Exchange in the synthetic zeolites Linde X and Y, *Journal of Physical Chemistry* **78** (1968) 4086-4094.

Shibue, Y., Cation-exchange reactions of siliceous and aluminous phillipsites, *Clays and Clay Minerals* **29** (1981) 397-402.

Siegel, M.D., Leckie, J.O., Park, S.W., Phillips, S.L., Sewards, T., *Studies of radionuclide sorption by clays in the Culebra dolomite at the Wipp Site, Southeastern New Mexico*, Technical Report SAND-89-2387, Sandia National Labs., Albuquerque, NM (USA) (1990) 893-900.

Sig Ko, Y., Seung Ahn, W., Crystallization of zeolite L from Na_2O-K_2O-A_2O_3-SiO_2-H_2O system, *Powder Technology* **145** (2004) 10-19.

Sing, K.S.W., Everett, D.H., Haul, R.A.W., Moscou, L., Pierotti, R.A., Rouquerol, J., Siemieniewska, T., Reporting physisorption data for gas/ solid systems, *Pure and Applied Chemistry* **57** (1985) 603-619.

Slade, P.G., Quirk, J.P., Norrish, K., Crystalline swelling of smectite samples in concentrated NaCl solutions in relation to layer charge, *Clays and Clay Minerals* **39** (1991) 234-238.

Slaty, F., Khoury, H., Wastiels, J., Rahier, H., Characterization of alkali activated kaolinitic clay, *Applied Clay Science* **75-76** (2013) 120-125.

Smart, L.E., Moore, E.A., Solid state chemistry – An introduction, CRC Press, Taylor & Francis Group, Boca Raton (2005) 407pp.

Sposito, G., *The surface chemistry of soils*, Oxford University Press, New York (1984).

Steiger, M., Asmussen, S., Crystallization of sodium sulphate phases in porous materials: The phase diagram Na2SO4-H2O and the generation of stress, *Geochimica at Cosmochimica Acta* **72** (2008) 4291-4306

Stumm, W., Reactivity at the mineral-water interface: Dissolution and inhibition, *Colloids and Surfaces A* **120** (1997) 143-166.

Suarez Barrios, M., Vicente-Rodriguez, M.A., Martin Pozas, J.M., Intercalation compounds between nicotine and a high surface area saponite, *Journal of*

Inclusion Phenomenae and Molecular Recognition in Chemistry **24** (1996) 263-272.

Sutarno and Arryanto,Y., Synthesis of faujasite from fly ash and its application for hydrocracking of petroleum distillates, *Bulletin of Chemical Reaction Engineering and Catalysis* **2** (2007) 45-51.

Swanepoel, J.C., Strydom, C.A., Utilisation of fly ash in a geopolymeric material, *Applied Geochemistry* **17** (2002) 1143-1148.

Taubald, H., Bauer, A., Schäfer, T., Geckeis, H., Satir, M., Kim, J.I., Experimental investigation of the effect of high-pH solutions on the Opalinus Shale and Hammerschmiede smectite, *Clay Minerals* **35** (2000) 515-524.

Thomas, P.J., *Quantifying properties and variability of expansive soils in selected map units*, PhD Thesis, Virginia Polytechnique Institute and State University, USA, 1998.

Thommes, M, Chapter 15. Textural characterization of zeolites and ordered mesoporous materials by physical adsorption, *Studies in the Surface Science and Catalysis* **168** (2007) Pages 495–523.

Tiano, P., Delgado Rodrigues, J., De Witte, E., Verges-Belmin,V.,Massey, S., Snethlage, R.,Costa, D., Cadot-Leroux,L., Garrod, E., Singer, B., The conservation of monuments: A new method to evaluate consolidating treatments. *International Journal for Restoration of Buildings and Monuments* **6** (2000) 133-150.

Toranzo, R., Vicente, M.A., Bañares-Muñoz, M.A., Pillaring of a saponite with aluminium-chromium oligomers. Characterization of the solids obtained, *Chemistry of Mat*erials **9** (1997) 1829-1836.

Tombacz, E., Szekeres, M., Baranyi, L., Micheli, E., Surface modification of clay minerals by organic polyions, *Colloids and Surfaces A* **141** (1998) 379-384.

Tracy, S.L., Williams, D.A., Jennings, H.M., The growth of calcite spherulites from solution II.Kinetics of formation, *Journal of crystal growth* **193** (1998) 332-388.

UNE-EN 1015-11, Metodos de ensayo de los morteros para albañilería, AENOR Asociación Española de Normalización y Certificación (2000) 14pp.

Valverde, J.L., Cañizares, P., Sun Kou, M.R., Molina, C.B., Enhanced thermal stability of Al-pillared smectites modified with Ce and La, *Clays and Clay Minerals* **48** (2000) 424-432.

van Jaarsveld, J.G.S., van Deventer, J.S.J., Lorenzen, L., The potential use of geopolymeric materials to immobilise toxic metals: Part I. Theory and applications, *Minerals Engineering* **10** 7 (1997) 659-669.

van Jaarsveld, J.G.S., van Deventer, J.S.J., Effect of the alkali metal activator on the properties of fly ash-based geopolymers, *Industrial and Engineering Chemistry Research* **38** (1999) 3932-3941.

van Jaarsveld, J.G.S., van Deventer, J.S.J., Lukey, G.C., The effect of composition and temperature on the properties of fly-ash and kaolinite-based geopolymers, *Chemical Engineering Journal* **89 (**2002) 63-73.

van Olphen, H., Dispersion and flocculation, in *Chemistry of Clay Minerals, Mineralogical Society Monograph No.6*, Newman, A.C.D. (ed.), Longman Scientific & Technical, London 1987, 203-224.

Velde, B., *Introduction to clay minerals: chemistry, origins, uses and environmental significance*, Chapman and Hall, London (1992), 198pp.

Velde, B., Meunier, A., *The origin of clay minerals in soils and weathered rocks*, Springer Verlag, Berlin (2008).

Vicente, M.A., Bañares-Muñoz, M.A., Gandía, L.M., Gil, A., On the structural changes of a saponite intercalated with various polycations upon thermal treatments, *Applied Catalysis A: General* **217** (2001) 191-204.

Vicente Valverde, I., *Synthesis of hectorites and saponites with microwaves and their application in catalysis and composites*, Doctoral thesis, Universidad Rovira I Virgili , Tarragona (2010) ISBN:/DL:T. 1033-2011.

Vigil de la Villa, R., Cuevas, J., Ramirez, S., Leguey, S., Zeolite formation during alkaline reaction of bentonite, *European Journal of Mineralogy* **13** (2001) 635-644.

Wang, H., Li, H., Yan, F., Synthesis and tribological behaviour of metakaoline-based geopolymer composites, *Materials Letters* **59** (2005) 3976-3981.

Wattel-Koekkoek, E., *Clay-associated organic matter in kaolinitic and smectitic soils*, PhD Thesis, Wageningen University, The Netherlands (2002),120pp.

White, A.F., Brantley, S.L., Chemical weathering rates of silicate minerals: An overview, *Reviews in Mineralogy Vol. 31, Chemical Weathering rates of silicate minerals*, White, A.F., Brantley, S.L., (eds.) Mineralogical Society of America, Washington D.C., (1995) 1-22.

Wild, S., Arabi, M. and Rowlands, G.O., Relation between poro size distribution, permeability, and cementitious gel formation in cured clay-lime systems, *Materials Science and Tech*nology **2** (1987) 1005-1011.

Wilson, J., Savage, D., Cuadros, J., Shibata, M., Vala Ragnarsdottir, K., The effect of iron on montmorillonite stability, I Background and thermodynamic considerations, *Geochimica et Cosmochimica Acta* **700** (2006) 306-322.

Wilson, M.J., (ed.), *A handbook of determinative methods in clay mineralogy*, Blackie and Son Ltd, London 1987.

Wolff-Boenisch, D., Gislason, S.R., Oelkers, E.H., The effect of crystallinity on dissolution rates and CO_2 consumption capacity of silicates, *Geochimica et Cosmochimica Acta* **70** (2006) 858-870.

Wongpa, J., Kiattikomol, K., Jaturapitakkul, C., Chindaprasirt, P., Compressive strength, modulus of elasticity, and water permeability of inorganic polymer concrete, *Materials and Design* **31** (2010) 4748-4754

Worden, R.H., Champness, P.E., Droop, G.T.R., Transmission electron microscopy of pyrometamorphic breakdown of phengite and chlorite, *Mineralogical Magazine*, **51** (1987) 107-121.

Xeidakis, G.S., Stabilization of swelling clays by $Mg(OH)_2$. Factors affecting hydroxy-Mg-interlayering in swelling clays, *Engineering Geology* **44** 1-4 (1996) 93-106.

Xie, Z., Walther, J.V., Incongruent dissolution and surface area of kaolinite, *Geochimica et Cosmochimica Acta* **56** (1992) 3357-3363.

Xu, H., van Deventer, J.S.J., The geopolymerisation of alumino-silicate minerals, *International Journal of Mineral Processing* **59** (2000) 247-266.

Yip, C.K., Lukey, G.C., van Deventer, J.S.J., The coexistence of geopolymeric gel and calcium silicate hydrate at the early stage of alkaline activation, *Cement and Concrete Research* **35** (2005) 1688-1697.

Yokoyama, S., Kuroda, M., Sato, T., Atomic force microscopy study of montmorillonite dissolution under highly alkaline conditions, *Clays and Clay Minerals*, **53** (2005) 147-154.

Yuang, P.C., Shen, Y.H., Determination of the surface area of smectite in water by ethylene oxide chain adsorption, *Journal of Colloid and Interface Science* **285** (2005) 443-447.

Zech, W., Senesi, N., Guggenberger, G., Kaiser, K., Lehmann, J., Miano, T.M., Miltner, A., Schroth, G., Factors controlling humification and mineralization of soil organic matter in the tropics, *Geoderma* **79** (1997) 117-161.

Zhang, G., Delgado-Lopez, J.M., Choquesillo-Lazarte, D., Garcia-Ruiz, J.M., Crystallization of monohydrocalcite in silica-rich alkaline solution, *CrystEngComm* **15** (2013) 6526-6532.

Zhang, W.Z., Chen, X.Q., Zhou, J.M., Liu,D.H., Wang, H.Y.,Du, C.W., Influence of humic acid on interaction of ammonium and potassium ions on clay minerals, *Pedosphere* **23** (2013) 493-502.

Zinder, B., Furrer, G., Stumm, W., The coordination chemistry of weathering: II. Dissolution of Fe(III) oxides, *Geochimica et Cosmochimica Acta* **50** (1986) 1861-1869.